

UCLA

UCLA Electronic Theses and Dissertations

Title

Metal-Mediated Transformations of Strained Intermediates

Permalink

<https://escholarship.org/uc/item/9fj6f9r9>

Author

Spence, Katie Anne

Publication Date

2023

Peer reviewed|Thesis/dissertation

UNIVERSITY OF CALIFORNIA

Los Angeles

Metal-Mediated Transformations of Strained Intermediates

A dissertation submitted in partial satisfaction of the
requirements for the degree Doctor of Philosophy
in Chemistry

by

Katie Anne Spence

2023

© Copyright by
Katie Anne Spence
2023

ABSTRACT OF THE DISSERTATION

Metal-Mediated Transformations of Strained Intermediates

by

Katie Anne Spence

Doctor of Philosophy in Chemistry

University of California, Los Angeles, 2023

Professor Neil K. Garg, Chair

This dissertation describes the study of metal-mediated transformations of strained cyclic alkynes and their applications to synthetic organic chemistry. Strained cyclic alkynes are in situ generated, fleeting intermediates with strain energies ranging from 40–50 kcal/mol. Harnessing the reactivity of these strained molecules, while challenging in many cases, offers a means to form multiple bonds in a single step, and generate products that may be inaccessible by other means. Herein, several synthetic endeavors are described that leverage strain release to advance our understanding of chemical reactivity and gain new entryways into important classes of organic and organometallic compounds. Finally, this dissertation describes a study towards the development

of marijuana breathalyzer technology, which focuses on performing electrochemical oxidations of Δ^9 -THC at low concentrations.

Chapter one gives an overview of metal-mediated transformations of strained intermediates. Whereas strained intermediates such as cyclic alkynes and allenes are typically utilized in cycloadditions and nucleophilic additions, a third major mode of strained intermediate chemistry involves transition metal catalysis. The merger of metal catalysis and strained intermediates has enabled rapid access to complex, polycyclic systems and the broad applicability of such transformations, including exciting future directions, are discussed.

Chapters two and three describe the development of new methodologies that exploit strained arynes in the synthesis of complex organic and organometallic materials. Both chapters investigate the controlled generation and reactivity of aryne intermediates, as well as engagement of these intermediates in Pd-catalysis to build new ring systems. Chapter two details the development of Pd-catalyzed reactions of indole and carbazole-based arynes (i.e., hetarynes) to access π -extended heterocyclic materials. The products obtained were applied as ligands in two-coordinate metal complexes to access new OLED emitters. Chapter three details the development of aryne chemistry “on-the-complex,” wherein fleeting aryne intermediates are reacted with pre-coordinated metal–ligand complexes to form new carbon–carbon bonds. These studies, performed in the context of privileged, photoactive polypyridyl metal complexes, provide an effective strategy to annulate organometallic complexes and access complex metal–ligand scaffolds, while furthering the synthetic utility of strained intermediates in chemical synthesis.

Chapter four details two total syntheses of tylophorine, a natural product with anti-cancer properties, via metal-mediated transformations of strained azacyclic alkynes. Such strained intermediates are relatively understudied in comparison to their aromatic counterparts. This

chapter explores access to strained azacyclic alkynes, including a new 'indolizidyne' intermediate, and demonstrates their use in a total synthesis effort. These studies should prompt the further exploration of these strained azacyclic alkyne intermediates.

Chapter five details research toward the development of marijuana breathalyzer technologies. Specifically, this chapter describes how electrochemical oxidation of Δ^9 -THC can be performed at nanomolar concentrations, which approaches the levels of Δ^9 -THC found on the breath of a THC-impaired individual. Moreover, this chapter describes how vaporized Δ^9 -THC can be captured directly in electrolyte medium, and subsequently subjected to electrochemical oxidation, thus paving the way for future technology development.

The dissertation of Katie Anne Spence is approved.

Kendall N. Houk

Abigail G. Doyle

Yi Tang

Neil K. Garg, Committee Chair

University of California, Los Angeles

2023

“When the world is in trouble, chemistry comes to the rescue.”

– Carolyn Bertozzi

For my family.

TABLE OF CONTENTS

ABSTRACT OF THE DISSERTATION	ii
COMMITTEE PAGE	v
DEDICATION PAGE	vi
TABLE OF CONTENTS.....	vii
LIST OF FIGURES AND SCHEMES	xii
LIST OF TABLES.....	xxi
LIST OF ABBREVIATIONS.....	xxii
ACKNOWLEDGEMENTS.....	xxviii
BIOGRAPHICAL SKETCH	xxxvi
CHAPTER ONE: Merging Metals and Strained Intermediates	1
1.1 Abstract.....	1
1.2 Introduction.....	1
1.3 Use of Arynes to Access Organometallic Complexes	6
1.4 Use of Cyclic Allenes in Enantioselective Metal-Catalyzed Annulations.....	9
1.5 Looking Forward	12
1.6 Notes and References.....	13
CHAPTER TWO: π -Extension of Heterocycles via a Pd-Catalyzed Heterocyclic Aryne Annulation: π -Extended Donors for TADF Emitters	23
2.1 Abstract.....	23
2.2 Introduction.....	24
2.3 Results and Discussion	28

2.3.1 Pd-Catalyzed Annulations of Indolyne.....	28
2.3.2 Carbazolyne Studies.....	30
2.3.3 Application of π -Extended Products as TADF Emitters	31
2.4 Conclusions.....	43
2.5 Experimental Section.....	45
2.5.1 Materials and Methods.....	45
2.5.2 Experimental Procedures	47
2.5.2.1 Scope of Pd-Catalyzed Annulation with <i>N</i> -Me-4,5-Indolyne.....	47
2.5.2.2 Synthesis of Silyl Triflate Precursor to 2,3-Carbazolyne	55
2.5.2.3 Annulation of <i>N</i> -Me-Carbazolyne	59
2.5.2.4 Synthesis of N–H Annulation Products for Metal Coordination ...	59
2.5.2.5 Synthesis of Two-Coordinate Metal Complexes	62
2.5.2.6 General Procedure for Photophysical Property Analyses.....	65
2.5.2.7 Absorption Spectra of Donor Ligands	66
2.5.2.8 Emission Spectra of Deprotonated Donor Ligands	66
2.6 Computational Methods.....	68
2.6.1 Complete Citation of Q-Chem 5.1	68
2.6.2 Calculated Frontier Molecular Orbital Energies.....	69
2.7 Photoluminescence (PL) Decay Lifetime Data.....	70
2.7.1 Lifetime Plots.....	70
2.8 Spectra Relevant to Chapter Two	75
2.9 Notes and References.....	97

CHAPTER THREE: A Platform for On-the-Complex Annulation Reactions with Transient Aryne Intermediates.....	108
3.1 Abstract.....	108
3.2 Introduction.....	108
3.3 Development of the Pd-Catalyzed On-the-Complex Aryne Reaction.....	113
3.4 Scope of the Pd-Catalyzed Annulation.....	116
3.5 Generation and Trapping of an Organometallic Aryne.....	119
3.6 Photophysical Studies.....	124
3.7 Conclusion.....	127
3.8 Experimental Section.....	128
3.8.1 Materials and Methods.....	128
3.8.2 Experimental Procedures.....	130
3.8.2.1 Synthesis of Halobipyridine Organometallic Complexes.....	130
3.8.2.2 Optimization of on-the-Complex Annulation with Benzyne.....	143
3.8.2.3 Crystallographic Data.....	145
3.8.2.4 Synthesis of Silyl Triflate Aryne Precursors.....	146
3.8.2.5 Scope of Pd-Catalyzed Aryne Annulation.....	149
3.8.2.6 Synthesis and Trapping Experiments of Ru-Centered Aryne.....	160
3.8.3 Photophysical Data.....	169
3.8.3.1 Compiled Photophysical Data Table.....	170
3.8.3.2 UV–Vis Spectra.....	171
3.8.3.3 Molar Extinction Coefficient Measurements.....	172
3.8.3.4 Quantum Yield Measurements.....	175

3.8.4 Computational Data	176
3.8.4.1 Complete Citation of Gaussian 16	176
3.8.4.2 Energy and Cartesian Coordinates for Optimized Structure.....	177
3.9 Spectra Relevant to Chapter Three	180
3.10 Notes and References.....	207
CHAPTER FOUR: Total Synthesis of Phenanthroindolizidines Using Strained Azacyclic Alkynes	
.....	218
4.1 Abstract.....	218
4.2 Introduction.....	218
4.3 Results and Discussion	222
4.3.1 Access to Tylophorine via a Piperidyne Annulation	222
4.3.2 Access to an Indolizidyne Precursor.....	223
4.3.3 Access to Phenanthroindolizidines via Indolizidyne Chemistry	225
4.4 Conclusions.....	227
4.5 Experimental Section	227
4.5.1 Materials and Methods.....	227
4.5.2 Experimental Procedures	229
4.5.2.1 Access to Tylophorine Through a Piperidyne	229
4.5.2.2 Access to the Silyl Tosylate Indolizidyne Precursor	234
4.5.2.3 Silyl Triflate Decomposition.....	239
4.5.2.4 Annulations of Indolizidyne to Access Natural Products	240
4.6 Spectra Relevant to Chapter Four	243

4.7 Notes and References.....	253
CHAPTER FIVE: Electrochemical Oxidation of Δ^9 -Tetrahydrocannabinol at Nanomolar Concentrations	264
5.1 Abstract.....	264
5.2 Introduction.....	264
5.3 Results and Discussion	267
5.4 Conclusions.....	273
5.5 Experimental Section.....	274
5.5.1 Materials and Methods.....	274
5.5.2 Experimental Procedures	276
5.5.2.1 LC-MS/MS Methods	276
5.5.2.2 General Procedure for Electrochemical Oxidation Reactions	277
5.5.2.3 Select Results from Electrochemical Oxidation Screening	278
5.5.2.4 Procedure for the Vaporization, Capture and Subsequent Oxidation of Δ^9 -THC	281
5.5.2.4.1 Vaporization	281
5.5.2.4.2 Electrochemical Oxidation	281
5.5.2.5 Chromatographic Comparison of <i>ortho</i> - and <i>para</i> - Isomers of Δ^9 -THCQ	283
5.5.2.6 Independent Chemical Oxidation of Δ^9 -THC to Δ^9 -THC <i>ortho</i> -Quinone (5.3)	284
5.5.2.7 Relevant Photophysical Data for 5.3	285

5.6 Spectra Relevant to Chapter Five	287
5.7 Notes and References.....	293

LIST OF FIGURES AND SCHEMES

CHAPTER ONE

<i>Figure 1.1</i> Seminal studies of strained, cyclic intermediates.....	3
<i>Figure 1.2</i> Transition metal-stabilized strained intermediates	4
<i>Figure 1.3</i> Transition metal-catalyzed reactions of arynes	5
<i>Figure 1.4</i> Arynes on-the-complex	8
<i>Figure 1.5</i> Transition metal-catalyzed annulations	11

CHAPTER TWO

<i>Figure 2.1</i> Examples of heteroatom-containing PAHs with applications in materials chemistry.....	24
<i>Figure 2.2</i> Approaches for π -extension of hetarynes.....	26
<i>Scheme 2.1</i> Mechanism for TADF emission in comparison to fluorescence and phosphorescence	28
<i>Figure 2.3</i> π -Extension of indolynes.....	30
<i>Figure 2.4</i> Synthesis of carbazolyne precursors.....	32
<i>Figure 2.5</i> Synthesis of N–H products 2.34 and 2.35	33

Figure 2.6 Heterocyclic PAHs as donor ligands in TADF complexes	35
Figure 2.7 Preparation (A) and structures (B) of two-coordinate gold complexes.....	26
Figure 2.8 Absorption (left) and emission spectra (right) for the carbene-Au-carbazolyl complexes	38
Figure 2.9 Absorption (left) and emission spectra (right) for carbene-Au-indolyl complexes	41
Figure 2.10 Extinction coefficients for the donor ligands in 2-MeTHF	66
Figure 2.11 Emission spectra of 2-methylindol-1-ide in 2-MeTHF	67
Figure 2.12 Emission spectra of ligand 2.34 ⁻ in 2-MeTHF	67
Figure 2.13 Emission spectra of ligand 2.35 ⁻ in 2-MeTHF	68
Figure 2.14 Emission lifetime decay for 2.36 + π	70
Figure 2.15 Emission lifetime decay for 2.37 + π	71
Figure 2.16 Emission lifetime decay for 2.38	72
Figure 2.17 Emission lifetime decay for 2.38 + π	73
Figure 2.18 ¹ H NMR (500 MHz, CDCl ₃) of compound 2.16	76
Figure 2.19 ¹³ C NMR (125 MHz, CDCl ₃) of compound 2.16	76
Figure 2.20 ¹ H NMR (500 MHz, C ₆ D ₆) of compounds 2.17 and 2.40	77
Figure 2.21 ¹³ C NMR (125 MHz, C ₆ D ₆) of compounds 2.17 and 2.40	77
Figure 2.22 ¹ H NMR (600 MHz, CDCl ₃) of compounds 2.18 and 2.42	78
Figure 2.23 ¹³ C NMR (125 MHz, CDCl ₃) of compounds 2.18 and 2.42	78
Figure 2.24 ¹ H NMR (500 MHz, CDCl ₃) of compounds 2.19 and 2.44	79
Figure 2.25 ¹³ C NMR (100 MHz, CDCl ₃) of compounds 2.19 and 2.44	79
Figure 2.26 NOESY NMR (500 MHz, CDCl ₃) of compounds 2.19 and 2.44	80

Figure 2.27 ^1H NMR (500 MHz, C_6D_6) of compounds 2.20 and 2.46	81
Figure 2.28 ^{13}C NMR (125 MHz, C_6D_6) of compounds 2.20 and 2.46	81
Figure 2.29 ^1H NMR (500 MHz, C_6D_6) of compounds 2.21 and 2.48	82
Figure 2.30 ^{13}C NMR (125 MHz, C_6D_6) of compounds 2.21 and 2.48	82
Figure 2.31 ^1H NMR (500 MHz, C_6D_6) of compounds 2.22 and 2.50	83
Figure 2.32 ^{13}C NMR (125 MHz, C_6D_6) of compounds 2.22 and 2.50	83
Figure 2.33 NOESY NMR (125 MHz, C_6D_6) of compounds 2.22 and 2.50	84
Figure 2.34 ^1H NMR (500 MHz, CDCl_3) of compound 2.25	85
Figure 2.35 ^{13}C NMR (125 MHz, CDCl_3) of compound 2.25	85
Figure 2.36 ^1H NMR (400 MHz, CDCl_3) of compound 2.28	86
Figure 2.37 ^{13}C NMR (150 MHz, CDCl_3) of compound 2.28	86
Figure 2.38 ^1H NMR (400 MHz, CDCl_3) of compound 2.29	87
Figure 2.39 ^{13}C NMR (125 MHz, CDCl_3) of compound 2.29	87
Figure 2.40 ^1H NMR (600 MHz, CDCl_3) of compound 2.30	88
Figure 2.41 ^{13}C NMR (125 MHz, CDCl_3) of compound 2.30	88
Figure 2.42 ^1H NMR (500 MHz, CDCl_3) of compound 2.31	89
Figure 2.43 ^{13}C NMR (125 MHz, CDCl_3) of compound 2.31	89
Figure 2.44 ^1H NMR (400 MHz, CDCl_3) of compound 2.32	90
Figure 2.45 ^{13}C NMR (100 MHz, CDCl_3) of compound 2.32	90
Figure 2.46 ^1H NMR (500 MHz, CDCl_3) of compound 2.34	91
Figure 2.47 ^{13}C NMR (125 MHz, CDCl_3) of compound 2.34	91
Figure 2.48 ^1H NMR (600 MHz, CDCl_3) of compound 2.35	92
Figure 2.49 ^{13}C NMR (125 MHz, CDCl_3) of compound 2.35	92

Figure 2.50 ^1H NMR (400 MHz, CDCl_3) of compound 2.36 + π	93
Figure 2.51 ^{13}C NMR (150 MHz, CDCl_3) of compound 2.36 + π	93
Figure 2.52 ^1H NMR (400 MHz, CDCl_3) of compound 2.37 + π	94
Figure 2.53 ^{13}C NMR (100 MHz, CDCl_3) of compound 2.37 + π	94
Figure 2.54 ^1H NMR (400 MHz, acetone- d_6) of compound 2.38	95
Figure 2.55 ^{13}C NMR (100 MHz, acetone- d_6) of compound 2.38	95
Figure 2.56 ^1H NMR (400 MHz, acetone- d_6) of compound 2.38 + π	96
Figure 2.57 ^{13}C NMR (150 MHz, acetone- d_6) of compound 2.38 + π	96

CHAPTER THREE

Figure 3.1 General synthetic approaches toward metal–ligand complexes.....	111
Figure 3.2 Arynes-on-the-complex approach to metal complexes	112
Figure 3.3 Optimization studies for Pd-catalyzed annulation of benzyne onto Ru-polypyridyl complex 3.14	115
Figure 3.4 Aryne scope of the Pd-catalyzed aryne annulation. Yields shown reflect the average of two isolation experiments	117
Figure 3.5 Pd-catalyzed aryne annulation of Ir-centered polypyridyl metal complexes. Yields shown reflect the average of two isolation experiments	118
Figure 3.6 Pd-catalyzed aryne annulation at multiple sites of Ru complexes. Yields shown reflect the average of two isolation experiments	119
Figure 3.7 Synthesis of an organometallic aryne precursor via masked bis(aryne) annulation	121
Figure 3.8 Mild generation and trapping of a Ru(II) aryne	123

Figure 3.9 Photophysical studies of bis(annulation) product 3.31 and tris(annulation) product 3.33 relative to [Ru(bpy) ₃] ²⁺ (3.17). Evaluation of luminescence quantum yield (Φ , %) and molar extinction coefficient (ϵ , mol ⁻¹ cm ⁻¹).....	126
Figure 3.10 Unsuccessful aryne annulation of free ligands 3.47 and 3.49	145
Figure 3.11 ORTEP representation of X-ray crystallographic structure 3.16 . (CCDC Registry #2048567).....	145
Figure 3.12 UV–vis absorption spectra of compounds 3.17 , 3.16 , 3.31 , and 3.33	171
Figure 3.13 UV–vis absorption spectra of compounds 3.17 , 3.41 , 3.42 , and 3.43	171
Figure 3.14 Beer-Lambert plot of 3.17 at 452 nm	172
Figure 3.15 Beer-Lambert plot of 3.16 at 452 nm	172
Figure 3.16 Beer-Lambert plot of 3.31 at 452 nm	173
Figure 3.17 Beer-Lambert plot of 3.33 at 452 nm	173
Figure 3.18 Beer-Lambert plot of 3.41 at 452 nm	174
Figure 3.19 Beer-Lambert plot of 3.42 at 452 nm	174
Figure 3.20 Beer-Lambert plot of 3.43 at 452 nm	175
Figure 3.21 ¹ H NMR (500 MHz, CDCl ₃) of compound 3.47	181
Figure 3.22 ¹ H NMR (500 MHz, CDCl ₃) of compound 3.49	181
Figure 3.23 ¹ H NMR (400 MHz, CDCl ₃) of compound 3.14a	182
Figure 3.24 ¹³ C NMR (125 MHz, CDCl ₃) of compound 3.14a	182
Figure 3.25 ¹ H NMR (400 MHz, CD ₃ CN) of compound 3.14b	183
Figure 3.26 ¹³ C NMR (125 MHz, CD ₃ CN) of compound 3.14b	183
Figure 3.27 ¹ H NMR (500 MHz, CD ₃ CN) of compound 3.26	184
Figure 3.28 ¹³ C NMR (125 MHz, CD ₃ CN) of compound 3.26	184

<i>Figure 3.29</i> ^1H NMR (500 MHz, CD_3CN) of compound 3.32	185
<i>Figure 3.30</i> ^{13}C NMR (125 MHz, CD_3CN) of compound 3.32	185
<i>Figure 3.31</i> ^1H NMR (500 MHz, CD_3CN) of compound 3.54	186
<i>Figure 3.32</i> ^{13}C NMR (125 MHz, CD_3CN) of compound 3.54	186
<i>Figure 3.33</i> ^1H NMR (500 MHz, CD_3CN) of compound 3.56	187
<i>Figure 3.34</i> ^{13}C NMR (125 MHz, CD_3CN) of compound 3.56	187
<i>Figure 3.35</i> ^1H NMR (500 MHz, CD_3CN) of compound 3.58	188
<i>Figure 3.36</i> ^{13}C NMR (125 MHz, CD_3CN) of compound 3.58	188
<i>Figure 3.37</i> ^1H NMR (500 MHz, CDCl_3) of compound 3.62	189
<i>Figure 3.38</i> ^1H NMR (600 MHz, CDCl_3) of compound 3.68	189
<i>Figure 3.39</i> ^1H NMR (500 MHz, CD_3CN) of compound 3.36	190
<i>Figure 3.40</i> ^{13}C NMR (125 MHz, CD_3CN) of compound 3.36	190
<i>Figure 3.41</i> ^1H NMR (500 MHz, CD_3CN) of compound 3.16	191
<i>Figure 3.42</i> ^{13}C NMR (125 MHz, CD_3CN) of compound 3.16	191
<i>Figure 3.43</i> ^1H NMR (600 MHz, CD_3CN) of compound 3.21	192
<i>Figure 3.44</i> ^{13}C NMR (125 MHz, CD_3CN) of compound 3.21	192
<i>Figure 3.45</i> ^1H NMR (500 MHz, CD_3CN) of compound 3.22	193
<i>Figure 3.46</i> ^{13}C NMR (125 MHz, CD_3CN) of compound 3.22	193
<i>Figure 3.47</i> ^1H NMR (600 MHz, CD_3CN) of compound 3.23	194
<i>Figure 3.48</i> ^{13}C NMR (125 MHz, CD_3CN) of compound 3.23	194
<i>Figure 3.49</i> ^1H NMR (500 MHz, CD_3CN) of compound 3.26	195
<i>Figure 3.50</i> ^{13}C NMR (125 MHz, CD_3CN) of compound 3.26	195
<i>Figure 3.51</i> ^1H NMR (500 MHz, CD_3CN) of compound 3.27	196

<i>Figure 3.52</i> ^{13}C NMR (125 MHz, CD_3CN) of compound 3.27	196
<i>Figure 3.53</i> ^1H NMR (500 MHz, CD_3CN) of compound 3.28	197
<i>Figure 3.54</i> ^{13}C NMR (125 MHz, CD_3CN) of compound 3.28	197
<i>Figure 3.55</i> ^1H NMR (500 MHz, CD_3CN) of compound 3.29	198
<i>Figure 3.56</i> ^{13}C NMR (125 MHz, CD_3CN) of compound 3.29	198
<i>Figure 3.57</i> ^1H NMR (500 MHz, CD_3CN) of compound 3.31	199
<i>Figure 3.58</i> ^{13}C NMR (125 MHz, CD_3CN) of compound 3.31	199
<i>Figure 3.59</i> ^1H NMR (600 MHz, CD_3CN) of compound 3.33	200
<i>Figure 3.60</i> ^{13}C NMR (125 MHz, CD_3CN) of compound 3.33	200
<i>Figure 3.61</i> ^1H NMR (500 MHz, CD_3CN) of compound 3.37	201
<i>Figure 3.62</i> ^{13}C NMR (100 MHz, CD_3CN) of compound 3.37	201
<i>Figure 3.63</i> ^1H NMR (500 MHz, CD_3CN) of compound 3.35	202
<i>Figure 3.64</i> ^{13}C NMR (125 MHz, CD_3CN) of compound 3.35	202
<i>Figure 3.65</i> ^1H NMR (500 MHz, CD_3CN) of compound 3.41	203
<i>Figure 3.66</i> ^{13}C NMR (125 MHz, CD_3CN) of compound 3.41	203
<i>Figure 3.67</i> ^1H NMR (500 MHz, CD_3CN) of compound 3.42	204
<i>Figure 3.68</i> ^{13}C NMR (125 MHz, CD_3CN) of compound 3.42	204
<i>Figure 3.69</i> ^1H NMR (500 MHz, CD_3CN) of compound 3.43	205
<i>Figure 3.70</i> ^{13}C NMR (125 MHz, CD_3CN) of compound 3.43	205
<i>Figure 3.71</i> ^1H NMR (500 MHz, CD_3CN) of compound 3.44	206
<i>Figure 3.72</i> ^{13}C NMR (125 MHz, CD_3CN) of compound 3.44	206

CHAPTER FOUR

Figure 4.1 Well-studied strained azacyclic alkynes 4.1–4.3 , azacyclic alkynes 4.4 and 4.5 , and examples of natural products synthesized using <i>N</i> -containing hetarynes	220
Figure 4.2 Strategies for the synthesis of tylophorine (4.9) using strained azacyclic alkynes 4.11 or 4.5 in Pd-catalyzed annulations	221
Figure 4.3 Concise total synthesis of tylophorine (4.9) using piperidyne 4.16	223
Figure 4.4 Unsuccessful attempt toward accessing an indolizidyne precursor.....	224
Figure 4.5 Synthesis of indolizidyne precursor 4.25	225
Figure 4.6 Pd-catalyzed annulation of indolizidyne 4.5 to furnish tylophorine (4.9) ...	226
Figure 4.7 Indolizidyne trapping provides tylocrebine (4.28) and isotylocrebine (4.29)	227
Figure 4.8 ¹ H NMR (600 MHz, CDCl ₃) of compound 4.14	244
Figure 4.9 ¹³ C NMR (125 MHz, CDCl ₃) of compound 4.14	244
Figure 4.10 ¹ H NMR (600 MHz, CDCl ₃) of compound 4.15	245
Figure 4.11 ¹³ C NMR (125 MHz, CDCl ₃) of compound 4.15	245
Figure 4.12 ¹ H NMR (500 MHz, CDCl ₃) of compound 4.17	246
Figure 4.13 ¹³ C NMR (125 MHz, CDCl ₃) of compound 4.17	246
Figure 4.14 ¹ H NMR (600 MHz, CDCl ₃) of tylophorine (4.9).....	247
Figure 4.15 ¹ H NMR (600 MHz, C ₆ D ₆) of compound 4.19	247
Figure 4.16 ¹³ C NMR (125 MHz, C ₆ D ₆) of compound 4.19	248
Figure 4.17 ¹ H NMR (500 MHz, C ₆ D ₆) of compound 4.23	248
Figure 4.18 ¹³ C NMR (125 MHz, C ₆ D ₆) of compound 4.23	249
Figure 4.19 ¹ H NMR (600 MHz, C ₆ D ₆) of compound 4.24	249

Figure 4.20 ^{13}C NMR (125 MHz, C_6D_6) of compound 4.24	250
Figure 4.21 ^1H NMR (600 MHz, C_6D_6) of compound 4.25	250
Figure 4.22 ^{13}C NMR (125 MHz, C_6D_6) of compound 4.25	251
Figure 4.23 ^1H NMR (600 MHz, C_6D_6) of compound 4.22	251
Figure 4.24 ^{13}C NMR (125 MHz, C_6D_6) of compound 4.22	252
Figure 4.25 ^1H NMR (600 MHz, CDCl_3) of tylocrebine (4.28) and isotylocrebine (4.29), 1:1 ratio	252

CHAPTER FIVE

Figure 5.1 Increasing marijuana legalization requires development of new tools to measure impairment due to Δ^9 -THC (5.1)	266
Figure 5.2 Previously reported electrochemical oxidation of Δ^9 -THC (5.1) and goals of present study	267
Figure 5.3 THCQ isomers 5.2 and 5.3 , with <i>ortho</i> quinone isomer 5.3 forming when the electrochemical oxidation is performed at low concentrations.....	269
Figure 5.4 Vaporized Δ^9 -THC (5.1) was captured in acetonitrile and then subjected to electrochemical oxidation to generate THCW (5.2 and 5.3)	273
Figure 5.5 Initial electrochemical oxidation reaction	278
Figure 5.6 Chromatograms of 5.2 , 5.3 , and 5.1	283
Figure 5.7 UV-Vis absorbance spectrum of 5.3	285
Figure 5.8 Beer–Lambert plot of 5.3 at 495 nm.....	286
Figure 5.9 ^1H NMR (500 MHz, CDCl_3) of compound 5.3	288
Figure 5.10 ^{13}C NMR (125 MHz, CDCl_3) of compound 5.3	288

<i>Figure 5.11</i> COSY NMR (125 MHz, CDCl ₃) of compound 5.3	289
<i>Figure 5.12</i> NOESY NMR (125 MHz, CDCl ₃) of compound 5.3	290
<i>Figure 5.13</i> HMBC NMR (125 MHz, CDCl ₃) of compound 5.3	291
<i>Figure 5.14</i> HSQC NMR (125 MHz, CDCl ₃) of compound 5.3	292

LIST OF TABLES

CHAPTER TWO

<i>Table 2.1</i> Photophysical data for carbene-Au-carbazolyl complexes	39
<i>Table 2.2</i> Photophysical data for carbene-Au-indolyl complexes.....	42
<i>Table 2.3</i> Calculated frontier molecular orbital, singlet (S ₁), and triplet (T ₁) energies....	69

CHAPTER THREE

<i>Table 3.1</i> Optimization studies of on-the-complex annulation with benzyne	144
<i>Table 3.2</i> Crystal data and structure refinement for compound 3.16	145
<i>Table 3.3</i> Photophysical data for selected Ru complexes.....	170

CHAPTER FIVE

<i>Table 5.1</i> Initial attempts to effect oxidation at lower concentrations	268
<i>Table 5.2</i> Electrochemical oxidation screening, altering headspace and voltage.....	271
<i>Table 5.3</i> Electrochemical oxidation at low concentrations.....	272
<i>Table 5.4</i> Effects of the anode material and electrochemical condition at μM concentrations of Δ ⁹ -THC (5.1)	279
<i>Table 5.5</i> Effects of applied potential at μM concentrations of Δ ⁹ -THC (5.1).	280
<i>Table 5.6</i> LC-MS/MS analysis at different timepoints for the electrochemical oxidation of vaporized, then captured Δ ⁹ -THC (5.1)	282

LIST OF ABBREVIATIONS

α	alpha
β	beta
γ	gamma
λ	wavelength
μ	micro
π	pi
δ	chemical shift
Δ	heat
(Het)	hetero
[H]	reduction
[O]	oxidation
$[\alpha]_D$	specific rotation at wavelength of sodium D line
$^{\circ}\text{C}$	degrees Celsius
\AA	angstrom
AcOH	acetic acid
AlCl_3	aluminum trichloride
Alk	alkyl
APCI	atmospheric-pressure chemical ionization
app.	apparent
aq.	aqueous
Ar	aryl
Au	gold
B(pin)	pinacol borane
Benz-ICy \cdot HCl	1,3-dicyclohexylbenzimidazolium chloride
$\text{BF}_3\cdot\text{Et}_2\text{O}$	boron trifluoride diethyl etherate
Bn	benzyl
BnNH ₂	benzylamine
Boc	<i>tert</i> -butoxycarbonyl
Boc ₂ O	di- <i>tert</i> -butyl dicarbonate
Bu	butyl
Bz	benzoyl
c	centi
<i>c</i>	concentration for specific rotation measurements

C	carbon
C ₆ D ₆	deuterated benzene
C ₆ H ₆	benzene
CaH ₂	calcium hydride
cal	calorie
calcd	calculated
cat.	catalytic or catalyst
CD ₃ CN	deuterated acetonitrile
CDCl ₃	deuterated chloroform
CF ₃	trifluoromethyl
CH ₂ Cl ₂	dichloromethane
CH ₃	methyl
CH ₃ CN	acetonitrile
CHCl ₃	chloroform
CO ₂	carbon dioxide
cod	1,5-cyclooctadiene
d	doublet
DART	direct analysis in real time
DMAP	4-dimethylaminopyridine
DMF	<i>N,N</i> -dimethylformamide
DMSO	dimethyl sulfoxide
dppf	1,1'-bis(diphenylphosphino)ferrocene
EDC	1-ethyl-3-(3-dimethylaminopropyl)carbodiimide
EDC•HCl	1-ethyl-3-(3-dimethylaminopropyl)carbodiimide hydrochloride
eds.	editors
EDTA	ethylenediaminetetraacetic acid
ee	enantiomeric excess
equiv	equivalent
ESI	electrospray ionization
Et	ethyl
Et ₂ O	diethyl ether
Et ₃ N	triethylamine
EtOAc	ethyl acetate
FAQ	frequently asked questions

FT	Fourier transform
g	gram(s)
GC-MS	gas chromatography mass spectrometry(er)
h	hour(s)
H	proton
$h\nu$	light
HCl	hydrochloric acid
Hf	hafnium
HMB	hexamethylbenzene
HOBt	hydroxybenzotriazole
HPLC	high-performance liquid chromatography
HRMS	high resolution mass spectroscopy
Hz	hertz
<i>i</i> -Bu	isobutyl
<i>i</i> -Pr	<i>iso</i> -propyl
<i>i</i> -PrNH ₂	<i>iso</i> -propyl amine
<i>i</i> -PrOAc	<i>iso</i> -propyl acetate
<i>i</i> -PrOH	<i>iso</i> -propyl alcohol
I ₂	iodine
ICy•HCl	1,3-dicyclohexylimidazolium chloride
IPr	1,3-Bis(2,6-diisopropylphenyl)-imidazol-2-ylidene
IR	infrared (spectroscopy)
<i>J</i>	coupling constant
K ₃ PO ₄	potassium phosphate tribasic
KO <i>t</i> -Bu	potassium <i>tert</i> -butoxide
KRED	ketoreductase
L	liter
LDA	lithium diisopropylamide
LiAlH ₄	lithium aluminum hydride
LiCl	lithium chloride
LiHMDS	lithium bis(trimethylsilyl)amide
m	multiplet or milli or meter
M	molecular mass, molar, or metal
<i>m</i> -	meta
<i>m/z</i>	mass to charge ratio

Me	methyl
MgSO ₄	magnesium sulfate
MHz	megahertz
min	minute(s)
Mo	molybdenum
mol	mole(s)
mp	melting point
MS	molecular sieves
N	normal
<i>n</i> -Bu	butyl (linear)
<i>n</i> -BuLi	butyl (linear) lithium
N ₂	nitrogen gas
Na ⁰	sodium metal
Na ₂ S ₂ O ₃	sodium thiosulfate
Na ₂ SO ₄	sodium sulfate
NADP	nicotinamide adenine dinucleotide phosphate
NaH	sodium hydride
NaHCO ₃	sodium bicarbonate
NaOH	sodium hydroxide
NaO <i>t</i> -Bu	sodium <i>tert</i> -butoxide
NH ₄ Cl	ammonium chloride
NHC	<i>N</i> -heterocyclic carbene
Ni	nickel
nM	nanomolar
NMR	nuclear magnetic resonance
NOESY	nuclear overhauser effect spectroscopy
<i>o</i> -	ortho
OMe	methoxy
<i>p</i> -	para
Pd	palladium
PDB	protein data bank
Ph	phenyl
PhCOCF ₃	2,2,2-trifluoroacetophenone
PhH	benzene
PhMe	toluene

Piv	pivaloyl
PPh ₃	triphenylphosphine
ppm	parts per million
Pr	Propyl
Pt	platinum
PTFE	polytetrafluoroethylene
q	quartet
quint.	quintet
rac	racemic
R _f	retention factor
rpm/RPM	revolutions per minute
Ru	ruthenium
s	singlet or second
sat.	saturated
sext.	sextet
SFC	supercritical fluid chromatography
SiPr	1,3-Bis(2,6-diisopropylphenyl)-1,3-dihydro-2 <i>H</i> -imidazol-2-ylidene
SiPr•HCl	1,3-Bis(2,6-diisopropylphenyl)-1,3-dihydro-2 <i>H</i> -imidazol-2-ylidene hydrochloride
SmI ₂	samarium diiodide
t	triplet
<i>t</i> -Bu	<i>tert</i> -butyl
<i>t</i> -BuNH ₂	<i>tert</i> -butyl amine
<i>t</i> -BuOH	<i>tert</i> -butyl alcohol
TA	teaching assistant
TBDPS	<i>tert</i> -butyldiphenylsilyl
TBDPSCl	<i>tert</i> -butyldiphenylchlorosilane
TCI	Tokyo Chemical Industry Co.
temp	temperature
THF	tetrahydrofuran
Ti	titanium
TLC	thin layer chromatography
TMB	1,3,5-trimethoxybenzene
TMSCl	chlorotrimethylsilane

t_R	retention time
Trit	trityl
Ts	tosyl
UATR	universal attenuated total reflectance
UHP	ultra-high purity
UV	ultraviolet
WT	wild-type
ZnEt ₂	diethyl zinc
Zr	zirconium

ACKNOWLEDGEMENTS

I am sincerely grateful for all of the incredible people who have supported me throughout my time in graduate school. They have stood by me through failures, challenged me, and inspired me to continue learning and growing each day. This thesis is a reflection of each of them, and is theirs too.

First and foremost, I would like to thank my thesis advisor Professor Neil Garg. Since joining the Garg lab in the summer of 2018, I have grown immeasurably as a chemist, critical thinker and professional. All throughout graduate school Neil has advocated for me, offered actionable feedback, and pushed me to become better. While serving as chair of the UCLA Chemistry Department and leading an organic chemistry lab cannot be easy, especially amidst a global pandemic, Neil has tackled every problem that he has faced with thoughtfulness and grace. I will be forever grateful for his support over the past five years.

I would also like to thank the rest of my doctoral committee: Professors Ken Houk, Abigail Doyle, and Yi Tang. Their mentorship, support and advice has been instrumental throughout my time at UCLA.

I am grateful for my undergraduate thesis advisor, Professor Anthony Carrasquillo. He gave me a first-hand look at what research entailed, and provided me with crucial hands-on mentorship. He taught me to think critically about all aspects of reactions and their set-up, and also played a crucial role in my decision to pursue graduate chemistry research. I am extremely grateful for Anthony's role in my career development.

Next, I would like to thank the many incredible individuals who I have overlapped with in the Garg lab during graduate school. They have made the long hours spent in lab manageable and rewarding. This begins with the post-doctoral scholars. Having completed their PhDs in different

labs, they each bring unique perspectives, techniques and modes of problem-solving. When I first joined the Garg group, Dr. Maude Giroud served as an example as a strong woman in chemistry. She was methodical, thoughtful and always willing to talk through any chemistry questions that I had. Dr. Evan Darzi was also a post-doc when I entered the lab. I have always respected Evan for his creativity, and his ability to prioritize family without lowering the standard that he holds himself to in his career. After he left the Garg lab, I continued to collaborate with Evan through ElectraTect, Inc. This experience has taught me about what goes into a start-up, and I am extremely grateful to him for this rewarding opportunity.

Drs. Logan Bachmann and Veronica Tona arrived next. Logan possesses an incredible chemical intuition and positive outlook on life that I have always admired. His kindness and humbleness are unparalleled, and I'm very excited to work with him after graduate school. Veronica is an exceptional chemist and brought with her infinite amounts of wisdom and advice. She is also one of the most effortlessly funny people that I have ever met and she brought an incredible amount of personality to the Garg lab. She is a powerful woman in organic chemistry who I will always admire.

I also had the opportunity to overlap with Drs. Daniel Nasrallah and Nathan Adamson. Dan's positive mentality and love for life have kept me grounded throughout graduate school. Dan is an incredible teacher, and anyone who has ever approached him with a question or problem is met with patience, kindness and a genuine desire to help. His future students are so lucky and I am excited to see what Dan's future holds. Nathan blessed the lab with total synthesis expertise and an unending slew of dad jokes. He met challenges with grace, and was always willing to thoughtfully answer any chemistry questions that I had.

Next, Drs. Jacob Sorrentino and Lukas Wein joined the lab during my final year as a graduate student. Jacob's medicinal chemistry expertise has been instrumental to the lab, and his willingness to provide thoughtful feedback has been greatly appreciated. Lukas' positivity and incredible sense of humor have uplifted everyone in the lab. He is an endless source of chemistry knowledge, and I have learned a lot from him through subgroups together.

This brings me to the graduate students of the Garg lab. The class of 2019 comprised of Drs. Joyann Barber, Bryan Simmons and Lucas Morrill. Joyann's technical expertise, positive attitude and kindheartedness significantly enriched my first year in the lab. During graduate school she competed as a professional roller skater, and her ability to balance these two commitments was inspiring. Bryan played a key role in honing my synthetic skills, and has continued to advocate for me long after leaving the Garg lab. He also instituted the Garg lab weight lifting club, and made me feel welcome in the lab as a first year. Finally, I am grateful for Lucas' positive presence and ability to bring light to any situation with his sharp sense of humor.

The class of 2020 graduated via Zoom amidst a global pandemic. They include Drs. Jacob Dander, Michael Yamano, Jordan Dotson and Robert Susick. Jacob is one of the greatest story tellers I have ever met, and made lab entertaining every single day. I will never forget his "My Favorite Murder" podcasts or our morning coffee runs. Michael, the king of Vegas, also made lab particularly fun. His love for practical jokes and open-ended questions like "is a pop tart a ravioli?" kept everyone laughing, and his sharp synthetic mind made him the go-to for some of the hardest synthetic questions. Jordan is extremely kind and humble, and I owe my current understanding of radical chemistry to him. I am excited for us to both be up in the Bay Area. Finally, as part of the "annulators" team in the Garg lab, Rob and I tackled many challenging projects together. I always valued our open communication and his love of upbeat music.

The next class was comprised of Drs. Melissa Ramirez, Sarah Anthony and Timothy Boit. Melissa is a master of computational chemistry, and was invaluable to our lab in that area. She is humble, patient and thoughtful, and anyone who joins her lab in the future will have the best mentor. Next, Sarah was always willing to help others in the group. She possesses a tireless work ethic, and I have missed hearing her sing to Abba in the lab. Finally, Tim's attention to detail is unmatched, and he was always willing to talk through complicated concepts. I can always count on Tim for a good "hot take," and even though he denies it, I know he did his L. L. Bean shopping on the lab computer.

I spent the vast majority of my graduate school career with the class of 2022: Drs. Rachel Knapp, Jason Chari and Francesca Ippoliti. As members of the class directly above me, they each played a pivotal role in my development as a chemist and professional. Rachel is one of my greatest friends and role models as a strong woman in organic chemistry. Rachel is a closer: she gets things done. She has supported me through some of my hardest moments of grad school, and always offers the best advice. I will always remember watching multiple historic events with her on the lab computer in 5234, wine nights, coffee walks, our infamous trips to San Jose, Minnesota and Kentucky, and so many more. Next is Jason Chari. As my mentor in the group, Jason has had one of the largest influences on my success as a graduate student. He is one of the most creative chemists I have ever met, and has an incredible eye for aesthetics. Outside of the lab, I consider Jason one of my good friends. I will never forget going to November Project together on Wednesday mornings or our chats at his hood. The final member of the class of 2022 is Francesca. Francesca is one of the most positive people I have ever met, and took every challenge that grad school presented her with in stride. I was so lucky to get to work in 5234 with her during her fifth

year, and will always remember her impressive knowledge of wine, bonding with her over our Italian heritage and Fran's daily "OKAY Katie."

I am so lucky to have gone through each step of grad school with two of the most incredible classmates and human beings: Milauni Mehta and Andrew Kelleghan. They have made each major milestone of graduate school more manageable, and infinitely more fun. Milauni has been one of my biggest (and loudest) cheerleaders throughout all of grad school. Her energy is contagious and it's hard to imagine not hearing her voice and laugh travel across the hallway every day. I deeply admire her vulnerability, ability to wear her heart on her sleeve, and the way that she truly cares for everyone around her. She is an incredible friend, scientific thinker and advocate for others. Although I am sad to not see her every day, I am so excited to cheer her on from afar at Amgen. Of all the people I have encountered in graduate school, Andrew has made me laugh the most. He is a deeply loyal friend, and someone who I have always counted on for meaningful advice. Andrew not only possesses an impressive understanding of organic chemistry, but his unparalleled ability to articulate complicated concepts in a straightforward manner makes him an incredible teacher. I have continued to learn from him throughout all of graduate school, and am so lucky to get to continue working with and hanging out with him next year.

Next are Ana Bulger, Laura Wonilowicz and Matt McVeigh. Ana is a gifted chemist, singer and friend. It is rare to meet someone who genuinely listens and cares for everyone around them in the way that Ana does, and I will miss walking into the office to find her under a heated blanket (Los Angeles does get cold sometimes) with a Celsius in hand. Laura has really grown into a leadership role in the lab over the past couple of years, and a listening ear for anyone needing advice (both professionally or personally). I appreciate her love for books with surprise twists, edgy podcasts and her dark sense of humor. I will miss popping into 5235 and chit chatting with

her. Finally, we have Matt. Matt is kind and humble, and his patience makes him a great mentor. I am impressed by his work ethic, and by the number of projects that he has tackled throughout graduate school – he has truly become an expert on all modes of strained, cyclic allene reactivity.

The class of 2025 is composed of Arismel Tena-Meza, Luca McDermott and Dominick Witkowski. Ari is an absolute firecracker, and you'd never see it coming. I'll always remember our chats at each other's hoods, goofing around in lab, tackling the VWR job together, and our infamous 5 hour commute to lab from San Francisco. Ari's people skills and chemical intuition will take her far in life, and I can't wait to watch her success continue. Next in the class is Luca. Luca's high energy has continued every day since he stepped foot in the lab, and I'm so glad for it. He is brimming with creativity, and I will miss seeing him with his bucket hat and mojito at lab events. Finally, we have Dom. I truly appreciate Dom's ability to remain calm while under stress. He has kept his composure through every hurdle of graduate school, and the results have been admirable. His humor, knowledge of cool music and ability to talk through chemistry have made our bay in 5234 a better place to work.

Next we have the dynamic duo that make up the class of 2026: Georgia Scherer and Jordan Gonzalez. Georgia is one of the most well-rounded people I have ever met. She is incredibly bright, a phenomenal athlete and an even better friend. Despite all of these attributes, she remains extremely humble. I am going to miss our Tuesday night Venice Run Club routine, and our conversations in the car rides there and back. Jordan has been a constant source of positivity in 5234. He is kind, thoughtful, and places a large emphasis on first principles which will serve him well as he heads into the seventh inning stretch of his PhD.

As I leave the lab, it is sad to realize that I only got to overlap with the first years for a small amount of time. I'm excited to watch Allison Hands become a quick leader in the lab. She

is incredibly thoughtful, has a strong grasp of organic chemistry and looks out for those around her. I will miss our Venice Run Club Tuesdays and playing today's top hits in lab with her. Zach and Dani are both creative, hard-working and enthusiastic which will serve them well as they continue on their graduate school journey.

Outside of the lab, I would like to thank my parents, Mark and Ellen Spence, for everything. You have always believed in me, even when I didn't believe in myself. You have pushed me to aim high, follow my dreams and put my best effort towards everything that I pursue. I would simply not be where I am without your unconditional love and support. You have brought so much love and laughter into my life, and helped me realize that not everything is as big of a deal as I make it out to be in my head. My mom has been a constant example of positivity for me. She has answered all of my phone calls, and offered me support at every corner of my professional journey. She has taught me empathy, kindness, and instilled in me her unique ability to problem-solve and think critically. My dad ingrained a deep scientific curiosity in me, and taught me to think about ways in which the world around me can be improved. He is one of the hardest working people I know, and taught me that nothing in life can be achieved without consistent effort and work. His support and encouragement have been instrumental to my professional journey.

Although he is my younger brother, Michael has been a constant role model to me throughout my life. I admire and have learned immensely from his ability to remain level-headed in stressful situations, natural people skills and determination in pursuing things that he is passionate about. He lights up every room that he walks into and people naturally gravitate towards him, which will serve him well in his future. Thank you for your unconditional support, and for teaching me to not take myself too seriously.

Finally, I want to acknowledge my partner, Mickey. Mickey came into my life in the middle of graduate school and has been a constant source of support and positivity for me. He has brought so much fun into my life, and I love the way he views the world in such a positive light. I am so excited for our future together in San Francisco.

Chapter 1 is a version of Spence, K. A.;† Tena Meza, A.;† Garg, N. K. Merging Metals and Strained Intermediates. *Chem Catalysis* **2022**, *2*, 1870–1879. Spence, Tena Meza, and Garg were responsible for the manuscript.

Chapter 2 is a version of Spence, K. A.;† Chari, J. V.;† Di Niro, M.; Susick, R. B.; Ukwitegetse, N.; Djurovich, P. I.; Thompson, M. E.; Garg, N. K. π -Extension of Heterocycles via a Pd-Catalyzed Heterocyclic Aryne Annulation: π -Extended Donors for TADF Emitters. *Chem. Sci.* **2022**, *13*, 5884–5892. Spence, Chari, Di Niro, Susick, and Ukwitegetse were responsible for experimental studies.

Chapter 3 is a version of Chari, J. V.;† Spence, K. A.;† Susick, R. B.; Garg, N. K. A Platform for On-the-Complex Annulation Reactions with Transient Aryne Intermediates. *Nat. Commun.* **2021**, *12*, 3706. Chari, Spence, and Susick were responsible for experimental studies.

Chapter 4 is a version of Spence, K. A.; Hoffmann, M.; Garg, N. K. Total Synthesis of Phenanthroindolizidines Using Strained Azacyclic Alkynes. *Manuscript Submitted*. Spence and Hoffmann were responsible for experimental studies.

Chapter 5 is a version of Forbes, C. R.; Spence, K. A.; Garg, N. K.; Darzi, E. R. Electrochemical Oxidation of Δ^9 -Tetrahydrocannabinol at Nanomolar Concentrations. *Manuscript Submitted*. Forbes and Spence were responsible for experimental studies.

BIOGRAPHICAL SKETCH

EDUCATION

University of California, Los Angeles (UCLA)
Ph.D. Candidate in Organic Chemistry (GPA 3.94)

Los Angeles, CA
June 2023

Williams College
B.A. in Chemistry with Honors and Psychology

Williamstown, MA
June 2018

RESEARCH EXPERIENCE

Graduate Student Researcher

UCLA, Los Angeles, CA

Advisor: Professor Neil Garg

July 2018 – present

- Developed arynes “on the complex” to synthesize unique, highly conjugated Ru and Ir complexes with tunable photophysical properties through the manipulation of strained intermediates
- Prepared highly conjugated, heterocyclic scaffolds for use in OLED technology using Pd-catalyzed annulations of arynes
- Conducted studies for the detection of Δ^9 -tetrahydrocannabinol (THC) using electrochemical oxidation in collaboration with ElectraTect, Inc.
- Synthesized complex fused-indoline containing compounds for the potential treatment of Parkinson’s disease
- Optimized large-scale procedures for the synthesis of 2,5-diaryloxadiazinones and triphenylene using strained intermediate chemistry
- Leveraged strained azacyclic alkynes to access tylophorine, tylocrebine and isotylocrebine

Undergraduate Thesis Student

Williams College, Williamstown, MA

Advisor: Professor Anthony Carrasquillo

September 2017 – May 2018

- Studied the role of functional group identity on the formation of low-volatility products from gas-phase oxidation reactions
- Identified products using a combination of mass spectrometry (GC-FID, LC-ESI-MS and MALDI) and spectroscopy (NMR and FTIR)

Medicinal Chemistry Summer Intern

Gilead Sciences, Inc., Foster City, CA

Advisor: Michael Sangi, Senior Associate Scientist

Summers 2016, 2017

- Designed, synthesized, purified and characterized new molecules for potential use in combatting life-threatening disease
- Developed SAR on a lead series of analogs focused on improving potency and physicochemical properties

TEACHING EXPERIENCE

Organic Chemistry Laboratory 1
Teaching Assistant under Dr. Amber Reilly

Los Angeles, CA
September 2018 – June 2019

- Led a weekly lab section, held regular office hours and graded students' exams and lab assignments
- Organic Chemistry II** **Williamstown, MA**
Teaching Assistant under Professor Thomas Smith September – December 2017
- Led a weekly lab section and graded students' lab assignments

HONORS AND AWARDS

- Ralph & Charlene Bauer Award (2023)
- Dissertation Year Fellowship, UCLA (2022 – 2023)
- Chemistry & Biochemistry Departmental Fellowship, UCLA (2022)
- Medicinal and Bioorganic Chemistry Foundation Scholar (2022)
- Charles J. Pedersen/E.I. Dupont Excellence in Research Award, UCLA (2021)
- Michael E. Jung Excellence in Teaching Award, UCLA (2020)
- University Fellowship, UCLA (2018 – 2022)
- The Degree with Honors, Chemistry, Williams College (2018)
- Associate Member of Sigma Xi, The Scientific Research Honor Society (2018)
- Biochemistry and Molecular Biology Class of 1960 Scholar, Williams College (2016, 2017)
- NCAA All-American, Track and Field (2016)
- 6x All-New England Athlete, Track and Field (2015 – 2017)

PUBLICATIONS AND PATENTS

1. **Total Synthesis of Phenanthroindolizidines Using Strained Azacyclic Alkynes.** Katie A. Spence, Marie Hoffmann, and Neil K. Garg. *Manuscript Submitted*.
2. **Electrochemical Oxidation of Δ^9 -Tetrahydrocannabinol at Nanomolar Concentrations.** Christina R. Forbes, Katie A. Spence, Neil K. Garg and Evan R. Darzi. *Manuscript Submitted*.
3. **Merging Metals and Strained Intermediates.** Katie A. Spence,[†] Arismel Tena-Meza[†] and Neil K. Garg. *Chem Catalysis* **2022**, *2*, 1–10.
4. **Synthesis of Triphenylene via the Palladium-catalyzed Annulation of Benzyne.** Katie A. Spence, Milauni M. Mehta and Neil K. Garg. *Org. Synth.* **2022**, *99*, 174–189.
5. **Heterocyclic Aryne Annulations for the π -Extension of Donor Ligands in Two-Coordinate Metal Complexes.** Katie A. Spence,[†] Jason V. Chari,[†] Mattia Di Niro, Robert B. Susick, Narcisse Ukwitegetse, Mark E. Thompson and Neil K. Garg. *Chem. Sci.* **2022**, *13*, 5884–5892.
6. **A Platform for On-the-Complex Annulation Reactions with Transient Aryne Intermediates.** Jason V. Chari,[†] Katie A. Spence,[†] Robert B. Susick and Neil K. Garg. *Nat. Commun.* **2021**, *12*, 3706.
7. **From Glovebox to Benchtop.** Timothy B. Boit, Katie A. Spence and Neil K. Garg. *Nat. Catal.* **2020**, *3*, 2–3.
8. **Synthesis of 2,5 Diaryloxadiazinones.** Andrew V. Kelleghan, Katie A. Spence and Neil K. Garg. *Org. Synth.* **2020**, *97*, 189–206.
9. **Methods for the Synthesis of Heteroatom Containing Polycyclic Aromatic Hydrocarbons.** Robert B. Susick, Jason V. Chari, Katie A. Spence, Neil K. Garg, Evan R. Darzi and Joyann S. Barber. *WO 2020041369*.

CHAPTER ONE

Merging Metals and Strained Intermediates

Katie A. Spence,[†] Arismel Tena Meza,[†] and Neil K. Garg.

Chem Catalysis **2022**, 2, 1870–1879.

1.1 Abstract

Strained intermediates such as cyclic alkynes and allenes are most commonly utilized in nucleophilic additions and cycloadditions, but have seen increased use in a third area of reactivity: metal-mediated transformations. The merger of strained intermediates and metal catalysis has enabled rapid access to complex, polycyclic systems. Following a discussion of relevant landmark studies involving metals and strained intermediates, this article highlights recent advances in transition metal-mediated transformations from our laboratory. Specifically, this includes the use of arynes in the synthesis of decorated organometallic complexes, and the utilization of cyclic allenes to access enantioenriched heterocycles. Moreover, the broad applicability of such transformations, and exciting future areas of research are discussed.

1.2 Introduction

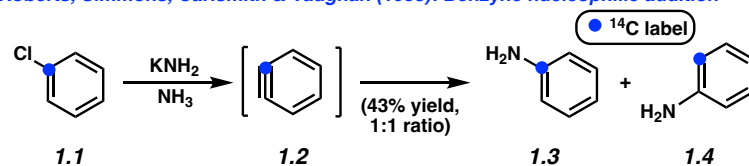
Can alkynes exist within small rings? This intriguing question, first asked in 1902,¹ was initially met with skepticism. Now, 120 years later, the existence of cyclic alkynes and related species is widely accepted.^{2,3,4,5,6,7,8,9,10,11,12,13,14,15,16,17} The strain associated with these species can be leveraged strategically to access a number of important compounds, including ligands,¹⁸ fungicides,¹⁹ medicinal agents,²⁰ and natural products.^{4,5,17,21,22}

To pay tribute to key historical advances and highlight two major modes of strained intermediate reactivity, we feature pioneering studies from the 1950s and 1960s. In a seminal study by Roberts and co-workers, ¹⁴C-labelled chlorobenzene **1.1** was treated with potassium amide in liquid ammonia (Figure 1.1A).²³ The formation of aniline products **1.3** and **1.4** in equal amounts provided strong evidence for the in situ formation of benzyne (**1.2**). Two years later, Wittig and co-workers reported the first generation and trapping of an aryne in a cycloaddition.²⁴ 1-Bromo-2-fluorobenzene (**1.5**) underwent lithium halogen exchange followed by 1,2-elimination to afford benzyne (**1.7**) in situ, which was subsequently trapped with furan (**1.6**) to access cycloaddition product **1.8** in an 88% yield (Figure 1.1B). Soon thereafter, it was demonstrated that 1,2-cyclohexadiene (**1.11**) could be generated and intercepted in cycloaddition processes with styrene (**1.10**) and diphenylisobenzofuran (**1.14**) to access cyclobutane **1.12** and fused tetracycle **1.15**, respectively (Figure 1.1C).^{25,26}

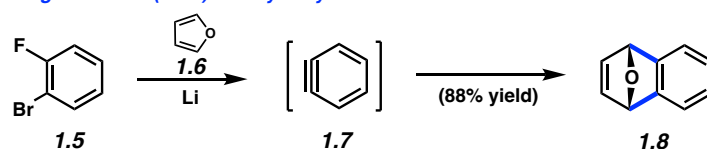
The examples shown in Figure 1.1 highlight two major modes of reactivity of strained intermediates: nucleophilic additions and cycloadditions. Indeed, the majority of synthetically useful transformations of arynes and related strained intermediates involve these types of reactions. Related modes of aryne reactivity, such as nucleophilic annulation reactions, insertion reactions and multicomponent reactions have subsequently arisen and have been reviewed.^{3,5,7} However, following the development of mild conditions for generating strained intermediates, such as Kobayashi's 1,2-elimination of silyl triflates,^{3,27,28} a third major mode of strained intermediate reactivity involving metal-catalyzed processes came to light. This perspective will highlight recent advances in metal-catalyzed transformations of arynes and strained, cyclic allenes to generate complexity in molecular scaffolds.

A. Validation of the intermediacy of benzyne through nucleophilic addition and cycloaddition experiments

Roberts, Simmons, Carlsmith & Vaughan (1953): Benzyne nucleophilic addition

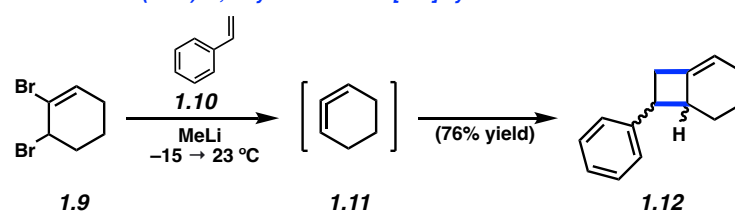


Wittig & Pohmer (1955): Benzyne cycloaddition



B. First reported cycloadditions of 1,2-cyclohexadiene

Moser & Moore (1964): 1,2-Cyclohexadiene [2+2] cycloaddition



Wittig & Fritze (1966): 1,2-Cyclohexadiene [4+2] cycloaddition

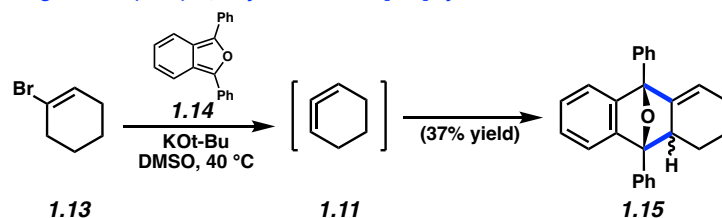


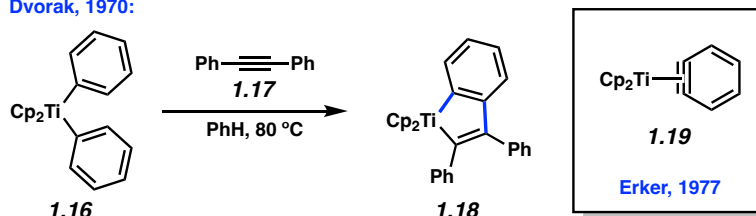
Figure 1.1. Seminal studies of strained, cyclic intermediates.

A number of landmark reports regarding the merger of arynes and metals were published in the late 20th century. It was reported by Dvorak and co-workers that subsection of titanium complex **1.16** to alkyne **1.17** at 80 °C led to formation of metallocycle **1.18** (Figure 1.2A).²⁹ A subsequent study by Erker and co-workers provided strong evidence for the intermediacy of titanium-stabilized benzyne complex **1.19** in this process.³⁰ The existence of metal-stabilized arynes was further validated by Schrock and co-workers in 1979, following the isolation and characterization of metal-stabilized benzyne **1.20** via X-ray crystallography (Figure 1.2B).³¹ Additional metal-stabilized arynes have since been reported,³² including zirconium complex **1.21**

which was characterized via X-ray crystallography and leveraged in a number of synthetic transformations.^{33,34,35} Moreover, in 1993, the first X-ray crystal structure of a metal-stabilized cyclic allene was reported (i.e. **1.22**).³⁶

A. Early studies support the existence of transition-metal-stabilized arynes

Dvorak, 1970:



B. Examples of isolated transition-metal-stabilized strained arynes and a transition-metal-stabilized cyclic allene

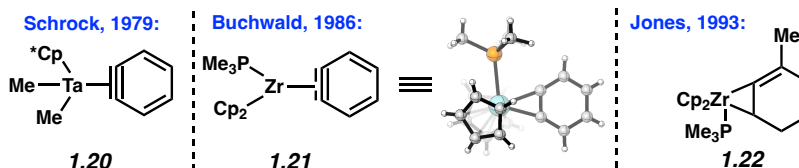


Figure 1.2. Transition metal-stabilized strained intermediates.

Since the aforementioned studies, the field has evolved to focus on synthetically useful transformations of arynes and cyclic allenes that use transition metals as catalysts. Leveraging strained intermediates in transition metal catalysis is powerful in complex molecule synthesis because it can allow for rapid access to a diverse set of scaffolds. However, numerous challenges can arise in developing such reactions, as they require merging of two reactive intermediates generated in situ. The first example of a metal-catalyzed reaction of arynes was not reported until 1998, roughly 50 years after the validation of benzyne. Guitián and co-workers reported a palladium-catalyzed cyclotrimerization reaction of in situ generated benzyne (**1.7**) using catalytic

palladium (0) tetrakis(triphenylphosphine) (Figure 1.3A).³⁷ Using this method, cyclotrimerization product **1.24** was obtained in an 83% yield.

Since Guitián and co-workers' seminal report, reactions that merge strained intermediates and metal catalysis have provided access to many unique scaffolds. For example, the naphthalene core of the natural product taiwanin C (**1.25**) was accessed via a late-stage palladium-catalyzed [2+2+2] cyclization involving an aryne.³⁸ In another example, the natural product flemichapparin C (**1.26**) was accessed via a palladium-catalyzed C–H activation of a 4-hydroxycoumarin, followed by C–C and C–O bond formation involving an aryne intermediate (Figure 1.3B).³⁹ Finally, the indoloquinoline core of isocryptolepine (**1.27**) was constructed via a copper-catalyzed cascade C–H/N–H annulation with benzyne.⁴⁰

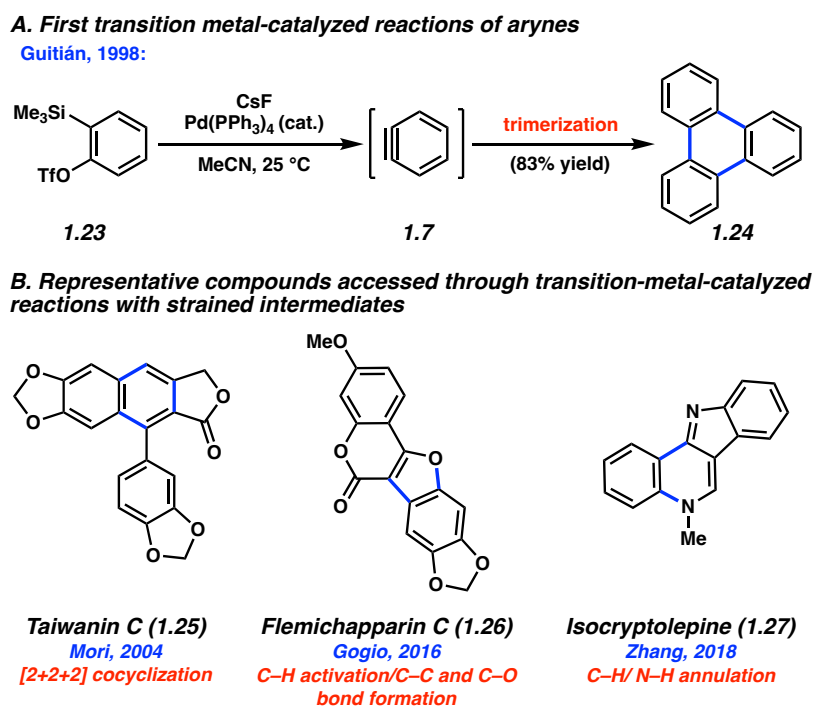


Figure 1.3. Transition metal-catalyzed reactions of arynes.

Recent advances in the merger of strained intermediates and transition metal catalysis have continued to allow access to increasingly complex scaffolds. This perspective highlights two recent advances from our laboratory. The first is the use of arynes to prepare complex organometallic compounds. The second is the use of strained, cyclic allenes to prepare polycyclic heterocycles bearing one or more stereocenters.

1.3 Use of Arynes to Access Organometallic Complexes

While arynes have been utilized to access a wide array of organic compounds, an area where arynes have seen limited use is in the synthesis and derivatization of organometallic compounds. Few examples exist of arynes being utilized in so-called “chemistry-on-the-complex” reactions,⁴¹ where ligands are modified while bound to a metal center. The two earliest examples demonstrate that arynes can be utilized in Diels–Alder reactions “on-the-complex” when the organometallic complex bears a reactive diene ligand.^{42,43} For example, Wang and co-workers reported a Diels–Alder reaction between benzyne (via silyl triflate **1.23**) and iron complex **1.28** to afford cycloadduct **1.29** in 23% yield (Figure 1.4A).

Our laboratory became interested in utilizing metal-catalyzed transformations of arynes for the direct p-extension of organometallic complexes.⁴⁴ Extended conjugation can impart important properties on metal complexes.⁴⁵ Metal complexes **1.30** (R = Ir or Ru) were found to undergo a palladium-catalyzed annulation with in situ-generated arynes **1.31** to access metal complexes **1.32** (Figure 1.4B). Iridium complex **1.33** and ruthenium complex **1.34** are depicted as examples of adducts that could both be accessed in good to excellent yields. Additionally, ruthenium complex **1.35** participated in a triple annulation process with benzyne to extend all three ligands concurrently (Figure 1.4C). This reaction provided **1.36** in 57% yield through the

formation of six C–C bonds in a single transformation. Of note, this product displays a significantly higher luminescence quantum yield and molar extinction coefficient compared to Ru(bpy)₃. Overall, this study demonstrates the ability of metal-catalyzed reactions of arynes to provide rapid access to organometallic complexes with extended conjugation. The scope of aryne-mediated transformations of organometallic complexes continues to expand. For example,⁴⁶ studies by Inger and Polarski, where ligands are modified via the formation of aryne intermediates, are ongoing.

1.4 Use of Cyclic Allenes in Enantioselective Metal-Catalyzed Annulations

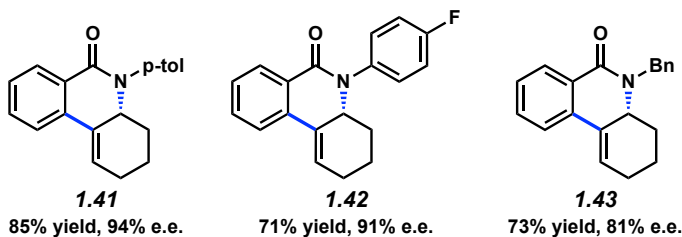
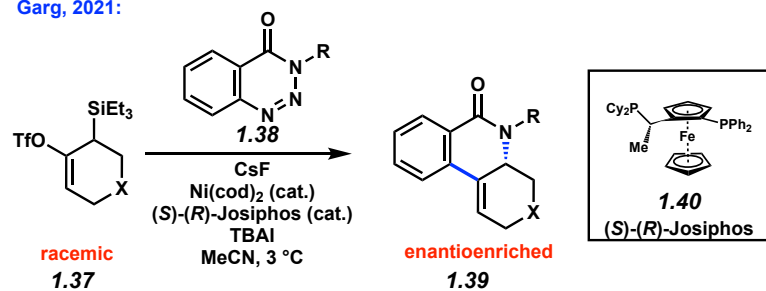
Strained cyclic allenes, despite being known since the 1960s, have only recently gained significant use in chemical synthesis.^{2,47,48,49,50,51,52,53,54,55,56,57,58,59,60,61,62,63,64,65,66,67,68,69,70,71,72} Like arynes, cyclic allenes can be used to generate two new bonds, offering a means for efficiently building polycyclic scaffolds. In addition, cyclic allenes are chiral, which can allow for the generation of sp³ centers, typically through cycloaddition reactions. In comparison to arynes, strained, cyclic allenes have seen far less use in metal-catalyzed transformations. The first examples of transition metal-mediated transformations of strained cyclic allenes were reported by Guitián in 2006 and 2009.^{47,48} Only recently have enantioselective annulations been discovered.

Two asymmetric transition metal-catalyzed annulations of strained, cyclic allenes were developed in our laboratory and are shown in Figure 1.5.^{50,52} Treatment of racemic cyclic allene precursors **1.37** and benzotriazinones **1.38**, in the presence of Ni and Josiphos ligand **1.40**, gave rise to enantioenriched tricycles **1.39** (Figure 1.5A). The transformation is thought to proceed by denitrogenation of **1.38**, to give an organometallic species in catalytic quantities, which, in turn, traps the fleeting cyclic allene intermediate. Formation of adducts **1.41–1.43** provide examples of compounds that were accessible using this methodology in synthetically useful yields and enantioselectivities. More recently, a palladium-catalyzed annulation involving strained, cyclic allene precursors **1.44** and iodoaniline pronucleophiles **1.45** was developed (Figure 1.5B). This methodology provided access to racemic compounds such as **1.48–1.50** in good to excellent yields using DavePhos ligand **1.47**. An enantioselective variant of this reaction, utilizing Mandyphos **1.54** as a ligand, was also demonstrated. In this case, racemic cyclic allene precursor **1.51** and iodopyridine **1.52** underwent palladium-catalyzed annulation to afford tricycle **1.53** in

64% yield and 90% ee (Figure 1.5C). Collectively these studies demonstrate the ability of strained, cyclic allenes to be leveraged in metal-catalyzed transformations to access heterocycles with stereocenters, including examples that proceed with high enantioselectivity.

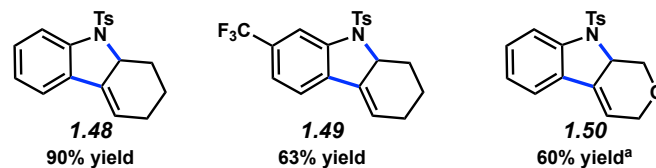
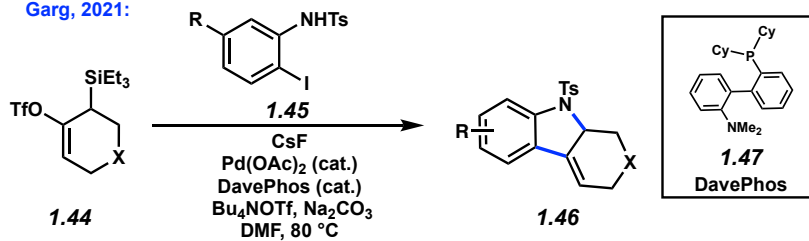
A. Selected examples of enantioselective nickel-catalyzed annulation with cyclic allenes

Garg, 2021:



B. Selected examples of palladium-catalyzed annulations of strained cyclic allenes

Garg, 2021:



C. Enantioselective variant of the palladium-catalyzed annulation methodology

Garg, 2021:

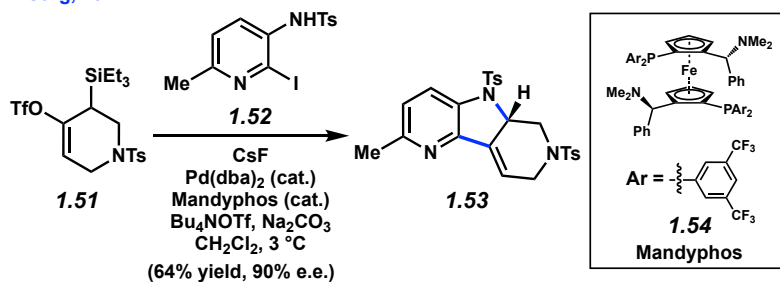


Figure 1.5. Transition metal-catalyzed annulations.

1.5 Looking Forward

Merging strained intermediates with transition metal catalysis can result in direct access to a variety of complex molecules. The recent studies highlighted herein specifically demonstrate that transition metal-catalyzed transformations of strained intermediates can be leveraged to access both organometallic complexes and enantioenriched heterocycles.

Despite these recent advances, there is much room for the continued expansion of metal-mediated transformations of strained intermediates. Looking forward, methods that merge strained intermediates with transition metal catalysis may push the boundaries on what types of molecules can be accessed synthetically. For example, new advances could allow access to chiral building blocks for the assembly of medicinal agents, materials, agrochemicals, or other compounds of importance. One area we are particularly excited about is the use of strained intermediates and metal catalysis in the total synthesis of natural products. Such efforts would not only prove useful in the preparation of target molecules, but could also serve to push the limits of known methods and spawn the invention of new ones. Finally, the use of metal-catalyzed reactions of strained intermediates could be leveraged to access unique chiral molecules, with recent relevant examples reported related to axially chiral helicenes.^{73,74} The merger of strained intermediates with transition metal catalysis is likely to provide access to increasingly diverse scaffolds with unique physical, chemical, and biological properties.

1.6 Notes and References

- (1) Stoermer, R.; Kahlert, B. Ueber Das 1- und 2-brom-cumaron. *Ber. Dtsch. Chem. Ges.* **1902**, *35*, 1633–1940.
- (2) Anthony, S. M.; Wonilowicz, L. G.; McVeigh, M. S.; Garg, N. K. Leveraging Fleeting Strained Intermediates to Access Complex Scaffolds. *JACS Au* **2021**, *1*, 897–912.
- (3) Shi, J.; Li, L.; Li, Y. *o*-Silylaryl Triflates: A Journey of Kobayashi Aryne Precursors. *Chem. Rev.* **2021**, *121*, 3892–4044.
- (4) Tadross, P. M.; Stoltz, B. M. A Comprehensive History of Arynes in Natural Product Total Synthesis. *Chem. Rev.* **2012**, *112*, 3550–3577.
- (5) Bhunia, A.; Yetra, S. R.; Biju, A. T. Recent Advances in Transition-Metal-Free Carbon–Carbon and Carbon–Heteroatom Bond-Forming Reactions Using Arynes. *Chem. Soc. Rev.* **2012**, *41*, 3140–3152.
- (6) Pérez, D.; Peña, D.; Guitián, E. Aryne Cycloaddition Reactions in the Synthesis of Large Polycyclic Aromatic Compounds. *Eur. J. Org. Chem.* **2013**, *52*, 5981–6013.
- (7) Bhojgude, S. S.; Bhunia, A.; Biju, A. T. Employing Arynes in Diels–Alder Reactions and Transition-Metal-Free Multicomponent Coupling and Arylation Reactions. *Acc. Chem. Res.* **2016**, *49*, 1658–1670.
- (8) Wenke, H. H.; Winkler, M.; Sander, W. One Century of Aryne Chemistry. *Angew. Chem., Int. Ed.* **2003**, *42*, 502–528.
- (9) Dubrovskiy, A. V.; Markina, N. A.; Larock, R. C. Use of Benzyne for the Synthesis of Heterocycles. *Org. Biomol. Chem.* **2013**, *11*, 191–218.

- (10) Hoffman, R. W.; Suzuki, K. A “Hot, Energized” Benzyne. *Angew. Chem., Int. Ed.* **2013**, *52*, 2655–2656.
- (11) Goetz, A. E.; Garg, N. K. Enabling the Use of Heterocyclic Arynes in Chemical Synthesis. *J. Org. Chem.* **2014**, *79*, 846–851.
- (12) Yoshida, S.; Hosoya, T. The Renaissance and Bright Future of Synthetic Aryne Chemistry. *Chem. Lett.* **2015**, *44*, 1450–1460.
- (13) Takikawa, H.; Nishii, A.; Sakai, T.; Suzuki, K. Aryne-Based Strategy in the Total Synthesis of Naturally Occurring Polycyclic Compounds. *Chem. Soc. Rev.* **2018**, *47*, 8030–8056.
- (14) Wittig, G. 1,2-Dehydrobenzene. *Angew. Chem. Int. Ed. Engl.* **1965**, *4*, 731–737.
- (15) Guitián, E.; Pérez, D.; Peña, D. Palladium-Catalyzed Cycloaddition Reactions of Arynes. *Top. Organomet. Chem.* **2005**, *14*, 109–146.
- (16) Bronner, S. M.; Goetz, A. E.; Garg, N. K. Understanding and Modulating Indolyne Regioselectivities. *Synlett* **2011**, *2011*, 2599–2604.
- (17) Goetz, A. E.; Shah, T. K.; Garg, N. K. Pyridynes and Indolynes as Building Blocks for Functionalized Heterocycles and Natural Products. *Chem. Commun.* **2015**, *51*, 34–45.
- (18) Mauger, C. C.; Mignani, G. A. An Efficient and Safe Procedure for the Large-Scale Pd-Catalyzed Hydrazonation of Aromatic Chlorides Using Buchwald Technology. *Org. Process Res. Dev.* **2004**, *8*, 1065–1071.
- (19) Schleth, F.; Vettiger, T.; Rommel, M.; Tobler, H. Process for the Preparation of Pyrazole Carboxylic Acid Amides. WO2011131544A1.

- (20) Coe, J. W.; Brooks, P. R.; Wirtz, M. C.; Bashore, C. G.; Bianco, K. E.; Vetelino, M. G.; Arnold, E. P.; Lebel, L. A.; Fox, C. B.; Tingley, F. D.; Schulz, D. W.; Davis, T. I.; Sands, S. B.; Mansbach, R. S.; Rollema, H.; O'Neill, B. T. 3,5-Bicyclic Aryl Piperidines: A Novel Class of $\alpha 4\beta 2$ Neuronal Receptor Partial Agonist for Smoking Cessation. *Bioorg. Med. Chem. Lett.* **2005**, *15*, 4889–4897.
- (21) Corsello, M. A.; Kim, J.; Garg, N. K. Total Synthesis of (-)-Tubingensin B Enabled by the Strategic Use of Aryne Cyclization. *Nat. Chem.* **2017**, *9*, 944–949.
- (22) Gampe, C. M.; Carreira, E. M. Arynes and Cyclohexyne in Natural Product Synthesis. *Angew. Chem., Int. Ed.* **2012**, *51*, 3766–3778.
- (23) Roberts, J. D.; Simmons, H. E.; Carlsmith, L. A.; Vaughan, C. W. Rearrangement in the Reaction of Chlorobenzene-1- C^{14} with Potassium Amide. *J. Am. Chem. Soc.* **1953**, *75*, 3290–3291.
- (24) Wittig, G.; Pohmer, L. Intermediäre Bildung von Dehydrobenzol (Cyclohexadienin). *Angew. Chem.* **1955**, *67*, 348.
- (25) Moser, W. R. PhD Thesis, Massachusetts Institute of Technology, Cambridge, MA, 1964.
- (26) Wittig, G.; Fritze, P. On the Intermediate Occurrence of 1,2-Cyclohexadiene. *Angew. Chem., Int. Ed.* **1966**, *5*, 846.
- (27) Dhokale, R. A.; Mhaske, S. B. Transition-Metal-Catalyzed Reactions Involving Arynes. *Synthesis* **2018**, *50*, 1–16.

- (28) Yoshio, H.; Takaaki, S.; Kobayashi, H. Fluoride-Induced 1,2-Elimination of *o*-Trimethylsilylphenyl Triflate to Benzyne Under Mild Conditions. *Chem. Lett.* **1983**, *12*, 1211–1214.
- (29) Dvorak, J.; O'Brien, J.; Santo, W. A Reinvestigation of the Thermal Decomposition of $(C_5H_5)_2TiPh_2$. *Chem. Commun.* **1970**, *7*, 411–412.
- (30) Erker, G. The Reaction of Intermediate Zirconocene–Aryne Complexes with C–H Bonds in the Thermolysis of Diarylzirconocenes. *J. Org. Chem.* **1977**, *134*, 189–202.
- (31) McLain, S. J.; Schrock, R. P.; Sharp, P. R.; Churchill, M. R.; Youngs, W. J. Synthesis of Monomeric Niobium- and Tantalum-Benzyne Complexes and the Molecular Structure of $Ta(\eta^5-C_5Me_5)(C_6H_4)Me_2$. *J. Am. Chem. Soc.* **1977**, *101*, 263–265.
- (32) For more examples of metal-stabilized arynes, see: Bennett, M. A.; Schwemlein, H. P. Metal Complexes of Small Cycloalkynes and Arynes. *Angew. Chem., Int. Ed. Engl.* **1989**, *28*, 1296–1320.
- (33) Buchwald, S. L.; Watson, B. T.; Huffman, J. C. Trimethylphosphine Adduct of the Zirconocene-Benzyne Complex: Synthesis, Reactions and X-ray Crystal Structure. *J. Am. Chem. Soc.* **1986**, *108*, 7411–7413.
- (34) Buchwald, S. L.; Watson, B. T.; Lum, R. T.; Nugent, W. A. A General Method for the Preparation of Zirconocene Complexes of Substituted Benzyne: in situ Generation, Coupling Reactions, and Use in the Synthesis of Polyfunctionalized Aromatic Compounds. *J. Am. Chem. Soc.* **1987**, *109*, 7137–7141.
- (35) Buchwald, S. L.; Nielsen, R. B. Group 4 Metal Complexes of Benzyne, Cycloalkynes, Acyclic Alkynes, and Alkenes. *Chem. Rev.* **1988**, *88*, 1047–1058.

- (36) Yin, J.; Abboud, K. A.; Jones, W. M. Synthesis and Structure of (Trimethylphosphine)zirconocene-3-methyl-1,2-cyclohexadiene: First Metal Complex of a Six-Membered Allene. *J. Am. Chem. Soc.* **1993**, *115*, 3810–3811.
- (37) Peña, D.; Escudero, S.; Pérez, D.; Guitián, E.; Castedo, L. Efficient Palladium-Catalyzed Cyclotrimerization of Arynes: Synthesis of Triphenylenes. *Angew. Chem., Int. Ed.* **1998**, *37*, 2659–2661.
- (38) Sato, Y.; Tamura, T.; Mori, M. Arylnaphthalene Ligands through Pd-Catalyzed [2+2+2] Cocyclization of Arynes and Diynes: Total Synthesis of Taiwanins C and E. *Angew. Chem., Int. Ed.* **2004**, *43*, 2436–2440.
- (39) Neog, K.; Borah, A.; Gogoi, P. J. Palladium(II)-Catalyzed C–H Bond Activation/C–C and C–O Bond Formation Reaction Cascade: Direct Synthesis of Coumestans. *J. Org. Chem.* **2016**, *81*, 11971.
- (40) Zhang, T.-Y.; Liu, C.; Chen, C.; Liu, J.-X.; Xiang, H.-Y.; Jiang, W.; Ding, T.-M.; Zhang, S.-Y. Copper-Mediated Cascade C–H/N–H Annulation of Indolocarboxamides with Arynes: Construction of Tetracyclic Indoloquinoline Alkaloids. *Org. Lett.* **2018**, *20*, 220–223.
- (41) Mede, T.; Jäger, M.; Schubert, U. S. “Chemistry-on-the-Complex”: Functional Ru(II) Polypyridyl-Type Sensitizers as Divergent Building Blocks. *Chem. Soc. Rev.* **2018**, *47*, 7577–7627.
- (42) Wang, B.; Mu, B.; Chen, D.; Xu, S.; Zhou, X. Diels–Alder Reactions of Benzyne with Indenyl Iron Complexes. *Organometallics*, **2004**, *23*, 6225–6230.

- (43) Luo, S.; Zhao, X.; Mu, B.; Song, H.; Xu, S.; Wang, B. Diels–Alder Reactions of Benzyne with Indenyl and Fluorenyl Ruthenium Complexes. *Organometallics* **2009**, *28*, 4602–4605.
- (44) Chari, J. V.; Spence, K. A.; Susick, R. B.; Garg, N. K. A Platform for On-the-Complex Annulation Reactions with Transient Aryne Intermediates. *Nat. Commun.* **2021**, *12*, 3706.
- (45) Twilton, J.; Le, C.; Zhang, P.; Shaw, M. H.; Evans, R. W.; MacMillan, D. W. C. The Merger of Transition Metal and Photocatalysis. *Nat. Rev. Chem.* **2017**, *1*, 0052.
- (46) Inger, F. PhD Thesis, Uppsala University, Uppsala, Sweden, 2022.
- (47) Peña, D.; Iglesias, B.; Quintana, I.; Pérez, D.; Guitián, E.; Castedo L. Synthesis and Reactivity of New Strained Cyclic Allene and Alkyne Precursors. *Pure Appl. Chem.* **2006**, *78*, 451–455.
- (48) Quintana, I.; Peña, D.; Pérez, D.; Guitián, E. Generation and Reactivity of 1,2-Cyclohexadiene under Mild Reaction Conditions. *Eur. J. Org. Chem.* **2009**, *2009*, 5519–5524.
- (49) Barber, J. S.; Yamano, M. M.; Ramirez, M.; Darzi, E. R.; Knapp, R. R.; Liu, F.; Houk, K. N.; Garg, N. K. Diels–Alder Cycloadditions of Strained Azacyclic Allenes. *Nat. Chem.* **2018**, *10*, 953–960.
- (50) Yamano, M. M.; Kelleghan, A. V.; Shao, Q.; Giroud, M.; Simmons, B. J.; Li, B.; Chen, S.; Houk, K. N.; Garg, N. K. Intercepting Fleeting Cyclic Allenes with Asymmetric Nickel Catalysis. *Nature* **2021**, *586*, 242–247.
- (51) Yamano, M. M.; Knapp, R. R.; Ngamnithiporn, A.; Ramirez, M.; Houk, K. N.; Stoltz, B. M.; Garg, N. K. Cycloadditions of Oxacyclic Allenes and a Catalytic Asymmetric

- Entryway to Enantioenriched Cyclic Allenes. *Angew. Chem., Int. Ed.* **2019**, *58*, 5653–5657.
- (52) Kelleghan, A. V.; Witkowski, D. C.; McVeigh, M. S.; Garg, N. K. Palladium-Catalyzed Annulations of Strained Cyclic Allenes. *J. Am. Chem. Soc.* **2021**, *25*, 9338–9342.
- (53) McVeigh, M. S.; Garg, N. K. Interception of 1,2-Cyclohexadiene with TEMPO Radical. *Tetrahedron Lett.* **2021**, *87*, 153539–153543.
- (54) Engels, B.; Schöneboom, J. C.; Munster, A. F.; Groetsch, S.; Christl, M. Computational Assessment of the Electronic Structures of Cyclohexa-1,2,4-triene, 1-Oxacyclohexa-2,3,5-triene (3 δ^2 -Pyran), Their Benzo Derivatives, and Cyclohexa-1,2-diene. An Experimental Approach to 3 δ^2 -Pyran. *J. Am. Chem. Soc.* **2002**, *124*, 287–297.
- (55) Schmidt, M. W.; Angus, R. O.; Johnson, R. P. Small Ring Cyclic Allenes: An ab Initio Study of the Structure of 1,2-Cyclohexadiene. *J. Am. Chem. Soc.* **1982**, *104*, 6838–6839.
- (56) Hänninen, M. M.; Peuronen, A.; Tuononen, H. M. Do Extremely Bent Allenes Exist? *Chem. Eur. J.* **2009**, *15*, 7287–7291.
- (57) Taskesenligil, Y.; Kashyap, R. P.; Watson, W. H.; Balci, M. Is the Intermediate in the Reaction of 3-Bromo-6,7-benzobicyclo[3.2.1]octa-2,6-diene with Potassium tert-Butoxide an Allene or an Alkyne? *J. Org. Chem.* **1993**, *58*, 3216–3218.
- (58) Daoust, K. J.; Hernandez, S. M.; Konrad, K. M.; Mackie, I. D.; Winstanley, J.; Johnson, R. P. Strain Estimates for Small-Ring Cyclic Allenes and Butatrienes. *J. Org. Chem.* **2006**, *71*, 5708–5714.

- (59) Dillon, P. W.; Underwood, G. R. Cyclic Allenes. I. The Electronic Structure and Probable Deformation of the Allene Linkage When Included in a Ring. An INDO–MO Study. *J. Am. Chem. Soc.* **1974**, *96*, 779–787.
- (60) Angus, R. O.; Schmidt, M. W.; Johnson, R. P. Small-Ring Cyclic Cumulenes: Theoretical Studies of the Structure and Barrier to Inversion in Cyclic Allenes. *J. Am. Chem. Soc.* **1985**, *107*, 532–537.
- (61) Nendel, M.; Tolbert, L. M.; Herring, L. E.; Islam, M. N.; Houk, K. N. Strained Allenes as Dienophiles in the Diels–Alder Reaction: An Experimental and Computational Study. *J. Org. Chem.* **1999**, *64*, 976–983.
- (62) Christl, M.; Braun, M.; Fischer, H.; Groetsch, S.; Muller, G.; Leusser, D.; Deuerlein, S.; Stalke, D.; Arnone, M.; Engels, B. The Stereochemical Course of the Generation and Interception of a Six Membered Cyclic Allene: 3 δ 2-1H-Naphthalene (2,3-Didehydro-1,2-dihydronaphthalene). *Eur. J. Org. Chem.* **2006**, *2006*, 5045–5058.
- (63) Christl, M.; Fischer, H.; Arnone, M.; Engels, B. 1-Phenyl-1,2-cyclohexadiene: Astoundingly High Enantioselectivities on Generation in a Doering–Moore–Skattebøl Reaction and Interception by Activated Olefins. *Chem.-Eur. J.* **2009**, *15*, 11266–11272.
- (64) Christl, M.; Schreck, M.; Fischer, T.; Rudolph, M.; Moigno, D.; Fischer, H.; Deuerlein, S.; Stalke, D. 1-Phenyl-1,2-cyclohexadiene: Generation, Interception by Activated Olefins, Dimerisation and Trimerisation. *Chem.-Eur. J.* **2009**, *15*, 11256–11265.
- (65) Christl, M.; Schreck, M. 7-Arylbicyclo[4.2.0]oct-1-ene – Synthese durch [2 + 2]-Cycloadditionen von 1,2-Cyclohexadien Sowie 1-Methyl-1,2-cyclohexadien und Thermische Aquilibrierung der Exo/Endo-Isomeren. *Chem. Ber.* **1987**, *120*, 915–920.

- (66) Hioki, Y.; Mori, A.; Okano, K. Steric Effects on Deprotonative Generation of Cyclohexynes and 1,2-Cyclohexadienes from Cyclohexenyl Triflates by Magnesium Amides. *Tetrahedron* **2020**, *76*, 131103.
- (67) Inoue, K.; Nakura, R.; Okano, K.; Mori, A. One-Pot Synthesis of Silylated Enol Triflates from Silyl Enol Ethers for Cyclohexynes and 1,2-Cyclohexadienes. *Eur. J. Org. Chem.* **2018**, *2018*, 3343–3347.
- (68) Barber, J. S.; Styduhar, E. D.; Pham, H. V.; McMahon, T. C.; Houk, K. N.; Garg, N. K. Nitrene Cycloadditions of 1,2-Cyclohexadiene. *J. Am. Chem. Soc.* **2016**, *138*, 2512–2515.
- (69) Lofstrand, V. A.; West, F. G. Efficient Trapping of 1,2-Cyclohexadienes with 1,3-Dipoles. *Chem. Eur. J.* **2016**, *22*, 10763–10767.
- (70) Wang, B.; Constantin, M.-G.; Singh, S.; Zhou, Y.; Davis, R. L.; West, F. G. Generation and Trapping of Electron-Deficient 1,2-Cyclohexadienes. Unexpected Hetero-Diels–Alder Reactivity. *Org. Biomol. Chem.* **2021**, *19*, 399–405.
- (71) Almealmadi, Y. A.; West, F. G. A Mild Method for the Generation and Interception of 1,2-Cycloheptadienes with 1,3-Dipoles. *Org. Lett.* **2020**, *22*, 6091–6095.
- (72) Lofstrand, V. A.; McIntosh, K. C.; Almealmadi, Y. A.; West, F. G. Strain-Activated Diels–Alder Trapping of 1,2-Cyclohexadienes: Intramolecular Capture by Pendant Furans. *Org. Lett.* **2019**, *21*, 6231–6234.
- (73) Caeiro, J.; Peña, D.; Cobas, A.; Pérez, D.; Guitián, E. Asymmetric Catalysis in the [2+2+2] Cycloaddition of Arynes and Alkynes: Enantioselective Synthesis of a Pentahelicene. *Adv. Synth. Catal.* **2016**, *348*, 2466–2474.

- (74) Yubuta, A.; Hosokawa, T.; Gon, M.; Tanaka, K.; Chujo, Y.; Tsurusaki, A.; Kamikawa, K. Enantioselective Synthesis of Triple Helicenyl Aryne and Alkynes via Dynamic Kinetic Resolution. *J. Am. Chem. Soc.* **2021**, *22*, 10025–10033.

CHAPTER TWO

π -Extension of Heterocycles via a Pd-Catalyzed Heterocyclic Aryne Annulation:

π -Extended Donors for TADF Emitters

Katie A. Spence,[†] Jason V. Chari,[†] Mattia Di Niro, Robert B. Susick, Narcisse Ukwitegetse,
Peter I. Djurovich, Mark E. Thompson, and Neil K. Garg.

Chem. Sci. **2022**, *13*, 5884–5892.

2.1 Abstract

We report the annulation of heterocyclic building blocks to access π -extended polycyclic aromatic hydrocarbons (PAHs). The method involves the trapping of short-lived hetarynes with catalytically-generated biaryl palladium intermediates and allows for the concise appendage of three or more fused aromatic rings about a central heterocyclic building block. Our studies focus on annulating the indole and carbazole heterocycles through the use of indolyne and carbazolyne chemistry, respectively, the latter of which required the synthesis of a new carbazolyne precursor. Notably, these represent rare examples of transition metal-catalyzed reactions of *N*-containing hetarynes. We demonstrate the utility of our methodology in the synthesis of heterocyclic π -extended PAHs, which were then applied as ligands in two-coordinate metal complexes. As a result of these studies, we identified a new thermally-activated delayed fluorescence (TADF) emitter that displays up to 81% photoluminescence efficiency, along with insight into structure-property relationships. These studies underscore the utility of heterocyclic strained intermediates in the synthesis and study of organic materials.

2.2 Introduction

Polycyclic aromatic hydrocarbons (PAHs) have had a remarkable impact on materials science due to their desirable electronic and self-assembly properties.¹ A privileged subset of PAHs, heterocyclic PAHs, are highly valued in solar cells,² electroluminescent materials³ and organic light emitting diodes (OLEDs)⁴ (e.g., **2.1–2.3**, Figure 2.1). Indeed, heteroatom incorporation in these systems provides several functional and electronic advantages. This includes the introduction of nitrogen functional handles for synthetic manipulations, capacity for *N*-coordination to metal centers, the potential for donor-acceptor systems and usage as stimuli-responsive materials.⁵ Accordingly, concise and diversifiable synthetic methods for accessing heterocyclic PAHs are highly desirable.⁶

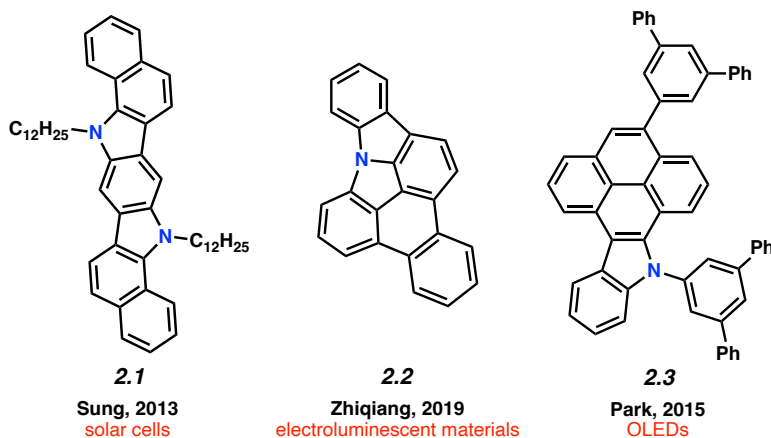
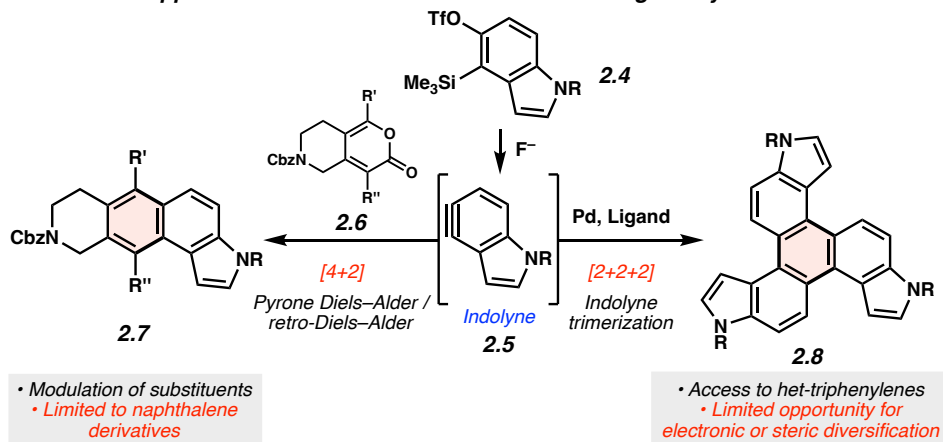


Figure 2.1. Examples of heteroatom-containing PAHs with applications in materials chemistry.

An attractive approach toward heterocyclic PAHs involves assembling fused rings about a central heterocyclic building block through annulative π -extension (APEX).⁶ A compelling means to achieve this objective involves the use of in situ generated arynes, although such intermediates were historically avoided because of their high reactivity. However, the strain driven reactivity of

arynes, along with the ability to form multiple bonds in a single step under mild conditions, has prompted the recent usage of arynes as modular building blocks in a wide array of applications, including in the synthesis of PAHs.^{7,8,9,10,11} In contrast, heterocyclic arynes (hetarynes) have only been used sparingly in PAH synthesis. This is in part due to the mild, fluoride-mediated generation of heterocyclic arynes (hetarynes) only becoming widespread in the past decade.¹² Moreover, the ability to access and manipulate indole-derived arynes (indolynes) and their derivatives differs considerably from that of benzyne chemistry. The pyrrole ring can influence aryne structure and reactivity,¹³ and its nucleophilicity can often result in side reactions,¹⁴ posing numerous challenges for methodology development. Specifically, the reaction rate of pyrrole in electrophilic aromatic substitution reactions has been approximated to be roughly 3×10^{18} times faster than that of benzene.¹⁵ Figure 2.2A highlights two recent examples of the generation and capture of indolyne **2.5**, which arises from indolyne silyl triflate precursor **2.4**.^{16,17,18}

A. Previous approaches toward π -extended materials using hetarynes



B. This study: Pd-catalyzed π -extension using hetarynes

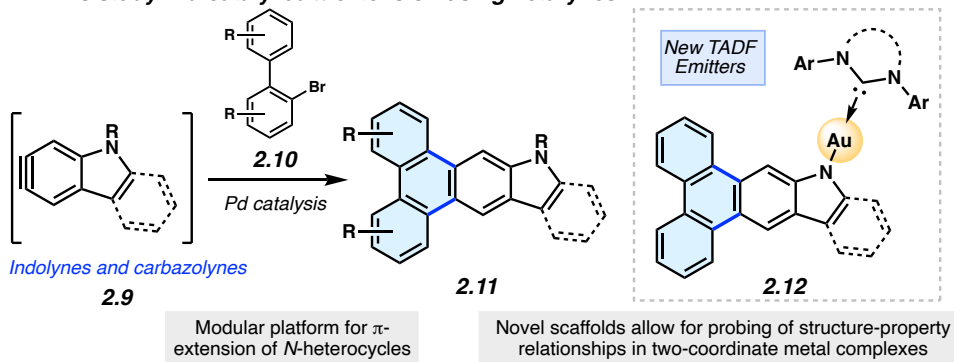
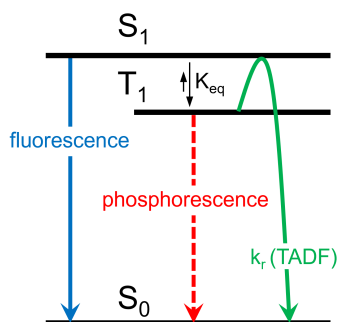


Figure 2.2. Approaches for π -extension of hetarynes.

In the present study, we aimed to develop a rapid, convergent approach to access heteroatom-containing PAH scaffolds. In particular, a method was devised that allows for the appendage of multiple aromatic rings to important heterocyclic building blocks in a controlled bimolecular reaction. This reaction provides access to a diverse set of aromatic products with electronic and steric modifications. The sequence we devised, inspired by pioneering studies by Larock,¹⁹ is shown in Figure 2.2B. In situ generated hetarynes **2.9** would be united with bromobiphenyl partners **2.10** using palladium catalysis to furnish heterocyclic PAHs **2.11**.²⁰ This annulative π -extension of hetarynes would expand on existing applications of hetaryne chemistry, create two new carbon-carbon (C-C) bonds, allow for the addition of three aromatic rings (shown

in blue) to important heterocycles, and permit rapid access to heterocyclic triphenylene derivatives. Of note, this type of Larock annulation¹⁹ had not previously been achieved using nitrogen-containing, hetaryne intermediates. Additionally, metal-catalyzed transformations that utilize hetarynes are rare. Iwayama and Sato have reported [2+2+2] reactions of pyridynes.²¹ Only one study involving metal-catalyzed reactions of electron-rich *N*-containing hetarynes is available in the literature, as developed by our laboratory.¹⁷

Herein, we describe the development of this methodology to access π -extended heterocyclic adducts, in addition to a concise synthetic route to a new carbazolyne precursor. We also show the utility of our methodology in the synthesis of π -extended ligands, which were utilized in novel two-coordinate metal complexes **2.12**. Rapid access to complexes **2.12** allowed us to study the influence of extended conjugation on the efficiency of thermally activated delayed fluorescence (TADF) processes, which have received notable interest in recent years in the context of OLEDs.²² As described in Scheme 2.1, in OLEDs, singlets (S_1) and triplets (T_1) are generated upon hole and electron recombination. Fluorescence describes prompt decay from the S_1 state, whereas phosphorescence describes delayed decay from the T_1 state. In TADF emitters, T_1 is thermally promoted to the S_1 state, followed by radiative decay from S_1 . We show that extended π -conjugation can influence the performance of the TADF complex by modulating either the steric or electronic features of the ligand. Moreover, our studies permit access to a new TADF emitter that displays up to 81% photoluminescence efficiency.



Scheme 2.1. Mechanism for TADF emission in comparison to fluorescence and phosphorescence.

2.3 Results and Discussion

2.3.1 Pd-Catalyzed Annulations of Indolyne

We initiated our synthetic studies by pursuing a Pd-catalyzed annulation reaction of bromobiaryls **2.13**²³ with *N*-Me-4,5-indolyne precursor **2.14** (Figure 2.3), the latter of which is accessible in a single step from its commercially available N–H derivative. In our initial studies, we used 2-bromobiphenyl as the aryl halide coupling partner and examined conditions reported by Larock for the annulation of carbocyclic arynes.¹⁹ This led to the formation of **2.16** in only 43% yield, highlighting the aforementioned challenges associated with using *N*-containing hetarynes in metal-catalyzed reactions, as compared to simpler arynes. In prior studies,^{24,25,26} we found that metal-catalyzed trappings of heterocyclic strained intermediates necessitate careful optimization, as such reactions require that a transient strained intermediate be generated at a rate that allows for efficient reaction with an in situ generated organometallic species (i.e., after **2.13** undergoes oxidative addition with Pd), while minimizing decomposition pathways commonly seen in strained intermediate chemistry. We ultimately found the desired reaction took place more efficiently by employing 5 mol% Pd(dba)₂, 5 mol% P(*o*-tolyl)₃, a 1:1 ratio of co-solvents acetonitrile and toluene, and 10 equivalents of cesium fluoride (CsF). The mixture of co-solvents, in particular, is thought

to be important for modulating the rate of heteraryne formation.²⁷ With optimal conditions, **2.16** could be accessed in 90% yield. Substituted biaryls could also be employed in the methodology. For example, methoxy- and nitro-substituted biaryls underwent the annulation smoothly to deliver adducts **2.17** and **2.18** in 62% and 80% yields, respectively. In these cases, mixtures of regioisomers are formed in roughly equal quantities.²⁸ We also sought to incorporate additional heteroatoms into the products by employing heterocyclic derivatives of 2-bromobiphenyls. Use of a pyridyl substrate furnished **2.19** in 76% yield, which is an interesting aza-analog of parent compound **2.16**. We were also able to replace one of the phenyl rings with pyrrole or indole units, as exemplified by the formation of **2.20–2.22**. Lastly, we performed the annulation of 2-bromobiphenyl (**2.23**) with 5,6-indolyne precursor **2.24**, which delivered adduct **2.25** in 81% yield. The results shown in Figure 2.3 not only provide access to electronically and structurally diverse heteroatom-containing PAHs, but also validate our strategy to achieve the π -extension of heterocyclic building blocks.

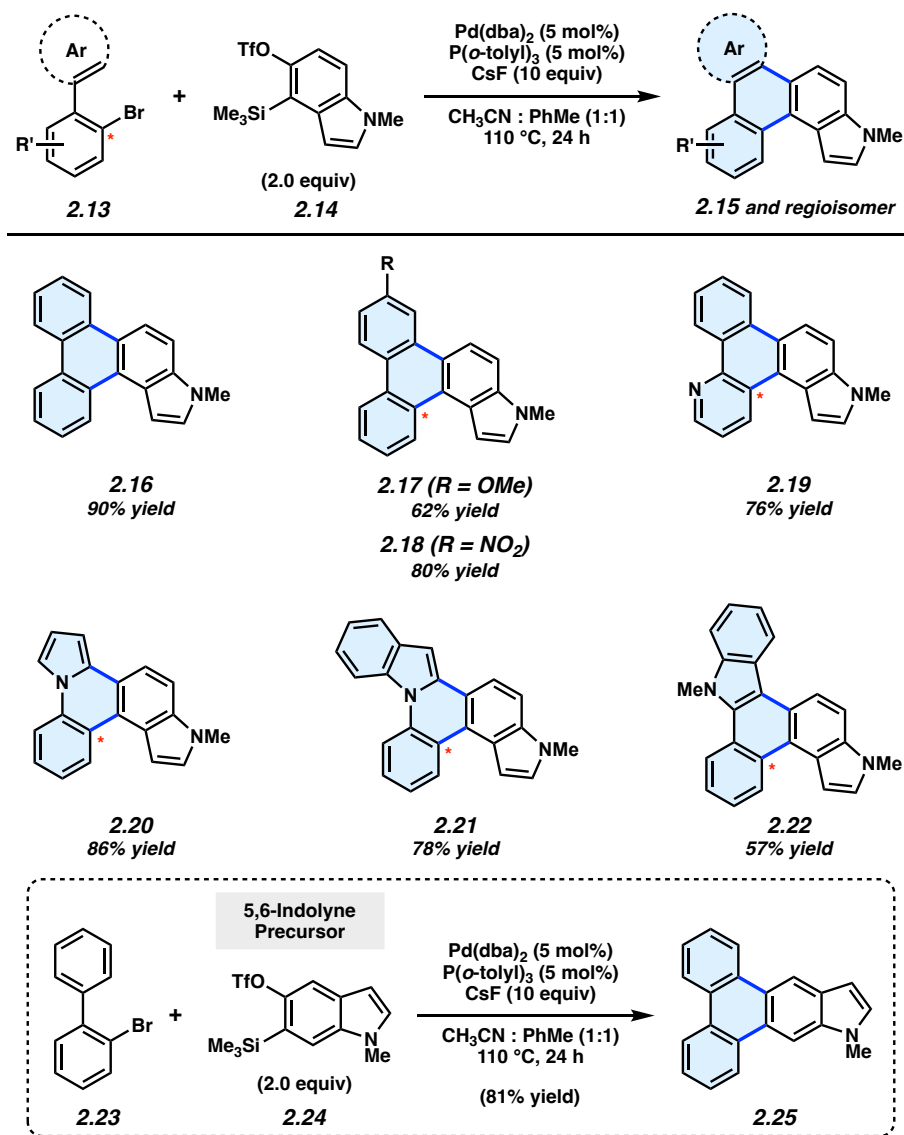


Figure 2.3. π -Extension of indolynes. Yields for **2.17–2.22** reflect isolated yields of a mixture of regioisomers (1–1.5:1; see Section 2.5.2.1 for details).

2.3.2 Carbazolyne Studies

Having validated the π -extension of indoles via the use of indolynes, we sought to develop analogous chemistry using the carbazole heterocycle. Carbazoles bear an additional aromatic ring in comparison to their indole counterparts and are valuable in materials-based applications,²⁹

medicinal chemistry,³⁰ and natural product total synthesis.³¹ However, aryne-derived carbazoles (carbazolynes) have seen sparse use in chemical synthesis. Recent examples involve carbazolyne generation from the hexadehydro-Diels–Alder reaction,³² the use of a silyl nonaflate precursor,³³ and via classic dehydrohalogenation chemistry.^{31,34}

As silyl triflate precursors to carbazolynes were not known in the literature, we developed the concise approach to carbazolyne precursors **2.29–2.31** shown in Figure 2.4. 3-Bromo-2-hydroxycarbazole (**2.26**)^{31,34} was treated with HMDS to afford silyl ether **2.27**, which, in turn, was carried forward in a retro-Brook rearrangement sequence to afford silyl alcohol **2.28**. Triflation proceeded smoothly to deliver silyl triflate **2.29** in 69% yield. N–H compound **2.29** was elaborated to protected derivatives **2.30** and **2.31** via methylation and Boc-protection, respectively. *N*-Me-carbazolyne precursor **2.30** was employed in our π -extension methodology using our previously optimized conditions. We were delighted to find that reaction of 2-bromobiphenyl (**2.23**) and *N*-Me-carbazolyne precursor **2.30** using Pd-catalysis furnished π -extended carbazole **2.32** in 86% yield. This is the first example of a transition metal-catalyzed trapping of a carbazolyne intermediate. Notably, this permits the one-step installment of a carbazole moiety into a π -extended system.

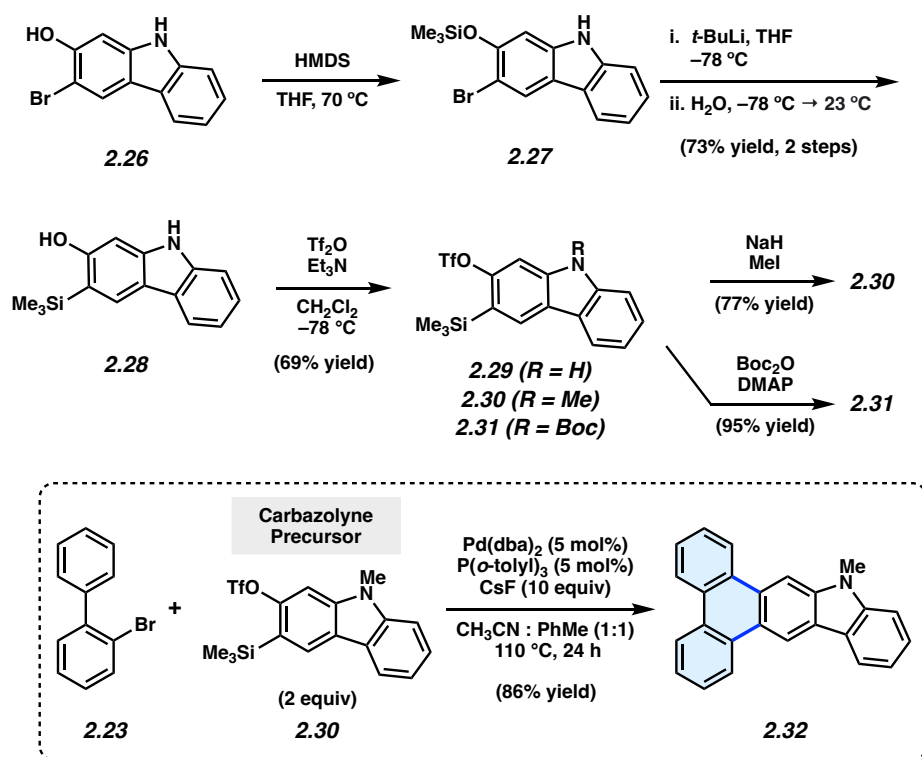


Figure 2.4. Synthesis of carbazolyne precursors.

We also sought to determine if N–H derivatives of our indole and carbazole annulation products could be accessed using our methodology. It was ultimately found that N–H products were accessible by employing *N*-Boc protected hetaryne precursors in our methodology (Figure 2.5).³⁵ Subjection of **2.23** and indolyne precursor **2.33** to our standard reactions conditions, followed by treatment with trifluoroacetic acid (TFA) to remove the Boc protecting group, gave deprotected indole scaffold **2.34** in 34% yield. Similarly, N–H carbazole adduct **2.35** was accessed in 65% yield via the corresponding reaction of **2.23** and *N*-Boc-carbazolyne precursor **2.31**. The ability to access π -extended N–H products (e.g., **2.34** and **2.35**) is expected to prove generally useful, as the *N*-position can be easily substituted. PAHs **2.34** and **2.35** also proved useful in our subsequent studies (vide infra) pertaining to the synthesis and evaluation of thermally activated delayed fluorescence (TADF) complexes.

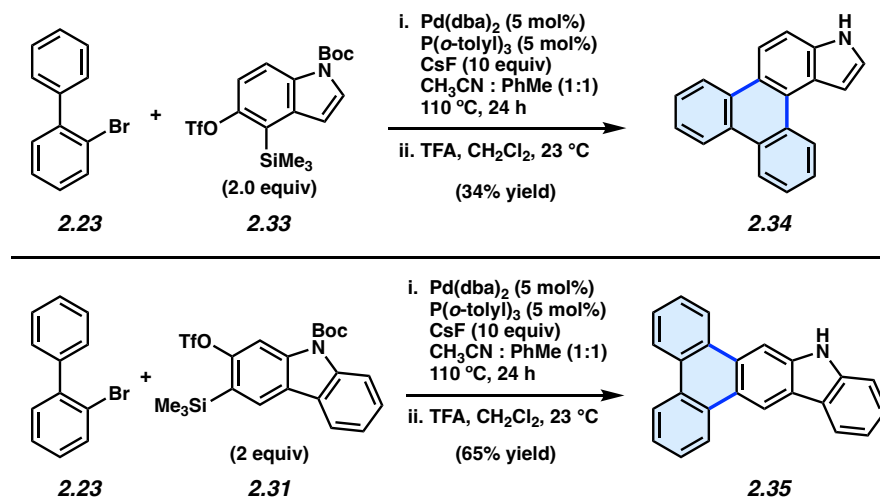


Figure 2.5. Synthesis of N–H products **2.34** and **2.35**.

2.3.3 Application of π -Extended Products as TADF Emitters

A potential application of indole- and carbazole-based PAHs is in organic light emitting diodes (OLEDs), which are crucial for high-performance display technologies and solid-state lighting applications. Specifically, the recent development of TADF complexes of the general structure donor–M–acceptor, where M is Cu(I), Ag(I), or Au(I), and where the donor and acceptor are amide and carbene ligands, respectively, (e.g., **2.36** and **2.37**, Figure 2.6),^{36,37,38,39,40} has allowed access to emissive dopants with high photoluminescence efficiencies (Φ_{PLQY} up to 100% in both solution and in the solid state) and short-lived excited states ($\tau < 1$ ms). These compounds also offer potential economic advantages over Ir- or Pt-centered phosphorescent dopants.^{41,42}

The photophysical properties of these two-coordinate complexes can be manipulated by altering either the donor or acceptor ligands.⁴³ For example, compounds **2.36** and **2.37** have the same amide donor ligand (carbazolyl) but different acceptor carbene ligands. Consequently, the energy for the interligand charge transfer (ICT) transition is different in each complex. Compound

2.36, with the carbene BZI (1,3-bis(2,6-diisopropylphenyl)-1-H-benzo[d]imidazole-2-ylidene) as an acceptor ligand emits at 432 nm when doped in polystyrene (PS) films whereas **2.37**, which has MAC (1,3-bis(2,6-diisopropylphenyl)-5,5-dimethyl-4-keto-tetrahydropyridylidene) as an acceptor, emits at 506 nm in the same media. The difference in energy for the ICT state is due to the poorer electrophilicity of BZI (**2.36**, $E_{\text{red}} = -2.82$ V vs. Fc^+/Fc) relative to MAC (**2.37**, $E_{\text{red}} = -2.50$ V). The low electron affinity of BZI raises the energy of the ^3ICT state such that it is near resonant with that of the locally excited triplet state (^3LE) of carbazolyl ($^3\text{LE} = 415$ nm). It follows that altering the nature of amide donor will also modify the energy of the ICT state, and consequently the photophysical properties of the complex.

Previous studies on carbazolyl donor ligands have focused on electronic modifications of carbazole using electron-donating or withdrawing groups, steric hindrance, and structural flexibility, leading to important structure-property relationships.^{36c,40,43,44,45} Moreover, extending the conjugation in aromatic π -systems by benzannulation has been shown to impact relative HOMO and LUMO energy levels in ways that sometimes lead to counterintuitive changes in emission color.^{42,46,47} Thus, the effect of similar π -extension on the photophysical properties of donor–M–acceptor complexes may not be obvious. Heterocyclic PAHs accessible by our π -extension methodology provide an opportunity to study and compare new π -extended TADF complexes.

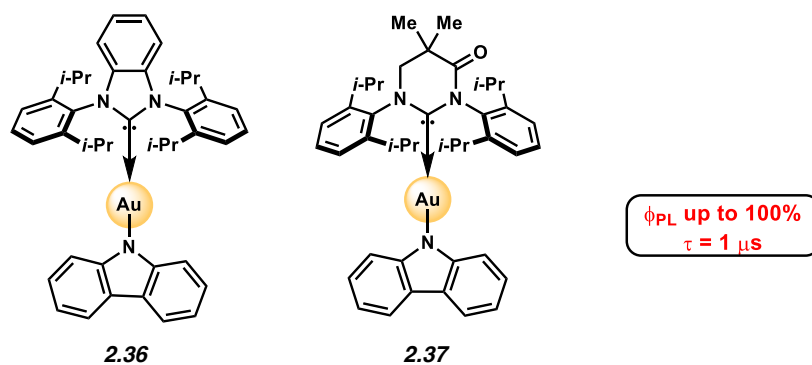


Figure 2.6. Heterocyclic PAHs as donor ligands in TADF complexes.^{48,49}

Two-coordinate donor-Au-acceptor complexes were prepared by treatment of **2.34** or **2.35** with sodium *tert*-butoxide in the presence of the NHC-Au-Cl complex (Figure 2.7A). The metal complexes evaluated in the present study (Figure 2.7B) are Au complexes due to their superior stability compared to Ag or Cu analogs.⁴⁰ Complexes **2.36**+ π and **2.37**+ π were obtained in 68% and 78% yields, respectively, whereas the respective indolyl complexes **2.38** and **2.38**+ π were prepared in 60% and 45% yields using this protocol. Complexes **2.36**+ π and **2.37**+ π enable comparison of the new π -extended phenanthrocarbazoyl donors to their respective carbazoyl counterparts, **2.36**⁴⁸ and **2.37**.^{43,49} The methyloindolyl (**2.38**) and phenanthroindolyl (**2.38**+ π) derivatives allow us to assess the impact of π -extension within a new indole series of complexes, as well as compare the carbazoyl and indolyl complexes.

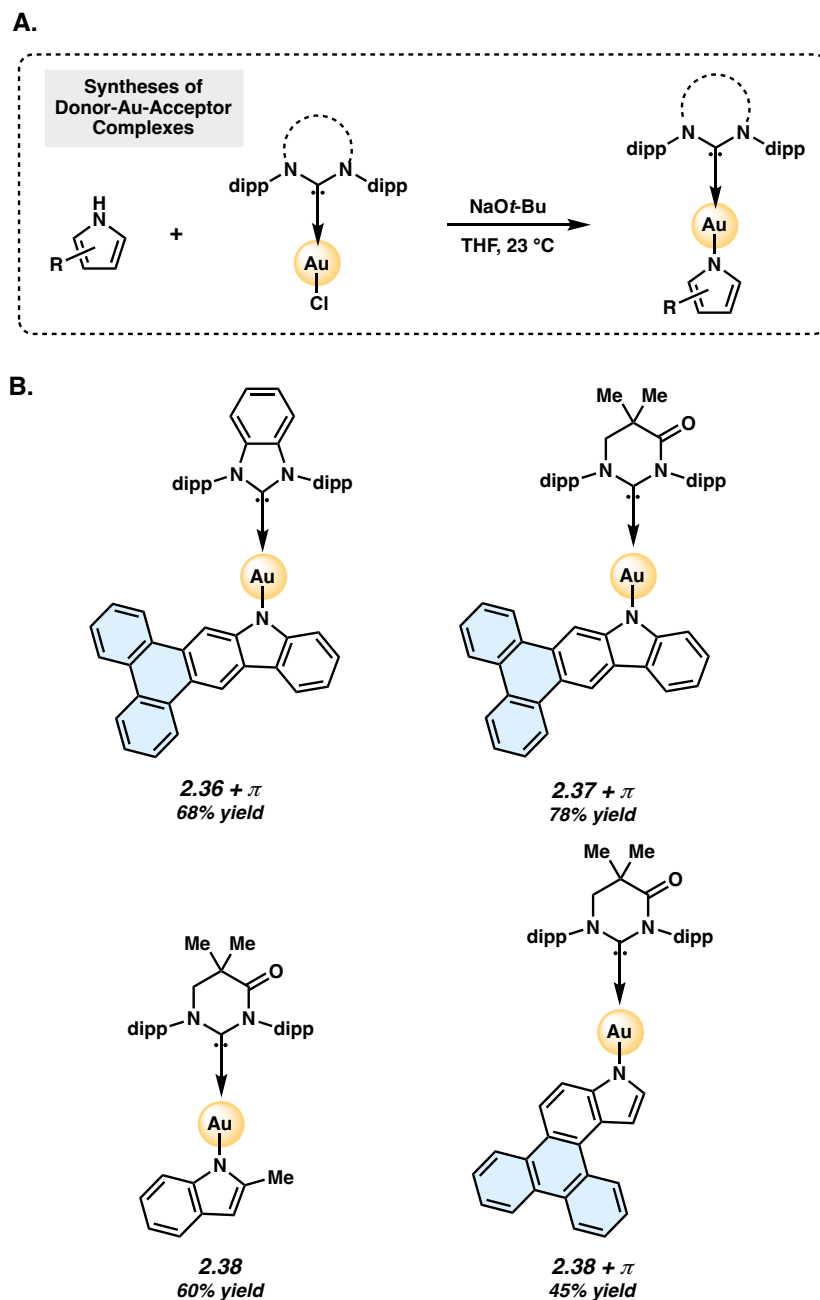


Figure 2.7. Preparation (A) and structures (B) of two-coordinate gold complexes. dipp = 2,6-diisopropylphenyl, as shown in Figure 2.6.

The photophysical properties of the π -extended carbazoyl-based complexes, **2.36+ π** and **2.37+ π** , were examined in different media (Figure 2.8) and compared to data of the parent

carbazole-containing complexes **2.36** and **2.37** (Table 2.1).^{43,49,49} The UV-visible absorption spectra of **2.36**+ π and **2.37**+ π display a strong solvent-independent band at 320 nm attributed to a π - π^* transition localized on the phenanthrocarbazolyl ligand. Weaker bands at lower energy are more structured and display a pronounced negative solvatochromism (e.g., **2.36**+ π at 416 nm in MeCy and 382 nm in MeTHF; **2.37**+ π at 460 nm in MeCy and 417 nm in MeTHF). This band is assigned to the ICT transition between the π -extended carbazole donor and carbene acceptor ligand that is overlapped with π - π^* transitions on the phenanthrocarbazolyl ligand. The solvatochromic behavior of the ICT band is ascribed to the dipole moment interactions between the solvent and complex molecules, in which the dipole of the excited state is larger and is oriented in the opposite direction as that of the ground state. The energy of the ICT transition in **2.36**+ π and **2.37**+ π is comparable to values for **2.36** and **2.37** (see Table 2.1) indicating that the donor strength of the phenanthrocarbazolyl and carbazolyl ligands are nearly equivalent.

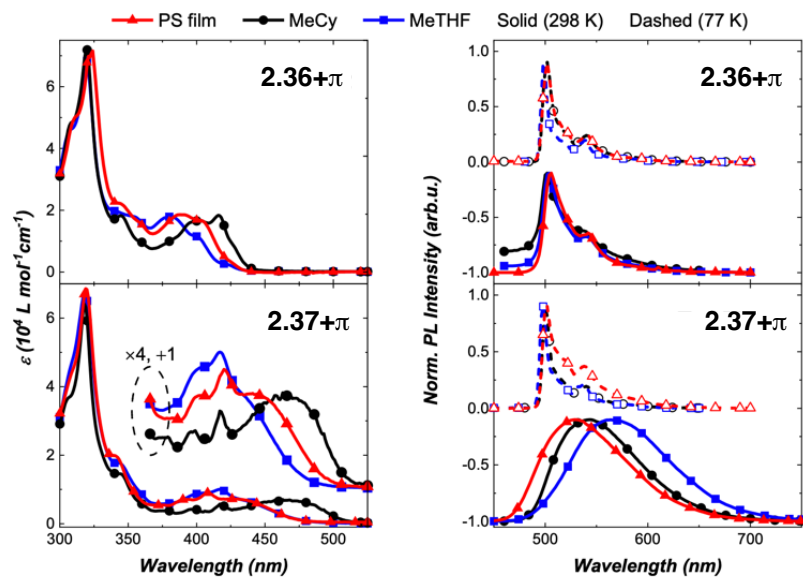


Figure 2.8. Absorption (left) and emission spectra (right) for the carbene-Au-carbazolyl complexes. Note that the absorption spectra of the PS films were scaled to match the intensity of the MeCy solution at $\lambda_{\text{max}} = 320$ nm. This feature is assigned to a solvent insensitive transition localized on the carbazolyl ligand.

Table 2.1. Photophysical data for carbene-Au-carbazolyl complexes.

complex	solvent	λ_{abs}^a	$\lambda_{\text{em, 298K}} (\lambda_{77\text{K}})$	Φ_{PLQY}	$\tau_{298\text{K}} (10^{-6} \text{ s})$	$k_r (10^5 \text{ s}^{-1})$	$k_{nr} (10^5 \text{ s}^{-1})$	$\tau_{77\text{K}} (10^{-3} \text{ s})$
2.36 ⁴⁸	1% PS film	385	452 (426)	1.00	3.6 (54%) 0.74 (46%)	4.4 ^b	<0.04 ^b	0.19
	MeCy	405	424 (424)	0.89	1.2	7.8	0.9	0.34
	MeTHF	365	452 (426)	0.79	2.6	3.0	0.8	0.64
2.36+π	1% PS film	388	506 (502)	0.52	5.1 (70%) 6.7 (30%)	3.1 ^b	11 ^b	1.8
	MeCy	416	502 (504)	0.03	30.0	0.01	0.3	2.9 (90%) 14 (8%) 100 (2%)
	MeTHF	382	504 (498)	0.02	57	0.004	0.2	3.2 (94%) 33 (6%)
2.37 ⁴⁹	1% PS film	425 ^c	512 (506)	0.85	0.83	10.0	1.8	0.043
	MeCy	450	522 (456)	0.88	1.1	8.0	1.1	0.068
	MeTHF	412	544 (428)	0.50	0.79	6.3	6.3	0.26
2.37+π	1% PS film	420	529 (500)	0.74	3.3 (47%) 1.0 (45%) ^d	3.4 ^b	1.2 ^b	4.4 (43%) 2.2 (33%) 0.7 (24%)
	MeCy	460	544 (500)	0.81	0.9 (91%) ^d	9.1	2.1	1.8 (59%) 3.1 (41%)
	MeTHF	417	566 (498)	0.39	0.6 (96%) ^d	6.9	11	2.4 (72%) 5.3 (28%)

^a ICT band. ^b Calculated from the weighted averages of both contributions. ^c Obtained from excitation spectrum. ^d An additional minor contribution from a longer lifetime component is needed to fit the observed data and assigned to *p*-type delayed fluorescence. See Section 2.6.2.

The effect of π -extension on the amide ligand is manifested more evidently in the luminescence properties of the complexes. In particular, whereas luminescence from **2.36** is broad and solvatochromic, emission spectra of **2.36+ π** are narrow, red-shifted and independent of solvent polarity. Radiative (k_r) and non-radiative (k_{nr}) rate constants are calculated using the relationship $k_r = \Phi_{\text{PL}}/\tau$, where $\Phi_{\text{PL}} = k_r/(k_r + k_{nr})$. The radiative rate for emission from **2.36** is rapid ($k_r = 3.0 \times 10^5 \text{ s}^{-1}$ in MeTHF) as opposed to being markedly slow in **2.36+ π** ($k_r = 4 \times 10^2 \text{ s}^{-1}$ in MeTHF). Unlike the photophysical properties of **2.36**, which are characteristic of emission from an ICT state, luminescence from **2.36+ π** indicates that the excited state transitions are localized on the donor ligand, and hence undergo conventional phosphorescence rather than TADF. This

assignment for the luminescence is confirmed by the minimal shift in energy and millisecond emission lifetime found upon cooling to 77 K. The difference in properties for **2.36**+ π versus **2.36** is caused by the lower energy for ^3LE state of the phenanthrocarbazolyl moiety (see section 2.6) compared to that for the carbazolyl ligand. In contrast, complex **2.37**+ π is capable of efficient TADF from the ICT state as borne out by emission spectra (Figure 2.8) that are similar, albeit redshifted, to spectra reported for **2.37**. The fast radiative rate ($k_r = 9.1 \times 10^5 \text{ s}^{-1}$) and high photoluminescence efficiency ($\Phi_{\text{PLQY}} = 0.81$) at room temperature in MeCy, along with luminescence that is redshifted from polar solvent (MeTHF) to non-polar solvent (MeCy and polystyrene film), is also consistent with emission from an ICT state.⁵⁰ Emission at 77 K (500 nm) is structured and polarity-independent. In this case, solvent molecules are frozen as a glass around the complex molecules, thus restricting stabilization of the excited ICT triplet.⁴³ Therefore, the triplet state localized on the donor becomes the lowest-lying emissive state and precludes ICT events. Notably, **2.37**+ π achieved 81% photoluminescence efficiency in MeCy (Figure 2.8).

Next, we compared the optical properties of **2.38** and **2.38**+ π (Figure 2.9 and Table 2.2). The ICT and π - π^* absorption bands are more resolved in complex **2.38** than in **2.38**+ π . The high extinction coefficients for the ICT band of **2.38** suggest strong electronic coupling between the acceptor carbene and the 2-methylindolyl donor ligands. Emission spectra for both complexes at 298 K show broad featureless bands and radiative rates are relatively fast ($k_r > 10^5 \text{ s}^{-1}$), both characteristics consistent with decay from an ICT excited state. The luminescence from **2.38** is slightly red-shifted (e.g., $\lambda_{\text{MeTHF}} = 600 \text{ nm}$) relative to spectra from **2.38**+ π (e.g., $\lambda_{\text{MeTHF}} = 566 \text{ nm}$), indicating that 2-methylindole is a stronger donor than the phenanthroindolyl ligand, which can be attributed to the different position of the π -extension in **2.38**+ π compared to **2.36**+ π and **2.37**+ π . Luminescence from the methylindolyl-based complex remains broad and

featureless upon cooling from 298 K to 77 K, indicating that the transition retains ICT character even in frozen matrix. For **2.38**, note that the destabilization of the ICT state upon going from 298 K to 77 K is greater in MeCy and MeTHF than in the PS film. This is likely due to enhanced solute-solute interactions on cooling the fluid solutions to 77 K, whereas the relative orientations of the solutes are fixed in a more random fashion at room temperature in the PS film. In contrast, the emission spectrum of **2.38+ π** is structured at 77 K and assigned to a low-lying ^3LE transition on the phenanthroindolyl ligand. The short lifetime measured for **2.38** at 77 K in MeTHF ($\tau = 1.1 \times 10^{-4}$ s) compared to that for **2.38+ π** ($\tau = 1.5 \times 10^{-2}$ s) is consistent with an ^3ICT transition for the former complex and ^3LE phosphorescence for the latter derivative.

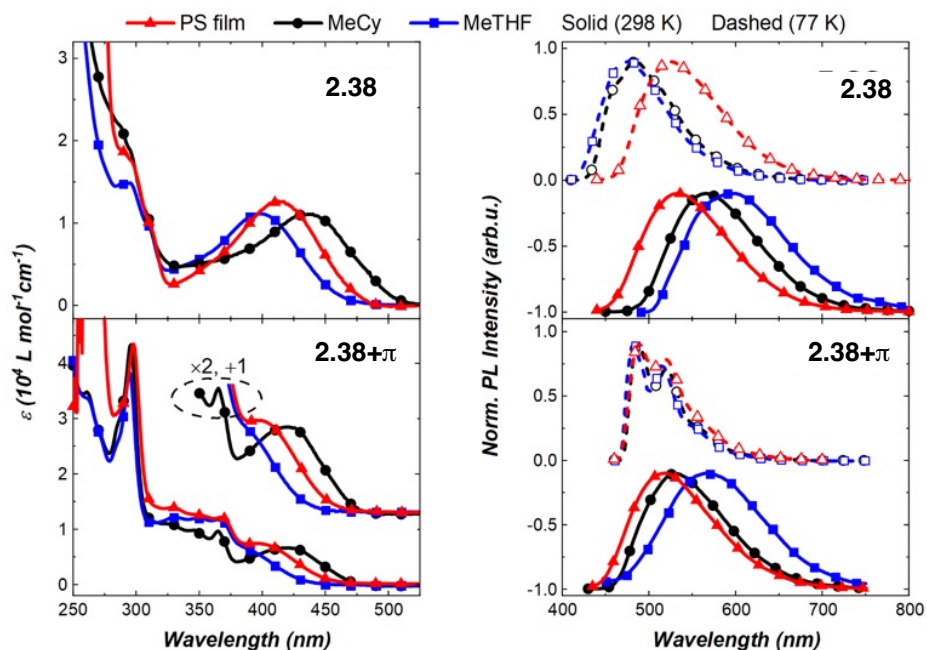


Figure 2.9. Absorption (left) and emission spectra (right) for carbene-Au-indolyl complexes.

Note that the absorption spectra of the PS films were scaled to match the peak at $\lambda_{\text{max}} = 295$ nm in MeCy solution, which is assigned to a solvent insensitive transition localized on the indolyl ligand.

Complex **2.38**+ π exhibits higher photoluminescence quantum yields in all media compared to **2.38**. The yields increase from MeTHF ($\Phi_{\text{PLQY}} = 1.4\%$) to MeCy ($\Phi_{\text{PLQY}} = 24.2\%$) to the PS film ($\Phi_{\text{PLQY}} = 49\%$). The lower emission efficiency in polar solvents is attributed to the greater reorganization of the excited state structure in polar solvents. Generally, complex **2.38** displays comparable, although slower radiative rates (k_r) and faster non-radiative rates (k_{nr}) in all solvents relative to **2.38**+ π . The slower k_{nr} of **2.38**+ π is likely due to a slower rate of rotation or exchange caused by the larger free volume of the **2.38**+ π ligand.

Table 2.2. Photophysical data for carbene-Au-indolyl complexes.

complex	solvent	λ_{abs}^a	$\lambda_{\text{em, 298K}} (\lambda_{77\text{K}})$	Φ_{PLQY}	$\tau_{298\text{K}}$ (10^{-6} s)	k_r (10^5 s^{-1})	k_{nr} (10^5 s^{-1})	$\tau_{77\text{K}}$ (10^{-3} s)
2.38	1% PS film	414	534 (525)	0.12	0.71 (80%) 0.25 (20%)	2.5 ^b	14 ^b	0.067 (78%) 0.025 (22%)
	MeCy	435	565 (484)	0.03	0.13	2.5	74	0.10
	MeTHF	399	600 (476)	0.004	0.011	3.6	910	0.11
2.38 + π	1% PS film	394	519 (495)	0.49	1.7 (65%) 0.41 (35%)	3.9 ^b	2.1 ^b	7.0 (74%) 3.0 (26%)
	MeCy	420	530 (486)	0.24	0.54	4.1	14	9.3 (62%) 13 (38%)
	MeTHF	380 ^a	566 (482)	0.01	0.024	5.8	4100	14 (73%) 19 (27%)

^a ICT band. ^b Calculated from the weighted averages of both contributions.

Comparing the carbazolyl and indolyl MAC complexes, it is noted that both appear to undergo TADF emission; however, the former (carbazolyl) family exhibits higher photoluminescence efficiencies due to lower rates of non-radiative decay. In comparing **2.38** to **2.38**+ π , the low steric profile about the indolyl ligand appears to have a greater influence on the photophysical performance than any energetic differences. In contrast, the discrepancy in performance between **2.36** and **2.36**+ π is attributed primarily to the energetics induced by π -

conjugation. In other words, the photophysical properties of indolyl-based complexes are primarily influenced by decreased steric hindrance of the indolyl ligand, whereas the performance of the carbazolyl-based complexes is primarily dictated by the π -conjugation thermodynamics.

2.4 Conclusions

In summary, we have developed a modular platform to access *N*-heterocycles with extended π -conjugation by leveraging hetarynes and Pd-catalysis. Of note, these represent rare examples of metal-mediated transformations of *N*-heterocyclic arynes. Through the construction of two C–C bonds in a single operation, this methodology allows for the direct π -extension of heterocyclic scaffolds through the appendage of three or more aromatic rings. The methodology offers a convergent platform for accessing important heterocycles with structural and electronic diversity. Notably, a new carbazolyne precursor, whose synthesis relies on a key retro-Brook rearrangement, can also be leveraged in this reaction to access carbazole derivatives. Heterocycles accessed in our methodology were ligated to Au-NHC complexes to give new two-coordinate metal complexes.

We find that extending the π -conjugation of the donor ligand influences the photophysical properties of the two-coordinate Au(I)-NHC complexes. The principal effect of π -extension in these compounds is stabilization of the triplet energy as opposed to only a minor perturbation of the donor strength. Therefore, depending on the nature of the carbene paired with the donor ligand, luminescence can be tuned to achieve emission from either the ^3LE or ICT state. Thus, a relatively weak electron accepting carbene such as BZI in **2.36** and **2.36+ π** gives only inefficient ^3LE emission, whereas the stronger electron accepting MAC carbene in **2.37** and **2.37+ π** leads to efficient emission from the ICT state. The carbazolyl (**2.37** and **2.37+ π**) and indolyl (**2.38** and

2.38+ π) complexes allow for the direct comparison of two systems that undergo TADF emission from the ICT state. The π -extension of the carbazolyl ligand in **2.37+ π** leads to a red-shift in emission. However, π -extending the indolyl-based ligand in **2.38+ π** results in an unexpected blue-shift in emission energy that may owe to the different position of substitution.⁴²

These studies should prompt further structure–photophysical property studies of donor ligands in these metal complexes to enhance OLED stability and efficiency. Furthermore, these studies demonstrate that hetarynes can be strategically leveraged as central building blocks for accessing π -extended scaffolds with notable properties.

2.5 Experimental Section

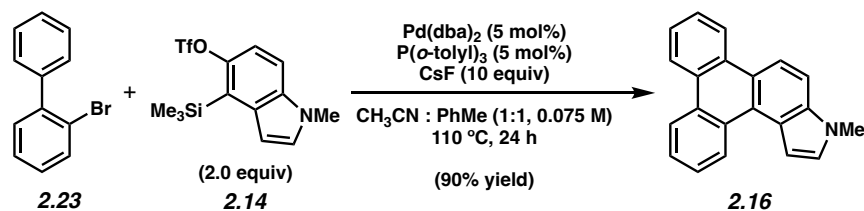
2.5.1 Materials and Methods

Unless stated otherwise, reactions were conducted in flame-dried glassware under an atmosphere of nitrogen or argon and commercially obtained reagents were used as received. Anhydrous solvents were either freshly distilled or passed through activated alumina columns, unless otherwise stated. Reaction temperatures were controlled using an IKAmag temperature modulator and, unless stated otherwise, reactions were performed at room temperature (approximately 23 °C). Cesium Fluoride (CsF) and Bis(dibenzylideneacetone)palladium(0) (Pd(dba)₂) were obtained from Strem Chemicals and stored in a desiccator. Tri(*o*-tolyl)phosphine (P(*o*-tolyl)₃), 1,1,1,3,3,3-hexamethyldisilazane (HMDS), *tert*-butyllithium (*t*-BuLi), sodium hydride (NaH), and sodium *ter*-butoxide (NaO*t*-Bu) were obtained from Sigma Aldrich. Methyl iodide (MeI) was acquired from Spectrum Chemical. Triflic anhydride was purchased from Oakwood Chemical and distilled over phosphorous pentoxide prior to use. Di-*tert*-butyl decarbonate and 4-dimethylaminopyridine (DMAP) were obtained from Oakwood Chemical. Triethylamine was purchased from Fischer Scientific and passed through an activated alumina column prior to use. 2-Bromobiphenyl (**2.23**) was obtained from Combi-Blocks and purified by flash chromatography (100% Hexanes) prior to use. 3-Bromo-2-phenylpyridine (**2.43**) was obtained from Combi-Blocks. Bromobiaryls **2.39**,⁵¹ **2.41**,⁵² **2.45**,⁵³ **2.47**,⁵⁴ and **2.49**,⁵⁵ were prepared according to literature procedures. The silyl triflates **2.14**,¹⁶ **2.33**,⁵⁶ and **2.24**⁵⁶ were prepared following literature procedures. 3-Bromo-2-hydroxycarbazole (**2.26**) was prepared in one step from 2-hydroxycarbazole following a literature protocol.³¹ NHC–Au–Cl complexes **2.51**⁴⁸ and **2.52**⁴³ were prepared following literature procedures. Regioisomeric ratios for indolyne annulation products were determined by analysis of the ¹H NMR spectra of the crude reaction mixtures. Thin-layer chromatography (TLC) was

conducted with EMD gel 60 F254 pre-coated plates (0.25 mm for analytical chromatography and 0.50 mm for preparative chromatography) and visualized using UV(254 nm). Celite[®] was purchased from Fischer Scientific and used as received. Silicycle Siliaflash P60 (particle size 0.040–0.063 mm) was used for flash column chromatography. ¹H NMR spectra were recorded on Bruker spectrometers (at 400, 500 and 600 MHz) and are reported relative to residual solvent signals. Data for ¹H NMR spectra are reported as follows: chemical shift (δ ppm), multiplicity, coupling constant (Hz), integration. Data for ¹³C NMR are reported in terms of chemical shift (at 101 and 125 MHz). IR spectra were recorded on a Perkin-Elmer UATR Two FT-IR spectrometer and are reported in terms of frequency absorption (cm^{-1}). DART-MS spectra were collected on a Thermo Exactive Plus MSD (Thermo Scientific) equipped with an ID-CUBE ion source and a Vapor Interface (IonSense Inc.). Both the source and MSD were controlled by Excalibur software v. 3.0. The analyte was spotted onto OpenSpot sampling cards (IonSense Inc.) using CH₂Cl₂ as the solvent. Ionization was accomplished using UHP He plasma with no additional ionization agents. The mass calibration was carried out using Pierce LTQ Velos ESI (+) and (–) Ion calibration solutions (Thermo Fisher Scientific). UV-visible absorption spectra were recorded by using Hewlett-Packard 4853 diode array spectrometer. Steady state emission spectra were recorded on Quanta-Master Photon Technology International phosphorescence/fluorescence spectrofluorometer. Emission quantum yields were measured using Hamamatsu C9920 system equipped with a xenon lamp, integrating sphere and model C10027 photonic multichannel analyzer (PMA). Emission lifetimes were acquired on IBH Fluorocube instrument by using time-correlated single photon counting (TCSPC) method.

2.5.2 Experimental Procedures

2.5.2.1 Scope of Pd-Catalyzed Annulation with *N*-Me-4,5-Indolyne



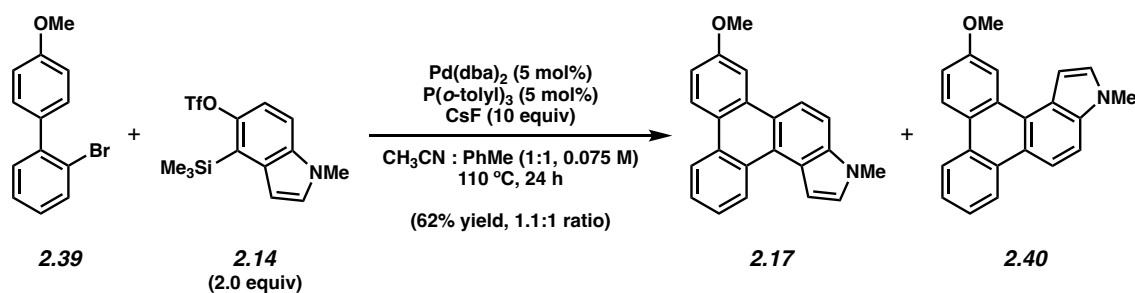
Representative Procedure A for hetaryne annulations (Figure 2.3, annulation product 2.16 used as an example).

A 1-dram vial was charged with Pd(dba)₂ (3.7 mg, 0.064 mmol, 5 mol%). Next, toluene (0.86 mL), P(*o*-tolyl)₃ (2.0 mg, 0.064 mmol, 5 mol%), 2-bromobiphenyl (**2.23**) (30.0 mg, 0.129 mmol, 1.0 equiv), silyl triflate **2.14** (90.5 mg, 0.257 mmol, 2.0 equiv), and acetonitrile (0.86 mL) were added, followed by an oven-dried magnetic stirbar and then CsF (195 mg, 1.29 mmol, 10 equiv). The vial was purged with nitrogen for 3 minutes, then sealed with a Teflon-lined screw cap and stirred at 110 °C for 24 h. Then, after cooling to 23 °C, the mixture was transferred with CH₂Cl₂ (10 mL) and H₂O (2 mL) to a 150 mL separatory funnel containing brine (15 mL). The layers were separated and the aqueous layer was extracted with CH₂Cl₂ (3 x 15 mL). The combined organic layers were dried over MgSO₄, filtered, and concentrated *in vacuo*. The resulting crude product was purified by flash chromatography (100% Hexanes → 200:1 Hexanes:EtOAc) to afford annulation product **2.16** (90% yield, average of two experiments) as an off-white solid.

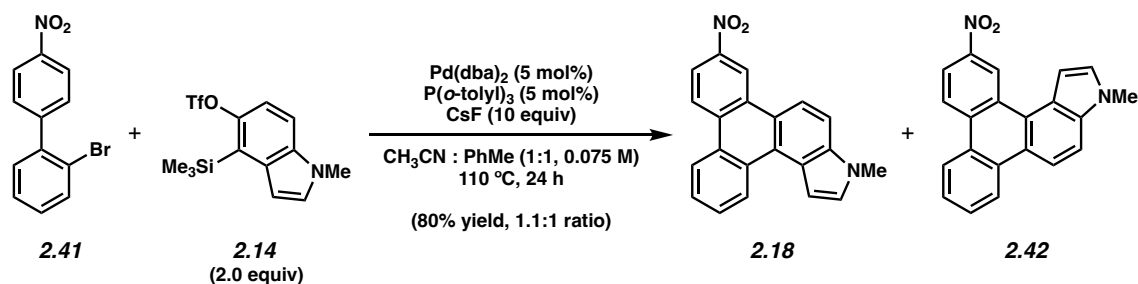
Indole **2.16**: mp: 139–144 °C; R_f 0.41 (4:1 Hexanes:EtOAc); ¹H NMR (500 MHz, CDCl₃): δ 9.24 (d, *J* = 8.0, 1H), 8.78 (d, *J* = 8.0, 1H), 8.72 (t, *J* = 7.0, 2H), 8.57 (d, *J* = 9.0, 1H), 7.74 (t, *J* = 7.4, 1H), 7.73–7.62 (m, 4H), 7.53 (d, *J* = 2.8, 1H), 7.28 (d, *J* = 3.0, 1H), 3.92 (s, 3H); ¹³C NMR (125 MHz, CDCl₃): δ 136.4, 131.3, 131.2, 130.4, 128.9, 128.8, 127.17, 127.15, 126.7, 126.4, 125.9, 124.6, 124.1, 123.8, 123.6, 123.28, 123.25, 117.7, 110.5, 104.0, 33.3; IR (film): 3069, 2924, 2850,

1514, 1492, 1441, 1417, 1351, 1248, 754, 740, 718 cm^{-1} ; HRMS-APCI (m/z) $[\text{M} + \text{H}]^+$ calcd for $\text{C}_{21}\text{H}_{16}\text{N}^+$, 282.12773; found 282.12717.

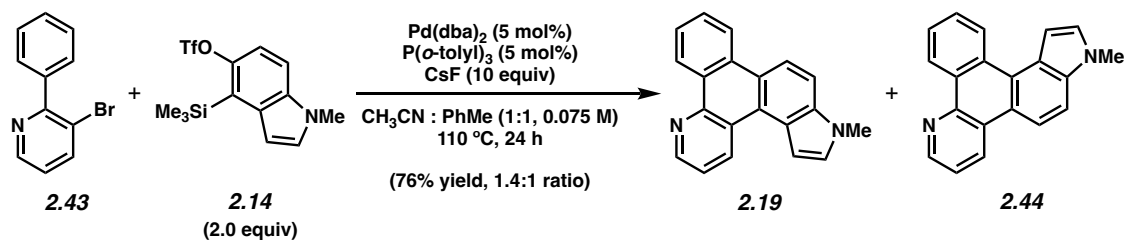
Any modifications of the conditions shown in the representative procedure above are specified in the following schemes, which depict all of the results shown in Figure 2.3.



Indoles 2.17 and 2.40. Followed representative procedure A. Purification by flash chromatography (50:1 Hexanes:EtOAc) afforded an inseparable mixture of indoles **2.17** and **2.40** (62% yield, average of two experiments, 1.1:1 ratio, unassigned) as a white solid. Indoles **2.17** and **2.40**: R_f 0.27 (4:1 Hexanes:EtOAc); ^1H NMR (500 MHz, C_6D_6 , combined): δ 9.42 (dd, $J = 8.3$, 1.3, 1H), 8.93 (d, $J = 2.6$, 1H), 8.69 (dd, $J = 7.9$, 1.3, 1H), 8.57–8.50 (m, 5H), 8.48 (d, $J = 9.0$, 1H), 8.22 (d, $J = 2.5$, 1H), 7.60–7.47 (m, 6H), 7.30–7.26 (m, 3H), 7.21 (dd, $J = 9.2$, 2.6, 1H), 6.72 (d, $J = 6.7$, 1H), 6.69 (d, $J = 3.2$, 1H), 3.61 (s, 3H), 3.55 (s, 3H), 3.001 (s, 3H), 2.995 (s, 3H); ^{13}C NMR (125 MHz, C_6D_6 , combined): δ 159.6, 159.3, 136.8, 136.6, 133.32, 133.31, 131.2, 131.0, 130.8, 129.7, 128.6, 128.5, 127.6, 126.6, 126.4, 126.2, 126.0, 125.8, 125.4, 125.3, 125.2, 125.1, 125.0, 124.6, 124.5, 124.4, 124.0, 123.6, 123.27, 123.25, 118.1, 118.0, 115.5, 115.0, 110.8, 110.5, 110.1, 106.5, 104.5, 104.0, 55.0, 54.9, 32.31, 32.28; IR (film): 2934, 2834, 1614, 1510, 1414, 1246, 1227 cm^{-1} ; HRMS-APCI (m/z) $[\text{M} + \text{H}]^+$ calcd for $\text{C}_{22}\text{H}_{18}\text{NO}^+$, 312.13829; found 312.13897.

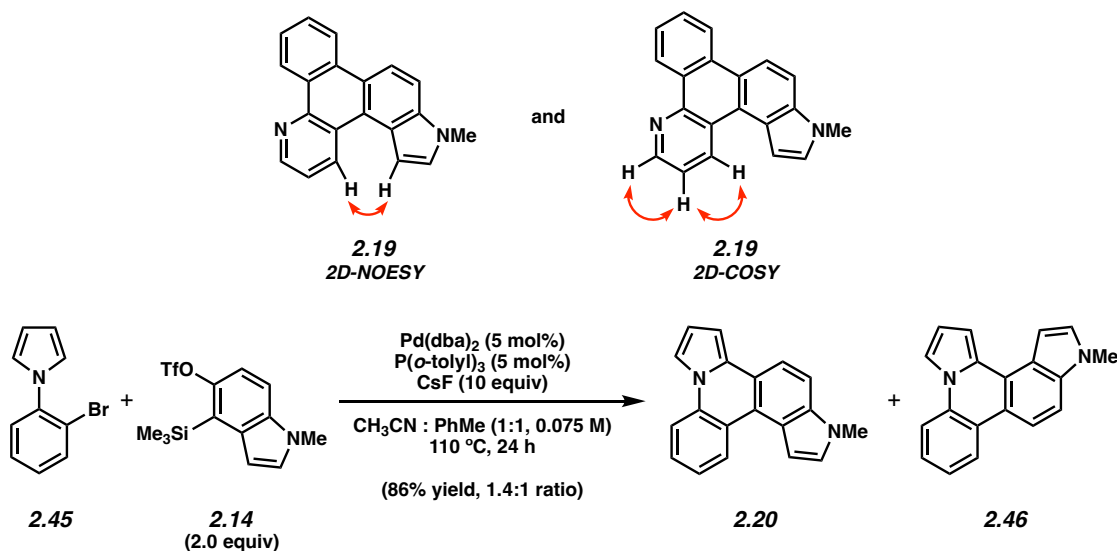


Indoles 2.18 and 2.42. Followed representative procedure A. Purification by flash chromatography (50:1 Hexanes:EtOAc → 20:1 Hexanes:EtOAc) afforded an inseparable mixture of indoles **2.18** and **2.42** (80% yield, average of two experiments, 1.4:1 ratio, unassigned) as a yellow solid. Indoles **2.18** and **2.42**: R_f 0.45 (4:1 Hexanes:EtOAc); $^1\text{H NMR}$ (600 MHz, CDCl_3 , major): δ 10.10 (d, $J = 2.4$, 1H), 8.79 (d, $J = 9.1$, 1H), 8.71 (d, $J = 8.3$, 1H), 8.66 (d, $J = 8.2$, 1H), 8.55 (d, $J = 9.2$, 1H), 8.41 (dd, $J = 9.0$, 2.3, 1H), 7.78–7.72 (m, 2H), 7.67 (ddd, $J = 8.1$, 7.0, 1.2, 1H), 7.54 (d, $J = 3.1$, 1H), 7.39 (d, $J = 3.2$, 1H), 4.00 (s, 3H); $^1\text{H NMR}$ (600 MHz, CDCl_3 , minor): δ 9.54 (d, $J = 2.3$, 1H), 9.21 (d, $J = 8.3$, 1H), 8.75 (d, $J = 9.1$, 1H), 8.70 (d, $J = 8.3$, 1H), 8.55 (d, $J = 8.9$, 1H), 8.35 (dd, $J = 9.0$, 2.3, 1H), 7.82 (ddd, $J = 8.1$, 7.0, 1.3, 1H), 7.76–7.71 (m, 2H), 7.51 (d, $J = 3.1$, 1H), 7.36 (d, $J = 3.2$, 1H), 4.00 (s, 3H); $^{13}\text{C NMR}$ (125 MHz, CDCl_3 , combined): δ 146.4, 146.0, 136.8, 136.4, 134.8, 133.3, 132.51, 132.48, 131.3, 131.0, 129.9, 129.4, 129.0, 128.7, 128.6, 127.4, 127.3, 126.8, 126.4, 125.2, 124.6, 124.4, 124.21, 124.17, 124.1, 123.8, 123.60, 123.55, 123.5, 123.1, 122.8, 119.9, 119.53, 119.47, 117.5, 117.4, 111.7, 111.1, 104.0, 103.4, 33.4, 33.3; IR (film): 2919, 2852, 1597, 1515, 1346, 854, 747 cm^{-1} ; HRMS-APCI (m/z) [$M + \text{H}^+$] calcd for $\text{C}_{21}\text{H}_{15}\text{N}_2\text{O}_2^+$, 327.11280; found 327.11387.

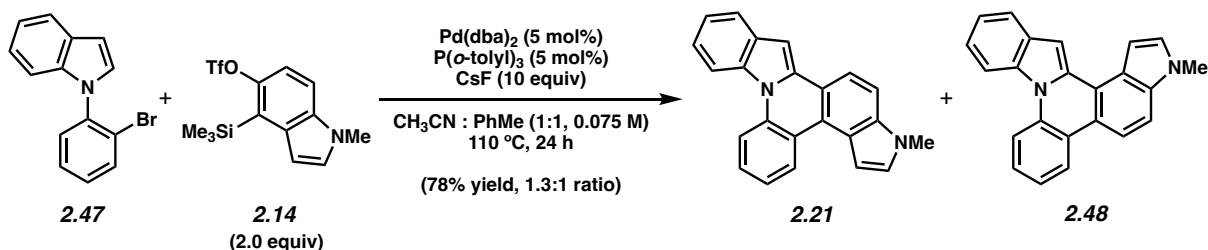


Indoles 2.19 and 2.44. Followed representative procedure A. Purification by flash chromatography (100% Hexanes \rightarrow 50:1 Hexanes:EtOAc \rightarrow 9:1 Hexanes:EtOAc) afforded an inseparable mixture of indoles **2.19** and **2.44** (76% yield, 1.4:1 ratio, average of two experiments) as a pale yellow solid. Indole **2.19**: R_f 0.34 (4:1 Hexanes:EtOAc); $^1\text{H NMR}$ (500 MHz, CDCl_3): δ 9.40 (ddd, $J = 8.2, 4.7, 1.4$, 2H), 8.99 (dd, $J = 4.3, 1.6$, 1H), 8.66 (d, $J = 8.2$, 1H), 8.54 (d, $J = 8.5$, 1H), 7.76 (ddd, $J = 8.1, 6.9, 1.6$, 1H), 7.71 (ddd, $J = 8.3, 6.8, 1.2$, 1H), 7.65 (d, $J = 9.0$, 1H), 7.64–7.60 (m, 1H), 7.38 (d, $J = 2.9$, 1H), 7.27 (d, $J = 3.2$, 1H), 3.90 (s, 3H). Indole **2.44**: R_f 0.34 (4:1 Hexanes:EtOAc); $^1\text{H NMR}$ (500 MHz, CDCl_3): δ 9.46 (dd, $J = 8.1, 1.3$, 1H), 9.18 (d, $J = 8.2$, 1H), 8.95 (dd, $J = 4.3, 1.6$, 1H), 8.89 (dd, $J = 8.4, 1.3$, 1H), 8.41 (d, $J = 9.0$, 1H), 7.83 (ddd, $J = 8.2, 7.0, 1.7$, 1H), 7.77 (ddd, $J = 7.2, 5.6, 1.2$, 1H), 7.64–7.60 (m, 1H), 7.55 (dd, $J = 8.3, 4.3$, 1H), 7.53 (d, $J = 3.1$, 1H), 7.29 (d, $J = 3.2$, 1H), 3.91 (s, 3H); $^{13}\text{C NMR}$ (125 MHz, CDCl_3 , combined): 147.69, 147.66, 146.9, 145.6, 136.6, 136.3, 134.2, 132.8, 132.7, 131.4, 131.0, 130.1, 129.3, 129.2, 128.8, 128.4, 126.6, 126.4, 126.2, 126.1, 125.8, 125.4, 125.2, 124.6, 124.2, 124.0, 123.9, 123.2, 122.9, 122.8, 122.1, 121.5, 117.7, 117.3, 111.1, 110.6, 104.0, 103.2, 33.3 (2C); IR (film): 3059, 2920, 1739, 1609, 1579, 1513, 1477, 1444, 1418, 1399, 1349, 1290, 1241 cm^{-1} ; HRMS-APCI (m/z) [$\text{M} + \text{H}^+$] calcd for $\text{C}_{20}\text{H}_{15}\text{N}_2^+$, 283.12297; found 283.11932.

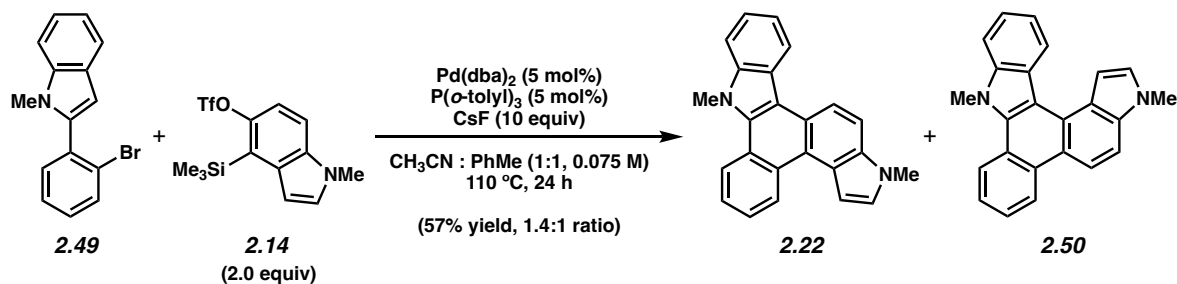
The structure of **2.19** was verified by 2D-NOESY and 2D-COSY of the mixture, as the following interactions were observed:



Pyrroles 2.20 and 2.46. Followed representative procedure A. Purification by flash chromatography (20:1 Hexanes:Benzenes) afforded an inseparable mixture of pyrroles **2.20** and **2.46** (86% yield, 1.4:1 ratio, average of two experiments, unassigned) as a yellow solid. Pyrroles **2.20** and **2.46**: *R_f* 0.56 (4:1 Hexanes:EtOAc); ¹H NMR (500 MHz, C₆D₆, combined): δ 9.01 (dd, *J* = 8.0, 1.5, 1H), 8.33–8.28 (m, 1H), 8.13 (d, *J* = 8.9, 1H), 8.01 (d, *J* = 8.7, 1H), 7.65 (dd, *J* = 3.0, 1.4, 1H), 7.58 (dd, *J* = 3.0, 1.4, 1H), 7.4 (m, 3H), 7.28 (dd, *J* = 3.2, 0.7, 1H), 7.27–7.23 (m, 2H), 7.22–7.19 (m, 1H), 7.19–7.17 (m, 2H), 7.10 (t, *J* = 0.9, 1H), 7.09 (m, 2H), 6.92 (dd, *J* = 4.0, 2.9, 1H), 6.84 (dd, *J* = 3.9, 2.8, 1H), 6.67 (d, *J* = 3.0, 1H), 6.62 (d, *J* = 3.3, 1H), 2.96 (s, 3H), 2.92 (s, 3H); ¹³C NMR (125 MHz, C₆D₆, combined): δ 136.7, 136.2, 134.0, 132.9, 131.5, 129.6, 128.9, 128.8, 127.60, 127.58, 127.0, 124.3, 124.2, 124.0, 123.7, 123.5, 123.4, 122.9, 121.5, 120.4, 118.9, 118.6, 117.9, 117.0, 115.3, 115.2, 113.0, 112.9, 112.7, 112.2, 111.5, 108.8, 105.6, 102.94, 102.88, 101.0, 32.22, 32.19; IR (film): 3102, 2923, 1500, 1441, 1355 cm⁻¹; HRMS-APCI (*m/z*) [*M* + H⁺] calcd for C₁₉H₁₅N₂⁺, 271.12297; found 271.12191.

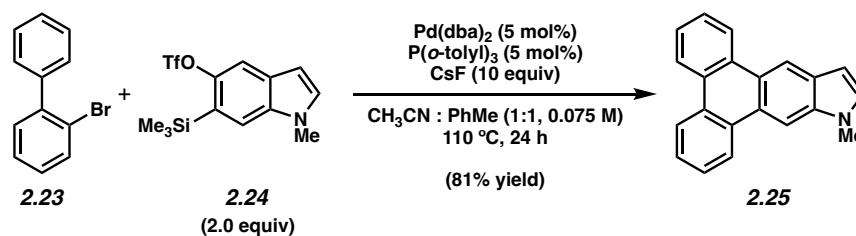
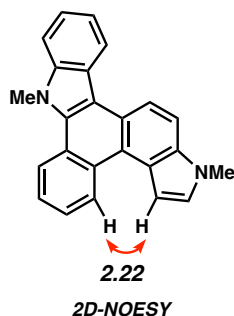


Indoles 2.21 and 2.48. Followed representative procedure A. Purification by flash chromatography (100% Hexanes \rightarrow 100:1 Hexanes:EtOAc \rightarrow 25:1 Hexanes:EtOAc \rightarrow 9:1 Hexanes:EtOAc, followed by a second column of 9:1 Hexanes:EtOAc) afforded an inseparable mixture of indoles **2.21** and **2.48** (78% yield, 1.3:1 ratio, average of two experiments, unassigned) as a bright yellow solid. Indoles **2.21** and **2.48**: R_f 0.32 (4:1 Hexanes:EtOAc); $^1\text{H NMR}$ (500 MHz, C_6D_6 , major): δ 8.43 (dd, $J = 8.2, 1.0$, 1H), 8.28 (dd, $J = 8.0, 1.1$, 2H), 8.04 (d, $J = 9.0$, 1H), 7.98 (d, $J = 8.6$, 1H), 7.79 (s, 1H), 7.41 (ddd, $J = 7.8, 6.8, 0.9$, 1H), 7.36–7.31 (m, 1H), 7.30–7.17 (m, 3H), 7.08 (dd, $J = 8.9, 0.6$, 1H), 6.63 (d, $J = 3.2$, 1H), 2.94 (s, 3H); $^1\text{H NMR}$ (500 MHz, C_6D_6 , minor): δ 8.95 (dd, $J = 8.0, 1.6$, 1H), 8.41 (dd, $J = 8.0, 1.1$, 1H), 8.23 (d, $J = 8.4$, 1H), 7.98 (d, $J = 7.6$, 1H), 7.91 (d, $J = 7.9$, 1H), 7.41 (ddd, $J = 7.5, 6.9, 0.9$, 1H), 7.36–7.31 (m, 1H), 7.30–7.17 (m, 4H), 7.04 (dd, $J = 8.7, 0.7$, 1H), 6.58 (d, $J = 3.2$, 1H), 2.92 (s, 3H); $^{13}\text{C NMR}$ (125 MHz, C_6D_6 , combined; 44 of 46 signals observed): δ 137.6, 137.2, 136.7, 136.5, 135.6, 135.5, 134.1, 133.9, 131.7, 131.6, 129.3, 129.2, 127.6, 127.3, 124.6, 124.3, 124.0, 123.8, 123.7, 123.04, 122.95, 122.3, 122.11, 122.06, 121.6, 121.5, 121.4, 121.1, 121.0, 120.7, 119.9, 118.7, 116.8, 116.7, 116.6, 114.8, 111.3, 110.5, 103.2, 102.9, 99.8, 95.2, 32.21, 32.18; IR (film): 3040, 2923, 1738, 1601, 1550, 1509, 1490, 1447, 1419, 1355; HRMS-APCI (m/z) $[\text{M} + \text{H}]^+$ calcd for $\text{C}_{23}\text{H}_{17}\text{N}_2^+$, 321.13862; found 321.13951.



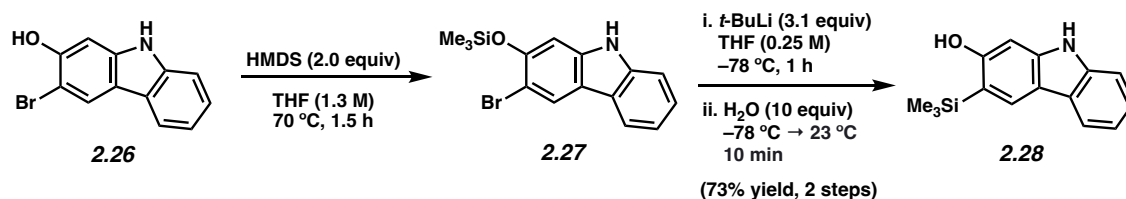
Indoles 2.22 and 2.50. Followed representative procedure A. Purification by flash chromatography (100% Hexanes \rightarrow 200:1 Hexanes:EtOAc \rightarrow 100:1 Hexanes:EtOAc) afforded an inseparable mixture of indoles **2.22** and **2.50** (57% yield, 1.4:1 ratio, average of two experiments) as a yellow amorphous solid. Indole **2.22**: R_f 0.40 (3:1 Hexanes:EtOAc); ^1H NMR (500 MHz, C_6D_6): δ 9.74 (d, $J = 8.5$, 1H), 9.09 (d, $J = 8.8$, 1H), 8.92–8.88 (m, 1H), 8.48 (dd, $J = 8.3$, 0.9, 1H), 7.70–7.65 (m, 2H), 7.59–7.43 (m, 4H), 7.29 (dd, $J = 7.5$, 1.5, 1H), 6.81 (d, $J = 3.1$, 1H), 3.57 (s, 3H), 3.11 (s, 3H); ^{13}C NMR (125 MHz, C_6D_6 ; 22 of 24 signals observed): 141.8, 134.8, 134.2, 132.7, 125.7, 125.3, 125.2, 124.4, 123.9, 123.8, 123.6, 123.3, 122.6, 122.1, 120.3, 118.8, 115.7, 111.4, 109.9, 103.9, 34.0, 32.4. Indole **2.50**: R_f 0.40 (3:1 Hexanes:EtOAc); ^1H NMR (500 MHz, C_6D_6): δ 9.37 (d, $J = 8.1$, 1H), 8.92–8.88 (m, 1H), 8.68 (d, $J = 9.1$, 1H), 8.38 (dd, $J = 8.4$, 0.9, 1H), 7.95 (d, $J = 3.1$, 1H), 7.59–7.43 (m, 3H), 7.40 (ddd, $J = 7.9$, 7.1, 1.1, 1H), 7.34 (dd, $J = 9.1$, 0.6, 1H), 7.26 (d, $J = 8.1$, 1H), 6.72 (d, $J = 3.1$, 1H), 3.54 (s, 3H), 3.10 (s, 3H); ^{13}C NMR (125 MHz, C_6D_6 ; 23 of 24 signals observed): 141.5, 136.5, 136.2, 132.8, 126.3, 125.8, 125.1, 124.8, 124.54, 124.51, 124.46, 123.7, 123.6, 123.1, 121.7, 119.2, 118.3, 115.3, 109.7, 108.1, 105.8, 34.0, 32.4; IR (film, entire mixture): 3055, 2923, 2854, 1737, 1509, 1472, 1374, 1342, 1245, 1102 cm^{-1} ; HRMS-APCI (m/z) [$\text{M} + \text{H}$] $^+$ calcd for $\text{C}_{24}\text{H}_{19}\text{N}_2^+$, 335.15428; found 335.15396.

The structure of **2.22** was verified by 2D-NOESY of the mixture, as the following interaction was observed:



Indole 2.25. Followed representative Procedure A. Purification by flash chromatography (Hexanes \rightarrow 1:1 Hexanes:Benzenes) afforded indole **2.25** (81% yield, average of two experiments) as an off-white solid. Indole **2.25**: mp 169.6–172.0 $^\circ\text{C}$; R_f 0.25 (9:1 Hexanes:EtOAc); ^1H NMR (500 MHz, CDCl_3): δ 8.92 (s, 1H), 8.73 (d, $J = 8.3$, 2H), 8.62 (t, $J = 7.7$, 2H), 8.51 (s, 1H), 7.66–7.56 (m, 4H), 7.27 (d, $J = 2.6$, 1H), 6.70 (dd, $J = 0.8, 3.1$, 1H), 3.99 (s, 3H); ^{13}C NMR (125 MHz, CDCl_3 ; 27 of 28 signals observed): δ 137.4, 132.0, 131.4, 131.2, 129.6, 129.3, 129.0, 127.3, 127.1, 126.6, 126.1, 125.7, 123.56, 123.55, 123.4, 123.22, 123.15, 115.1, 102.3, 101.1, 33.2; IR (film): 3081, 2928, 2811, 1628, 1601, 1520, 1446, 1218, 1085, 754 cm^{-1} ; HRMS–APCI (m/z) $[\text{M}]^+$ calcd for $\text{C}_{21}\text{H}_{16}\text{N}^+$, 281.11990; found 281.12065.

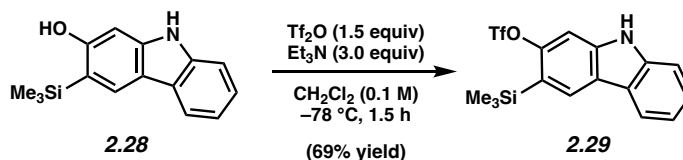
2.5.2.2 Synthesis of Silyl Triflate Precursor to 2,3-Carbazolyne



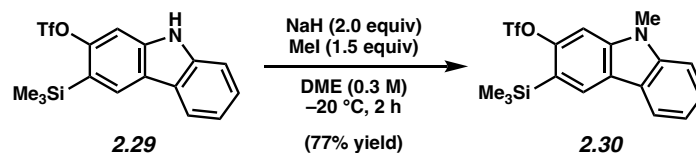
Silyl alcohol 2.28. A 20 mL scintillation vial was charged with 3-bromo-2-hydroxycarbazole (**2.26**, 4.3 g, 16 mmol, 1.0 equiv) and THF (5.6 mL, 1.3 M). HMDS (6.9 mL, 2.0 equiv, 33 mmol) was added in one portion. The vial was sealed with a Teflon cap, and subsequently placed in an aluminum block preheated to 70 °C, where it was allowed to stir for 1.5 h. After stirring for 1.5 h, the reaction mixture was cooled to 23 °C and concentrated under reduced pressure to afford the intermediate silyl enol ether **2.27** as a pink solid. This was carried forward without further purification.

The crude solid was dissolved in THF (8.5 mL, 0.25 M) and purged with nitrogen for 3 minutes, before being cooled to -78 °C. *tert*-Butyllithium (1.70 M, 4.17 mL, 7.09 mmol, 3.1 equiv) was then added dropwise over 10 min. The solution was allowed to stir for 1 hour at -78 °C. After the allotted time, deionized H₂O (408 μL, 22.5 mmol, 10 equiv) was added dropwise over 2 min. The solution was then allowed to warm to 23 °C over 10 min and the mixture was transferred to a separatory funnel with H₂O (20 mL) and CH₂Cl₂ (20 mL). The layers were then separated and the aqueous layer was extracted with CH₂Cl₂ (2 x 20 mL). The combined organic layers were dried over MgSO₄, filtered, and concentrated under reduced pressure. The crude residue was then purified by flash chromatography (100% Benzene) to afford silyl alcohol **2.28** as a white solid (3.1 g, 73% yield over two steps). Silyl alcohol **2.28**: mp: >200 °C; R_f 0.15 (100% Benzene); ¹H NMR (600 MHz, CDCl₃): δ 8.03 (s, 1H), 8.00 (d, *J* = 7.7, 1H), 7.84 (s, 1H), 7.36–7.32 (m, 2H), 7.21 (dd, *J* = 6.6, 2.2, 1H), 6.72 (d, *J* = 2.4, 1H), 4.94 (s, 1H), 0.39 (s, 9H); ¹³C NMR (125 MHz, CDCl₃): δ

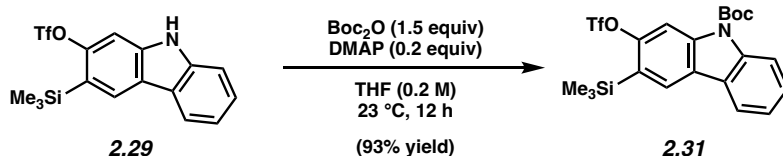
159.4, 141.8, 139.2, 126.9, 124.4, 123.4, 119.6, 119.3, 117.5, 117.2, 110.2, 96.0, -0.7; IR (film): 3416, 3016, 2970, 2926, 2854, 1738, 1366 cm^{-1} ; HRMS-APCI (m/z) $[\text{M} + \text{H}]^+$ calcd for $\text{C}_{13}\text{H}_{18}\text{NOSi}^+$, 256.1152; found 256.1171.



Silyl triflate 2.29. Silyl alcohol **2.28** (403 mg, 1.58 mmol, 1.00 equiv) was suspended in CH_2Cl_2 (15 mL). The solution was purged with nitrogen for 3 minutes, then cooled to -78°C . Triethylamine (0.66 mL, 4.7 mmol, 3.0 equiv) was then added in one portion followed by trifluoromethanesulfonic anhydride (400 μL , 2.37 mmol, 1.5 equiv), which was added dropwise over 5 min. The solution was allowed to stir for 1.5 h at -78°C . After the allotted time, saturated aqueous NaHCO_3 (20 mL) was added over 1 minute. The solution was then allowed to warm to 23°C over 10 min and the mixture was transferred to a separatory funnel with H_2O (10 mL) and CH_2Cl_2 (20 mL). The layers were then separated and the aqueous layer was extracted with CH_2Cl_2 (2 x 20 mL). The combined organic layers were dried over MgSO_4 , filtered, and concentrated under reduced pressure. The crude residue was then purified by flash chromatography (100% Benzene) to afford silyl triflate **2.29** as a clear oil (375 mg, 69% yield). Silyl triflate **2.29**: $R_f = 0.59$ (100% Benzene); ^1H NMR (500 MHz, CDCl_3): δ 8.22 (s, 1H), 8.16 (s, 1H), 8.08 (d, $J = 7.9$, 1H), 7.46–7.44 (m, 3H), 7.28 (ddd, $J = 7.8, 5.0, 3.1$, 1H), 0.44 (s, 9H); ^{13}C NMR (125 MHz, CDCl_3): δ 153.3, 140.4, 140.2, 127.5, 126.6, 122.7, 122.3, 121.9, 120.43, 120.41, 110.9, 102.0, 0.40; IR (film): 3443, 3016, 2970, 2948, 1739, 1217 cm^{-1} ; HRMS-APCI (m/z) $[\text{M} + \text{H}]^+$ calcd for $\text{C}_{16}\text{H}_{17}\text{NO}_3\text{F}_3\text{SSi}^+$, 388.0645; found 388.0659.

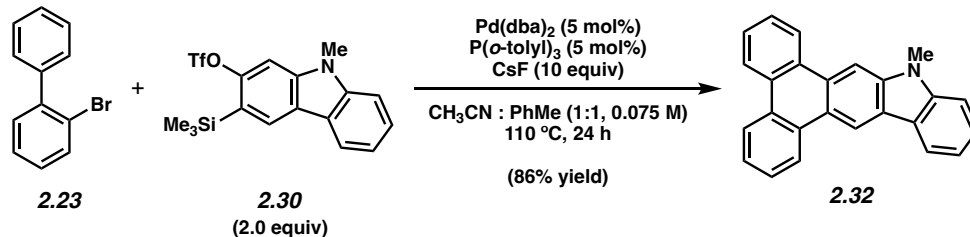


***N*-Me-Carbazole Silyl Triflate 2.30.** To a 2-dram vial was added carbazole silyl triflate **2.29** (196 mg, 0.506 mmol, 1.00 equiv) and DME (1.7 mL, 0.3 M). The resulting mixture was stirred under positive nitrogen pressure. The mixture was cooled to $-20\text{ }^\circ\text{C}$ in a dry ice and water/methanol (7:3) bath for 5 min. To the cooled solution was added iodomethane (48 μL , 0.76 mmol, 1.5 equiv) in a single portion. Next, the septum was removed and NaH (60% dispersion in mineral oil, 40.5 mg, 1.01 mmol, 2.0 equiv) was added in a single portion, then the septum was quickly replaced. The reaction continued to stir under nitrogen at $-20\text{ }^\circ\text{C}$ for 2 h, at which point the reaction was quenched with sat. aq. NH_4Cl (5 mL) and allowed to stir at $23\text{ }^\circ\text{C}$ for 5 min. The mixture was transferred to a separatory funnel containing water (10 mL) and EtOAc (10 mL). The layers were separated and the aqueous layer was extracted with EtOAc (3 x 10 mL). The organic layers were combined, dried over MgSO_4 , filtered, and concentrated under reduced pressure to afford a yellow solid. The crude residue was purified by flash chromatography (16:1 Hexanes:Benzene) to afford *N*-Me-carbazole silyl triflate **2.30** (156 mg, 77% yield) as a white solid. *N*-Me-carbazole silyl triflate **2.30**: mp $128.2\text{--}130.3\text{ }^\circ\text{C}$; R_f 0.79 (9:1 Hexanes:EtOAc); ^1H NMR (600 MHz, CDCl_3): δ 8.18 (s, 1H), 8.11 (d, $J = 7.9$, 1H), 7.53–7.50 (m, 1H), 7.43 (d, $J = 8.3$, 1H), 7.38 (s, 1H), 7.30 (td, $J = 7.5$, 0.9, 1H), 3.85 (s, 3H), 0.44 (s, 9H); ^{13}C NMR (125 MHz, CDCl_3 ; 14 of 15 signals observed): δ 153.5, 142.1, 141.9, 127.4, 126.4, 122.1, 121.9, 121.0, 120.4, 119.9, 108.8, 100.0, 29.3, -0.4 ; IR (film): 3017, 2955, 1739, 1596, 1414, 1206 cm^{-1} ; HRMS-APCI (m/z) $[\text{M} + \text{H}]^+$ calcd for $\text{C}_{17}\text{H}_{19}\text{F}_3\text{NO}_3\text{SSi}^+$, 402.0802; found 402.0690.



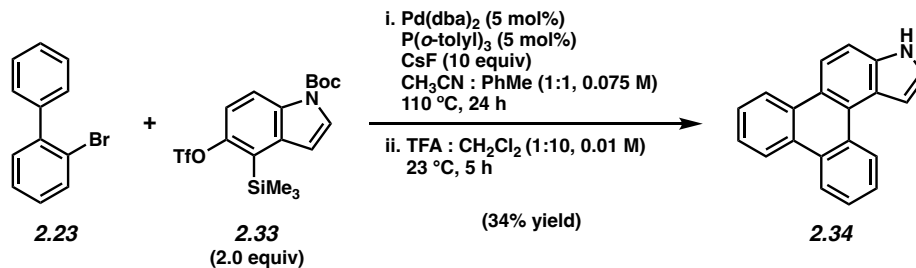
***N*-Boc-Carbazole Silyl Triflate 2.31.** To a 50 mL round bottom flask was added carbazole silyl triflate **2.29** (1.00 g, 2.58 mmol, 1.0 equiv), THF (13 mL, 0.2 M), 4-dimethylaminopyridine (63 mg, 0.51 mmol, 0.2 equiv), and di-*tert*-butyl dicarbonate (839 mg, 3.84 mmol, 1.5 equiv). The resulting mixture was purged with nitrogen for 3 minutes, then allowed to stir under positive nitrogen pressure at 23 °C for 2 h. The mixture was then quenched with deionized water (10 mL). The solution was transferred to a separatory funnel and the layers were separated. The aqueous layer was subsequently extracted with CH₂Cl₂ (3 x 10 mL). The organic layers were combined, dried over Na₂SO₄, filtered, and concentrated under reduced pressure to afford a crude, yellow solid. The crude material was purified by flash chromatography (100:1 Hexanes:EtOAc) to yield *N*-Boc-carbazole silyl triflate **2.31** (1.17 g, 93% yield) as a white solid. *N*-Boc-carbazole silyl triflate **2.31**: mp: 170.5–172.3 °C; *R_f* 0.57 (9:1 Hexanes:EtOAc); ¹H NMR (600 MHz, CDCl₃): δ 8.36 (d, *J* = 8.6, 1H), 8.35 (s, 1H), 8.08 (s, 1H), 8.00 (d, *J* = 7.9, 1H), 7.51 (td, *J* = 7.6, 1.0, 1H), 7.39 (td, *J* = 7.5, 1.0, 1H), 1.76 (s, 9H), 0.44 (s, 9H); ¹³C NMR (125 MHz, CDCl₃; 16 of 17 signals observed): δ 153.9, 150.6, 139.6, 127.8, 126.6, 126.4, 124.9, 124.5, 123.6, 119.9, 119.8, 116.5, 108.3, 85.1, 28.4, –0.5; IR (film): 2983, 1728, 1393, 1355, 1212, 1155, 1140 cm⁻¹; HRMS-APCI (*m/z*) [M + H]⁺ calcd for C₂₁H₂₅F₃NO₅SSi⁺, 488.1169; found 488.1198.

2.5.2.3 Annulation of *N*-Me-Carbazolyne



Carbazole 2.32. Followed representative procedure A. Purification by flash chromatography (100% Hexanes → 1:1 Hexanes:Benzenes) afforded carbazole **2.32** (86% yield) as an off-white solid. Carbazole **2.32**: mp >200 °C; *R_f* 0.74 (4:1 Hexanes:EtOAc); ¹H NMR (400 MHz, CDCl₃): δ 9.38 (s, 1H), 8.86 (d, *J* = 8.2, 1H), 8.81 (d, *J* = 7.8, 1H), 8.68 (td, *J* = 8.6, 1.5, 2H), 8.54 (s, 1H), 8.31 (dt, *J* = 7.8, 0.9, 1H), 7.72–7.60 (m, 4H), 7.63 (td, *J* = 7.8, 1.1, 1H), 7.58 (td, *J* = 7.8, 1.1, 1H), 7.47 (d, *J* = 8.1, 1H), 7.33 (td, *J* = 7.4, 0.8, 1H), 4.03 (s, 3H); ¹³C NMR (100 MHz, CDCl₃; 27 of 28 signals observed): δ 142.9, 141.3, 131.1, 130.6, 130.0, 128.85, 128.78, 127.4, 127.1, 127.0, 126.8, 126.1, 123.9, 123.6, 123.5, 123.4, 123.1, 123.0, 122.9, 120.8, 119.2, 114.8, 108.5, 101.1, 29.3; IR (film): 3049, 2923, 2854, 1638, 1603, 1500, 1443, 1258, 754 cm⁻¹; HRMS-APCI (*m/z*) [M]⁺ calcd for C₂₅H₁₇N⁺, 331.13555; found 331.13609.

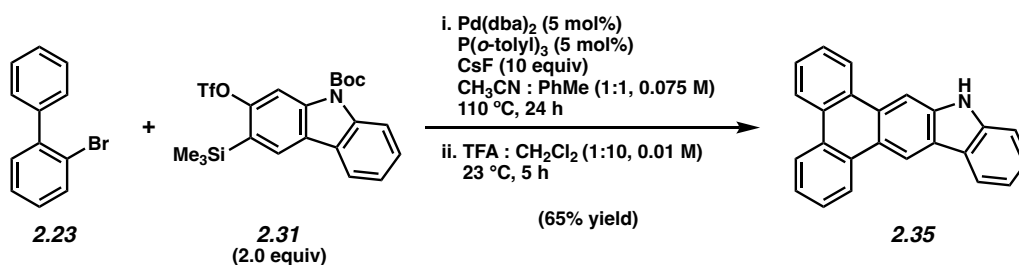
2.5.2.4 Synthesis of *N*-H Annulation Products for Metal Coordination



Indole 2.34. A 2-dram vial was charged with Pd(dba)₂ (7.0 mg, 0.012 mmol, 5 mol%). Next, toluene (1.5 mL), P(*o*-tolyl)₃ (3.7 mg, 0.012 mmol, 5 mol%), 2-bromobiphenyl (**2.23**) (56.4 mg, 0.242 mmol, 1.0 equiv), silyl triflate **2.33** (318 mg, 0.495 mmol, 2.0 equiv), and acetonitrile (1.5

mL) were added sequentially, followed by an oven-dried magnetic stirbar and then CsF (333 mg, 8.26 mmol, 10.0 equiv). The vial was purged with nitrogen for 3 minutes, then sealed with a Teflon-lined screw cap and stirred at 110 °C for 24 h. After allowing to cool to 23 °C, the mixture was transferred with CH₂Cl₂ (20 mL) and H₂O (10 mL) to a separatory funnel containing brine (15 mL). The layers were separated and the aqueous layer was extracted with CH₂Cl₂ (3 x 30 mL). The combined organic layers were dried over Na₂SO₄, filtered, and concentrated under reduced pressure to afford a brown residue that was carried forward without further purification.

The crude material was dissolved in 10:1 CH₂Cl₂:TFA (24.2 mL, 0.01 M) and stirred at 23 °C for 5 h. The reaction was then slowly transferred to a separatory funnel containing sat. aq. sodium bicarbonate (30 mL). The mixture was further diluted with CH₂Cl₂ (10 mL) and the layers were separated. The organic phase was dried over Na₂SO₄ and filtered. To the filtrate was added silica (500 mg). The resulting mixture was dried under reduced pressure until a free-flowing solid was obtained. The crude material purified by flash chromatography (2:3 CH₂Cl₂:Hexanes → 3:1 CH₂Cl₂:Hexanes) to afford indole **2.34** (22.0 mg, 34% yield) as a yellow solid. Indole **2.34**. mp: >200 °C; R_f 0.22 (2:3 CH₂Cl₂:Hexanes); ¹H NMR (600 MHz, DMSO-d₆): δ 9.23 (dd, *J* = 8.6, 1.4, 1H), 8.77 (dd, *J* = 8.3, 1.7, 1H), 8.74–8.79 (m, 2H), 8.55 (d, *J* = 8.9, 1H), 8.50 (s, 1H), 7.76–7.60 (m, 6H), 7.41 (t, *J* = 3.6, 2.8, 1H); ¹³C NMR (100 MHz, CDCl₃): δ 135.5, 131.1, 131.0, 130.3, 128.9, 127.1, 127.0, 126.7, 126.3, 125.9, 124.5, 124.4, 124.1, 123.5, 123.19, 123.18, 123.13, 118.1, 112.3, 105.6; IR (film): 3416, 3026, 3073, 2956, 1725, 1350 cm⁻¹; HRMS-APCI (*m/z*) [M + H]⁺ calcd for C₂₀H₁₄N⁺, 268.1121; found 267.6527.

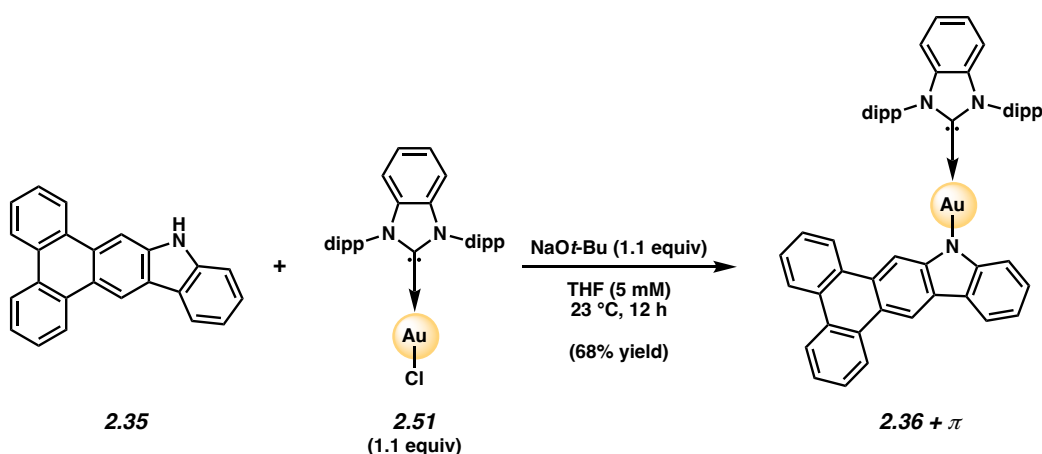


Carbazole 2.35. A 2-dram vial was charged with Pd(dba)₂ (7.1 mg, 0.012 mmol, 5 mol%). Next, toluene (1.3 mL), P(*o*-tolyl)₃ (3.8 mg, 0.012 mmol, 5 mol%), 2-bromobiphenyl (**2.23**) (58.0 mg, 0.248 mmol, 1.0 equiv), silyl triflate **2.31** (241 mg, 0.495 mmol, 2.0 equiv), and acetonitrile (1.6 mL) were added, followed by an oven-dried magnetic stirbar and then CsF (376 mg, 2.48 mmol, 10 equiv). The vial was purged with nitrogen for 3 minutes, then sealed with a Teflon-lined screw cap and stirred at 110 °C for 24 h. After allowing to cool to 23 °C, the mixture was transferred with CH₂Cl₂ (20 mL) and H₂O (10 mL) to a separatory funnel containing brine (15 mL). The layers were separated and the aqueous layer was extracted with CH₂Cl₂ (3 x 30 mL). The combined organic layers were dried over Na₂SO₄, filtered, and concentrated under reduced pressure to afford a brown residue that was carried forward without further purification.

The crude material was dissolved in 10:1 CH₂Cl₂:TFA (24.2 mL, 0.01 M) and stirred at 23 °C for 5 h. The reaction was then slowly transferred to a separatory funnel containing sat. aq. sodium bicarbonate (30 mL). The mixture was further diluted with CH₂Cl₂ (10 mL) and the layers were separated. The organic phase was dried over Na₂SO₄ and filtered. To the filtrate was added silica (500 mg). The resulting mixture was dried under reduced pressure until a free-flowing solid was obtained. The crude material purified by flash chromatography (100% Hexanes → 9:1 Hexanes:EtOAc → 1:1 Hexanes:Benzene) to yield carbazole **2.35** (51 mg, 65% yield) as an off-white solid. Carbazole **2.35**. mp >200 °C; R_f 0.63 (4:1 Hexanes:EtOAc); ¹H NMR (600 MHz, CDCl₃): δ 11.35 (s, 1H), 9.62 (s, 1H), 9.0 (d, *J* = 8.0, 1H), 8.82 (d, *J* = 8.3, 1H), 8.76 (dd, *J* = 12.5,

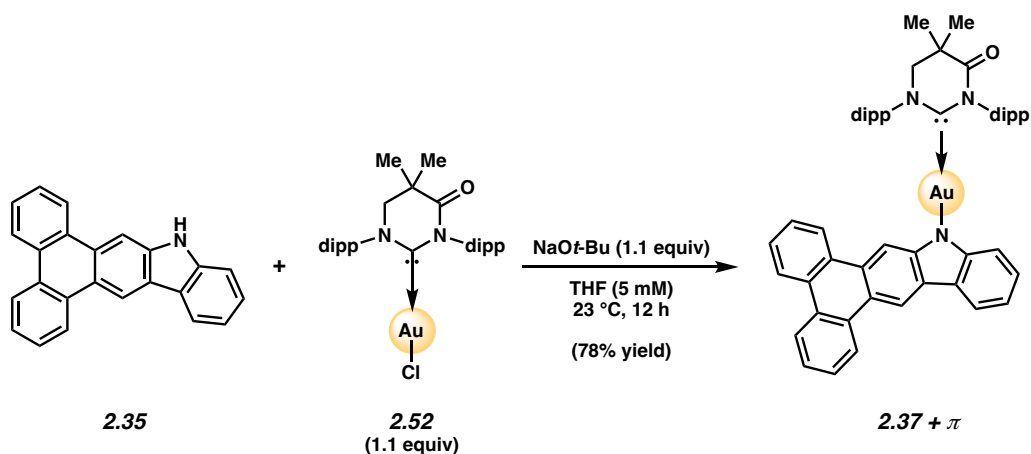
8.3, 2H), 8.72 (s, 1H), 8.43 (d, $J = 7.5$, 1H), 7.73–7.69 (m, 2H), 7.67 (t, $J = 6.9$, 1H), 7.62 (t, $J = 7.5$, 1H), 7.55 (d, $J = 8.0$, 1H), 7.46 (t, $J = 7.5$, 1H), 7.24 (t, $J = 7.5$, 1H); ^{13}C NMR (100 MHz, CDCl_3 ; 22 of 24 signals observed): δ 141.3, 139.8, 131.0, 130.3, 129.9, 129.0, 128.8, 127.3, 127.1, 127.0, 126.9, 126.2, 124.4, 123.5, 123.43, 123.36, 123.0, 120.8, 119.8, 114.8, 110.6, 103.4; IR (film): 3413, 2923, 2852, 1611, 1435, 751 cm^{-1} ; HRMS-APCI (m/z) $[\text{M} + \text{H}]^+$ calcd for $\text{C}_{24}\text{H}_{16}\text{N}^+$, 318.12773; found 318.12843.

2.5.2.5 Synthesis of Two-Coordinate Metal Complexes



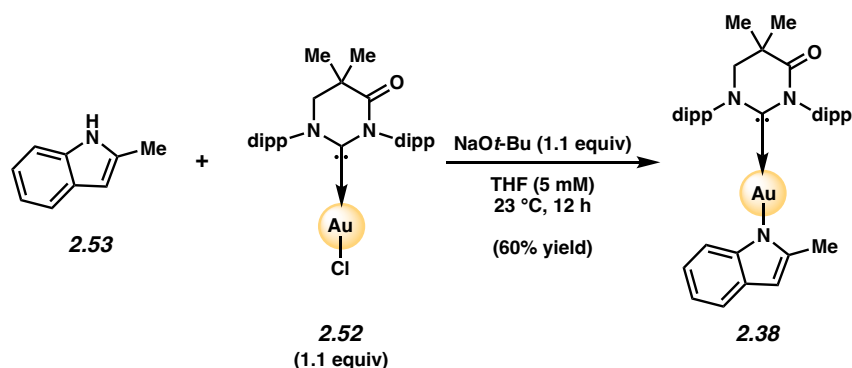
Representative Procedure B for metal coordination (Figure 2.7, complex **2.36 + π used as an example).** Sodium *tert*-butoxide (6.4 mg, 67 μmol , 1.1 equiv) was added to a solution of ligand **2.35** (20 mg, 63 μmol , 1.0 equiv) in THF (10 mL). **2.51** (44.4 mg, 66.2 μmol , 1.1 equiv) was added to the reaction flask in one portion and the mixture was left stirring under inert gas at 23 °C for 12 hours. The solution was filtered through a plug of celite (2 cm in a 15 mL fritted funnel), washed with THF (10 mL), and the volatiles were removed under reduced pressure. The resulting product was recrystallized from CH_2Cl_2 and hexanes to afford an off-white precipitate (47 mg, 68% yield). Carbazole–Au–BZI **2.36 + π** : ^1H NMR (400 MHz, CDCl_3): δ 9.25 (s, 1H), 8.77 (dd, $J = 8.5$, 1.3, 1H), 8.60 (ddd, $J = 16.7$, 8.4, 1.4, 2H), 8.28 (dd, $J = 8.5$, 1.4, 1H), 8.17 (dd, $J = 7.6$, 1.0, 1H), 8.13

(s, 1H), 7.86 (t, $J = 7.8$, 2H), 7.72 (ddd, $J = 8.2, 6.9, 1.3$, 1H), 7.65–7.56 (m, 6H), 7.52–7.47 (m, 3H), 7.29–7.26 (m, 2H), 7.16 (ddd, $J = 8.2, 7.0, 1.3$, 1H), 7.01 (ddd, $J = 7.9, 7.0, 1.0$, 1H), 6.67 (dd, $J = 8.1, 0.9$, 1H), 2.60 (hept, $J = 6.9$, 4H), 1.40 (d, $J = 6.9$, 12H), 1.19 (d, $J = 6.8$, 12H). ^{13}C NMR (150 MHz, CDCl_3): δ 207.21, 206.89, 185.66, 151.68, 149.68, 147.17, 146.43, 134.96, 132.19, 131.63, 131.44, 131.04, 129.51, 128.02, 127.23, 126.88, 126.05, 125.74, 125.54, 125.33, 124.75, 124.64, 123.80, 123.73, 123.17, 123.07, 122.78, 120.55, 119.85, 116.11, 113.50, 111.90, 105.58, 30.89, 29.19, 24.64, 24.08. Anal. Calcd for $\text{C}_{55}\text{H}_{52}\text{AuN}_3$: C, 69.39; N, 4.41; H, 5.51. Found: C, 68.05; N, 4.27; H, 5.30. MALDI-TOF (m/z) $[\text{M}]^+$ calcd for $\text{C}_{55}\text{H}_{52}\text{AuN}_3^+$, 951.38; found, 951.22.

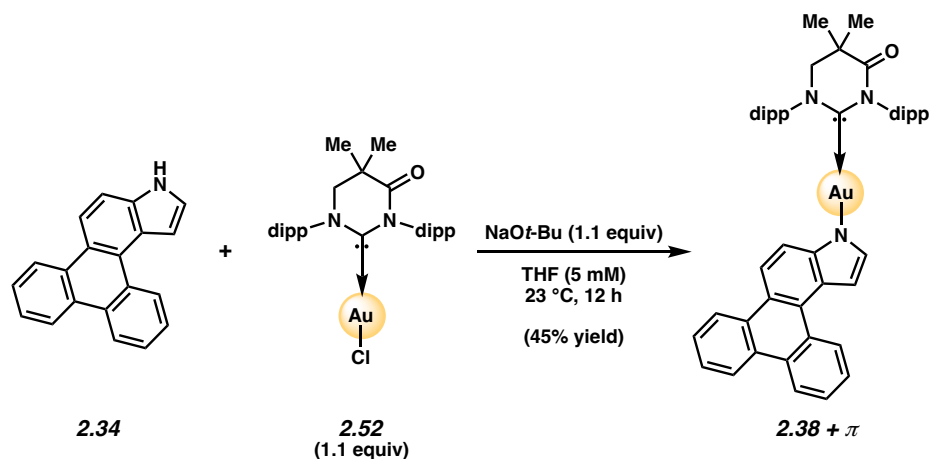


Annulated Carbazole–Au–MAC 2.37+ π . Representative procedure B was followed to yield **2.37+ π** (42 mg, 78% yield) as a yellow solid. Annulated Carbazole–Au–MAC **2.37+ π** : ^1H NMR (400 MHz, CDCl_3): δ 9.17 (s, 1H), 8.73 (d, $J = 7.8$ Hz, 1H), 8.57 (ddd, $J = 18.5, 8.3, 1.1$ Hz, 2H), 8.38 (d, $J = 8.1$ Hz, 1H), 8.08 (d, $J = 0.7$ Hz, 1H), 7.82 – 7.70 (m, 3H), 7.65 – 7.44 (m, 8H), 7.04 – 6.91 (m, 2H), 5.81 (d, $J = 7.6$ Hz, 1H), 3.86 (s, 2H), 3.36 (hept, $J = 6.5$ Hz, 2H), 3.08 (hept, $J = 6.8$ Hz, 2H), 1.56 (s, 6H), 1.45 – 1.33 (m, 18H), 1.26 (d, $J = 6.8$ Hz, 6H). ^{13}C NMR (100 MHz, CDCl_3): δ 204.87, 171.43, 151.72, 149.54, 146.05, 144.95, 140.12, 135.57, 132.07, 131.35, 130.60,

130.44, 129.45, 127.98, 127.33, 126.87, 125.86, 125.79, 125.65, 125.63, 124.82, 124.73, 124.54, 124.16, 123.54, 123.14, 123.02, 122.80, 120.63, 119.41, 116.24, 114.06, 113.35, 105.48, 77.19, 62.27, 37.95, 29.35, 28.98, 24.70, 24.61, 24.58, 24.13, 23.93. Anal. Calcd for $C_{54}H_{56}AuN_3O$: C, 67.56; N, 4.38; H, 5.88. Found: C, 67.41; N, 4.35; H, 5.93. MALDI-TOF (m/z) $[M]^+$ calcd for $C_{54}H_{56}AuN_3O^+$, 959.41; found, 959.16.



2-Methyl Indole–Au–MAC 2.38. Representative procedure B was followed to yield **2.38** (110 mg, 60% yield) as an off-white solid. 2-Methylindole–Au–MAC **2.38**: ^1H NMR (400 MHz, acetone- d_6): δ 7.64 (dt, $J = 17.7, 7.7$, 2H), 7.52 (d, $J = 7.8$, 2H), 7.46 (d, $J = 7.7$, 2H), 7.09 (dd, $J = 7.6, 1.2$, 1H), 6.62–6.53 (m, 1H), 6.49 (td, $J = 7.5, 1.3$, 1H), 5.84 (d, $J = 8.0$, 1H), 5.74 (d, $J = 1.0$, 1H), 4.25 (s, 2H), 3.50 (hept, $J = 6.8$, 2H), 3.24 (hept, $J = 6.8$, 2H), 1.69 (s, 6H), 1.48–1.43 (m, 8H), 1.42 (d, $J = 3.2$, 7H), 1.40 (d, $J = 6.8$, 6H), 1.25 (d, $J = 6.8$, 6H). ^{13}C NMR (100 MHz, acetone- d_6): δ 205.18, 171.91, 146.16, 145.94, 144.96, 144.43, 140.69, 136.56, 130.54, 130.07, 129.77, 125.29, 124.30, 117.03, 116.77, 116.13, 113.55, 98.29, 61.12, 37.98, 28.49, 23.94, 23.70, 23.65, 23.25, 15.60. Anal. Calcd for $C_{39}H_{50}AuN_3O$: C, 60.54; N, 5.43; H, 6.51. Found: C, 60.49; N, 5.32; H, 6.67. MALDI-TOF (m/z) $[M]^+$ calcd for $C_{39}H_{50}AuN_3O^+$, 773.36; found, 773.45.



Annulated Indole–Au–MAC 2.38+ π . Representative procedure B was followed to yield **2.38** (120 mg, 45% yield) as an off-white solid. Annulated Indole–Au–MAC **2.38+ π** : ^1H NMR (400 MHz, acetone- d_6): δ 9.18–9.11 (m, 1H), 8.77–8.62 (m, 3H), 8.05 (d, $J = 9.1$ Hz, 1H), 7.72 (dt, $J = 20.8, 7.8$ Hz, 2H), 7.65–7.45 (m, 8H), 7.16–7.10 (m, 1H), 6.52 (d, $J = 2.8$ Hz, 1H), 6.49 (dd, $J = 8.9, 1.0$ Hz, 1H), 4.29 (s, 2H), 3.48 (h, $J = 6.8$ Hz, 2H), 3.24 (hept, $J = 6.8$ Hz, 2H), 1.68 (s, 6H), 1.50–1.31 (m, 18H), 1.22 (d, $J = 6.8$ Hz, 6H). ^{13}C NMR (150 MHz, acetone- d_6): δ 205.19, 203.69, 171.81, 146.27, 145.07, 145.00, 140.59, 136.57, 135.92, 132.09, 131.87, 130.31, 129.95, 129.45, 128.12, 126.78, 126.61, 126.17, 125.36, 125.10, 124.71, 124.37, 124.18, 124.05, 123.32, 123.20, 122.94, 122.74, 122.49, 117.26, 113.45, 103.02, 60.96, 38.13, 28.85, 28.35, 24.04, 23.97, 23.92, 23.86, 23.79, 23.72, 23.53, 23.21, 23.07. Anal. Calcd for $\text{C}_{50}\text{H}_{54}\text{AuN}_3\text{O}$: C, 66.00; N, 4.62; H, 5.98. Found: C, 65.50; N, 4.49; H, 6.09. MALDI-TOF (m/z) $[\text{M}]^+$ calcd for $\text{C}_{50}\text{H}_{54}\text{AuN}_3\text{O}^+$, 909.39; found, 909.27.

2.5.2.6 General Procedure for Photophysical Property Analyses

General Procedure for 1% Polystyrene Films. A mixture of polystyrene pellets (99 mg) and toluene (2 mL) was sonicated for 1 h, until all pellets are dissolved. Two-coordinate metal complex (1 mg) was dissolved in the solution. Using a pipet, ~ 0.5 mL of the solution was drop-casted onto

a glass substrate (2 cm x 2 cm) to achieve an even surface. The film was left to air-dry for 30 min and then placed in the vacuum chamber for further drying overnight. The resulting film was used to acquire the photophysical data.

2.5.2.7 Absorption Spectra of Donor Ligands

The extinction coefficient for the donor ligands was measured in 2-MeTHF. The molar absorptivity values for the donor ligands are comparable in magnitude to the molar absorptivity values for the transitions localized on the donor ligands in the metal complexes.

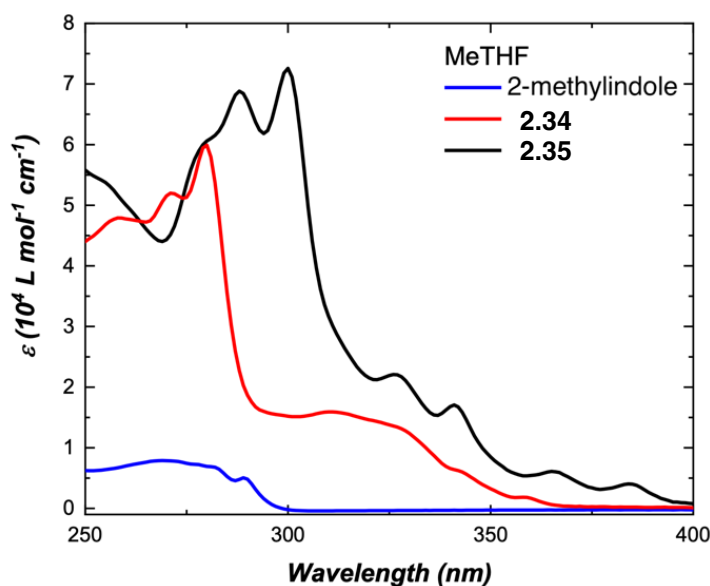


Figure 2.10. Extinction coefficients for the donor ligands in 2-MeTHF.

2.5.2.8 Emission Spectra of Deprotonated Donor Ligands

A few milligrams of donor ligand (1–3 mg) were dissolved in THF (10 mL). The solution was cooled in an ice bath. Once completely dissolved, a solution containing 1.2 equivalents of *n*-BuLi diluted in THF was added. Although a color change was immediately observable, the reaction was

allowed to stir for 1 h. The solvent was then evaporated under reduced pressure, and the solid obtained was dissolved in 2-MeTHF.

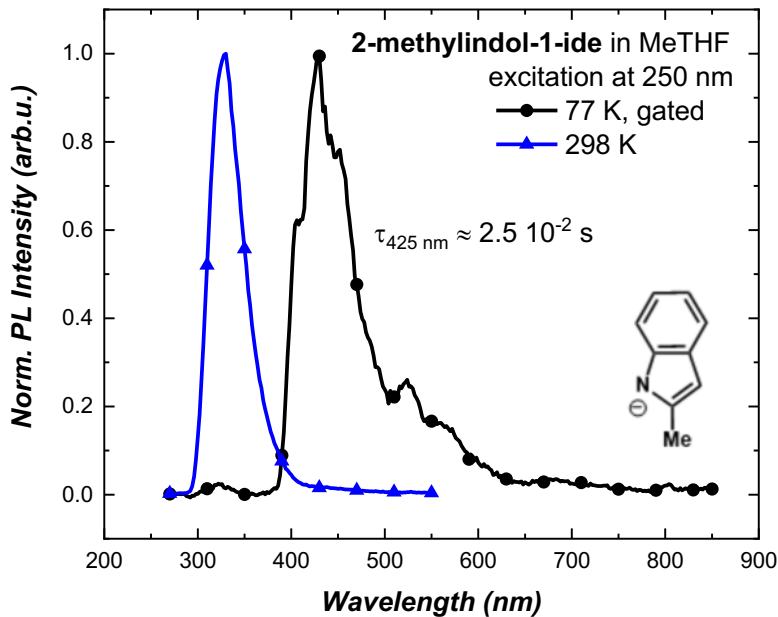


Figure 2.11. Emission spectra of 2-methylindol-1-ide in 2-MeTHF.

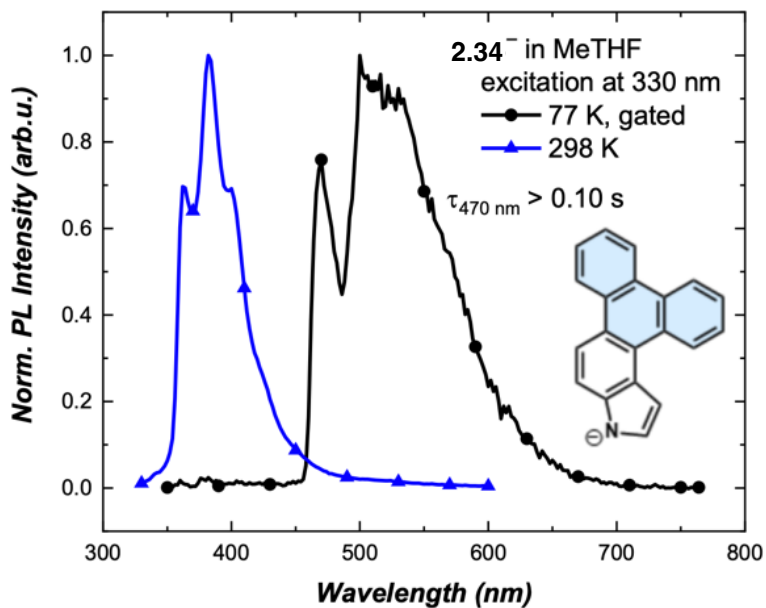


Figure 2.12. Emission spectra of ligand 2.34⁻ in 2-MeTHF.

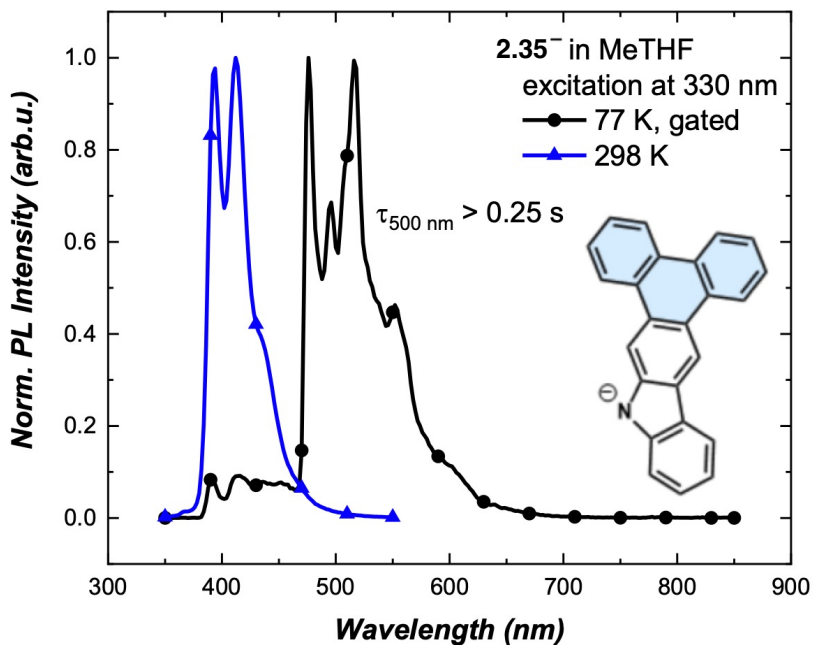


Figure 2.13. Emission spectra of ligand **2.35⁻** in 2-MeTHF.

2.6 Computational Methods

2.6.1 Complete Citation of Q-Chem 5.1

Density functional theory (DFT) calculations were executed using Q-Chem 5.1 program⁵⁷ at the B3LYP/6-31G** level for ground state geometry optimization of the organic ligands and at the B3LYP/LACVP level for the metal complexes. Time-dependent density functional theory (TD-DFT) calculations were performed on the ground state optimized geometries at the CAM-B3LYP/LACVP** level for a balanced description of both charge-transfer and locally excited (LE) states (Table 2.3).

2.6.2 Calculated Frontier Molecular Orbital Energies

Table 2.3. Calculated frontier molecular orbital, singlet (S₁), and triplet (T₁) energies.

CT = Charge Transfer state, LE = Locally Excited state.

	HOMO (eV)	LUMO (eV)	$\Delta E_{\text{HOMO-LUMO}}$ (eV)	S ₁ (eV)	Nature of S ₁ transition	T ₁ (eV)	Nature of T ₁ transition
2-methylindole	-5.28	0.00	5.28	5.21	-	3.16	-
2.34	-5.28	-0.90	4.38	4.24	-	2.55	-
carbazole	-5.47	-0.65	4.82	4.58	-	3.09	-
2.35	-5.28	-1.20	4.08	4.04	-	2.53	-
2.36	-4.22	-1.44	2.78	3.50	CT	3.07	LE
2.36+π	-4.27	-1.52	2.75	3.46	CT	2.48	LE
2.37	-4.30	-1.96	2.34	3.10	CT	2.85	CT
2.37+π	-4.35	-2.07	2.29	3.07	CT	2.48	LE
2.38	-4.16	-1.96	2.20	3.11	CT	2.87	CT
2.38+π	-4.38	-2.10	2.29	3.27	CT	2.51	LE

2.7 Photoluminescence (PL) Decay Lifetime Data

2.7.1 Lifetime Plots

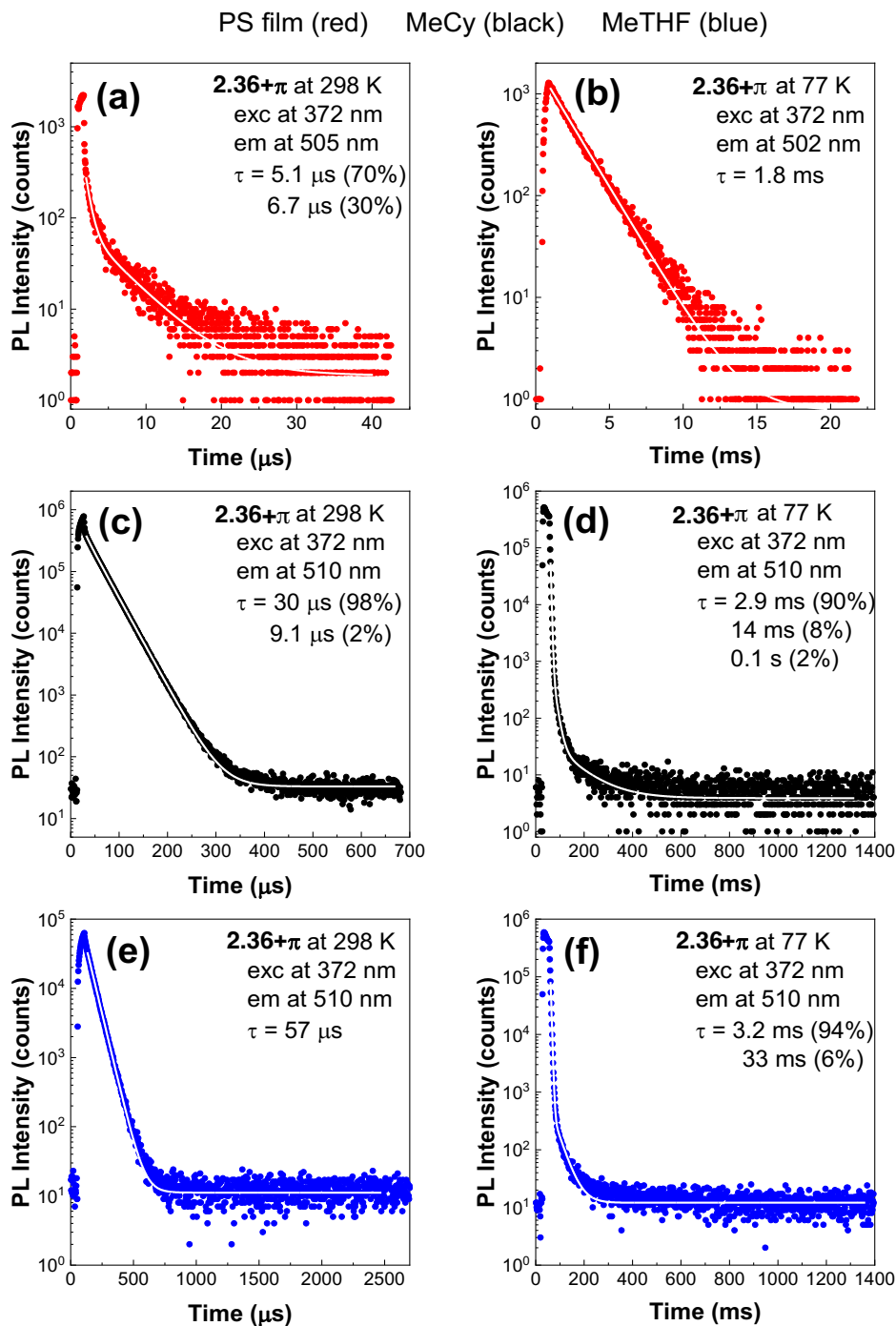


Figure 2.14. Emission lifetime decay for $2.36+\pi$ in (a-b) PS film, (c-d) MeCy, and (e-f) MeTHF at 298 K (left side) and 77 K (right side).

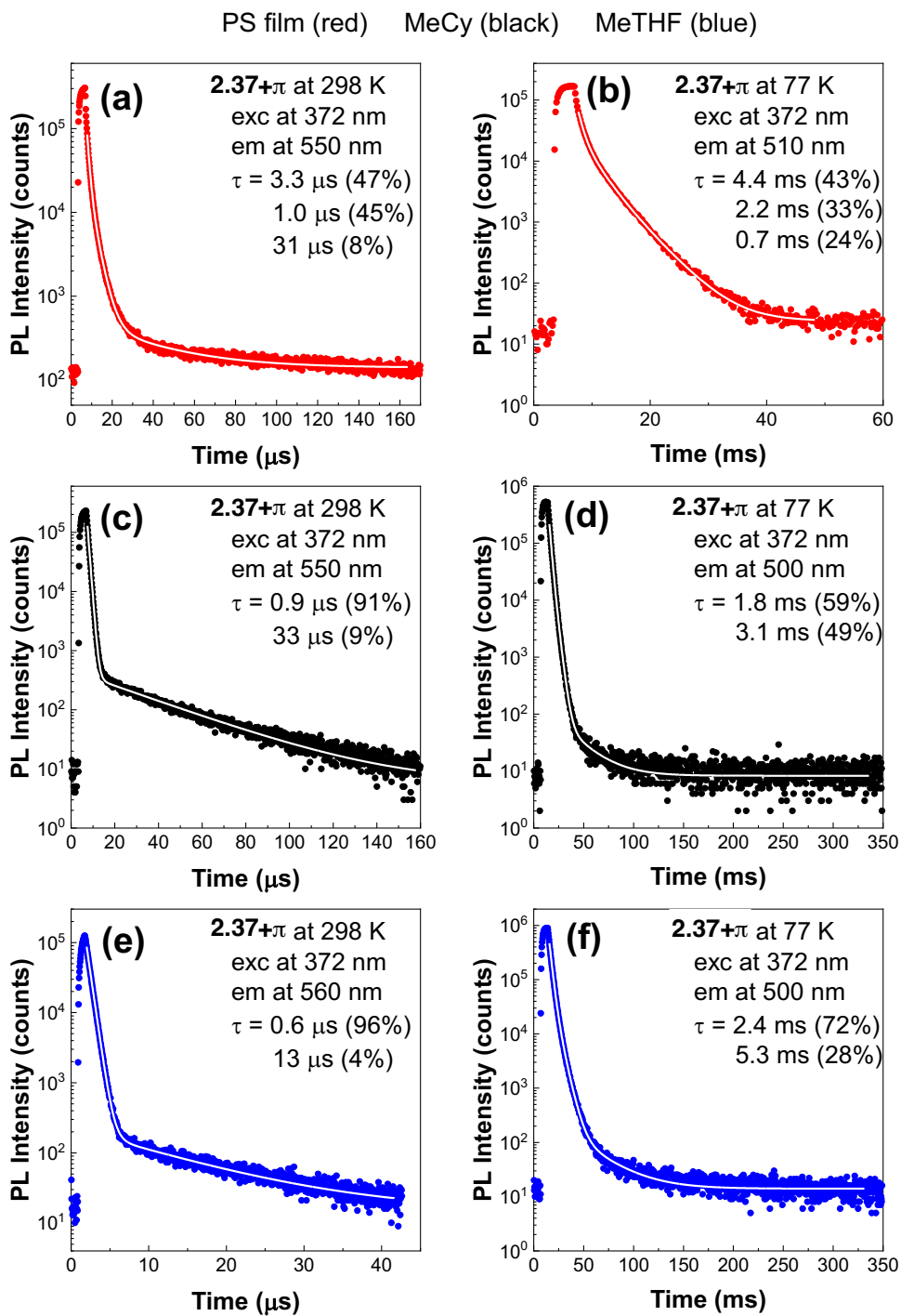


Figure 2.15. Emission lifetime decay for $2.37+\pi$ in (a-b) PS film, (c-d) MeCy, and (e-f) MeTHF at 298 K (left side) and 77 K (right side).

2.38

PS film (red) MeCy (black) MeTHF (blue)

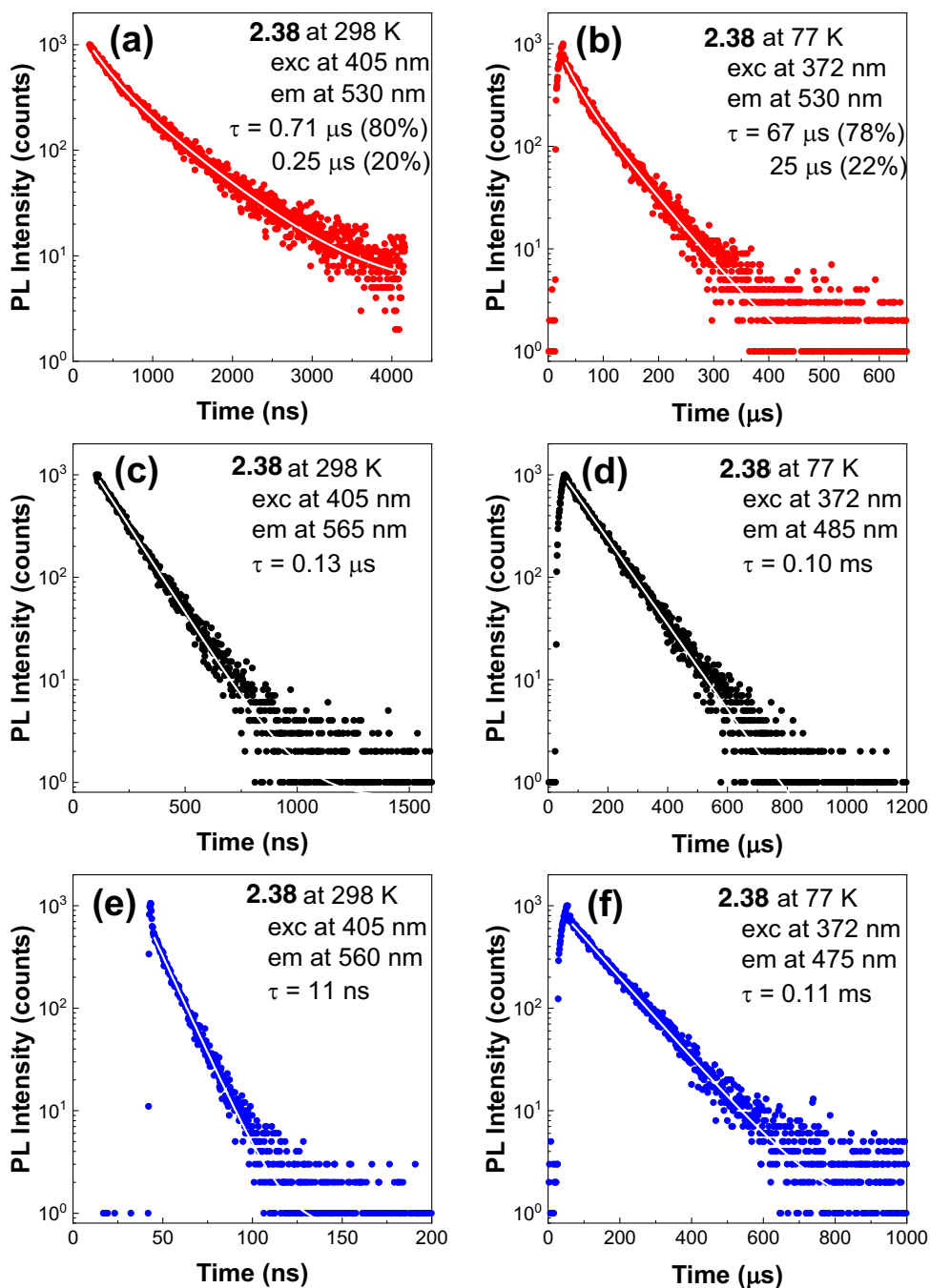


Figure 2.16. Emission lifetime decay for **2.38** in (a-b) PS film, (c-d) MeCy, and (e-f) MeTHF at 298 K (left side) and 77 K (right side).

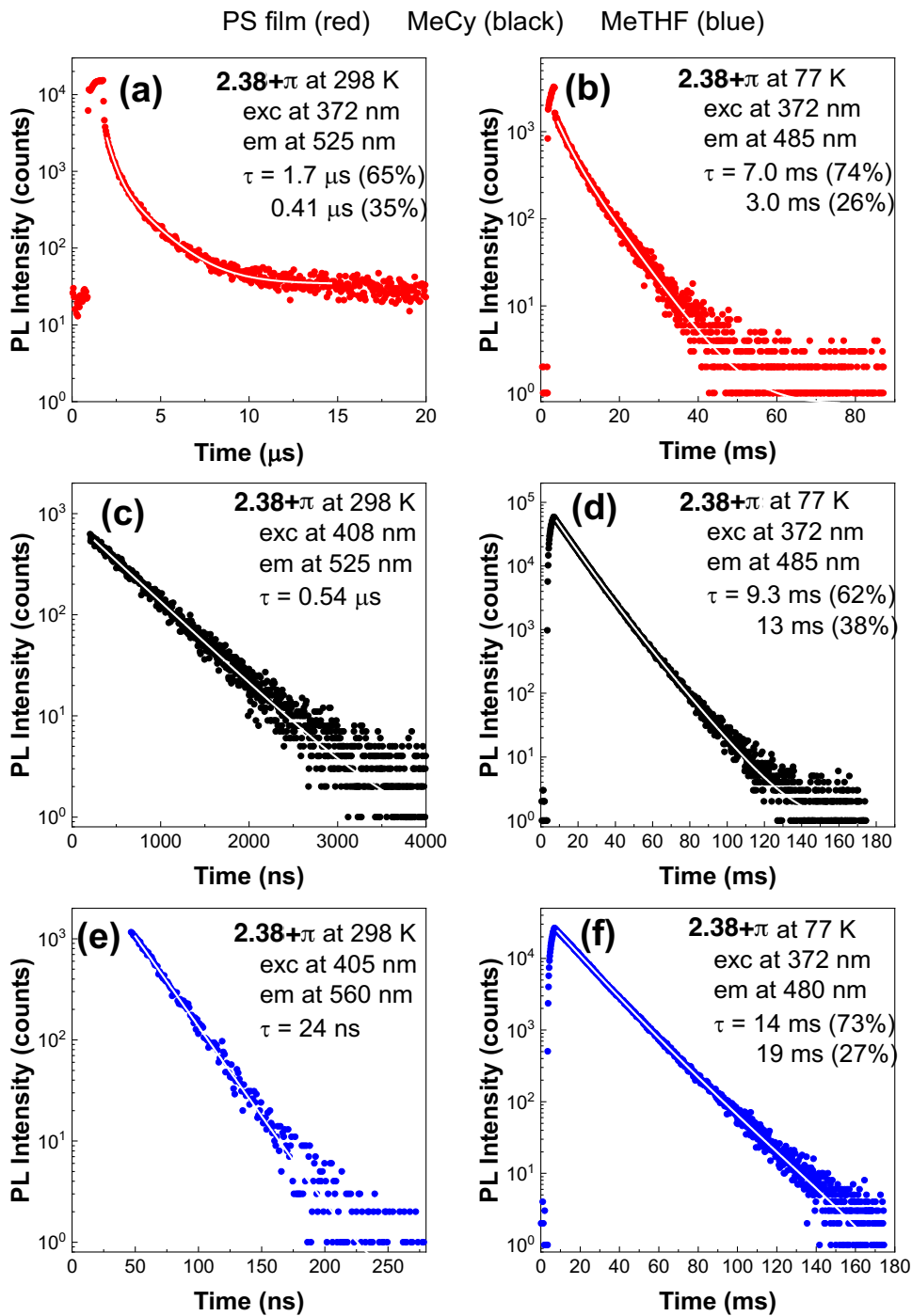


Figure 2.17. Emission lifetime decay for $2.38+\pi$ in (a-b) PS film, (c-d) MeCy, and (e-f) MeTHF at 298 K (left side) and 77 K (right side). In $2.37+\pi$, in both MeCy and MeTHF at 298 K a

biexponential decay is observed. The slow lifetime is in the range of tens of microseconds. It is assigned to p-type delayed fluorescence caused by a bimolecular triplet-triplet annihilation.

2.8 Spectra Relevant to Chapter Two:

π -Extension of Heterocycles via a Pd-Catalyzed Heterocyclic Aryne Annulation: π - Extended Donors for TADF Emitters

Katie A. Spence,[†] Jason V. Chari,[†] Mattia Di Niro, Robert B. Susick, Narcisse Ukwitegetse,
Peter I. Djurovich, Mark E. Thompson, and Neil K. Garg.

Chem. Sci. **2022**, *13*, 5884–5892.

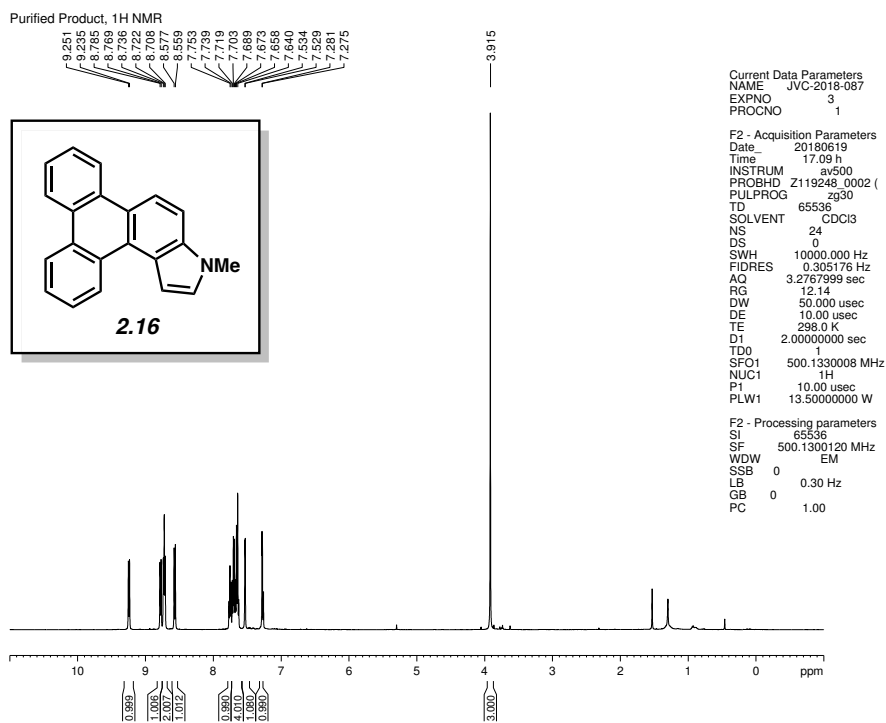


Figure 2.18 ¹H NMR (500 MHz, CDCl₃) of compound **2.16**.

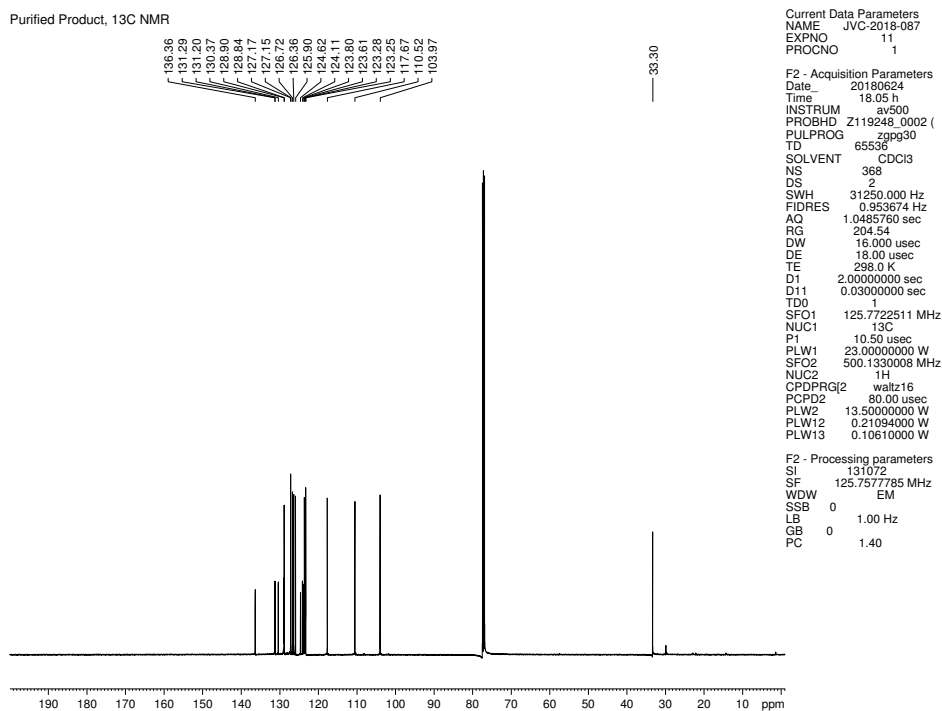


Figure 2.19 ¹³C NMR (125 MHz, CDCl₃) of compound **2.16**.

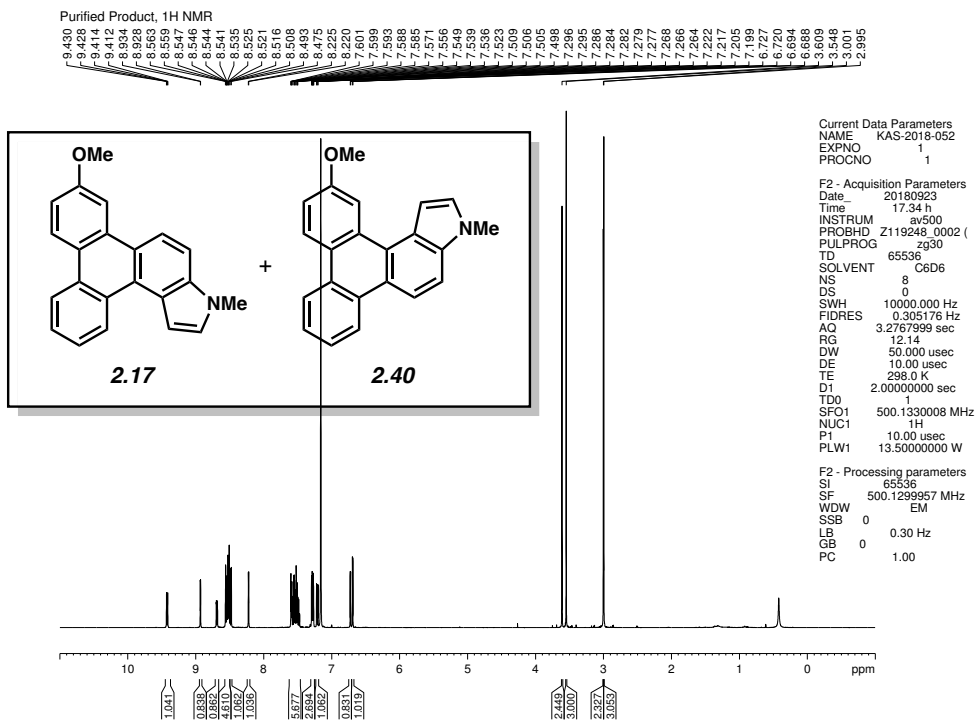


Figure 2.20 ¹H NMR (500 MHz, C₆D₆) of compounds **2.17** and **2.40**.

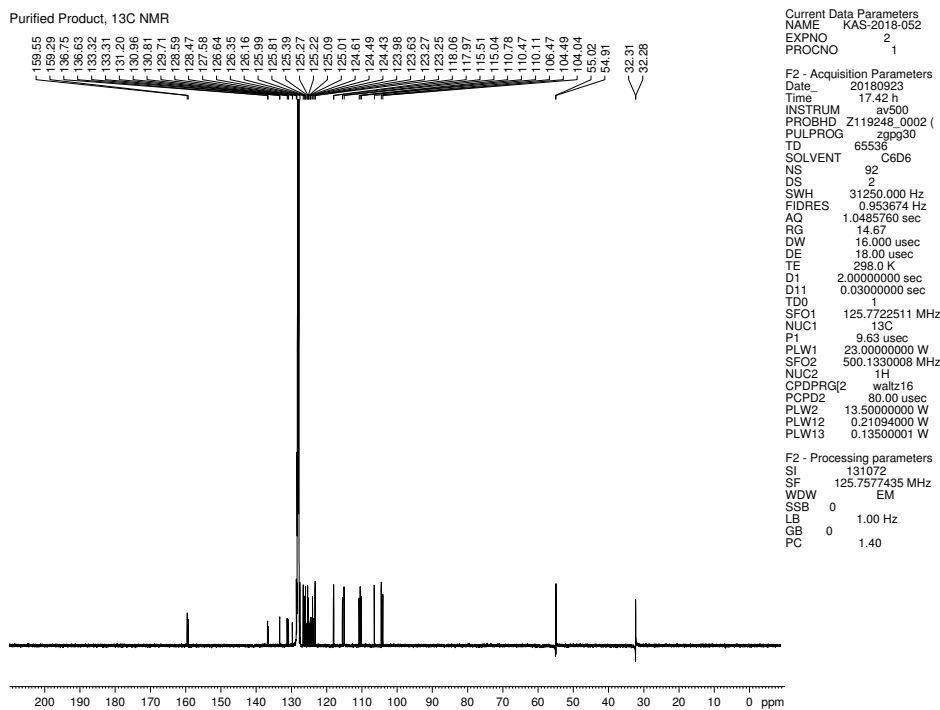


Figure 2.21 ¹³C NMR (125 MHz, C₆D₆) of compounds **2.17** and **2.40**.

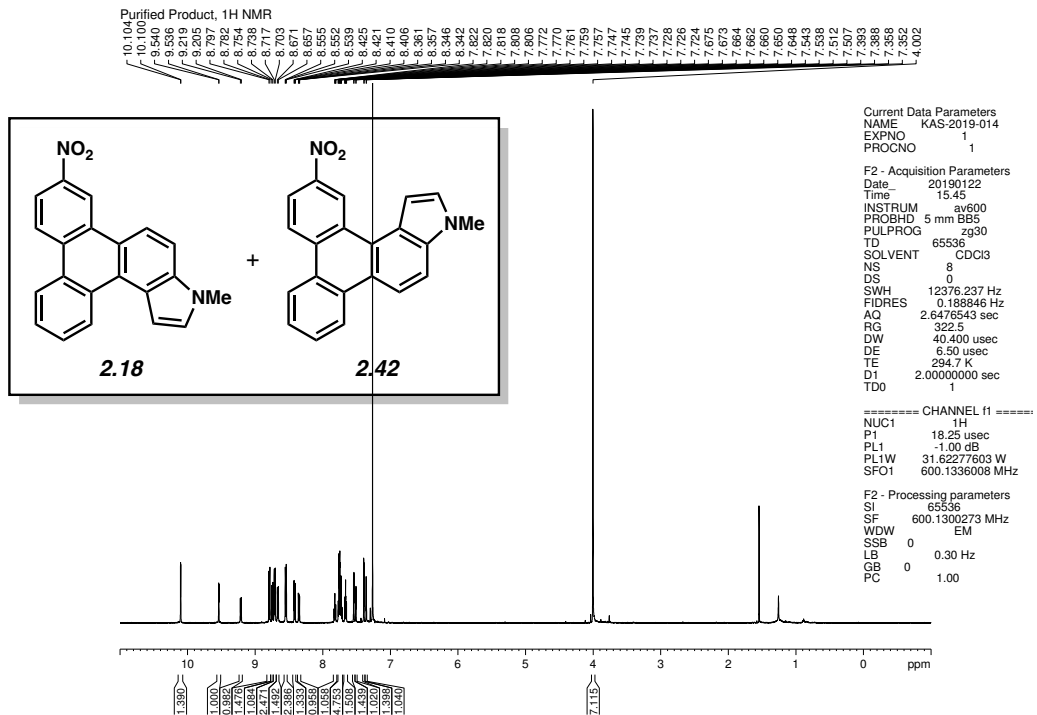


Figure 2.22 ¹H NMR (600 MHz, CDCl₃) of compounds **2.18** and **2.42**.

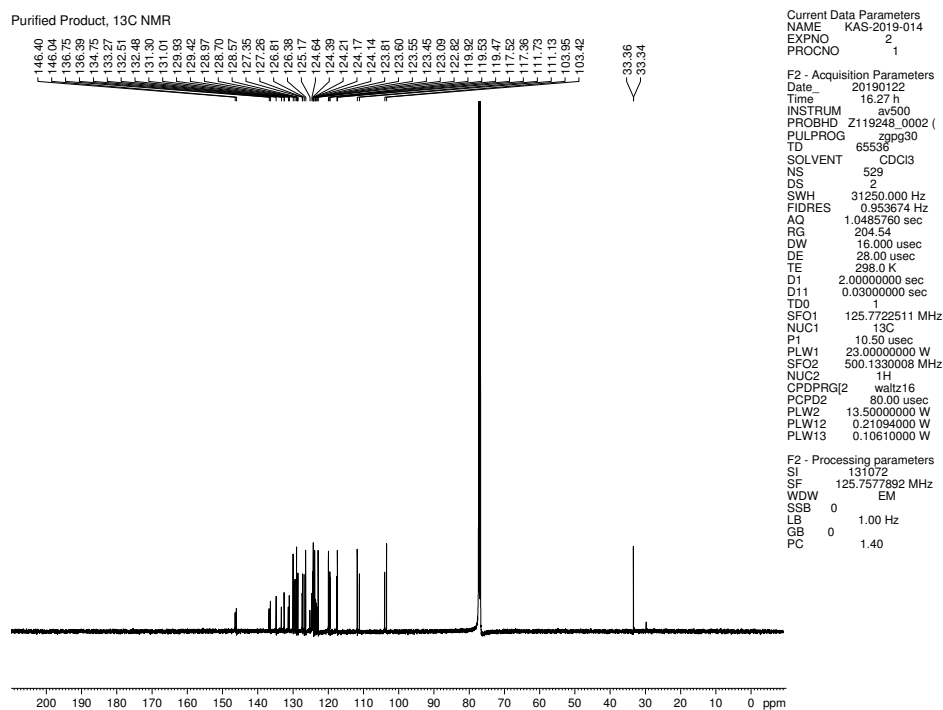


Figure 2.23 ¹³C NMR (125 MHz, CDCl₃) of compounds **2.18** and **2.42**.

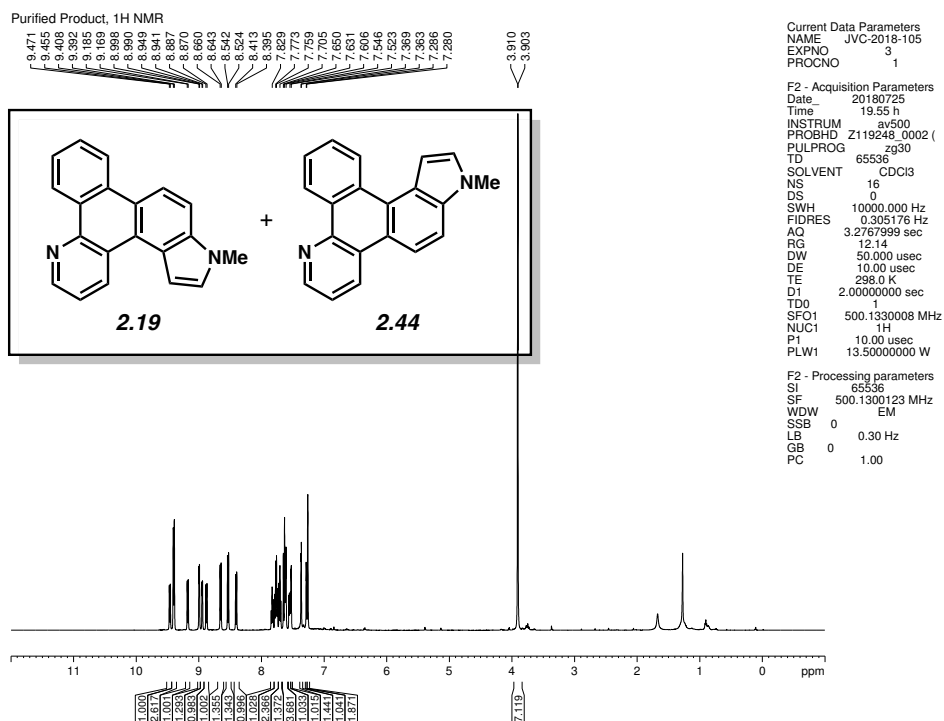


Figure 2.24 ¹H NMR (500 MHz, CDCl₃) of compounds **2.19** and **2.44**.

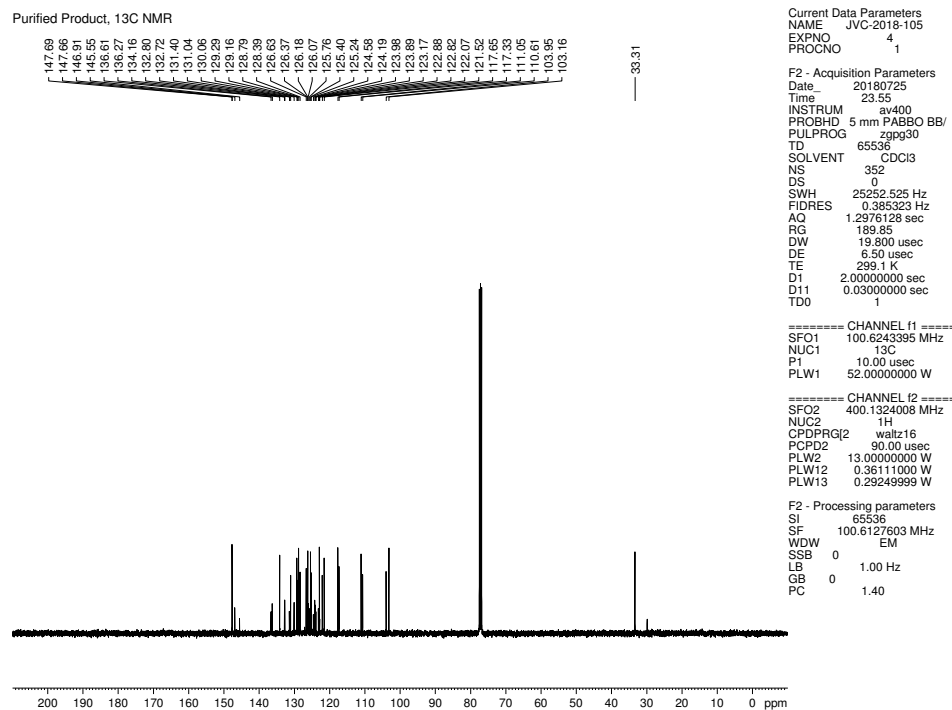


Figure 2.25 ¹³C NMR (100 MHz, CDCl₃) of compounds **2.19** and **2.44**.

NOESY

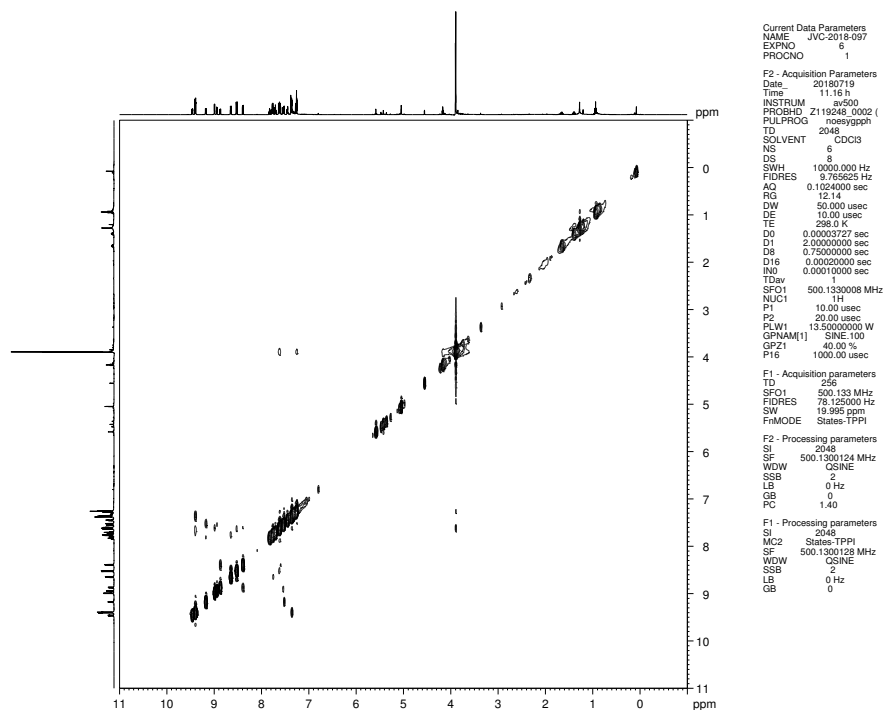
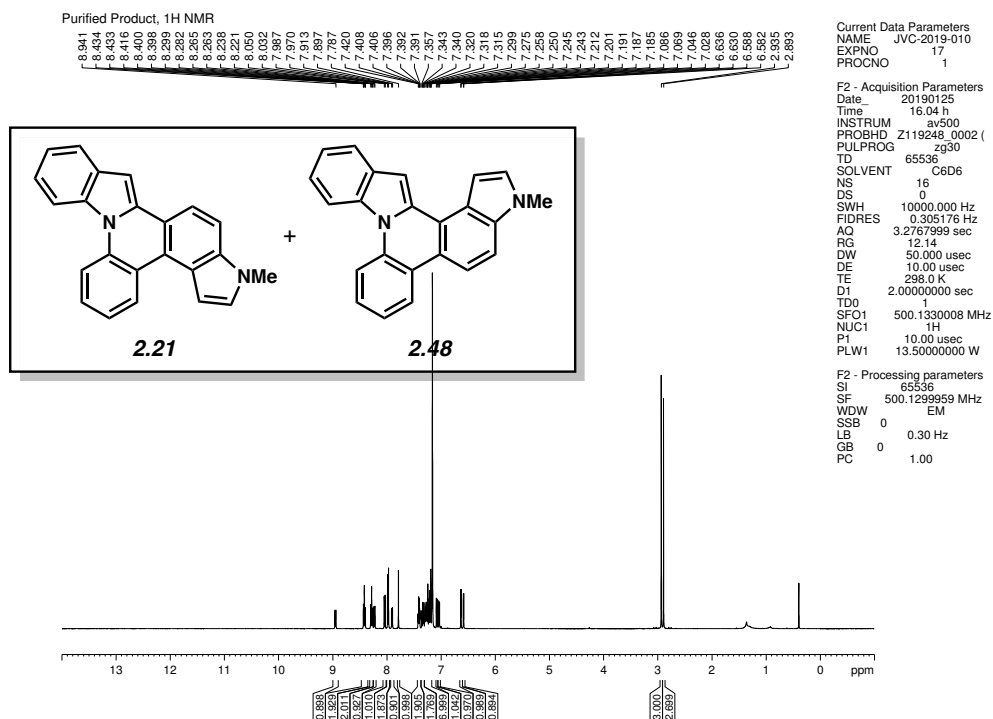


Figure 2.26 NOESY NMR (500 MHz, CDCl₃) of compounds **2.19** and **2.44**.



NOESY

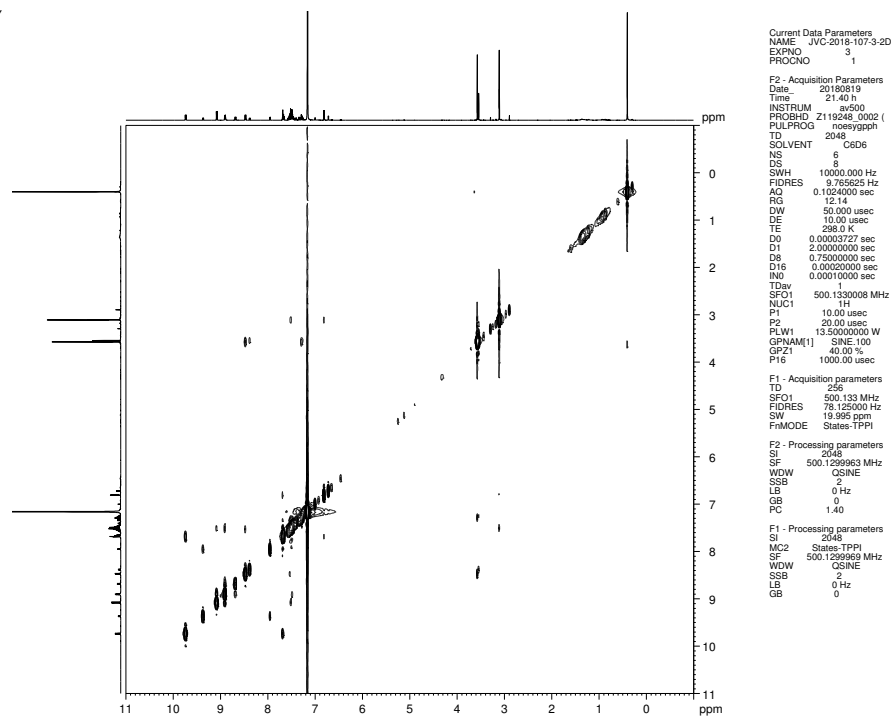


Figure 2.33 NOESY NMR (125 MHz, C₆D₆) of compounds **2.22** and **2.50**.

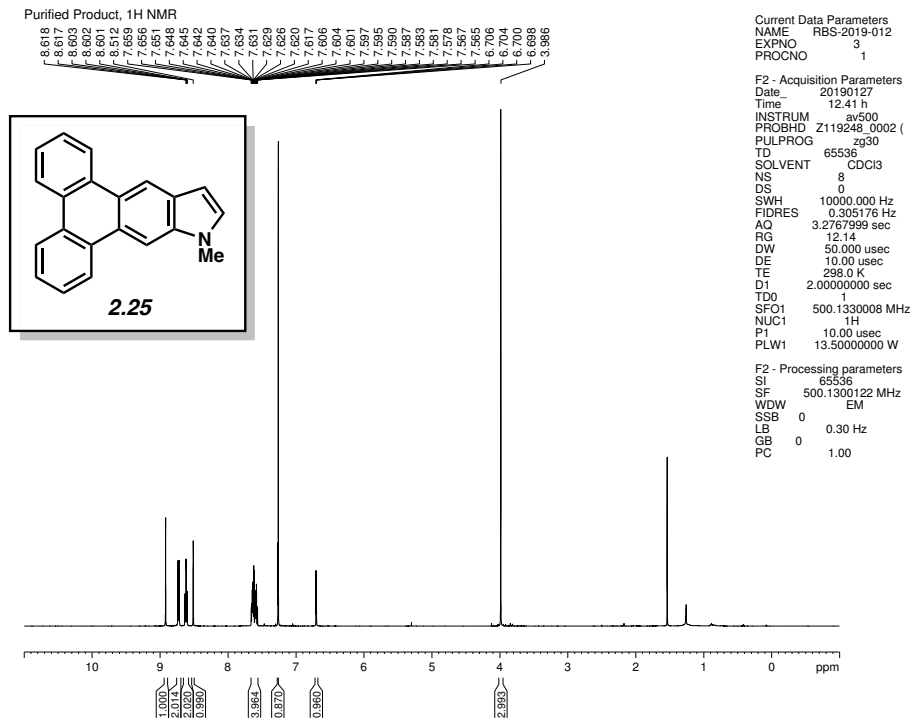


Figure 2.34 ¹H NMR (500 MHz, CDCl₃) of compound 2.25.

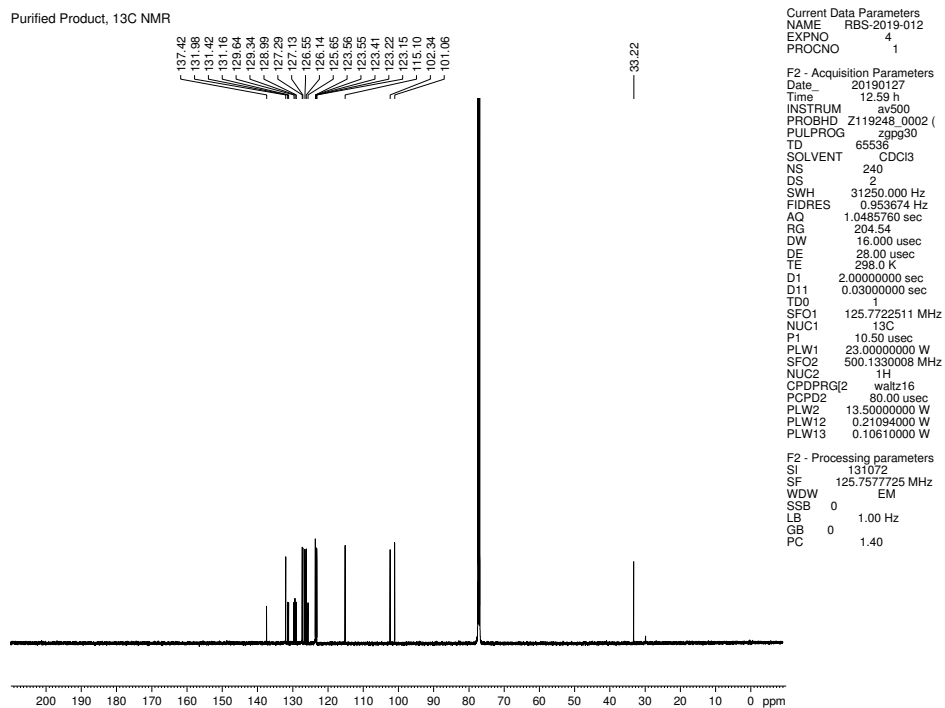


Figure 2.35 ¹³C NMR (125 MHz, CDCl₃) of compound 2.25.

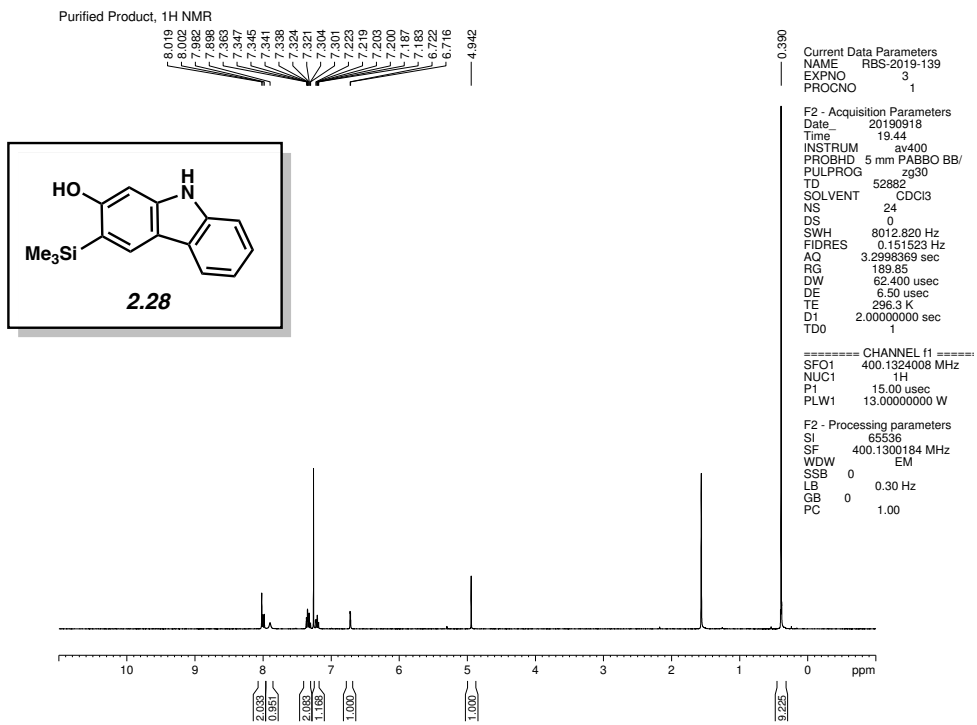


Figure 2.36 ¹H NMR (400 MHz, CDCl₃) of compound **2.28**.

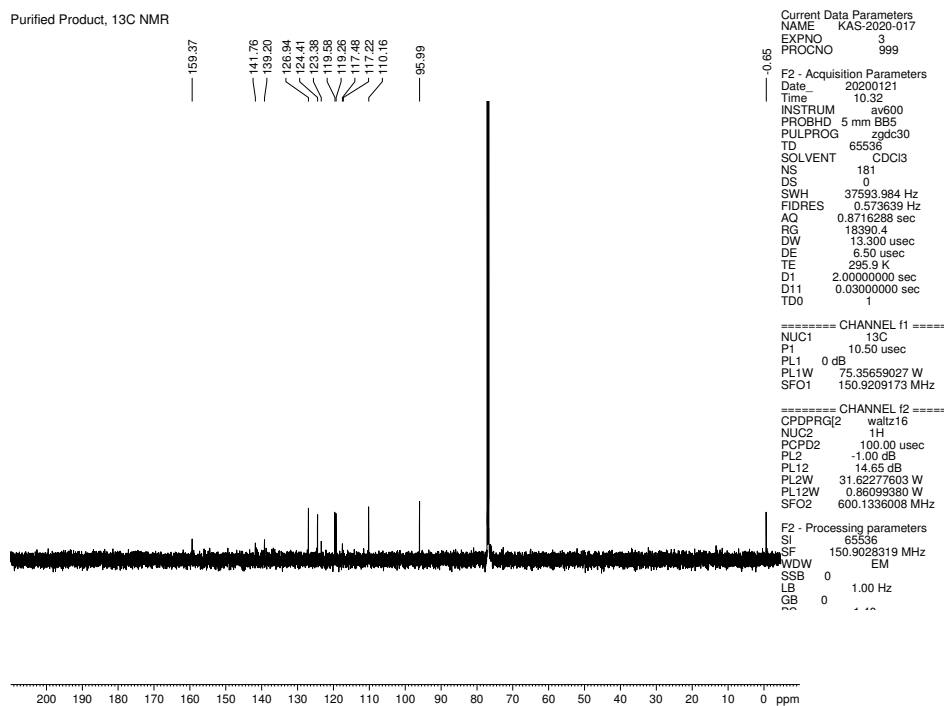


Figure 2.37 ¹³C NMR (150 MHz, CDCl₃) of compound **2.28**.

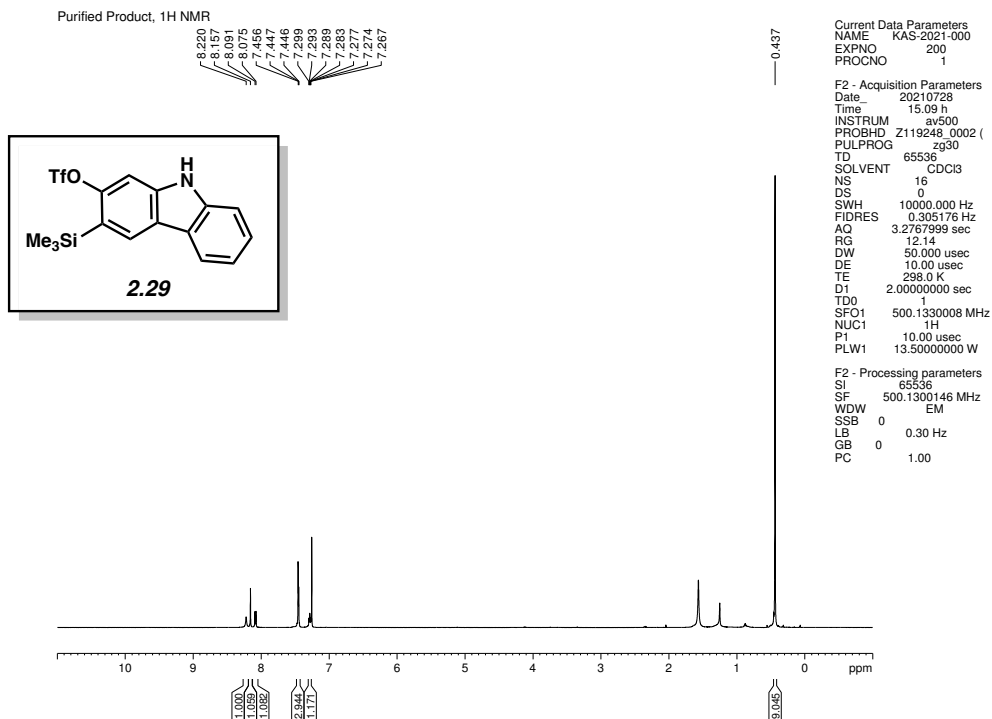


Figure 2.38 ¹H NMR (400 MHz, CDCl₃) of compound **2.29**.

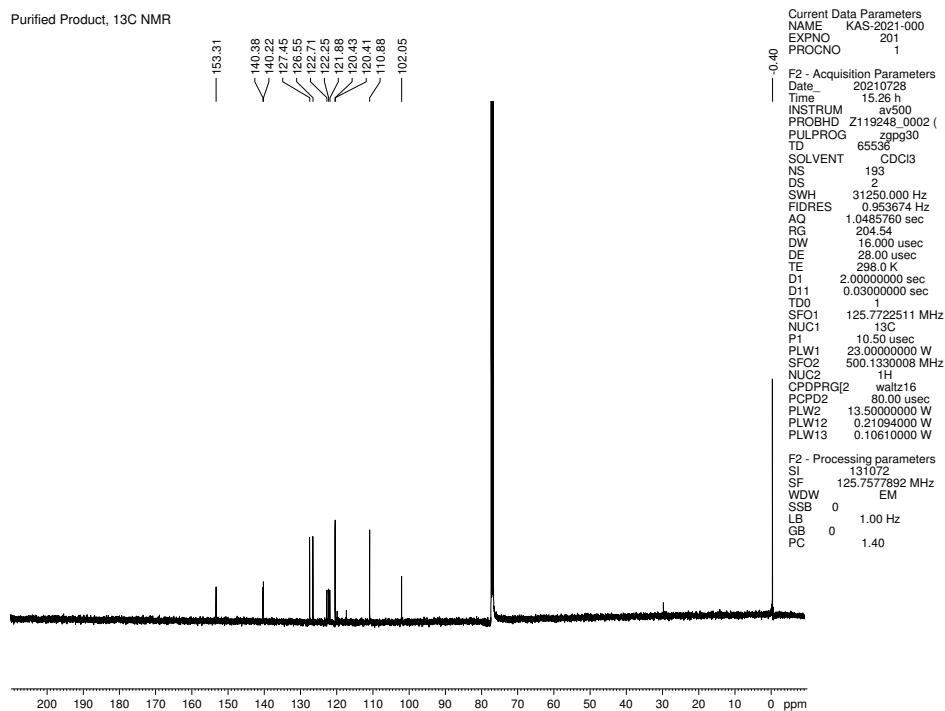


Figure 2.39 ¹³C NMR (125 MHz, CDCl₃) of compound **2.29**.

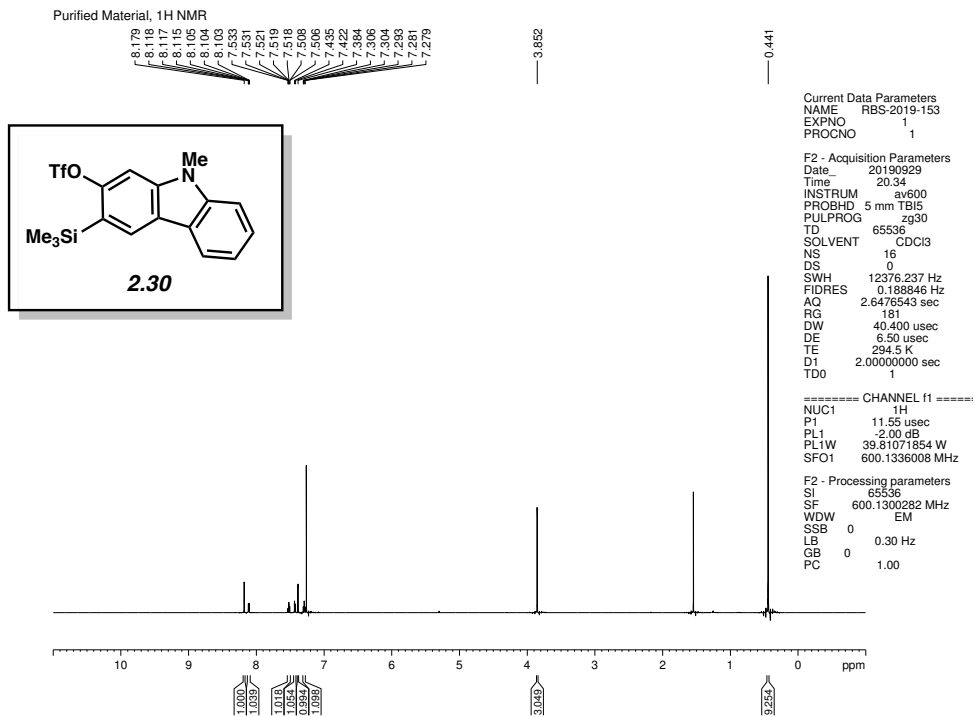


Figure 2.40 ¹H NMR (600 MHz, CDCl₃) of compound **2.30**.

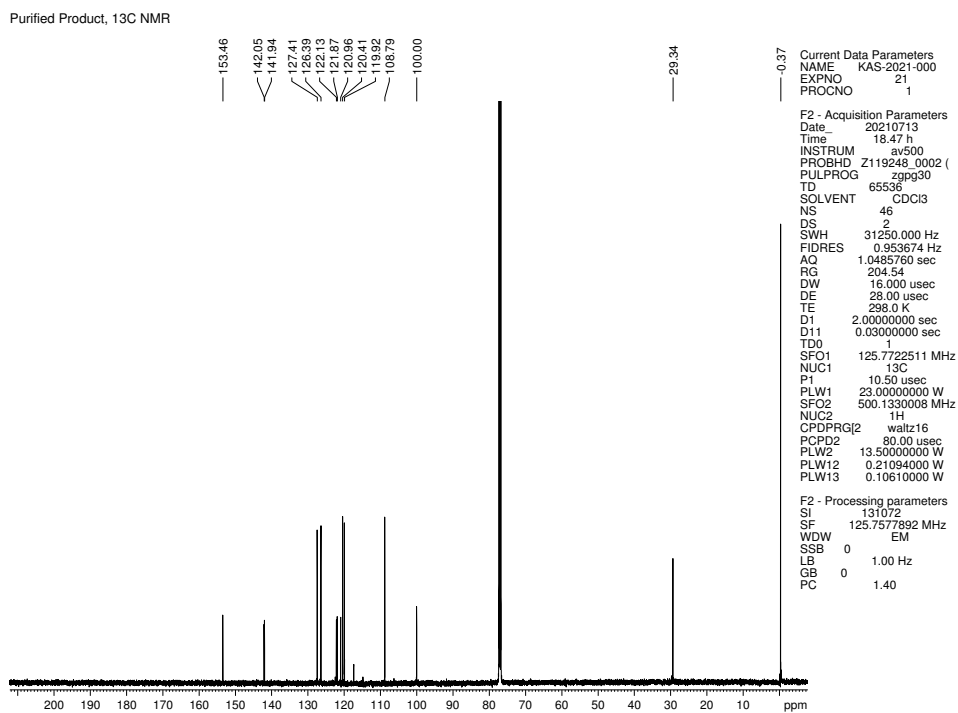


Figure 2.41 ¹³C NMR (125 MHz, CDCl₃) of compound **2.30**.

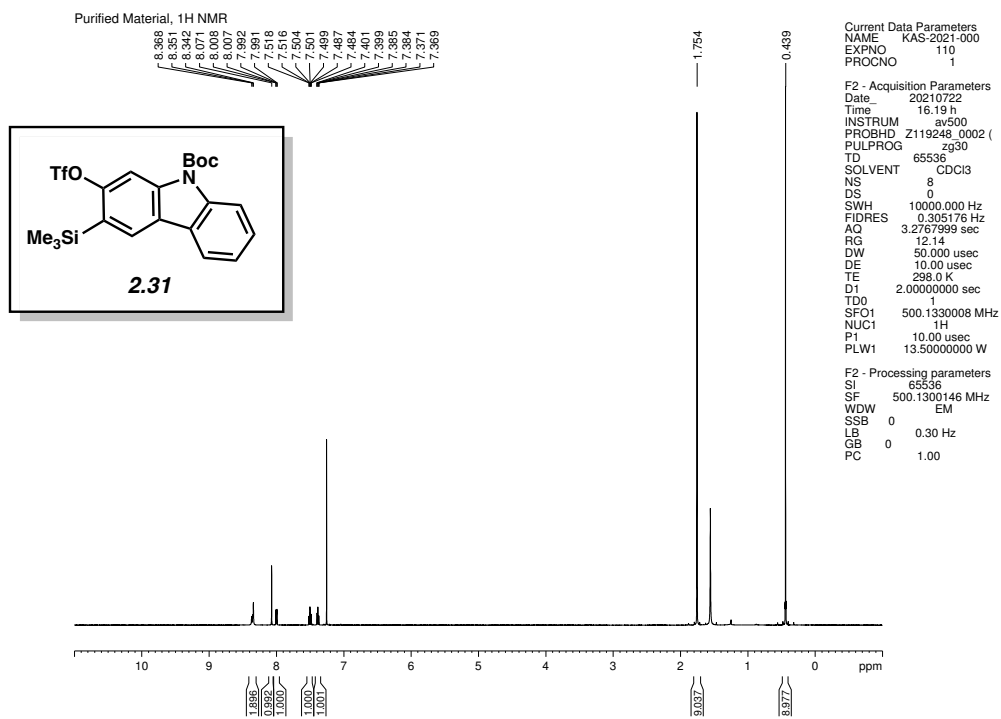


Figure 2.42 ¹H NMR (500 MHz, CDCl₃) of compound **2.31**.

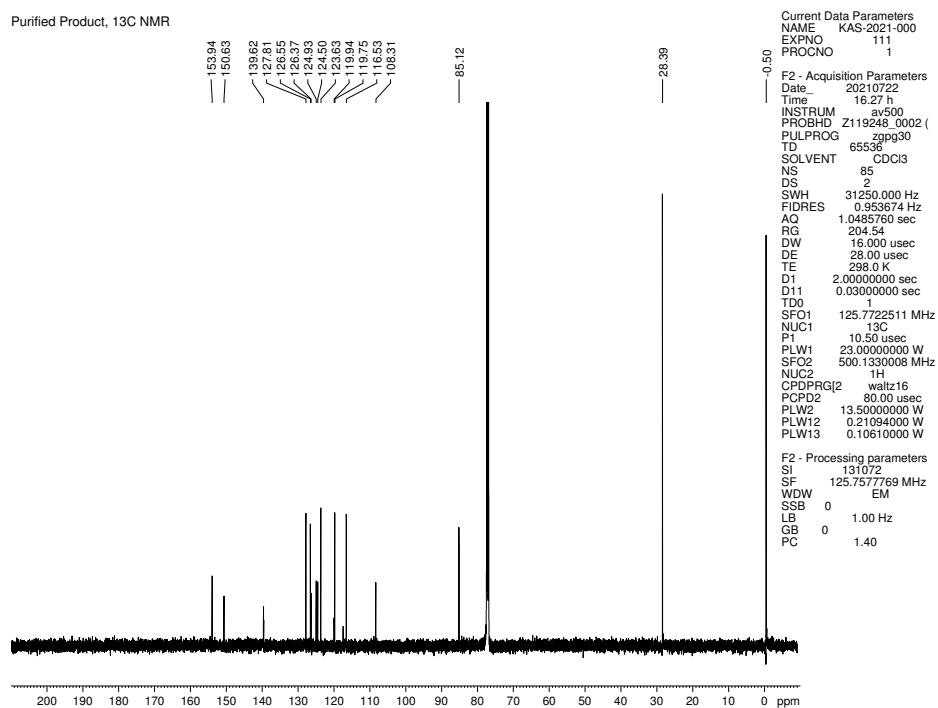


Figure 2.43 ¹³C NMR (125 MHz, CDCl₃) of compound **2.31**.

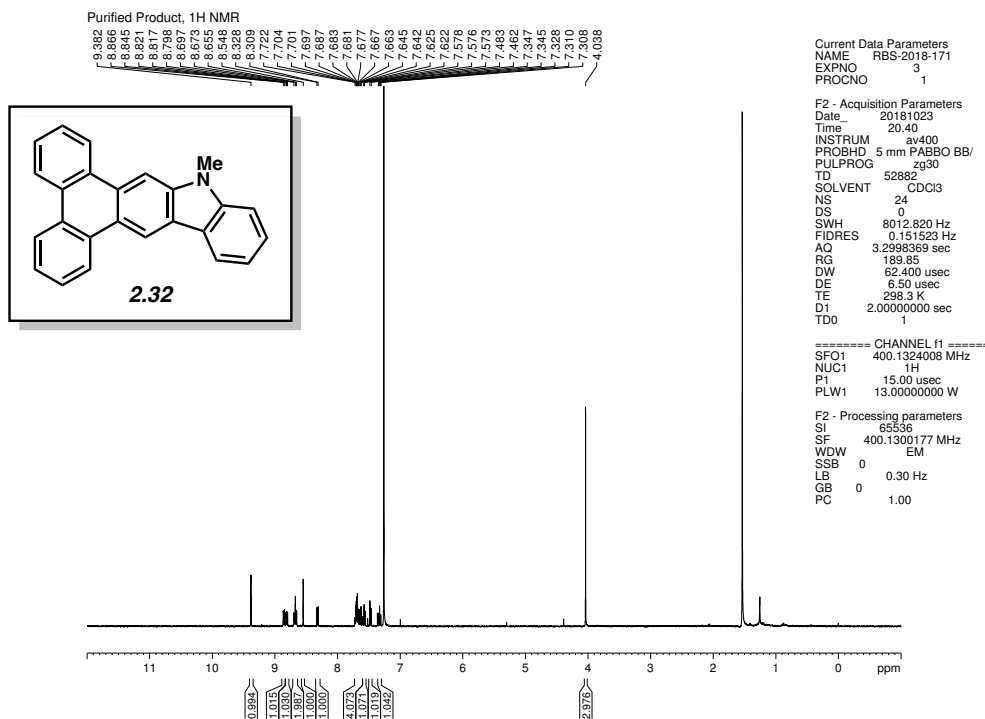


Figure 2.44 ¹H NMR (400 MHz, CDCl₃) of compound **2.32**.

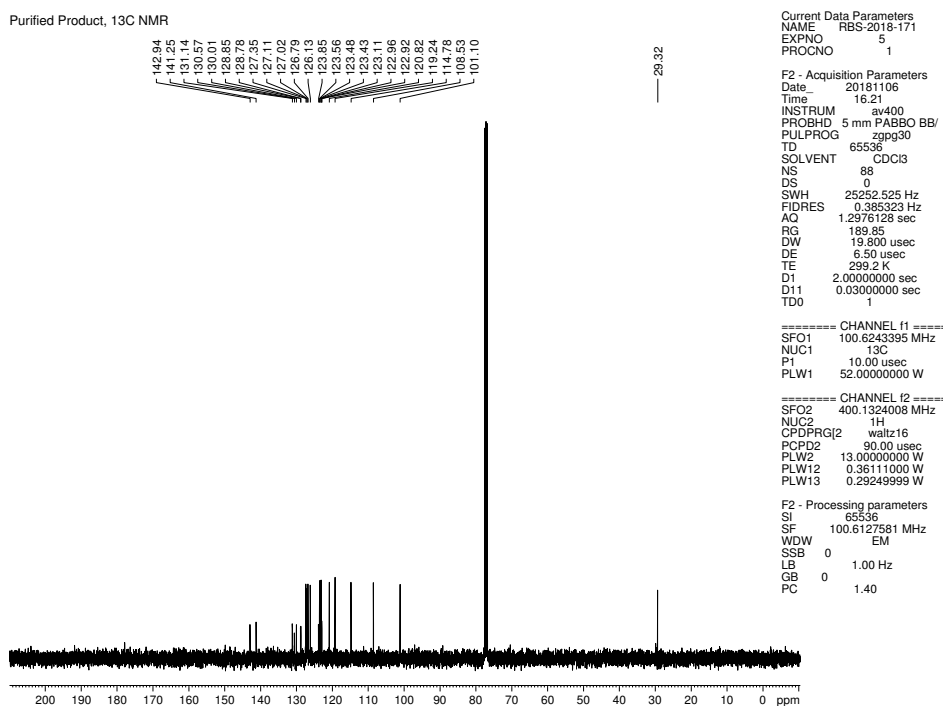


Figure 2.45 ¹³C NMR (100 MHz, CDCl₃) of compound **2.32**.

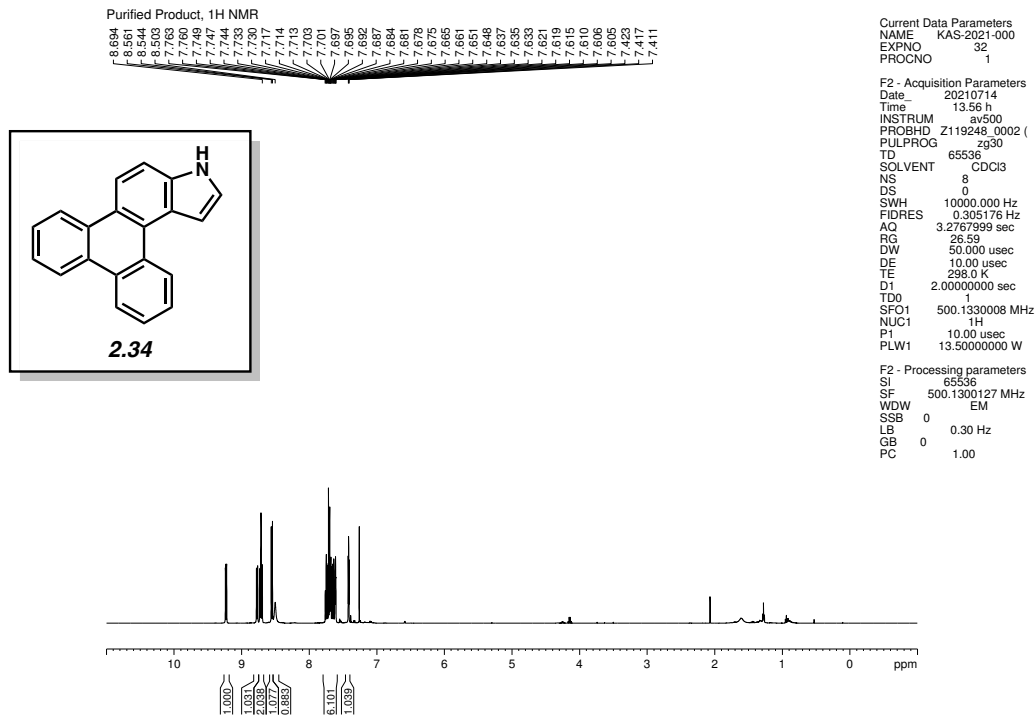


Figure 2.46 ¹H NMR (500 MHz, CDCl₃) of compound **2.34**.

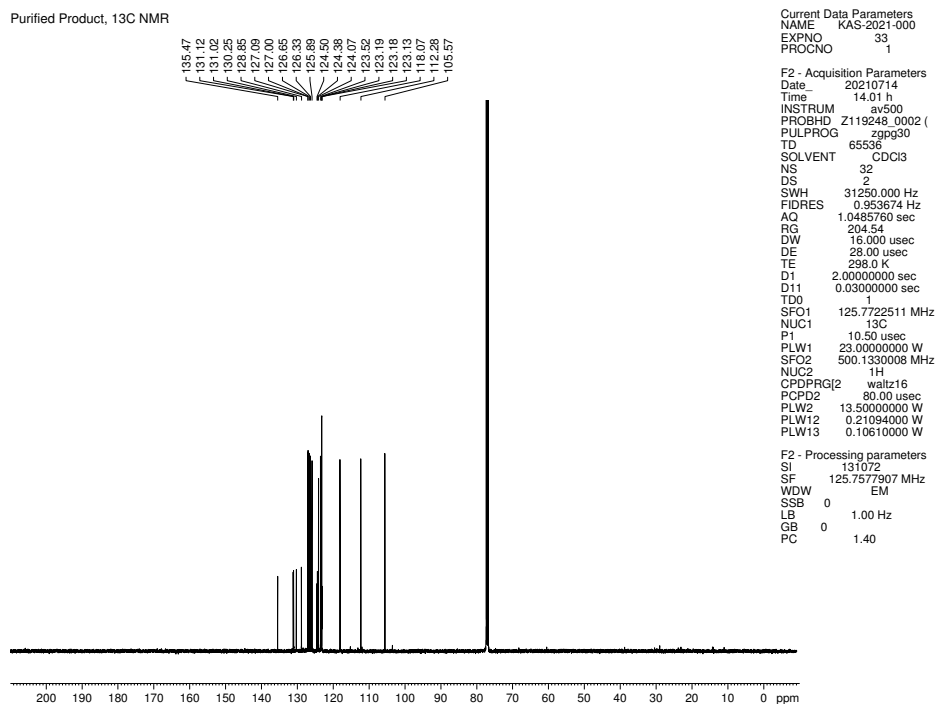


Figure 2.47 ¹³C NMR (125 MHz, CDCl₃) of compound **2.34**.

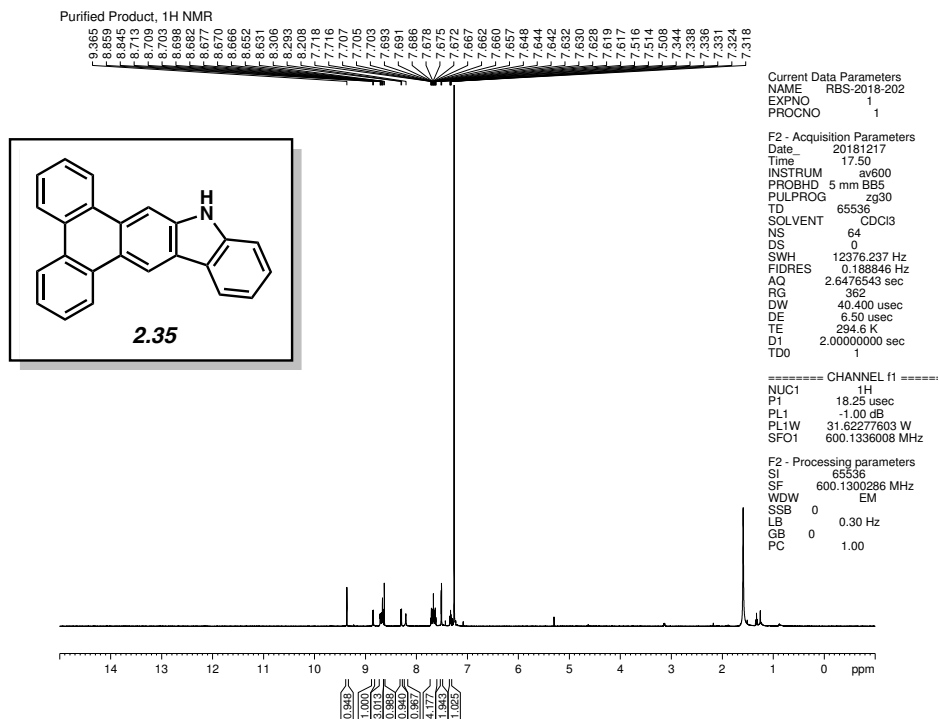


Figure 2.48 ^1H NMR (600 MHz, CDCl_3) of compound **2.35**.

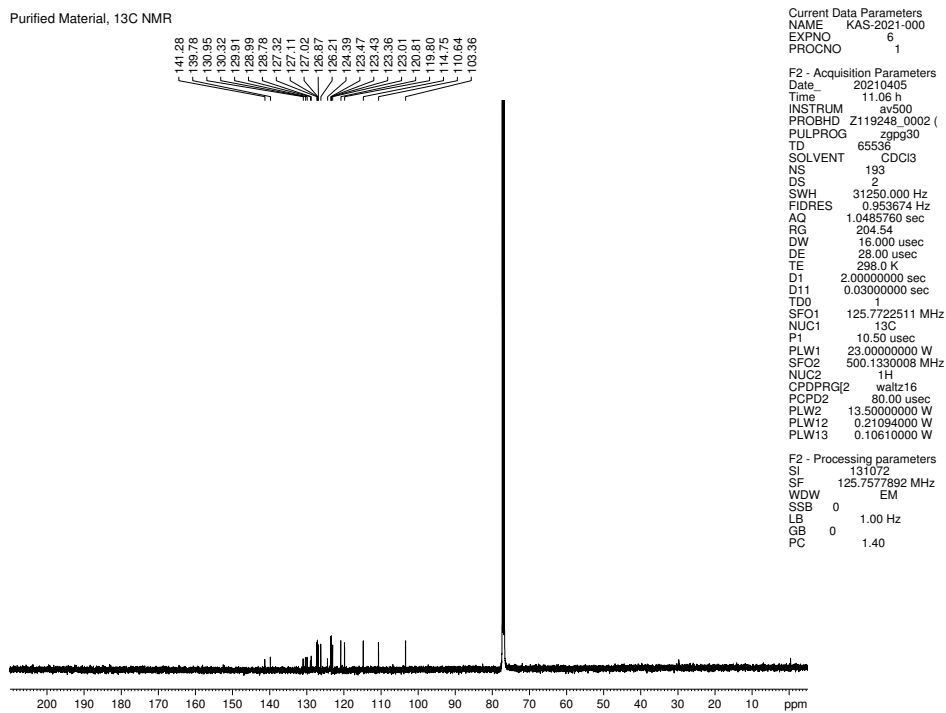


Figure 2.49 ^{13}C NMR (125 MHz, CDCl_3) of compound **2.35**.

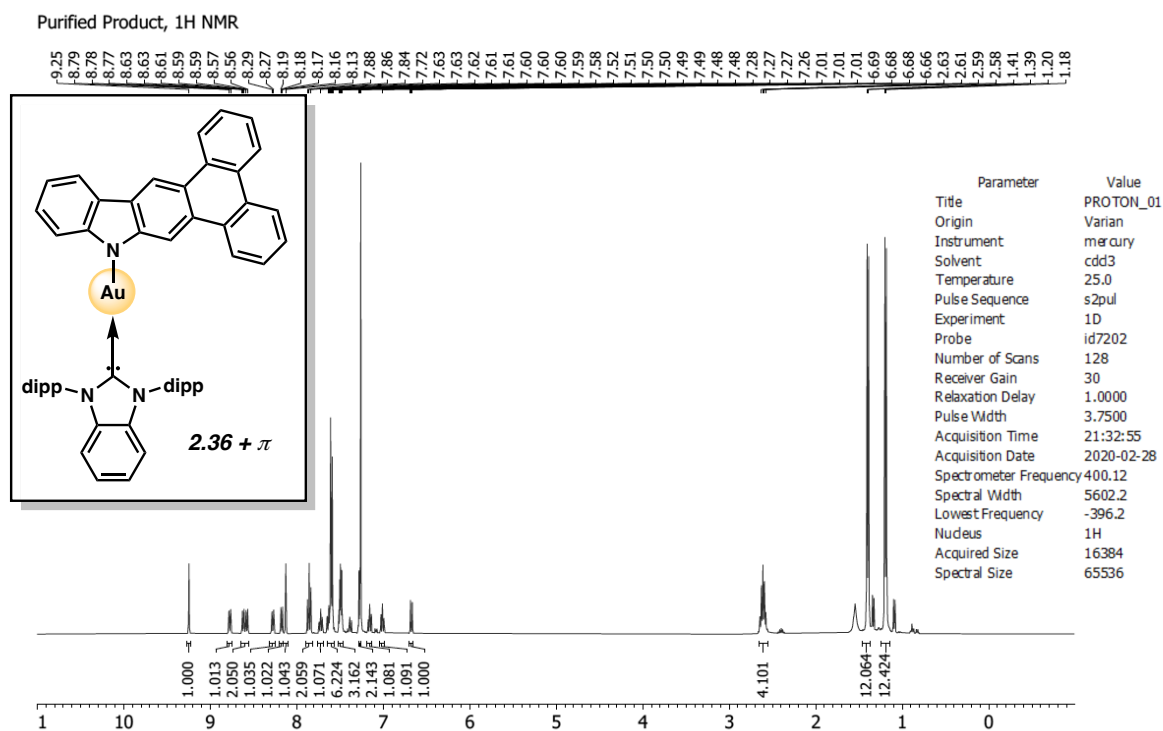


Figure 2.50 ^1H NMR (400 MHz, CDCl_3) of compound **2.36 + π** .

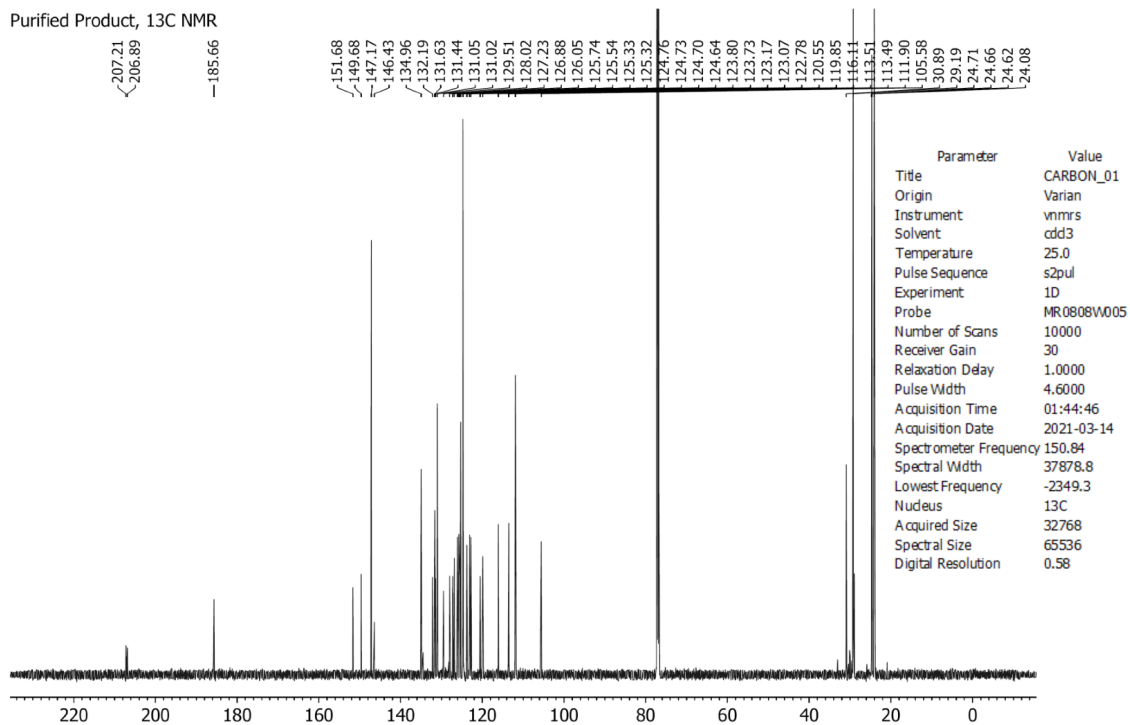


Figure 2.51 ^{13}C NMR (150 MHz, CDCl_3) of compound **2.36 + π** .

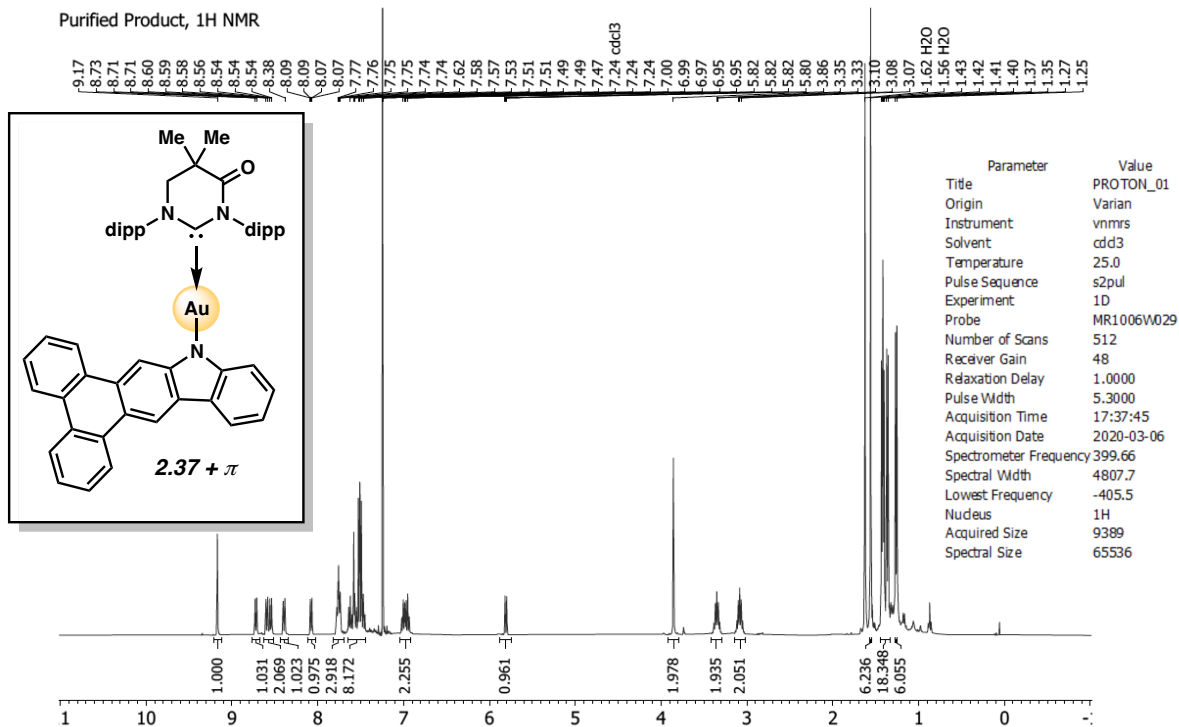


Figure 2.52 ^1H NMR (400 MHz, CDCl_3) of compound **2.37 + π** .

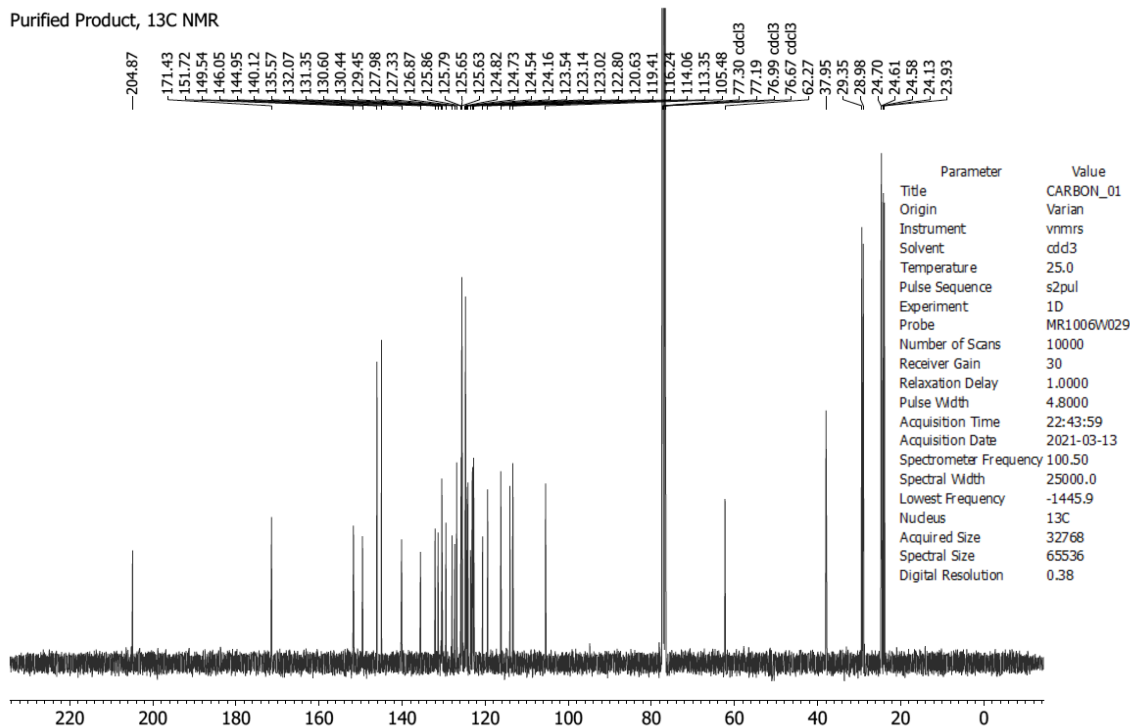


Figure 2.53 ^{13}C NMR (100 MHz, CDCl_3) of compound **2.37 + π** .

Purified Product, ¹H NMR

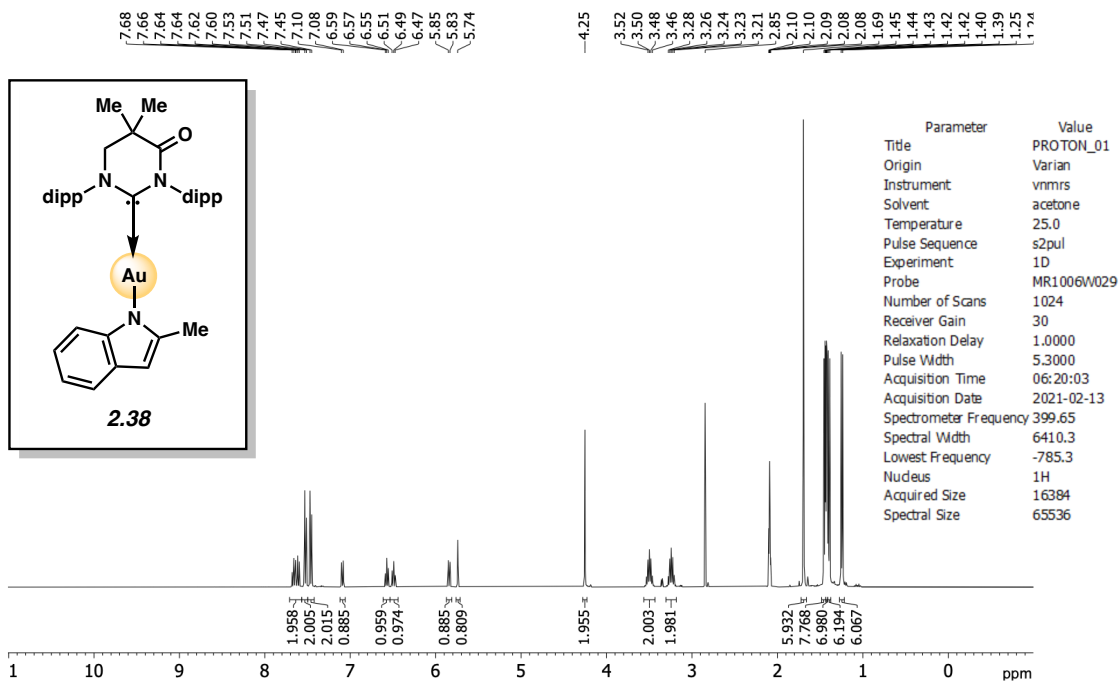


Figure 2.54 ¹H NMR (400 MHz, acetone-*d*₆) of compound **2.38**.

Purified Product, ¹³C NMR

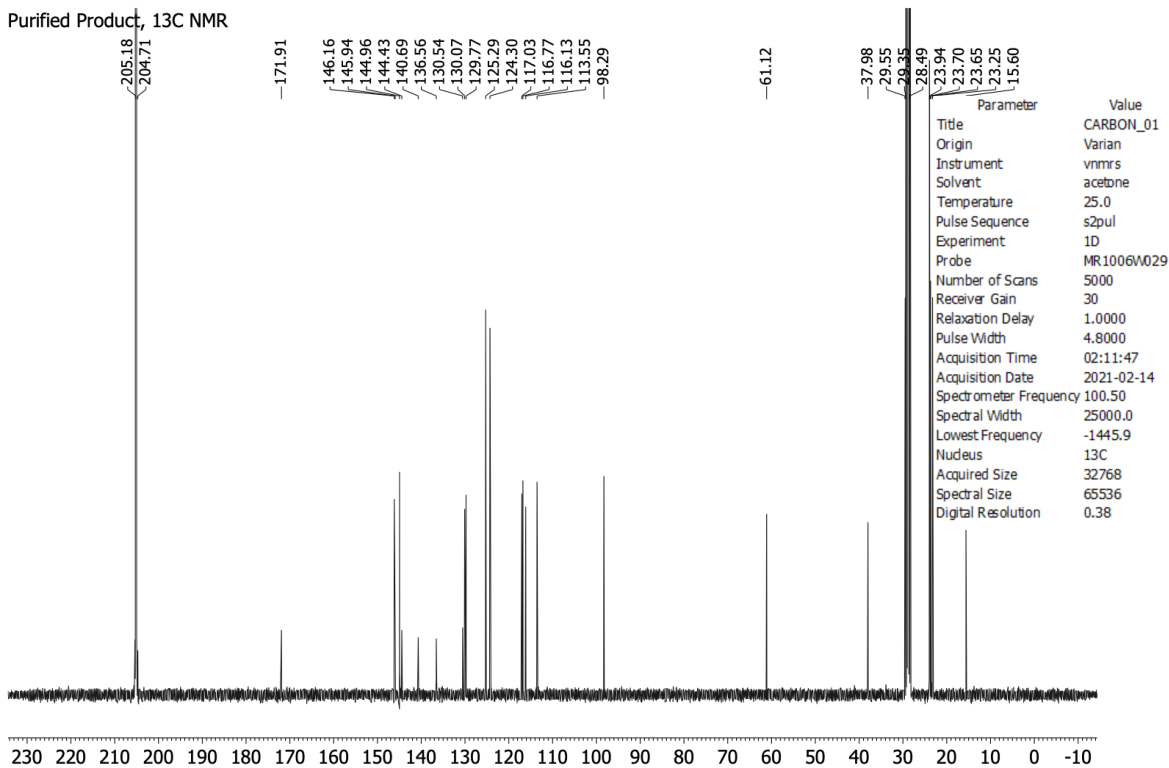


Figure 2.55 ¹³C NMR (100 MHz, acetone-*d*₆) of compound **2.38**.

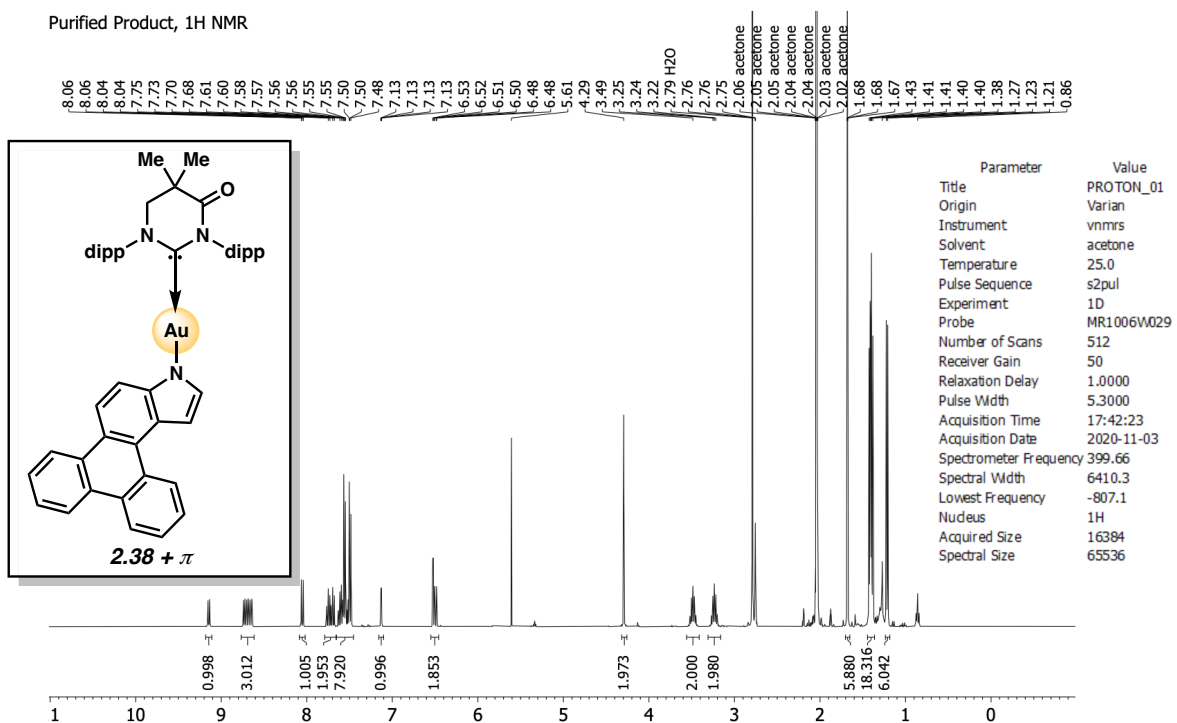


Figure 2.56 ^1H NMR (400 MHz, acetone- d_6) of compound **2.38 + π** .

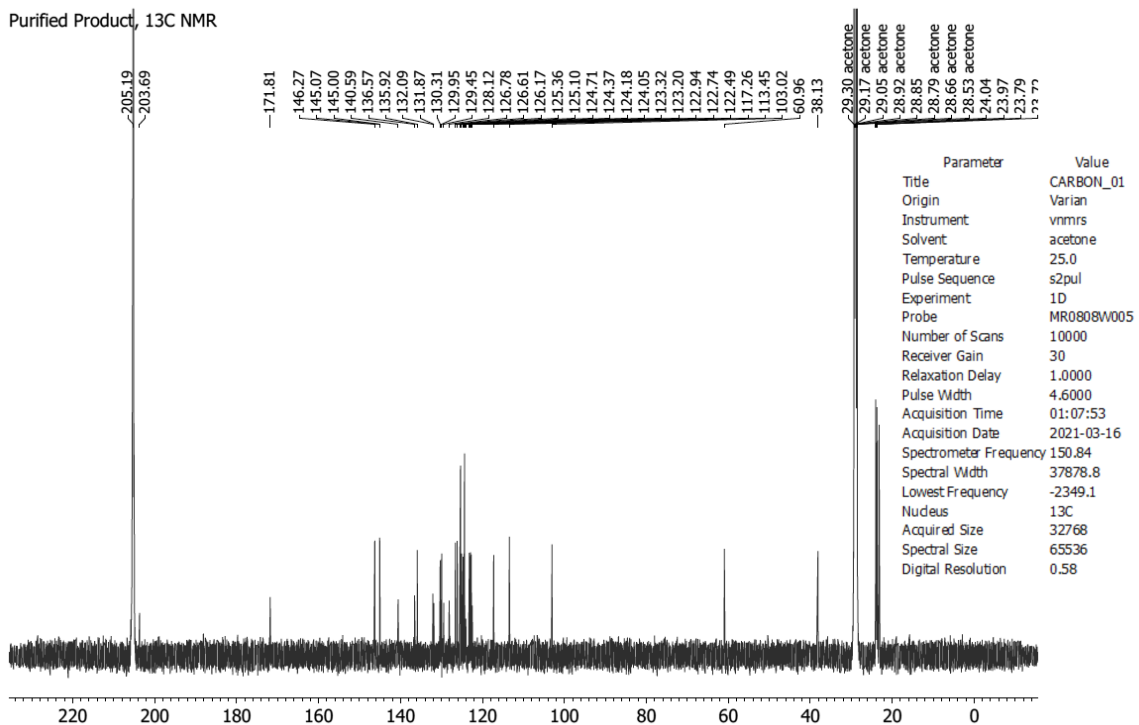


Figure 2.57 ^{13}C NMR (150 MHz, acetone- d_6) of compound **2.38 + π** .

2.9 Notes and References

- (1) Keyte, I. J.; Harrison, R. M.; Lammel, G. Chemical Reactivity and Long-Range Transport Potential of Polycyclic Aromatic Hydrocarbons – A Review. *Chem. Soc. Rev.* **2013**, *42*, 9333–9391.
- (2) Park, K. S.; Salunkhe, S. M.; Lim, I.; Cho, C.-G.; Han, S. H.; Sung, M. High-Performance Air-Stable Single-Crystal Organic Nanowires Based on a New Indolocarbazole Derivative for Field-Effect Transistors. *Adv. Mater.* **2013**, *25*, 3351–3356.
- (3) Ji, Z.; Layek, S.; Ma, B. *US Pat.*, 0315759 A1, 2019.
- (4) Lee, J.; Park, J. Synthesis and Electroluminescence of Novel Pyrene-Fused Chromophores. *Org. Lett.* **2015**, *17*, 3960–3963.
- (5) Wang, Y.; Zhang, Y.-M.; Zhang, S. X.-A. Stimuli-Induced Reversible Proton Transfer for Stimuli-Responsive Materials and Devices. *Acc. Chem. Res.* **2021**, *54*, 2216–2226.
- (6) Traditional synthetic approaches to heterocyclic PAH scaffolds rely on sequential C–C bond formation. For a review of recent advances, see: Ito, H.; Ozaki, K.; Itami, K. Annulative π -Extension (APEX): Rapid Access to Fused Arenes, Heteroarenes, and Nanographenes. *Angew. Chem., Int. Ed.* **2017**, *56*, 11144–11164.
- (7) Nakamura, Y.; Yoshida, S.; Hosoya, T. Recent advances in synthetic heterocyclic chemistry. *Heterocycles* **2019**, *98*, 1623–1677.
- (8) Pellissier, H.; Santelli, M. The use of arynes in organic synthesis. *Tetrahedron* **2003**, *59*, 701–730.
- (9) Wenk, H. H.; Winkler, M.; Sander, W. One century of aryne chemistry. *Angew. Chem., Int. Ed.* **2003**, *42*, 502–528.

- (10) Sanz, R. Recent applications of aryne chemistry to organic synthesis. A review. *Org. Prep. Proced. Int.* **2008**, *40*, 215–291.
- (11) Perez, D.; Pena, D.; Guitian, E. Aryne Cycloaddition Reactions in the Synthesis of Large Polycyclic Aromatic Compounds. *Eur. J. Org. Chem.* **2013**, *27*, 5981–6013.
- (12) Goetz, A. E.; Shah, T. K.; Garg, N. K. Pyridynes and indolynes as building blocks for functionalized heterocycles and natural products. *Chem. Commun.* **2015**, *51*, 34–45.
- (13) Cheong, P. H.-Y.; Paton, R. S.; Bronner, S. M.; Im, G.-Y. J.; Garg, N. K.; Houk, K. N. Indolyne and Aryne Distortions and Nucleophilic Regioselectivities. *J. Am. Chem. Soc.* **2010**, *132*, 1267–1269.
- (14) Lakhdar, S.; Westermaier, M.; Terrier, F.; Goumont, R.; Boubaker, T.; Ofial, A. R.; Mayr, H. Nucleophilic Reactivities of Indoles. *J. Org. Chem.* **2006**, *71*, 9088–9095.
- (15) Loudon, G. M.; Parise, J. *Organic Chemistry*, 6th ed.; Roberts and Company Publishers, Inc., 2016.
- (16) Bronner, S. M.; Bahnck, K. B.; Garg, N. K. Indolynes as Electrophilic Indole Surrogates: Fundamental Reactivity and Synthetic Applications. *Org. Lett.* **2009** *11*, 1007–1010.
- (17) Lin, J. B.; Shah, T. K.; Goetz, A. E.; Garg, N. K.; Houk, K. N. Conjugated Trimeric Scaffolds Accessible from Indolyne Cyclotrimerizations: Synthesis, Structures, and Electronic Properties. *J. Am. Chem. Soc.* **2017**, *139*, 10447–10455.
- (18) Darzi, E. R.; Barber, J. S.; Garg, N. K. Cyclic Alkyne Approach to Heteroatom-Containing Polycyclic Aromatic Hydrocarbon Scaffolds. *Angew. Chem., Int. Ed.* **2019**, *58*, 9419–9424.
- (19) a) Liu, Z.; Zhang, X.; Larock, R. C. Synthesis of Fused Polycyclic Aromatics by Palladium-Catalyzed Annulation of Arynes Using 2-Halobiaryls. *J. Am. Chem. Soc.* **2005**, *127*,

- 15716–15717. b) Liu, Z.; Larock, R. C. Highly Efficient Route to Fused Polycyclic Aromatics via Palladium-Catalyzed Aryne Annulation by Aryl Halides. *J. Org. Chem.* **2007**, *72*, 223–232.
- (20) For examples of Pd-catalyzed transformations of arynes, see: a) Peña, D.; Pérez, D.; Guitián, E.; Castedo, L. Palladium-Catalyzed Cocyclization of Arynes with Alkynes: Selective Synthesis of Phenanthrenes and Naphthalenes. *J. Am. Chem. Soc.* **1999**, *121*, 5827–5828. b) Yoshida, H.; Ikadai, J.; Shudo, M.; Ohshita, J.; Kunai, A. Palladium-Catalyzed Bissilylation of Arynes with Cyclic Disilanes: Synthesis of Benzo-Annulated Disilacarbo-cycles. *J. Am. Chem. Soc.* **2003**, *125*, 6638–6639. c) Jeganmohan, M.; Bhuvanewari, S.; Cheng, C.-H. A Cooperative Copper- and Palladium-catalyzed Three-Component Coupling of Benzyne, Allylic Epoxides, and Terminal Alkynes. *Angew. Chem., Int. Ed.* **2009**, *48*, 391–394. d) Liu, Y.-L.; Liang, Y.; Pi, S.-F.; Huang, X.-C.; Li, J.-H. Palladium-Catalyzed Cocyclotrimerization of Allenes with Arynes: Selective Synthesis of Phenanthrenes. *J. Org. Chem.* **2009**, *74*, 3199–3202. e) Garve, L. K. B.; Werz, D. B. Pd-Catalyzed Three-Component Coupling of Terminal Alkynes, Arynes, and Vinyl Cyclopropane Dicarboxylate. *Org. Lett.* **2015**, *17*, 596–599. f) Feng, M.; Tang, B.; Xu, H.-X.; Jiang, X. Collective Synthesis of Phenanthridinone through C–H Activation Involving a Pd-Catalyzed Aryne Multicomponent Reaction. *Org. Lett.* **2016**, *18*, 4352–4355. g) Yao, T.; He, D. Palladium-Catalyzed Domino Heck/Aryne Carbopalladation/C–H Functionalization: Synthesis of Heterocycle-Fused 9,10-Dihydrophenanthrenes. *Org. Lett.* **2017**, *19*, 842–845. h) Pozo, I.; Guitián, E.; Pérez, D.; Peña, D. Synthesis of

- Nanographenes, Starphenes, and Sterically Congested Polyarenes by Aryne Cyclotrimerization. *Acc. Chem. Res.* **2019**, *52*, 2472–2481.
- (21) For notable examples, see ref. 16 and a) Iwayama, T.; Sato, Y. Nickel(0)-catalyzed [2 + 2 + 2] cycloaddition of diynes and 3,4-pyridynes: novel synthesis of isoquinoline derivatives. *Chem. Commun.* **2009**, 5245–5247. b) Iwayama, T.; Sato, Y. Synthesis of Substituted Isoquinolines via Nickel-Catalyzed [2+2+2] Cycloaddition of Alkynes and 3,4-Pyridynes. *Heterocycles* **2010**, *80*, 917–924.
- (22) For a review on yellow/orange phosphors, see: a) Fan, C.; Yang, C. Yellow/Orange Emissive Heavy-Metal Complexes as Phosphors in Monochromatic and White Organic Light-Emitting Devices. *Chem. Soc. Rev.* **2014**, *43*, 6439–6469. For a review on blue phosphors, see: b) Im, Y.; Byun, S. Y.; Kim, J. H.; Lee, D. R.; Oh, C. S.; Yook, K. S.; Lee, J. Y. Recent Progress in High-Efficiency Blue-Light-Emitting Materials for Organic Light-Emitting Diodes. *Adv. Funct. Mater.* **2017**, *27*, 1603007.
- (23) We elected to utilize aryl bromides for our studies due to their ease of preparation and success in our preliminary studies. Other studies have demonstrated the viability of using aryl iodides (see ref. 19). Our laboratory has also demonstrated the use of aryl chlorides, albeit in the context of metal-complexed bipyridyl ligands (see ref. 24).
- (24) Chari, J. V.; Spence, K. A.; Susick, R. B.; Garg, N. K. A Platform for On-the-Complex Annulation Reactions with Transient Aryne Intermediates. *Nat. Commun.* **2021**, *12*, 3706.
- (25) Yamano, M. M.; Kelleghan, A. V. Shao, Q.; Giroud, M.; Simmons, B. J.; Li, B.; Chen, S.; Houk, K. N.; Garg, N. K. Intercepting Fleeting Cyclic Allenes with Asymmetric Nickel Catalysis. *Nature* **2020**, *586*, 242–247.

- (26) Kelleghan, A. V.; Witkowski, D. C.; McVeigh, M. S.; Garg, N. K. Palladium-Catalyzed Annulations of Strained Cyclic Allenes. *J. Am. Chem. Soc.* **2021**, *143*, 9338–9342.
- (27) We have experimentally observed that the addition of toluene leads to slower consumption of silyltriflate precursors, presumably by reducing the solubility of CsF in the reaction medium. The solubility of CsF in acetonitrile is roughly 5000x greater compared to the solubility of CsF in benzene, a close relative of toluene with a comparable dielectric constant. For a study of CsF solubility, see: Wynn, D. A.; Roth, M. M.; Pollard, B. D. The solubility of alkali-metal fluorides in non-aqueous solvents with and without crown ethers, as determined by flame emission spectrometry. *Talanta* **1984**, *31*, 1036–1040.
- (28) In prior studies of indolynes, we have observed lower regioselectivities for processes that are concerted. As such, we believe the reaction proceeds by oxidative addition, followed by a concerted insertion across the reactive triple bond of the indolyne. This step is also consistent with the general mechanism proposed by Larock (see ref. 19a).
- (29) Cha, M. S.; Park, J. E.; Kim, S.; Han, S.-H.; Shin, S.-H.; Yang, S. H.; Kim, T.-H.; Yu, D. M.; So, S.; Hong, Y. T.; Yoon, S. J.; Oh, S.-G.; Kang, S. Y.; Kim, O.-H.; Park, H. S.; Bae, B.; Sung, Y.E.; Cho, Y.-H.; Lee, J. Y. Poly(carbazole)-based Anion-Conducting Materials with High Performance and Durability for Energy Conversion Devices. *Energy Environ. Sci.* **2020**, *13*, 3633–3645.
- (30) Tsutsumi, L. S.; Gündisch, D.; Sun, D. Carbazole Scaffolds in Medicinal Chemistry and Natural Products: A Review from 2010–2015. *Curr. Top. Med. Chem.* **2016**, *16*, 1290–1313.

- (31) Goetz, A. E.; Silberstein, A. L.; Corsello, M. A.; Garg, N. K. Concise Enantiospecific Total Synthesis of Tubingensin A. *J. Am. Chem. Soc.* **2014**, *136*, 3036–3039.
- (32) Wang, T.; Hoye, T. R. Hexadehydro-Diels–Alder (HDDA)-Enabled Carbazolyne Chemistry: Single Step, de Novo Construction of the Pyranocarbazole Core of Alkaloids of the *Murraya koenigii* (Curry Tree) Family. *J. Am. Chem. Soc.* **2016**, *138*, 13870–13873.
- (33) Devaraj, K.; Ingner, F. J. L.; Sollert, C.; Gates, P. J.; Orthaber, A.; Pilarski, L. T. Arynes and Their Precursors from Arylboronic Acids via Catalytic C–H Silylation. *J. Org. Chem.* **2019**, *84*, 5863–5871.
- (34) Corsello, M. A.; Kim, J.; Garg, N. K. Total Synthesis of (–)-Tubingensin B Enabled by the Strategic Use of an Aryne Cyclization. *Nat. Chem.* **2017**, *9*, 944–949.
- (35) When the N–H variant of the 4,5-indolyne precursor was utilized in our general annulation conditions, only minimal amounts of the desired product were observed.
- (36) Jones, S.; Thomas, T. H.; Jalebi, M. A.; Friend, R. H.; Linnolahti, M.; Bochmann, M.; Credgington, D. High-Performance Light-Emitting Diodes Based on Carbene-Metal-Amides. *Science* **2017**, *356*, 159–163. b) Hamze, R.; Peltier, J. L.; Sylvinson, D.; Jun, M.; Cardenas, J.; Haiges, R.; Soleilhavoup, M.; Jazzar, R.; Djurovich, P. I.; Bertrand, G.; Thompson, M. E. Eliminating Nonradiative Decay in Cu(I) Emitters: >99% Quantum Efficiency and Microsecond Lifetime. *Science* **2019**, *363*, 601–606. c) Hamze, R.; Shi, S.; Kapper, S. C.; Ravinson, D. S. M.; Estergreen, L.; Jung, M.-C.; Tadle, A. C.; Haiges, R.; Djurovich, P. I.; Peltier, J. L.; Jazzar, R.; Bertrand, G.; Bradforth, S. E.; Thompson, M. E. “Quick-Silver” from a Systematic Study of Highly Luminescent, Two-Coordinate, d¹⁰ Coinage Metal Complexes. *J. Am. Chem. Soc.* **2019**, *141*, 8616–8626.

- (37) Gernert, M.; Balles-Wolf, L.; Kerner, F.; Müller, U.; Schmiedel, A.; Holzapfel, M.; Marian, C. M.; Pflaum, J.; Lambert, C.; Steffen, A. Cyclic (Amino)(aryl)carbenes Enter the Field of Chromophore Ligands: Expanded π System Leads to Unusually Deep Red Emitting Cu^I Compounds. *J. Am. Chem. Soc.* **2020**, *142*, 8897–8909.
- (38) Romanov, A. S.; Becker, C. R.; James, C. E.; Di, D.; Credginton, D.; Linnolahti, M.; Bochmann, M. Copper and Gold (Alkyl)(amino)carbene Complexes with Sub-Microsecond Photoemissions: Structure and Substituent Effects on Redox and Luminescent Properties. *Chem. Eur. J.* **2017**, *23*, 4625–4637.
- (39) Conaghan, P. J.; Matthews, C. S. B.; Chotard, F.; Jones, S. T. E.; Greenham, N. C.; Bochmann, M.; Credginton, D.; Romanov, A. S. Highly Efficient Blue Organic Light-Emitting Diodes Based on Carbene-Metal-Amides. *Nat. Commun.* **2020**, *11*, 1758.
- (40) Chotard, F.; Sivchik, V.; Linnolahti, M.; Bochmann, M.; Romanov, A. S. Mono- versus Bicyclic Carbene Metal Amide Photoemitters: Which Design Leads to the Best Performance? *Chem. Mater.* **2020**, *32*, 6114–6122.
- (41) Yersin, H.; Rausch, A. F.; Czerwieniec, R.; Hofbek, T.; Fischer, T. The Triplet State of Organo-Transition Metal Compounds. Triplet Harvesting and Singlet Harvesting for Efficient OLEDs. *Coord. Chem. Rev.* **2011**, *255*, 2622–2652.
- (42) Hanson, K.; Roskop, L.; Djurovich, P. I.; Zahariev, F.; Gordon, M. S.; Thompson, M. E. A Paradigm for Blue- or Red-Shifted Absorption of Small Molecules Depending on the Site of π -Extension. *J. Am. Chem. Soc.* **2010**, *132*, 16247–16255.
- (43) Shi, S.; Jung, M. C.; Coburn, C.; Tadler, A.; Ravinson, D. S. M.; Djurovich, P. I.; Forrest, S. R.; Thompson, M. E. Highly Efficient Photo- and Electroluminescence from Two-

- Coordinate Cu(I) Complexes Featuring Nonconventional *N*-Heterocyclic Carbenes. *J. Am. Chem. Soc.* **2019**, *141*, 3576–3588.
- (44) Romanov, A. S.; Yang, L.; Jones, S. T. E.; Di, D.; Morley, O. J.; Drummond, B. H.; Reponen, A. P. M.; Linnolahti, M.; Credginton, D.; Bochmann, M. Dendritic Carbene Metal Carbazole Complexes as Photoemitters for Fully Solution-Processed OLEDs. *Chem. Mater.* **2019**, *31*, 3613–3623.
- (45) Ying, A.; Huang, Y.-H.; Lu, C.-H.; Chen, Z.; Lee, W.-K.; Zeng, X.; Chen, T.; Cao, X.; Wu, C.-C.; Gong, S.; Yang, C. High-Efficiency Red Electroluminescence Based on a Carbene-Cu(I)-Acridine Complex. **2021**, *13*, 13478–13486.
- (46) Bossi, A.; Rausch, A. F.; Leitl, M. J.; Czerwieniec, R.; Whited, M. T.; Djurovich, P. I.; Yersin, H.; Thompson, M. E. Photophysical Properties of Cyclometalated Pt(II) Complexes: Counterintuitive Blue Shift in Emission with an Expanded Ligand π System. *Inorg. Chem.* **2013**, *52*, 12403–12415.
- (47) Mandapati, P.; Giesbrecht, P. K.; Davis, R. L.; Herbert, D. E. Phenanthridine-Containing Pincer-like Amido Complexes of Nickel, Palladium, and Platinum. *Inorg. Chem.* **2017**, *56*, 3674–3685.
- (48) Hamze, R.; Idris, M.; Ravinson, D. S. M.; Jung, M. C.; Haiges, R.; Djurovich, P. I.; Thompson, M. E. Highly Efficient Deep Blue Luminescence of 2-Coordinate Coinage Metal Complexes Bearing Bulky NHC Benzimidazolyl Carbene. *Front. Chem.* **2020**, *8*, 401.
- (49) Hamze, R.; Shi, S.; Kapper, S.; Ravinson, D. S. M.; Estergreen, L.; Jung, M.-C.; Tadde, A. C.; Haiges, R.; Djurovich, P. I.; Peltier, J. L.; Jazzar, R.; Bertrand, G.; Bradforth, S. E.;

- Thompson, M. E. "Quick-Silver" from a Systematic Study of Highly Luminescent, Two-Coordinate, d¹⁰ Coinage Metal Complexes. *J. Am. Chem. Soc.* **2019**, *141*, 8616–8626.
- (50) See Section 5.5.2.6 for preparation of 1 wt% polystyrene film.
- (51) Zhang, Q.-W.; An, K.; Liu, L.-C.; Guo, S.; Jiang, C.; Guo, H.; He, W. Rhodium-Catalyzed Intramolecular C–H Silylation by Silacyclobutanes. *Angew. Chem., Int. Ed.* **2016**, *55*, 6319–6323.
- (52) Wang, T.-F.; Lin, C.-L.; Chen, C.-N.; Wang, T.-C. Easily Accessible 2-(2-Bromophenyl)-4,4,5,5-Tetramethyl-[1,3,2]Dioxaborolane for Suzuki-Miyaura Reactions. *J. Chin. Chem. Soc.* **2007**, *54*, 811–816.
- (53) Wu, D.; Chen, L.; Ma, S.; Luo, H.; Cao, J.; Chen, R.; Duan, Z.; Mathey, F. Synthesis of 1,3-Azaphospholes with Pyrrolo[1,2-*a*]quinoline Skeleton and Their Optical Applications. *Org. Lett.* **2018**, *20*, 4103–4106.
- (54) Pantelev, J.; Geyer, K.; Aguilar-Aguilar, A.; Wang, L.; Lautens, M. C–H Bond Functionalization in the Synthesis of Fused 1,2,3-Triazoles. *Org. Lett.* **2010**, *12*, 5092–5095.
- (55) Wong, S. M.; Yuen, O. Y.; Choy, P. Y.; So, C. M.; Kwong, F. Y. Preparation of 2-(2-(Dicyclohexylphosphino)phenyl)-1-methyl-1H-indole (CM-phos). *Org. Synth.* **2016**, *93*, 14–28.
- (56) Im, G.-Y. J.; Bronner, S. M.; Goetz, A. E.; Paton, R. S.; Cheong, P. H.-Y.; Houk, K. N.; Garg, N. K. Indolyne Experimental and Computational Studies: Synthetic Applications and Origins of Selectivities of Nucleophilic Additions. *J. Am. Chem. Soc.* **2010**, *132*, 17933–17944.

(57) Shao, Y. H.; Gan, Z. T.; Epifanovsky, E.; Gilbert, A. T. B.; Wormit, M.; Kussmann, J.; Lange, A. W.; Behn, A.; Deng, J.; Feng, X. T.; Ghosh, D.; Goldey, M.; Horn, P. R.; Jacobson, L. D.; Kaliman, I.; Khaliullin, R. Z.; Kus, T.; Landau, A.; Liu, J.; Proynov, E. I.; Rhee, Y. M.; Richard, R. M.; Rohrdanz, M. A.; Steele, R. P.; Sundstrom, E. J.; Woodcock, H. L.; Zimmerman, P. M.; Zuev, D.; Albrecht, B.; Alguire, E.; Austin, B.; Beran, G. J. O.; Bernard, Y. A.; Berquist, E.; Brandhorst, K.; Bravaya, K. B.; Brown, S. T.; Casanova, D.; Chang, C. M.; Chen, Y. Q.; Chien, S. H.; Closser, K. D.; Crittenden, D. L.; Diedenhofen, M.; DiStasio, R. A.; Do, H.; Dutoi, A. D.; Edgar, R. G.; Fatehi, S.; Fusti-Molnar, L.; Ghysels, A.; Golubeva-Zadorozhnaya, A.; Gomes, J.; Hanson-Heine, M. W. D.; Harbach, P. H. P.; Hauser, A. W.; Hohenstein, E. G.; Holden, Z. C.; Jagau, T. C.; Ji, H. J.; Kaduk, B.; Khistyayev, K.; Kim, J.; King, R. A.; Klunzinger, P.; Kosenkov, D.; Kowalczyk, T.; Krauter, C. M.; Lao, K. U.; Laurent, A. D.; Lawler, K. V.; Levchenko, S. V.; Lin, C. Y.; Liu, F.; Livshits, E.; Lochan, R. C.; Luenser, A.; Manohar, P.; Manzer, S. F.; Mao, S. P.; Mardirossian, N.; Marenich, A. V.; Maurer, S. A.; Mayhall, N. J.; Neuscamman, E.; Oana, C. M.; Olivares-Amaya, R.; O'Neill, D. P.; Parkhill, J. A.; Perrine, T. M.; Peverati, R.; Prociuk, A.; Rehn, D. R.; Rosta, E.; Russ, N. J.; Sharada, S. M.; Sharma, S.; Small, D. W.; Sodt, A.; Stein, T.; Stuck, D.; Su, Y. C.; Thom, A. J. W.; Tsuchimochi, T.; Vanovschi, V.; Vogt, L.; Vydrov, O.; Wang, T.; Watson, M. A.; Wenzel, J.; White, A.; Williams, C. F.; Yang, J.; Yeganeh, S.; Yost, S. R.; You, Z. Q.; Zhang, I. Y.; Zhang, X.; Zhao, Y.; Brooks, B. R.; Chan, G. K. L.; Chipman, D. M.; Cramer, C. J.; Goddard, W. A.; Gordon, M. S.; Hehre, W. J.; Klamt, A.; Schaefer, H. F.; Schmidt, M. W.; Sherrill, C. D.; Truhlar, D. G.; Warshel, A.; Xu, X.; Aspuru-Guzik, A.; Baer, R.; Bell, A. T.; Besley, N. A.; Chai, J. D.;

Dreuw, A.; Dunietz, B. D.; Furlani, T. R.; Gwaltney, S. R.; Hsu, C. P.; Jung, Y. S.; Kong, J.; Lambrecht, D. S.; Liang, W. Z.; Ochsenfeld, C.; Rassolov, V. A.; Slipchenko, L. V.; Subotnik, J. E.; Van Voorhis, T.; Herbert, J. M.; Krylov, A. I.; Gill, P. M. W.; Head-Gordon, M. Advances in Molecular Quantum Chemistry Contained in the Q-Chem 4 Program Package. *Mol. Phys.* **2015**, *113*, 184–215.

CHAPTER THREE

A Platform for On-the-Complex Annulation Reactions with Transient Aryne Intermediates

Jason V. Chari,[†] Katie A. Spence,[†] Robert B. Susick, and Neil K. Garg.

Nat. Commun. **2021**, *12*, 3706.

3.1 Abstract

Organometallic complexes are ubiquitous in chemistry and biology. Whereas their preparation has historically relied on ligand synthesis followed by coordination to metal centers, the ability to efficiently diversify their structures remains a synthetic challenge. A promising yet underdeveloped strategy involves the direct manipulation of ligands that are already bound to a metal center, also known as chemistry-on-the-complex. Herein, we introduce a versatile platform for on-the-complex annulation reactions using transient aryne intermediates. In one variant, organometallic complexes undergo transition metal-catalyzed annulations with in situ generated arynes to form up to six new carbon–carbon bonds. In the other variant, an organometallic complex bearing a free aryne is generated and intercepted in cycloaddition reactions to access unique scaffolds. Our studies, centered around privileged polypyridyl metal complexes, provide an effective strategy to annulate organometallic complexes and access complex metal–ligand scaffolds, while furthering the synthetic utility of strained intermediates in chemical synthesis.

3.2 Introduction

Organometallic complexes are prevalent in chemistry and biology, with applications ranging from usage as highly selective catalysts¹ to therapeutics² and enzyme cofactors.³ Key to

this versatility is the ability to tune function through manipulation of ligand structure. Fine tuning of the ligand sphere can lead to profound changes in the properties of an organometallic complex, including stereoelectronic and photophysical properties, catalyst turnover rate and stability.⁴ Thus, the continued growth of organometallic chemistry is contingent on the capacity to access metal–ligand architectures with increased structural diversity and complexity.

Conventional synthetic approaches toward organometallic complexes involve reliance on ligand synthesis followed by coordination to a metal center (Figure 3.1a). This general approach remains modular and adaptable, accounting for the syntheses of the majority of known metal–ligand complexes. Nonetheless, this general strategy can have drawbacks in the syntheses of notable ligand classes. For example, the synthesis of strongly chelating ligands can be challenging due to their propensity to form stable metal–ligand chelates and, in turn, prevent the use of metal-mediated transformations such as cross-couplings, C–H functionalization, and annulation reactions.⁵ In addition, highly rigid ligand systems can also have poor solubility in organic solvents, thus complicating their syntheses and subsequent coordination to metal centers.^{6,7} Finally, ligand synthesis may require long, linear reaction sequences, which can render the process of synthesizing large libraries of organometallic derivatives cumbersome or impractical.

Divergent synthetic routes to organometallic complexes, analogous to those which have proven valuable in medicinal chemistry, are important for generating structurally diverse libraries of compounds. Toward this end, a nascent synthetic approach that complements traditional coordination chemistry is chemistry-on-the-complex,⁸ whereby ligands are modified after being bound to a metal center. This strategy provides an attractive means for rapid

structural diversification of metal–ligand complexes and can serve to circumvent the aforementioned challenges often encountered in ligand synthesis.

Chemistry-on-the-complex has proven effective in the synthesis of heterodimetallic complexes,⁹ with applications in artificial photosynthesis,¹⁰ along with the synthesis and elaboration of ferrocenyl^{11,12} and porphyrin¹³ structures. These studies demonstrate the value of on-the-complex approaches in diversity-oriented synthesis, but also expose the need for further reaction development in this area. One illustrative example of chemistry-on-the-complex is highlighted in Figure 3.1b, where Davies and co-workers strategically utilized Suzuki–Miyaura cross-coupling reactions of pre-coordinated dimeric rhodium complexes toward the discovery of catalysts **3.1** used for the functionalization of unactivated C–H bonds.¹⁴ This case demonstrates the value of the general design, but also highlights that chemistry-on-the-complex is most often used to introduce one bond relative to a given functional group. Methods that allow for the formation of more than one bond using chemistry-on-the-complex remain more limited. Examples include azide cycloadditions (click chemistry) and well-established condensation reactions, resulting in products such as **3.2**¹⁵ and **3.3**¹⁶, respectively.

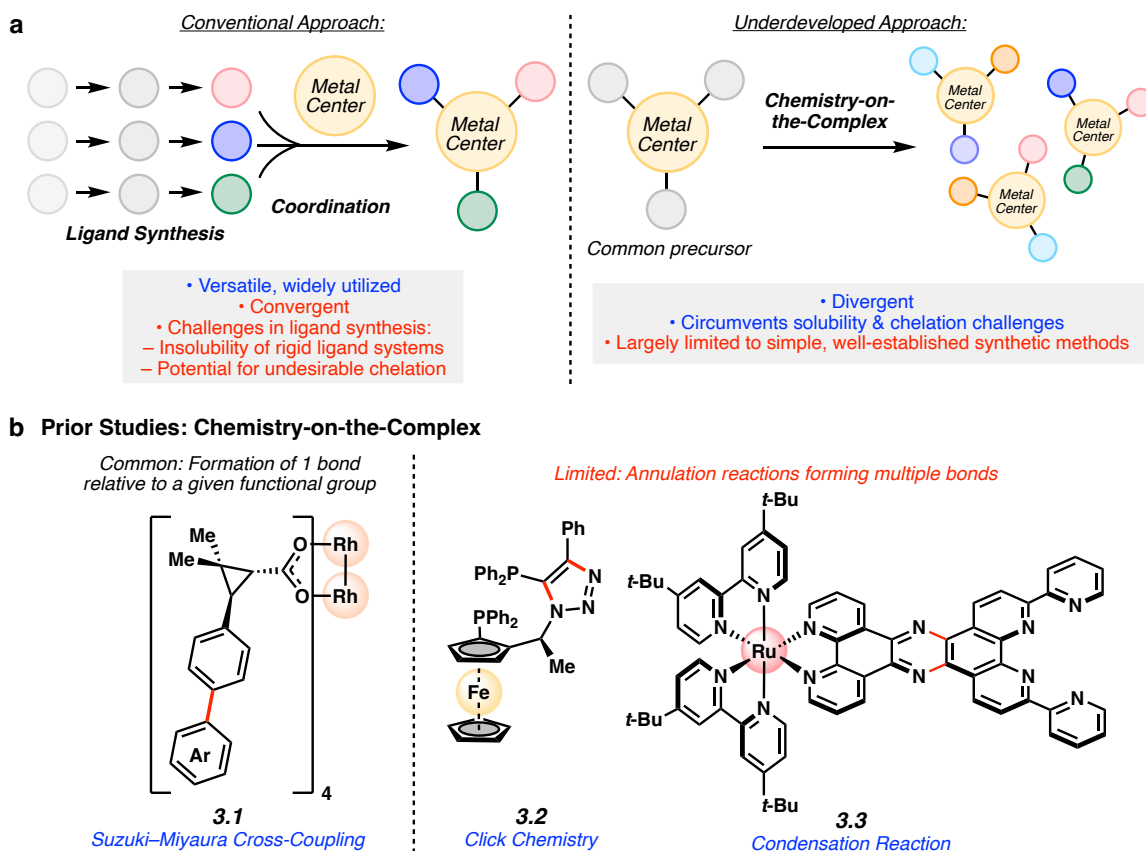
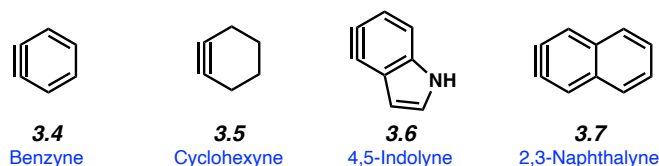


Figure 3.1. General synthetic approaches toward metal–ligand complexes. (a) Comparison of coordination chemistry and chemistry-on-the-complex. (b) Prior studies involving chemistry-on-the-complex. Me, methyl; Ph, phenyl; *t*-Bu, *tert*-butyl.

In considering the strategic generation of new ring systems on-the-complex, transient aryne intermediates provide a compelling entryway (Figure 3.2). Although arynes and related species were once avoided due to their high reactivity, they have recently gained popularity in a number of applications as useful synthons for building molecular complexity.^{17,18,19,20,21,22,23,24,25,26} For example, strained cyclic intermediates such as **3.4–3.7** (Figure 3.2a) have been used to access heterocycles of value to medicinal chemistry,²⁷ widely used phosphine ligands,^{28,29} agrochemicals,³⁰ and natural products,³¹ Nonetheless, the usage of

transient aryne intermediates in chemistry-on-the-complex approaches has remained limited, with only two reports in the literature to date.^{32,33} Both examples demonstrate the feasibility of aryne Diels–Alder trappings, but require that the organometallic complex bear a reactive diene ligand.

a In-Situ Generated Aryne and Cyclic Alkyne Intermediates as Valuable Synthons



- Form multiple bonds in one step
 - Mild generation possible
- Underexplored usage in synthesis of organometallic complexes

b This study: Platform for On-the-Complex Annulations using Arynes

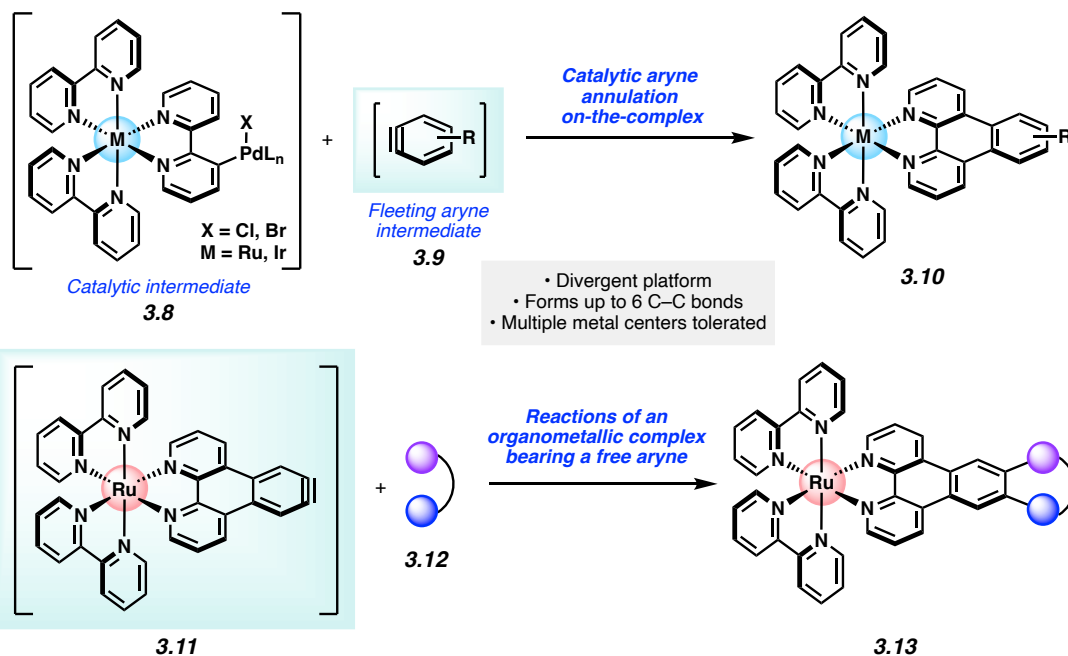


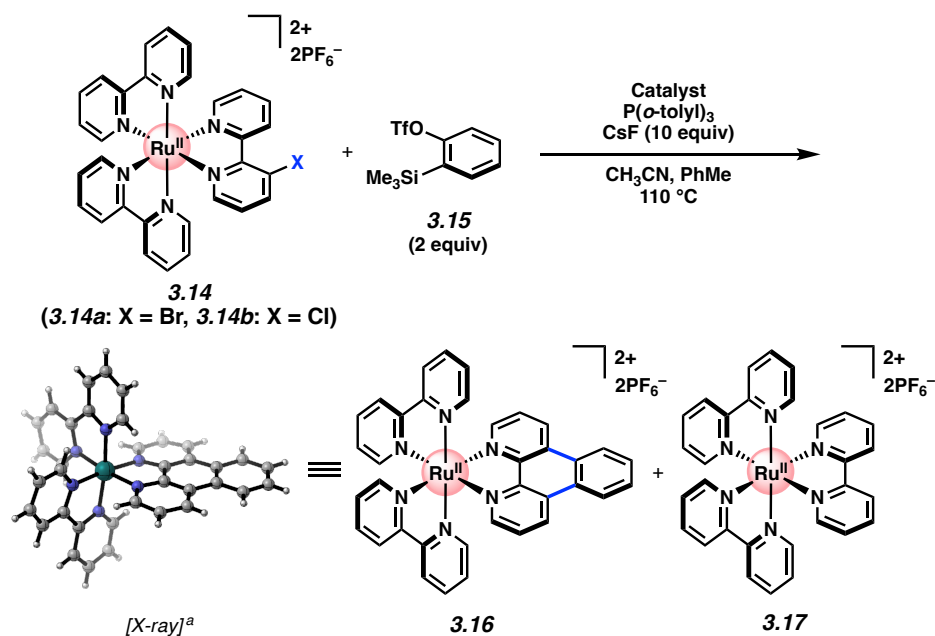
Figure 3.2. Arynes-on-the-complex approach to metal complexes. (a) Aryne and cyclic alkyne intermediates. (b) Our approach to the direct manipulation of polypyridyl metal complexes using arynes.

Herein, we show that intercepting arynes on-the-complex provides a versatile platform for the strategic manipulation of organometallic compounds. We evaluate this approach in the context of photoactive polypyridyl metal complexes, whose applications span various chemical, biological, and therapeutic disciplines^{34,35,36,37,38,39,40,41,42,43} (Figure 3.2b). We disclose two variants. In the first, readily available aryl halides are embedded in the ligand framework and enable palladium-catalyzed annulations with in situ generated arynes. This proceeds via the reaction of catalytically-generated bis(metallic) species **3.8** and fleeting aryne intermediates **3.9** to give annulated products **3.10**. In the other variant, compound **3.11**, a unique organometallic complex that bears an unligated aryne, is generated transiently. In situ trapping with cycloaddition partners **3.12** gives cycloadducts **3.13**. Our approaches enable the formation of multiple carbon–carbon (C–C) bonds in a single operation, offer a means to access functionalized polypyridyl metal complexes, underscore the utility of traditionally avoided aryne intermediates, and validate the aryne on-the-complex approach for accessing a diverse range of organometallic compounds.

3.3 Development of the Pd-Catalyzed On-the-Complex Aryne Reaction

To initiate our studies, we sought to identify a versatile functional group handle for aryne on-the-complex manipulations. We settled on the use of aryl halides, given their ready availability and their prevalence in transition metal-catalyzed reactions, and prepared halogenated Ru(bpy)₃ derivatives **3.14** (Figure 3.3 and see Section 3.8.2.1). Although many impressive examples of Pd-catalyzed transformations of arynes have now been reported^{44,45,46,47,48,49,50,51} use of this chemistry in the manipulation of organometallic complexes has remained unexplored. Inspired by Larock’s impressive annulation of biaryl halides,^{52,53} we

sought to perform a Pd-catalyzed annulation of **3.14** with commercially available benzyne precursor **3.15**. Initial attempts involved the use of Pd(dba)₂ and P(*o*-tolyl)₃, in the presence of CsF, but were met with limited success, as we observed formation of the desired π -extended adduct **3.16**, albeit in only 2% yield (entry 1). Instead, undesired protodehalogenation product, Ru(bpy)₃ (**3.17**), was observed in 48% yield. Efforts to prevent this dehalogenation pathway via reduced temperatures and rigorous exclusion of air and moisture proved unfruitful,⁵⁴ as did the use of other Pd⁰ sources such as Pd(PPh₃)₄ (e.g., entry 2). Alternatively, the use of Pd(OAc)₂ led to an improved 26% yield of the desired π -extended adduct **3.16** (entry 3). By increasing the catalyst and ligand loadings to 10 mol%, we observed a further increase in yield of **3.16** to 71%, with a reaction time of just 30 minutes (entry 4). Employing modified ratios of the co-solvents, acetonitrile and toluene, resulted in decreased reaction efficiency (entries 5 and 6).⁵⁵ Finally, shifting from brominated substrate **3.14a** to chlorinated derivative **3.14b** effectively shut down the dehalogenation pathway and provided the desired product in 78% yield (entry 7). We surmise that the conversion of **3.14** + **3.15** to **3.16** proceeds via initial oxidative addition and aryne formation occurring concomitantly (see Fig 3.2b, **3.8** and **3.9**), followed by aryne insertion, palladation, and reductive elimination.⁵⁶ It is worth noting that attempts to perform the analogous annulation on uncoordinated bromo- or chlorobipyridine ligands proved unproductive, potentially owing to *N,N*-chelation of palladium (see Section 3.8.2.2), thus highlighting an aforementioned benefit of on-the-complex chemistry.



Entry	Catalyst	X	Catalyst Loading	Ligand Loading	CH ₃ CN : PhMe	Time	Yield of 3.16 ^b	Yield of 3.17 ^b
1	Pd(dba) ₂	Br	5 mol%	5 mol%	1 : 1	2 h	2%	48%
2	Pd(PPh ₃) ₄	Br	5 mol%	5 mol%	1 : 1	2 h	2%	48%
3	Pd(OAc) ₂	Br	5 mol%	5 mol%	1 : 1	2 h	26%	24%
4	Pd(OAc) ₂	Br	10 mol%	10 mol%	1 : 1	30 min	71%	16%
5	Pd(OAc) ₂	Br	10 mol%	10 mol%	3 : 1	30 min	61%	19%
6	Pd(OAc) ₂	Br	10 mol%	10 mol%	1 : 3	30 min	35%	28%
7	Pd(OAc) ₂	Cl	10 mol%	10 mol%	1 : 1	30 min	78%	0%

Figure 3.3. Optimization studies for Pd-catalyzed annulation of benzyne onto Ru-polypyridyl complex **3.14**. ^a PF₆⁻ counterions have been removed from the X-ray crystal structure for clarity. ^b

Yields were determined by ¹H NMR analysis, using 1,3,5-trimethoxybenzene as an external standard. OTf, trifluoromethanesulfonate.

3.4 Scope of the Pd-Catalyzed Annulation

Variation of either the aryne or organometallic component was tolerated in the annulation, thus giving rise to a range of polypyridyl metal complexes in synthetically useful yields. With regard to the aryne component (Figure 3.4), benzyne adduct **3.16** was isolated in 81% yield (X = Cl) or 69% yield (X = Br) using standard column chromatography. Notably, the only available protocol to access the diazatriphenylene ligand found in **3.16** involves the use of hazardous reagents and exceptionally forcing conditions.⁵⁷ *N*-Me-4,5-indolyne could also be employed to deliver adduct **3.21** in 80% yield (X = Cl) or 75% yield (X = Br), thus demonstrating the expedient incorporation of a heterocycle into the π -framework of the metal complex. Naphthalynes were also deemed competent reaction partners, as judged by the formation of **3.22** and **3.23**. Prior routes to synthesize the naphthophenanthroline ligand present in **3.22** are lengthy or low yielding,⁵⁸ in part due to poor solubility of the free ligand.⁶

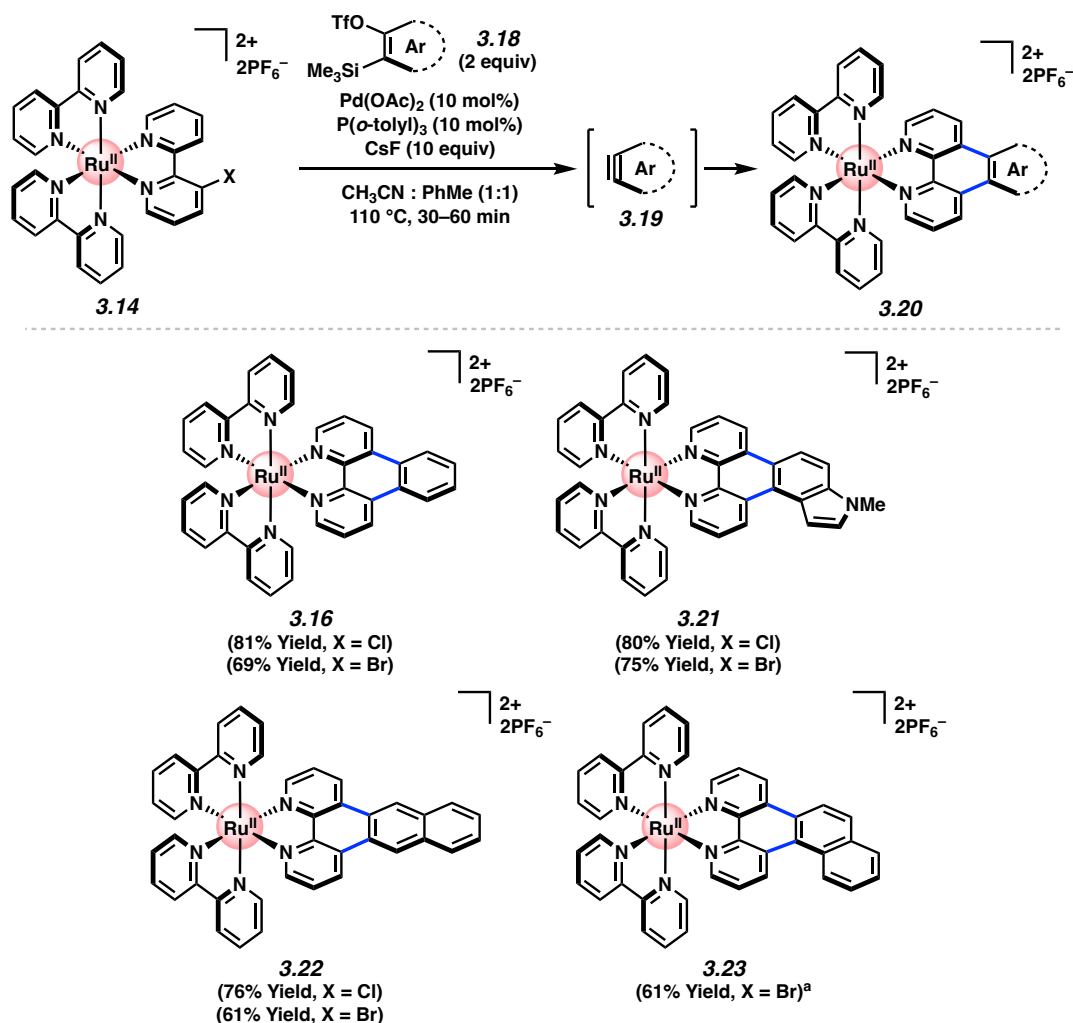


Figure 3.4. Aryne scope of the Pd-catalyzed aryne annulation. Yields shown reflect the average of two isolation experiments. ^a Significant decomposition was observed when X = Cl. Me, methyl; OTf, trifluoromethanesulfonate.

Although we primarily focused the current study on Ru complexes, we opted to probe the methodology in the context of Ir-centered polypyridyl complexes as well. Ir-centered polypyridyl complexes are prevalent in photochemistry,^{59,60,61,62} with documented value of extended π -conjugation in structure–property relationship studies.⁶³ We were gratified to find that the methodology could be used to access several Ir(ppy)₂bpy derivatives, as delineated in Figure 3.5.

Via the intermediacy of benzyne and 2,3-naphthalene, **3.26** and **3.27** could be accessed in 75% and 71% yield, respectively. Excellent yields were also observed upon varying the phenylpyridine ligands of the substrate, as isoquinolinyln annulation product **3.28** and tetrafluorinated adduct **3.29** could each be obtained in high yields from the corresponding chloride substrates.

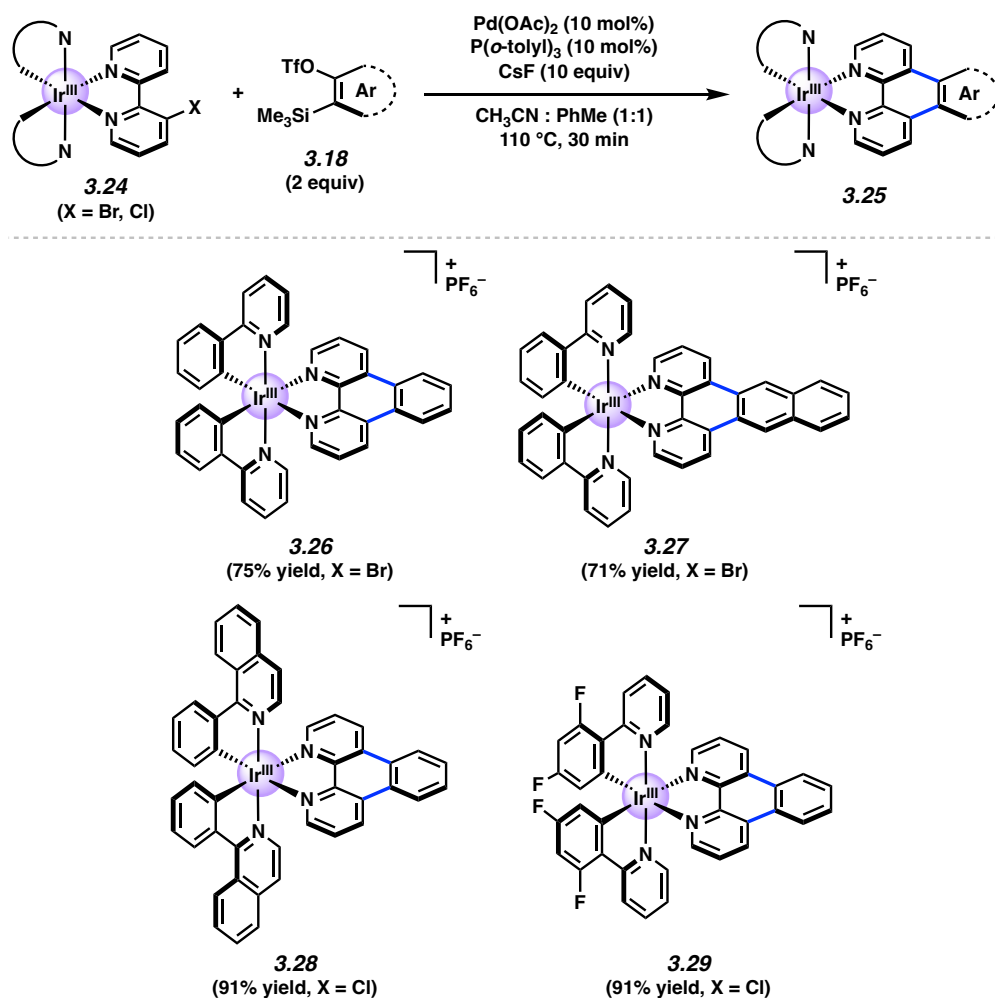


Figure 3.5. Pd-catalyzed aryne annulation of Ir-centered polypyridyl metal complexes. Yields shown reflect the average of two isolation experiments. OTf, trifluoromethanesulfonate.

To assess the possibility of carrying out multiple annulations on a given organometallic complex and test the limits of our aryne on-the-complex chemistry, we prepared Ru complexes **3.30** and **3.32**, bearing two or three chlorides, respectively (Figure 3.6). Subjecting these complexes independently to slightly modified reaction conditions delivered double and triple annulation products **3.31** and **3.33**, via the efficient formation of four or six new C–C bonds, respectively. Half of the bonds formed in either process arise from arene C–H functionalization.

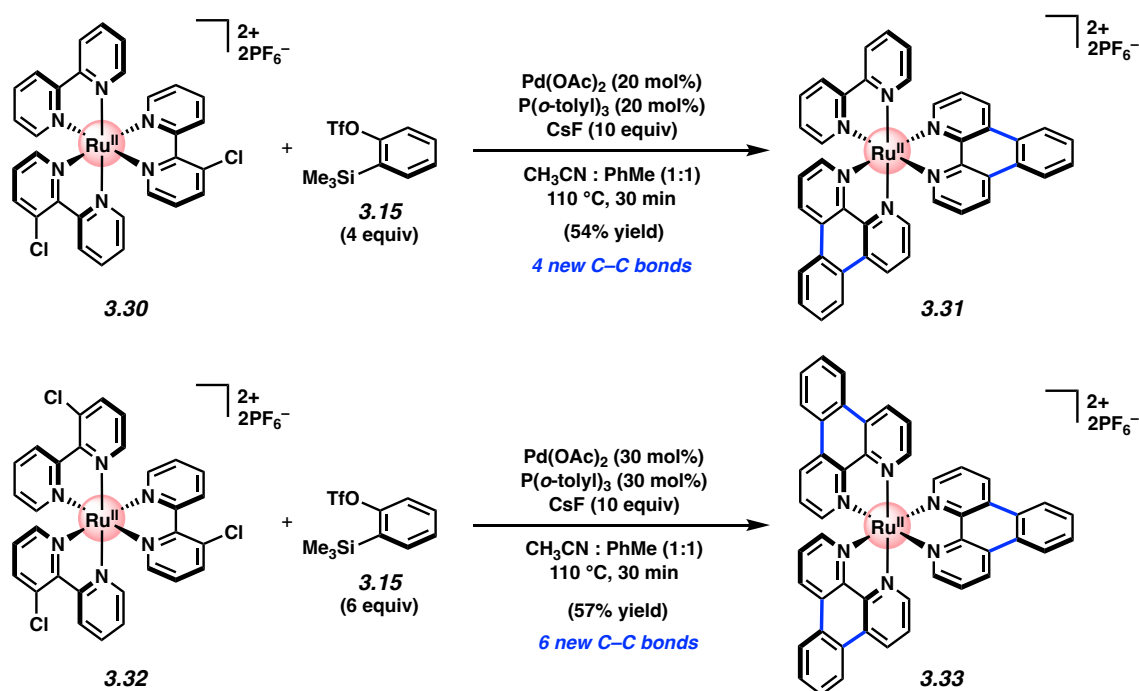


Figure 3.6. Pd-catalyzed aryne annulation at multiple sites of Ru complexes. Yields shown reflect the average of two isolation experiments. OTf, trifluoromethanesulfonate.

3.5 Generation and Trapping of an Organometallic Aryne

With an aryne-driven method for the annulation of organometallic complexes in hand, we sought to exploit this methodology to further extend the utility of aryne chemistry in accessing organometallic complexes. In particular, we sought to generate a free aryne on the

organometallic complex itself and trap it in cycloaddition reactions. In contrast to arynes coordinated directly to metal centers (e.g., Zr, Ti),⁶⁴ which are well-studied, free arynes embedded in an organometallic framework have remained elusive. Notably, previous efforts toward organometallic species bearing a free aryne have been met with difficulty,⁶⁵ and we therefore viewed the development of strategies in this area as an opportunity for advances in both aryne chemistry and chemistry on-the-complex. As shown in Figure 3.7, we targeted silyl triflate **3.35** as the suitable aryne precursor. Unfortunately, initial efforts to access **3.35** via the annulation of Ru-complex **3.14b** with bis(silyl triflate) **3.34**⁶⁶ proved unsuccessful. As a workaround, we employed methoxymethyl (MOM) ether **3.36**, prepared in two steps from commercially available materials, in the annulation reaction. After careful tuning of reaction conditions, adduct **3.37** could be generated in 80% yield with retention of both the MOM ether and trimethylsilyl group.⁶⁷ Subsequent cleavage of the MOM group, followed by triflation, delivered the desired silyl triflate **3.35** in 73% yield over two steps.

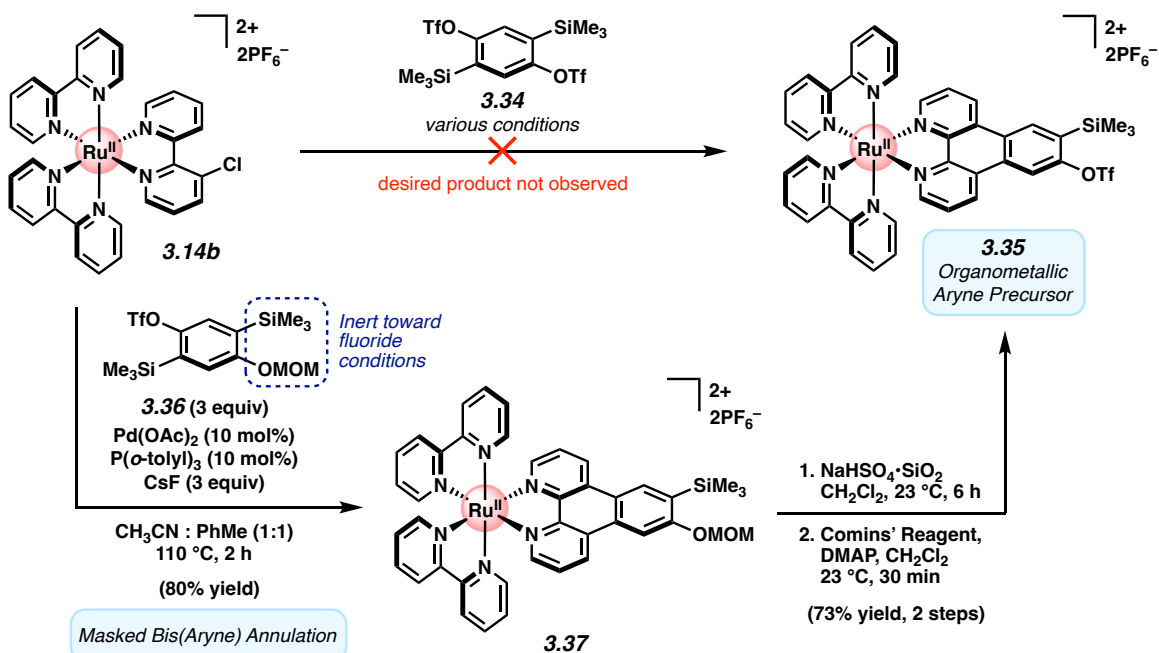


Figure 3.7. Synthesis of an organometallic aryne precursor via masked bis(aryne) annulation.

OTf, trifluoromethanesulfonate; MOM, methoxymethyl; DMAP, 4-dimethylaminopyridine.

As highlighted in Figure 3.8a, we found that silyl triflate **3.35** indeed served as a suitable precursor to aryne **3.11**, which, in turn, underwent cycloaddition in situ with trapping partners **3.12**. Trapping of **3.11** in the presence of 2,5-dimethylfuran (**3.38**) gave Diels–Alder adduct **3.41** in 50% yield. In addition, a formal [2+2] cycloaddition of **3.11** with diketene acetal **3.39** was achieved, generating adduct **3.42** bearing a carbonyl functional handle. Finally, trapping of **3.11** with tetraphenylcyclopentadienone (**3.40**) gave rise to the unusual adduct **3.43** via a Diels–Alder and subsequent cheletropic cycloreversion to extrude CO. Complex **3.43** displays an excited state lifetime that is roughly two-fold longer than that of Ru(bpy)₃ (see Section 3.8.3.1). Overall, the ability to access **3.41**–**3.43** from aryne precursor **3.35** showcases a free aryne being generated directly on an organometallic complex and demonstrates the utility of such species to access metal complexes with a diverse array of ring systems. Moreover, the results shown in Figures 3.7

and 3.8a provide an unconventional strategy to access unique coordination complexes via two iterations of aryne on-the-complex chemistry (i.e., **3.14b** → **3.37** and **3.35** → **3.41–3.43**), which collectively enables the formation of four C–C bonds in each organometallic complex made.

Lastly, we explored the possibility of further manipulating the interesting organometallic complex **3.43**. Geometry optimization of **3.43** via DFT calculations suggests that its four phenyl substituents are oriented perpendicular to the plane of the bipyridyl ligand (see Figure 3.8a and Section 3.8.4). We therefore questioned whether these rings could be joined through an oxidative cyclization reaction (Figure 3.8b). Gratifyingly, treatment of **3.43** with DDQ and triflic acid facilitated triple C–C bond formation to give **3.44** in 46% yield, which notably occurs without oxidation of the Ru center. This approach to **3.44** circumvents solubility challenges historically encountered in efforts to access similar π -extended complexes through off-the-complex protocols,⁶⁸ while providing access to a unique scaffold via a Scholl reaction⁶⁹ of a Ru-centered organometallic complex.⁷⁰

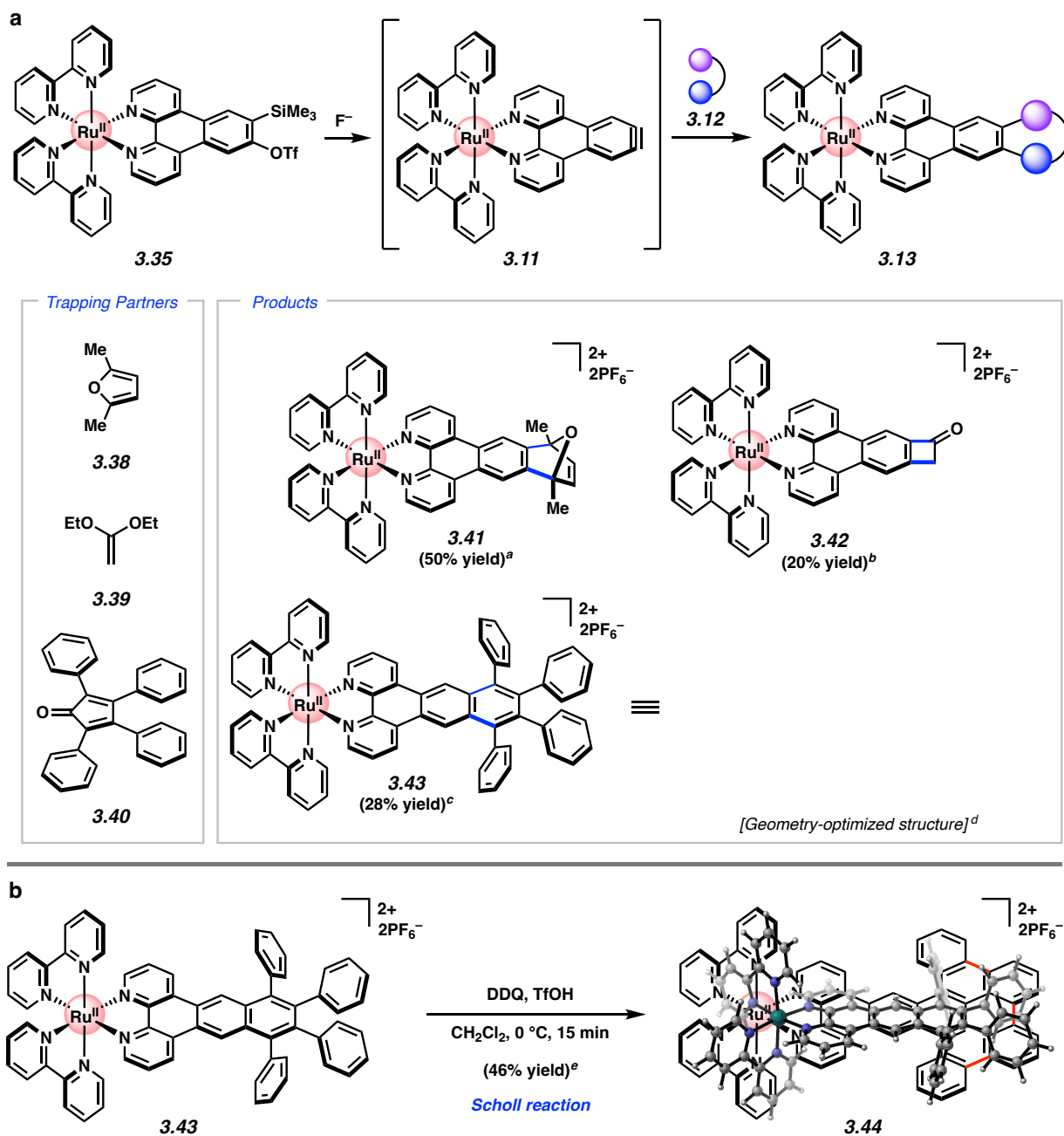


Figure 3.8. Mild generation and trapping of a Ru(II) aryne. (a) Cycloaddition reactions of organometallic aryne **3.11**. (b) Scholl reaction of **3.43** to give **3.44**. ^a Conditions: **3.35** (1 equiv), **3.38** (10 equiv), CsF (5 equiv), CH₃CN, 23 °C, 12 h. ^b Conditions: **3.35** (1 equiv), **3.39** (5 equiv), CsF (3 equiv), CH₃CN, 23 °C, 1.5 h; TFA. ^c Conditions: **3.35** (1 equiv), **3.40** (2 equiv), CsF (5 equiv), CH₃CN:CH₂Cl₂ (2:1), 50 °C, 1.5 h. ^d Geometry optimization of **3.43** (without

counterions) was performed using B3LYP/6-31G(d)/LANL2DZ/CPCM(MeCN). ^e Conditions:

3.43 (1 equiv), DDQ (20 equiv), CH₂Cl₂:TfOH (40:1), 0 °C, 15 min. OTf, trifluoromethanesulfonate; Me, methyl; Et, ethyl; DDQ, 2,3-dichloro-5,6-dicyano-1,4-benzoquinone.

3.6 Photophysical Studies

Although our primary objective was to develop the fundamental synthetic methodology described above, we also sought to identify and evaluate trends in photophysical properties of the products obtained. We deemed this particularly important given the broad impact of [Ru(bpy)₃]²⁺ (**3.17**) and other polypyridyl metal complexes in light-based applications, as mentioned earlier. Thus, we compared the photophysical properties of [Ru(bpy)₃]²⁺ (**3.17**) to that of annulation products obtained through our methodology. Examining luminescence quantum yield and molar extinction coefficients provided useful insights and revealed adducts **3.31** and **3.33** as being particularly interesting (Figure 3.9). First, a positive trend in luminescence quantum yield was observed from [Ru(bpy)₃]²⁺ (**3.17**) to bis(annulation) product **3.31** to tris(annulation) product **3.33**. In particular, **3.33** exhibits a high luminescence quantum yield of 24%, which is notably 2.5-fold greater than that of [Ru(bpy)₃]²⁺ (**3.17**) at 9.5%. A high luminescence quantum yield indicates more efficient formation of a reactive excited state upon photon absorption, and is desirable in such applications as luminescence sensing, solar energy conversion, and photoredox catalysis.³⁶ Additionally, **3.33** displays a higher molar extinction coefficient across the visible region (e.g., 23,500 mol⁻¹ cm⁻¹ at 452 nm) than that of [Ru(bpy)₃]²⁺ (**3.17**) (e.g., 18,100 mol⁻¹ cm⁻¹ at 452 nm), which suggests that it exhibits stronger ground state absorption of light in the visible region, a desirable quality in the aforementioned applications. All three compounds

exhibit a strong visible absorption peak at 452 nm, which is characteristic of the metal-to-ligand charge transfer (MLCT)-based luminescence that is typically observed in Ru(II) polypyridyl complexes. Of note, a shoulder also emerges in the region from 370–410 nm in compounds **3.31** and, more prominently, in **3.33**, and can likely be ascribed to delocalized $^1\pi-\pi^*$ transitions that are characteristic of other π -expansive ligands (e.g., phenazine derivatives).⁷¹ These findings bode well for the future use of our methodology to access complexes with promising and improved photophysical properties.

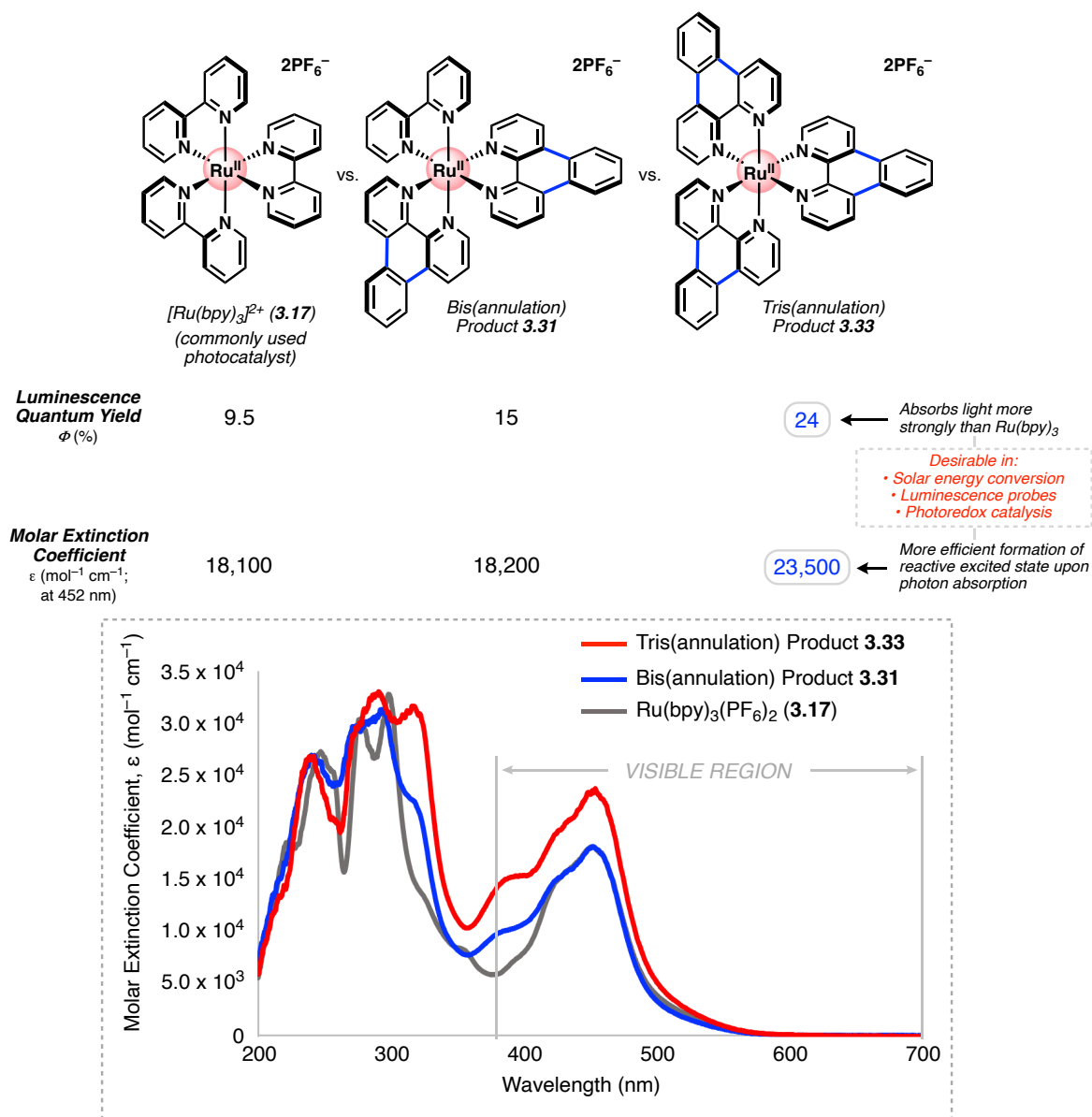


Figure 3.9. Photophysical studies of bis(annulation) product **3.31** and tris(annulation) product **3.33** relative to [Ru(bpy)₃]²⁺ (**3.17**). Evaluation of luminescence quantum yield (Φ , %) and molar extinction coefficient (ϵ , mol⁻¹ cm⁻¹). Experimental absorption spectra (molar extinction coefficient) are shown from 200–700 nm.

3.7 Conclusion

We have developed two variants of elusive aryne on-the-complex chemistry in the context of privileged polypyridyl metal complexes. In one variant, organometallic complexes bearing aryl halides undergo transition metal-catalyzed annulations with in situ, transiently-generated arynes. In the second version, an organometallic complex bearing a free aryne is intercepted in cycloaddition reactions to access complex scaffolds. Multiple C–C bonds (i.e., up to 6) can be formed in single synthetic operations, thus providing access to metal complexes bearing unique substitution patterns. These studies not only underscore the utility of traditionally avoided aryne intermediates and the value of on-the-complex aryne chemistry, but should also stimulate the development of on-the-complex reactions that enable transformations that are challenging by other means. Further studies will aim to evaluate and expand the utility of this methodology in accessing other valuable classes of organometallic complexes. From the standpoint of synthetic strategy, we hope these studies encourage the use of pre-coordinated ligands as synthons in the pursuit of complex organometallic architectures.

3.8 Experimental Section

3.8.1 Materials and Methods

Unless stated otherwise, reactions were conducted in flame-dried glassware under an atmosphere of nitrogen or argon and commercially obtained reagents were used as received. Anhydrous solvents were either freshly distilled or passed through activated alumina columns, unless otherwise stated. Reaction temperatures were controlled using an IKAmag temperature modulator, and unless stated otherwise, reactions were performed at room temperature (approximately 23 °C). Cesium fluoride (CsF), palladium(II) acetate (Pd(OAc)₂), and di- μ -chlorotetrakis[2-(2-pyridinyl-kN)phenyl-kC]diiridium(III) (**3.53**) were obtained from Strem Chemicals. Methyl iodide was obtained from Spectrum Chemical. Ruthenium(III) chloride trihydrate (**3.51**), 3-(trimethylsilyl)-2-naphthyl trifluoromethanesulfonate (**3.71**), 2,5-dibromohydroquinone (**3.63**), 2,5-dimethylfuran (**3.38**), and 2,3-dichloro-5,6-dicyano-1,4-benzoquinone (DDQ) were obtained from Combi-Blocks. 1-(trimethylsilyl)-2-naphthyl trifluoromethanesulfonate (**3.72**) was obtained from TCI America. Tri(*o*-tolyl)phosphine (P(*o*-tolyl)₃), Garg 4,5-indolyne precursor (**3.61**), *cis*-bis(2,2'-bipyridine)dichlororuthenium(II) hydrate (**3.50**), phosphorus trichloride (PCl₃), 1,1,1,3,3,3-hexamethyldisilazane (HMDS), bromomethyl methyl ether (MOMBr), tetraphenylcyclopentadienone (**3.40**), di- μ -chlorotetrakis[2-(1-isoquinolinyl-N)phenyl-C]diiridium(III) (**3.55**), and dichlorotetrakis[3,5-difluoro-2-(2-pyridinyl)phenyl]diiridium(III) (**3.57**) were obtained from Sigma-Aldrich. *N*-bromosuccinimide and *N*-chlorosuccinimide were obtained from Acros Organics. Phosphorus tribromide (PBr₃) and trifluoromethanesulfonic acid (TfOH) was obtained from Oakwood Chemical. 1,1'-Diethoxyethene (**3.39**) was obtained from Fluka. 2,2'-bipyridine *N*-oxide (**3.45**) was prepared according to literature procedures,⁷² and is also commercially available. Thin-layer

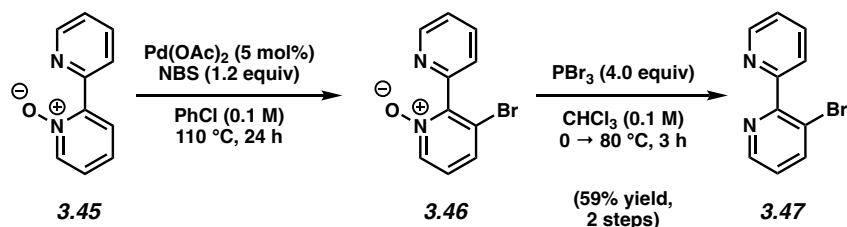
chromatography (TLC) was conducted with EMD gel 60 F254 pre-coated plates (0.25 mm for analytical chromatography and 0.50 mm for preparative chromatography) and visualized using UV. Silicycle Siliaflash P60 (particle size 0.040–0.063 mm) was used for flash column chromatography. ¹H NMR spectra were recorded on Bruker spectrometers (at 400, 500 and 600 MHz) and are reported relative to residual solvent signals. Data for ¹H NMR spectra are reported as follows: chemical shift (δ ppm), multiplicity, coupling constant (Hz), integration. Data for ¹³C NMR are reported in terms of chemical shift (at 100 Hz and 125 MHz). IR spectra were recorded on a Perkin-Elmer UATR Two FT-IR spectrometer and are reported in terms of frequency absorption (cm^{-1}). ESI-TOF measurements were carried out in positive ionization mode on a Waters LCT-Premier XE Time of Flight Instrument controlled by MassLynx 3.1 software (Waters Corporation, Milford MA). The instrument was equipped with the Multi Mode Ionization source operated in the electrospray mode. A solution of Leucine Enkephalin (Sigma Chemical, L9133) was used in the Lock-Spray to obtain accurate mass measurements. Samples were infused using direct loop injection on a Waters Acquity UPLC system. GC-MS measurements were carried out using an Agilent Model 7693 Autosampler, 7890B Gas Chromatograph, and 7250 Q-TOF Mass Selective Detector in the Electron Ionization mode. Sample injection was carried out in split mode with inlet temperature set to 280 °C. Separation was carried out on an Agilent HP5-MS column with dimensions 30m x 250 μm x 0.25 μm . Ultra High Purity Grade He (Airgas) was used as carrier gas with the flow set to 1.1 mL/min in constant flow mode. The initial oven temperature was set to 70 °C for 1 min followed by a 20 °C/min ramp to a final temperature of 300 °C which was maintained for 4 min. A 3.0 min solvent delay was used. EI energy was set to 70 eV. The MSD was set to scan the 50–500 m/z

range. Data collection and analysis were performed using Mass Hunter Acquisition and Qualitative Analysis software (Agilent).

3.8.2 Experimental Procedures

3.8.2.1 Synthesis of Halobipyridine Organometallic Complexes

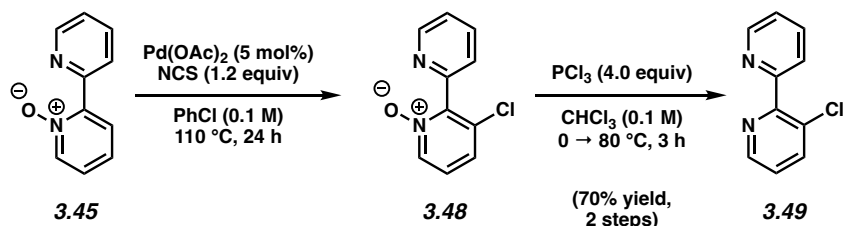
Note: The following procedures for the synthesis of halobipyridines were adapted from a published literature protocol⁵ to facilitate gram-scale synthesis.



Bromobipyridine 3.47. To a flask containing 2,2'-bipyridyl *N*-oxide (**3.45**, 1.00 g, 5.81 mmol), $\text{Pd}(\text{OAc})_2$ (65.4 mg, 0.291 mmol, 5 mol%), and *N*-Bromosuccinimide (1.24 g, 6.97 mmol, 1.2 equiv) was added PhCl (58 mL, 0.10 M). This suspension was then heated to $110\text{ }^\circ\text{C}$ and stirred for 24 h. The reaction was then allowed to cool to $23\text{ }^\circ\text{C}$, at which point it was transferred with CH_2Cl_2 (30 mL) to a separatory funnel containing 1.0 M saturated aqueous NaOH (30 mL). The layers were separated and the aqueous layer was extracted with CH_2Cl_2 (3 x 30 mL). The combined organic layers were then dried over Na_2SO_4 , filtered, and concentrated under reduced pressure to afford the corresponding bromobipyridine *N*-oxide **3.46** as a brown oil. This was carried forward without further purification.

The crude oil was dissolved in CHCl_3 (50 mL, 0.10 M) and cooled to $0\text{ }^\circ\text{C}$. To this stirred solution was added PBr_3 (2.0 mL, 21.0 mmol, 4.0 equiv) dropwise over 8 min. The cooling bath was then removed and the reaction was warmed to $80\text{ }^\circ\text{C}$ and stirred for 3 h. It was then allowed

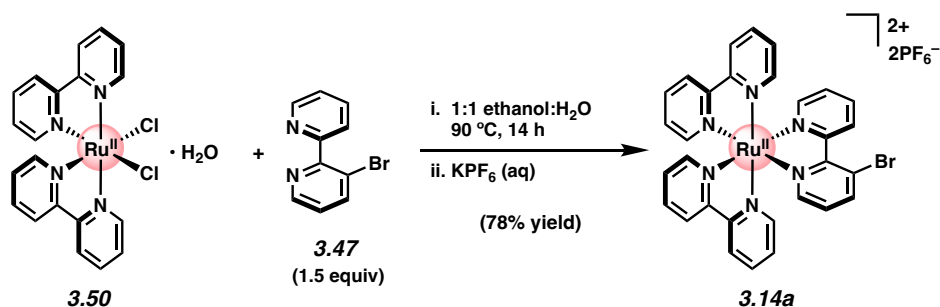
to cool to 23 °C before being cooled further to 0 °C. The reaction was then quenched by addition of aqueous NaOH (1.0 M, 40 mL) over 1 min before being warmed to 23 °C. 6.0 M NaOH (40 mL) was then added in one portion and the mixture was stirred at 23 °C for 5 min before being transferred to a separatory funnel. The layers were separated and the aqueous layer was extracted with CH₂Cl₂ (3 x 50 mL). The combined organic layers were then dried over Na₂SO₄, filtered, and concentrated under reduced pressure. The resulting oil was purified by flash chromatography (5% Et₃N in 9:1 hexanes:EtOAc → 5% Et₃N in 7:2 hexanes:EtOAc) using silica gel neutralized with Et₃N to afford bromobipyridine **3.47** as a beige solid (800 mg, 59% yield over two steps). **Bromobipyridine 3.47**: *R_f* 0.25 (3:1 EtOAc:Hexanes); ¹H NMR (500 MHz, CDCl₃): δ 8.75 (dd, *J* = 4.9, 0.8, 1H), 8.66 (d, *J* = 4.6, 1H), 8.03 (d, *J* = 7.9, 1H), 7.83 (td, *J* = 7.6, 1.4, 1H), 7.73 (d, *J* = 7.7, 1H), 7.36 (dd, *J* = 7.6, 4.9, 1H), 7.22 (dd, *J* = 8.3, 4.7, 1H). Spectral data match those previously reported in the literature.⁵



Chlorobipyridine 3.49. To a flask containing 2,2'-bipyridyl *N*-oxide (**3.45**, 3.81 g, 22.1 mmol), Pd(OAc)₂ (248 mg, 1.11 mmol, 5 mol%), and *N*-chlorosuccinimide (3.55 g, 26.6 mmol, 1.2 equiv) was added PhCl (220 mL, 0.10 M). This suspension was then heated to 110 °C and stirred for 24 h. The reaction mixture was then allowed to cool to 23 °C, at which point it was transferred with CH₂Cl₂ (15 mL) to a separatory funnel containing aqueous NaOH (1.0 M, 100 mL). The layers were separated and the aqueous layer was extracted with CH₂Cl₂ (3 x 60 mL). The combined organic layers were then dried over Na₂SO₄, filtered, and concentrated under

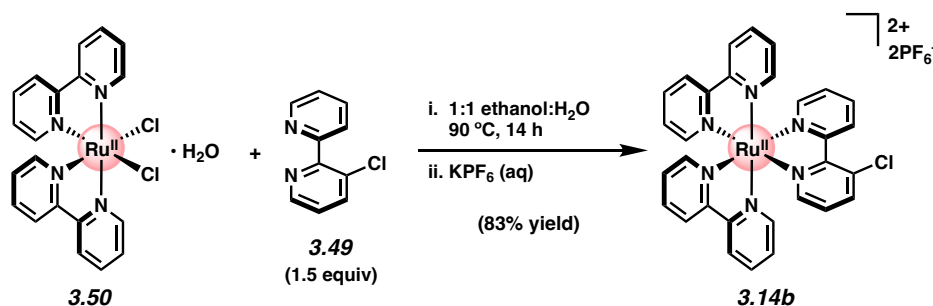
reduced pressure to afford the corresponding chlorobipyridine *N*-oxide **3.48** as a brown oil. This was carried forward without further purification.

The crude oil was dissolved in CHCl₃ (200 mL, 0.10 M) and cooled to 0 °C. To this stirred solution was added PCl₃ (7.28 mL, 83.2 mmol, 4.0 equiv) dropwise at 0 °C over 12 min. The cooling bath was then removed and the reaction was warmed to 80 °C and stirred for 3 h. It was then allowed to cool to 23 °C before being cooled further to 0 °C. The reaction was then quenched by addition of aqueous NaOH (1.0 M, 100 mL) over 2 min before being warmed to 23 °C. Aqueous NaOH (6.0 M, 50 mL) was then added in one portion and the mixture was stirred at 23 °C for 5 min before being transferred to a separatory funnel. The layers were separated and the aqueous layer was extracted with CH₂Cl₂ (3 x 100 mL). The combined organic layers were then dried over Na₂SO₄, filtered, and concentrated under reduced pressure. The resulting brown oil was purified by flash chromatography (5% Et₃N in 3:1 hexanes:EtOAc → 5% Et₃N in 1:1 hexanes:EtOAc → 5% Et₃N in 1:3 hexanes:EtOAc) using silica gel neutralized with Et₃N to afford chlorobipyridine **3.49** as an off-white solid (2.96 g, 70% yield over two steps). **Chlorobipyridine 3.49**: R_f 0.30 (3:1 EtOAc:hexanes); ¹H NMR (400 MHz, CD₃CN): δ 8.77 (d, *J* = 4.8, 1H), 8.64 (dd, *J* = 4.8, 1.4, 1H), 7.83 (td, *J* = 8.7, 1.4, 2H), 7.77 (d, *J* = 7.9, 1H), 7.36 (ddd, *J* = 7.7, 3.9, 1.3, 1H), 7.31 (dd, *J* = 8.31, 4.7, 1H). Spectral data match those previously reported in the literature.⁵



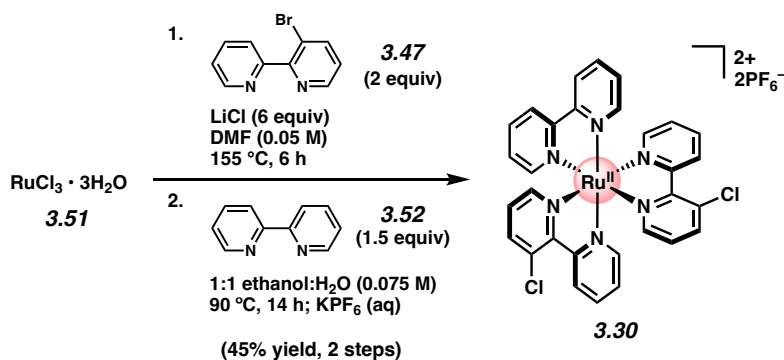
Bromo-Ru(bpy)₃[PF₆]₂ 3.14a. To a flask containing *cis*-bis(2,2'-bipyridine)dichlororuthenium(II) hydrate (**3.50**, 899 mg, 1.86 mmol, 1.0 equiv) and bromobipyridine **3.47** (667 mg, 2.84 mmol, 1.5 equiv) was added EtOH (120 mL) and H₂O (120 mL). The flask was topped with an air condenser and the system placed under N₂. The reaction was heated to 90 °C and stirred for 14 h, during which the solution changed in color from deep purple to red. The reaction was then allowed to cool to 23 °C before saturated aqueous KPF₆ (50 mL) was added over 1 min while stirring to produce a red precipitate. The mixture was then filtered over a pad of celite (packed with Et₂O), washed with Et₂O (3 x 20 mL), and the filtrate was discarded. The remaining solid residue was then redissolved in CH₃CN (90 mL) and passed through the same celite plug. The resulting deep red filtrate was then concentrated under reduced pressure and then passed through a pad of neutral alumina with CH₃CN (250 mL). The red band was collected and concentrated under reduced pressure to afford a red semi-solid. This material was then recrystallized from 1:1 MeOH:H₂O (10 mL) and the resulting red crystals were washed with 1:1 MeOH:H₂O (2 x 2 mL, cooled to 0 °C) and dried under reduced pressure (<1 torr) for 12 h at 60 °C to afford bromo-Ru(bpy)₃[PF₆]₂ **3.14a** as a red crystalline solid (1.36 g, 78% yield based on anhydrous **3.50**). **Bromo-Ru(bpy)₃[PF₆]₂ 3.14a:** mp >250 °C; R_f 0.64 (7:2:1 MeCN:H₂O:sat. aq. KNO₃); ¹H NMR (400 MHz, CD₃CN): δ 9.56 (dq, *J* = 8.6, 0.7, 1H), 8.49 (dd, *J* = 8.3, 3.4, 4H), 8.30 (dd, *J* = 8.3, 1.3, 1H), 8.10–8.02 (m, 5H), 7.84 (dd, *J* = 5.5, 1.4, 2H), 7.76 (dq, *J* = 5.7, 0.7, 1H), 7.70 (dq, *J* = 5.7, 0.7, 1H), 7.68–7.63 (m, 2H); ¹³C NMR (125 MHz,

CD₃CN, 26 of 30 signals observed): δ 157.79, 157.78, 157.69, 157.65, 157.5, 154.9, 153.2, 152.8, 152.7, 152.5, 152.3, 145.7, 138.93, 138.91, 138.90, 138.0, 129.3, 128.7, 128.64, 128.58, 128.55, 128.46, 127.9, 125.29, 125.28, 121.8; IR (film): 1606, 1467, 1447, 1425, 837, 762 cm⁻¹; HR-ESI-MS (m/z) [M – PF₆]⁺ calcd for C₃₀H₂₃N₆BrPF₆Ru⁺, 792.98529; found 792.9849.



Chloro-Ru(bpy)₃[PF₆]₂ 3.14b. To a flask containing *cis*-bis(2,2'-bipyridine)dichlororuthenium(II) hydrate (**3.50**, 4.00 g, 8.26 mmol, 1.0 equiv) and chlorobipyridine **3.49** (2.36 g, 12.4 mmol, 1.5 equiv) was added EtOH (330 mL) and H₂O (330 mL). The flask was topped with an air condenser and the system placed under N₂. The reaction was heated to 90 °C and stirred for 14 h, during which the solution changed in color from deep purple to red. The reaction was then allowed to cool to 23 °C before saturated aqueous KPF₆ (300 mL) was added over 5 min while stirring to produce a red precipitate. The mixture was then filtered over a pad of celite (packed with Et₂O), washed with Et₂O (3 x 50 mL), and the filtrate was discarded. The remaining solid residue was redissolved in CH₃CN (200 mL) and passed through the same celite plug. The resulting deep red filtrate was then concentrated under reduced pressure and then passed through a pad of neutral alumina with CH₃CN (600 mL). The red band was collected and concentrated under reduced pressure to afford a red semi-solid. The purified material was then divided into three portions and each was recrystallized from 1:1 MeOH:H₂O (10 mL) and the resulting red crystals were washed with 1:1 MeOH:H₂O (2 x 2 mL for each

portion, cooled to 0 °C) and dried under reduced pressure (<1 torr) for 12 h at 50 °C to afford chloro-Ru(bpy)₃[PF₆]₂ **3.14b** as a red crystalline solid (6.13 g, 83% yield based on anhydrous **3.50**). **Chloro-Ru(bpy)₃[PF₆]₂ 3.14b**: mp >250 °C; R_f 0.60 (7:2:1 MeCN:H₂O:sat. aq. KNO₃); ¹H NMR (400 MHz, CD₃CN): δ 9.41 (dq, *J* = 8.5, 0.8, 1H), 8.50 (dd, *J* = 8.2, 1.0, 4H), 8.12–8.02 (m, 6H), 7.86 (dq, *J* = 5.6, 0.7, 1H), 7.81 (dd, *J* = 5.5, 1.3, 1H), 7.76 (dq, *J* = 5.6, 0.7, 1H), 7.70 (dq, *J* = 5.6, 0.7, 1H), 7.68–7.64 (m, 2H), 7.44–7.35 (m, 5H), 7.31 (dd, *J* = 8.4, 5.5, 1H); ¹³C NMR (125 MHz, CD₃CN, 24 of 30 signals observed) δ 157.80, 157.78, 157.71, 157.67, 157.1, 154.0, 153.2, 152.8, 152.47, 152.45, 151.9, 142.0, 138.94, 138.91, 138.4, 134.2, 129.4, 128.7, 128.65, 128.61, 128.57, 128.5, 128.1, 125.30, 125.29; IR (film): 1604, 1467, 1447, 1427, 1243, 837 cm⁻¹; HR-ESI-MS (*m/z*) [M – PF₆]⁺ calcd for C₃₀H₂₃N₆ClPF₆Ru⁺, 749.03580; found 749.0350.



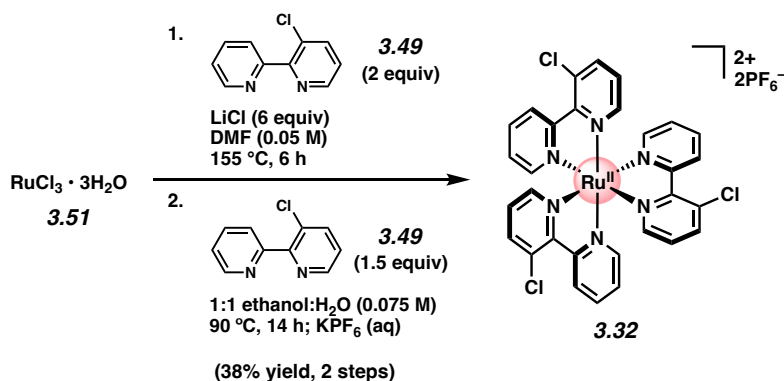
Bis(chloro)-Ru(bpy)₃[PF₆]₂ 3.30. To a flask containing ruthenium(III) chloride trihydrate (**3.51**, 309 mg, 1.18 mmol, 1.0 equiv), bromobipyridine **3.47** (559 mg, 2.38 mmol, 2.0 equiv), and LiCl (301 mg, 7.10 mmol, 6.0 equiv) was added DMF (25 mL, 0.05 M). The flask was topped with an air condenser and the system placed under N₂. The reaction was heated to 155 °C and stirred for 6 h. The reaction mixture was then allowed to cool to 23 °C before acetone (25 mL) was added in one portion and the solution was added dropwise to vigorously stirring Et₂O (300 mL). The

resultant mixture was then filtered over a pad of celite (packed with Et₂O) and washed with Et₂O (3 x 30 mL). The solid residue was then redissolved in CH₂Cl₂ (200 mL) and concentrated under reduced pressure to afford a deep purple solid. This was carried forward without further purification.

To the crude solid was added 2,2'-bipyridine (**3.52**, 281 mg, 1.80 mmol, 1.5 equiv), EtOH (80 mL), and H₂O (80 mL) sequentially. The flask was topped with an air condenser and the system placed under N₂. The reaction was heated to 90 °C and stirred for 14 h, during which the solution changed in color from deep purple to red. The reaction was then allowed to cool to 23 °C before saturated aqueous KPF₆ (70 mL) was added over 2 min while stirring to produce a red precipitate. The mixture was then filtered over a pad of celite (packed with Et₂O), washed with Et₂O (3 x 30 mL), and the solid residue was redissolved in MeCN (200 mL). The deep red filtrate was then concentrated under reduced pressure and then purified by flash chromatography on neutral alumina (100% MeCN). The red band was collected and concentrated under reduced pressure to afford a red semi-solid. This material was then recrystallized from 1:1 MeOH:H₂O (5 mL) and the resulting red crystals were washed with 1:1 MeOH:H₂O (2 x 2 mL, cooled to 0 °C) and dried under reduced pressure (<1 torr) for 12 h at 60 °C to afford bis(chloro)-Ru(bpy)₃[PF₆]₂ **3.30** as a red crystalline solid (491 mg, 45% yield over 2 steps). **Bis(chloro)-Ru(bpy)₃[PF₆]₂ 3.30**: mp >250 °C; R_f 0.63 (7:2:1 MeCN:H₂O:sat. aq. KNO₃); ¹H NMR (500 MHz, CD₃CN): δ 9.43–9.39 (m, 2H), 8.50 (d, *J* = 8.2, 2H), 8.13–8.04 (m, 6H), 7.88 (dq, *J* = 5.6, 0.7, 1H), 7.85–7.82 (m, 1H), 7.81–7.77 (m, 1H), 7.75 (ddd, *J* = 5.6, 3.7, 1.4, 1H) 7.71 (app. d, *J* = 5.6, 1H), 7.67–7.63 (m, 1H), 7.45–7.37 (m, 4H), 7.34–7.28 (m, 2H); ¹³C NMR (125 MHz, CD₃CN) δ 157.59, 157.57, 157.56, 157.5, 156.92, 156.85, 156.81, 153.85, 153.78, 153.75, 153.3, 153.04, 153.01, 152.64, 152.63, 152.03, 152.02, 151.74, 151.71, 142.24, 142.22, 142.21, 139.13, 139.11,

139.10, 139.09, 138.58, 138.57, 134.32, 134.29, 129.53, 129.51, 128.8, 128.72, 128.67, 128.61, 128.60, 128.5, 128.2, 128.1, 128.0, 125.41, 125.39, 125.37; IR (film): 1603, 1468, 1447, 1419, 1214, 835, 797 cm^{-1} ; HR-ESI-MS (m/z) $[\text{M} - \text{PF}_6]^+$ calcd for $\text{C}_{30}\text{H}_{22}\text{N}_6\text{Cl}_2\text{PF}_6\text{Ru}^+$, 782.99683; found 782.9984.

Note: Though unexpected, it is postulated that LiCl facilitates chloro-debromination during the reaction. 3.30 was obtained as a mixture of geometric isomers; these data represent empirically observed chemical shifts from the ^{13}C NMR spectrum.

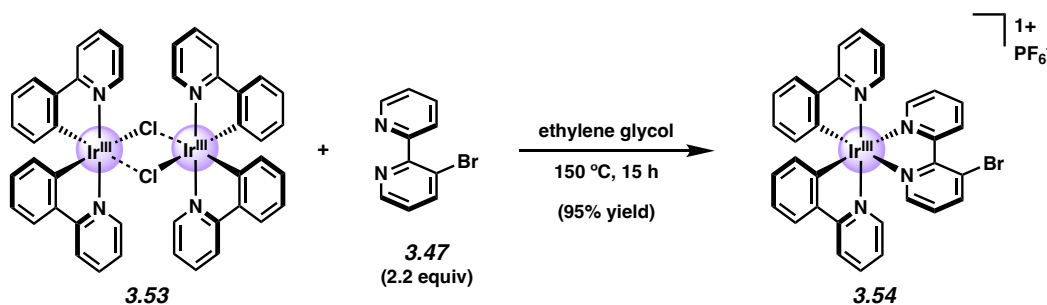


Tris(chloro)-Ru(bpy) $_3$ [PF $_6$] $_2$ 3.32. To a flask containing ruthenium(III) chloride trihydrate (**3.51**, 401 mg, 1.54 mmol, 1.0 equiv), chlorobipyridine **3.49** (584 mg, 3.07 mmol, 2.0 equiv), and LiCl (390 mg, 9.21 mmol, 6.0 equiv) was added DMF (30 mL, 0.05 M). The flask was topped with an air condenser and the system placed under N_2 . The reaction was heated to 155°C and stirred for 6 h. The reaction mixture was then allowed to cool to 23°C before acetone (35 mL) was added in one portion and the mixture was added dropwise to vigorously stirring Et_2O (300 mL). The resultant mixture was then filtered over a pad of celite (packed with Et_2O) and washed with Et_2O (4 x 30 mL). The solid residue was then redissolved in CH_2Cl_2 (250 mL) and

concentrated under reduced pressure to afford a deep purple solid. This was carried forward without further purification.

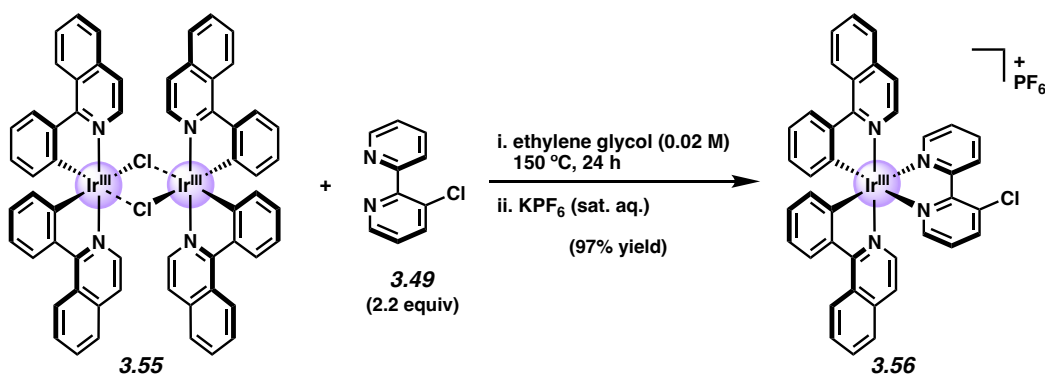
To the crude solid material was added chlorobipyridine **3.49** (443 mg, 2.32 mmol, 1.5 equiv), EtOH (100 mL), and H₂O (100 mL) sequentially. The flask was topped with an air condenser and the system placed under N₂. The reaction was heated to 90°C and stirred for 14 h, during which the solution changed in color from deep purple to red. The reaction was then allowed to cool to 23 °C before saturated aqueous KPF₆ (70 mL) was added over 2 min while stirring to produce a red precipitate. The mixture was then filtered over a pad of celite (packed with Et₂O), washed with Et₂O (3 x 30 mL), and the solid residue was redissolved in MeCN (250 mL). The deep red filtrate was then concentrated under reduced pressure and then purified by flash chromatography on neutral alumina (100% MeCN). The red band was collected and concentrated under reduced pressure to afford a red semi-solid. This material was then recrystallized from 1:1 MeOH:H₂O (5 mL) and the resulting red crystals were washed with 1:1 MeOH:H₂O (2 x 2 mL, cooled to 0 °C) and dried under reduced pressure (<1 torr) for 12 h at 60 °C to afford tris(chloro)-Ru(bpy)₃[PF₆]₂ **3.32** as a red crystalline solid (567 mg, 38% yield over 2 steps). **Tris(chloro)-Ru(bpy)₃[PF₆]₂ 3.32**: mp >250 °C; R_f 0.69 (7:2:1 MeCN:H₂O:sat. aq. KNO₃); ¹H NMR (500 MHz, CD₃CN): δ 9.41 (d, *J* = 8.5, 3H), 8.14–8.06 (m, 6H), 7.85–7.72 (m, 6H), 7.41–7.38 (qd, *J* = 6.8, 1.3, 3H), 7.35–7.28 (m, 3H); ¹³C NMR (125 MHz, CD₃CN) δ 156.7, 156.5, 153.63, 153.62, 153.59, 153.20, 153.18, 151.89, 151.87, 142.40, 142.38, 142.37, 138.74, 138.71, 134.38, 134.36, 134.35, 134.34, 129.61, 129.60, 129.57, 128.83, 128.79, 128.70, 128.66, 128.3, 128.2, 128.13, 128.07; IR (film): 1473, 1428, 1420, 1215, 837, 797 cm⁻¹; HR-ESI-MS (*m/z*) [M – PF₆]⁺ calcd for C₃₀H₂₁N₆Cl₃PF₆Ru⁺, 816.95786; found 816.9572.

Note: **3.32** was obtained as a mixture of geometric isomers. These data represent empirically observed chemical shifts from the ^{13}C NMR spectrum.



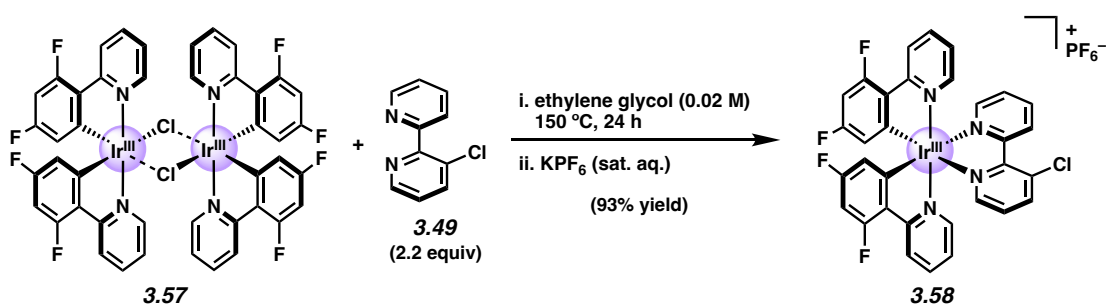
Bromo-Ir(ppy)₂bpy 3.54. To a 20 mL scintillation vial was added di- μ -chlorotetrakis[2-(2-pyridinyl-kN)phenyl-kC]diiridium(III) (**3.53**, 100.0 mg, 0.093 mmol, 1.0 equiv) in a glovebox. The vial was removed from the glovebox and placed under nitrogen. To a separate 1-dram vial was added bromobipyridine **3.47** (48.2 mg, 0.205 mmol, 2.2 equiv) and ethylene glycol (4.0 mL, 0.023 M), and the mixture was then sparged with N_2 for 15 minutes. This solution was then transferred to the vial containing **3.53**. The septa cap was replaced with a Teflon-lined screw cap and the reaction was transferred to an Al-block and stirred at 150 °C for 15 h. After cooling to 23 °C, the reaction was transferred to a separatory funnel containing deionized water (48 mL). The aqueous phase was washed with hexanes (2 x 24 mL) and then Et_2O (24 mL). The aqueous layer was then heated to 85 °C for 5 minutes to evaporate any remaining organic solvent. The solution cooled to 23 °C, and then then aqueous NH_4PF_6 (0.27 M, 12 mL) was added, resulting in an orange-yellow precipitate. This mixture was filtered through a plug of celite and washed with water (20 mL) to remove ethylene glycol. The celite pad was then eluted with acetonitrile (50 mL) to redissolve the product, and the resulting filtrate was collected and concentrated under reduced pressure to afford bromo-Ir(ppy)₂bpy complex **3.54** as a dark yellow solid (156 mg, 95% yield). **Bromo-Ir(ppy)₂bpy 3.54.** R_f 0.60 (7:2:1 $\text{CH}_3\text{CN}:\text{H}_2\text{O}:\text{sat. aq. KNO}_3$); ^1H NMR (500

MHz, CD₃CN): δ 9.42 (dt, $J = 8.3, 1.6, 0.9, 1\text{H}$), 8.36 (dd, $J = 8.4, 1.4, 1\text{H}$), 8.13 (ddd, $J = 8.7, 7.9, 1.8, 1\text{H}$), 8.09–8.04 (m, 4H), 7.88–7.83 (m, 2H), 7.78 (ddd, $J = 7.9, 3.3, 1.1, 2\text{H}$), 7.73–7.70 (m, 2H), 7.49 (ddd, $J = 7.7, 5.5, 1.2, 1\text{H}$), 7.29 (dd, $J = 8.6, 5.4, 1\text{H}$), 7.06–7.01 (m, 4H), 6.90 (tdd, $J = 7.4, 2.4, 1.3, 2\text{H}$), 6.22 (ddd, $J = 7.6, 4.6, 1.0, 2\text{H}$); ¹³C NMR (125 MHz, CD₃CN) δ 168.6, 168.5, 156.2, 154.9, 152.6, 151.7, 151.5, 150.83, 150.79, 150.7, 147.5, 145.4, 145.3, 140.1, 140.0, 139.8, 132.9, 132.8, 131.9, 131.8, 130.2, 129.9, 129.5, 126.3, 124.9, 124.8, 124.1, 124.0, 123.8, 123.0, 121.3, 121.2; IR (film): 3064, 2921, 1607, 1478, 1420, 1342 cm⁻¹; HR-ESI-MS (m/z) [M – PF₆]⁺ calcd for C₃₂H₂₃BrN₄Ir⁺, 735.0735; found 735.0738.



Isoquinolinyl Complex 3.56. To an 8-dram vial containing di- μ -chlorotetrakis[2-(1-isoquinolinyl-N)phenyl-C]diiridium(III) (**3.55**, 200.0 mg, 0.157 mmol, 1.0 equiv) and chlorobipyridine **3.49** (65.9 mg, 0.346 mmol, 2.2 equiv) was added ethylene glycol (6.8 mL, 0.023 M). The resulting suspension was then sparged with N₂ for 15 minutes before being transferred to an Al-block and stirred at 150 °C for 24 h. After cooling to 23 °C, the reaction was diluted with water (20 mL) before being transferred with water (5 mL) to a flask containing sat. aq. KPF₆ (50 mL), resulting in formation of a red precipitate. This mixture was then filtered through a plug of celite and washed sequentially with water (300 mL), hexanes (200 mL), and Et₂O (200 mL). The celite pad was then eluted with CH₂Cl₂ (200 mL) to redissolve the product,

and the resulting filtrate was collected, dried over Na₂SO₄, concentrated under reduced pressure, and dried under reduced pressure (<1 torr) at 100 °C for 12 h to afford Ir(ppy)₂bpy complex **3.56** as a red solid (286.3 mg, 97% yield). **Isoquinolinyl Complex 3.56.** *R_f* 0.62 (14:1:1 CH₃CN:H₂O:sat. aq. KNO₃); ¹H NMR (500 MHz, CD₃CN): δ 9.34 (dt, *J* = 8.5, 1.0, 1H), 9.06–8.94 (m, 2H), 8.37 (d, *J* = 8.1, 2H), 8.16–8.08 (m, 2H), 8.02–7.98 (m, 2H), 7.97 (ddd, *J* = 5.4, 1.7, 0.8, 1H), 7.93 (dd, *J* = 5.3, 1.4, 1H), 7.87–7.80 (m, 4H), 7.63 (d, *J* = 6.4, 1H), 7.61 (d, *J* = 6.5, 1H), 7.47–7.40 (m, 3H), 7.35 (dd, *J* = 8.3, 5.2, 1H), 7.11 (dddd, *J* = 8.8, 6.6, 1.6, 1.4, 2H), 6.86 (t, *J* = 7.4, 2H), 6.25 (ddd, *J* = 7.7, 4.4, 1.1, 2H); ¹³C NMR (125 MHz, CD₃CN, 35 of 40 signals observed) δ 169.3, 169.1, 155.2, 154.4, 153.7, 153.2, 152.2, 150.8, 146.5, 146.4, 143.4, 141.93, 141.90, 139.7, 138.1, 138.05, 134.8, 132.92, 132.87, 132.7, 131.8, 131.53, 131.47, 129.9, 129.8, 129.4, 129.2, 128.51, 128.50, 127.7, 127.1, 123.4, 123.3, 122.9, 122.8; IR (film): 3080, 3045, 1576, 1541, 1433, 840 cm⁻¹; HR-ESI-MS (*m/z*) [M – PF₆]⁺ calcd for C₄₀H₂₇ClN₄Ir⁺, 791.1553; found 791.1603.



Fluorinated Ir Complex 3.58. To an 8-dram vial containing dichlorotetrakis[3,5-difluoro-2-(2-pyridinyl)phenyl]diiridium(III) (**3.57**, 200.0 mg, 0.165 mmol, 1.0 equiv) and chlorobipyridine **3.49** (69.0 mg, 0.362 mmol, 2.2 equiv) was added ethylene glycol (7.2 mL, 0.023 M). The resulting suspension was then sparged with N₂ for 15 minutes before being transferred to an Al-block and stirred at 150 °C for 24 h. After cooling to 23 °C, the reaction was diluted with water

(20 mL) before being transferred with water (5 mL) to a flask containing sat. aq. KPF_6 (50 mL), resulting in formation of a red precipitate. This mixture was then filtered through a plug of celite and washed sequentially with water (300 mL), hexanes (200 mL), and Et_2O (200 mL). The celite pad was then eluted with CH_2Cl_2 (200 mL) to redissolve the product, and the resulting filtrate was collected, dried over Na_2SO_4 , concentrated under reduced pressure, and dried under reduced pressure (<1 torr) at 100 °C for 12 h to afford $\text{Ir}(\text{ppy})_2\text{bpy}$ complex **3.58** as a yellow solid (277.7 mg, 93% yield). **Fluorinated Ir Complex 3.58.** R_f 0.64 (14:1:1 $\text{CH}_3\text{CN}:\text{H}_2\text{O}:\text{sat. aq. KNO}_3$); ^1H NMR (500 MHz, CD_3CN): δ 9.36 (dt, $J = 8.4, 0.9$, 1H), 8.31 (d, $J = 8.5$, 2H), 8.23–8.15 (m, 2H), 8.12 (ddd, $J = 5.4, 1.7, 0.7$, 1H), 8.07 (dd, $J = 5.3, 1.4$, 1H), 7.95–7.87 (dddd, $J = 8.5, 7.9, 4.2, 1.6, 0.7$, 2H), 7.71 (d, $J = 5.8$, 2H), 7.54 (ddd, $J = 7.8, 5.5, 1.2$, 1H), 7.45 (dd, $J = 8.6, 5.3$, 1H), 7.09 (dddd, $J = 10.9, 7.8, 5.9, 1.4$, 2H), 6.69 (dddd, $J = 12.8, 9.4, 2.5, 2.1$), 5.69 (ddd, $J = 8.6, 7.2, 2.4$); ^{13}C NMR (125 MHz, CD_3CN) δ 165.5, 165.4, 164.43, 164.38, 164.34, 164.28, 163.5, 163.43, 163.40, 163.38, 163.3, 161.31, 161.26, 155.21, 155.15, 155.1, 154.43, 154.37, 153.0, 152.6, 151.3, 150.84, 150.75, 144.1, 140.59, 140.57, 140.4, 135.1, 130.0, 129.8, 129.5, 128.91, 128.89, 128.87, 128.85, 128.81, 128.79, 128.77, 128.75, 125.0, 124.8, 124.7, 114.81, 114.79, 114.67, 114.65, 114.6, 114.51, 114.48, 100.03, 99.98, 99.81, 99.76, 99.6, 99.5; IR (film): 3088, 2973, 1739, 1604, 1575, 1479, 1430, 1406, 840 cm^{-1} ; HR-ESI-MS (m/z) $[\text{M} - \text{PF}_6]^+$ calcd for $\text{C}_{32}\text{H}_{19}\text{ClF}_4\text{N}_4\text{Ir}^+$, 763.0864; found 763.0864.

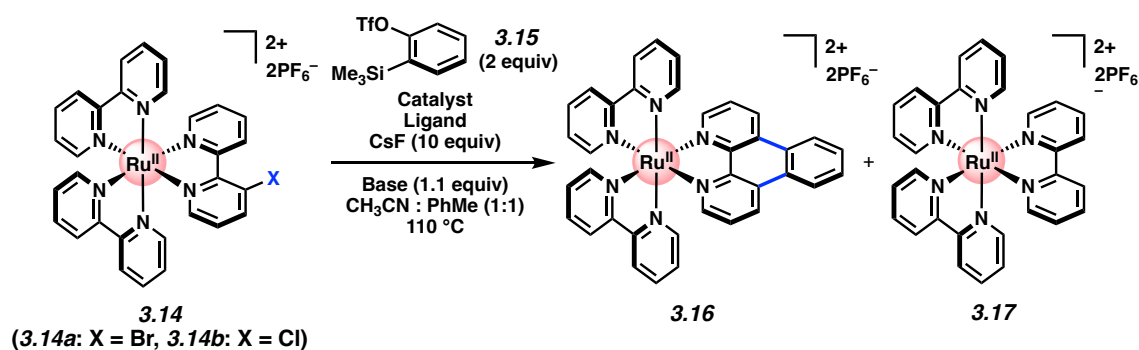
(Note: Complex splitting patterns observed due to presence of fluorine atoms; these data represent empirically observed chemical shifts from the ^{13}C NMR spectrum)

3.8.2.2 Optimization of on-the-Complex Annulation with Benzyne

Representative Procedure for reaction optimization. Benzyne adduct 3.16 (Table 3.1, entry 11): To a 1-dram vial was added Pd(OAc)₂ (1.6 mg, 7.3 μmol, 10 mol%), bromo-Ru(bpy)₃[PF₆]₂ **3.14a** (68.6 mg, 73.1 μmol, 1.0 equiv), P(*o*-tolyl)₃ (2.2 mg, 7.3 μmol, 10 mol%), MeCN (0.50 mL, 0.15 M), PhMe (0.50 mL, 0.15 M), silyl triflate (43.6 mg, 73.1 μmol, 2.0 equiv, **3.15**), an oven-dried magnetic stir bar, and CsF (111 mg, 731 μmol, 10.0 equiv) sequentially. The reaction was then purged with N₂ for 5 min before being sealed with a Teflon-lined screw cap under a flow of N₂, sealed with Teflon tape and electrical tape, transferred to an Al-block, and stirred at 110 °C for 30 min. After cooling to 23 °C, the mixture was filtered through a plug of celite with MeCN (6 mL) and concentrated under reduced pressure. The yield was determined by ¹H NMR analysis with 1,3,5-trimethoxybenzene as an external standard.

Optimization efforts that deviate from the above conditions are indicated below.

Table 3.1. Optimization studies of on-the-complex annulation with benzyne. Yields were determined using ^1H NMR analysis with 1,3,5-trimethoxybenzene (TMB) as an external standard.



Entry	Catalyst	Ligand	X	Catalyst Loading	Ligand Loading	Base	CH ₃ CN : PhMe	Time	3.16	3.17
1	Pd(dba) ₂	P(<i>o</i> -tolyl) ₃	Br	5 mol%	5 mol%	–	1 : 1	2 h	2%	48%
2	Pd(PPh ₃) ₄	P(<i>o</i> -tolyl) ₃	Br	5 mol%	5 mol%	–	1 : 1	2 h	2%	48%
3	XPhos Pd G2		Br	5 mol%	5 mol%	–	1 : 1	2 h	4%	40%
4	Pd(OAc) ₂	P(<i>o</i> -tolyl) ₃	Br	5 mol%	5 mol%	–	1 : 1	2 h	26%	24%
5	Pd(OAc) ₂	P(<i>o</i> -tolyl) ₃	Br	10 mol%	30 mol%	–	1 : 1	2 h	60%	18%
6	Pd(OAc) ₂	P(<i>o</i> -tolyl) ₃	Br	10 mol%	30 mol%	Ag ₂ CO ₃	1 : 1	2 h	54%	16%
7	Pd(OAc) ₂	P(<i>o</i> -tolyl) ₃	Br	10 mol%	30 mol%	K ₂ CO ₃	1 : 1	2 h	41%	19%
8	Pd(OAc) ₂	P(4-ClC ₆ H ₄) ₃	Br	10 mol%	30 mol%	–	1 : 1	2 h	32%	29%
9	Pd(OAc) ₂	P(4-MeOC ₆ H ₄) ₃	Br	10 mol%	30 mol%	–	1 : 1	2 h	16%	35%
10	Pd(OAc) ₂	SPhos	Br	10 mol%	30 mol%	–	1 : 1	2 h	44%	26%
11	Pd(OAc) ₂	P(<i>o</i> -tolyl) ₃	Br	10 mol%	10 mol%	–	1 : 1	30 min	71%	16%
12	Pd(OAc) ₂	P(<i>o</i> -tolyl) ₃	Br	10 mol%	10 mol%	–	3 : 1	30 min	61%	19%
13	Pd(OAc) ₂	P(<i>o</i> -tolyl) ₃	Br	10 mol%	10 mol%	–	9 : 1	30 min	44%	18%
14	Pd(OAc) ₂	P(<i>o</i> -tolyl) ₃	Br	10 mol%	10 mol%	–	100% CH ₃ CN	30 min	47%	16%
15	Pd(OAc) ₂	P(<i>o</i> -tolyl) ₃	Br	10 mol%	10 mol%	–	1 : 3	30 min	35%	28%
16	Pd(OAc) ₂	P(<i>o</i> -tolyl) ₃	Cl	10 mol%	10 mol%	–	1 : 1	30 min	78%	0%

Significant decomposition was observed when the halogenated bipyridyl ligand was not pre-ligated to the Ru complex (see below). It is postulated that deleterious intermediates such as **3.51**

may form under these conditions due to the propensity for bipyridyl ligands to undergo *N,N'*-chelation to transition metals.

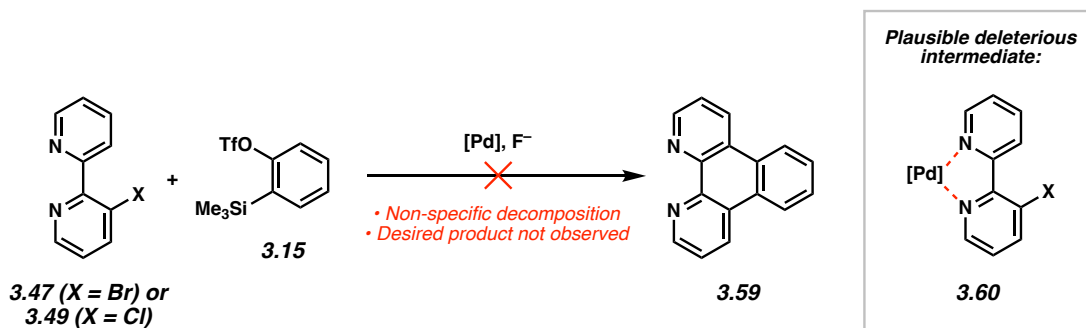


Figure 3.10. Unsuccessful aryne annulation of free ligands 3.47 and 3.49.

3.8.2.3 Crystallographic Data

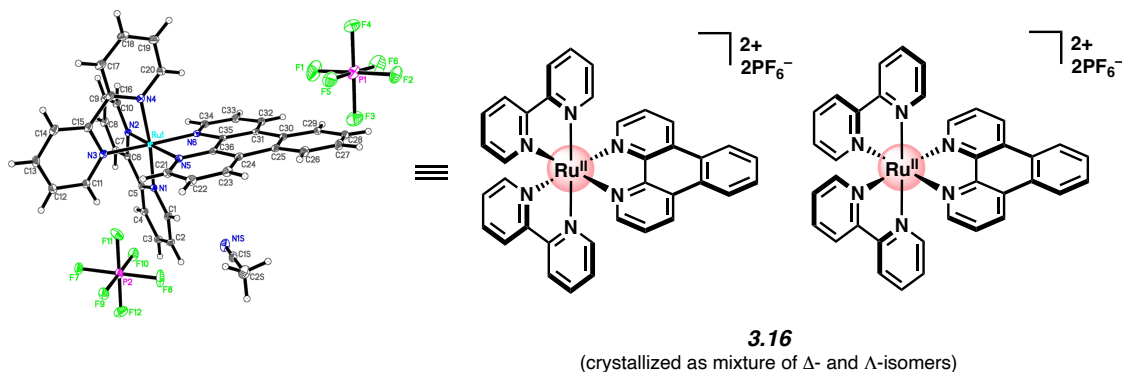


Figure 3.11. ORTEP representation of X-ray crystallographic structure 3.16.

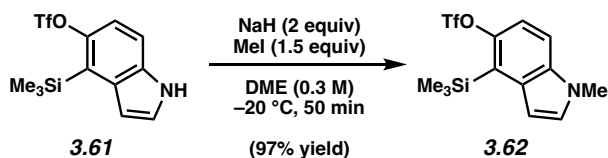
(CCDC Registry #2048567).

Table 3.2. Crystal data and structure refinement for compound 3.16.

Identification code	cu_garg1904_a_sq_s
Empirical formula	C38 H29 F12 N7 P2 Ru
Formula weight	974.69
Temperature	100(2) K

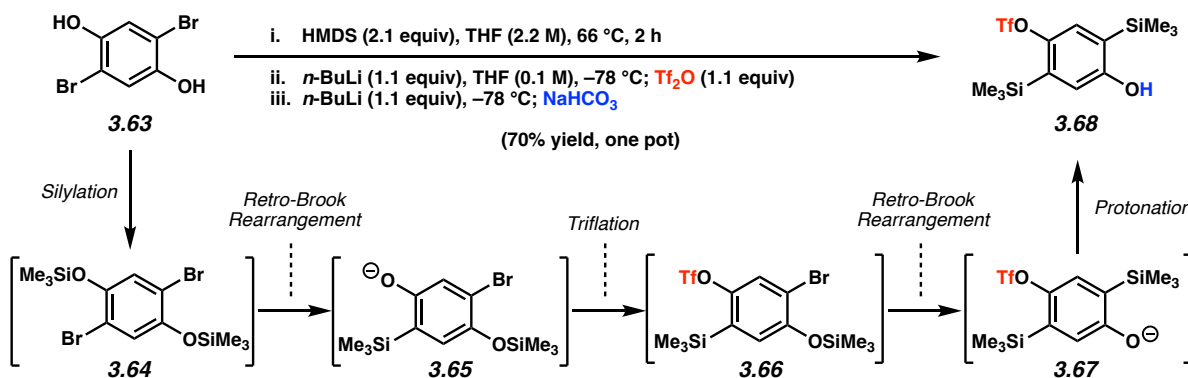
Wavelength	1.54178 Å	
Crystal system	Monoclinic	
Space group	P2 ₁ /c	
Unit cell dimensions	a = 11.6931(3) Å	α = 90°.
	b = 30.8685(9) Å	β = 112.4510(10)°.
	c = 12.4524(3) Å	γ = 90°.
Volume	4154.01(19) Å ³	
Z	4	
Density (calculated)	1.559 Mg/m ³	
Absorption coefficient	4.611 mm ⁻¹	
F(000)	1952	
Crystal size	.16 x .08 x .04 mm ³	
Theta range for data collection	2.863 to 70.067°.	
Index ranges	-13 ≤ h ≤ 12, -36 ≤ k ≤ 37, -14 ≤ l ≤ 15	
Reflections collected	34574	
Independent reflections	7544 [R(int) = 0.0345]	
Completeness to theta = 67.679°	96.9 %	
Absorption correction	Semi-empirical from equivalents	
Max. and min. transmission	0.75 and 0.62	
Refinement method	Full-matrix least-squares on F ²	
Data / restraints / parameters	7544 / 0 / 542	
Goodness-of-fit on F ²	1.060	
Final R indices [I > 2σ(I)]	R1 = 0.0259, wR2 = 0.0644	
R indices (all data)	R1 = 0.0302, wR2 = 0.0657	
Extinction coefficient	n/a	
Largest diff. peak and hole	0.464 and -0.490 e.Å ⁻³	

3.8.2.4 Synthesis of Silyl Triflate Aryne Precursors



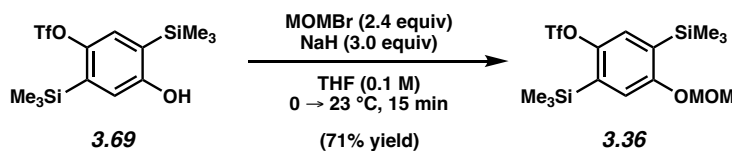
Silyl triflate 3.62. To a solution of Garg 4,5-indolyne precursor (**3.61**, 913 mg, 2.71 mmol, 1.0 equiv) in DME (9 mL, 0.3 M) at -20°C was added MeI (256 μL , 4.10 mmol, 1.5 equiv) and NaH (60 wt% dispersion in mineral oil; 215 mg, 5.41 mmol, 2.0 equiv) sequentially. The reaction mixture was then stirred at -20°C for 50 min before being quenched by addition of saturated aqueous NH_4Cl (5 mL). It was then allowed to warm to 23°C before being transferred

to a separatory funnel with H₂O (10 mL) and EtOAc (10 mL). The layers were then separated and the aqueous layer was extracted with EtOAc (3 x 15 mL). The combined organic layers were dried over MgSO₄, filtered, and concentrated under reduced pressure. The crude residue was then purified by flash chromatography (100% hexanes → 100:1 hexanes:EtOAc → 50:1 hexanes:EtOAc) to afford silyl triflate **3.62** as a viscous, pale yellow oil (927 mg, 97% yield). *N*-Me silyl triflate **3.62**: R_f 0.63 (4:1 hexanes:EtOAc); ¹H NMR (500 MHz, CDCl₃): δ 7.33 (d, *J* = 9.0, 0.9, 1H), 7.20–7.14 (m, 2H), 6.68 (dd, *J* = 3.4, 0.6, 1H), 3.81 (s, 3H), 0.50 (s, 9H). Spectral data match those previously reported in the literature.⁷³



Silyl alcohol 3.68. To a stirred solution of 2,5-dibromohydroquinone (**3.63**, 2.60 g, 9.71 mmol, 1.0 equiv) in THF (4.40 mL, 2.20 M) was added HMDS (4.25 mL, 20.4 mmol, 2.1 equiv). The flask was topped with an air condenser and the system placed under N₂. The reaction was heated to 66 °C and stirred for 2 h. Then, the reaction mixture was allowed to cool to 23 °C and the volatiles were removed. THF (69 mL, 0.14 M) was then added and the mixture was cooled to -78 °C. *n*-BuLi (2.49 M in hexanes; 3.29 mL, 10.7 mmol, 1.1 equiv) was then added dropwise over 8 min. The reaction mixture was then stirred at -78 °C for 25 min. Tf₂O (1.80 mL, 10.7 mmol, 1.1 equiv) was then added dropwise over 5 min at -78 °C, and the mixture was allowed to stir at this temperature for 25 min. *n*-BuLi (2.49 M in hexanes; 4.29 mL, 10.7 mmol, 1.1 equiv)

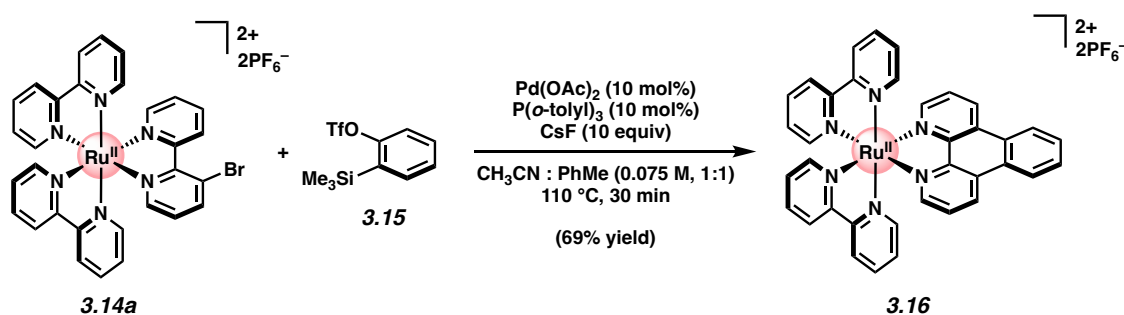
was then added dropwise over 8 min. The reaction mixture was then stirred at $-78\text{ }^{\circ}\text{C}$ for 25 min. Finally, the reaction was quenched by addition of saturated aqueous NaHCO_3 (40 mL) in one portion and the mixture was allowed to warm to $23\text{ }^{\circ}\text{C}$ before being transferred to a separatory funnel with Et_2O (100 mL) and the layers were separated. The aqueous layer was then extracted with Et_2O (2 x 100 mL) and the combined organic layers were dried over Na_2SO_4 , filtered, and concentrated under reduced pressure. The crude residue was then purified by flash chromatography (100% hexanes \rightarrow 3% EtOAc in hexanes \rightarrow 5% EtOAc in hexanes) to afford silyl alcohol **3.68** as a viscous yellow oil (2.62 g, 70% yield). **Silyl alcohol 3.68**: R_f 0.39 (9:1 hexanes:EtOAc) $^1\text{H NMR}$ (600 MHz, CDCl_3): δ 7.23 (s, 1H), 6.74 (s, 1H), 4.88 (s, 1H), 0.35 (s, 9H), 0.31 (s, 9H). Spectral data match those previously reported in the literature.⁶⁷



Methoxymethyl ether 3.36. To a stirred solution of silyl alcohol **3.69** (1.03 g, 2.66 mmol, 1.0 equiv) in THF (25 mL, 0.10 M) at $0\text{ }^{\circ}\text{C}$ was added sodium hydride (dry, 95%; 202 mg, 7.99 mmol, 3.0 equiv) in one portion. The solution was then stirred at $0\text{ }^{\circ}\text{C}$ for 15 min, followed by dropwise addition of bromomethyl methyl ether (522 μL , 6.39 mmol, 2.40 equiv) over 1 minute. Following addition, the reaction was allowed to warm to $23\text{ }^{\circ}\text{C}$ and stirred for 15 min before being diluted with Et_2O (30 mL). H_2O (30 mL) was then added over 30 seconds and the mixture was transferred with Et_2O (5 mL) to a separatory funnel. The layers were separated and the aqueous layer was extracted with Et_2O (3 x 30 mL). The combined organic layers were then washed with H_2O (30 mL), dried over Na_2SO_4 , and concentrated under reduced pressure. The crude residue was then purified by flash chromatography (100% hexanes) to afford methoxy

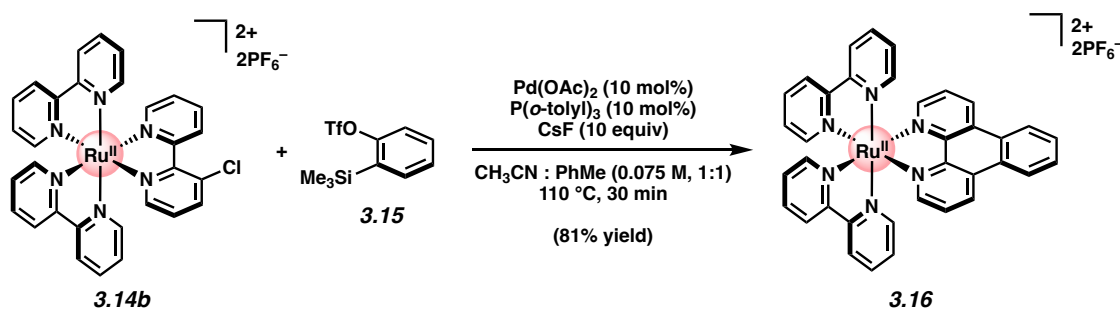
methyl ether **3.36** as a white solid (814 mg, 71% yield). **Methoxymethyl ether 3.36**: mp: 37.5–38.5 °C; R_f 0.56 (9:1 hexanes:EtOAc); ^1H NMR (500 MHz, CDCl_3): δ 7.25 (s, 1H), 7.14 (s, 1H), 5.19 (s, 2H), 3.48 (s, 3H), 0.36 (s, 9H), 0.28 (s, 9H); ^{13}C NMR (125 MHz, CD_3CN) δ 160.5, 149.6, 135.3, 132.8, 126.1, 126.0, 119.2, 118.7 (q, $J = 320.5$ Hz), 94.3, 56.3, -0.7 , -1.2 ; IR (film): 2957, 1468, 1420, 1341, 1246, 1210, 1144, 1082, 1013, 945, 841, 757, 633 cm^{-1} ; HR-GC-MS (m/z) $[\text{M}]^+$ calcd for $\text{C}_{15}\text{H}_{25}\text{F}_3\text{O}_5\text{SSi}_2^+$ 430.09133; found 430.0908.

3.8.2.5 Scope of Pd-Catalyzed Aryne Annulation



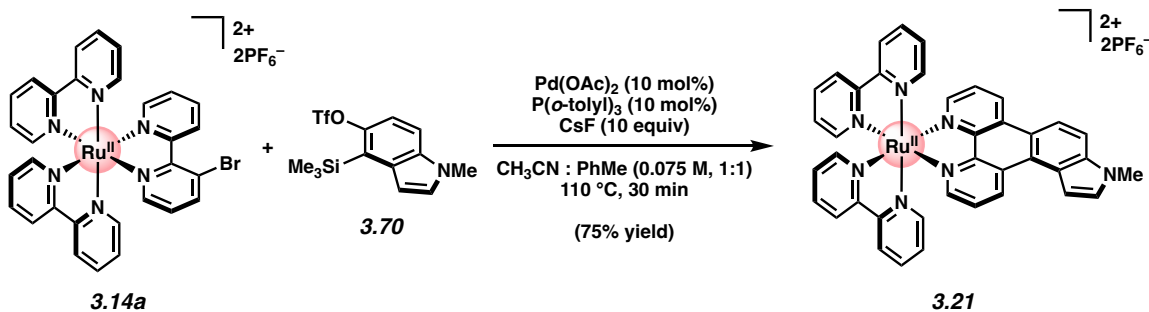
Representative Procedure A for aryne annulations (Figure 3.3, benzyne adduct 3.16 used as an example). To a 1-dram vial was added $\text{Pd}(\text{OAc})_2$ (1.5 mg, 6.7 μmol , 10 mol%), Bromo- $\text{Ru}(\text{bpy})_3[\text{PF}_6]_2$ **3.14a** (62.2 mg, 0.066 mmol, 1.0 equiv), $\text{P}(\text{o-tolyl})_3$ (2.2 mg, 7.2 μmol , 10 mol%), MeCN (0.50 mL, 0.15 M), PhMe (0.50 mL, 0.15 M), silyl triflate **3.15** (40.1 mg, 0.134 mmol, 2.0 equiv), an oven-dried magnetic stir bar, and CsF (101 mg, 0.663 mmol, 10.0 equiv) sequentially. The reaction was then purged with N_2 for 5 min before being capped with a Teflon-lined screw cap under a flow of N_2 , sealed with Teflon tape and electrical tape, transferred to an Al-block, and stirred at $110\text{ }^\circ\text{C}$ for 30 min. After cooling to $23\text{ }^\circ\text{C}$, the mixture was filtered through a plug of celite with MeCN (6 mL), and concentrated under reduced pressure. The crude residue was adsorbed onto silica gel (500 mg) under reduced pressure and purified by flash

chromatography (100% EtOAc \rightarrow 14:1:1 MeCN:H₂O:sat. aq. KNO₃). To the concentrated aqueous mixture was added saturated aqueous KPF₆ (50 mL) to precipitate the desired product, and the resultant mixture was transferred to a separatory funnel with CH₂Cl₂ (50 mL). The layers were separated and the aqueous layer was extracted with CH₂Cl₂ (2 x 50 mL). The combined organic layers were then dried over Na₂SO₄, concentrated under reduced pressure and dried under reduced pressure (<1 torr) at 100 °C for 12 h to afford benzyne adduct **3.16** as a deep red solid (69% yield, average of two experiments). **Benzyne adduct 3.16**: mp >250 °C; R_f 0.68 (7:2:1 MeCN:H₂O:sat. aq. KNO₃); ¹H NMR (500 MHz, CD₃CN): δ 9.23 (dd, *J* = 8.4, 0.9, 2H), 8.92–8.88 (m, 2H), 8.55 (d, *J* = 8.3, 2H), 8.51 (d, *J* = 8.3, 2H), 8.11 (td, *J* = 7.9, 1.5, 2H), 8.07 (dd, *J* = 5.3, 0.9, 2H), 8.02–7.98 (m, 4H), 7.85 (d, *J* = 5.8, 2H), 7.79 (dd, *J* = 8.2, 5.3, 2H), 7.63 (d, *J* = 5.6, 2H), 7.46 (td, *J* = 6.9, 1.3, 2H), 7.23 (td, *J* = 6.9, 1.2, 2H); ¹³C NMR (125 MHz, CD₃CN) δ 158.09, 153.11, 152.91, 152.82, 149.00, 148.82, 138.70, 133.18, 133.03, 131.32, 131.26, 131.21, 129.14, 128.34, 127.42, 127.28, 125.64, 125.60, 125.13; IR (film): 1604, 1466, 1447, 1437, 838, 761, 731, 557 cm⁻¹; HR-ESI-MS (*m/z*) [M – PF₆]⁺ calcd for C₃₆H₂₆F₆N₆PRu⁺, 789.09043; found 789.0905.

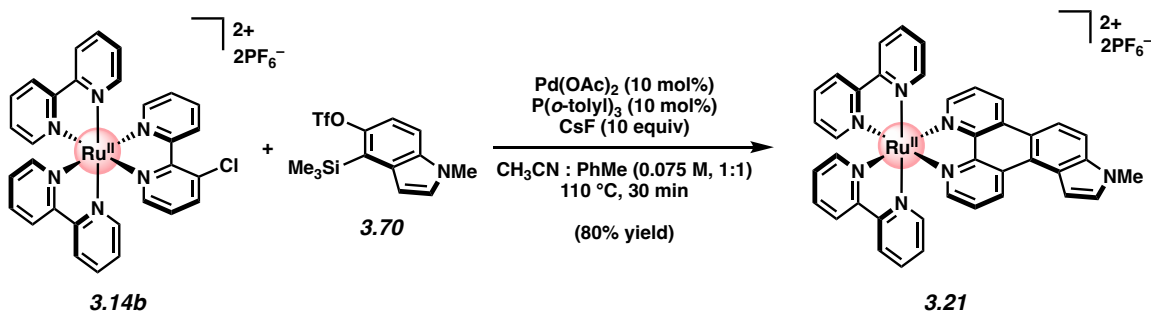


Benzyne adduct 3.16. Followed representative procedure A. Purification by flash chromatography (100% EtOAc \rightarrow 14:1:1 CH₃CN:H₂O:sat. aq. KNO₃) afforded benzyne adduct

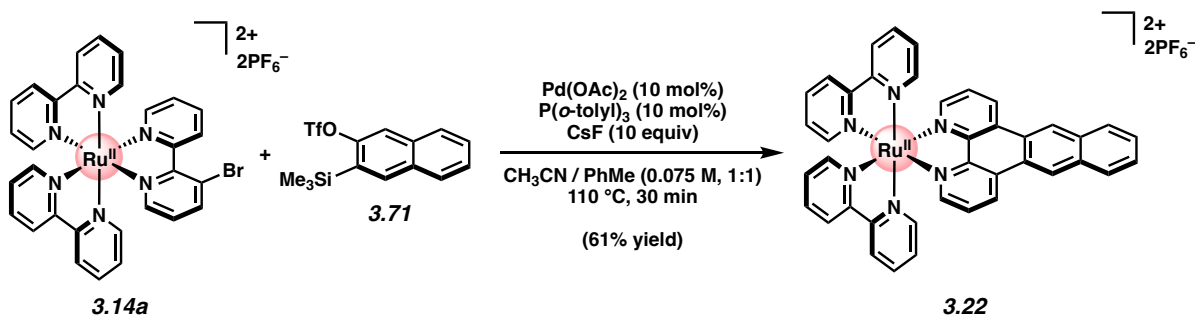
3.16 (81% yield, average of two experiments) as a red solid. Spectral data matched those provided above.



Indolyne adduct 3.21. Followed representative procedure A. Purification by flash chromatography (7:2:1 CH₃CN:H₂O:sat. aq. KNO₃) afforded indolyne adduct **3.21** (75% yield, average of two experiments) as a red solid. **Indolyne adduct 3.21**: mp >250 °C; R_f 0.63 (7:2:1 CH₃CN:H₂O:sat. aq. KNO₃); ¹H NMR (600 MHz, CD₃CN): δ 9.71 (dd, *J* = 8.8, 1.1, 1H), 9.27 (d, *J* = 8.8, 1H), 8.73 (d, *J* = 9.1, 1H), 8.54 (ddt, *J* = 8.3, 4.4, 1.1, 2H), 8.51–8.48 (m, 2H), 8.12–8.07 (m, 3H), 8.06 (dd, *J* = 5.2, 1.1, 1H), 8.01 (dd, *J* = 5.3, 1.1, 1H), 8.00–7.96 (m, 2H), 7.87–7.81 (m, 3H), 7.75 (dd, *J* = 8.6, 5.2, 1H), 7.67 (d, *J* = 3.3, 1H), 7.64–7.60 (m, 2H), 7.57 (d, *J* = 3.3, 1H), 7.57–7.43 (m, 2H), 7.22–7.18 (m, 2H), 4.04 (s, 3H); ¹³C NMR (125 MHz, CD₃CN): δ 158.6, 158.5, 158.4, 153.23, 153.22, 151.71, 151.66, 149.1, 147.8, 139.1, 139.0, 138.7, 136.2, 133.6, 133.4, 132.8, 132.6, 128.92, 128.90, 128.76, 128.75, 127.6, 127.3, 125.61, 125.60, 125.5, 125.1, 123.9, 123.6, 115.2, 103.9, 34.4; IR (film): 3707, 2681, 2973, 2923, 1055, 1033; HR-ESI-MS (*m/z*) [M – PF₆]⁺ calcd for C₃₉H₂₉N₇P F₆Ru⁺, 842.1180; found 842.1110.

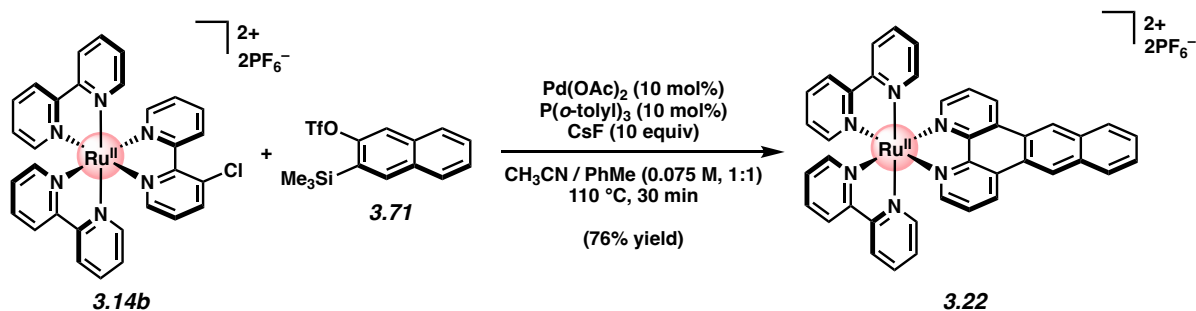


Indolyne adduct 3.21. Followed representative procedure A. Purification by flash chromatography (7:2:1 $\text{CH}_3\text{CN}:\text{H}_2\text{O}:\text{sat. aq. KNO}_3$) afforded indolyne adduct **3.21** (80% yield, average of two experiments) as a red solid. Spectral data matched those provided above.

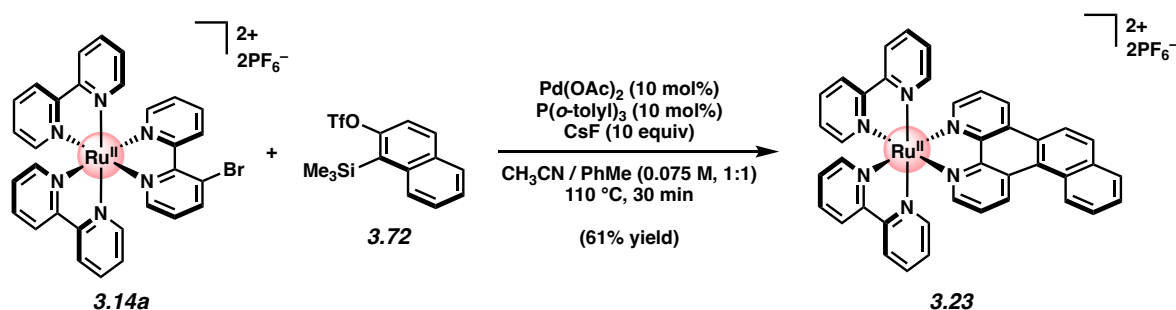


Representative Procedure B for aryne annulations (Figure 3.4, naphthalene adduct 3.22 used as an example). To a 1-dram vial was added $\text{Pd}(\text{OAc})_2$ (1.4 mg, 6.4 μmol , 10 mol%), Bromo-Ru(bpy) $_3$ [PF_6] $_2$ **3.14a** (60.0 mg, 0.064 mmol, 1.0 equiv), $\text{P}(\text{o-tolyl})_3$ (2.0 mg, 6.4 μmol , 10 mol%), MeCN (0.50 mL, 0.15 M), PhMe (0.50 mL, 0.15 M), silyl triflate **3.71** (44.6 mg, 0.128 mmol, 2.0 equiv), an oven-dried magnetic stir bar, and CsF (97.1 mg, 0.639 mmol, 10.0 equiv) sequentially. The reaction was then purged with N_2 for 5 min before being sealed with a Teflon-lined screw cap under a flow of N_2 , sealed with Teflon tape and electrical tape, transferred to an Al-block, and stirred at 110 °C for 30 min. After cooling to 23 °C, the mixture was filtered through a plug of celite with MeCN (6 mL), and concentrated under reduced pressure. The crude residue was adsorbed onto silica gel (500 mg) under reduced pressure and

purified by flash chromatography (100% EtOAc \rightarrow 7:2:1 MeCN:H₂O:sat. aq. KNO₃). To the concentrated aqueous mixture was added saturated aqueous KPF₆ (50 mL) to precipitate the desired product, and the resultant mixture was transferred to a separatory funnel with CH₂Cl₂ (50 mL). The layers were separated and the aqueous layer was extracted with CH₂Cl₂ (2 x 50 mL). The combined organic layers were then concentrated under reduced pressure before being redissolved in CH₃CN (10 mL). Activated charcoal (150 mg) was then added the mixture was agitated for 10 seconds before being filtered over celite, concentrated under reduced pressure, and dried under reduced pressure (<1 torr) at 100 °C for 12 h to afford naphthalene adduct **3.22** as a deep red solid (61% yield, average of two experiments). **Naphthalene adduct 3.22**: mp >250 °C; *R_f* 0.57 (7:2:1 CH₃CN:H₂O:saturated aqueous KNO₃); ¹H NMR (500 MHz, CD₃CN): δ 9.41 (s, 2H), 9.29 (dd, *J* = 8.0, 1.2, 2H), 8.56–8.51 (m, 4H), 8.30–8.27 (m, 2H), 8.11 (td, *J* = 10, 1.4, 2H), 8.03–7.99 (m, 4H), 7.85 (dd, *J* = 5.5, 0.5, 2H), 7.79–7.76 (m, 4H), 7.72 (dd, *J* = 5.6, 0.5, 2H), 7.46 (ddd, *J* = 7.8, 5.7, 1.3, 2H), 7.27 (ddd, *J* = 7.8, 5.7, 1.3, 2H); ¹³C NMR (125 MHz, CD₃CN): δ 158.0, 157.9, 152.9, 152.8, 152.3, 149.5, 138.8, 138.6, 133.9, 133.0, 132.2, 129.3, 129.1, 128.5, 128.4, 127.7, 126.4, 125.5, 125.2, 125.1; IR (film): 3681, 2981, 2923, 1332, 1054, 1033, 1013 cm⁻¹; HR-ESI-MS (*m/z*) [M – PF₆]⁺ calcd for C₄₀H₂₇N₆PF₆Ru⁺, 839.1061; found 839.1050.

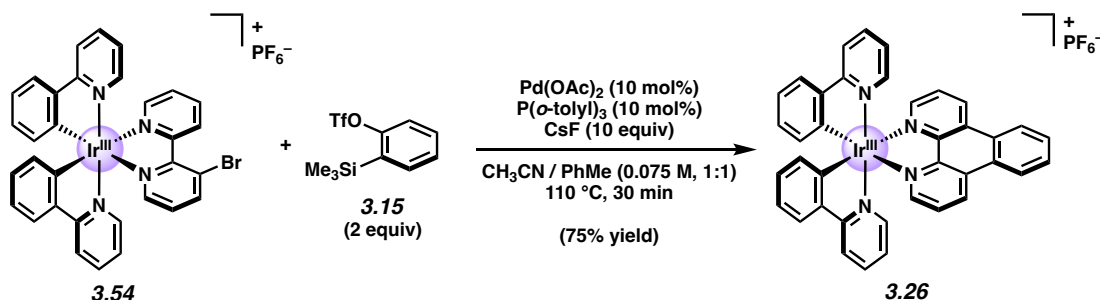


Naphthalene adduct 3.22. Followed representative procedure B. Purification by flash chromatography (7:2:1 $\text{CH}_3\text{CN}:\text{H}_2\text{O}:\text{sat. aq. KNO}_3$) afforded naphthalene adduct **3.22** (76% yield, average of two experiments) as a red solid. Spectral data matched those provided above.

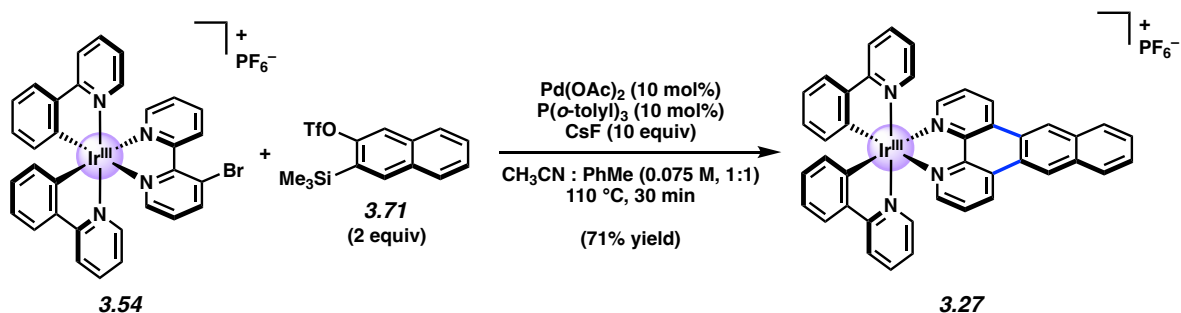


Naphthalene adduct 3.23. Followed representative procedure B. Purification by flash chromatography (14:2:1 $\text{CH}_3\text{CN}:\text{H}_2\text{O}:\text{sat. aq. KNO}_3$) afforded naphthalene adduct **3.23** (61% yield, average of two experiments) as a red solid. **Naphthalene adduct 3.23:** mp $>250\text{ }^\circ\text{C}$; R_f 0.70 (7:2:1 $\text{CH}_3\text{CN}:\text{H}_2\text{O}:\text{sat. aq. KNO}_3$); ^1H NMR (600 MHz, CD_3CN): δ 9.52 (d, $J = 8.7$, 1H), 9.29 (d, $J = 8.7$, 1H), 8.96 (d, $J = 8.3$, 1H), 8.82 (d, $J = 8.7$, 1H), 8.57–8.50 (m, 4H), 8.37 (d, $J = 8.8$, 1H), 8.24 (d, $J = 7.9$, 1H), 8.15–8.09 (m, 4H) 8.00 (t, $J = 7.8$, 2H), 7.89–7.78 (m, 6H), 7.69 (d, $J = 5.2$, 1H), 7.64 (d, $J = 5.6$, 1H), 7.49–7.44 (m, 2H), 7.23–7.20 (m, 2H); ^{13}C NMR (125 MHz, CD_3CN): δ 158.1, 157.9, 152.92, 152.86, 152.8, 152.0, 149.1, 148.6, 138.8, 138.7, 138.0, 135.3, 133.7, 132.0, 130.8, 130.6, 130.5, 130.0, 129.1, 128.9, 128.6, 128.5, 128.3, 127.3, 126.9,

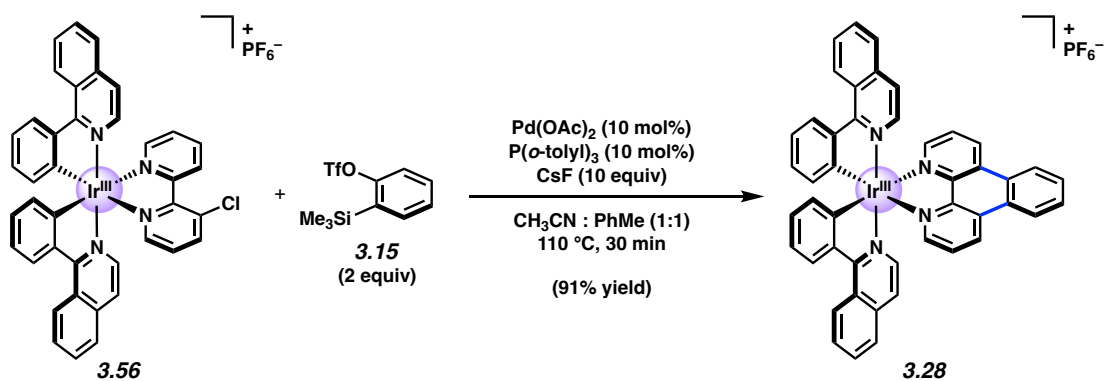
126.3, 125.2, 125.1, 121.6; IR (film): 3663, 3589, 3084, 2925, 2854 cm^{-1} ; HR-ESI-MS (m/z) [$M - \text{PF}_6$] $^+$ calcd for $\text{C}_{40}\text{H}_{27}\text{N}_6\text{PF}_6\text{Ru}^+$, 839.1061; found 839.1119.



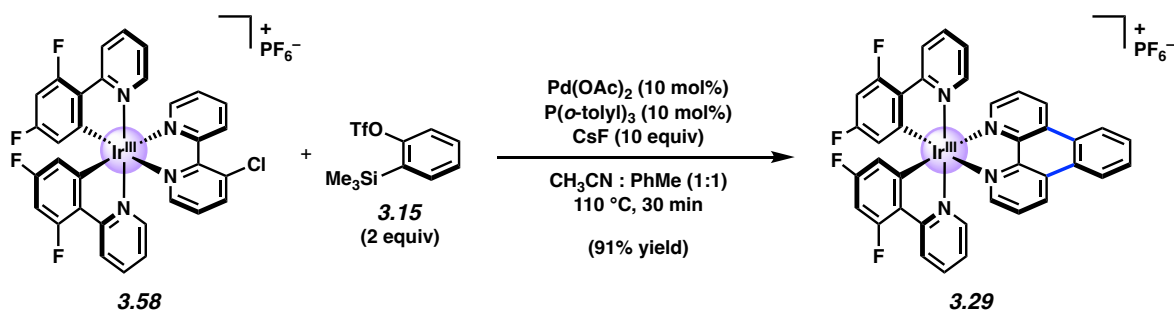
Ir-benzyne adduct 3.26. Followed representative procedure A. Purification by flash chromatography (9:1 benzene:acetonitrile \rightarrow 3:2 benzene:acetonitrile) afforded Ir-benzyne adduct **3.26** (75% yield, average of two experiments) as a dark orange solid. **Ir-benzyne adduct 3.26:** mp $>250\text{ }^\circ\text{C}$; R_f 0.59 (7:2:1 $\text{CH}_3\text{CN}:\text{H}_2\text{O}:\text{sat. aq. KNO}_3$); ^1H NMR (600 MHz, CD_3CN): δ 9.30 (dd, $J = 8.6, 0.9$, 1H), 8.92–8.88 (m, 1H), 8.29 (dd, $J = 5.1, 1.3$, 1H), 8.06 (d, $J = 8.3$, 1H), 8.00–7.98 (m, 1H), 7.89 (dd, $J = 8.6, 5.1$, 1H), 7.84 (dd, $J = 8.0, 1.1$, 1H), 7.79 (ddd, $J = 8.2, 7.6, 1.5$, 1H), 7.49 (ddd, $J = 6.0, 1.5, 0.7$, 1H), 7.29 (dd, $J = 8.4, 5.3$, 1H), 7.06–7.00 (m, 4H), 6.90 (tdd, $J = 7.5, 2.5, 1.3$, 2H), 6.22 (ddd, 7.5, 4.8, 1.2, 2H); ^{13}C NMR (125 MHz, CD_3CN): δ 168.33, 151.5, 151.2, 150.4, 147.9, 145.1, 139.3, 134.7, 132.6, 131.7, 131.3, 131.1, 129.1, 128.2, 125.8, 125.5, 124.3, 123.5, 120.7; IR (film): 2981, 1735, 1689, 1368, 1149 cm^{-1} ; HR-ESI-MS (m/z) [$M - \text{PF}_6$] $^+$ calcd for $\text{C}_{38}\text{H}_{26}\text{N}_4\text{Ir}^+$, 731.1787; found 731.1704.



Ir-naphthalylene adduct 3.27. Followed representative procedure B. Purification by flash chromatography (100% EtOAc → 14:2:1 MeCN:H₂O:sat. aq. KNO₃) afforded naphthalylene adduct **3.27** as an orange solid (71% yield, average of two experiments). **Naphthalylene adduct 3.27:** mp >200 °C; *R_f* 0.70 (14:2:1 CH₃CN:H₂O:saturated aqueous KNO₃); ¹H NMR (500 MHz, CD₃CN): δ 9.41 (s, 2H), 9.36 (dd, *J* = 8.6, 1.2, 2H), 8.30–8.27 (m, 2H), 8.24 (dd, *J* = 5.4, 1.3, 2H), 8.07 (d, *J* = 8.3, 2H), 7.89–7.77 (m, 10H), 7.59 (ddd, *J* = 6.0, 1.5, 0.8, 2H), 7.09 (td, *J* = 7.2, 1.5, 2H), 6.97 (td, *J* = 7.7, 1.4, 2H), 6.91 (td, *J* = 6.8, 1.5, 2H), 6.38 (dd, *J* = 7.5, 0.8, 2H); ¹³C NMR (125 MHz, CD₃CN): δ 167.8, 150.71, 150.65, 149.8, 148.1, 144.6, 138.8, 134.0, 133.4, 132.2, 132.0, 130.7, 128.7, 128.5, 128.0, 125.8, 125.2, 124.9, 123.7, 122.9, 120.2; IR (film): 3050, 2924, 2855, 1608, 1479 cm⁻¹; HR-ESI-MS (*m/z*) [M – PF₆]⁺ calcd for C₄₂H₂₇N₄Ir⁺, 780.1859; found 780.1835.

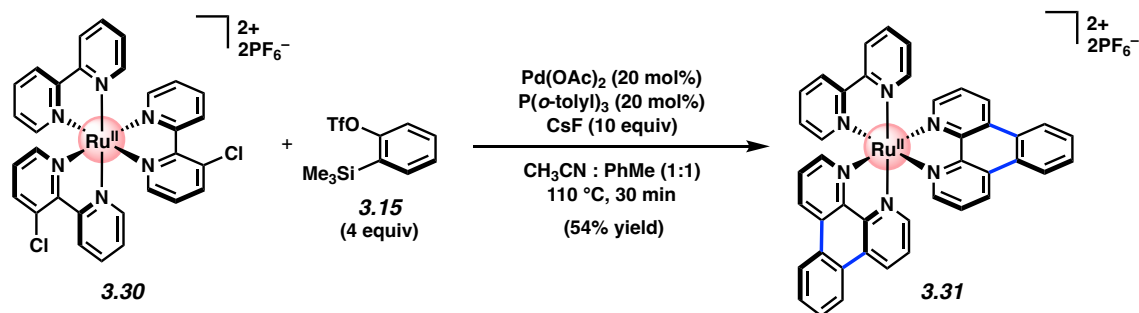


Isoquinolinyl adduct 3.28. Followed representative procedure A. Purification by flash chromatography (100% EtOAc → 14:1:1 MeCN:H₂O:sat. aq. KNO₃) afforded isoquinolinyl adduct **3.28** as a red solid (91% yield, average of two experiments). **Isoquinolinyl adduct 3.28:** mp >200 °C; R_f 0.63 (14:1:1 CH₃CN:H₂O:saturated aqueous KNO₃); ¹H NMR (500 MHz, CD₃CN): δ 9.30 (dd, *J* = 8.5, 1.3, 2H), 9.04 (d, *J* = 8.5, 2H), 8.92–8.84 (m, 2H), 8.42 (d, *J* = 8.0, 2H), 8.18 (dd, *J* = 5.1, 1.3, 2H), 8.01–7.97 (m, 2H), 7.93–7.90 (m, 2H), 7.87–7.78 (m, 6H), 7.40 (d, *J* = 6.5, 2H), 7.26 (d, *J* = 6.5, 2H), 7.18 (ddd, *J* = 8.1, 7.0, 1.3, 2H), 6.93 (td, *J* = 7.5, 1.2, 2H), 6.40 (dd, *J* = 7.6, 1.2, 2H); ¹³C NMR (125 MHz, CD₃CN): δ 169.5, 154.6, 151.6, 147.8, 146.7, 141.9, 138.0, 134.8, 133.1, 132.8, 131.8, 131.4, 131.2, 129.9, 129.1, 128.4, 128.3, 127.7, 127.1, 125.5, 123.3, 122.7; IR (film): 3047, 1577, 1541, 1435, 841 cm⁻¹; HR-ESI-MS (*m/z*) [M – PF₆]⁺ calcd for C₄₆H₃₀N₄Ir⁺, 831.2100; found 831.2111.

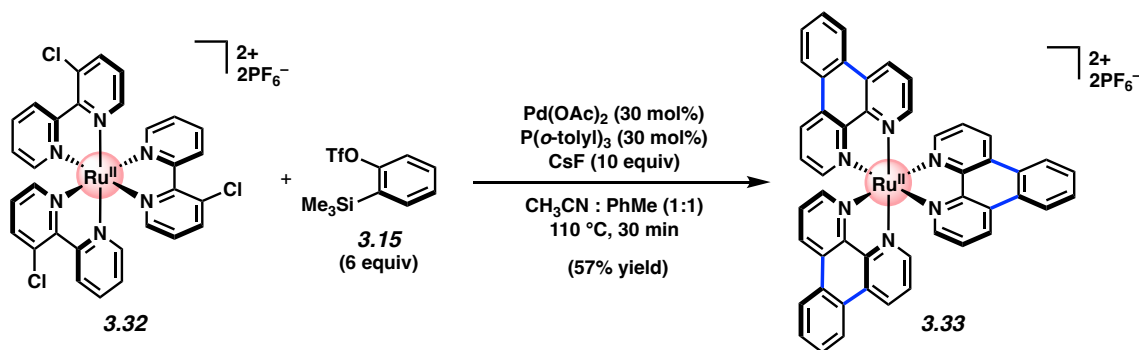


Fluorinated Ir adduct 3.29. Followed representative procedure A. Purification by flash chromatography (100% EtOAc \rightarrow 14:1:1 MeCN:H₂O:sat. aq. KNO₃) afforded fluorinated Ir adduct **3.29** as a golden solid (91% yield, average of two experiments). **Fluorinated Ir adduct 3.29:** mp >200 °C; R_f 0.64 (14:1:1 CH₃CN:H₂O:saturated aqueous KNO₃); ¹H NMR (500 MHz, CD₃CN): δ 9.33 (dd, $J = 8.6, 1.3, 2\text{H}$), 8.94–8.82 (m, 2H), 8.35–8.30 (m, 4H), 8.01–7.97 (m, 2H), 7.92 (dd, $J = 8.5, 5.1, 2\text{H}$), 7.85 (td, $J = 8.0, 1.3, 2\text{H}$), 7.54 (ddd, $J = 5.9, 1.6, 0.7, 2\text{H}$), 6.93 (ddd, $J = 7.8, 6.0, 1.4, 2\text{H}$), 6.72 (ddd, $J = 12.5, 9.5, 2.5, 2\text{H}$), 5.84 (dd, $J = 8.6, 2.4, 2\text{H}$); ¹³C NMR (125 MHz, CD₃CN): δ 165.5, 165.4, 164.7, 164.6, 163.5, 163.43, 163.40, 163.3, 161.4, 161.3, 155.33, 155.28, 151.9, 150.8, 147.6, 140.4, 135.3, 132.0, 131.3, 129.12, 129.11, 129.09, 129.05, 128.4, 125.5, 124.8, 124.7, 124.5, 114.91, 114.89, 114.77, 114.75, 99.9, 99.7, 99.5; IR (film): 3082, 1739, 1603, 1406, 1105, 840 cm⁻¹; HR-ESI-MS (m/z) [$\text{M} - \text{PF}_6$]⁺ calcd for C₃₈H₂₂F₄N₄Ir⁺, 803.1410; found 803.1416.

(Note: Complex splitting patterns observed due to presence of fluoride substituents; these data represent empirically observed chemical shifts from the ¹³C NMR spectrum)



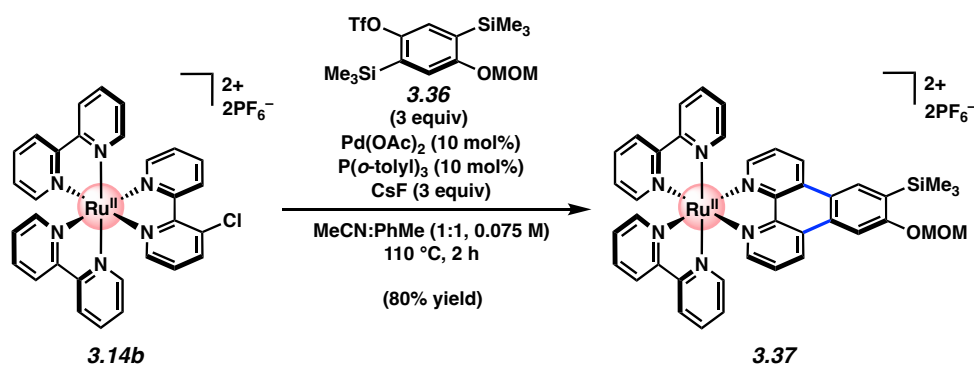
Bis(annulation) adduct 3.31. Followed representative procedure A. Purification by flash chromatography (100% EtOAc \rightarrow 14:1:1 CH₃CN:H₂O:sat. aq. KNO₃) afforded adduct **3.31** (54% yield, average of two experiments) as a red solid. **Bis(annulation adduct) 3.31:** mp >250 °C; *R_f* 0.77 (7:2:1 MeCN:H₂O:sat. aq. KNO₃); ¹H NMR (500 MHz, CD₃CN): δ 9.27 (d, *J* = 8.6, 1H), 9.16 (d, *J* = 8.6, 1H), 8.96–8.85 (m, 2H), 8.54 (d, *J* = 8.4, 1H), 8.17 (d, *J* = 5.2, 1H), 8.07–7.92 (m, 4H), 7.83 (dd, *J* = 8.5, 5.3, 1H), 7.74 (d, *J* = 5.3, 1H), 7.61 (dd, *J* = 8.2, 5.4, 1H), 7.28 (t, *J* = 6.4, 1H); ¹³C NMR (125 MHz, CD₃CN, 19 of 21 signals observed) δ 158.1, 153.1, 152.9, 152.8, 149.0, 148.8, 138.7, 133.2, 133.0, 131.32, 131.26, 131.2, 129.14, 128.3, 127.4, 127.3, 125.64, 125.60, 125.1; IR (film): 1467, 1436, 1407, 840, 762 cm⁻¹; HR-ESI-MS (*m/z*) [M – PF₆]⁺ calcd for C₄₂H₂₈N₆F₆PRu⁺, 863.10662; found 863.1080.



(Tris)annulation adduct 3.33. Followed representative procedure B. Purification by flash chromatography (100% EtOAc \rightarrow 14:1:1 CH₃CN:H₂O:sat. aq. KNO₃) afforded adduct **3.33**

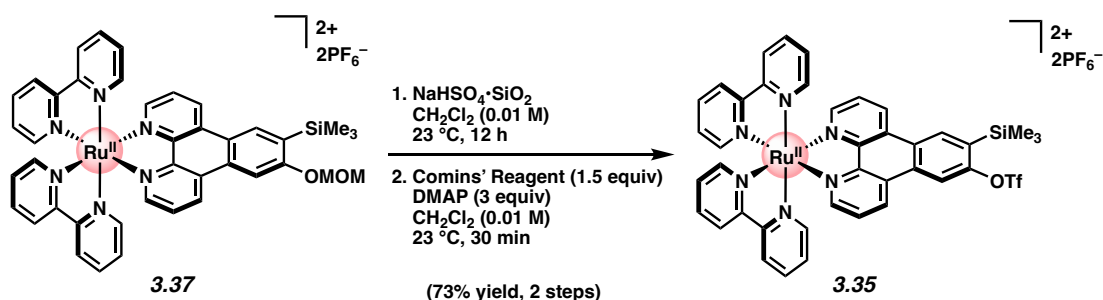
(57% yield, average of two experiments) as a red solid. (**Tris**)annulation adduct **3.33**: mp >250 °C; R_f 0.78 (7:2:1 CH₃CN:H₂O:sat. aq. KNO₃); ¹H NMR (500 MHz, CD₃CN): δ 9.22 (dd, J = 8.7, 0.7, 6H), 8.93–8.90 (m, 6H), 8.08 (dd, J = 5.3, 1.0, 6H), 8.03–7.99 (m, 6H), 7.68 (dd, J = 8.3, 5.3, 6H); ¹³C NMR (125 MHz, CD₃CN) δ 153.1, 149.0, 133.1, 131.3, 131.2, 129.2, 127.3, 125.6; IR (film): 2962, 1435, 1407, 1260, 1211, 1084, 1021, 840, 805, 758, 557; HR-ESI-MS (m/z) [M – PF₆]⁺ calcd for C₄₈H₃₀F₆N₆PRu⁺, 937.12227; found 937.12227.

3.8.2.6 Synthesis and Trapping Experiments of Ru-Centered Aryne



Methoxymethyl ether adduct 3.37. To a 20 mL scintillation vial was added Pd(OAc)₂ (10.1 mg, 44.8 μmol, 10 mol%), chloro-Ru(bpy)₃[PF₆]₂ **3.14b** (400.5 mg, 0.448 mmol, 1.0 equiv), P(*o*-tolyl)₃ (13.6 mg, 44.8 μmol, 10 mol%), MeCN (3.0 mL), PhMe (3.0 mL), silyl triflate **3.36** (564 mg, 1.31 mmol, 3.0 equiv), an oven-dried magnetic stir bar, and CsF (204 mg, 1.34 mmol, 3.0 equiv) sequentially. The reaction was then purged with N₂ for 5 min before being sealed with a Teflon-lined screw cap under a flow of N₂, sealed with Teflon tape and electrical tape, transferred to an Al-block, and stirred at 110 °C for 2 h. After cooling to 23 °C, the mixture was filtered through a plug of celite with MeCN (10 mL), and concentrated under reduced pressure. The crude residue was adsorbed onto SiO₂ and purified by flash chromatography (100% EtOAc

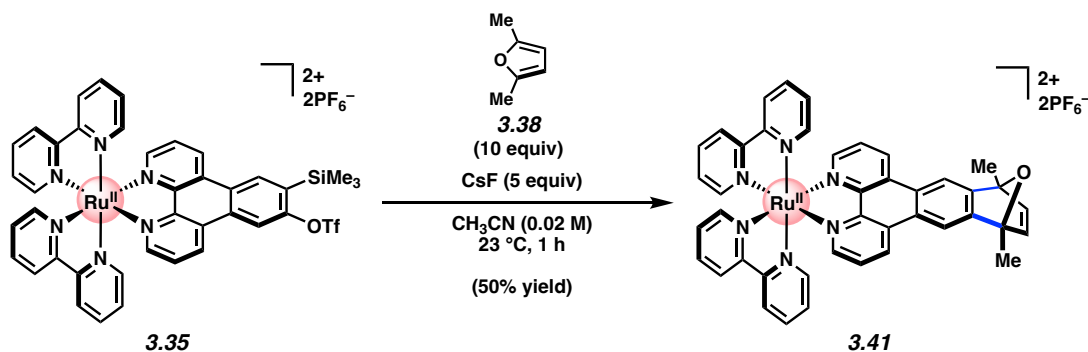
→ 14:1:1 MeCN:H₂O:sat. aq. KNO₃). To the concentrated aqueous mixture was added saturated aqueous KPF₆ (100 mL) to precipitate the desired product, and the resultant mixture was transferred to a separatory funnel with CH₂Cl₂ (50 mL). The layers were separated and the aqueous layer was extracted with CH₂Cl₂ (2 x 50 mL). The combined organic layers were then concentrated under reduced pressure before being redissolved in CH₃CN (10 mL). Activated charcoal (500 mg) was then added and the mixture was agitated for 10 seconds before being filtered over celite, concentrated under reduced pressure, and dried under reduced pressure (<1 torr) at 100 °C for 12 h to afford methoxymethyl ether adduct **3.37** as a red solid (380 mg, 80% yield). **Methoxymethyl ether adduct 3.37**: mp >250 °C; R_f 0.79 (7:2:1 CH₃CN:H₂O:saturated aqueous KNO₃); ¹H NMR (500 MHz, CD₃CN): δ 9.25 (dd, *J* = 12.0, 8.5, 2H), 8.88 (s, 1H), 8.60 (dd, *J* = 8.2, 2H), 8.56 (dd, *J* = 8.2, 2H), 8.34 (s, 1H), 8.16–8.11 (m, 3H), 8.08 (d, *J* = 5.2, 1H), 8.03 (tt, *J* = 7.9, 1.7, 2H), 7.91 (d, *J* = 5.8, 2H), 7.82 (td, *J* = 8.4, 5.3, 2H), 7.69 (t, *J* = 6.8, 2H), 7.50 (td, *J* = 6.6, 1.0, 2H), 7.28 (dd, *J* = 12.9, 5.5, 2H), 5.58 (q, *J* = 5.5, 2H), 3.54 (s, 3H), 0.48 (s, 9H); ¹³C NMR (100 MHz, CD₃CN) δ 163.8, 158.1, 157.9, 152.9, 152.84, 152.79, 152.8, 152.7, 151.6, 149.2, 147.7, 138.7, 138.6, 134.4, 133.2, 132.7, 132.6, 131.8, 131.2, 130.8, 128.5, 128.3, 128.3, 127.3, 127.1, 125.2, 125.1, 122.6, 106.7, 94.9, 57.0, 55.2, -1.02; IR (film): 3464, 3079, 1604, 1369, 1345 cm⁻¹; HR-ESI-MS (*m/z*) [M - PF₆]⁺ calcd for C₄₁H₃₈F₆N₆O₂PRuSi⁺, 921.15163; found 921.1541.



Silyl triflate 3.35. To a stirred solution of methoxymethyl ether **3.37** (259 mg, 0.243 mmol, 1.0 equiv) in CH_2Cl_2 (25 mL, 0.01 M) at $23\text{ }^\circ C$ was added solid supported catalyst⁷⁴ $NaHSO_4 \cdot SiO_2$ (2.63 g, stored in the oven for >48 h and added while hot) in one portion. The reaction mixture was then stirred for 6 h at $23\text{ }^\circ C$. The mixture was then filtered through a plug of silica gel with 7:2:1 MeCN:H₂O:sat. aq. KNO_3 (100 mL). The eluate was concentrated under reduced pressure before being crashed out with sat. aq. KPF_6 (100 mL) and transferred to a separatory funnel with CH_2Cl_2 (100 mL). The layers were separated and the aqueous layer was extracted with CH_2Cl_2 (2 x 100 mL). The combined organic layers were then concentrated under reduced pressure to afford the intermediate silyl alcohol as a red solid.

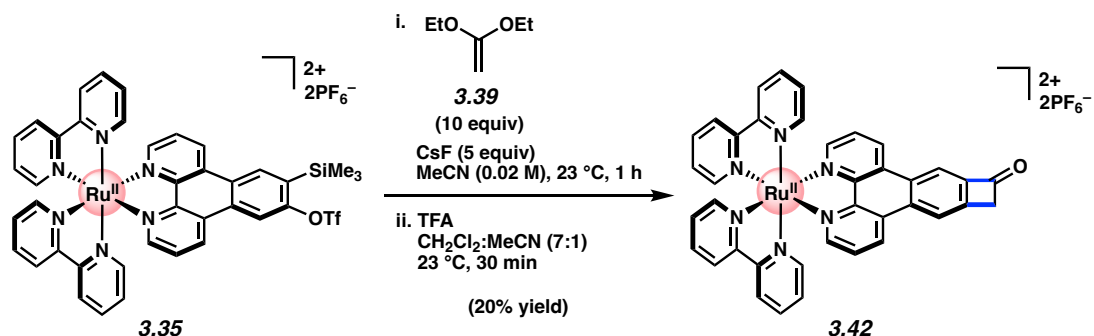
The intermediate silyl alcohol was then dissolved in CH_2Cl_2 (25 mL, 0.01 M) and while stirring at $23\text{ }^\circ C$, DMAP (89.3 mg, 0.731 mmol, 3.0 equiv) and Comins' reagent (144 mg, 0.366 mmol, 1.5 equiv) were added sequentially, each in single portions. After stirring at $23\text{ }^\circ C$ for 30 min, the reaction was concentrated under reduced pressure and then loaded onto a silica plug. The silica plug was washed with EtOAc (200 mL; eluate discarded) before being eluted with 7:2:1 MeCN:H₂O:sat. aq. KNO_3 (100 mL). The red eluate was then concentrated under reduced pressure and transferred with CH_2Cl_2 (100 mL) to a separatory funnel containing aqueous HCl (2.0 M, 100 mL). The layers were separated and the organic layer was washed with aqueous HCl (2.0 M, 2 x 40 mL). The combined aqueous layers were then extracted with CH_2Cl_2 (2 x 100 mL). The organic layers were then combined, dried over Na_2SO_4 , and concentrated under

reduced pressure. The residue was then filtered over a pad of neutral alumina (200 mL CH₃CN eluent) and concentrated under reduced pressure before being dried under reduced pressure (<1 torr) at 100 °C for 1 h to afford silyl triflate **3.35** as a red solid (204 mg, 73% yield). **Silyl triflate 3.35**: mp: >250 °C; *R_f* 0.34 (14:1:1 MeCN:H₂O:sat. aq. KNO₃); ¹H NMR (500 MHz, CD₃CN): δ 9.29 (d, *J* = 8.6, 1H), 9.11 (d, *J* = 8.5, 1H), 9.02 (s, 1H), 8.69 (s, 1H), 8.53 (d, *J* = 8.2, 2H), 8.49 (d, *J* = 8.2, 2H), 8.13–8.08 (m, 4H), 8.00 (tt, *J* = 7.9, 1.7, 2H), 7.84–7.78 (m, 4H), 7.60 (t, *J* = 5.3, 2H), 7.45 (t, *J* = 6.8, 2H), 7.22 (qt, *J* = 6.6, 1.3, 2H), 0.55 (s, 9H); ¹³C NMR (125 MHz, CD₃CN) δ 158.1, 157.9, 156.2, 153.7, 153.3, 153.00, 152.97, 152.9, 152.8, 149.5, 149.1, 138.9, 138.7, 136.7, 134.7, 133.6, 133.2, 131.8, 130.3, 130.1, 128.5, 128.4, 128.0, 127.7, 125.24, 125.16, 116.1; IR (film): 3359, 3310, 3193, 2920, 2851, 1632 cm⁻¹; HR-ESI-MS (*m/z*) [M – PF₆]⁺ calcd for C₄₀H₃₃F₉N₆O₃PRuSSi⁺, 1009.07470; found 1009.0704.



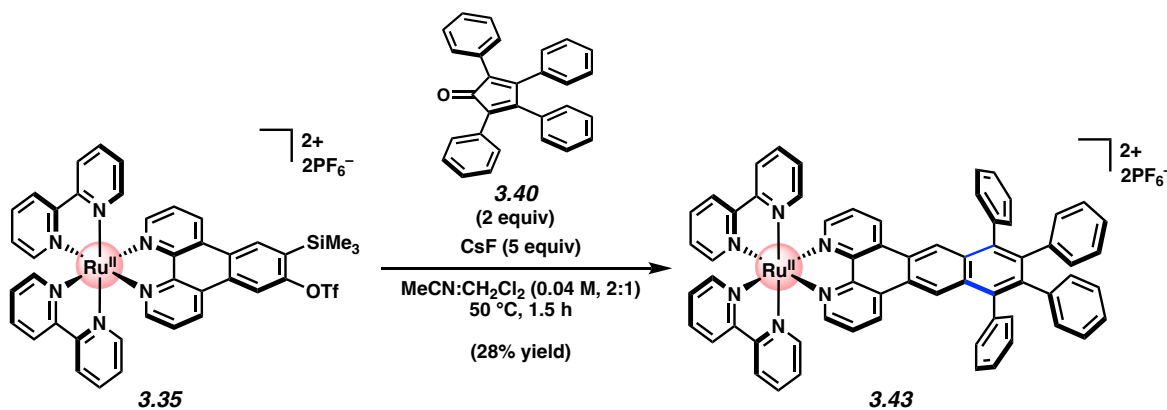
Cycloadduct 3.41. To a 1-dram vial was added silyl triflate **3.35** (19.5 mg, 16.9 μmol) and dissolved in MeCN (0.8 mL, 0.02 M). 2,5-dimethylfuran (**3.38**) (16.2 mg, 0.17 mmol, 10 equiv) was then added in one portion. While stirring, CsF (12.8 mg, 0.085 mmol, 5 equiv) was added in one portion and the reaction was stirred at 23 °C for 1 h. After 1 h, the reaction mixture was then filtered through a plug of celite with MeCN (10 mL), adsorbed onto silica gel (500 mg) under reduced pressure, and purified by flash chromatography (100% EtOAc → 14:1:1

MeCN:H₂O:sat. aq. KNO₃). To the resultant concentrated aqueous mixture was added saturated aqueous KPF₆ (50 mL) to precipitate the desired product, and the resultant mixture was transferred to a separatory funnel with CH₂Cl₂ (50 mL). The layers were separated and the aqueous layer was extracted with CH₂Cl₂ (2 x 50 mL). The combined organic layers were then concentrated under reduced pressure, dried over sodium sulfate, and dried under reduced pressure (<1 torr) at 100 °C for 12 h to afford cycloadduct **3.41** as a red solid (4.1 mg, 25% yield). **Cycloadduct 3.41**: mp: >250 °C; R_f 0.31 (14:1:1 MeCN:H₂O:sat. aq. KNO₃); ¹H NMR (500 MHz, CD₃CN): δ 9.23 (dt, *J* = 8.6, 1.3, 2H), 8.59 (d, *J* = 1.4, 2H), 8.52 (dq, *J* = 8.3, 0.8, 2H), 8.49 (ddt, *J* = 8.3, 3.0, 1.1, 2H), 8.09 (td, *J* = 8.0, 1.4, 2H), 8.04 (ddd, *J* = 5.2, 4.3, 1.1, 2H), 8.01–7.94 (m, 2H), 7.83 (dddd, *J* = 5.6, 3.3, 1.5, 0.8, 2H), 7.76 (dd, *J* = 8.6, 5.2, 2H), 7.57 (dddd, *J* = 11.8, 5.7, 1.6, 0.7, 2H), 7.44 (ddt, *J* = 7.7, 5.6, 1.3, 2H), 7.19 (dddd, *J* = 11.1, 7.8, 5.8, 1.3, 2H), 6.92 (app dd, *J* = 5.4, 3.4, 2H), 2.044 (s, 3H), 2.037 (s, 3H); ¹³C NMR (125 MHz, CD₃CN): δ 158.1, 157.90, 157.88, 156.2, 152.90, 152.89, 152.8, 152.3, 148.6, 147.41, 147.38, 138.8, 138.62, 138.59, 133.3, 131.3, 128.5, 128.33, 128.32, 127.2, 127.1, 125.2, 125.11, 125.09, 114.9, 114.8, 89.6; IR (film): 2931, 1467, 1447, 1390, 1141, 839, 762, 558 cm⁻¹; HR-ESI-MS (*m/z*) [M – PF₆]⁺ calcd for C₄₂H₃₂F₆N₆OPRu⁺, 883.13284; found 883.1326.



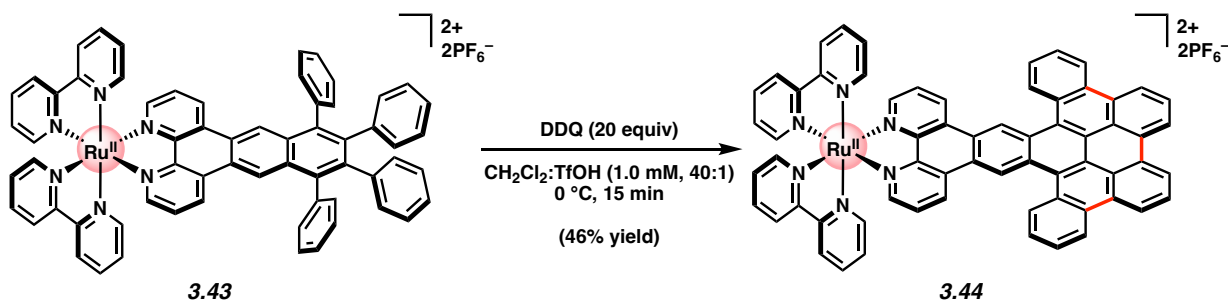
Cyclobutanone 3.42. To a stirred solution of silyl triflate **3.35** (20.5 mg, 17.8 μmol , 1.0 equiv) and 1,1-diethoxyethene (**3.39**) (24.9 μL , 178 μmol , 10.0 equiv) in MeCN (0.9 mL, 0.02 M) at 23 °C was added CsF (13.5 mg, 88.8 μmol , 5.0 equiv) in one portion. After stirring at 23 °C for 1 h, the reaction was filtered through a plug of celite with MeCN (10 mL) and then concentrated under reduced pressure. To the resulting residue was added CH₂Cl₂ (2.1 mL) and MeCN (0.3 mL) and while stirring at 23 °C, TFA (0.5 mL) was added dropwise over 20 seconds and the mixture was stirred at 23 °C for 30 min. The reaction was then quenched by slow addition of saturated aqueous NaHCO₃ (2.5 mL) over 30 seconds. The reaction was then transferred to a separatory funnel with CH₂Cl₂ (25 mL) and saturated aqueous KPF₆ (20 mL). The layers were separated and the aqueous layer was extracted with CH₂Cl₂ (3 x 50 mL). The combined organic layers were then dried over Na₂SO₄, filtered, and concentrated under reduced pressure. Purification by preparative TLC (14:1:1 MeCN:H₂O:sat. aq. KNO₃) afforded cyclobutanone **3.42** as a red solid (3.4 mg, 20% yield). **Cyclobutanone 3.42**: mp >250 °C; R_f 0.34 (14:1:1 MeCN:H₂O:sat. aq. KNO₃); ¹H NMR (500 MHz, CD₃CN): δ 9.29 (d, $J = 8.4$, 1H), 9.21 (d, $J = 8.4$, 1H), 9.07 (s, 1H), 8.89 (s, 1H), 8.53 (d, $J = 8.4$, 2H), 8.50 (d, $J = 8.4$, 2H), 8.14–8.05 (m, 4H), 8.00 (t, $J = 8.2$, 2H), 7.84–7.76 (m, 4H), 7.62 (d, $J = 5.0$, 2H), 7.45 (t, $J = 6.4$, 2H), 7.23 (t, $J = 6.0$, 2H), 4.37 (s, 2H); ¹³C NMR (125 MHz, CD₃CN): δ 189.2, 158.1, 157.9, 153.7, 153.1, 152.99, 152.95, 152.83, 152.81, 151.7, 150.7, 149.7, 148.7, 138.9, 138.7, 134.7, 134.1, 133.3,

131.9, 131.1, 130.1, 128.5, 128.4, 127.63, 127.58, 125.23, 125.16, 120.5, 117.3; IR (film): 2923, 1772, 1618, 1469, 1449, 839, 558 cm^{-1} ; HR-ESI-MS (m/z) $[\text{M} - \text{PF}_6]^+$ calcd for $\text{C}_{38}\text{H}_{26}\text{F}_6\text{N}_6\text{OPRu}^+$, 829.08589; found 829.0845.



Cycloadduct 3.43. To a 1-dram vial was added silyl triflate **3.35** (99.7 mg, 86.4 μmol , 1.0 equiv), tetraphenylcyclopentadienone (**3.40**, 66.4 mg, 173 μmol , 2.0 equiv), MeCN (1.4 mL, 0.06 M), CH₂Cl₂ (0.7 mL, 0.12 M), and CsF (65.6 mg, 432 μmol , 5.0 equiv) were added sequentially. The reaction vessel was purged with N₂, sealed with a Teflon cap, and placed in a preheated, 50 °C aluminum heating block. After stirring for 1.5 h, the reaction was cooled to 23 °C. The reaction mixture was then filtered through a plug of celite with MeCN (10 mL), adsorbed onto silica gel (750 mg) under reduced pressure, and purified by flash chromatography (100% EtOAc \rightarrow 14:1:1 MeCN:H₂O:sat. aq. KNO₃). To the concentrated aqueous mixture was added saturated aqueous KPF₆ (50 mL) to precipitate the desired product, and the resultant mixture was transferred to a separatory funnel with CH₂Cl₂ (50 mL). The layers were separated and the aqueous layer was extracted with CH₂Cl₂ (1 x 50 mL). The combined organic layers were then dried over sodium sulfate, filtered, concentrated under reduced pressure, and dried under reduced pressure (<1 torr) at 100 °C for 12 h to afford cycloadduct **3.43** as a red solid

(30.7 mg, 28% yield). **Cycloadduct 3.43**: mp >250 °C; R_f 0.84 (7:2:1 MeCN:H₂O:sat. aq. KNO₃); ¹H NMR (600 MHz, CD₃CN): δ 8.94 (s, 2H), 8.60 (dd, J = 8.6, 1.1, 2H), 8.51 (dt, J = 8.2, 1.0, 2H), 8.48 (dt, J = 8.2, 1.0, 2H), 8.08 (td, J = 8.0, 1.4, 2H), 8.00 (td, J = 7.9, 1.5, 2H), 7.94 (dd, J = 5.3, 1.1, 2H), 7.79 (ddd, J = 5.6, 1.4, 0.6, 2H), 7.64 (ddd, J = 5.7, 1.4, 0.6, 2H), 7.60 (dd, J = 8.3, 5.4, 2H), 7.44–7.34 (m, 12H), 7.23 (ddd, J = 7.7, 5.8, 1.3, 2H), 7.06–6.97 (m, 4H), 6.96–6.89 (m, 6H); ¹³C NMR (125 MHz, CD₃CN): δ 158.0, 157.9, 152.8, 152.7, 152.4, 149.6, 142.2, 141.1, 140.0, 139.5, 138.8, 138.7, 133.0, 132.6, 132.24, 132.18, 132.00, 131.98, 131.8, 128.91, 128.88, 128.5, 128.4, 128.2, 127.8, 127.6, 126.8, 126.2, 125.2, 125.1, 124.2; IR (film): 2929, 1606, 1469, 1447, 840, 763, 701, 558 cm⁻¹; HR-ESI-MS (m/z) [M – PF₆]⁺ calcd for C₆₄H₄₄F₆N₆PRu⁺, 1143.23182; found 1443.2338.



Scholl Product 3.44. To a stirred solution of **3.43** (6.3 mg, 3.9 μmol, 1.0 equiv), in CH₂Cl₂ (4.0 mL) at 0 °C was added DDQ (22 mg, 98 μmol, 20 equiv) in one portion. Then, TfOH (0.1 mL) was added dropwise over 1 min, whereupon the reaction turned deep green in color. The reaction was then stirred at 0 °C for 15 min, followed by addition of saturated aqueous NaHCO₃ (4.0 mL) slowly, over 10 seconds. The resulting mixture was then stirred at 0 °C for 5 min before being allowed to warm to 23 °C. It was then transferred with CH₂Cl₂ (30 mL) to a separatory funnel containing saturated aqueous KPF₆ (30 mL). The layers were separated and the aqueous layer was extracted with CH₂Cl₂ (2 x 30 mL). The combined organic layers were then concentrated

under reduced pressure and loaded onto a silica plug, which was washed with EtOAc (25 mL) before being eluted with 7:2:1 MeCN:H₂O:sat. aq. KNO₃ (30 mL). The red eluate was then concentrated under reduced pressure, saturated aqueous KPF₆ (30 mL) was added to precipitate the desired product, and the resultant mixture was transferred to a separatory funnel with CH₂Cl₂ (30 mL). The layers were separated and the aqueous layer was extracted with CH₂Cl₂ (1 x 30 mL). The combined organic layers were then concentrated under reduced pressure, dried over Na₂SO₄, filtered, and concentrated under reduced pressure to afford **Scholl Product 3.44** as a red solid (2.9 mg, 46% yield). **Scholl Product 3.44**: R_f 0.41 (14:1:1 MeCN:H₂O:sat. aq. KNO₃); ¹H NMR (500 MHz, CD₃CN): δ 10.03 (s, 2H), 9.05 (d, *J* = 8.3, 2H), 8.75 (d, *J* = 8.3, 2H), 8.71–8.64 (m, 4H), 8.61 (d, *J* = 8.2, 2H), 8.57 (d, *J* = 8.2, 2H), 8.50 (d, *J* = 7.8, 2H), 8.16 (td, *J* = 8.1, 1.4, 2H), 8.08 (dd, *J* = 5.3, 0.8, 2H), 8.05 (td, *J* = 8.0, 1.4, 2H), 7.91 (d, *J* = 5.5, 2H), 7.87–7.81 (m, 4H), 7.75 (t, *J* = 7.8, 2H), 7.69 (t, *J* = 7.6, 2H), 7.61 (t, *J* = 7.4, 2H), 7.51 (ddd, *J* = 7.8, 5.5, 1.3, 2H), 7.35 (t, *J* = 6.8, 2H); ¹³C NMR (125 MHz, CD₃CN, 31 of 32 signals observed): δ 157.20, 157.19, 152.0, 151.9, 151.5, 148.6, 138.0, 137.9, 132.2, 131.0, 130.9, 129.9, 129.5, 129.1, 128.7, 127.9, 127.7, 127.6, 127.41, 127.37, 126.9, 124.6, 124.5, 124.42, 124.39, 124.3, 124.0, 123.3, 122.9, 122.2, 122.0; IR (film): 2925, 1468, 1447, 1425, 841, 761, 558 cm⁻¹; HR-ESI-MS (*m/z*) [M – PF₆]⁺ calcd for C₆₄H₄₄F₆N₆PRu⁺, 1143.23182; found 1143.2338.

Note: 3.44 readily decomposes upon removal of solvent, and must therefore be carefully handled as a dilute solution. We surmise that its instability may be a consequence of its highly π-expansive nature, which introduces numerous sites for oxidation or dimerization.

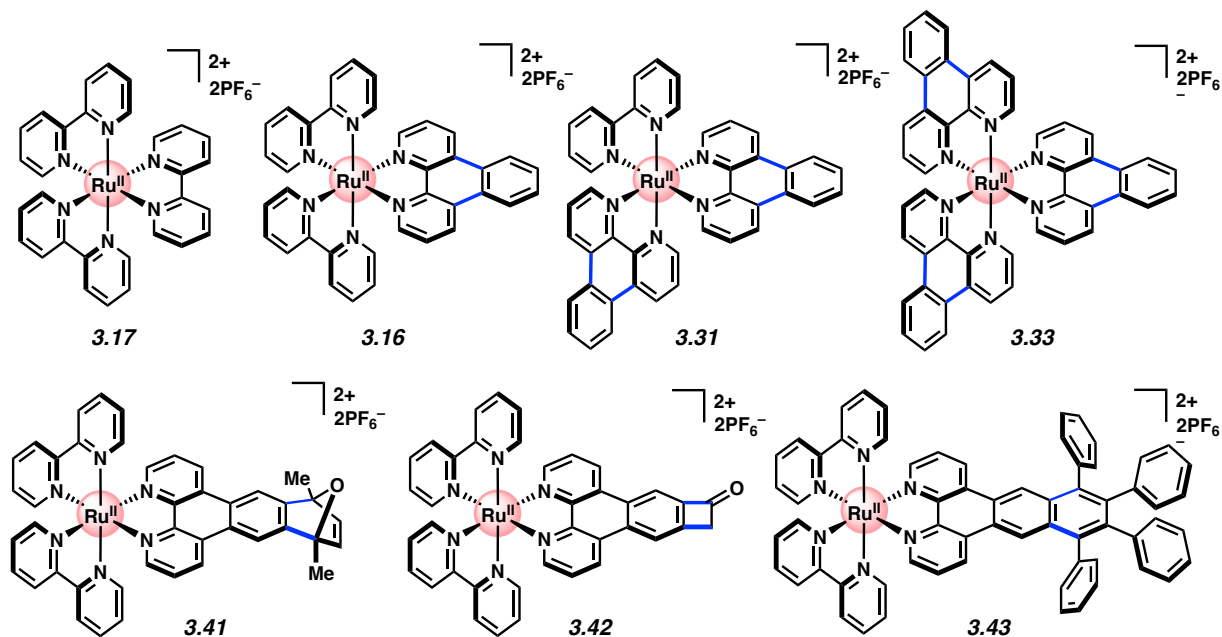
3.8.3 Photophysical Data

UV–vis absorption spectra were recorded on an Ocean Optics Flame-T spectrometer with the OceanView software package. Dynamic light scattering (DLS) data were collected using a Beckman-Coulter N4 Plus particle analyzer. Quartz cuvettes (1 cm) were used for absorbance and photoluminescence measurements. Relative quantum yields were determined in degassed acetonitrile relative to Ru(bpy)₃[PF₆]₂.

Nanosecond transient absorption experiments were performed using an Edinburgh Instruments LP920 laser flash photolysis spectrometer in conjunction with a Q-switched Nd:YAG Brilliant b laser from Quantel with a 266 nm output wavelength, a 5–8 ns pulse width, a 1 Hz repetition rate, and a 36–40 mJ pulse energy. Transient absorption detection is based on a 450 W pulsed xenon arc lamp, a Czerny-Turner TMS300 monochromator, a Hamamatsu R928 photomultiplier detector, and a Tektronix TDS3012C digital oscilloscope. Transient absorption data were collected and processed using the L900 software package provided by Edinburgh Instruments. Samples were prepared as solutions in acetonitrile and degassed by sparging with argon in a quartz cuvette. Reported transient absorption lifetime (τ_{TA}) values are reported as the average of three experiments. Phosphorescence spectra were recorded using an Edinburgh Instruments FLSP920 fluorimeter with a 450 W xenon lamp in CW (continuous wave) emission source.

3.8.3.1 Compiled Photophysical Data Table

Table 3.3. Photophysical data for selected Ru complexes. Samples were prepared as solutions in acetonitrile and degassed by sparging with argon in a quartz cuvette.



<i>Ru Complex</i>	$\lambda_{\max \text{ em.}}$ (nm)	$\epsilon \times 10^3$ (mol ⁻¹ cm ⁻¹ ; at 452 nm)	Φ_P (%)	τ_{TA} (ns)
3.17	593	18.1	9.5 (lit.) ⁶	1115
3.16	592	7.7	15	1077
3.31	589	18.2	15	1382
3.33	586	23.5	24	1479
3.41	592	14.7	14	1100
3.42	594	11.5	14	1339
3.43	591	15.8	16	2006

3.8.3.2 UV–Vis Spectra

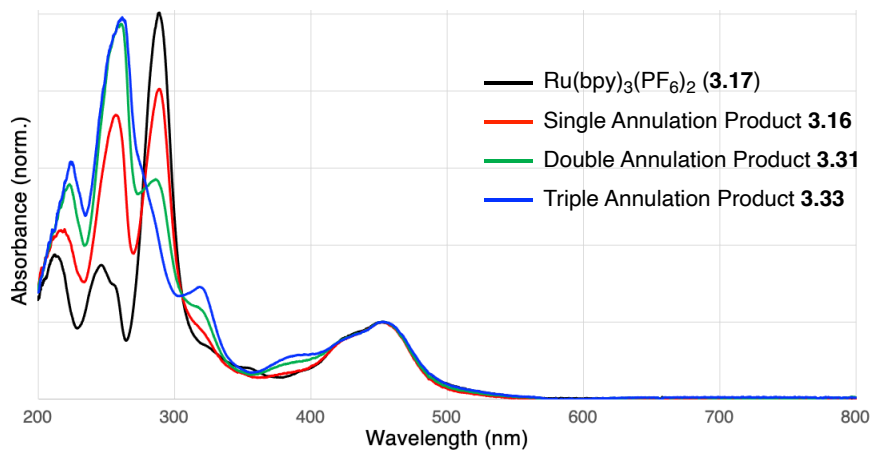


Figure 3.12. UV–vis absorption spectra of compounds **3.17**, **3.16**, **3.31**, and **3.33**. Spectra are normalized to OD = 1 at the MLCT maximum (452 nm) to compare the band shapes.

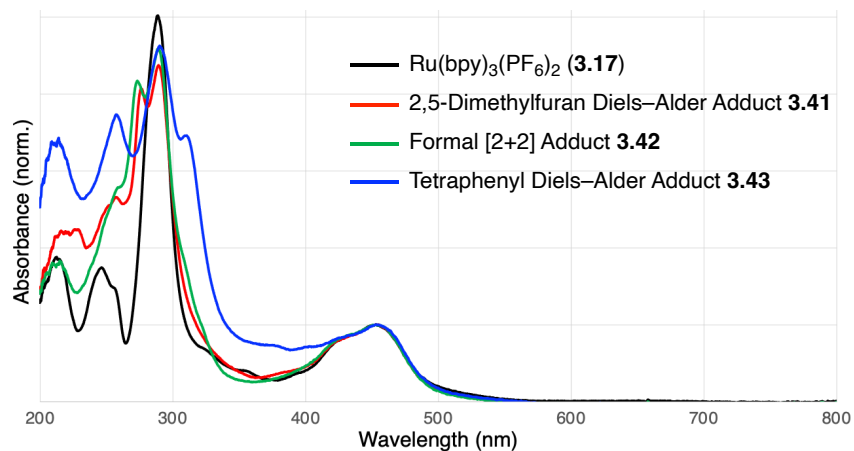


Figure 3.13. UV–vis absorption spectra of compounds **3.17**, **3.41**, **3.42**, and **3.43**. Spectra are normalized to OD = 1 at the MLCT maximum (452 nm) to compare the band shapes.

3.8.3.3 Molar Extinction Coefficient Measurements

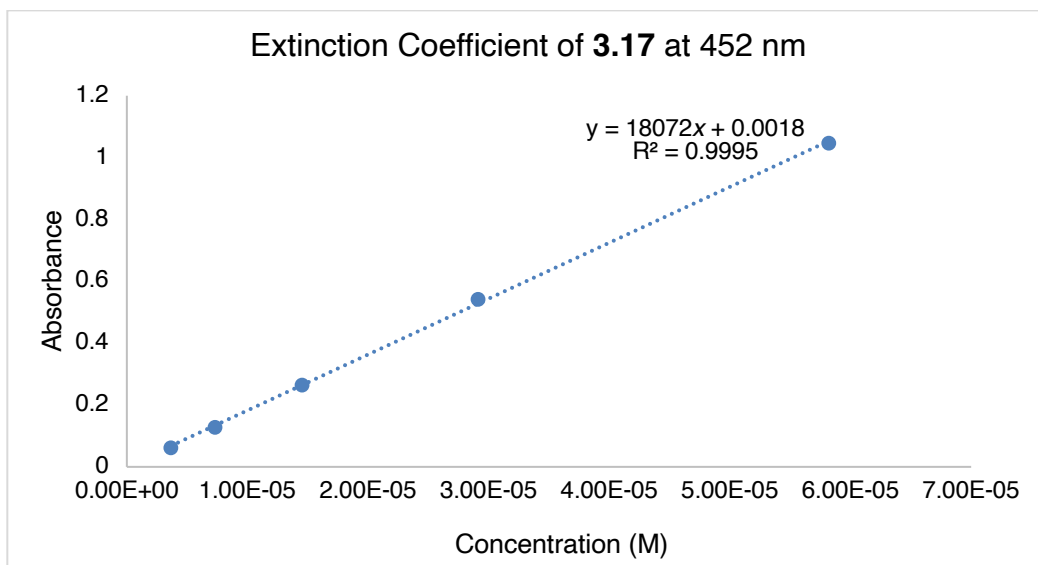


Figure 3.14. Beer-Lambert plot of **3.17** at 452 nm. ($\epsilon = 18.1 \times 10^4 \text{ M}^{-1} \text{ cm}^{-1}$).

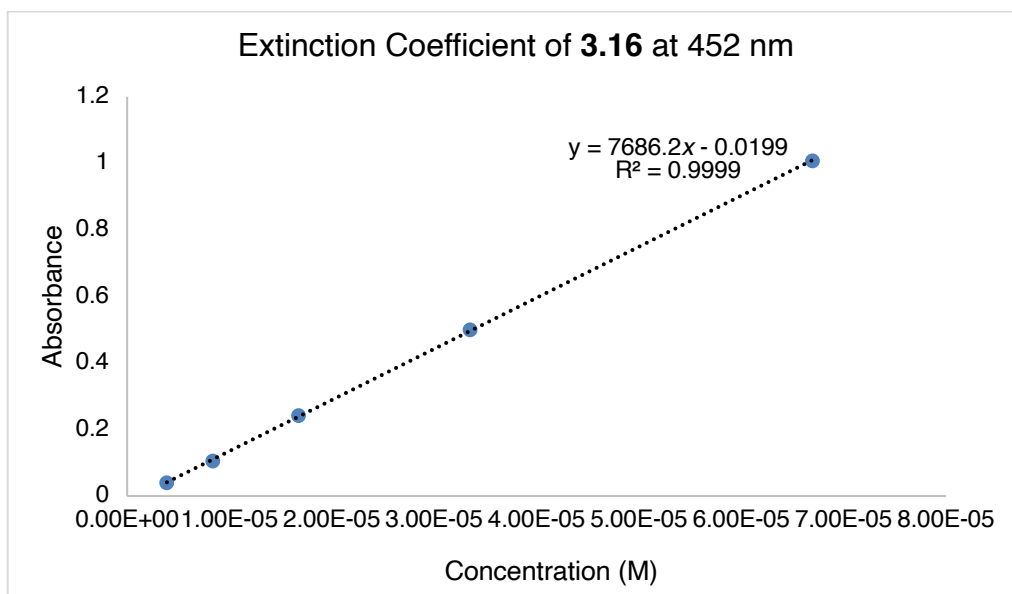


Figure 3.15. Beer-Lambert plot of **3.16** at 452 nm. ($\epsilon = 7.69 \times 10^3 \text{ M}^{-1} \text{ cm}^{-1}$).

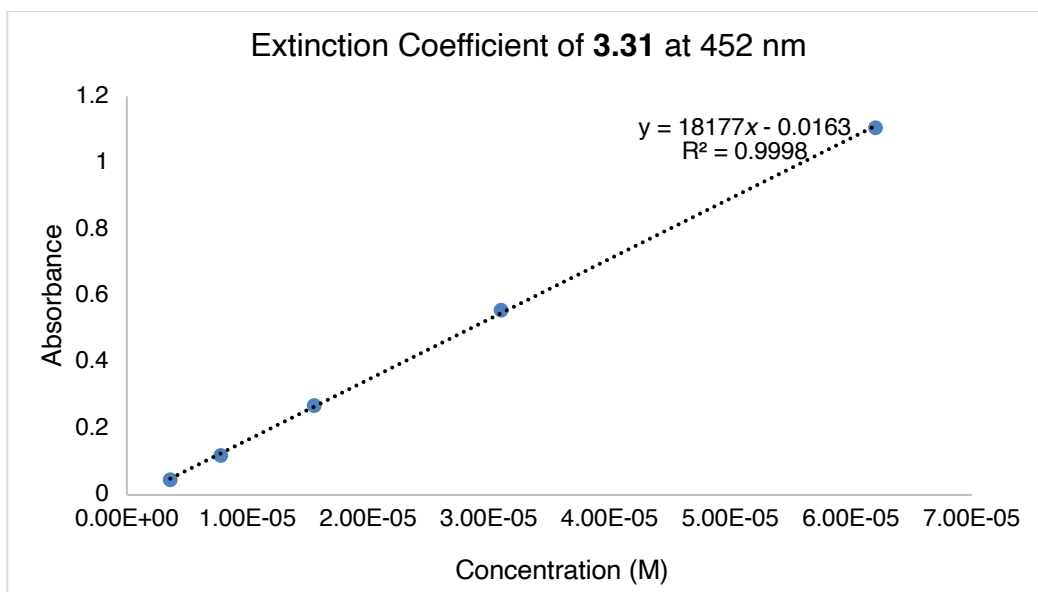


Figure 3.16. Beer-Lambert plot of **3.31** at 452 nm. ($\epsilon = 18.2 \times 10^4 \text{ M}^{-1} \text{ cm}^{-1}$).

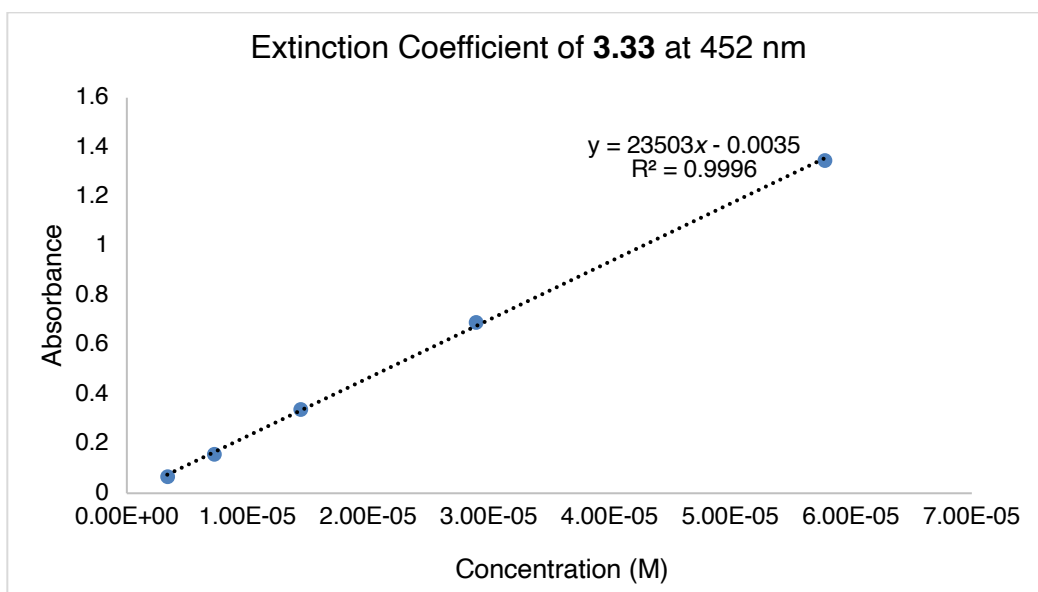


Figure 3.17. Beer-Lambert plot of **3.33** at 452 nm. ($\epsilon = 23.5 \times 10^4 \text{ M}^{-1} \text{ cm}^{-1}$).

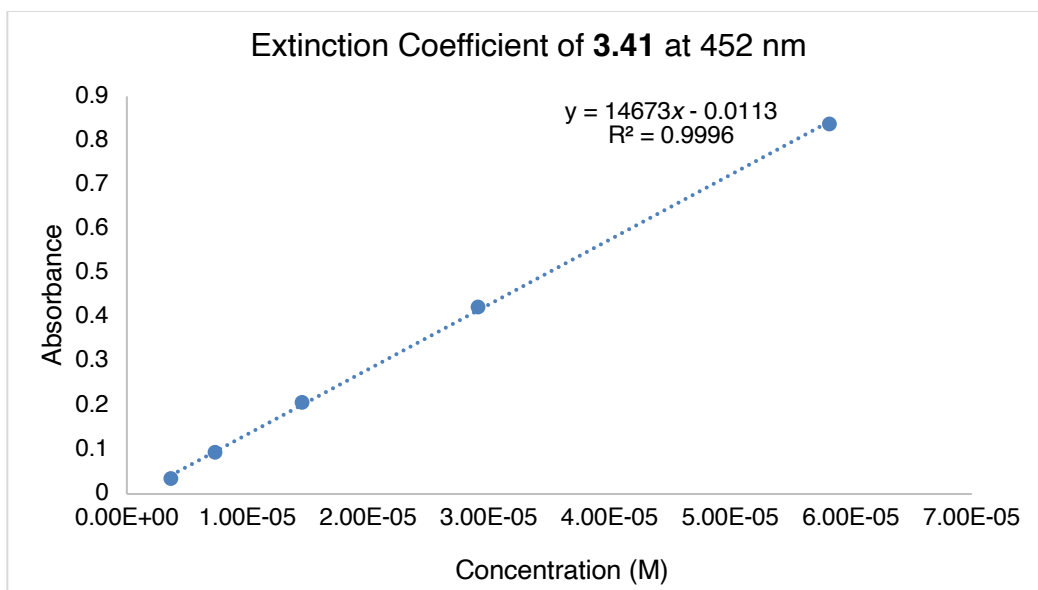


Figure 3.18. Beer-Lambert plot of **3.41** at 452 nm. ($\epsilon = 14.7 \times 10^4 \text{ M}^{-1} \text{ cm}^{-1}$).

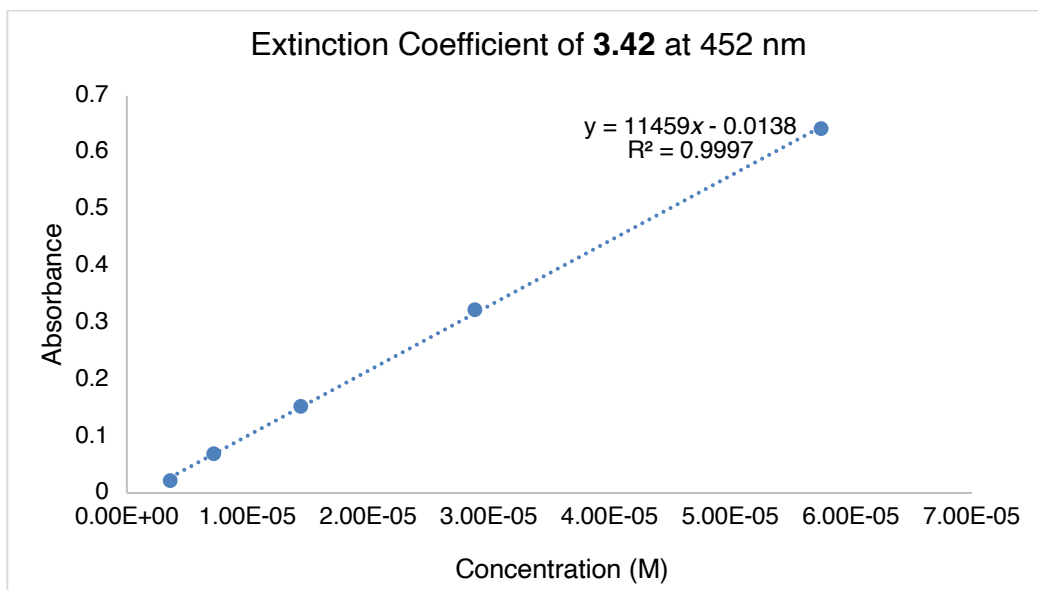


Figure 3.19. Beer-Lambert plot of **3.42** at 452 nm. ($\epsilon = 11.5 \times 10^3 \text{ M}^{-1} \text{ cm}^{-1}$).

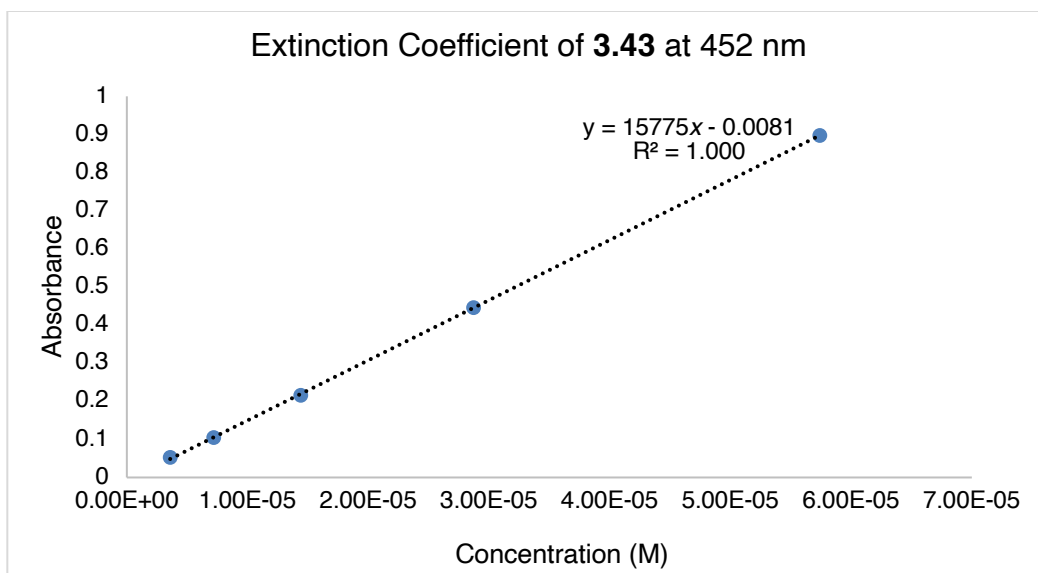


Figure 3.20. Beer-Lambert plot of **3.43** at 452 nm. ($\epsilon = 15.8 \times 10^4 \text{ M}^{-1} \text{ cm}^{-1}$).

3.8.3.4 Quantum Yield Measurements

The phosphorescence quantum yield (Φ_P) of a molecule or material is defined as follows:

$$\Phi_P = \frac{PE}{PA}$$

Where PE and PA represent the number of photons emitted and absorbed, respectively. To determine the quantum yield, we used a relative method with $\text{Ru}(\text{bpy})_3[\text{PF}_6]_2$ as a known standard in the same region of the electromagnetic spectrum.

To compare an unknown to a reference with a known quantum yield, the following relationship was used:

$$\Phi_{P,x} = \Phi_{P,r} \left(\frac{m_x}{m_r} \right) \left(\frac{n_x}{n_r} \right)$$

Where m represents the slope of the line ($y = mx + b$) obtained from graphing integrated phosphorescence intensity versus optical density across a series of samples, n is the refractive index of the solvent and the subscripts x and r represent values of the unknown and reference,

respectively. The $\Phi_{P,r}$ of Ru(bpy)₃[PF₆]₂ in degassed acetonitrile was taken to be 9.5%, as previously determined.⁷⁵

To obtain a plot of integrated phosphorescence intensity versus absorbance for the reference and unknown, five solutions and a solvent blank were prepared with absorbance at 452 nm between 0.02 and 0.30 au. Absorbance and emission spectra (with an excitation wavelength of 450 nm) were acquired for all samples. Ru(bpy)₃[PF₆]₂ and the unknown Ru complexes were diluted in acetonitrile to concentrations with optical densities at 452 nm of less than 0.3 to minimize effects of reabsorption. The phosphorescence traces were integrated, and the raw integrals were corrected by subtracting the integral over an identical range from phosphorescence traces of the blank solvent. The integrated phosphorescence intensities were then plotted against the baseline corrected absorbance values at the relevant wavelength (450 nm), and the slope and error in slope were obtained ($R^2 > 0.98$ for all traces).

3.8.4 Computational Data

Calculations were carried out with the Gaussian 16 package. Geometry optimization was performed with B3LYP with LANL2DZ basis set for Ru atom and 6-31G(d) basis set for all other atoms (C, H, N); CPCM (MeCN) solvation model was utilized.⁷⁶ Computed structures are illustrated using CYLView.⁷⁷

3.8.4.1 Complete Citation of Gaussian 16

M. J. Frisch, G. W. Trucks, H. B. Schlegel, G. E. Scuseria, M. A. Robb, J. R. Cheeseman, G. Scalmani, V. Barone, G. A. Petersson, H. Nakatsuji, X. Li, M. Caricato, A. V. Marenich, J. Bloino, B. G. Janesko, R. Gomperts, B. Mennucci, H. P. Hratchian, J. V. Ortiz, A. F. Izmaylov, J. L. Sonnenberg, D. Williams-Young, F. Ding, F. Lipparini, F. Egidi, J. Goings, B. Peng, A.

Petrone, T. Henderson, D. Ranasinghe, V. G. Zakrzewski, J. Gao, N. Rega, G. Zheng, W. Liang, M. Hada, M. Ehara, K. Toyota, R. Fukuda, J. Hasegawa, M. Ishida, T. Nakajima, Y. Honda, O. Kitao, H. Nakai, T. Vreven, K. Throssell, J. A. Montgomery, Jr., J. E. Peralta, F. Ogliaro, M. J. Bearpark, J. J. Heyd, E. N. Brothers, K. N. Kudin, V. N. Staroverov, T. A. Keith, R. Kobayashi, J. Normand, K. Raghavachari, A. P. Rendell, J. C. Burant, S. S. Iyengar, J. Tomasi, M. Cossi, J. M. Millam, M. Klene, C. Adamo, R. Cammi, J. W. Ochterski, R. L. Martin, K. Morokuma, O. Farkas, J. B. Foresman, and D. J. Fox, Gaussian, Inc., Wallingford CT, **2016**.

3.8.4.2 Energy and Cartesian Coordinates for Optimized Structure

Diels–Alder Product **3.43**:

Ru	4.40809	-0.00012	-0.00007
C	6.22913	2.03055	-1.16572
C	6.57862	1.88488	1.13838
C	7.22284	3.00866	-1.27044
C	7.57559	2.85342	1.09803
H	6.28918	1.4164	2.07072
C	7.90368	3.42517	-0.13021
H	7.46637	3.44296	-2.23182
H	8.0771	3.1454	2.01373
H	8.67631	4.18324	-0.20307
C	3.79384	0.04896	-3.03046
C	5.45287	1.52931	-2.31722
C	3.91518	0.47135	-4.34978
H	3.08641	-0.72173	-2.75111
C	5.62078	1.99568	-3.62464
C	4.8463	1.46386	-4.65154
H	3.28956	0.02634	-5.11515
H	6.34779	2.76764	-3.84278
H	4.97009	1.82056	-5.66857
N	5.91592	1.4774	0.03975
N	4.54011	0.55823	-2.03255
C	2.82646	2.63885	0.39094
C	1.54248	0.71709	0.10359
C	1.67673	3.42417	0.49829
H	3.81553	3.07389	0.46351
C	0.33237	1.43315	0.2052
C	0.432	2.82417	0.40613

H	1.77165	4.49286	0.65347
H	-0.45666	3.43751	0.48978
C	1.54243	-0.71674	-0.10598
C	2.82622	-2.63856	-0.39372
C	0.33226	-1.43263	-0.20813
C	1.67643	-3.42364	-0.50206
H	3.81525	-3.07373	-0.46595
C	0.43176	-2.82352	-0.40997
H	1.77126	-4.49225	-0.65788
H	-0.45695	-3.43667	-0.49444
N	2.76551	1.31566	0.19906
N	2.76539	-1.31546	-0.20122
C	6.57918	-1.8862	-1.13547
C	6.22731	-2.03073	1.16837
C	7.57612	-2.85472	-1.09362
H	6.29059	-1.41823	-2.06831
C	7.22103	-3.00865	1.2746
C	7.90306	-3.4257	0.13528
H	8.07852	-3.14723	-2.00866
H	7.46367	-3.44245	2.23641
H	8.67569	-4.18365	0.20936
C	3.78911	-0.04915	3.02935
C	5.44945	-1.52931	2.31874
C	3.90846	-0.4715	3.34886
H	3.0819	0.72136	2.74891
C	5.61538	-1.99563	3.62644
C	4.83922	-1.46387	3.65211
H	3.28151	-0.02659	5.1132
H	6.34199	-2.76762	3.8458
H	4.96142	-1.82058	5.66933
N	4.53702	-0.55834	2.03263
N	5.91542	-1.47812	-0.0377
C	-0.94068	-0.7112	-0.10227
C	-2.15871	-1.37413	-0.19101
C	-0.94063	0.71175	0.09983
C	-3.40002	-0.71029	-0.0907
H	-2.17855	-2.44455	-0.34277
C	-2.15863	1.37467	0.18934
C	-3.40002	0.71086	0.08954
H	-2.17834	2.44503	0.34148
C	-4.64711	-1.41775	-0.17557
C	-4.64718	1.41819	0.17521
C	-5.84149	0.71582	0.08873
C	-5.84144	-0.71559	-0.0883
C	-4.63266	2.90284	0.38001
C	-4.86062	3.45042	1.6518

C	-4.36913	3.77147	-0.69099
C	-4.8351	4.83305	1.84646
H	-5.05974	2.78886	2.49018
C	-4.34524	5.15448	-0.49708
H	-4.18771	3.36037	-1.68052
C	-4.57877	5.68918	0.77241
H	-5.01456	5.24032	2.83779
H	-4.14515	5.81256	-1.3383
H	-4.56001	6.76491	0.9238
C	-7.14919	1.4443	0.18504
C	-7.91079	1.39474	1.36243
C	-7.63273	2.1922	-0.89888
C	-9.12462	2.07862	1.45487
H	-7.54854	0.82046	2.21048
C	-8.84906	2.87265	-0.80915
H	-7.05386	2.23849	-1.81699
C	-9.59862	2.81872	0.36851
H	-9.69914	2.03299	2.37618
H	-9.20965	3.44464	-1.65989
H	-10.54421	3.34923	0.43948
C	-7.14903	-1.44432	-0.18437
C	-7.63259	-2.19184	0.89979
C	-7.9104	-1.39549	-1.36194
C	-8.84875	-2.87261	0.81015
H	-7.05387	-2.23758	1.81802
C	-9.12407	-2.07969	-1.45429
H	-7.54813	-0.82149	-2.21017
C	-9.59811	-2.81939	-0.36768
H	-9.20936	-3.4443	1.66108
H	-9.69843	-2.03462	-2.37573
H	-10.54355	-3.35015	-0.43858
C	-4.6325	-2.9024	-0.38056
C	-4.85892	-3.44969	-1.65275
C	-4.37033	-3.77125	0.69058
C	-4.83324	-4.83229	-1.84767
H	-5.057	-2.78793	-2.49123
C	-4.34628	-5.15422	0.49641
H	-4.19003	-3.36036	1.6804
C	-4.57825	-5.68864	-0.77348
H	-5.01154	-5.23934	-2.83929
H	-4.14723	-5.81249	1.33773
H	-4.55935	-6.76434	-0.92507

3.9 Spectra Relevant to Chapter Three:

A Platform for On-the-Complex Annulation Reactions with Transient Aryne Intermediates

Jason V. Chari,[†] Katie A. Spence,[†] Robert B. Susick, and Neil K. Garg.

Nat. Commun. **2021**, *12*, 3706.

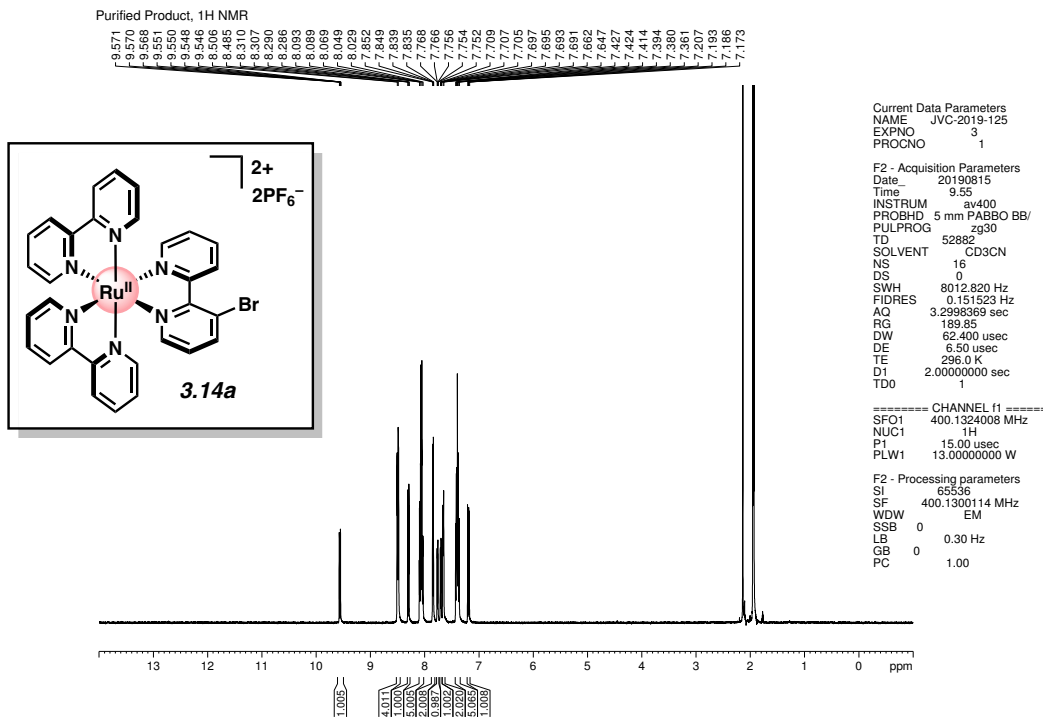


Figure 3.23 ¹H NMR (400 MHz, CDCl₃) of compound **3.14a**.

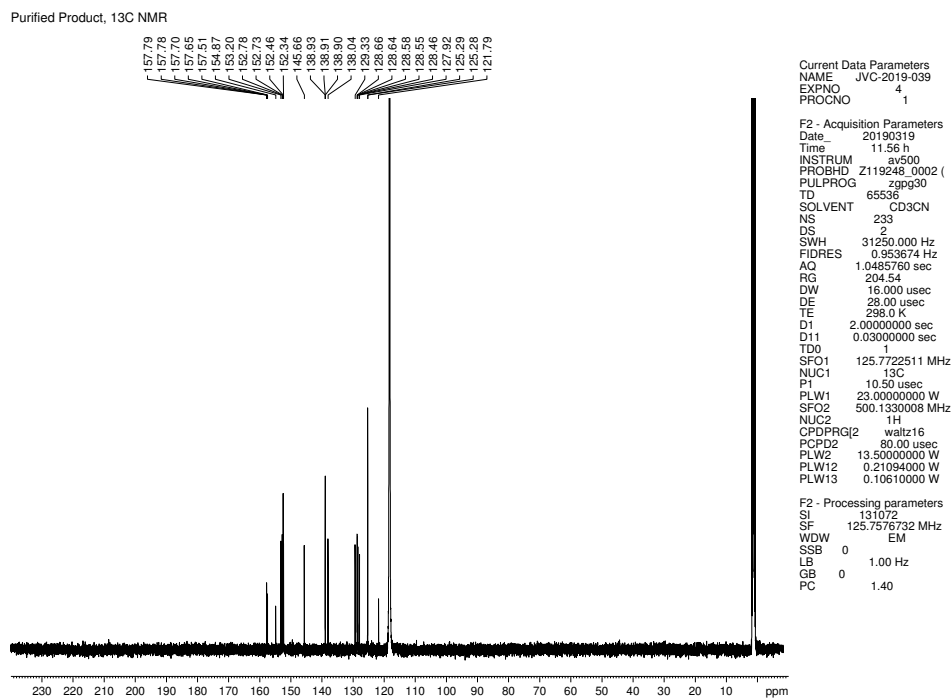


Figure 3.24 ¹³C NMR (125 MHz, CDCl₃) of compound **3.14a**.

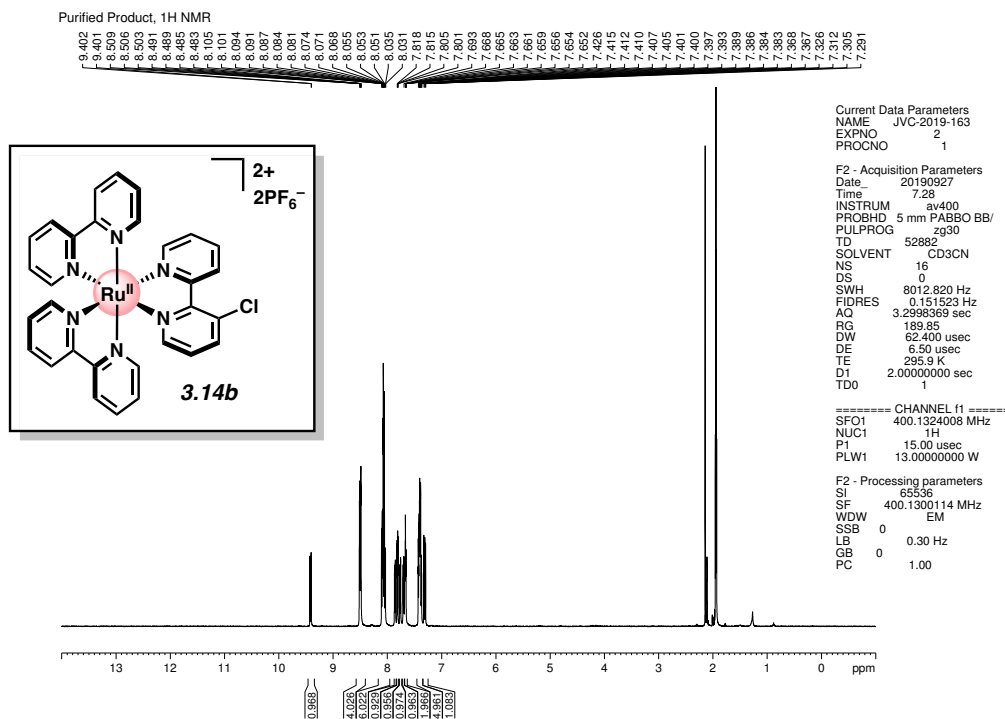


Figure 3.25 ¹H NMR (400 MHz, CD₃CN) of compound **3.14b**.

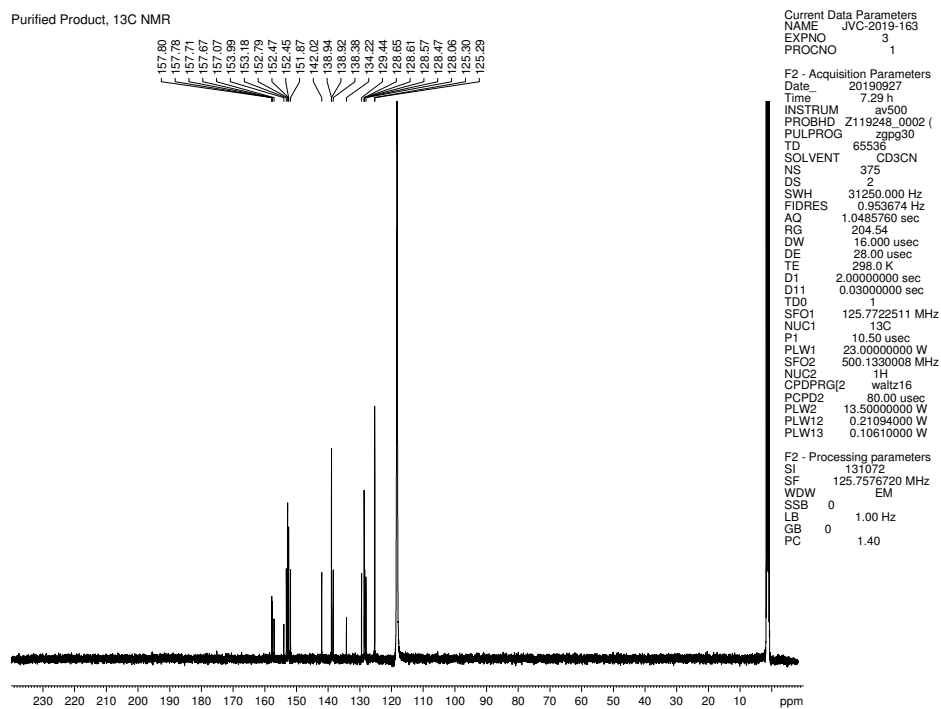


Figure 3.26 ¹³C NMR (125 MHz, CD₃CN) of compound **3.14b**.

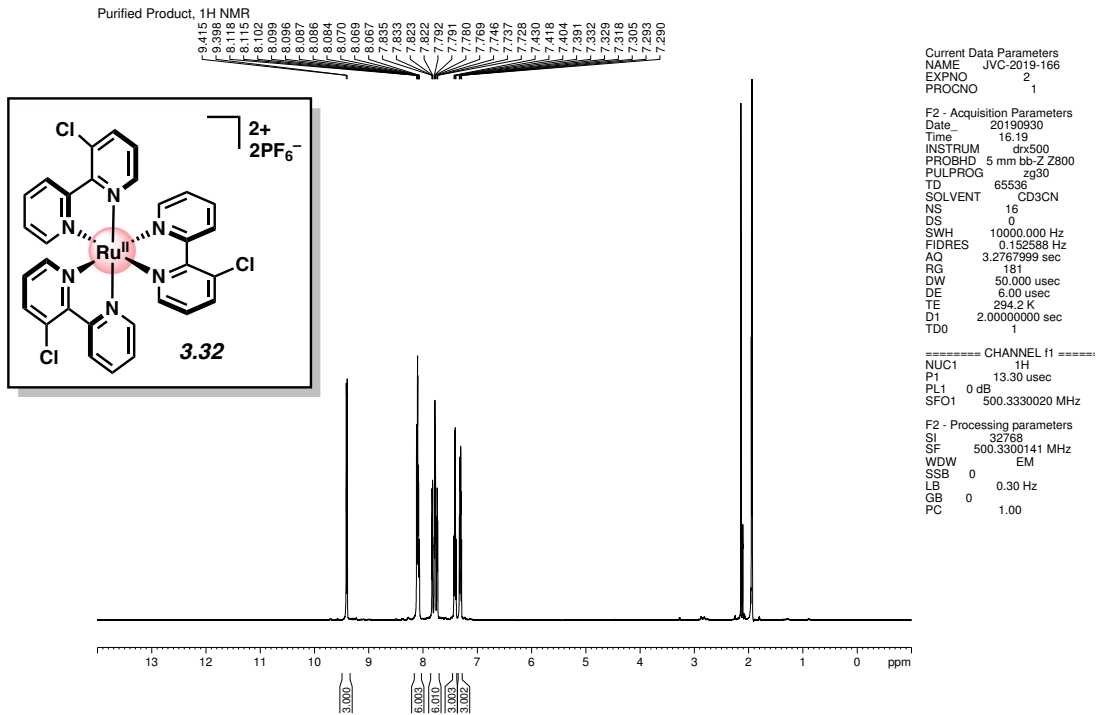


Figure 3.29 ¹H NMR (500 MHz, CD₃CN) of compound **3.32**.

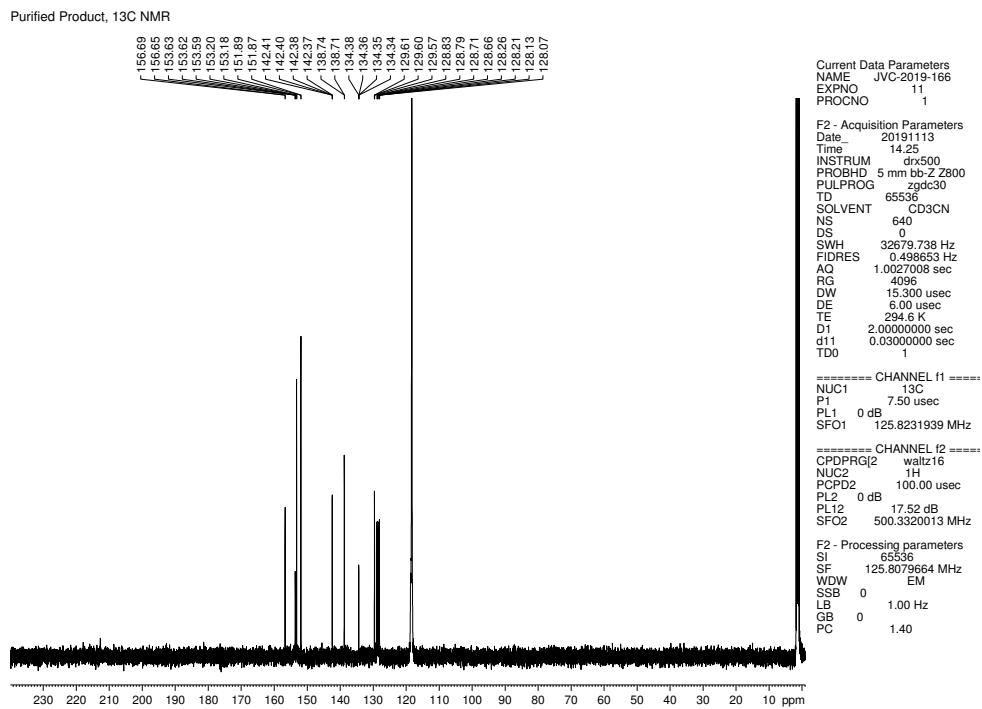


Figure 3.30 ¹³C NMR (125 MHz, CD₃CN) of compound **3.32**.

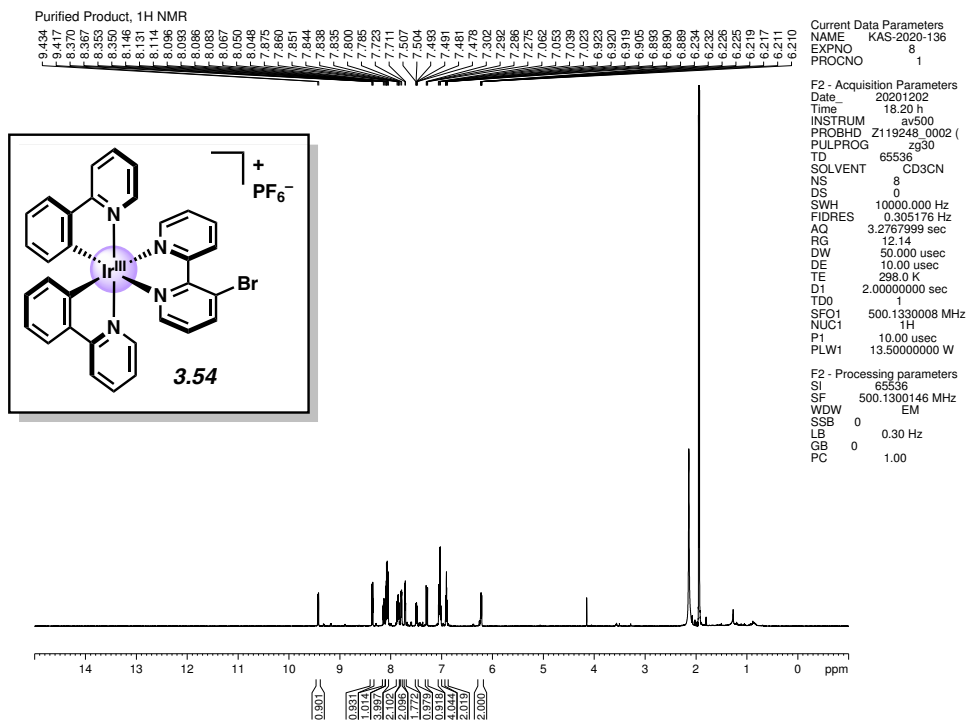


Figure 3.31 ¹H NMR (500 MHz, CD₃CN) of compound 3.54.

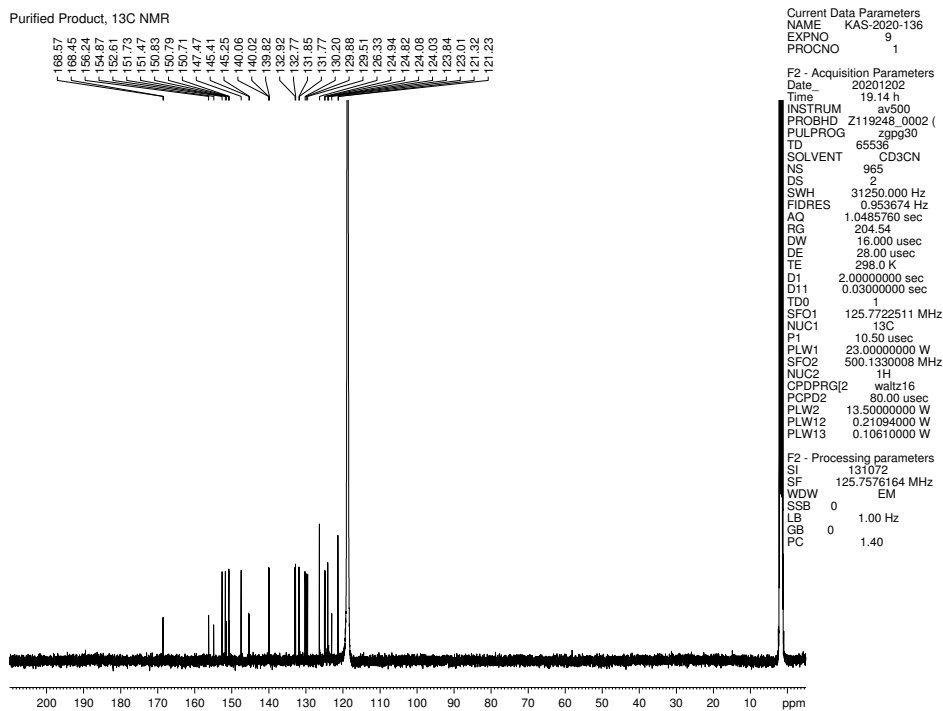


Figure 3.32 ¹³C NMR (125 MHz, CD₃CN) of compound 3.54.

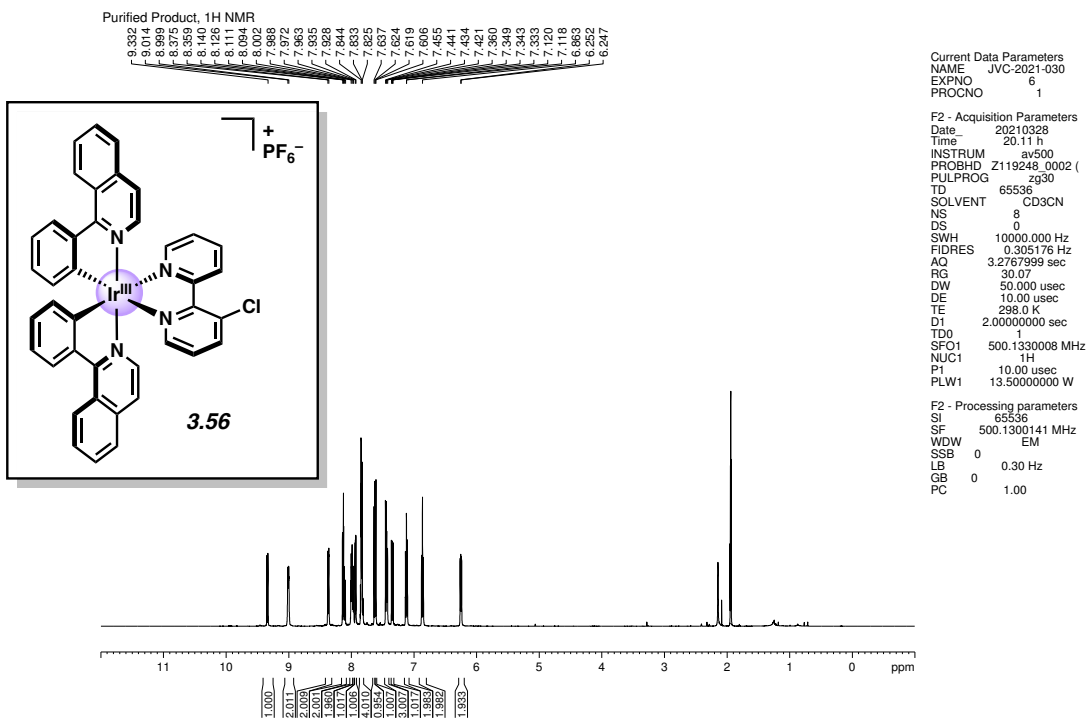


Figure 3.33 ¹H NMR (500 MHz, CD₃CN) of compound **3.56**.

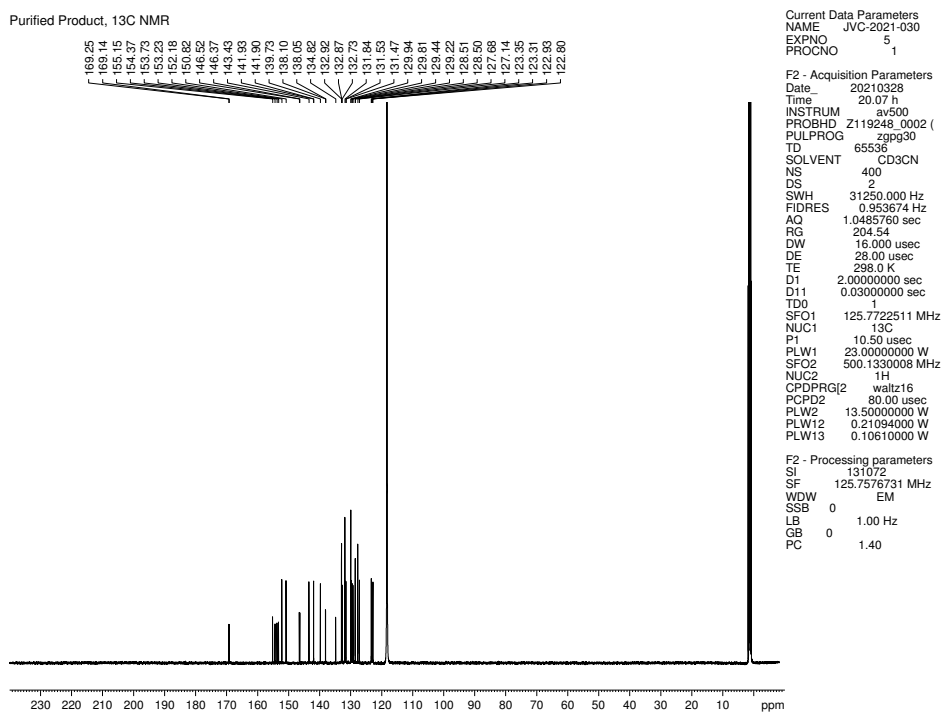


Figure 3.34 ¹³C NMR (125 MHz, CD₃CN) of compound **3.56**.

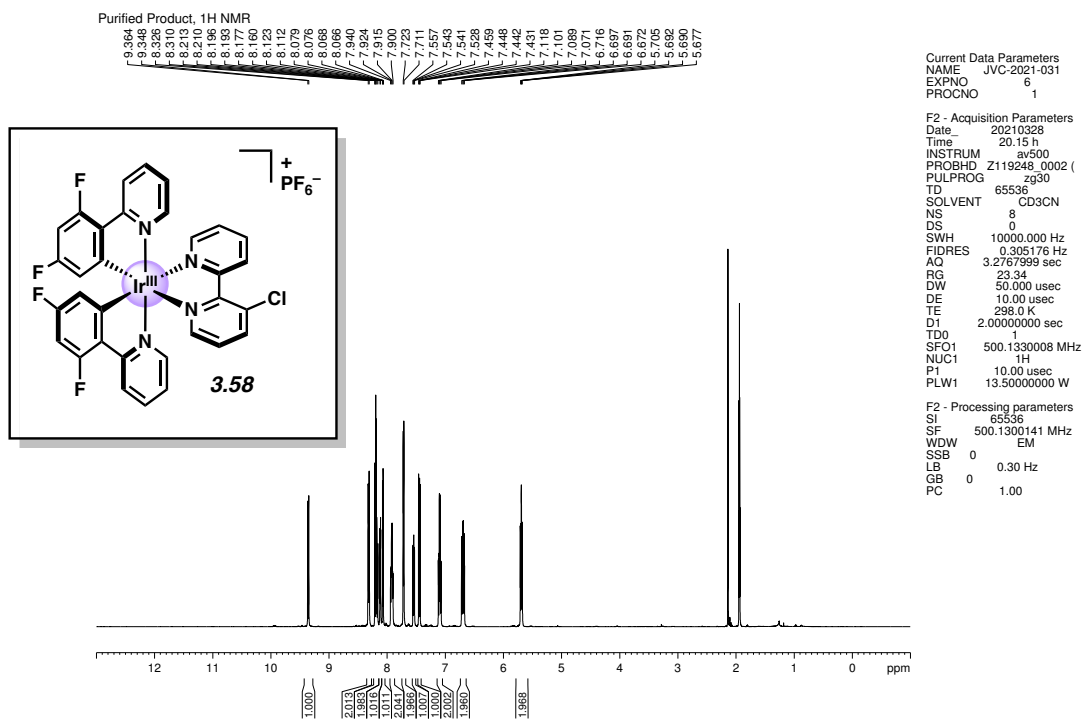


Figure 3.35 ¹H NMR (500 MHz, CD₃CN) of compound **3.58**.

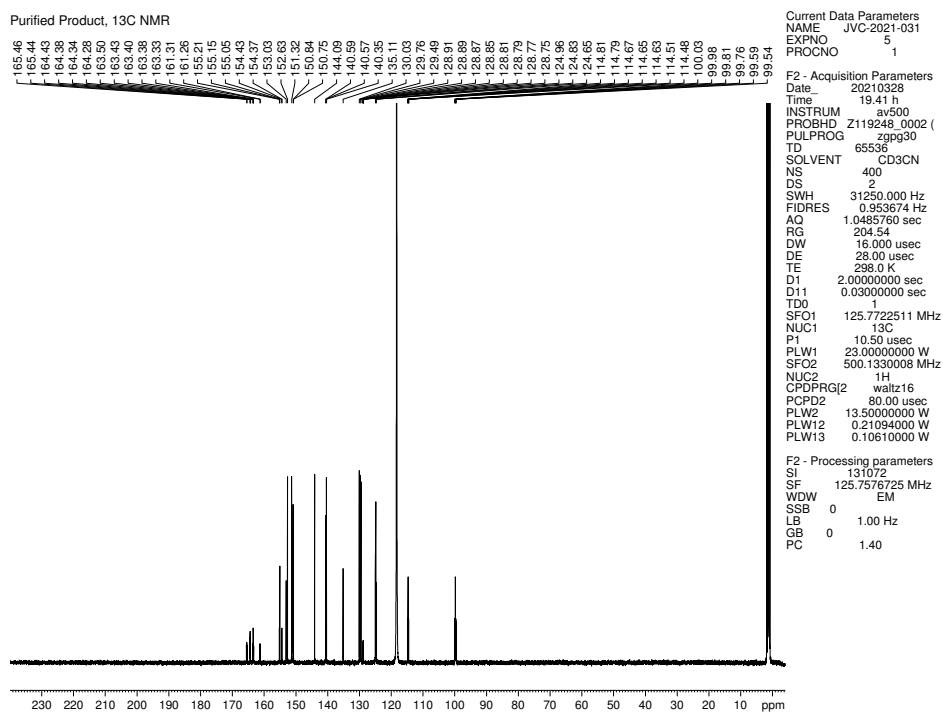


Figure 3.36 ¹³C NMR (125 MHz, CD₃CN) of compound **3.58**.

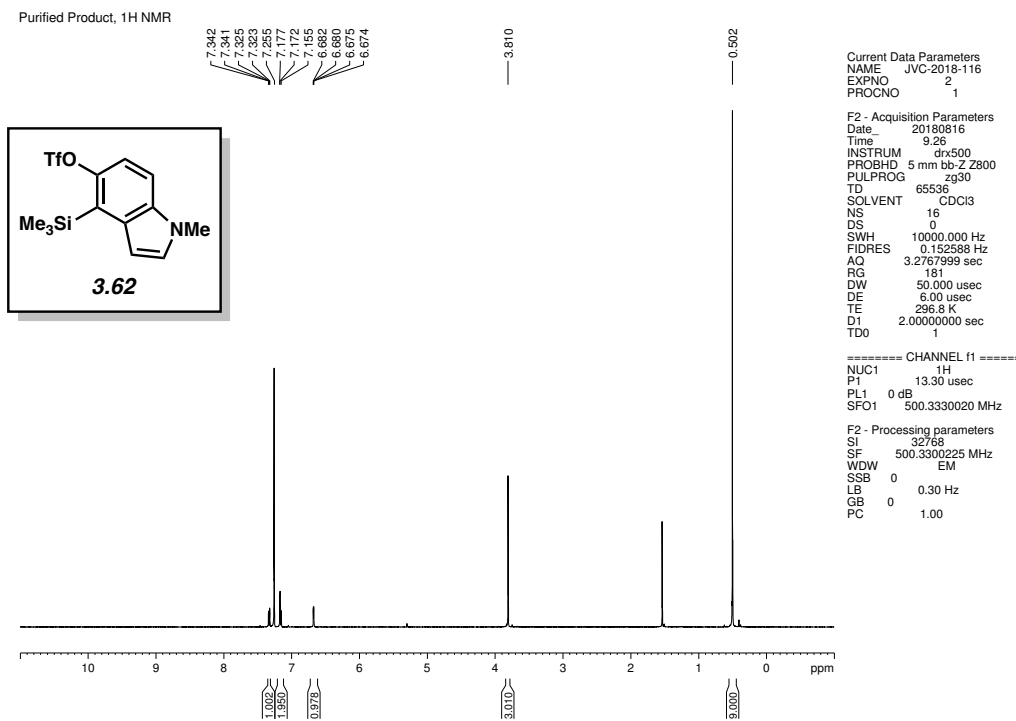


Figure 3.37 ¹H NMR (500 MHz, CDCl₃) of compound **3.62**.

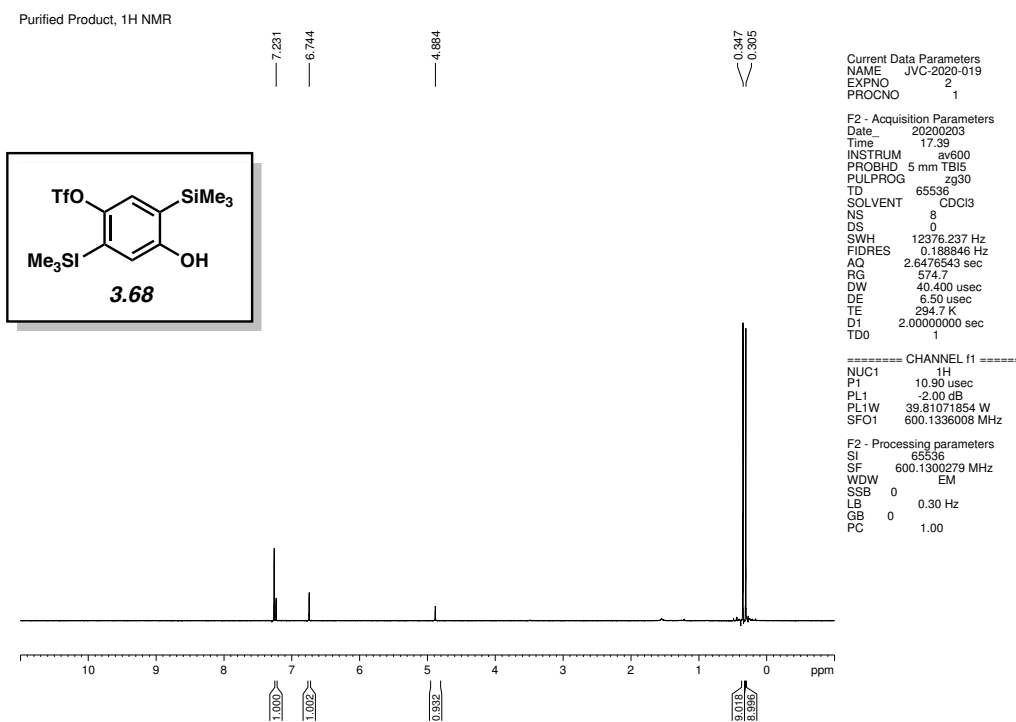


Figure 3.38 ¹H NMR (600 MHz, CDCl₃) of compound **3.68**.

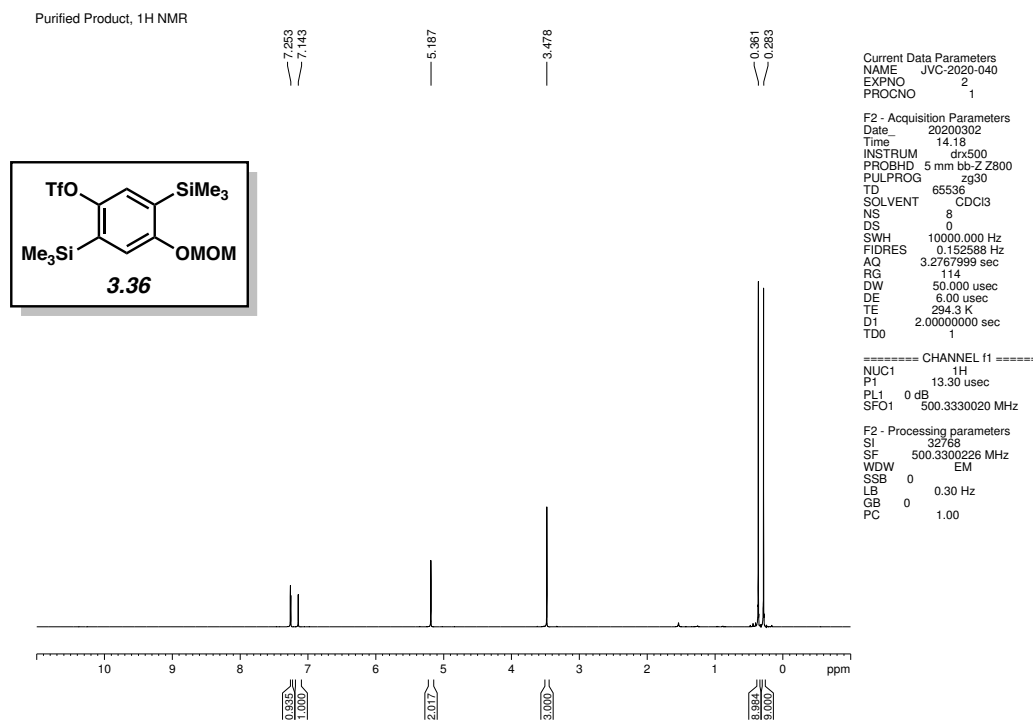


Figure 3.39 ¹H NMR (500 MHz, CD₃CN) of compound **3.36**.

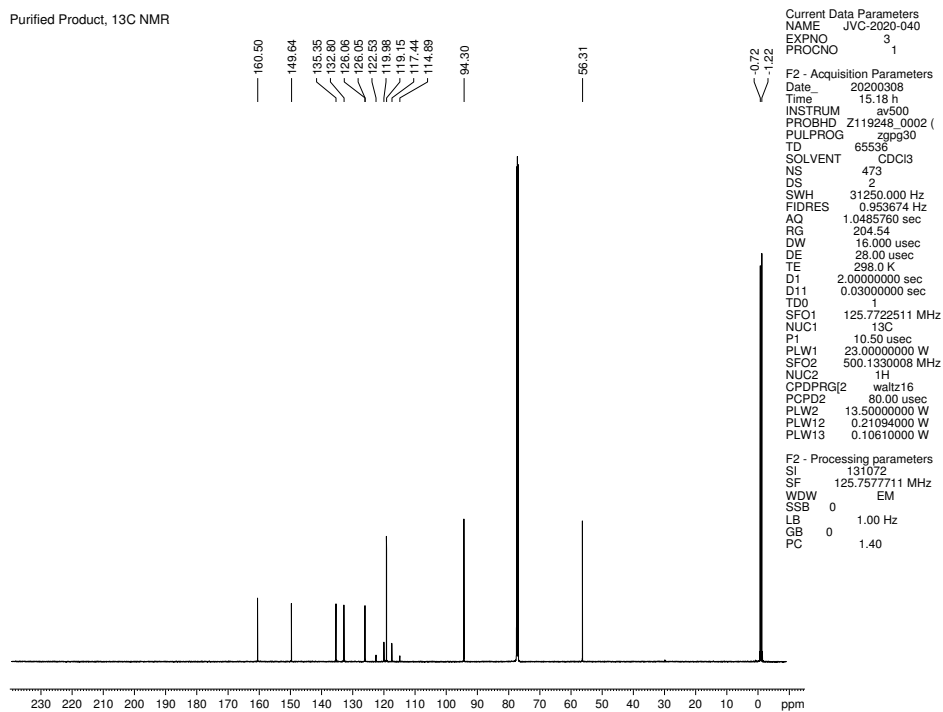


Figure 3.40 ¹³C NMR (125 MHz, CD₃CN) of compound **3.36**.

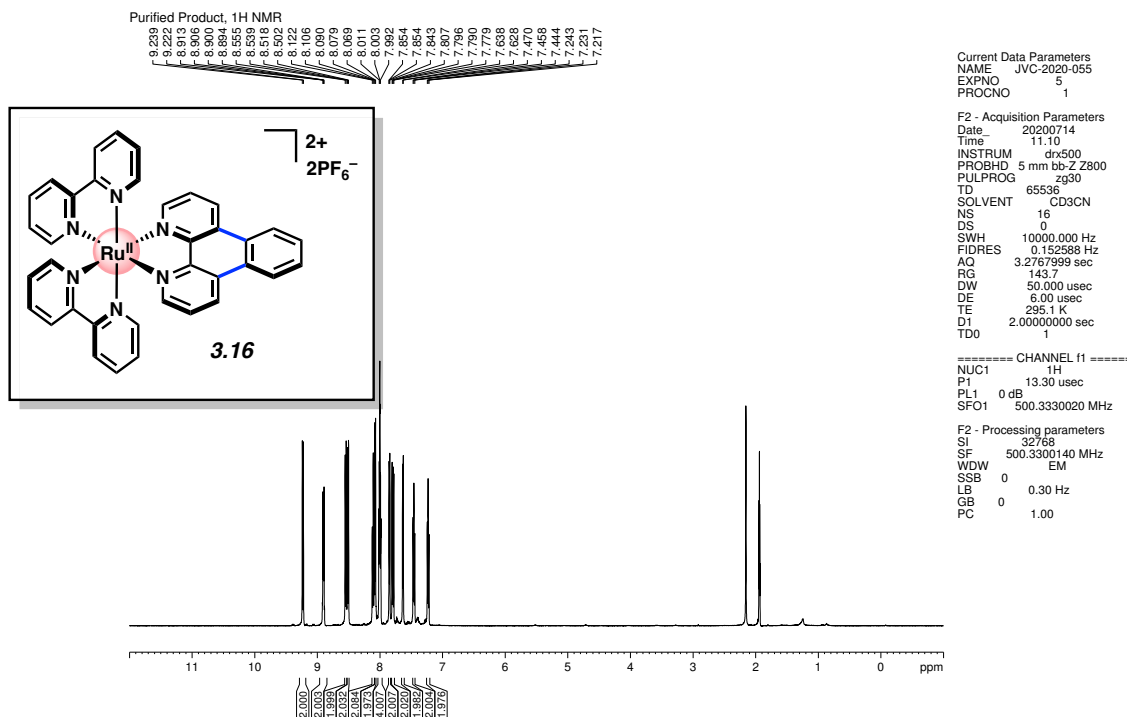


Figure 3.41 ¹H NMR (500 MHz, CD₃CN) of compound **3.16**.

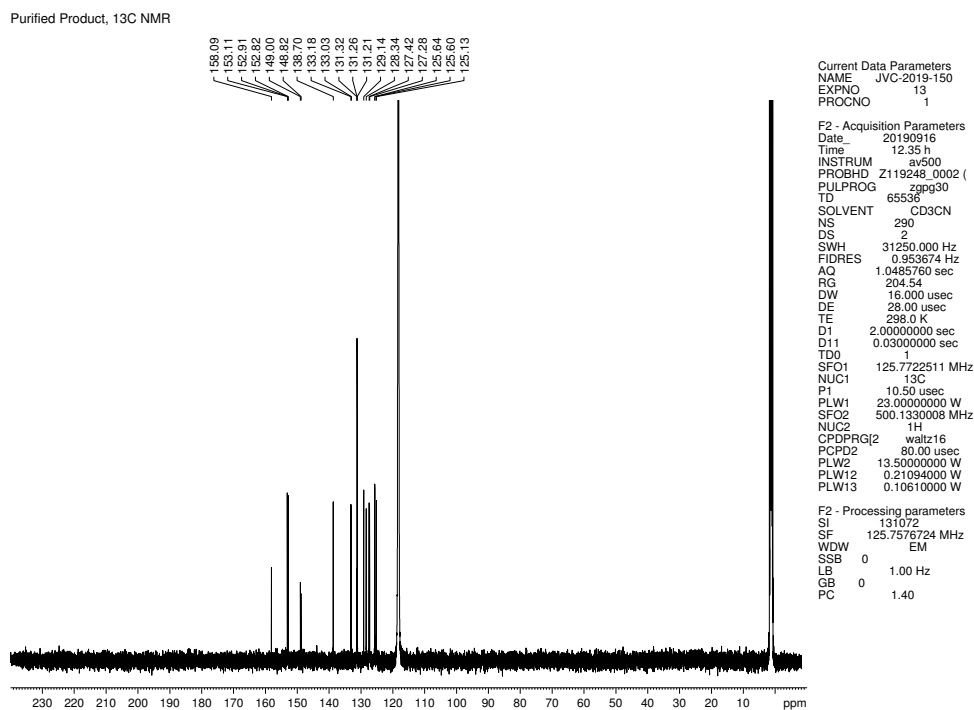


Figure 3.42 ¹³C NMR (125 MHz, CD₃CN) of compound **3.16**.

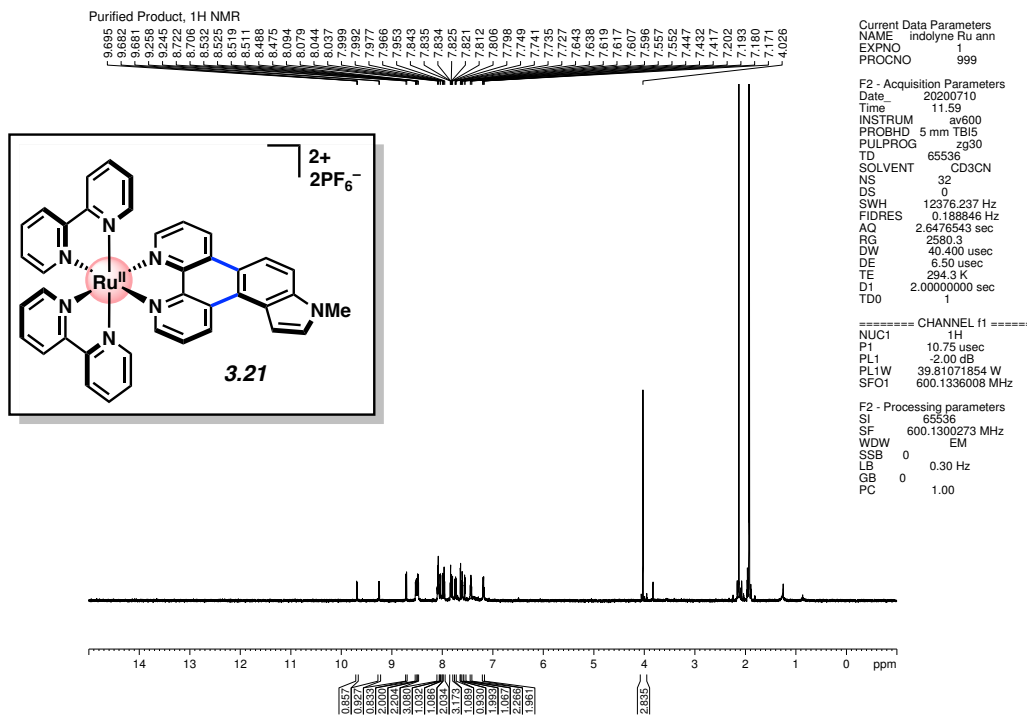


Figure 3.43 ¹H NMR (600 MHz, CD₃CN) of compound **3.21**.

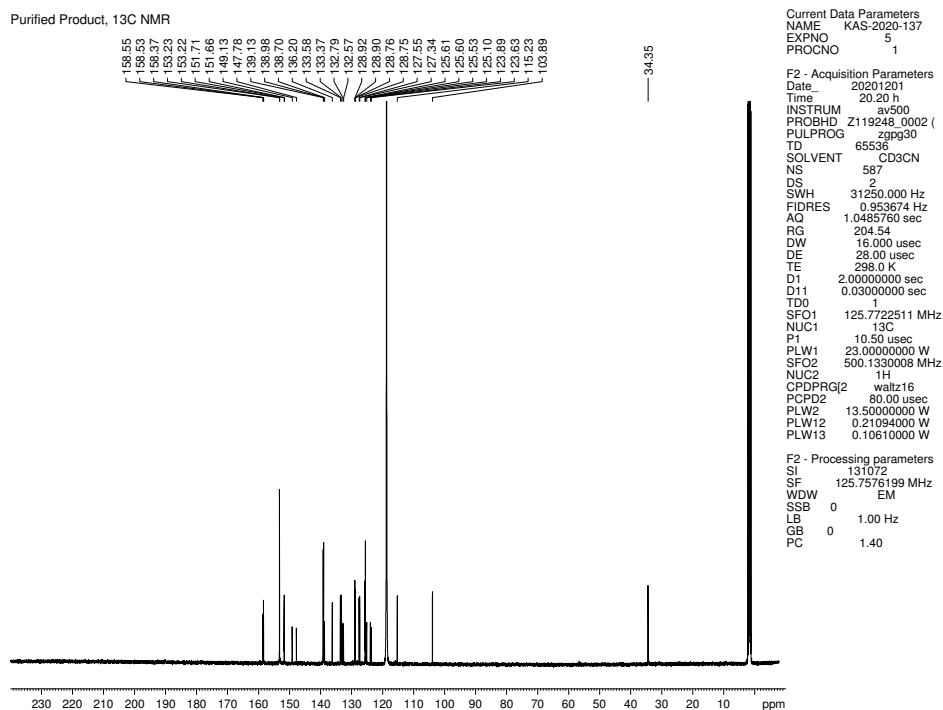


Figure 3.44 ¹³C NMR (125 MHz, CD₃CN) of compound **3.21**.

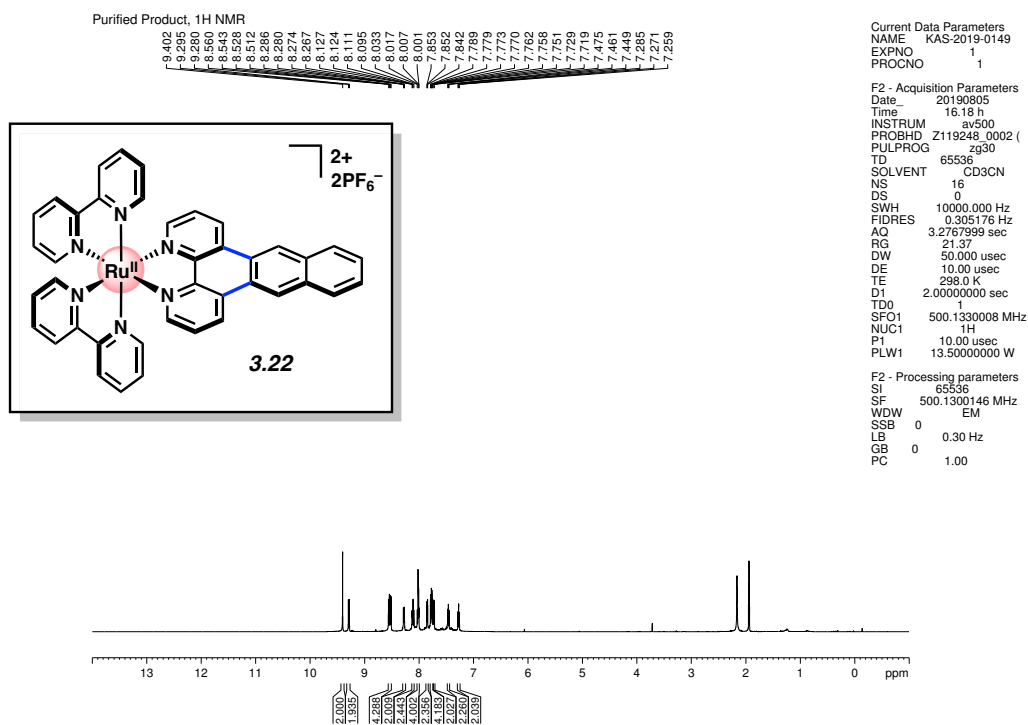


Figure 3.45 ¹H NMR (500 MHz, CD₃CN) of compound 3.22.

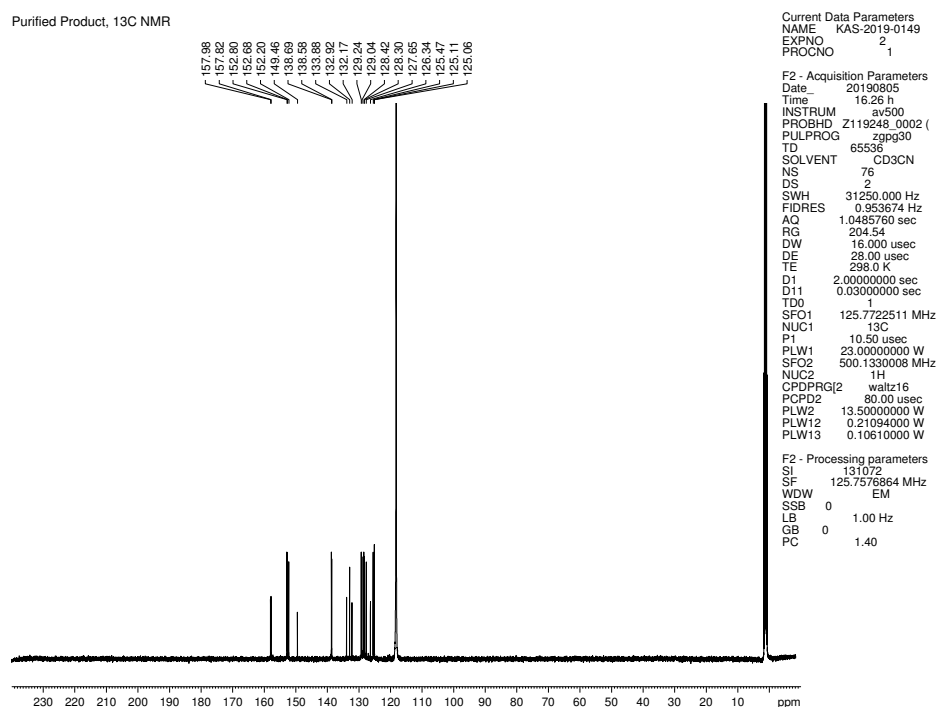


Figure 3.46 ¹³C NMR (500 MHz, CD₃CN) of compound 3.22.

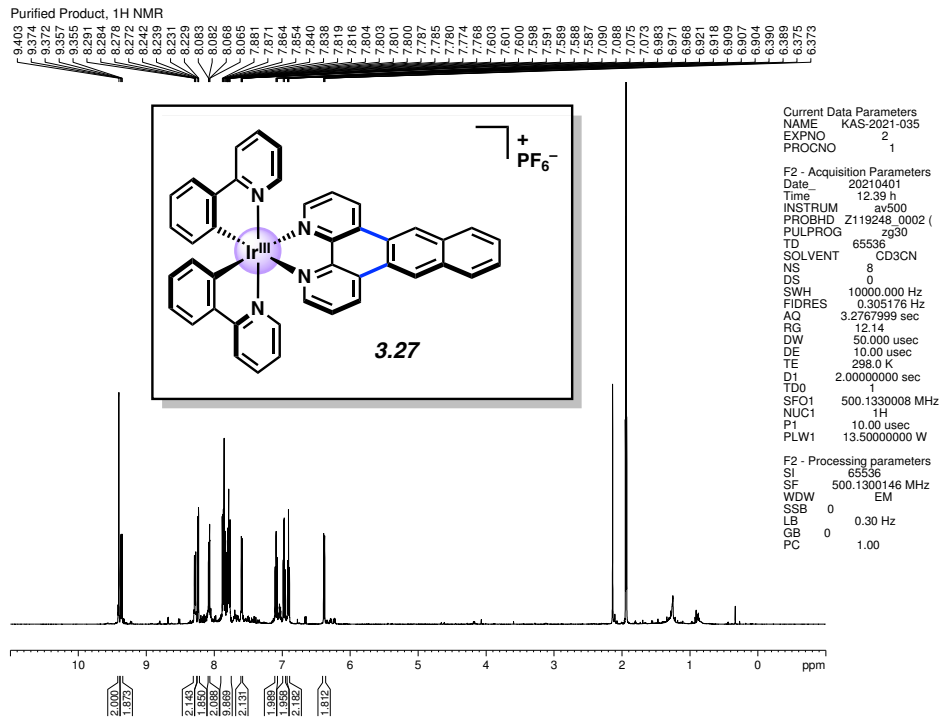


Figure 3.51 ¹H NMR (500 MHz, CD₃CN) of compound **3.27**.

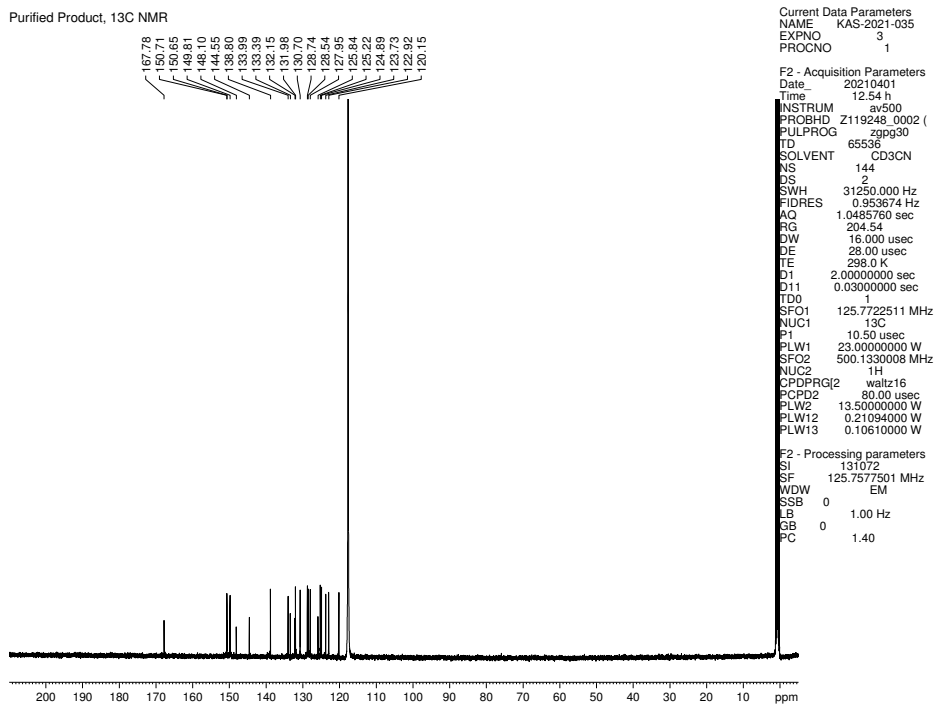


Figure 3.52 ¹³C NMR (125 MHz, CD₃CN) of compound **3.27**.

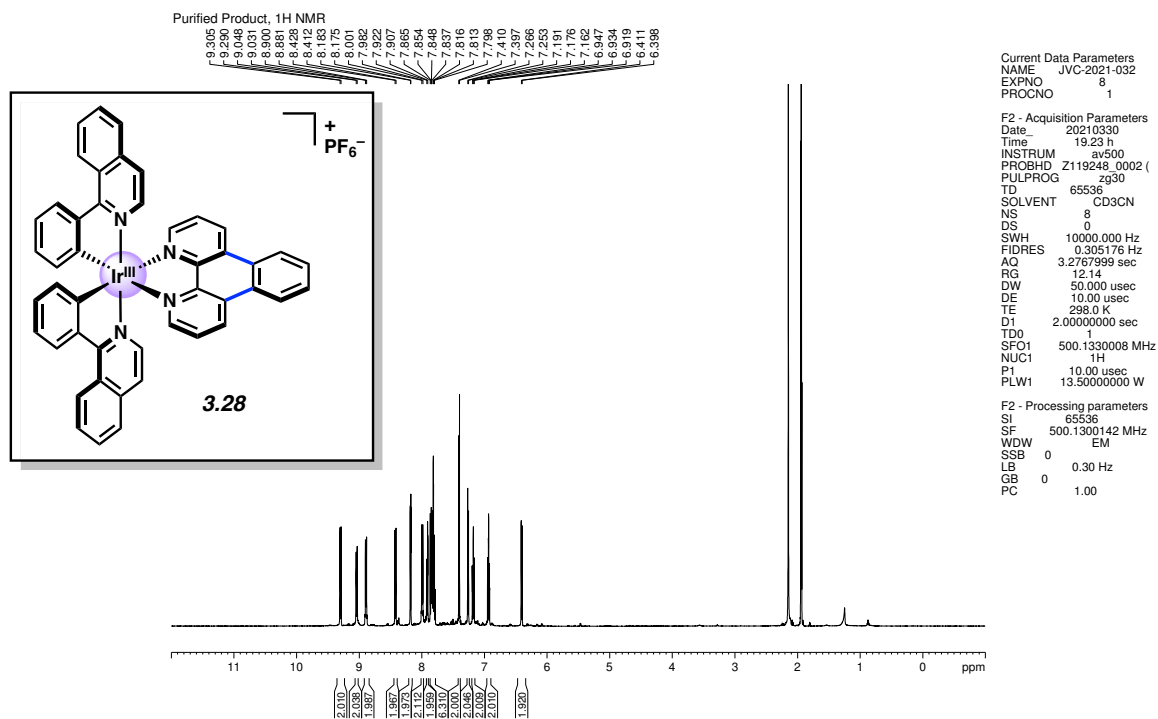


Figure 3.53 ¹H NMR (500 MHz, CD₃CN) of compound **3.28**.

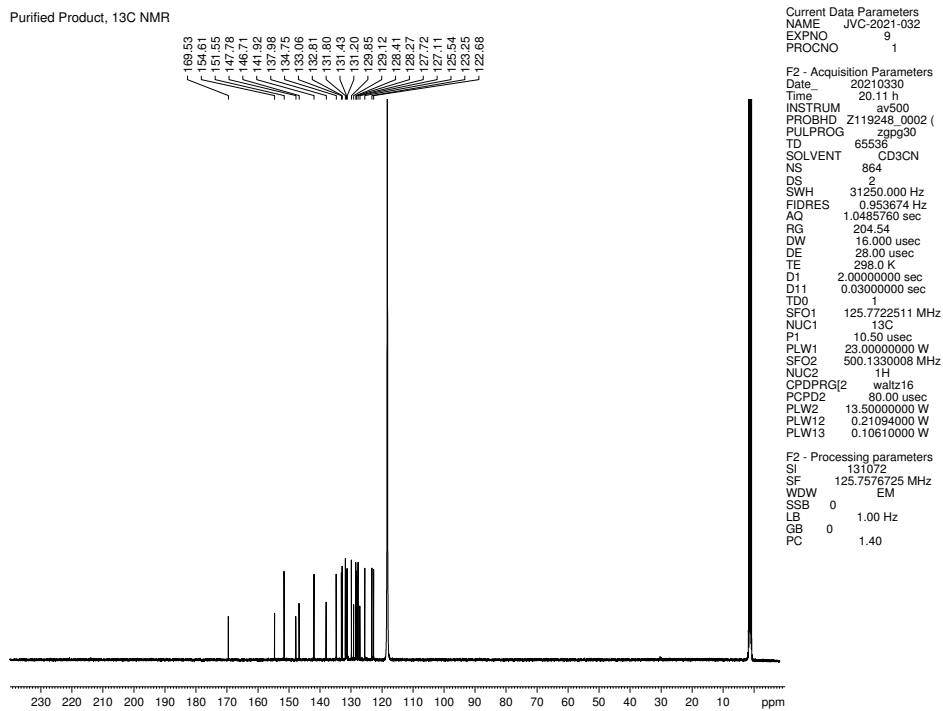


Figure 3.54 ¹³C NMR (125 MHz, CD₃CN) of compound **3.28**.

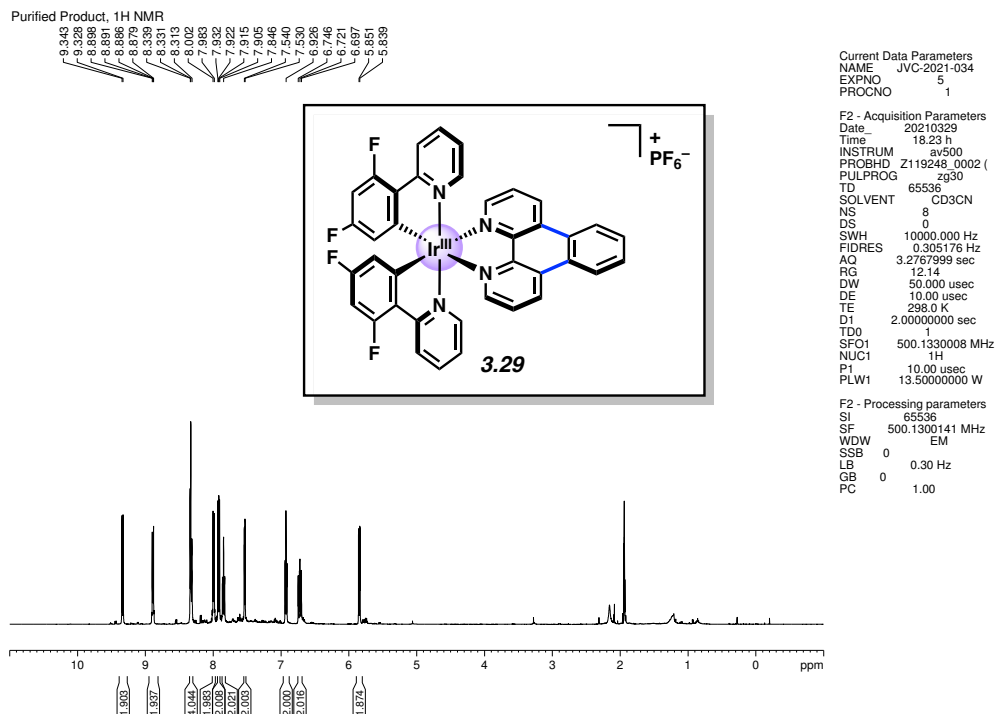


Figure 3.55 ¹H NMR (500 MHz, CD₃CN) of compound 3.29.

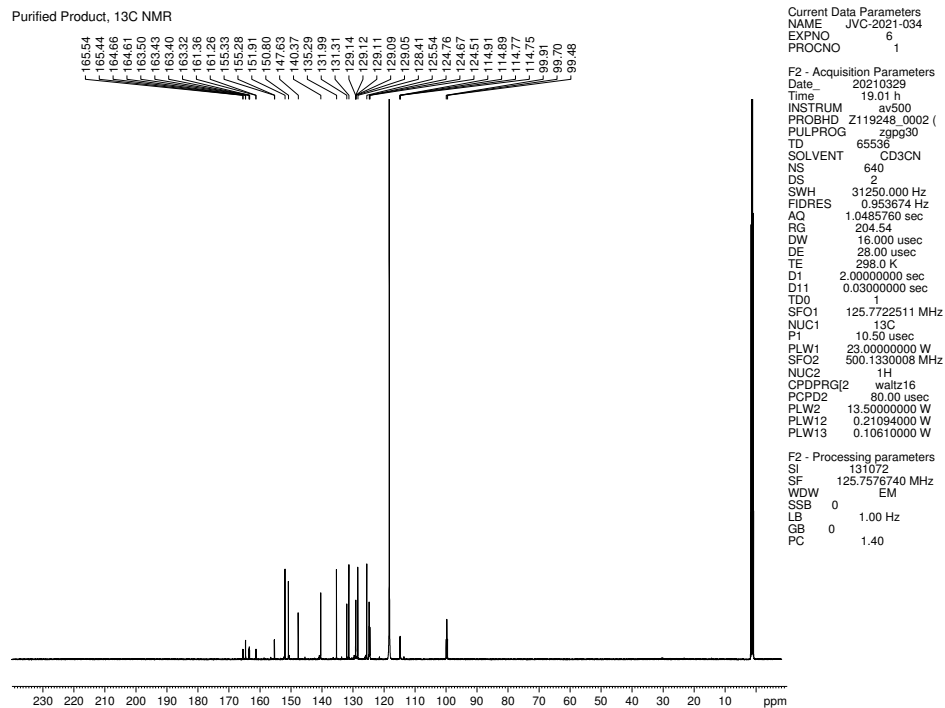


Figure 3.56 ¹³C NMR (125 MHz, CD₃CN) of compound 3.29.

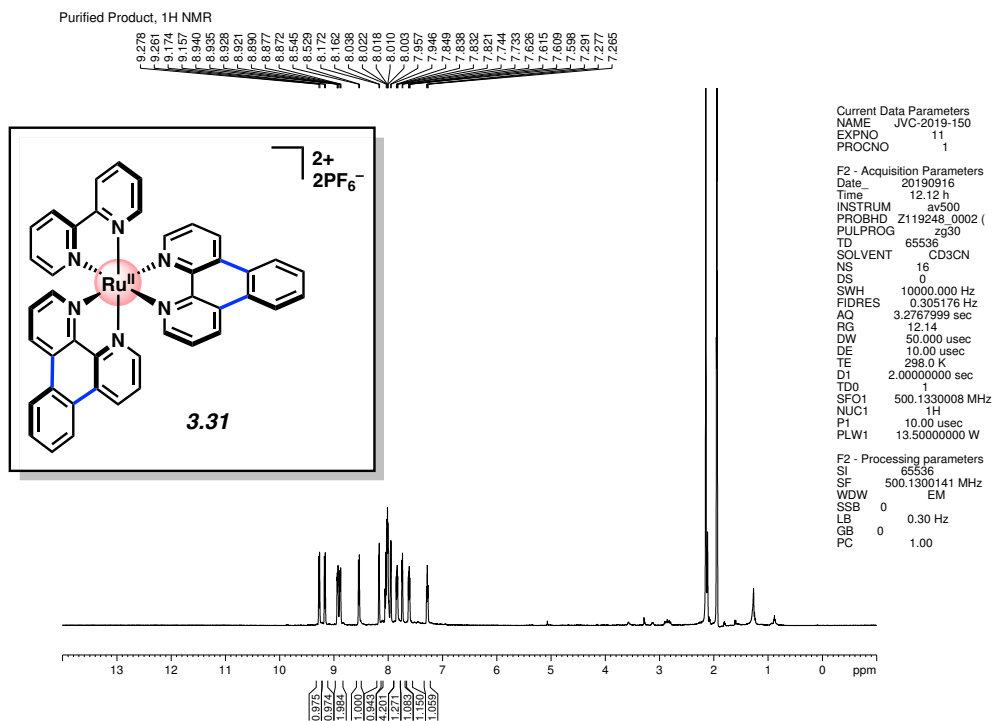


Figure 3.57 ¹H NMR (500 MHz, CD₃CN) of compound **3.31**.

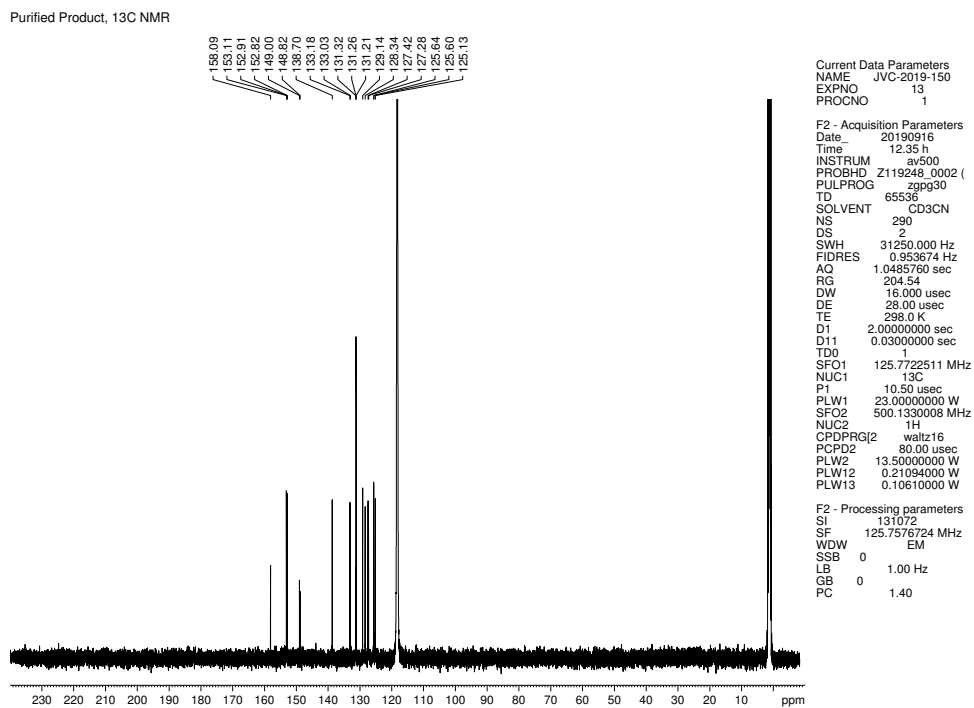


Figure 3.58 ¹³C NMR (125 MHz, CD₃CN) of compound **3.31**.

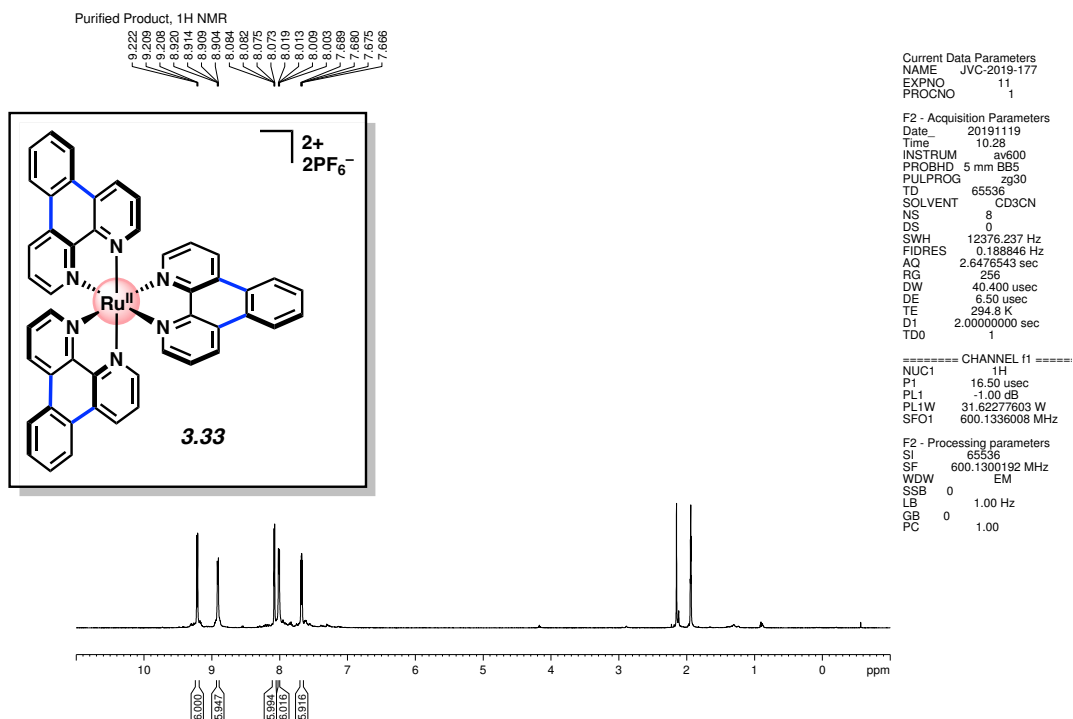


Figure 3.59 ¹H NMR (600 MHz, CD₃CN) of compound **3.33**.

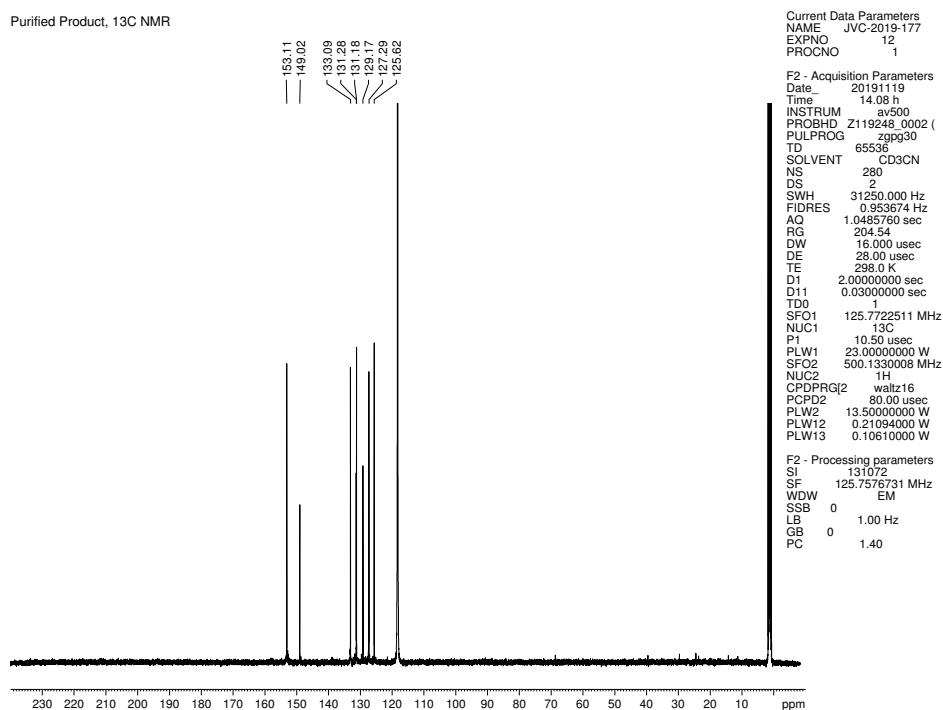


Figure 3.60 ¹³C NMR (125 MHz, CD₃CN) of compound **3.33**.

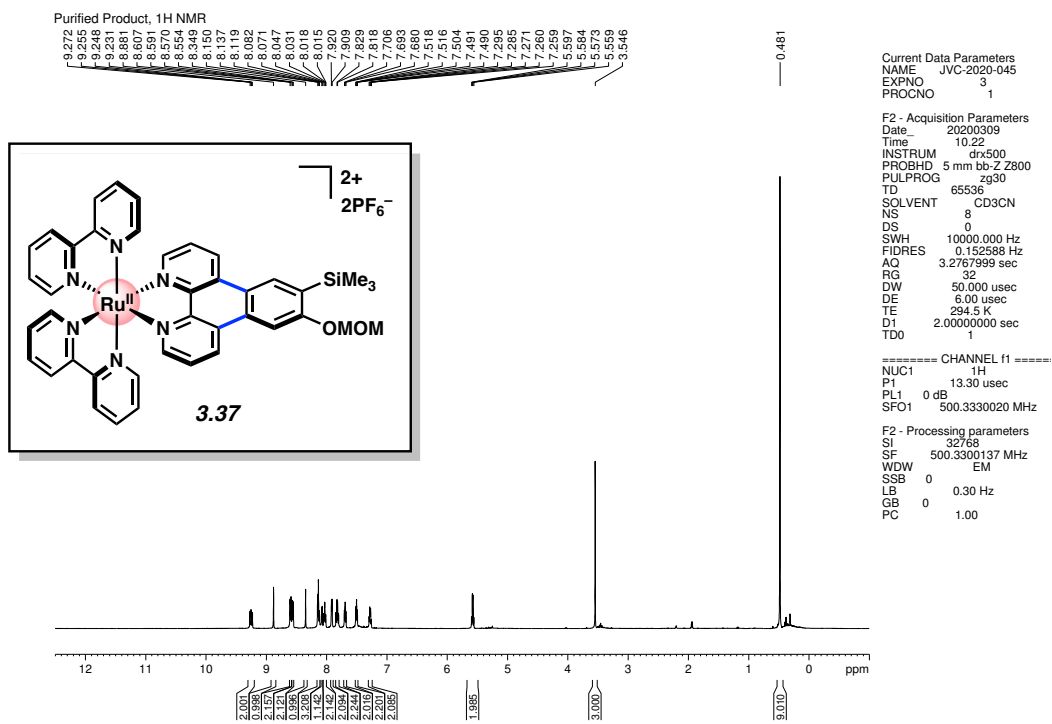


Figure 3.61 ¹H NMR (500 MHz, CD₃CN) of compound **3.37**.

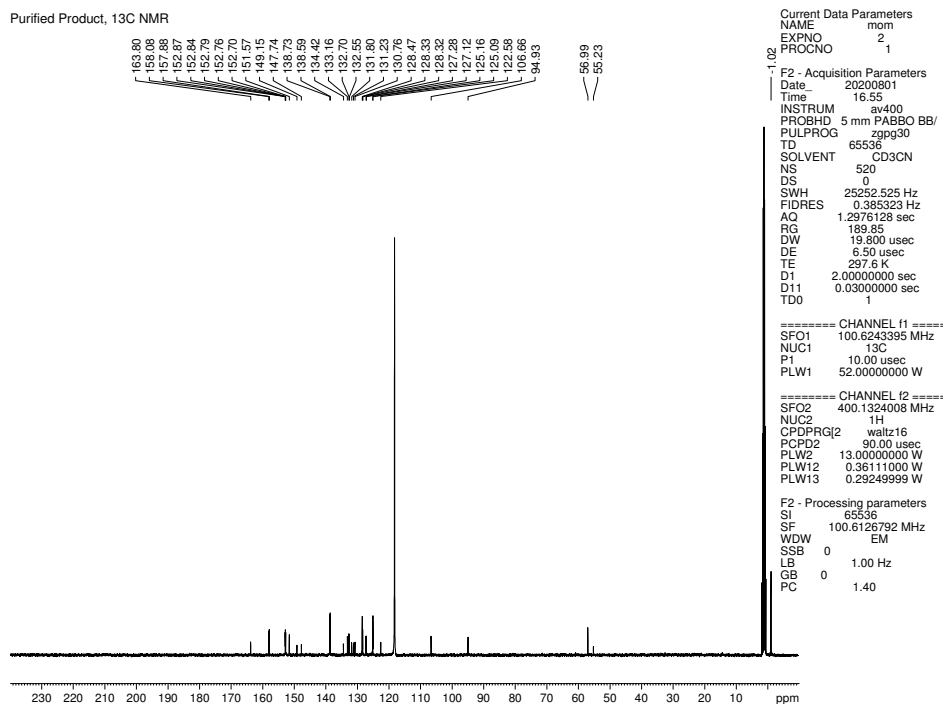


Figure 3.62 ¹³C NMR (100 MHz, CD₃CN) of compound **3.37**.

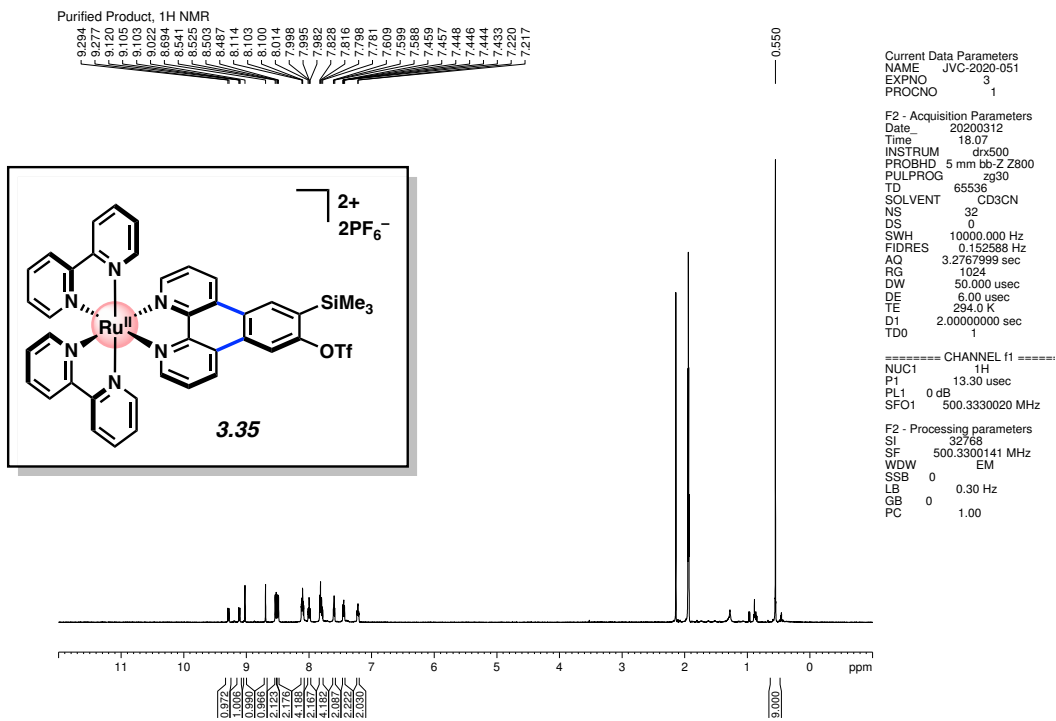


Figure 3.63 ¹H NMR (500 MHz, CD₃CN) of compound **3.35**.

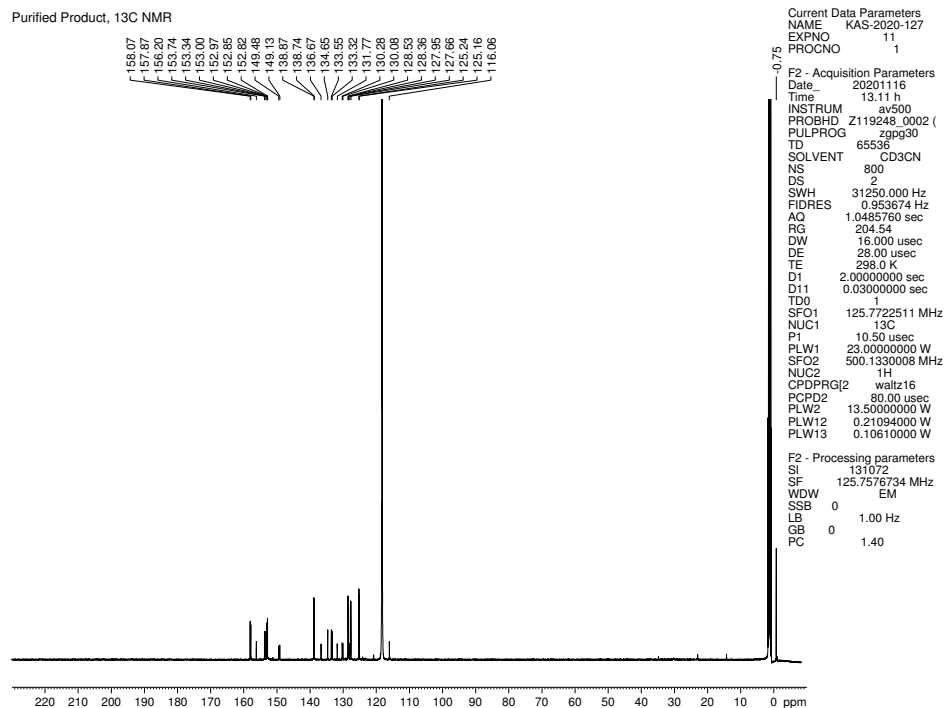


Figure 3.64 ¹³C NMR (125 MHz, CD₃CN) of compound **3.35**.

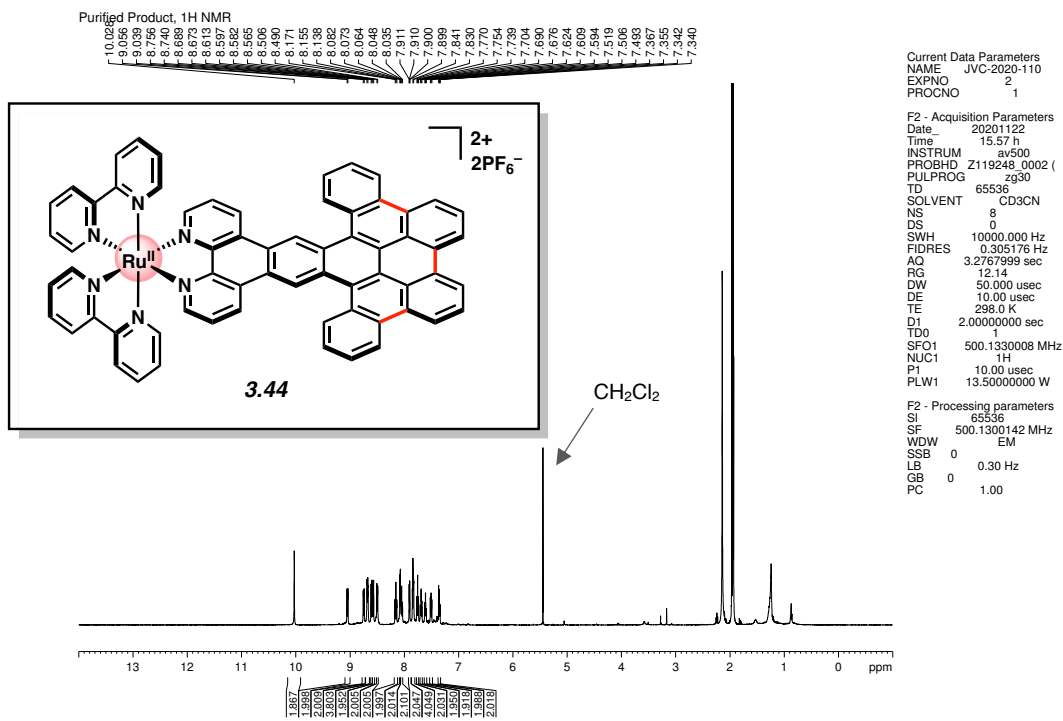


Figure 3.71 ¹H NMR (500 MHz, CD₃CN) of compound 3.44.

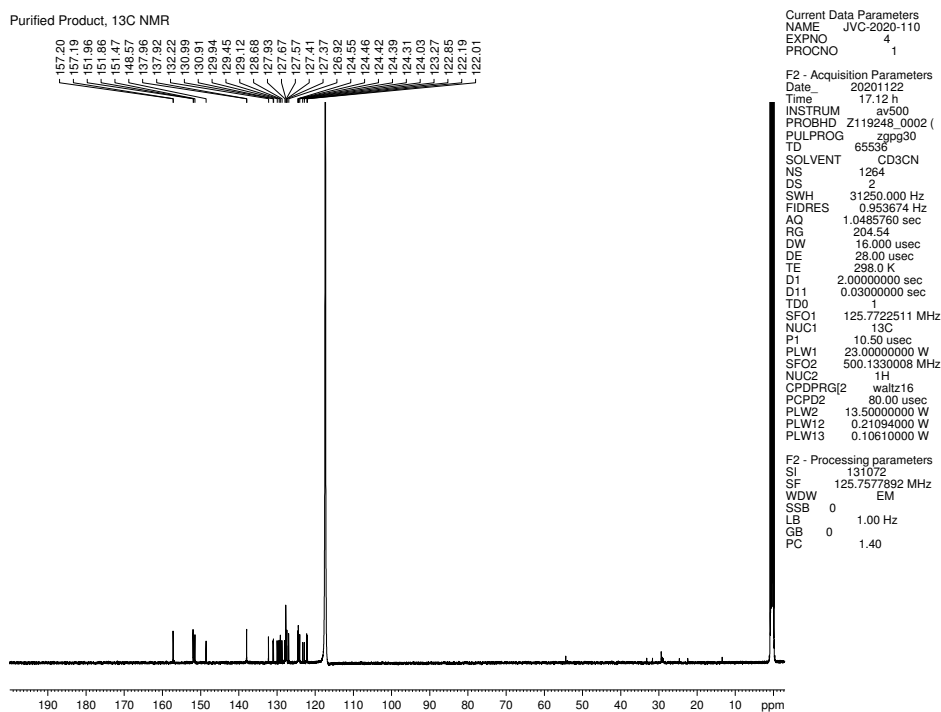


Figure 3.72 ¹³C NMR (125 MHz, CD₃CN) of compound 3.44.

3.10 Notes and References

- (1) Noyori, R.; Kitamura, M.; Ohkuma, T. Toward Efficient Asymmetric Hydrogenation: Architectural and Functional Engineering of Chiral Molecular Catalysts. *Proc. Natl. Acad. Sci. U.S.A.* **2004**, *101*, 5356–5362.
- (2) Monro, S.; Colón, K. L.; Yin, H.; Roque, J., III.; Konda, P.; Gujar, S.; Thummel, R. P.; Lilge, L.; Cameron, C. G.; McFarland, S. A. Transition Metal Complexes and Photodynamic Therapy from a Tumor-Centered Approach: Challenges, Opportunities, and Highlights from the Development of TLD1433. *Chem. Rev.* **2019**, *119*, 797–828.
- (3) Linck, R. C.; Rauchfuss, T. B. *Bioorganometallics: Biomolecules, Labeling, Medicine*; Wiley–VCH; Weinheim, 2005; pp 403–435.
- (4) Braunstein, P. Functional Ligands and Complexes for New Structures, Homogeneous Catalysts and Nanomaterials. *J. Organomet. Chem.* **2004**, *689*, 3953–3967.
- (5) Zucker, S. P.; Wossidlo, F.; Weber, M.; Lentz, D.; Tzschucke, C. C. Palladium-Catalyzed Directed Halogenation of Bipyridine *N*-Oxides. *J. Org. Chem.* **2017**, *82*, 5616–5635.
- (6) Soulis, K.; Gourlaouen, C.; Daniel, C.; Quatela, A.; Odobel, F.; Blart, E.; Pellegrin, Y. New Luminescent Copper(I) Complexes with Extended π -Conjugation. *Polyhedron* **2018**, *140*, 42–50.
- (7) Bolger, J.; Gourdon, A.; Ishow, E.; Launay, J.-P. Stepwise Syntheses of Mono- and Dinuclear Ruthenium tpphz Complexes $[(bpy)_2Ru(tpphz)]^{2-}$ and $[(bpy)_2Ru(tpphz)Ru(bpy)_2]^{4+}$ {tpphz = tetrapyrido[3,2-a: 2',3'-c: 3'',2''-h: 2'',3'''-j]phenazine}. *J. Chem. Soc., Chem. Commun.* **1995**, 1799–1800.

- (8) Mede, T.; Jäger, M.; Schubert, U. S. “Chemistry-on-the-Complex”: Functional Ru^{II} Polypyridyl-Type Sensitizers as Divergent Building Blocks. *Chem. Soc. Rev.* **2018**, *47*, 7577–7627.
- (9) Fang, Y.-Q.; Polson, M. I. J.; Hanan, G. S. Creating New Binding Sites in Ligands and Metal Complexes Using the Negishi Cross-Coupling Reaction. *Inorg. Chem.* **2003**, *42*, 5–7.
- (10) Zedler, L.; Mengele, A. K.; Ziems, K. M.; Zhang, Y.; Wächtler, M.; Gräfe, S.; Pascher, T.; Rau, S.; Kupfer, S.; Dietzek, B. Unraveling the Light-Activated Reaction Mechanism in a Catalytically Competent Key Intermediate of a Multifunctional Molecular Catalyst for Artificial Photosynthesis. *Angew. Chem., Int. Ed.* **2019**, *58*, 13140–13148.
- (11) Anderson, S. C.; Grounds, H.; Szalóki, G. Synthesis of Planar Chiral Ferrocenyl Cyclopentadienyl Chelate Ligand Precursors. *Tetrahedron: Asymmetry* **2013**, *24*, 1023–1034.
- (12) Teimuri-Mofrad, R.; Mirzaei, F.; Abbasi, H.; Safa, K. D. Synthesis of New Binuclear Ferrocenyl Compounds by Hydrosilylation Reactions. *C. R. Chimie.* **2017**, *20*, 197–205.
- (13) Hiroto, S.; Miyake, Y.; Shinokubo, H. Synthesis and Functionalization of Porphyrins through Organometallic Methodologies. *Chem. Rev.* **2017**, *117*, 2910–3043.
- (14) Liao, K.; Yang, Y.-F.; Li, Y.; Sanders, J. N.; Houk, K. N.; Musaev, D. G.; Davies, H. M. L. Design of Catalysts for Site-Selective and Enantioselective Functionalization of Non-Activated Primary C–H Bonds. *Nat. Chem.* **2018**, *10*, 1048–1055.
- (15) Fukuzawa, S.; Oki, H.; Hosaka, M.; Sugawara, J.; Kikuchi, S. ClickFerrophos: New Chiral Ferrocenyl Phosphine Ligands Synthesized by Click Chemistry and the Use of

- Their Metal Complexes as Catalysts for Asymmetric Hydrogenation and Allylic Substitution. *Org. Lett.* **2007**, *9*, 5557–5560.
- (16) Huber, F. L.; Nauroozi, D.; Mengele, A. K.; Rau, S. Synthesis and Characterization of a Ruthenium(II) Complex for the Development of Supramolecular Photocatalysts Containing Multidentate Coordination Spheres. *Eur. J. Inorg. Chem.* **2017**, 4020–4027.
- (17) Nakamura, Y.; Yoshida, S.; Hosoya, T. Recent Advances in Synthetic Hetaryne Chemistry. *Heterocycles* **2019**, *98*, 1623–1677.
- (18) Pellissier, H.; Santelli, M. The Use of Arynes in Organic Synthesis. *Tetrahedron* **2003**, *59*, 701–730.
- (19) Wenk, H. H.; Winkler, M.; Sander, W. One Century of Aryne Chemistry. *Angew. Chem., Int. Ed.* **2003**, *42*, 502–528.
- (20) Sanz, R. Recent Applications of Aryne Chemistry to Organic Synthesis. A Review. *Org. Prep. Proced. Int.* **2008**, *40*, 215–291.
- (21) Gampe, C. M.; Carreira, E. M. Arynes and Cyclohexyne in Natural Product Synthesis. *Angew. Chem., Int. Ed.* **2012**, *51*, 3766–3778.
- (22) Bhunia, A.; Yetra, S. R.; Biju, A. T. Recent Advances in Transition-Metal-Free Carbon–Carbon and Carbon–Heteroatom Bond-Forming Reactions Using Arynes. *Chem. Soc. Rev.* **2012**, *41*, 3140–3152.
- (23) Yoshida, H.; Takaki, K. Aryne Insertion Reactions into Carbon–Carbon σ -bonds. *Synlett* **2012**, 1725–1732.
- (24) Dubrovskiy, A. V.; Markina, N. A.; Larock, R. C. Use of Benzyne for the Synthesis of Heterocycles. *Org. Biomol. Chem.* **2013**, *11*, 191–218.

- (25) Wu, C.; Shi, F. A Closer Look at Aryne Chemistry: Details that Remain Mysterious. *Asian J. Org. Chem.* **2013**, *2*, 116–125.
- (26) Hoffmann, R. W.; Suzuki, K. A “Hot, Energized” Benzyne. *Angew. Chem., Int. Ed.* **2013**, *52*, 2655–2656.
- (27) Goetz, A. E.; Garg, N. K. Enabling the Use of Heterocyclic Arynes in Chemical Synthesis. *J. Org. Chem.* **2014**, *79*, 846–851.
- (28) Surry, D. S.; Buchwald, S. L. Biaryl Phosphane Ligands in Palladium-Catalyzed Amination. *Angew. Chem., Int. Ed.* **2008**, *47*, 6338–6361.
- (29) Mauger, C. C.; Mignani, G. A. An Efficient and Safe Procedure for the Large-Scale Pd-Catalyzed Hydrazonation of Aromatic Chlorides using Buchwald Technology. *Org. Process Res. Dev.* **2004**, *8*, 1065–1071.
- (30) Schleth, F.; Vettiger, T.; Rommel, M.; Tobler, H. Process for the Preparation of Pyrazole Carboxylic Acid Amides. WO2011131544 A1, 2011.
- (31) Tadross, P. M.; Stoltz, B. M. A Comprehensive History of Arynes in Natural Product Total Synthesis. *Chem. Rev.* **2012**, *112*, 3550–3577.
- (32) Wang, B.; Mu, B.; Chen, D.; Xu, S.; Zhou, X. Diels–Alder Reactions of Benzyne with Indenyl Iron Complexes. *Organometallics* **2004**, *23*, 6225–6230.
- (33) Luo, S.; Zhao, X.; Mu, B.; Song, H.; Xu, S.; Wang, B. Diels–Alder Reactions of Benzyne with Indenyl and Fluorenyl Ruthenium Complexes. *Organometallics* **2009**, *28*, 4602–4605.
- (34) Grätzel, M. Dye-Sensitized Solar Cells. *J. Photochem. Photobiol., C* **2003**, *4*, 145–154.

- (35) Shaw, M. H.; Twilton, J.; MacMillan, D. W. C. Photoredox Catalysis in Organic Chemistry. *J. Org. Chem.* **2016**, *81*, 6898–6926.
- (36) Arias-Rotondo, D. M.; McCusker, J. K. The Photophysics of Photoredox Catalysis: a Roadmap for Catalyst Design. *Chem. Soc. Rev.* **2016**, *45*, 5804–5820.
- (37) Balzani, V.; Bergamini, G.; Marchioni, F.; Ceroni, P. Ru(II)-Bipyridine Complexes in Supramolecular Systems, Devices and Machines. *Coord. Chem. Rev.* **2006**, *250*, 1254–1266.
- (38) McAtee, R. C.; McClain, E. J.; Stephenson, C. R. J. Illuminating Photoredox Catalysis. *Trends Chem.* **2019**, *1*, 111–125.
- (39) Gill, M. R.; Thomas, J. A. Ruthenium(II) Polypyridyl Complexes and DNA – From Structural Probes to Cellular Imaging and Therapeutics. *Chem. Soc. Rev.* **2012**, *41*, 3179–3192.
- (40) Zeglis, B.; Pierre, V. C.; Barton, J. K. Metallo-Intercalators and Metallo-insertors. *Chem. Commun.* **2007**, 4565–4579.
- (41) Song, H.; Kaiser, J. T.; Barton, J. K. Crystal Structure of Δ -[Ru(bpy)₂dppz]²⁺ Bound to Mismatched DNA Reveals Side-by-Side Metalloinsertion and Intercalation. *Nat. Chem.* **2012**, *4*, 615–620.
- (42) Keefe, M. H.; Benkstein, K. D.; Hupp, J. T. Luminescent Sensor Molecules Based on Coordinated Metals: A Review of Recent Developments. *Coord. Chem. Rev.* **2000**, *205*, 201–228.
- (43) Kozhenvnikov, V. N.; Deary, M. E.; Mantso, T.; Panayiotidis, M. I.; Sims, M. T. Iridium(III) Complexes of 1,2,4-Triazines as Potential Bioorthogonal Reagents: Metal

- Coordination Facilitates Luminogenic Reaction with Strained Cyclooctynes. *Chem. Commun.* **2019**, 55, 14283–14286.
- (44) Peña, D.; Pérez, D.; Guitián, E.; Castedo, L. Palladium-Catalyzed Cocyclization of Arynes with Alkynes: Selective Synthesis of Phenanthrenes and Naphthalenes. *J. Am. Chem. Soc.* **1999**, 121, 5827–5828.
- (45) Yoshida, H.; Ikadai, J.; Shudo, M.; Ohshita, J.; Kunai, A. Palladium-Catalyzed Bissilylation of Arynes with Cyclic Disilanes: Synthesis of Benzo-Annulated Disilacarborocycles. *J. Am. Chem. Soc.* **2003**, 125, 6638–6639.
- (46) Jeganmohan, M.; Bhuvaneshwari, S.; Cheng, C.-H. A Cooperative Copper- and Palladium-catalyzed Three-Component Coupling of Benzynes, Allylic Epoxides, and Terminal Alkynes. *Angew. Chem., Int. Ed.* **2009**, 48, 391–394.
- (47) Liu, Y.-L.; Liang, Y.; Pi, S.-F.; Huang, X.-C.; Li, J.-H. Palladium-Catalyzed Cocyclotrimerization of Allenes with Arynes: Selective Synthesis of Phenanthrenes. *J. Org. Chem.* **2009**, 74, 3199–3202.
- (48) Garve, L. K. B.; Werz, D. B. Pd-Catalyzed Three-Component Coupling of Terminal Alkynes, Arynes, and Vinyl Cyclopropane Dicarboxylate. *Org. Lett.* **2015**, 17, 596–599.
- (49) Feng, M.; Tang, B.; Xu, H.-X.; Jiang, X. Collective Synthesis of Phenanthridinone through C–H Activation Involving a Pd-Catalyzed Aryne Multicomponent Reaction. *Org. Lett.* **2016**, 18, 4352–4355.
- (50) Yao, T.; He, D. Palladium-Catalyzed Domino Heck/Aryne Carbopalladation/C–H Functionalization: Synthesis of Heterocycle-Fused 9,10-Dihydrophenanthrenes. *Org. Lett.* **2017**, 19, 842–845.

- (51) Pozo, I.; Guitián, E.; Pérez, D.; Peña, D. Synthesis of Nanographenes, Starphenes, and Sterically Congested Polyarenes by Aryne Cyclotrimerization. *Acc. Chem. Res.* **2019**, *52*, 2472–2481.
- (52) Liu, Z.; Zhang, X.; Larock, R. C. Synthesis of Fused Polycyclic Aromatics by Palladium-Catalyzed Annulation of Arynes using 2-Halobiaryls. *J. Am. Chem. Soc.* **2005**, *127*, 15716–15717.
- (53) Liu, Z.; Larock, R. C. Highly Efficient Route to Fused Polycyclic Aromatics via Palladium-Catalyzed Aryne Annulation by Aryl Halides. *J. Org. Chem.* **2007**, *72*, 223–232.
- (54) For a prior report of dehalogenation in Ru(bpy)₃ derivatives, see: Iranmanesh, H.; Arachchige, K. S. A.; Bhadbhade, M.; Donald, W. A.; Liew, J. Y.; Liu, K. T.-C.; Luis, E. T.; Moore, E. G.; Price, J. R.; Yan, H.; Yang, J.; Beves, J. E. Chiral Ruthenium(II) Complexes as Supramolecular Building Blocks for Heterometallic Self-Assembly. *Inorg. Chem.* **2016**, *55*, 12737–12751.
- (55) CsF, which governs aryne formation, has sparing solubility in organic solvents. By modulating the solvent mixture, one can tune the effective concentration of aryne in solution. In a catalytic reaction, such as that reported herein, it is critical to balance the amount of aryne in solution relative to the reactive organometallic species.
- (56) For a pertinent report and proposed mechanism for Pd-catalyzed annulation of arynes with halobiaryl substrates, see reference 64.

- (57) Verhoeven, J. W.; van der Tol, E. B.; Steemers, F. J.; Verboom, W.; Reinhoudt, D. N.; Hofstraat, J. W. Complex Comprising a Rare-Earth Metal Ion and a Complexing Moiety. EP1019401 B1, 1998.
- (58) Lu, W.; Vicic, D. A.; Barton, J. K. Reductive and Oxidative DNA Damage by Photoactive Platinum(II) Intercalators. *Inorg. Chem.* **2005**, *44*, 7970–7980.
- (59) Geri, J. B.; Oakley, J. V.; Reyes-Robles, T.; Wang, T.; McCarver, S. J.; White, C. H.; Rodriguez-Rivera, F. P.; Parker, D. L., Jr.; Hett, E. C.; Fadeyi, O. O.; Oslund, R. C.; MacMillan, D. W. C. Microenvironment Mapping via Dexter Energy Transfer on Immune Cells. *Science* **2020**, *367*, 1091–1097.
- (60) Colombo, M. G.; Hauser, A.; Guedel, H. U. Evidence for Strong Mixing Between the LC and MLCT Excited States in Bis(2-phenylpyridinato-C2,N')(2,2'-bipyridine)iridium(III). *Inorg. Chem.* **1993**, *32*, 3088–3092.
- (61) Wang, C.; deKrafft, K. E.; Lin, W. Pt Nanoparticles@Photoactive Metal–Organic Frameworks: Efficient Hydrogen Evolution via Synergistic Photoexcitation and Electron Injection. *J. Am. Chem. Soc.* **2012**, *134*, 7211–7214.
- (62) Bolink, H. J.; Coronado, E.; Costa, R. D.; Ortí, E.; Sessolo, M.; Graber, S.; Doyle, K.; Neuburger, M.; Housecroft, C. E.; Constable, E. C. Long-Living Light-Emitting Electrochemical Cells – Control through Supramolecular Interactions. *Adv. Mater.* **2008**, *20*, 3910–3913.
- (63) Li, Y.; Dandu, N.; Liu, R.; Li, Z.; Kilina, S.; Sun, W. Effects of Extended π -Conjugation in Phenanthroline (N^N) and Phenylpyridine (C^N) Ligands on the Photophysics and

- Reverse Saturable Absorption of Cationic Heteroleptic Iridium(III) Complexes. *J. Phys. Chem. C* **2014**, *118*, 6372–6384.
- (64) Bennett, M. A.; Schwemlein, H. P. Metal Complexes of Small Cycloalkynes and Arynes. *Angew. Chem., Int. Ed. Engl.* **1989**, *28*, 1296–1320.
- (65) Werner, G.; Lehmann, C. W.; Butenschön, H. The First Anionic Thia-Fries Rearrangements at Ferrocene: Ready Access to Trifluoromethylsulfonyl-Substituted Hydroxyferrocenes and an Extremely High Interannular Stereinduction Between Cyclopentadienyl Ligands. *Adv. Synth. Catal.* **2010**, *352*, 1345–1355.
- (66) Duong, H. M.; Bendikov, M.; Steiger, D.; Zhang, Q.; Sonmez, G.; Yamada, J.; Wudl, F. Efficient Synthesis of a Novel, Twisted and Stable, Electroluminescent “Twistacene.” *Org. Lett.* **2003**, *5*, 4433–4436.
- (67) Suzuki, S.; Itami, K.; Yamaguchi, J. Synthesis of Octaaryl Naphthalenes and Anthracenes with Different Substituents. *Angew. Chem., Int. Ed.* **2017**, *56*, 15010–15013.
- (68) Graczyk, A.; Murphy, F. A.; Nolan, D.; Fernández-Moreira, V.; Lundin, N. J.; Fitchett, C. M.; Draper, S. M. Terpyridine-Fused Polyaromatic Hydrocarbons Generated via Cyclodehydrogenation and used as Ligands in Ru(II) Complexes. *Dalton Trans.* **2012**, *41*, 7746–7754.
- (69) Grzybowski, M.; Sadowski, B.; Butenschön, H.; Gryko, D. T. Synthetic Applications of Oxidative Aromatic Coupling—from Biphenols to Nanographenes. *Angew. Chem., Int. Ed.* **2020**, *59*, 2998–3027.
- (70) Polypyridyl metal complexes bearing highly π -expanded ligand systems have historically demonstrated unique coordinating properties and photophysical characteristics. For a

- notable example, see: Draper, S. M.; Gregg, D. J.; Schofield, E. R.; Browne, W. R.; Duati, M.; Vos, J. G.; Passaniti, P. Complexed Nitrogen Heterosuperbenzene: The Coordinating Properties of a Remarkable Ligand. *J. Am. Chem. Soc.* **2004**, *126*, 8694–8701.
- (71) Reichardt, C.; Monro, S.; Sobotta, F. H.; Colón, K. L.; Sainuddin, T.; Stephenson, M.; Sampson, E.; Roque, J., III.; Yin, H.; Brendel, J. C.; Cameron, C. G.; McFarland, S.; Dietzek, B. Predictive Strength of Photophysical Measurements for in Vitro Photobiological Activity in a Series of Ru(II) Polypyridyl Complexes Derived from π -Extended Ligands. *Inorg. Chem.* **2019**, *58*, 3156–3166.
- (72) Young, M. C.; Liew, E.; Ashby, J.; McCoy, K. E.; Hooley, R. J. Spin State Modulation of Iron Spin Crossover Complexes via Hydrogen Bonding Self-Assembly. *Chem. Commun.* **2013**, *49*, 6331–6333.
- (73) Cheong, P. H.-Y.; Paton, R. S.; Bronner, S. M.; Im, G.-Y. J.; Garg, N. K.; Houk, K. N. Indolyne and Aryne Distortions and Nucleophilic Regioselectivities. *J. Am. Chem. Soc.* **2010**, *132*, 1267–1269.
- (74) Breton, G. W. Selective Monoacetylation of Unsymmetrical Diols Catalyzed by Silica Gel Supported Sodium Hydrogen Sulfate. *J. Org. Chem.* **1997**, *62*, 8952–8954.
- (75) Suzuki, K.; Kobayashi, A.; Kaneko, S.; Takehira, K.; Yoshihara, T.; Ishida, H.; Shiina, Y.; Oishi, S.; Tobita, S. Reevaluation of Absolute Luminescence Quantum Yields of Standard Solutions using a Spectrometer with an Integrating Sphere and a Back-Thinned CCD Detector. *Phys. Chem. Chem. Phys.* **2009**, *11*, 9850–9860.

- (76) Méndez-Hernández, D. D.; Gillmore, J. G.; Montano, L. A.; Gust, D.; Moore, T. A.; Moore, A. L.; Mujica, V. Building and Testing Correlations for the Estimation of One-Electron Reduction Potentials of a Diverse Set of Organic Molecules. *J. Phys. Org. Chem.* **2015**, *28*, 320–328.
- (77) CYLview20; Legault, C. Y., Université de Sherbrooke, 2020 (<http://www.cylview.org>).

CHAPTER FOUR

Total Synthesis of Phenanthroindolizidines Using Strained Azacyclic Alkynes

Katie A. Spence, Marie Hoffmann, and Neil K. Garg.

Manuscript Submitted.

4.1 Abstract

We report a concise approach to phenanthroindolizidine alkaloids. This involves the interception of strained azacyclic alkynes in Pd-catalyzed annulation reactions. Two types of strained intermediates were evaluated in the key step: a functionalized piperidyne, as well as a previously unknown type of strained intermediate, an indolizidyne. We show that both types of strained intermediates can be employed to efficiently access phenanthroindolizidines. The indolizidyne, despite possessing a basic nitrogen substituent, was used in the final step to synthesize three natural products: tylophorine, tylocrebine, and isotylocrebine. This study represents the first use of non-aromatic, strained azacyclic alkynes in total synthesis. Moreover, these efforts demonstrate the successful merger of strained azacyclic alkyne chemistry with transition-metal catalysis for the construction of complex heterocycles.

4.2 Introduction

Nitrogen-containing heterocycles are commonly present in many important molecules, including natural products,¹ medicinal agents,^{2,3} agrochemicals,⁴ materials,⁵ polymers,⁶ and organometallic compounds.⁷ As such, new strategies for their syntheses remain highly valuable. One promising tactic involves the use of heterocyclic arynes, such as **4.1–4.3** (Figure 4.1). These short-lived intermediates can be manipulated in ways reminiscent of aryne functionalization

processes^{8,9,10,11,12,13} but come with the added benefit of having an *N*-substituent incorporated in their core.^{14,15,16} Pyridynes (e.g., **4.1**) have been most thoroughly studied and have been used in a number of total syntheses.^{17,18,19,20,21,22,23,24,25,26} For example, Moody's 1984 total synthesis of ellipticine (**4.6**) was enabled by a Diels–Alder reaction with an in-situ generated pyridyne.¹⁹ Indolynes (e.g., **4.2**), and their π -extended carbazolyne counterparts (e.g., **4.3**) are also highly valuable synthetic building blocks, with several applications in total synthesis being reported.^{27,28,29,30,31,32,33,34,35,36,37} For example, the interception of an indolyne and carbazolyne, respectively, was instrumental in enabling the total syntheses of *N*-methylwelwitindolinone C isothiocyanate (**4.7**)²⁹ and tubingensin B (**4.8**).³⁶

Non-aromatic heterocyclic alkynes are far less studied compared to their aromatic counterparts. Two methodology studies on piperidynes (e.g., **4.4**, Figure 4.1) are available^{38,39} that demonstrate cycloadditions and nucleophilic trappings. These, as well as other scattered examples,^{40,41,42,43,44,45,46} show that piperidynes can be used to access functionalized, sp^3 -rich heterocycles. However, piperidynes have never been utilized in total synthesis or metal-catalyzed annulations. Another interesting aspect of piperidyne chemistry is that the *N*-atom bears an electron-withdrawing group (e.g., Ts, Cbz) in known trapping experiments as a means to mitigate the basicity and nucleophilicity of the piperidine nitrogen. As such, indolizidyne intermediate **4.5**, bearing a basic tertiary amine, has remained unknown. This was of particular interest to us given the presence of indolizidines in natural product scaffolds, including in the phenanthroindolizidine alkaloids.⁴⁷

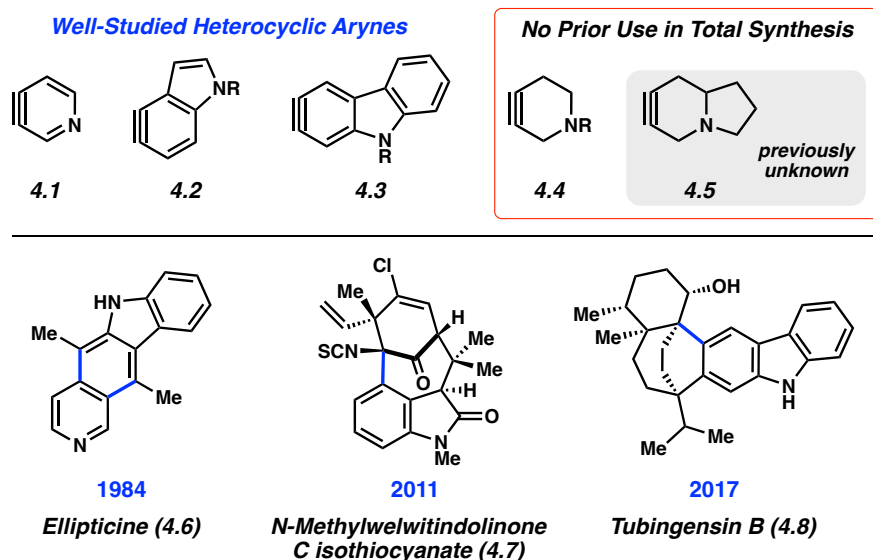


Figure 4.1. Well-studied strained azacyclic alkynes **4.1–4.3**, azacyclic alkynes **4.4** and **4.5**, and examples of natural products synthesized using *N*-containing hetarynes.

The most well-known family member of the phenanthroindolizidine alkaloids is tylophorine (**4.9**, Figure 4.2), which was first isolated from *Tylophora indica* in 1935.⁴⁸ Tylophorine (**4.9**) and many of its derivatives have garnered significant attention due to their important biological activities, including anti-cancer,^{49,50} anti-inflammatory,⁵¹ and anti-viral properties,⁵² which include significant activity against SARS-CoV-2.⁵³ Select examples of prior syntheses include the works of Georg,⁵⁴ Opatz,^{55,56} Zhao,⁵⁷ and Chemler.⁵⁸ In considering alternative strategic disconnections of tylophorine (**4.9**), we wondered whether strained, azacyclic alkyne chemistry could offer a uniquely convergent approach.

Our retrosynthetic strategy for accessing tylophorine (**4.9**) is shown in Figure 4.2. Disconnection of the B ring at two sites provides fragment **4.10** for the western portion of the molecule, as well as strained intermediates **4.11** or **4.5** for the eastern portion. In the forward sense, the fragments would be coupled via a palladium-catalyzed Larock annulation.^{59,60} Metal-

mediated transformations of strained alkynes are known,^{61,62,63} and provide powerful tools for constructing multiple bonds in efficient transformations. However, examples involving strained, azacyclic alkynes are less common,^{64,65,66} and metal-catalyzed reactions of piperidynes remain unknown.

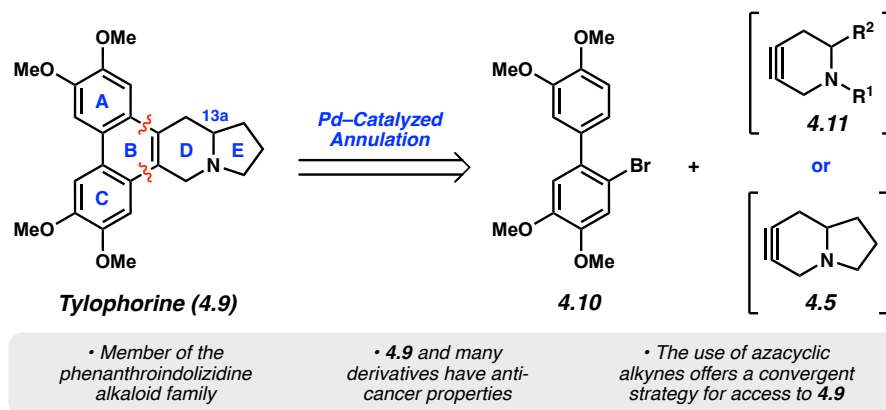


Figure 4.2. Strategies for the synthesis of tylophorine (**4.9**) using strained azacyclic alkynes **4.11** or **4.5** in Pd-catalyzed annulations.

Herein, we disclose access to phenanthroindolizidines using the aforementioned Pd-mediated coupling reaction of strained azacyclic alkynes. We demonstrate that either intermediates of the type **4.11** or **4.5** (see Figure 4.2) can be employed in the key step. For the latter case, we prepare the first indolizidine precursor **4.5** and harness it to synthesize three natural products, including (\pm)-tylophorine (**4.9**). This study illustrates the first use of a piperidine or indolizidine in natural product synthesis and should prompt further synthetic studies of these non-traditional intermediates.

4.3 Results and Discussion

4.3.1 Access to Tylophorine via a Piperidyne Annulation

In our first approach to tylophorine (**4.9**), we sought to utilize a piperidyne intermediate **4.11** (see Figure 4.2), which would bear an electron-withdrawing substituent on the nitrogen (R^1), akin to known piperidynes.³⁹ This intermediate would possess functionality at R^2 , which could allow for late-stage introduction of the E ring. We ultimately developed the concise route shown in Figure 4.3. Silyl methoxy pyridine **4.12**, prepared in one step from commercially available 4-methoxypyridine,⁶⁷ was treated sequentially with CbzCl, Grignard reagent **13**, and aqueous HCl. This delivered vinylogous amide **14** in 99% yield via nucleophilic addition into an in situ generated pyridinium salt at C13a, and hydrolysis.⁶⁸ Subsequent 1,4-reduction of **4.14** was achieved using L-selectride, and trapping with Tf_2O gave piperidyne precursor **4.15**.³⁹ Notably, our strategy to elaborate **4.12** to **4.15** is scalable and should be amenable to the synthesis of other substituted piperidyne precursors.

With **4.15** in hand, we directed our attention to the key Pd-catalyzed annulation with known biaryl bromide **4.10** (see Figure 4.2). In previous studies, we have found that metal-catalyzed trappings of heterocyclic strained intermediates require careful optimization.^{65,66,69,70,71} This is due to the inherent requirement that the transient, strained intermediate intercept a species only present in catalytic quantities. Indeed, the coupling proved challenging using conditions developed for benzyne annulations. Ultimately, we found that the reaction between piperidyne precursor **4.15** and biaryl bromide **4.10** proceeded most effectively when using 10 mol% $Pd(dba)_2$ and $P(o\text{-tolyl})_3$, 3 equivalents of cesium carbonate, 10 equivalents of cesium fluoride, and a 1:20 ratio⁷² of acetonitrile to toluene at 110 °C. After the coupling was complete, quenching with aqueous acid at 23 °C facilitated removal of the acetal protecting group.

Annulated product **4.17** bearing a pendant aldehyde was obtained in 60% yield. To complete the total synthesis of tylophorine (**4.9**), **4.17** was treated with H₂ and Pd/C in methanol. This allowed for hydrogenolysis, followed by reductive amination, to deliver (±)-tylophorine (**4.9**) in 90% yield. The route is four steps from **4.12** and establishes the viability of using piperidynes in total synthesis.

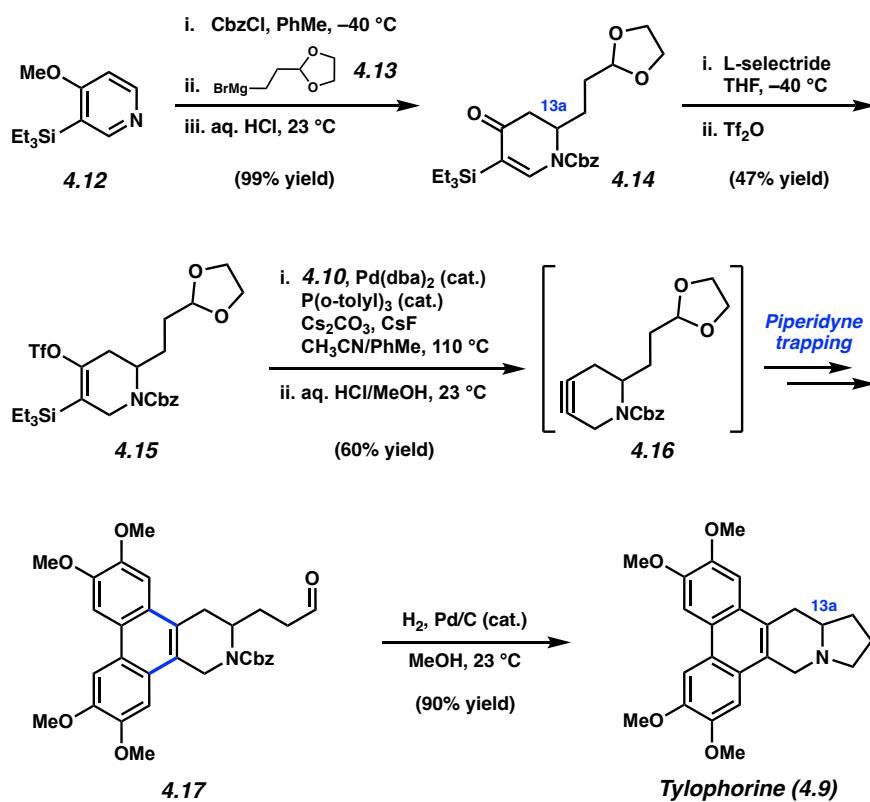


Figure 4.3. Concise total synthesis of tylophorine (**4.9**) using piperidine **4.16**.

4.3.2 Access to an Indolizidine Precursor

After establishing that a strained, azacyclic alkyne could be used in a metal-mediated Larock annulation to access to the phenanthroindolizidine core, we sought to synthesize a novel indolizidine precursor. Such an intermediate could offer a uniquely divergent approach to phenanthroindolizidines in just one synthetic step. Although many of our attempts proved

unsuccessful, the route described in Figure 4.4 showed some initial promise. The strategy parallels the general approach shown in Figure 4.3, but with provisions to introduce the necessary 5-membered ring. Treatment of pyridine **4.12** with allyl bromide gave pyridinium salt **4.18**, which was directly subjected to vinylmagnesium bromide. Subsequent hydrolysis afforded product **4.19** bearing allyl and vinyl substituents on N and C13a, respectively. With the hope of accessing silyl triflate **4.20**, **4.19** was treated with L-selectride, followed by Comins' reagent. However, instead of obtaining the desired silyl triflate **4.20**, fragmentation product **4.22** was isolated in 71% yield. It is hypothesized that silyl triflate **4.20** initially forms, but undergoes rapid and irreversible loss of triflate with C–C bond cleavage to form **4.21**. Upon aqueous workup, iminium **4.21** is hydrolyzed to give **4.22**.⁷³

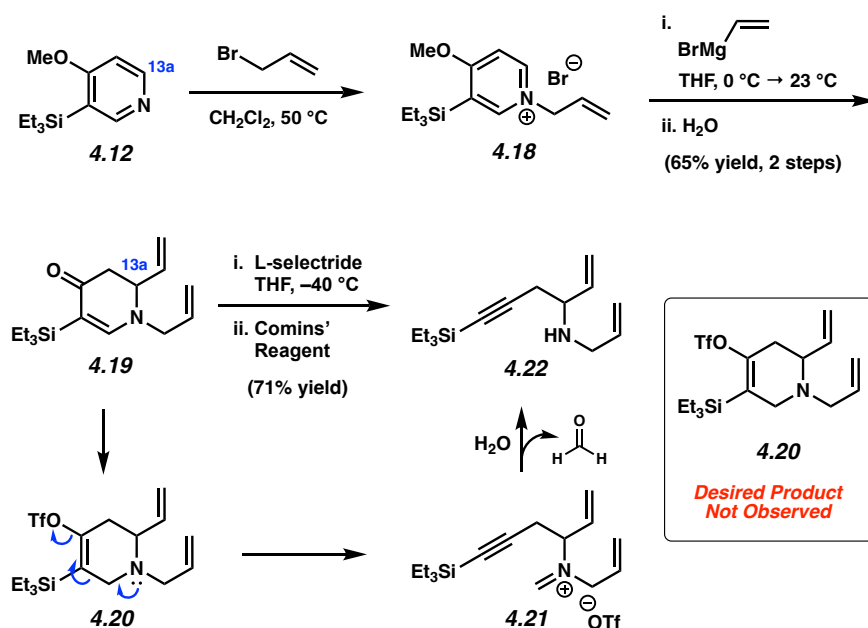


Figure 4.4. Unsuccessful attempt toward accessing an indolizidine precursor.

To circumvent the undesired pathway shown in Figure 4.4, we targeted silyl tosylate **4.25** as a precursor to **4.5** (Figure 4.5). The lower leaving group ability of tosylates in comparison to triflates⁷⁴ was expected to suppress the undesired fragmentation; in addition, silyl tosylates have

been used as precursors to other strained intermediates.⁷⁵ We were pleased to find that treatment of **4.19** with L-selectride, followed by *p*-toluenesulfonic anhydride (Ts₂O), gave **4.23** in 80% yield. Fragmentation product **4.22** was not observed. Next, the basic amine in **4.23** was protonated with *p*-toluenesulfonic acid (TsOH) prior to treatment with Grubbs II catalyst,⁷⁶ which yielded metathesis product **4.24** in 63% yield. Hydrogenation yielded the desired indolizidyne precursor **4.25**.

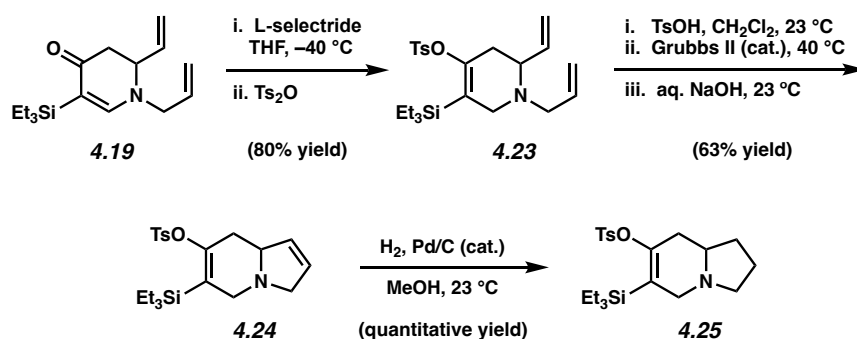


Figure 4.5. Synthesis of indolizidyne precursor **4.25**.

4.3.3 Access to Phenanthroindolizidines via Indolizidyne Chemistry

With access to silyl tosylate **4.25**, we were eager to evaluate indolizidyne generation and the key Pd-catalyzed annulation, as this would provide direct access to tylophorine (**4.9**) (Figure 4.6). We first attempted the key step using conditions developed for annulating piperidyne **4.16** (see Figure 4.3), but only observed trace conversion to tylophorine (**4.9**). We ultimately found that by altering the solvent to 1:4 DMF/PhMe, and adding tetrabutylammonium triflate to modulate fluoride solubility, the yield of **4.9** increased to 57%. Overall, this strategy provides highly convergent access to tylophorine (**4.9**) via a novel indolizidyne intermediate. Only one example of a piperidyne possessing a basic tertiary amine has been proposed in the literature,

arising from a flash vacuum pyrolysis experiment.⁷⁷ Moreover, catalyst activity in the annulation is not detrimentally hampered by the presence of the basic amine.

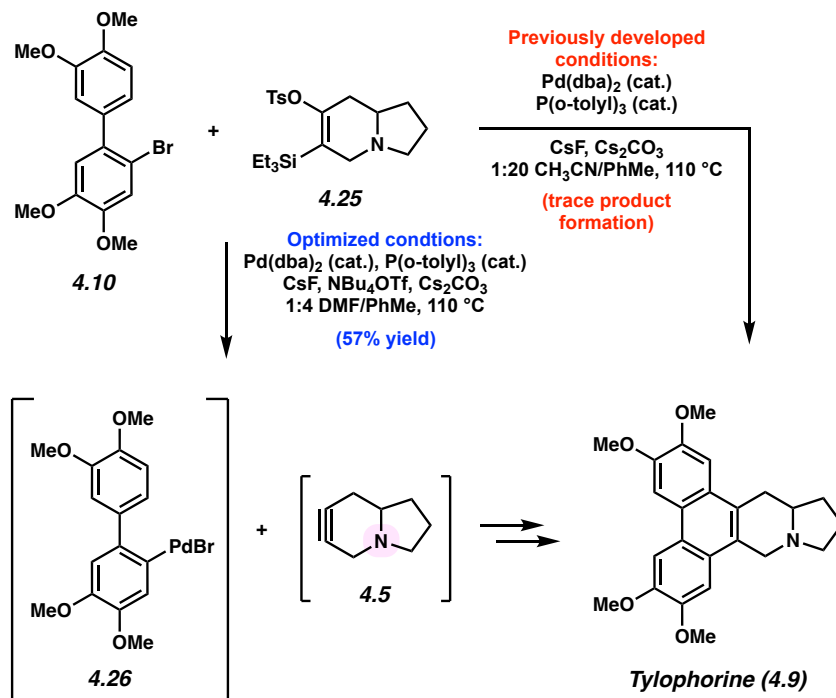


Figure 4.6. Pd-catalyzed annulation of indolizidine 4.5 to furnish tylophorine (4.9).

As highlighted in Figure 4.7, the indolizidine annulation provides a strategy to directly access other phenanthroindolizidines as a final step. Use of biaryl bromide 4.27 in the annulation reaction with indolizidine precursor 4.25 furnished a 1:1 ratio of tylocrebine (4.28) and isotylocrebine (4.29) in 68% yield. Both of these natural products demonstrate anti-cancer properties.^{78,79} Overall, the indolizidine approach obviates the need for protecting groups and late-stage manipulations, while providing advances in azacyclic alkyne chemistry.

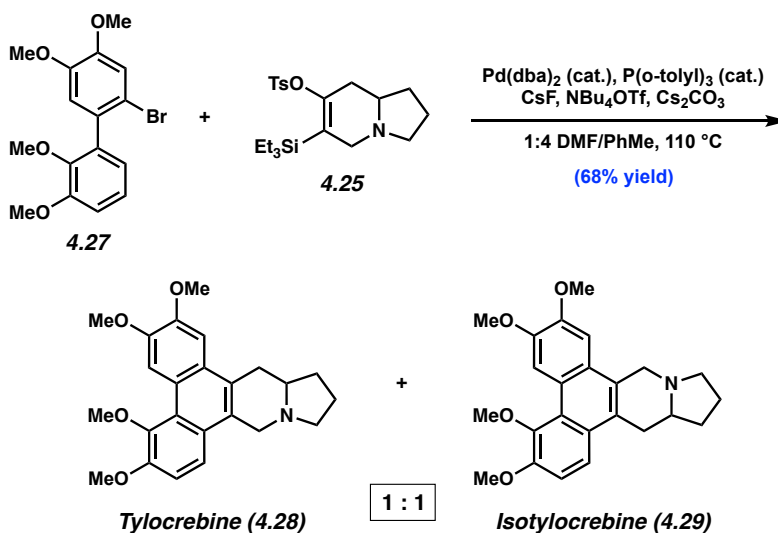


Figure 4.7. Indolizidine trapping provides tylocrebine (4.28) and isotylocrebine (4.29).

4.4 Conclusions

This study demonstrates that strained azacyclic alkynes (i.e., piperidynes and indolizidynes) serve as valuable building blocks in total synthesis. We hope these efforts will prompt the further investigation and usage of strained azacyclic alkynes for the synthesis of complex molecules.

4.5 Experimental Section

4.5.1 Materials and Methods

Unless stated otherwise, reactions were conducted in flame-dried glassware under an atmosphere of nitrogen and commercially obtained reagents were used as received. Anhydrous solvents were either freshly distilled or passed through activated alumina columns, unless otherwise specified. Reaction temperatures were controlled using an IKAmag temperature modulator, and unless stated otherwise, reactions were performed at room temperature (approximately 23 °C). Magnesium turnings, 1,2-dibromoethane, L-selectride, trifluoroacetic

anhydride, cesium carbonate (Cs_2CO_3), tri(*o*-tolyl)phosphine ($\text{P}(\textit{o}\text{-tolyl})_3$), Grubbs 2nd generation catalyst and vinylmagnesium bromide were purchased from Sigma Aldrich. Trifluoroacetic anhydride was distilled prior to use. 2-(2-bromoethyl)-1,3-dioxolane, *p*-toluenesulfonic acid (TsOH) and Comins' Reagent were purchased from Combi Blocks. Benzyl chloroformate (CbzCl) was purchased from Acros Organics. Hydrochloric acid (12 molar in water) was purchased from Fischer Chemical. Cesium fluoride, bis(dibenzylideneacetone)palladium(0) ($\text{Pd}(\text{dba})_2$) and palladium (10% on activated carbon, 50–70% wetted powder) were obtained from Strem Chemicals and stored in a desiccator. *p*-Toluenesulfonic anhydride (Ts_2O) was purchased from Acros Chemicals and recrystallized from benzene prior to use. Allyl bromide was obtained from Alfa Aesar. Known 4-Methoxy-3-(triethylsilyl)pyridine (**4.12**),⁸⁰ 2-bromo-3',4,4',5-tetramethoxy-1,1'-biphenyl (**4.10**)⁸¹ and 2'-bromo-2,3,4',5'-tetramethoxy-1,1'-biphenyl (**4.27**)⁸² were prepared following literature procedures.

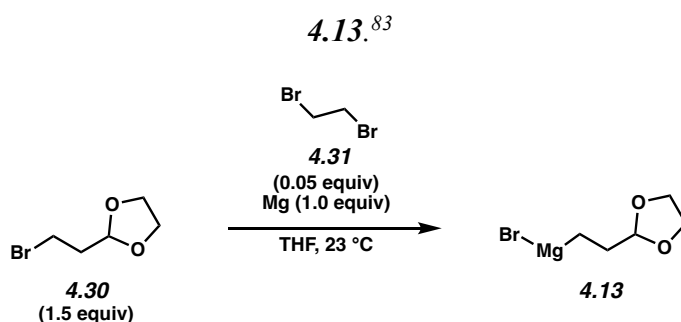
Thin-layer chromatography (TLC) was conducted with EMD gel 60 F254 pre-coated plates (0.25 mm for analytical chromatography and 0.50 mm for preparative chromatography) and visualized using a combination of UV light and potassium permanganate staining techniques. Silicycle Siliaflash P60 (particle size 0.040–0.063 mm) was used for flash column chromatography. ¹H NMR spectra were recorded on Bruker spectrometers (at 400, 500 and 600 MHz) and are reported relative to residual solvent signals. Data for ¹H NMR spectra are reported as follows: chemical shift (δ ppm), multiplicity, coupling constant (Hz), integration. Data for ¹³C NMR are reported in terms of chemical shift (125 MHz). IR spectra were recorded on a Perkin-Elmer UATR Two FT-IR spectrometer and are reported in terms of frequency absorption (cm^{-1}). DART-MS spectra were collected on a Thermo Exactive Plus MSD (Thermo Scientific) equipped with an ID-CUBE ion source and a Vapor Interface (IonSense Inc.). Both the source

and MSD were controlled by Excalibur software v. 3.0. The analyte was spotted onto OpenSpot sampling cards (IonSense Inc.) using volatile solvents (e.g., chloroform, dichloromethane). Ionization was accomplished using UHP He plasma with no additional ionization agents. The mass calibration was carried out using Pierce LTQ Velos ESI (+) and (-) Ion calibration solutions (Thermo Fisher Scientific).

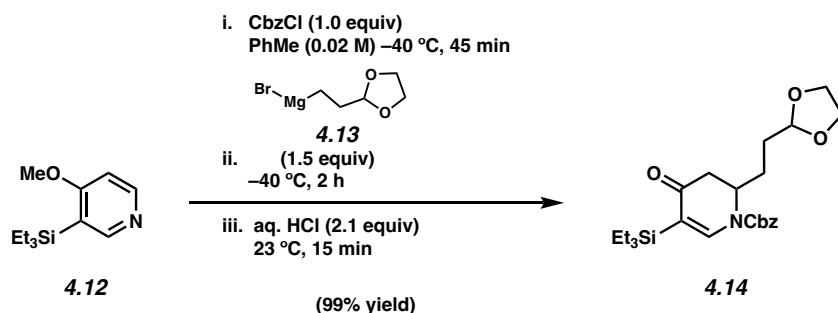
4.5.2 Experimental Procedures

4.5.2.1 Access to Tylophorine Through a Piperidine

Note: This procedure was modified from a previously reported synthesis of Grignard reagent



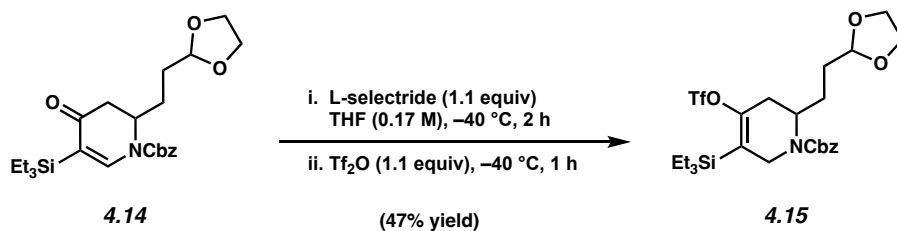
Grignard 4.13. To a flask containing magnesium (163 mg, 1.00 equiv, 6.71 mmol) was added THF (12.5 mL). 1,2-dibromoethane (**4.31**, 29.0 μ L, 0.05 equiv, 0.336 mmol) was then added drop-wise and the reaction mixture was allowed to stir for 5 minutes. The THF in the flask was then removed and the magnesium was resuspended in fresh THF (12.5 mL). 2-(2-bromoethyl)-1,3-dioxolane (**4.30**, 1.20 mL, 1.50 equiv, 10.1 mmol) was then added drop-wise and the solution was allowed to stir at 23 °C for 1.5 hours. After this time, the magnesium was completely consumed. The resulting yellow Grignard solution was used as is in the subsequent step, assuming a quantitative yield (0.54 M in THF, 1.38 g).



Oxo-dihydropyridine 4.14. To a flask containing 4-methoxy-3-(triethylsilyl)pyridine (**4.12**, 1.00 g, 1.00 equiv, 4.48 mmol) was added toluene (200 mL). The solution was then cooled to –40 °C while stirring over 10 minutes. CbzCl (639 μ L, 1.00 equiv, 4.48 mmol) was then added drop-wise and the solution was allowed to stir at –40 °C for 45 minutes. After this time, Grignard **4.13** (0.54 M in THF, 1.38 g, 1.50 equiv, 6.71 mmol) was added drop-wise and the solution was allowed to stir for an additional 2 hours. 12M aq. HCl (780 μ L, 2.10 equiv, 9.41 mmol) was then added drop-wise. The solution was warmed to 23 °C and stirred for an additional 15 minutes before sat. aq. NH₄Cl (15 mL) was added. The mixture was then transferred to a separatory funnel with sat. aq. NH₄Cl (50 mL) and Et₂O (50 mL). The layers were separated and the aqueous layer was extracted with Et₂O (2 x 75 mL). The organic layers were combined, dried over MgSO₄, filtered, then concentrated under reduced pressure. The resulting oil was purified by silica gel flash chromatography (1:5 ethyl acetate:hexanes) to afford oxo-dihydropyridine **4.14** as a clear oil (1.97 g, 99% yield). Oxo-dihydropyridine **4.14**: *R_f* 0.37 (4:1 hexanes:EtOAc); ¹H NMR (600 MHz, CDCl₃): δ 7.72 (s, 1H), 7.43 – 7.34 (m, 5H), 5.30 – 5.24 (m, 2H), 4.80 (br s, 1H), 4.62 (br s, 1H), 3.89 (br s, 2H), 3.79 (br s, 2H), 2.79 (dd, *J* = 16.0, 6.6, 1H), 2.42 (d, *J* = 16.2, 1H), 1.84 – 1.51 (m, 4H), 0.89 (t, *J* = 7.9, 9H), 0.74 – 0.63 (m, 6H); ¹³C NMR (125 MHz, CDCl₃): δ 201.1, 196.3, 152.9, 146.3, 135.3, 128.92, 128.86, 128.8, 128.5, 113.0, 103.8, 75.2, 69.3, 69.0, 65.1, 65.0, 54.1, 53.1, 40.3, 30.8, 30.0, 25.1, 7.6, 3.1, 3.0; IR (film): 2953, 1725,

1659, 1577, 1391 cm^{-1} ; HRMS-APCI (m/z) [$M + H^+$] calcd for $\text{C}_{24}\text{H}_{36}\text{NO}_5\text{Si}^+$, 446.2357; found 446.2358.

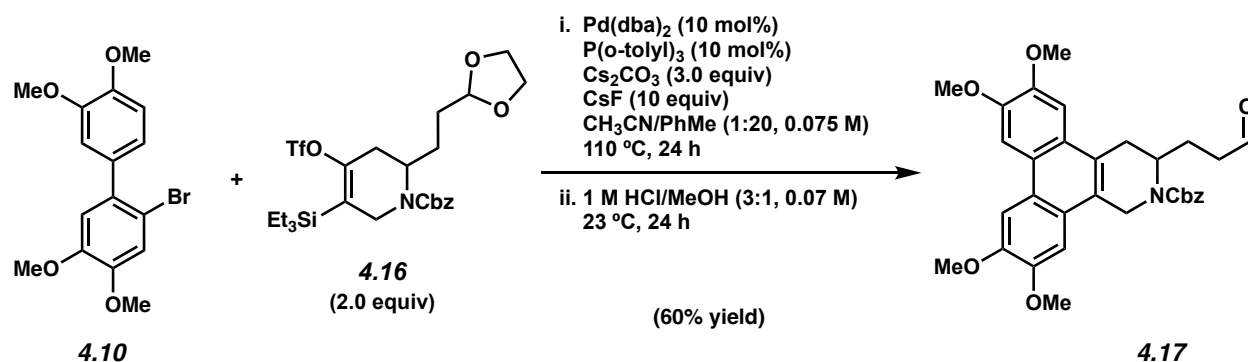
Note: 4.14 was obtained as a mixture of rotamers. These data represent empirically observed chemical shifts from ^1H and ^{13}C NMR spectra.



Silyl triflate 4.15. To a vial containing oxo-dihydropyridine **4.14** (150 mg, 1.00 equiv, 337 μmol) was added THF (1.52 mL). The solution was allowed to stir for 5 minutes before being cooled to $-40\text{ }^\circ\text{C}$. L-selectride (1.0 M in THF, 370 μL , 1.10 equiv, 370 μmol) was then added drop-wise and the solution was allowed to stir for 2 hours. After this time, triflic anhydride (62.6 μL , 1.10 equiv, 370 μM) was added and the solution was stirred for 1 hour at $-40\text{ }^\circ\text{C}$. Sat. aq. NaHCO_3 (1.5 mL) was then added in one portion and the solution was allowed to warm to $23\text{ }^\circ\text{C}$ where it was stirred for 1 hour. The mixture was then transferred to a separatory funnel with sat. aq. NaHCO_3 (20 mL) and EtOAc (20 mL). The layers were separated and the aqueous layer was extracted with EtOAc (2 x 20 mL). The organic layers were combined, dried over MgSO_4 , filtered, then concentrated under reduced pressure. The resulting oil was purified by silica gel flash chromatography (1:10 EtOAc:hexanes) to afford silyl triflate **4.15** as a clear oil (92.0 mg, 47% yield). Silyl triflate **4.15**: R_f 0.31 (1:4 EtOAc:hexanes); ^1H NMR (600 MHz, CDCl_3): δ 7.38 – 7.30 (m, 5H), 5.18 (d, $J = 12.5$, 1H), 5.11 (d, $J = 12.5$, 1H), 4.91 – 4.78 (m, 1H), 4.67 – 4.46 (m, 2H), 3.98 – 3.75 (m, 4H), 3.67 – 3.53 (m, 1H), 2.89 (d, $J = 14.6$, 1H), 2.23 (d, $J = 16.7$, 1H), 1.77 – 1.49 (m, 4H), 1.01 – 0.88 (m, 9H), 0.82 – 0.68 (m, 6H); ^{13}C NMR (125 MHz, CDCl_3): δ

155.0, 136.5, 128.7, 128.3, 127.9, 119.4, 117.3, 103.7, 67.7, 65.11, 65.06, 49.0, 42.0, 33.1, 32.6, 30.1, 25.2, 7.3, 2.8; IR (film): 2957, 2880, 1703, 1413, 1211 cm^{-1} ; HRMS-APCI (m/z) [$M + H^+$] calcd for $\text{C}_{25}\text{H}_{37}\text{F}_3\text{NO}_7\text{SSi}^+$, 580.2007; found 580.2010.

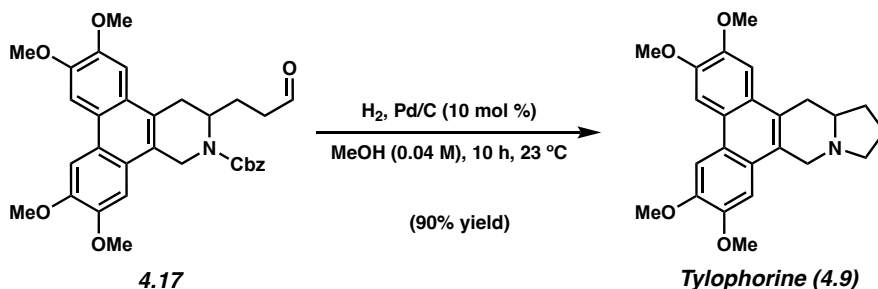
Note: 4.15 was obtained as a mixture of rotamers. These data represent empirically observed chemical shifts from ^1H and ^{13}C NMR spectra.



Phenanthrene 4.17. A 1-dram vial was charged sequentially with $\text{Pd}(\text{dba})_2$ (3.3 mg, 10 mol%, $5.7\ \mu\text{mol}$), biaryl bromide **4.10** (20 mg, 1.0 equiv, $57\ \mu\text{mol}$), $\text{P}(o\text{-tolyl})_3$ (1.7 mg, 10 mol%, $5.7\ \mu\text{mol}$), MeCN (0.017 mL), PhMe (0.34 mL), silyl triflate **4.16** (66 mg, 2.0 equiv, 0.11 mmol), an oven-dried magnetic stir bar, Cs_2CO_3 (55 mg, 3.0 equiv, 0.17 mmol) and CsF (86 mg, 10 equiv, 0.57 mmol). The reaction was then purged with N_2 for 5 min before being capped with a Teflon-lined screw cap under a flow of N_2 , sealed with Teflon tape and electrical tape, transferred to an Al-block, and stirred at 110°C for 24 hours. After cooling to 23°C , the mixture was filtered through a plug of celite, then concentrated under reduced pressure. The resulting mixture was resuspended in methanol (0.6 mL) and 1 M aq. HCl (0.2 mL). The mixture was allowed to stir vigorously at 23°C for 24 hours before being quenched with sat. aq. sodium bicarbonate (1 mL). The mixture was then suspended in sat. aq. sodium bicarbonate (15 mL) and extracted with EtOAc (3 x 15 mL). The organic layers were combined, dried over MgSO_4 , filtered, then

concentrated under reduced pressure. The crude residue was then purified by silica gel flash chromatography (1:1 hexanes:EtOAc) to afford phenanthrene **4.17** as a white solid (18 mg, 60% yield). Phenanthrene **4.17**: R_f 0.07 (2:1 hexanes:EtOAc); ^1H NMR (500 MHz, CDCl_3): δ 9.81–9.58 (m, 1H), 7.84 (s, 2H), 7.47–7.29 (m, 7H), 5.52–4.45 (m, 5H), 4.12 (s, 6H), 4.05 (s, 6H), 3.97–3.71 (m, 2H), 3.43–3.30 (m, 1H), 3.18–3.06 (m, 2H), 2.67–2.39 (m, 1H); ^{13}C NMR (125 MHz, CDCl_3): δ 201.3, 149.24, 149.17, 148.9, 129.6, 128.8, 128.4, 124.1, 123.6, 103.8, 103.6, 102.9, 67.6, 65.1, 56.2, 56.1, 56.0, 48.3, 46.0, 40.6, 39.0, 32.1, 30.8, 30.3, 29.8, 29.5, 29.3, 29.1, 25.6, 24.2, 24.0, 23.1; IR (film): 2927, 2852, 1693, 1514, 1250 cm^{-1} ; HRMS-APCI (m/z) [$\text{M} + \text{H}^+$] calcd for $\text{C}_{32}\text{H}_{34}\text{NO}_7^+$, 544.2330; found 544.2319.

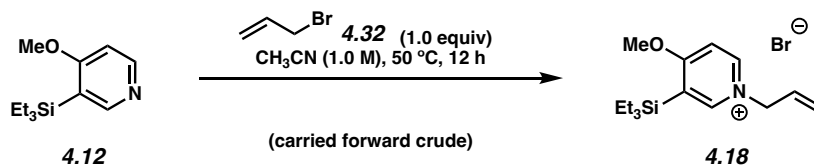
Note: 4.17 was obtained as a mixture of rotamers. These data represent empirically observed chemical shifts from ^1H and ^{13}C NMR spectra.



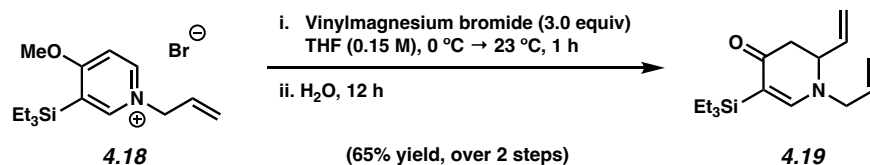
Tylophorine (4.9). A 1-dram vial was equipped with a magnetic stir bar, then charged with phenanthrene **4.17** (4.0 mg, 1.0 equiv, 7 μmol) and Pd/C (0.8 mg, 10 mol%, 0.7 μmol). The vial was purged with nitrogen for 5 minutes before its contents were suspended in methanol (0.2 mL). The reaction vial was then placed under an atmosphere of hydrogen via a balloon and vent needle. The vent needle was removed after 20 seconds of sparging, and the reaction mixture was allowed to stir at 23 °C for 10 hours under positive pressure of hydrogen from the balloon. After the allotted time, the reaction mixture was diluted with CH_2Cl_2 (1.0 mL) and passed through a

plug of celite. The crude reaction mixture was then concentrated under reduced pressure to afford the crude reaction mixture which was purified via preparative TLC (10:1 CH₂Cl₂:methanol) to afford tylophorine (**4.9**) as a white solid (2.5 mg, 90% yield). Spectral data matched those reported in the literature.⁸⁴ Tylophorine (**4.9**): R_f 0.48 (1:10 MeOH:CH₂Cl₂); ¹H NMR (600 MHz, CDCl₃): δ 7.84 (s, 1H), 7.83 (s, 1H), 7.32 (s, 1H), 7.17 (s, 1H), 4.64 (d, J = 14.4, 1H), 4.12 (s, 6H), 4.06 (s, 3H), 4.05 (s, 3H), 3.68 (dt, J = 14.6, 2.1, 1H), 3.48 (td, J = 8.7, 1.7, 1H), 3.38 (dd, J = 15.8, 2.4, 1H), 2.96 – 2.88 (m, 1H), 2.55 – 2.44 (m, 2H), 2.29 – 2.22 (m, 1H), 2.09 – 2.00 (m, 1H), 1.97 – 1.88 (m, 1H), 1.82 – 1.74 (m, 1H).

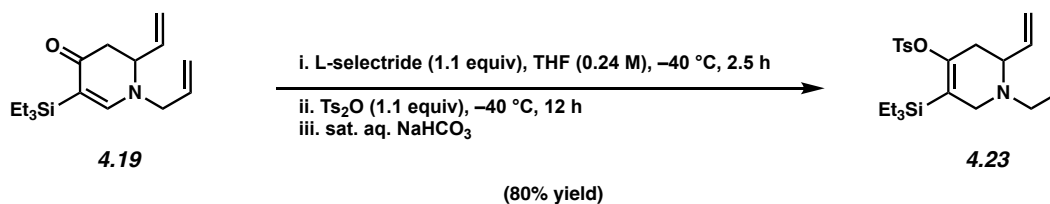
4.5.2.2 Access to the Silyl Tosylate Indolizidine Precursor



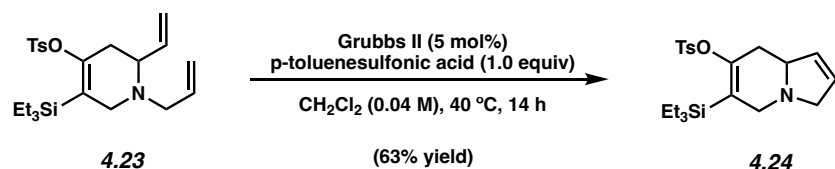
Pyridinium 4.18. To a flask containing 4-methoxy-3-(triethylsilyl)pyridine (**4.12**, 5.00 g, 1.00 equiv, 27.6 mmol) was added acetonitrile (24 mL). 3-Bromoprop-1-ene (**4.32**, 2.38 mL, 1.00 equiv, 27.6 mmol) was then added in one portion. The vial was purged with nitrogen for 5 minutes before being capped and transferred to an aluminum block pre-heated to 50 °C. The vial was allowed to stir for 12 hours at 50 °C. The vial was then allowed to cool to 23 °C before being concentrated under reduced pressure to afford an orange solid. The solid was then suspended in EtOAc (75 mL) and sonicated thoroughly before being filtered over a plug of celite. The product remained on top of the celite and was washed into a second flask using CH₂Cl₂ (75 mL). The product was concentrated and dried under high vacuum to afford **4.18** as a white solid. The yield was assumed to be quantitative and the crude material was carried forward to the next step.



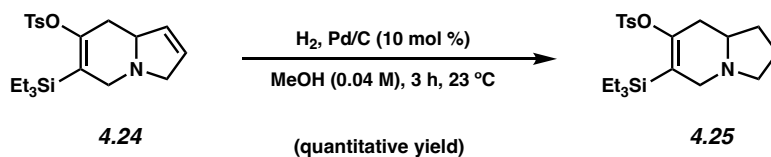
Oxo-dihydropyridine 4.19. To a flask containing crude pyridinium **4.18** (8.34 g, 1.0 equiv, 24.2 mmol) was added THF (125 mL). The flask was cooled to 0 °C, and vinylmagnesium bromide (1.0 M in THF, 48.4 mL, 2.0 equiv, 48.4 mmol) was added drop-wise. The vial was warmed to 23 °C and allowed to stir for 1 hour. The reaction mixture was cooled back down to 0 °C and water (10 mL) was added drop-wise (added slowly to avoid large exotherm). The vial was then warmed back up to 23 °C and allowed to stir for 12 hours. After this time, the mixture was transferred to a separatory funnel with sat. aq. NH₄Cl (40 mL) and EtOAc (40 mL). The layers were separated and the aqueous layer was extracted with EtOAc (2 x 40 mL). The organic layers were combined, dried over MgSO₄, filtered, then concentrated under reduced pressure. The resulting oil was purified by silica gel flash chromatography (0 → 60% EtOAc in hexanes) to afford oxo-dihydropyridine **4.19** as a yellow oil (4.35 g, 65% yield). Oxo-dihydropyridine **4.19**: *R_f* 0.28 (4:1 hexanes:EtOAc); ¹H NMR (500 MHz, C₆D₆): δ 6.70 (s, 1H), 5.48 (ddd, *J* = 17.0, 10.3, 7.5, 1H), 5.32 (dtd, *J* = 10.9, 10.8, 5.8, 1H), 5.89 – 4.81 (m, 3H), 4.75 (d, *J* = 17.4, 1H), 3.38 (q, *J* = 6.5, 1H), 3.15 – 3.05 (m, 2H), 2.53 (dd, *J* = 15.7, 6.8, 1H), 2.28 (dd, *J* = 15.7, 5.4, 1H), 1.13 (t, *J* = 7.7, 9H), 0.96 – 0.89 (m, 6H); ¹³C NMR (125 MHz, CDCl₃): δ 192.6, 156.3, 134.0, 133.7, 117.7, 117.2, 101.6, 59.5, 55.5, 42.0, 8.0, 3.8; IR (film): 2951, 2872, 1627, 1417, 718 cm⁻¹; HRMS-APCI (*m/z*) [M + H⁺] calcd for C₁₆H₂₈NOSi⁺, 278.1935; found 278.1928.



Silyl tosylate 4.23. To a flask containing oxo-dihydropyridine **4.19** (50 mg, 1.0 equiv, 180 μmol) was added THF (0.70 mL). The mixture was allowed to stir at 23 $^\circ\text{C}$ for 5 minutes before being cooled to $-40\text{ }^\circ\text{C}$. L-Selectride (0.97 M in THF, 200 μL , 1.1 equiv, 200 μmol) was then added drop-wise and the resulting solution was stirred at $-40\text{ }^\circ\text{C}$ for 2.5 hours. A solution of *p*-toluenesulfonic anhydride (65 mg, 1.1 equiv, 198 μmol) in THF (0.40 mL) was then added in a single portion. The resulting solution was allowed to stir at $-40\text{ }^\circ\text{C}$ for 12 hours. After the allotted time, sat. aq. NaHCO_3 (1 mL) was added to the reaction mixture which was allowed to warm to 23 $^\circ\text{C}$ while stirring over 30 minutes. The mixture was then transferred to a separatory funnel using water (10 mL) and EtOAc (10 mL). The layers were separated and the aqueous layer was extracted with EtOAc (2 x 10 mL). The organic layers were combined, washed with brine (10 mL), dried over MgSO_4 , filtered and concentrated under reduced pressure to obtain the crude reaction mixture. The crude reaction mixture was purified via basic alumina flash chromatography (14:1 hexanes:EtOAc) to afford silyl tosylate **4.23** as a yellow oil (63 mg, 80% yield). Silyl tosylate **4.23**: R_f 0.44 (4:1 hexanes:EtOAc); $^1\text{H NMR}$ (600 MHz, C_6D_6): δ 7.78 (d, $J = 8.2$, 2H), 6.64 (d, $J = 8.1$, 2H), 5.84 (ddt, $J = 17.3$, 10.3, 6.0, 1H), 5.73 (ddd, $J = 17.5$, 10.6, 7.8, 1H), 5.14 (dd, $J = 17.2$, 1.7, 1H), 5.05 – 4.96 (m, 3H), 3.32 (dt, $J = 16.9$, 2.5, 1H), 3.18 – 3.08 (m, 3H), 2.89 (dd, $J = 13.8$, 6.8, 1H), 2.74 – 2.68 (m, 1H), 2.52 – 2.46 (m, 1H), 1.78 (s, 3H), 1.04 (t, $J = 7.9$, 9H), 0.81 (q, $J = 7.7$, 6H); $^{13}\text{C NMR}$ (125 MHz, CDCl_3): δ 151.8, 144.3, 137.0, 136.6, 136.4, 129.8, 128.3, 120.2, 117.3, 117.1, 59.9, 56.5, 51.8, 34.1, 21.1, 7.8, 3.5; IR (film): 2953, 2874, 1645, 1599, 1179 cm^{-1} ; HRMS-APCI (m/z) [$\text{M} + \text{H}^+$] calcd for $\text{C}_{23}\text{H}_{36}\text{NO}_3\text{SSi}^+$, 434.2180; found 434.2163.

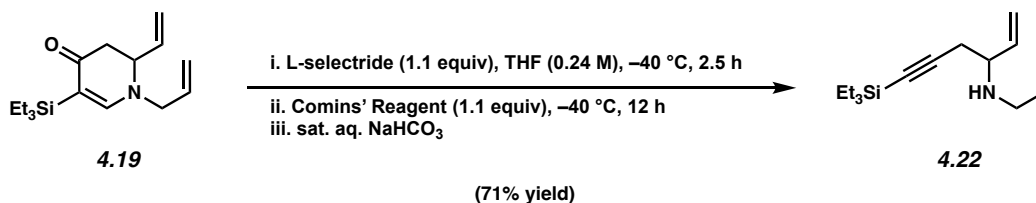


Tetrahydroindolizine silyl tosylate 4.24. In a nitrogen atmosphere glovebox, to a flask containing silyl tosylate **4.23** (210 mg, 1.0 equiv, 484 μmol) and *p*-toluenesulfonic acid (83.4 mg, 1.0 equiv, 484 μmol) was added methylene chloride (12.5 mL), which was sparged with nitrogen for 30 minutes prior to use. The vial was allowed to stir for 30 minutes before being charged with Grubbs II catalyst (41.1 mg, 10 mol%, 48.4 μmol). The vial was capped, removed from the glovebox and heated to 40 $^\circ\text{C}$. The vial was allowed to stir for 14 hours. After the allotted time, the reaction was cooled to 23 $^\circ\text{C}$. The contents of the vial were then transferred to a separatory funnel using CH_2Cl_2 (5 mL) and 1 M aq. NaOH (5 mL). The layers were separated and the aqueous layer was extracted with CH_2Cl_2 (2 x 5 mL). The organic layers were combined, dried over MgSO_4 , filtered and concentrated under reduced pressure to obtain the crude product. The crude material was purified via silica gel flash chromatography (4:1 hexanes:EtOAc with 2% triethylamine) to afford tetrahydroindolizine silyl tosylate **4.23** as a light yellow oil (125 mg, 63% yield). Tetrahydroindolizine silyl tosylate **4.24**: R_f 0.28 (2:1 hexanes:EtOAc); ^1H NMR (600 MHz, C_6D_6): δ 7.78 (d, $J = 8.2$, 2H), 6.63 (d, $J = 8.1$, 2H), 5.59 – 5.64 (m, 1H), 5.38 (dd, $J = 6.2$, 1.0, 1H), 3.54 (dt, $J = 12.8$, 1.9, 1H), 3.45 (dd, $J = 15.8$, 2.5, 1H), 3.16 – 3.10 (m, 1H), 3.07 (ddd, $J = 15.7$, 4.2, 2.9, 1H), 2.97 – 2.92 (m, 1H), 2.77 – 2.70 (m, 1H), 2.56 (dt, $J = 15.6$, 3.1, 1H), 1.77 (s, 3H), 1.05 (t, $J = 8.0$, 9H), 0.81 (q, $J = 4.3$, 6H); ^{13}C NMR (125 MHz, CDCl_3): δ 154.0, 144.3, 136.3, 131.2, 129.8, 129.3, 128.5, 122.4, 64.8, 57.7, 52.1, 36.0, 21.1, 7.8, 3.5; IR (film): 2953, 2878, 2745, 1632, 1370 cm^{-1} ; HRMS-APCI (m/z) [$\text{M} + \text{H}^+$] calcd for $\text{C}_{21}\text{H}_{32}\text{NO}_3\text{SSi}^+$, 406.1867; found 406.1866.



Silyl tosylate indolizidine precursor 4.25. To a flask containing tetrahydroindolizidine silyl tosylate **4.24** (80 mg, 1.0 equiv, 0.20 mmol) and Pd/C (10 wt%, 21 mg, 10 mol%, 20 μmol) was added methanol (4.6 mL). The reaction vial was then placed under an atmosphere of hydrogen via a balloon and vent needle. The vent needle was removed after 20 seconds of sparging, and the reaction mixture was allowed to stir at 23 $^\circ\text{C}$ for 3 hours under positive pressure of hydrogen from the balloon. After the allotted time, the reaction mixture was diluted with CH_2Cl_2 (1.0 mL) and passed through a plug of celite with 5.0 mL of CH_2Cl_2 . The eluent was then concentrated under reduced pressure to afford the silyl tosylate indolizidine precursor **4.25** as a light brown oil (80 mg, quantitative yield). Silyl tosylate indolizidine precursor **4.25**: R_f 0.31 (2:1 hexanes:EtOAc); ^1H NMR (600 MHz, C_6D_6): δ 7.81 (d, $J = 8.3$, 2H), 6.65 (d, $J = 8.0$, 2H), 3.56 (d, $J = 15.8$, 1H), 2.98 (td, $J = 8.6$, 2.1, 1H), 2.74 (dt, $J = 15.8$, 3.6, 1H), 2.62–2.57 (m, 2H), 2.02 (tt, $J = 8.8$, 6.5, 1H), 1.89 (q, $J = 9.0$, 1H), 1.78 (s, 3H), 1.69–1.61 (m, 1H), 1.59–1.38 (m, 1H), 1.24–1.16 (m, 1H), 1.04 (t, $J = 7.9$, 9H), 0.79 (q, $J = 4.0$, 6H); ^{13}C NMR (125 MHz, C_6D_6): δ 153.9, 144.3, 136.3, 129.7, 128.3, 120.7, 60.4, 54.4, 53.7, 37.0, 31.0, 22.4, 21.1, 7.8, 3.4; IR (film): 2954, 2874, 2788, 1641, 1192 cm^{-1} ; HRMS-APCI (m/z) [$\text{M} + \text{H}^+$] calcd for $\text{C}_{21}\text{H}_{34}\text{NO}_3\text{SSi}^+$, 408.2023; found 408.2007.

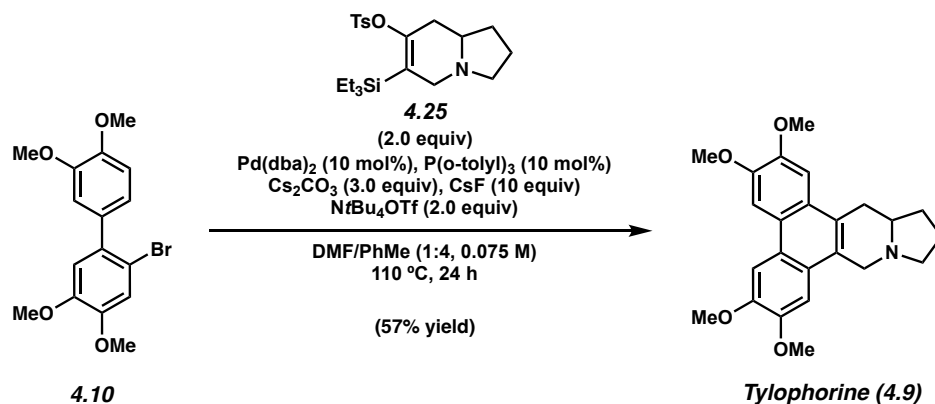
4.5.2.3 Silyl Triflate Decomposition



Silyl alkyne 4.22. To a flask containing oxo-dihydropyridine **4.19** (100 mg, 1.0 equiv, 360 μmol) was added THF (0.70 mL). The mixture was allowed to stir at 23 °C for 5 minutes before being cooled to -40 °C. L-selectride (156 mg, 1.1 equiv, 396 μmol) was then added to the mixture drop-wise and the resulting solution was allowed to stir at -40 °C for 2.5 hours. A solution of Comins' Reagent (65 mg, 1.1 equiv, 198 μmol) in THF (0.40 mL) was then added in a single portion. The resulting solution was allowed to stir at -40 °C for 12 hours. After the allotted time, sat. aq. NaHCO₃ (1 mL) was added to the reaction mixture which was allowed to warm to 23 °C while stirring over 30 minutes. The mixture was then transferred to a separatory funnel using water (10 mL) and EtOAc (10 mL). The layers were separated and the aqueous layer was extracted with EtOAc (2 x 10 mL). The organic layers were combined, washed with brine (10 mL), dried over MgSO₄, filtered and concentrated under reduced pressure to obtain the crude product. The crude reaction mixture was purified via basic alumina flash chromatography (4:1 hexanes:EtOAc, 1% triethylamine) to afford silyl alkyne **4.22** as a yellow oil (64 mg, 71% yield). R_f 0.17 (4:1 hexanes:EtOAc); Silyl alkyne **4.22**: ¹H NMR (600 MHz, C₆D₆): δ 5.87 (dddd, $J = 17.0, 10.3, 6.2, 5.3$), 5.63 (ddd, $J = 17.3, 10.2, 7.5, 1\text{H}$), 5.19 (dq, $J = 17.3, 1.9, 1\text{H}$), 5.08 (dq, $J = 17.2, 1.0, 1\text{H}$), 5.03 – 4.99 (m, 2H), 3.18 (ddt, $J = 14.4, 5.3, 1.6, 1\text{H}$), 3.13 (q, $J = 6.4, 1\text{H}$), 3.04 (ddt, $J = 14.3, 6.2, 1.4, 1\text{H}$), 2.30 (dd, $J = 6.0, 2.3, 1\text{H}$), 1.26 (br s, 1H), 1.08 (t, $J = 8.0, 9\text{H}$), 0.63 (q, $J = 7.8, 6\text{H}$); ¹³C NMR (125 MHz, C₆D₆): δ 140.3, 137.7, 116.1, 115.2, 105.8, 84.1,

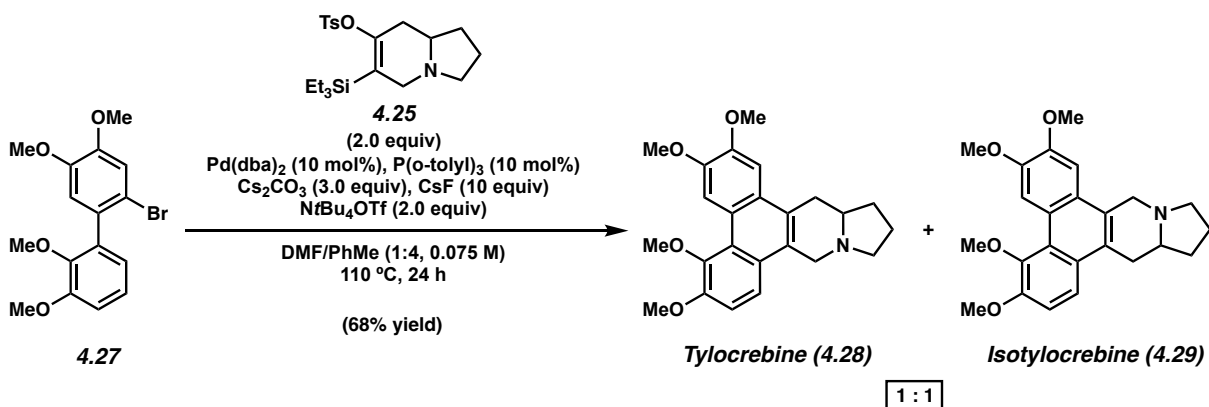
59.7, 49.9, 27.3, 7.8, 5.0; IR (film): 2876, 2956, 2174, 1463, 1315 cm^{-1} ; HRMS-APCI (m/z) [$M + H^+$] calcd for $\text{C}_{15}\text{H}_{28}\text{NSi}^+$, 250.1986; found 250.1979.

4.5.2.4 Annulations of Indolizidine to Access Natural Products



Tylophorine (4.9). A 1-dram vial was charged sequentially with Pd(dba)₂ (1.1 mg, 1.98 μmol , 10 mol%), biaryl bromide **4.10** (7.0 mg, 19.8 μmol , 1.0 equiv), P(*o*-tolyl)₃ (0.6 mg, 1.98 μmol , 10 mol%), DMF (55 μL), PhMe (220 μL), silyl triflate **4.25** (16.2 mg, 39.6 μmol , 2.0 equiv), an oven-dried magnetic stir bar, Cs₂CO₃ (19.4 mg, 59.5 μmol , 3.0 equiv), tetrabutylammonium trifluoromethanesulfonate (15.5 mg, 39.6 μmol , 2.0 equiv) and CsF (30.1 mg, 198 μmol , 10.0 equiv). The reaction was then purged with N₂ for 5 min before being capped with a Teflon-lined screw cap under a flow of N₂, sealed with Teflon tape and electrical tape, transferred to an Al-block, and stirred at 110 °C for 24 hours. After cooling to 23 °C, the mixture was concentrated under reduced pressure to afford the crude reaction mixture. The residue was then purified by preparative TLC (10:1 CH₂Cl₂:methanol) to afford tylophorine (**4.9**, 4.4 mg, 57% yield). Spectral data matched those reported in the literature.⁸⁴ Tylophorine (**4.9**): R_f 0.48 (1:10 MeOH:CH₂Cl₂); ¹H NMR (600 MHz, CDCl₃): δ 7.84 (s, 1H), 7.83 (s, 1H), 7.32 (s, 1H), 7.17 (s, 1H), 4.64 (d, $J = 14.4$, 1H), 4.12 (s, 6H), 4.06 (s, 3H), 4.05 (s, 3H), 3.68 (dt, $J = 14.6, 2.1$, 1H), 3.48 (td, $J = 8.7,$

1.7, 1H), 3.38 (dd, $J = 15.8, 2.4$, 1H), 2.96 – 2.88 (m, 1H), 2.55 – 2.44 (m, 2H), 2.29 – 2.22 (m, 1H), 2.09 – 2.00 (m, 1H), 1.97 – 1.88 (m, 1H), 1.82 – 1.74 (m, 1H).



Tylocrebine (4.28) and Isotylocrebine (4.29). A 1-dram vial was charged sequentially with Pd(dba)₂ (1.1 mg, 10 mol%, 2.0 μmol) biaryl bromide **4.27** (7.0 mg, 1.0 equiv, 20 μmol), P(*o*-tolyl)₃ (0.6 mg, 10 mol%, 2.0 μmol), DMF (55 μL), PhMe (220 μL), silyl triflate **4.25** (16.2 mg, 2.0 equiv, 39.6 μmol), an oven-dried magnetic stir bar, Cs₂CO₃ (19.4 mg, 3.0 equiv, 59.5 μmol), tetrabutylammonium trifluoromethanesulfonate (15.5 mg, 2.0 equiv, 39.6 μmol) and CsF (30.1 mg, 10.0 equiv, 198 μmol). The reaction was then purged with N₂ for 5 min before being capped with a Teflon-lined screw cap under a flow of N₂, sealed with Teflon tape and electrical tape, transferred to an Al-block, and stirred at 110 °C for 24 hours. After cooling to 23 °C, the mixture was concentrated under reduced pressure to afford the crude reaction mixture. The residue was then purified by preparative TLC (10:1 CH₂Cl₂:methanol) to afford a 1:1 mixture of tylocrebine:isotylocrebine (**4.28** + **4.29**, 5.3 mg, 68% yield, 1:1 ratio of regioisomers). Spectral data matched those reported in the literature.^{85,86} Tylocrebine (**4.28**): R_f 0.45 (1:10 MeOH:CH₂Cl₂); ¹H NMR (600 MHz, CDCl₃): δ 9.33 (s, 1H), 7.66 (d, $J = 9.1$ Hz, 1H), 7.33 (s, 1H), 7.28 (d, $J = 9.1$ Hz, 1H), 4.66 (d, $J = 14.8$ Hz, 1H), 4.07 (s, 3H), 4.03 (s, 3H), 3.92 (s, 3H), 3.70–3.67 (m, 1H), 3.50–3.45 (m, 1H), 3.33 (dd, $J = 15.8, 3.5$ Hz, 1H),), 2.91 (dd, $J = 14.8, 11.3$

Hz, 1H), 2.42–2.52 (m, 2H), 2.19–2.31 (m, 1H), 2.08–2.00 (m, 1H), 1.96–1.87 (m, 1H), 1.83–1.73 (m, 1H). Isotylocrebine (**4.29**): R_f 0.45 (1:10 MeOH:CH₂Cl₂); ¹H NMR: (600 MHz, CDCl₃): δ 9.33 (s, 1H), 7.81 (d, $J = 9.2$, 1H), 7.30 (d, $J = 9.2$, 1H), 7.17 (s, 1H), 4.60 (d, $J = 14.4$, 1H), 4.07 (s, 3H), 4.06 (s, 3H), 4.05 (s, 3H), 3.94 (s, 3H), 3.69 (d, $J = 12.4$, 1H), 3.50–3.45 (m, 1H), 3.40 (dd, $J = 16, 2$, 1H), 2.97–2.87 (m, 1H), 2.51–2.42 (m, 2H), 2.28–2.20 (m, 1H), 2.08 – 2.00 (m, 1H), 1.82–1.72 (m, 1H).

4.6 Spectra Relevant to Chapter Four:

Total Synthesis of Phenanthroindolizidines Using Strained Azacyclic Alkynes

Katie A. Spence, Marie Hoffmann, and Neil K. Garg.

Manuscript Submitted.

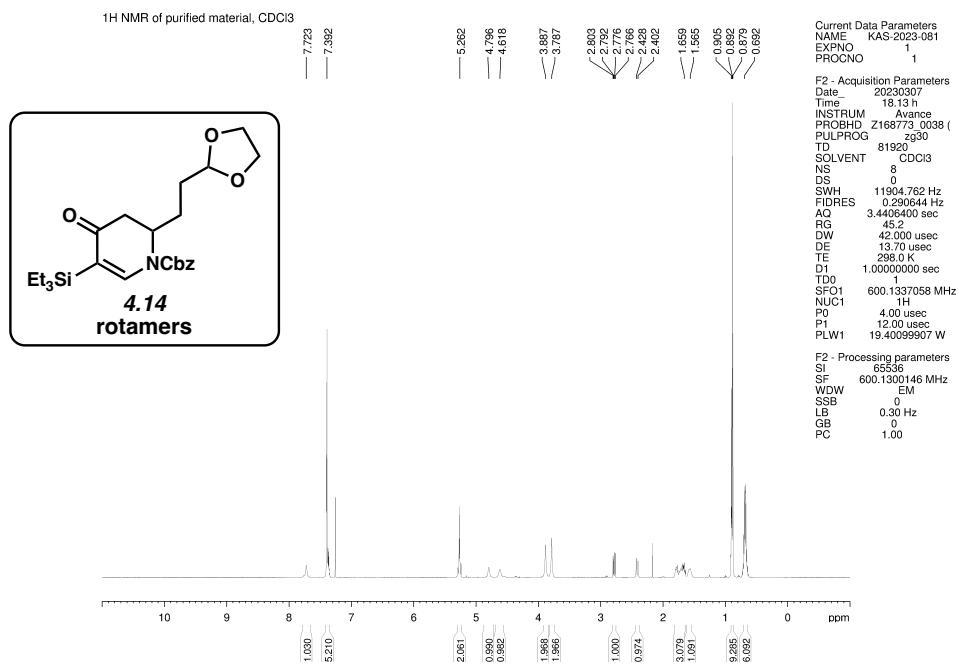


Figure 4.8. ¹H NMR (600 MHz, CDCl₃) of compound 4.14.

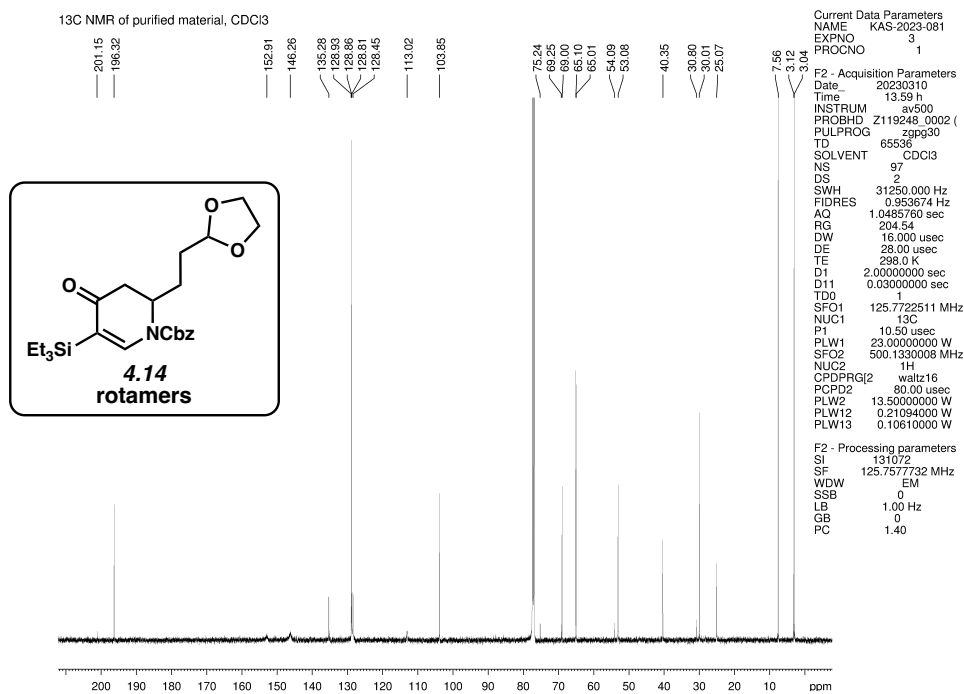


Figure 4.9. ¹³C NMR (125 MHz, CDCl₃) of compound 4.14.

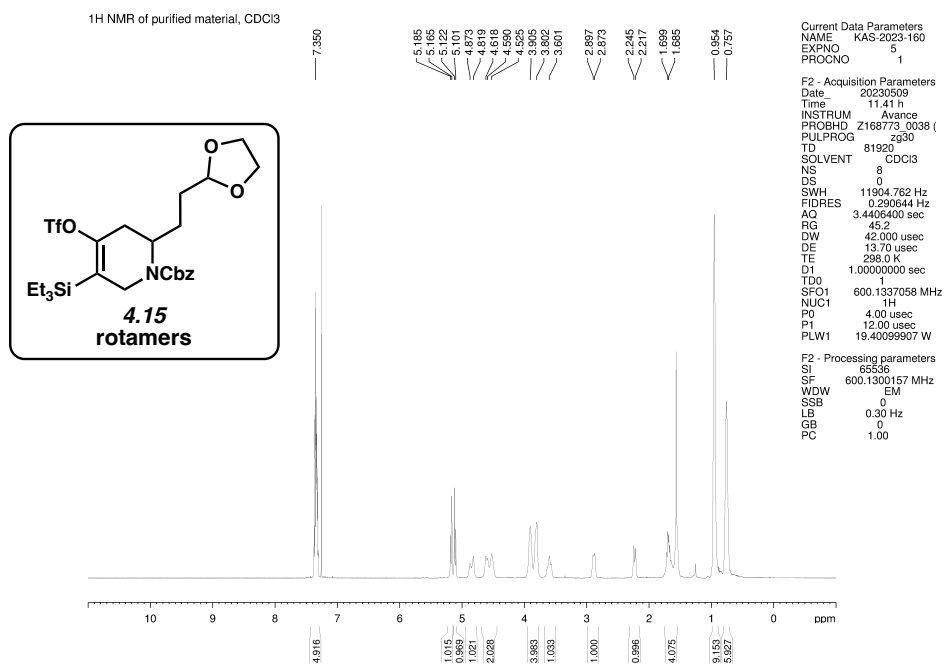


Figure 4.10. ¹H NMR (600 MHz, CDCl₃) of compound **4.15**.

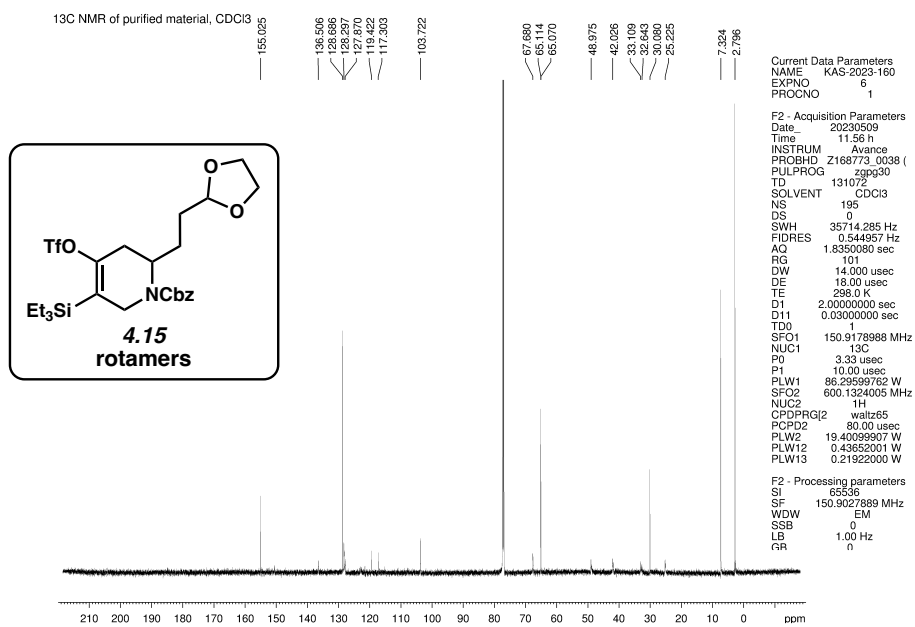


Figure 4.11. ¹³C NMR (125 MHz, CDCl₃) of compound **4.15**.

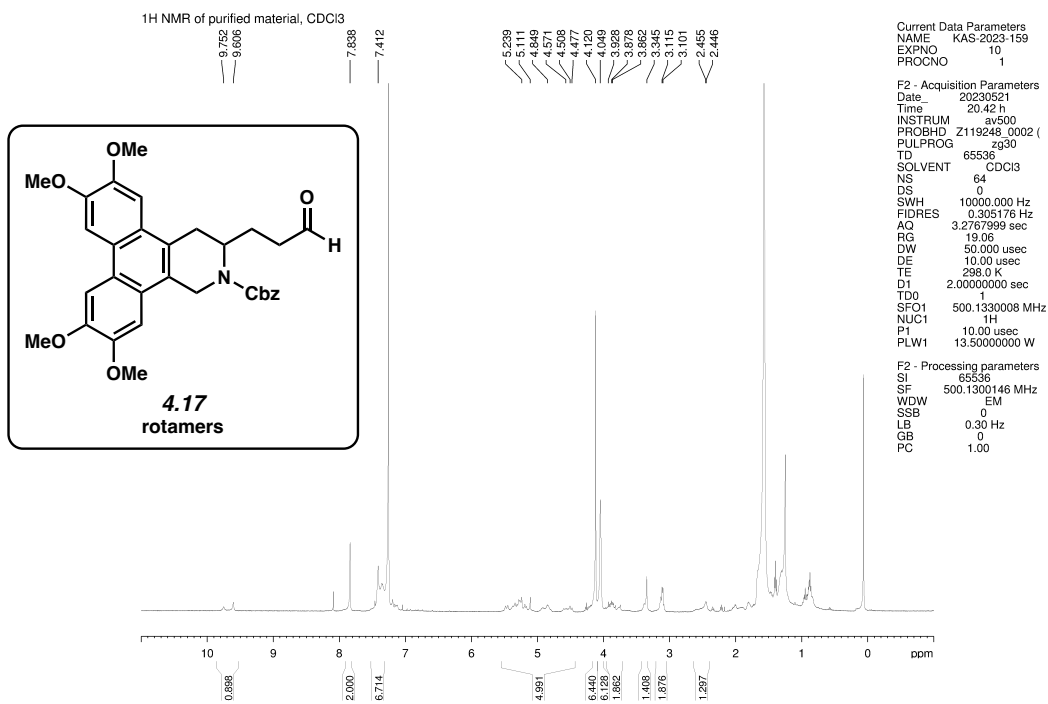


Figure 4.12. ¹H NMR (500 MHz, CDCl₃) of compound **4.17**.

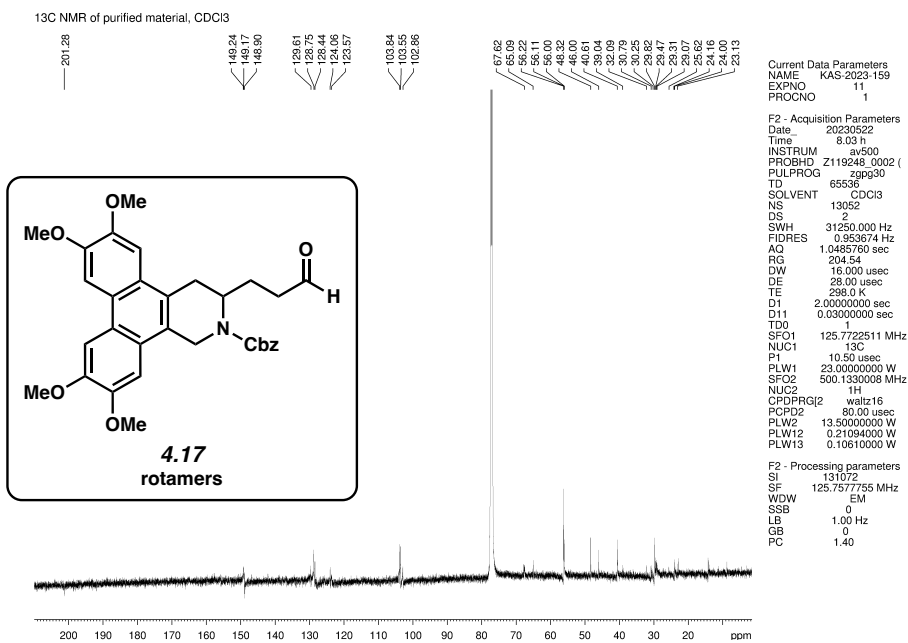


Figure 4.13. ¹³C NMR (125 MHz, CDCl₃) of compound **4.17**.

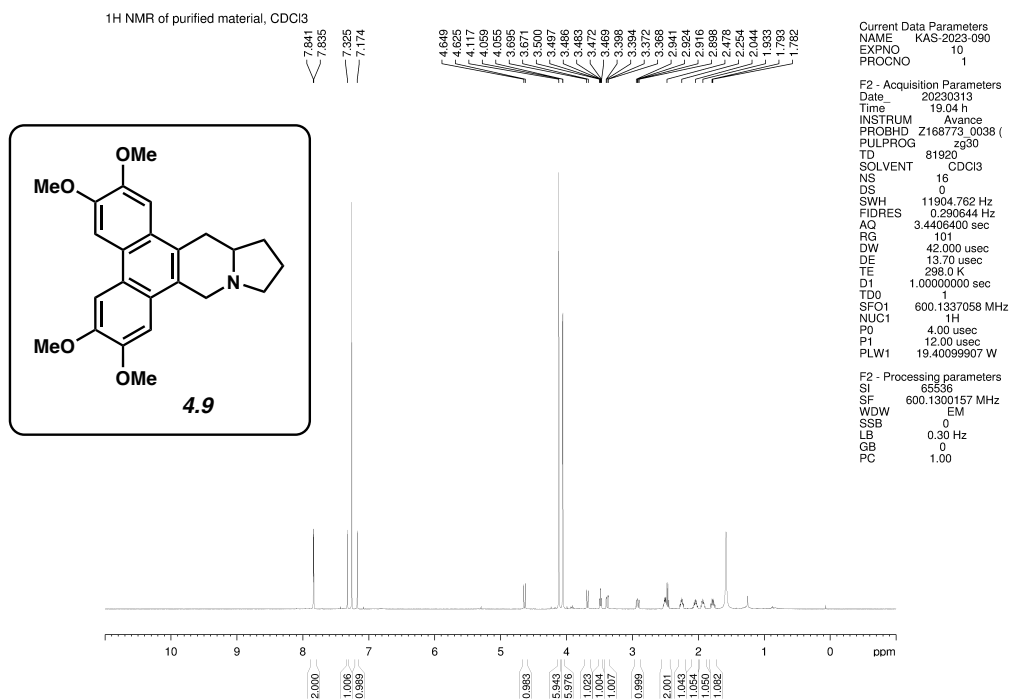


Figure 4.14. ¹H NMR (600 MHz, CDCl₃) of tylophorine (4.9).

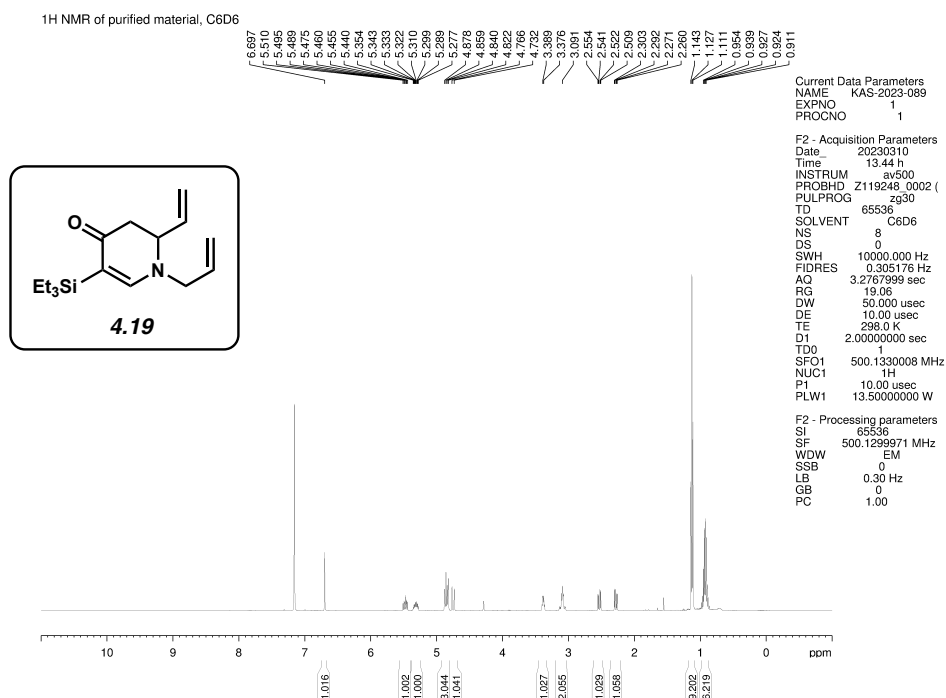


Figure 4.15. ¹H NMR (600 MHz, C₆D₆) of compound 4.19.

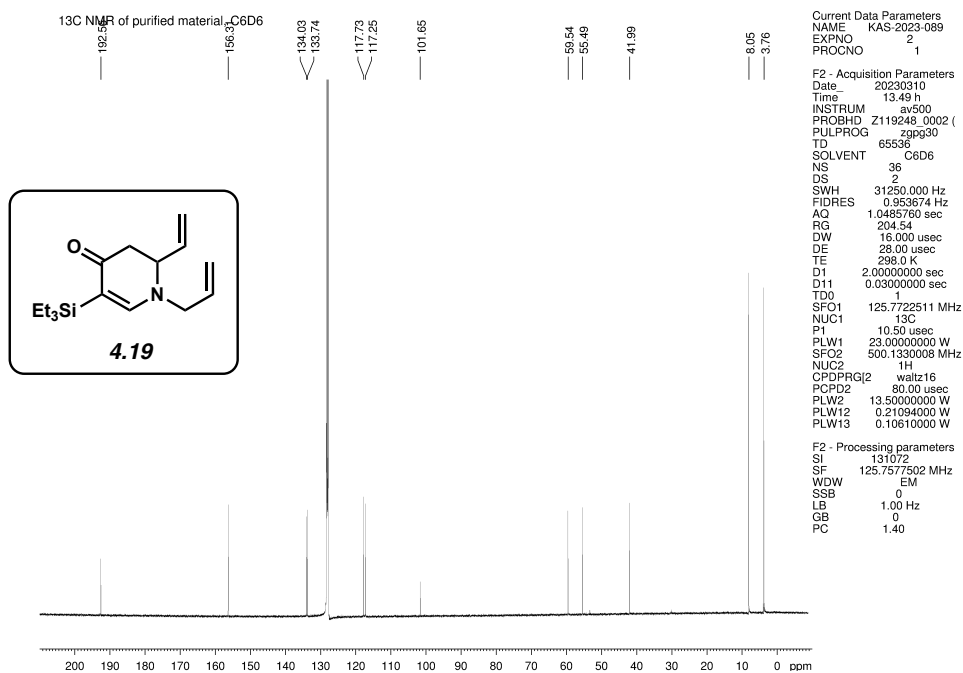


Figure 4.16. ¹³C NMR (125 MHz, C₆D₆) of compound **4.19**.

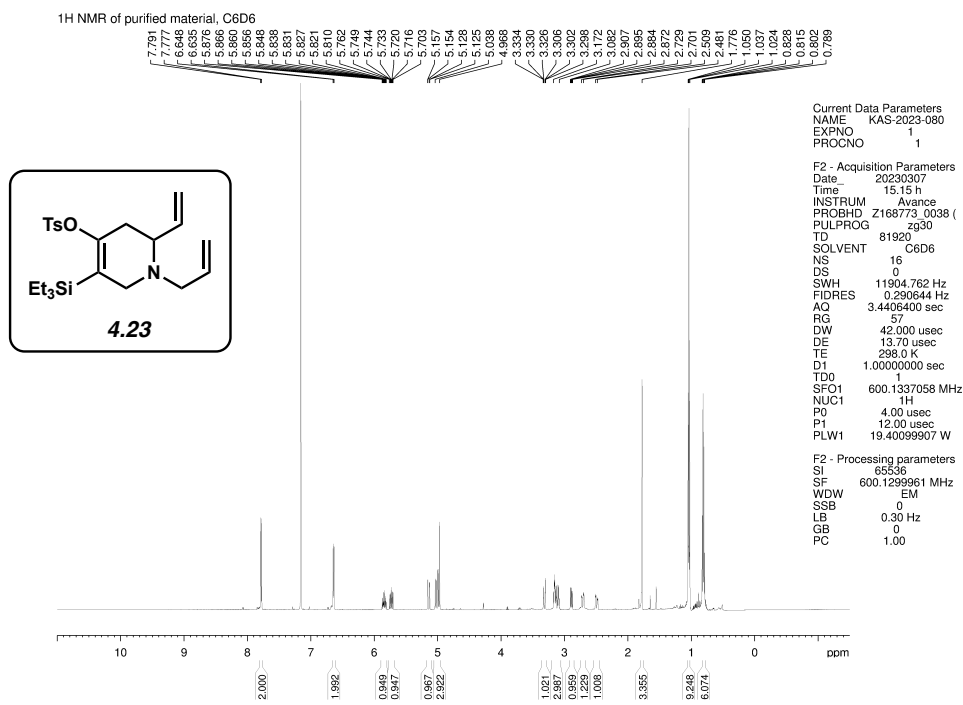


Figure 4.17. ¹H NMR (600 MHz, C₆D₆) of compound **4.23**.

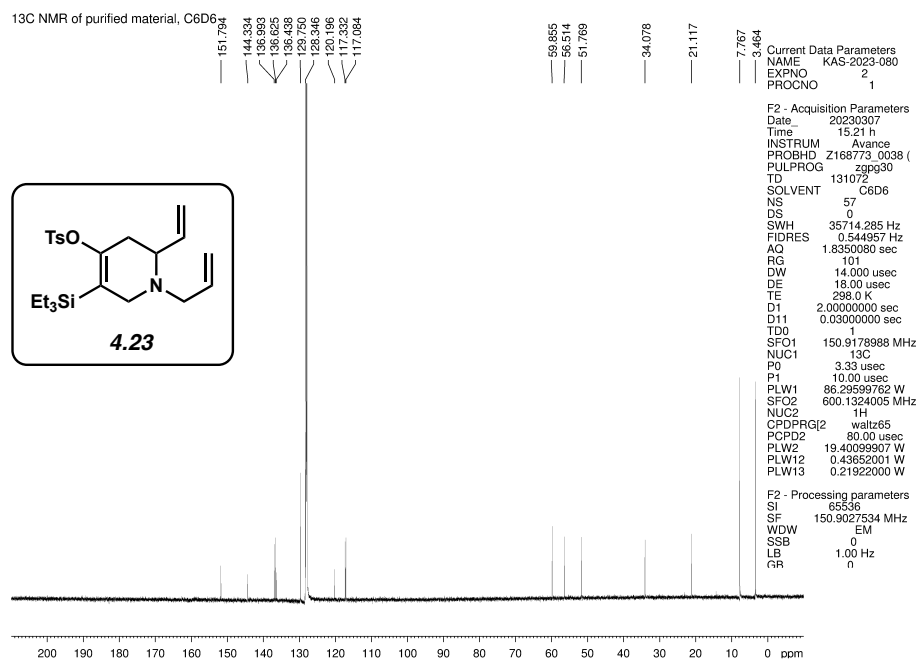


Figure 4.18. ^{13}C NMR (125 MHz, C_6D_6) of compound 4.23.

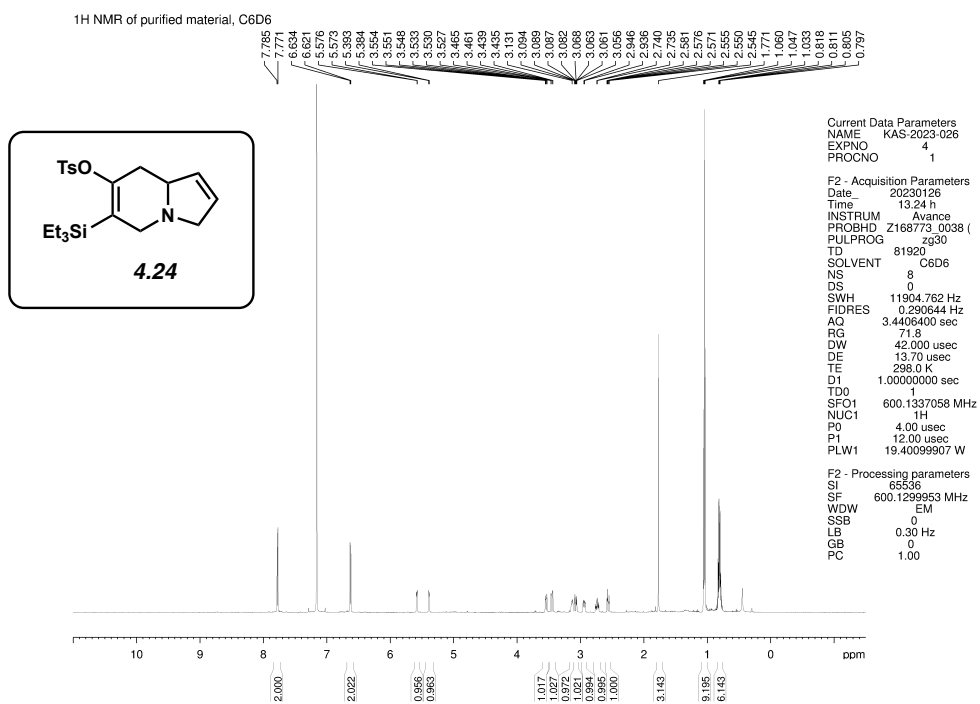


Figure 4.19. ^1H NMR (600 MHz, C_6D_6) of compound 4.24.



Figure 4.20. ^{13}C NMR (125 MHz, C_6D_6) of compound 4.24.

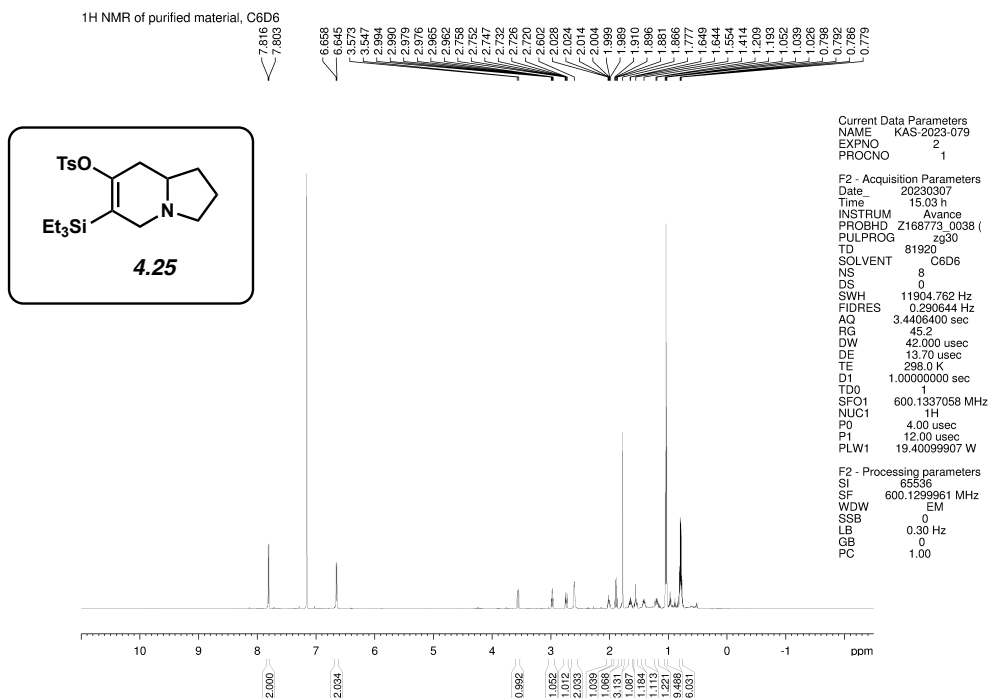


Figure 4.21. ^1H NMR (600 MHz, C_6D_6) of compound 4.25.

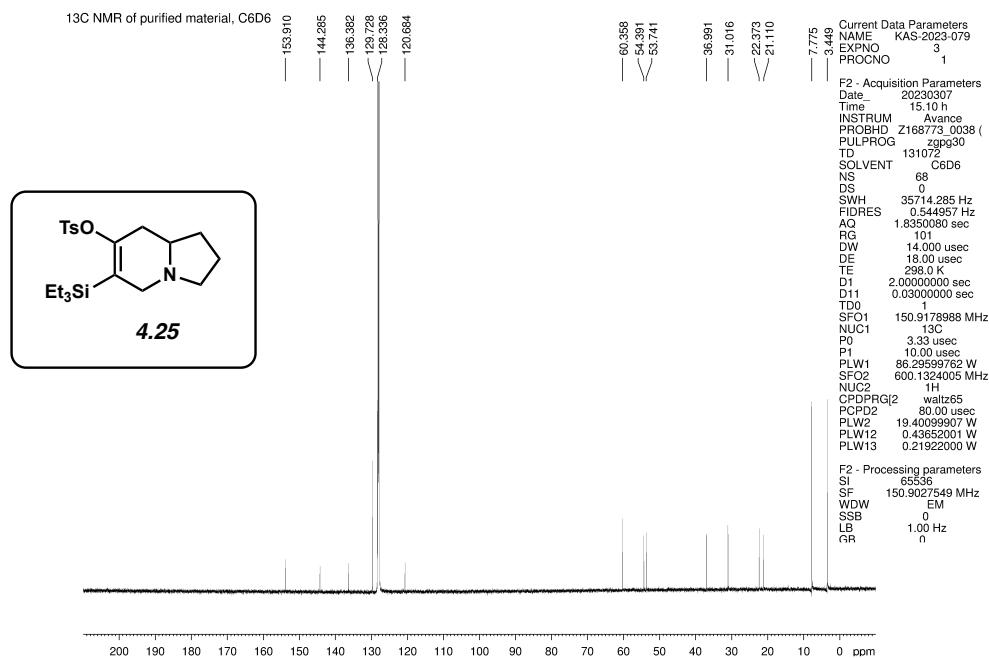


Figure 4.22. ¹³C NMR (125 MHz, C₆D₆) of compound 4.25.

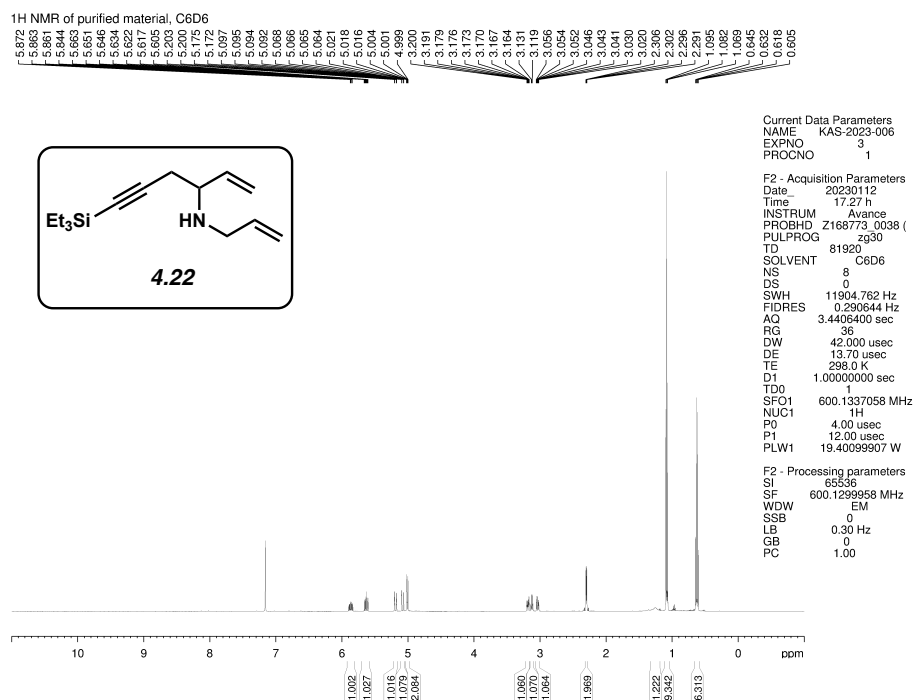


Figure 4.23. ¹H NMR (600 MHz, C₆D₆) of compound 4.22.

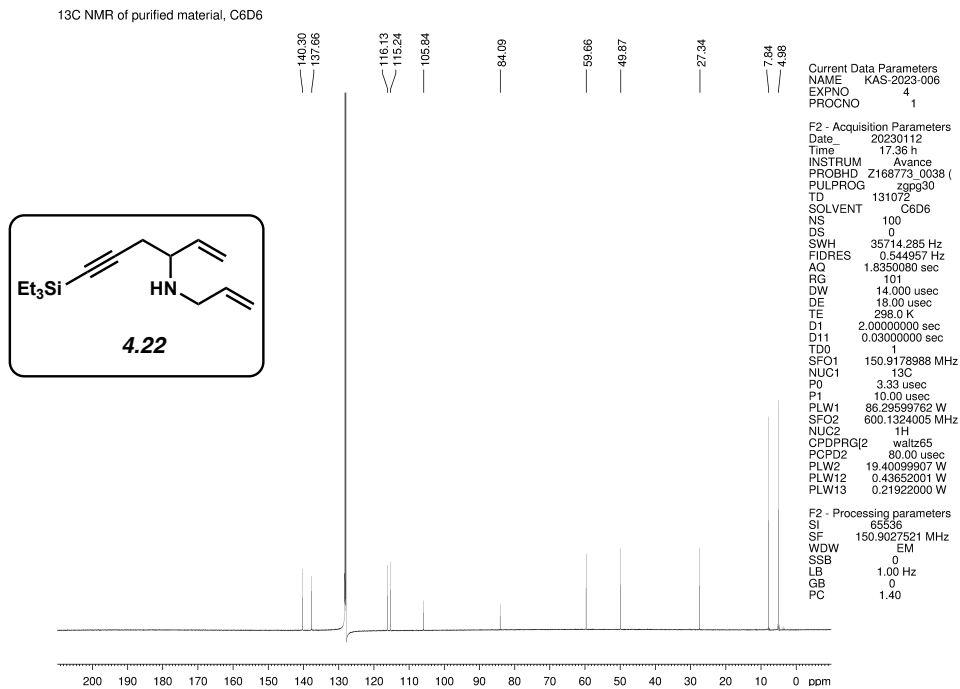


Figure 4.24. ¹³C NMR (125 MHz, C₆D₆) of compound 4.22.

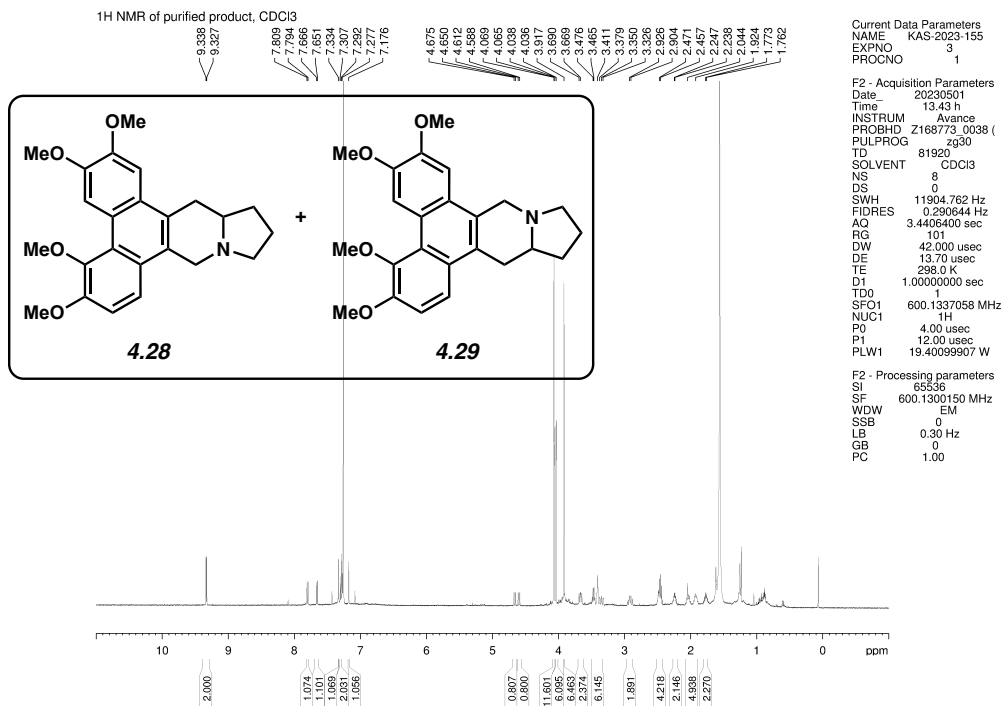


Figure 4.25. ¹H NMR (600 MHz, CDCl₃) of tylocrebine (4.28) and isotylocrebine (4.29), 1:1 ratio.

4.7 Notes and References

- (1) Joule, J. A. Natural Products Containing Nitrogen Heterocycles—Some Highlights 1990–2015. In *Advances in Heterocyclic Chemistry*; Elsevier Ltd, 2016; Vol. 119, pp. 81–106.
- (2) Vitaku, E.; Smith, D. T.; Njardarson, J. T. Analysis of the Structural Diversity, Substitution Patterns, and Frequency of Nitrogen Heterocycles Among U.S. FDA Approved Pharmaceuticals. *J. Med. Chem.* **2014**, *57*, 10257–10274.
- (3) Jampilek, J. Heterocycles in Medicinal Chemistry. *Molecules* **2019**, *24*, 3839.
- (4) Lamberth, C. Heterocyclic Chemistry of Crop Protection. *Pest Manag. Sci.* **2013**, *69*, 1106–1114.
- (5) Gao, H.; Zhang, Q.; Shreeve, J. M. Fused Heterocycle-Based Energetic Materials (2012–2019). *J. Mater. Chem. A* **2020**, *8*, 4193–4216.
- (6) Wang, T.; Zhang, N.; Bai, W.; Bao, Y. Fluorescent Chemosensors Based on Conjugated Polymers with N–Heterocyclic Moieties: Two Decades of Progress. *Polym. Chem.* **2020**, *11*, 3095–3114.
- (7) Chinchilla, R.; Nájera, C.; Yus, M. Metalated Heterocycles and Their Applications in Synthetic Organic Chemistry. *Chem. Rev.* **2004**, *104*, 2667–2722.
- (8) Tadross, P. M.; Stoltz, B. M. A Comprehensive History of Arynes in Natural Product Total Synthesis. *Chem. Rev.* **2012**, *112*, 3550–3577.
- (9) Gampe, C. M.; Carreira, E. M. Arynes and Cyclohexyne in Natural Product Synthesis. *Angew. Chem., Int. Ed.* **2012**, *51*, 3766–3778.
- (10) Wenk, H. H.; Winkler, M.; Sander, W. One Century of Aryne Chemistry. *Angew. Chem., Int. Ed.* **2003**, *42*, 502–528.

- (11) Shi, J.; Li, L.; Li, Y. *o*-Silylaryl Triflates: A Journey of Kobayashi Aryne Precursors. *Chem. Rev.* **2021**, *121*, 3892–4044.
- (12) Takikawa, H.; Nishii, A.; Sakai, T.; Suzuki, K. Aryne-Based Strategy in the Total Synthesis of Naturally Occurring Polycyclic Compounds. *Chem. Soc. Rev.* **2018**, *47*, 8030–8056.
- (13) Bhunia, A.; Yetra, S. R.; Biju, A. T. Recent Advances in Transition-Metal-Free Carbon–Carbon and Carbon–Heteroatom Bond-Forming Reactions Using Arynes. *Chem. Soc. Rev.* **2012**, *41*, 3140–3152.
- (14) Goetz, A. E.; Garg, N. K. Enabling the Use of Heterocyclic Arynes in Chemical Synthesis. *J. Org. Chem.* **2014**, *79*, 846–851.
- (15) Goetz, A. E.; Shah, T. K.; Garg, N. K. Pyridynes and Indolynes as Building Blocks for Functionalized Heterocycles and Natural Products. *Chem. Commun.* **2015**, *51*, 34–45.
- (16) Hosoya, T.; Yoshida, S.; Nakamura, Y. Recent Advances in Synthetic Hetaryne Chemistry. *Heterocycles* **2019**, *98*, 1623–1677.
- (17) Díaz, M. T.; Cobas, A.; Guitián, E.; Castedo, L. Polar Control of the Regioselectivity of Hetaryne Cycloadditions. Synthesis of Ellipticine. *Synlett* **1998**, 157–158.
- (18) Hoarau, C.; Couture, A.; Cornet, H.; Deniau, E.; Grandclaudon, P. A Concise Total Synthesis of the Azaphenanthrene Alkaloid Eupolauramine. *J. Org. Chem.* **2001**, *66*, 8064–8069.
- (19) May, C.; Moody, C. J. A Concise Synthesis of the Antitumor Alkaloid Ellipticine. *J. Chem. Soc., Chem. Commun.* **1984**, 926–927.

- (20) Díaz, M. T.; Cobas, A.; Guitián, E.; Castedo, L. Synthesis of Ellipticine by Hetaryne Cycloadditions – Control of Regioselectivity. *Eur. J. Org. Chem.* **2001**, 2001, 4543–4549.
- (21) Gribble, G. W.; Saulnier, M. G.; Sibi, M. P.; Obaza-Nutaitis, J. A. Synthesis and Diels–Alder Reactions of 1,3-Dimethyl-4-(phenylsulfonyl)-4H-furo[3,4-b]indole. A New Annulation Strategy for the Construction of Ellipticine and Isoellipticine. *J. Org. Chem.*, **1984**, *49*, 4518–4523.
- (22) May, C.; Moody, C. J. A New Precursor to 3,4-Didehydropyridine, and Its Use in the Synthesis of the Antitumor Alkaloid Ellipticine. *J. Chem. Soc., Perkin trans. 1*, **1988**, 247–250.
- (23) Sha, C. K.; Yang, J. F. Total Syntheses of Ellipticine Alkaloids and Their Amino Analogues. *Tetrahedron* **1992**, *48*, 10645–10654.
- (24) Enamorado, M. F.; Ondachi, P. W.; Comins, D. L. A Five-Step Synthesis of (*S*)-Macrostomine from (*S*)-Nicotine. *Org. Lett.*, **2010**, *12*, 4513–4515.
- (25) Kessar, S. V.; Gupta, Y. P.; Pahwa, P. S.; Singh, P. Synthesis of 2,9-Diazaphen Anthrene and Perlolidine through a Pyridyne Cyclisation Reaction. *Tetrahedron Lett.* **1976**, *17*, 3207–3208.
- (26) Kessar, S. V.; Singh, P. Synthesis of the Grass Alkaloid Perlolidine through a Pyridine Cyclisation Reaction. *Indian J. Chem.* **2001**, *40*, 1129–1131.
- (27) Julia, M.; Le Goffic, F.; Igolen, J.; Baillarge, M. Une Nouvelle Synthèse de l'Acide Lysergique. *Tetrahedron Lett.* **1969**, *10*, 1569–1572.

- (28) Iwao, M.; Motoi, O.; Fukuda, T.; Ishibashi, F. New Synthetic Approach to Pyrroloiminoquinone Marine Alkaloids. Total Synthesis of Makaluvamines A, D, I, and K. *Tetrahedron* **1998**, *54*, 8999–9010.
- (29) Hutters, A. D.; Quasdorf, K. W.; Styduhar, E. D.; Garg, N. K. Total Synthesis of (–)-N-Methylwelwitindolinone C Isothiocyanate. *J. Am. Chem. Soc.* **2011**, *133*, 15797–15799.
- (30) Styduhar, E. D.; Hutters, A. D.; Weires, N. A.; Garg, N. K. Enantiospecific Total Synthesis of N-Methylwelwitindolinone D Isonitrile. *Angew. Chem., Int. Ed.* **2013**, *52*, 12422–12425.
- (31) Bronner, S. M.; Goetz, A. E.; Garg, N. K. Overturning Indolyne Regioselectivities and Synthesis of Indolactam V. *J. Am. Chem. Soc.* **2011**, *133*, 3832–3835.
- (32) Fine Nathel, N.; Shah, T. K.; Bronner, S. M.; Garg, N. K. Total Syntheses of Indolactam Alkaloids (–)-Indolactam V, (–)-Pendolmycin, (–)-Lyngbyatoxin A, (–)-Teleocidin A-2. *Chem. Sci.* **2014**, *5*, 2184–2190.
- (33) Goetz, A. E.; Silberstein, A. L.; Corsello, M. A.; Garg, N. K. Concise Enantiospecific Total Synthesis of Tubingensin A. *J. Am. Chem. Soc.* **2014**, *136*, 3036–3039.
- (34) Weires, N. A.; Styduhar, E. D.; Baker, E. L.; Garg, N. K. Total Synthesis of (–)-N-Methylwelwitindolinone B Isothiocyanate via A Chlorinative Oxabicyclic Ring-Opening Strategy. *J. Am. Chem. Soc.* **2014**, *136*, 14710–14713.
- (35) Quasdorf, K. W.; Hutters, A. D.; Lodewyk, M. W.; Tantillo, D. J.; Garg, N. K. Total Synthesis of Oxidized Welwitindolinones and (–)-N-Methylwelwitindolinone C Isonitrile. *J. Am. Chem. Soc.* **2012**, *134*, 1396–1399.

- (36) Corsello, M. A.; Kim, J.; Garg, N. K. Total Synthesis of (–)-Tubingensin B Enabled by the Strategic Use of an Aryne Cyclization. *Nat. Chem.* **2017**, *9*, 944–949.
- (37) Bronner, S. M.; Goetz, A. E.; Garg, N. K. Understanding and Modulating Indolyne Regioselectivities. *Synlett* **2011**, *2011*, 2599–2604.
- (38) Tlais, S. F.; Danheiser, R. L. N-Tosyl-3-azacyclohexyne. Synthesis and Chemistry of a Strained Cyclic Ynamide. *J. Am. Chem. Soc.* **2014**, *136*, 15489–15492.
- (39) McMahon, T. C.; Medina, J. M.; Yang, Y.-F.; Simmons, B. J.; Houk, K. N.; Garg, N. K. Generation and Regioselective Trapping of a 3,4-Piperidyne for the Synthesis of Functionalized Heterocycles. *J. Am. Chem. Soc.* **2015**, *137*, 4082–4085.
- (40) Darzi, E. R.; Barber, J. S.; Garg, N. K. Cyclic Alkyne Approach to Heteroatom-Containing Polycyclic Aromatic Hydrocarbon Scaffolds. *Angew. Chem., Int. Ed.* **2019**, *58*, 9419–9424.
- (41) Picazo, E.; Anthony, S. M.; Giroud, M.; Simon, A.; Miller, M. A.; Houk, K. N.; Garg, N. K. Arynes and Cyclic Alkynes as Synthetic Building Blocks for Stereodefined Quaternary Centers. *J. Am. Chem. Soc.* **2018**, *140*, 7605–7610.
- (42) Li, L.; Shan, C.; Shi, J.; Li, W.; Lan, Y.; Li, Y. The Stannum–Ene Reactions of Benzyne and Cyclohexyne with Superb Chemoselectivity for Cyclohexyne. *Angew. Chem., Int. Ed.* **2022**, *61*, e202117351.
- (43) Takemura, H.; Goto, S.; Hosoya, T.; Yoshida, S. 2-Azidoacrylamides as Compact Platforms for Efficient Modular Synthesis. *Chem. Commun.* **2020**, *56*, 15541–15544.

- (44) Zhang, G.; Alshreimi, A. S.; Alonson, L.; Antar, A.; Yu, H.-C.; Islam, S. M.; Anderson, L. L. Nitrene and Alkyne Cascade Reactions for Regio- and Diastereoselective 1-Pyrroline Synthesis. *Angew. Chem. Int. Ed.* **2021**, *60*, 13089–13097.
- (45) Wezeman, T.; Comas-Barceló, J.; Nieger, M.; Harrity, J. P. A.; Bräse, S. Synthesis of Aminopyrazoles from Sydnone and Ynamides. *Org. Biomol. Chem.*, **2017**, *15*, 1575–1579.
- (46) Ramirez, M.; Darzi, E. R.; Donaldson, J. S.; Houk, K. N.; Garg, N. K. Cycloaddition Cascades of Strained Alkynes and Oxadiazinones. *Angew. Chem., Int. Ed.* **2021**, *60*, 18201–18208.
- (47) Zhang, J.; Morris-Natschke, S. L.; Ma, D.; Shang, X.-F.; Yang, C.-J.; Liu, Y.-Q. Biologically Active Indolizidine Alkaloids. *Med. Res. Rev.* **2021**, *41*, 928–960.
- (48) Ratnagiriswaran, A. N.; Venkatachalam, K. The Chemical Examination of *Tylophora Asthmatica* and Isolation of the Alkaloids Tylophorine and Tylophorinine. *Indian J. Med. Res.* **1935**, *22*, 433.
- (49) Omran, Z.; Guise, C. P.; Chen, L.; Rauch, C.; Abdalla, A. N.; Abdullah, O.; Sindi, I. A.; Fischer, P. M.; Smaill, J. B.; Patterson, A. V.; Liu, Y.; Wang, Q. Design, Synthesis and In-Vitro Biological Evaluation of Antofine and Tylophorine Prodrugs as Hypoxia-Targeted Anticancer Agents. *Molecules* **2021**, *26*, 3327–3337.
- (50) Saraswait, S.; Kanaujia, P. K.; Kumar, R.; Alhaider, A. A. Tylophorine, a Phenanthraindolizidine Alkaloid Isolated from *Tylophora Indica* Exerts Antiangiogenic and Antitumor Activity by Targeting Vascular Endothelial Growth Factor Receptor 2-Mediated Angiogenesis. *Molecular Cancer* **2013**, *12*, 82.

- (51) Gopalakrishnan, C.; Shankaranarayanan, D.; Nazimudeen, S. K.; Kameswaran. Effect of Tylophorine, a Major Alkaloid of *Tylophora Indica*, on Immunopathological and Inflammatory Reactions. *L. Indian J. Med. Res.* **1980**, *71*, 940–948.
- (52) Xi, Z.; Zhang, R.; Yu, Z.; Ouyang, D. The Interaction Between Tylophorine B and TMV RNA. *Biorg. Med. Chem. Lett.* **2006**, *16*, 4300–4304.
- (53) Wang, Z.; Fe, Y.; Feng, Y.; Xiao, W.; Song, H.; Zhao, L.; Lu, R.; Huang, B.; Liu, Y.; Wang, W.; Li, Y.; Ding, Y.; Zheng, Y.; Song, X.; Tan, W.; Wang, Q. Discovery and Nanosized Preparations of (*S,R*)-Tylophorine Malate as Novel Anti-SARS-CoV-2 Agents. *ACS Med. Chem. Lett.* **2021**, *12*, 1840–1846.
- (54) Niphakis, M. J.; Georg, G. I. Synthesis of Tylocrebrine and Related Phenanthroindolizidines by VOF₃-Mediated Oxidative Aryl-Alkene Coupling. *Org. Lett.* **2011**, *13*, 196–199.
- (55) Lahm, G.; Stoye, A.; Opatz, T. A Five-Step Synthesis of (±)-Tylophorine via a Nitrile-Stabilized Ammonium Ylide. *J. Org. Chem.* **2012**, *77*, 6620–6623.
- (56) Stoye, A.; Opatz, T. Racemization-Free Synthesis of (*S*)-(+)-Tylophorine from L-Proline by Radical Cyclization. *Org. Lett.* **2010**, *12*, 2140–2141.
- (57) Yao, T.; Zhang, H.; Zhao, Y. Synthesis of 9,10-Phenanthrenes via Palladium-Catalyzed Aryne Annulation by *o*-Halostyrenes and Formal Synthesis of (±)-Tylophorine. *Org. Lett.* **2016**, *18*, 2532–2535.
- (58) Zeng, W.; Chemler, S. R. Total Synthesis of (*S*)-(+)-Tylophorine Via Enantioselective Intramolecular Alkene Carboamination. *J. Org. Chem.* **2008**, *15*, 6045–6047.

- (59) A mechanism for a similar Pd-catalyzed annulation with an aryne has been proposed, see: Liu, Z.; Zhang, X.; Larock, R. C. Synthesis of Fused Polycyclic Aromatics by Palladium-Catalyzed Annulation of Arynes Using 2-Halobiaryls. *J. Am. Chem. Soc.*, **2005**, *127*, 15716–15717.
- (60) Liu, Z.; Larock, R. C. Highly Efficient Route to Fused Polycyclic Aromatics via Palladium-Catalyzed Aryne Annulation by Aryl Halides. *J. Org. Chem.* **2007**, *72*, 223–232.
- (61) Dhokale, R. A.; Mhaske, S. B. Transition-Metal-Catalyzed Reactions Involving Arynes. *Synthesis* **2018**, *50*, 1–16.
- (62) Anthony, S. M.; Wonilowicz, L. G.; McVeigh, M. S.; Garg, N. K. Leveraging Fleeting Strained Intermediates to Access Complex Scaffolds. *JACS Au* **2021**, *7*, 879–912.
- (63) Spence, K. A.; Tena Meza, A.; Garg, N. K. Merging Metals and Strained Intermediates. *Chem Catalysis* **2022**, *2*, 1870–1879.
- (64) Lin, J. B.; Shah, T. J.; Goetz, A. E.; Garg, N. K.; Houk, K. N. Conjugated Trimeric Scaffolds Accessible from Indolyne Cyclotrimerizations: Synthesis, Structures, and Electronic Properties. *J. Am. Chem. Soc.* **2017**, *139*, 10447–10455.
- (65) Spence, K. A.; Chari, J. V.; Di Niro, M.; Susick, R. B.; Ukwitegetse, N.; Djurovich, P. I.; Thompson, M. E.; Garg, N. K. π -Extension of Heterocycles via a Pd-Catalyzed Heterocyclic Aryne Annulation: π -Extended Donors for TADF Emitters. *Chem. Sci.* **2022**, *13*, 5884–5892.
- (66) Chari, J. V.; Spence, K. A.; Susick, R. B.; Garg, N. K. A Platform for On-the-Complex Annulation Reactions with Transient Aryne Intermediates. *Nat. Commun.* **2021**, *12*, 3706.

- (67) Barber, J. S.; Yamano, M. M.; Ramirez, M.; Darzi, E. R.; Knapp, R. R.; Liu, F.; Houk, K. N.; Garg, N. K. Diels–Alder Cycloadditions of Strained Azacyclic Allenes. *Nat. Chem.* **2018**, *10*, 953–960.
- (68) Comins, D. L.; Abdullah, A. H. Regioselective Addition of Grignard Reagents to 1-Acylpyridinium Salts. A Convenient Method for the Synthesis of 4-Alkyl(aryl)pyridines. *J. Org. Chem.* **1982**, *47*, 4315–4319.
- (69) Yamano, M. M.; Kelleghan, A. V.; Shao, Q.; Giroud, M.; Simmons, B. J.; Li, B.; Chen, S.; Houk, K. N.; Garg, N. K. Intercepting Fleeting Cyclic Allenes with Asymmetric Nickel Catalysis. *Nature* **2020**, 242–247.
- (70) Kelleghan, A. V.; Witkowski, D. C.; McVeigh, M. S.; Garg, N. K. Palladium-Catalyzed Annulations of Strained Cyclic Allenes. *J. Am. Chem. Soc.* **2021**, *143*, 9338–9342.
- (71) Witkowski, D. C.; McVeigh, M. S.; Scherer, G. M.; Anthony, S. M.; Garg, N. K. Catalyst-Controlled Annulations of Strained Cyclic Allenes with π -Allylpalladium Complexes. *J. Am. Chem. Soc.* **2023**, *145*, 10491–10496.
- (72) We have experimentally observed that the addition of toluene leads to slower consumption of silyl triflate precursors, presumably by reducing the solubility of CsF in the reaction medium. The solubility of CsF in acetonitrile is roughly 5000x greater compared to the solubility of CsF in benzene, a close relative of toluene with a comparable dielectric constant. For a study of CsF solubility, see: Wynn, D. A.; Rothand, M. M.; Pollard, B. D. The solubility of alkali-metal fluorides in non-aqueous solvents with and without crown ethers, as determined by flame emission spectrometry. *Talanta* **1984**, *31*, 1036–1040.

- (73) Notably, all reported examples of piperidine silyl triflate precursors possess an electron-withdrawing group on nitrogen, which presumably helps to mitigate the decomposition pathway we observe in attempting to access **4.20**.
- (74) Stang, P.; Anderson, A. G. Hammett and Taft Substituent Constants for the Mesylate, Tosylate, and Triflate Groups. *J. Org. Chem.* **1976**, *41*, 781–785.
- (75) McVeigh, M. S.; Kelleghan, A. V.; Yamano, M. M.; Knapp, R. R.; Garg, N. K. Silyl Tosylate Precursors to Cyclohexyne, 1,2-Cyclohexadiene, and 1,2-Cycloheptadiene. *Org. Lett.* **2020**, *22*, 4500–4504.
- (76) Lamor, A.; Uipanit, S.; Yakhampom, S.; Ngermmeesri, P.; Kongkathip, N.; Kongkathip, B.; Chuanopparat, N. Asymmetric Formal Synthesis of (–)-Swainsonine from Chiral-Pool Precursors D-Mannose and D-Arabinose. *Synlett* **2022**, *33*, 1463–1467.
- (77) Wentrup, C.; Blanch, R.; Briehl, H.; Gross, G. Benzyne, Cyclohexyne, and 3-Azacyclohexyne and the Problem of Cycloalkyne Versus Cycloalkylideneketene Genesis. *J. Am. Chem. Soc.* **1988**, *110*, 1874–1880.
- (78) Hartwell, J. L.; Abbott, B. J. Antineoplastic Principles in Plants: Recent Developments in the Field. *Advan. Pharm. Chemother.* **1969**, *7*, 117.
- (79) Wu, P.-L.; Rao, K. V.; Su, C.-H.; Kuoh, C.-S.; Wu, T.-S. Phenanthroindolizidine Alkaloids and Their Cytotoxicity from the Leaves of *Ficus Septica*. *Heterocycles* **2002**, *57*, 2401–2408.
- (80) Barber, J. S.; Yamano, M. M.; Ramirez, M.; Darzi, E. R.; Knapp, R. R.; Liu, F.; Houk, K. N.; Garg, N. K. Diels–Alder Cycloadditions of Strained Azacyclic Allenes. *Nat. Chem.* **2018**, *10*, 953–960.

- (81) Niphakis, M. J.; Gay, B. C.; Hong, K. H.; Bleeker, N. P.; Georg, G. I. Synthesis and Evaluation of the Anti-proliferative and NF- κ B Activities of a Library of Simplified Tylophorine Analogs. *Bioorg. Med. Chem.* **2012**, *20*, 5893–5900.
- (82) Niphakis, M. J.; Georg, G. I. Synthesis of Tylocrebine and Related Phenanthroindolizidines by VOF₃-Mediated Oxidative Aryl-Alkene Coupling. *Org. Lett.* **2011**, *13*, 196–199.
- (83) Fukumoto, K.; Suzuki, K.; Nemoto, H. An Efficient Synthesis of Cholanic Acids from 20-Ketopregnanes. *Tetrahedron* **1982**, *38*, 3701–3704.
- (84) Lahm, G.; Stoye, A.; Opatz, T. A Five-Step Synthesis of (\pm)-Tylophorine via a Nitrile-Stabilized Ammonium Ylide. *J. Org. Chem.* **2012**, *77*, 6620–6623.
- (85) Niphakis, M. J.; Georg, G. I. Synthesis of Tylocrebine and Related Phenanthroindolizidines by VOF₃-Mediated Oxidative Aryl-Alkene Coupling. *Org. Lett.* **2011**, *13*, 196–199.
- (86) Abe, F.; Iwase, Y.; Yamauchi, T.; Honda, K.; Hayashi, N. Phenanthroindolizidine Alkaloids from *Tylophora Tanake*. *Phytochemistry* **1995**, *39*, 695–699.

CHAPTER FIVE

Electrochemical Oxidation of Δ^9 -Tetrahydrocannabinol at Nanomolar Concentrations

Christina R. Forbes, Katie A. Spence, Neil K. Garg, and Evan R. Darzi.

Manuscript Submitted.

5.1 Abstract

With increasing marijuana legalization, there is a growing need for technology that can determine if an individual is impaired due to recent marijuana usage. An electrochemical oxidation of Δ^9 -THC to form its corresponding quinones can be used as a framework to develop an electrochemical sensor for Δ^9 -THC. This study describes an electrochemical oxidation of Δ^9 -THC that uses a copper anode, platinum cathode, and an atmosphere of oxygen. The oxidation is feasible at nanomolar concentrations, which is relevant to real-world sensor applications, such as marijuana breathalyzer technologies. Moreover, we show that vaporized Δ^9 -THC can be captured directly in an electrolyte medium and subjected to electrochemical oxidation, thus paving the way for use in future technology development.

5.2 Introduction

The legalization and decriminalization of marijuana in the United States has continued to expand over the past decade (Figure 5.1).¹ Currently, 39 states have legalized the use of medical marijuana, with 21 of these states also allowing recreational marijuana use.² Despite growing legal acceptance of marijuana-based products, a simple and accurate method for determining one's impairment level while under the influence of marijuana still does not exist.

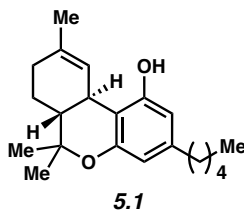
Current detection technologies for Δ^9 -tetrahydrocannabinol (Δ^9 -THC, **5.1**), the primary component of marijuana that is responsible for impairment, rely on blood, urine, or saliva tests.^{3,4} These methods cannot reliably distinguish between someone who is currently impaired from marijuana use, and someone who has used marijuana in the past days, weeks or sometimes months.^{5,6,7,8}

This puts responsible marijuana users at risk for wrongful DUI convictions, loss of employment, fines or imprisonment. Because Δ^9 -THC is only detectable on the breath for 3–4 hours, during the time in which impairment from marijuana use is most pronounced, a promising alternative method for assessing Δ^9 -THC impairment relies on breath analysis.^{9,10,11,12} One of the primary challenges associated with measuring Δ^9 -THC breath is the low concentration ranges of 1–1000 nM that are relevant to real world application. Several approaches toward breath-based Δ^9 -THC detection technologies have been reported, including those reliant on the use of fluorescence, chemiresistors, and mass spectrometry.^{13,14,15,16,17,18,19,20} Although promising, these methods each possess drawbacks, such as having non-reusable or non-portable components, or requiring costly instrumentation.

• *Marijuana legalized in 39 states*

• *Few options for rapid detection that correlate with the window of impairment*

An inexpensive, portable, and accurate forensic tool for THC detection is needed



(-)-*trans*- Δ^9 -tetrahydrocannabinol (THC)
Psychoactive component in cannabis products

Figure 5.1. Increasing marijuana legalization requires development of new tools to measure impairment due to Δ^9 -THC (**5.1**).

In 2020, we reported a strategy for Δ^9 -THC detection that relied on electrochemistry and could plausibly be translated to breath-based detection.²¹ The method is dependent on the selective electrochemical oxidation of Δ^9 -THC (**5.1**) to *p*-THCQ (**5.2**) (Figure 5.2) and was recently translated to establish the first cannabinoid fuel cell technology.²² Nonetheless, a number of questions remained regarding the applicability of this electrochemical-based strategy to real-world applications. For example, our initial experiments required 6.6 mM concentrations of Δ^9 -THC (**5.1**), which is significantly higher than what would be observed on breath samples. Studies have shown that only 5–500 ng of Δ^9 -THC (**5.1**) are present in 25 breaths during peak impairment, with the amount depending on numerous factors.^{23,24,25} In addition, our initial electrochemical oxidation was performed on liquid Δ^9 -THC (**5.1**) in solution, whereas a marijuana breathalyzer would rely on the use of captured Δ^9 -THC vapor or condensate.

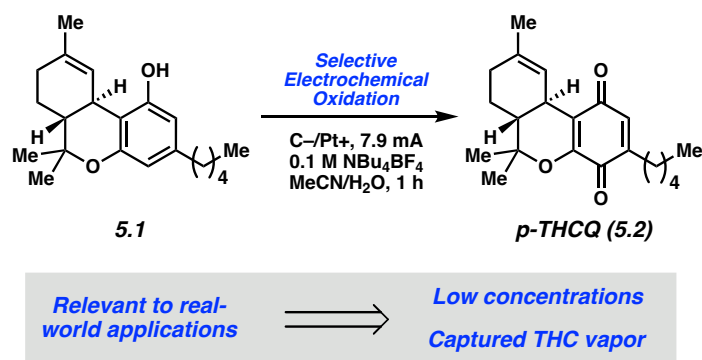


Figure 5.2. Previously reported electrochemical oxidation of Δ^9 -THC (**5.1**) and goals of present study.

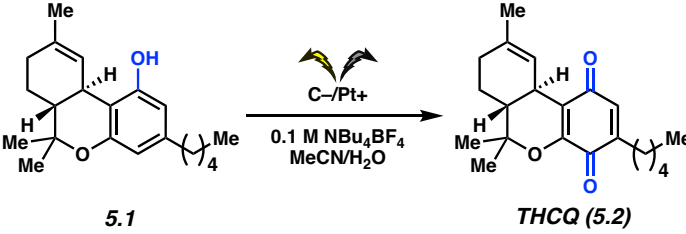
Herein, we describe the development of the electrochemical oxidation of Δ^9 -THC (**5.1**) at low concentrations, which involved the systematic evaluation of a number of different electrodes, electrolytes and concentrations. It was found that copper anode materials were most effective at improving oxidation of **5.1**, while avoiding undesired degradation. We show that oxidation can be achieved at concentrations as low as 1 nM, which provides a rare example of electrochemistry being achieved at such low concentrations. In addition, we demonstrate that vaporized **5.1** can be captured and subsequently oxidized using our low-concentration electrochemical oxidation conditions. Collectively, these studies address practical considerations for the electrochemical oxidation approach to Δ^9 -THC (**5.1**) detection, thus providing the impetus for further marijuana breathalyzer technology development.

5.3 Results and Discussion

We began the present study by examining our previously reported reaction conditions²¹ at lower concentrations (Table 5.1). All experiments were performed using the ElectraSyn 2.0 reactor. Using a concentration of 1.0 mM of Δ^9 -THC (**5.1**), a modest decrease compared to our

originally-used 6.6 mM concentration, only trace formation of quinone **5.2** was observed (1% yield, Table 5.1, entry 1). As substantial side-products were observed via HPLC analysis (see Figure 5.5), we tried reducing the reaction time from 60 to 10 min. Unfortunately, only a slight increase in yield was observed (entry 2). Recognizing that the observed current at a given potential depends on several factors, including substrate concentration,²⁶ we decreased the applied current (entry 3). This led to an increase in yield to 12% (entry 3). However, further decreasing the concentration of Δ^9 -THC (**5.1**), to high- and mid- μ M range, resulted again in low product formation (entries 4–5).

Table 5.1. Initial attempts to effect oxidation at lower concentrations.



Entry	[Δ^9 -THC] (mM)	Reaction Time (min)	Current (mA)	Yield
1	0.99	60	7.9	1%
2	0.97	10	7.9	4%
3	0.99	10	3.5	12%
4	0.13	10	3.5	1%
5 ^b	0.012	10	3.5	0%

^a Conditions: Reactions were performed on solutions of Δ^9 -THC in 0.1 M NBu₄BF₄ with 12% water in acetonitrile using a graphite anode and a platinum film cathode. Polarity was switched every 60 seconds. Yield and initial Δ^9 -THC concentration were determined via PDA mode of detection. ^b Determined from MRM mode of detection via LC-MS/MS.

To assess the difficulty in achieving the electrochemical oxidation of Δ^9 -THC (**5.1**) at low concentrations, we monitored reactions by LC-MS/MS. Using this sensitive analytical

technique, we found that a second THCQ product was being formed in addition to *p*-THCQ (**5.2**). This was ultimately identified as the ortho quinone isomer, *o*-THCQ (**5.3**) (Figure 5.3), by comparison to an authentic sample of **5.3** we prepared by chemical oxidation of Δ^9 -THC (**5.1**) using stabilized 2-iodobenzoic acid.²⁷ Fortuitously, each THCQ isomer shows slightly different retention times and distinctive UV-Vis signatures in the visible region. In addition, subtle differences in ionization behaviors exist (see Section 5.5 for details), which facilitated subsequent quantification of **5.2** and **5.3**.

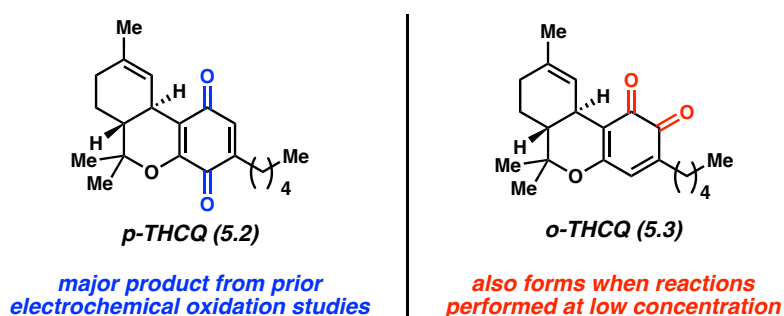
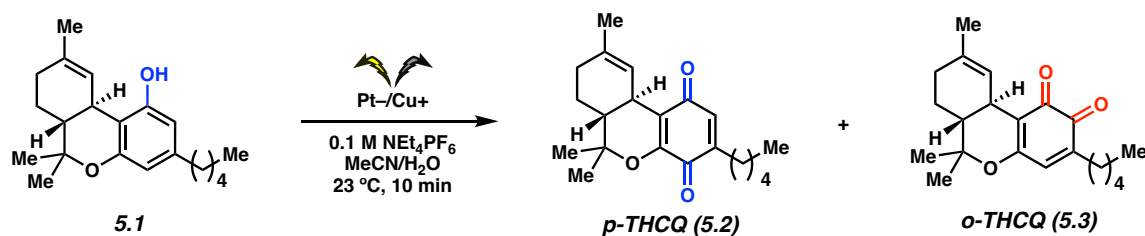


Figure 5.3. THCQ isomers **5.2** and **5.3**, with *ortho* quinone isomer **5.3** forming when the electrochemical oxidation is performed at low concentrations.

With both THCQ product isomers quantifiable by LC-MS/MS, we re-examined the electrochemical oxidation using 10 μ M concentration of THC (**5.1**). Many conditions were tested by varying parameters such as electrodes, current, potential, and electrolytes, but these efforts primarily led to unidentified byproducts and unreacted Δ^9 -THC (**5.1**) (See Section 5.5). Fortunately, we ultimately found that the use of copper anodes led to some quinone formation and fewer byproducts. Key results involving the use of copper anode, platinum cathode, NEt_4PF_6 as electrolyte, in acetonitrile and water under constant potential for 10 min are shown in Table 5.2. Applying a potential of +0.65 V under a headspace of air led to a slow, but relatively clean

reaction, yielding 89% of recovered **1** and 4% of quinones **5.2** and **5.3** (entry 1). Inspired by several reports^{28,29,30,31} detailing the important role of oxygen in copper-promoted phenol oxidations, we interrogated the role of oxygen in our electrochemical reaction. With N₂ sparging to omit oxygen from the reaction, quinones **5.2** and **5.3** were not observed (entry 2). Whereas sparging with air had a minimal effect (entry 3), we were delighted to find that sparging with O₂ led to significant improvement, affording quinones **5.2** and **5.3** in a combined yield of 41% (entry 4). To ensure consistent voltage, minimize the loss of potential, and ensure reproducibility,^{24,32} we also tested a three-electrode configuration with O₂ sparging. Using a non-aqueous Ag/AgCl reference electrode led to an increased 56% yield of **5.2** and **5.3**, albeit with greater unproductive degradation. Applying lower potentials with referencing gave slightly lower yields, but with greater recovery of Δ^9 -THC (**5.1**) and improved mass balance (entries 6 and 7). Applying +0.05 V vs. Ag/AgCl gave little conversion (entry 8). We elected to pursue entry 7 conditions for further study, given the notable conversion and overall mass recovery.

Table 5.2. Electrochemical oxidation screening, altering headspace and voltage.^a

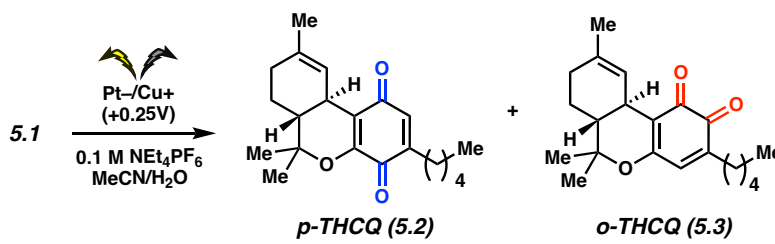


Entry	Applied Potential (V)	Cell Headspace	Δ^9 -THC Remaining ^b	Yield of 5.2 + 5.3 ^b
1	+0.65	Air, sealed	89%	4%
2	+0.65	N ₂ sparging	97%	0%
3	+0.65	air sparging	94%	3%
4	+0.65	O ₂ sparging	55%	41%
5	+0.65 vs Ag/AgCl	O ₂ sparging	28%	56%
6	+0.45 vs Ag/AgCl	O ₂ sparging	33%	53%
7	+0.25 vs Ag/AgCl	O ₂ sparging	56%	42%
8	+0.05 vs Ag/AgCl	O ₂ sparging	89%	8%

^aConditions: Reactions were performed by applying constant potential for 10 min on solutions of Δ^9 -THC (5.1) (measured to be 9.6–14 μM) in 0.1 M NEt₄PF₆ with 12% water in acetonitrile using platinum film cathode. Where noted, electrochemical cells were referenced with a jacketed Ag/AgCl reference electrode. Data reported are averaged over three independent experiments. ^bDetermined from MRM mode of detection via LC-MS/MS.

As shown in Table 5.3, the conditions we had identified using a three-electrode system and oxygen sparging were amenable to lower concentration. Entries 1–5 show key results where the concentration was lowered systematically from 8970 nM to 1.01 nM. In all cases, significant conversion to quinones **5.2** and **5.3** was observed. Of note, even at ~1 nM concentration, 43% yield of THCQs **5.2** and **5.3** was observed (entry 5). Although this data point approaches the limit of quantification for the LC-MS/MS instrumentation, we surmise that the use of lower concentrations is likely viable. Nonetheless, these data demonstrate that the electrochemical oxidation of Δ^9 -THC (**5.1**) is indeed viable at high dilution, as would be needed to analyze breath samples during peak impairment.

Table 5.3. Electrochemical oxidation at low concentrations.^a



Entry	$[\Delta^9\text{-THC}]$ (nM)	$\Delta^9\text{-THC}$ (5.1) remaining ^b	Yield THCQ (5.2 + 5.3) ^b
1	9.0E3	56%	28%
2	8.2E2	24%	43%
3	65	28%	35%
4	6.4	0%	52%
5	1.0	0%	43%

^a Conditions: Reactions were performed on solutions of 0.1 M NEt₄PF₆ 12% water in acetonitrile with constant potential applied (+0.25 V vs Ag/AgCl) for 10 min using a copper anode and a platinum film cathode. Electrochemical cells were referenced with a Ag/AgCl reference electrode. Data reported are averaged over three independent experiments. ^b Determined from MRM mode of detection via LC-MS/MS.

In order to establish the viability of these reaction conditions for samples that would come from breath, a simulated vapor transfer experiment was performed. A Volcano Vaporizer

(Storz & Bikel) was used to vaporize Δ^9 -THC (**5.1**), which was then captured in acetonitrile. The resulting solution was analyzed by LC-MS/MS, which showed a 94 nM concentration Δ^9 -THC (**5.1**) and the absence of quinones **5.2** and **5.3**. This sample was subjected to our optimized electrochemical oxidation conditions for 30 min affording THCQs **5.2** and **5.3** in 11% yield. Although the yield is lower compared to that seen in the solution-based study (see Table 5.3, entry 3), this experiment establishes the application of the electrochemical oxidation of Δ^9 -THC (**5.1**) to vapor-captured samples for the first time.

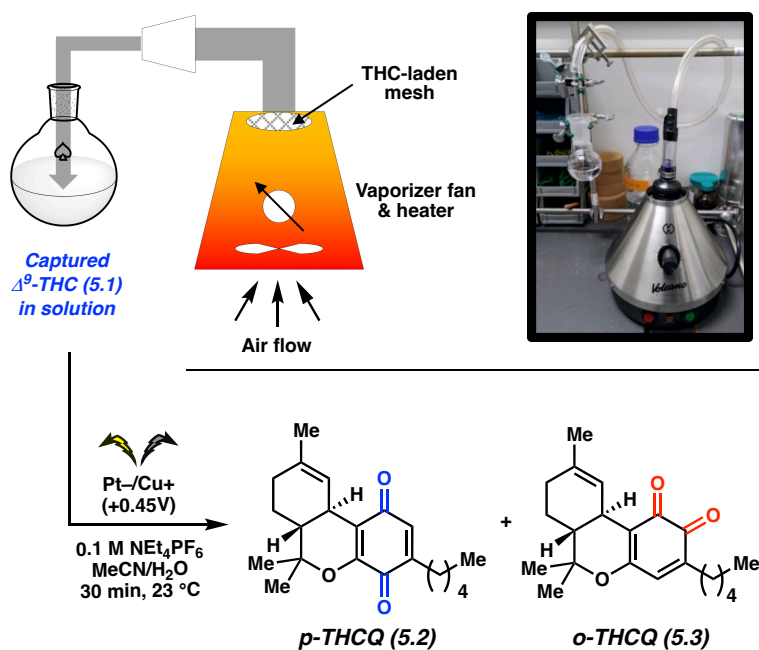


Figure 5.4. Vaporized Δ^9 -THC (**5.1**) was captured in acetonitrile and then subjected to electrochemical oxidation to generate THCQ (**5.2** and **5.3**).

5.4 Conclusions

In summary, we have demonstrated that the electrochemical oxidation of Δ^9 -THC (**5.1**) can be achieved at nM concentrations. The use of copper anode materials in the presence of

oxygen proved most effective. Two quinone products are observed: *p*-THCQ (**5.2**), the oxidation product observed under earlier reported conditions, and *o*-THCQ (**5.3**), an isomer not previously observed. We also demonstrate that the low concentration oxidation is operative using vapor-captured Δ^9 -THC (**5.1**). This study demonstrates a rare example of low-concentration organic electrochemistry and provides key advances toward the development of marijuana breathalyzer technologies.

5.5 Experimental Section

5.5.1 Materials and Methods

Synthesis reactions were conducted in flame-dried glassware under an atmosphere of nitrogen using anhydrous solvents (freshly distilled or passed through activated alumina columns). Electrochemical reactions were performed using an ElectraSyn 2.0 without flame-drying glassware or distilling solvents. All commercially obtained reagents were used as received unless otherwise specified. All commercially obtained reagents were used as received unless otherwise specified. Δ^9 -THC (**5.1**), was purchased from Sigma–Aldrich (www.sigmaaldrich.com; product number T2386) under DEA approval. 2-Iodoxybenzoic acid (IBX) was prepared according to a procedure described by Sputore.³³ Spectral data matched those reported in the literature. Thin layer chromatography (TLC) was conducted with EMD gel 60 F254 pre-coated plates (0.25 mm) and visualized using a combination of UV light, anisaldehyde, and potassium permanganate staining. Silicycle Siliaflash P60 (particle size 0.040–0.063 mm) was used for flash column chromatography. ¹H-NMR spectra were recorded on a Bruker spectrometer (at 500 MHz) and are reported relative to the residual solvent signal. Data for ¹H-NMR spectra are reported as follows: chemical shift (δ ppm) (multiplicity, coupling constant (Hz), integration, proton assignment).

¹³C-NMR spectra were recorded on a Bruker spectrometer (at 125 MHz) and chemical shifts are reported relative to the residual solvent signal. Carbons are numbered based on conventional numbering (See Section 5.5.2). Data for ¹³C-NMR spectra are reported in terms of chemical shift and carbon assignment. IR spectra were obtained on a Perkin-Elmer UATR Two FT-IR spectrometer and are reported in terms of frequency of absorption (cm⁻¹). DART-MS spectra were collected on a Thermo Exactive Plus MSD (Thermo Scientific) equipped with an ID-CUBE ion source and a Vapur Interface (IonSense Inc.). Both the source and MSD were controlled by Excalibur software v. 3.0. The analyte was spotted onto OpenSpot sampling cards (IonSense Inc.) using CH₂Cl₂ as the solvent. Ionization was accomplished using UHP He (Airgas Inc.) plasma with no additional ionization agents. The mass calibration was carried out using Pierce LTQ Velos ESI (+) and (-) Ion calibration solutions (Thermo Fisher Scientific). UV-Vis spectra were recorded using an JASCO C-770 UV-Visible/NIR spectrophotometer. The UV-Vis spectra were recorded using a 1-cm quartz cuvette, with ethanol. The concentration of Δ⁹-THC and quinone products from electrochemical reactions were measured using a liquid chromatograph tandem mass spectrometer (LC-MS/MS, Shimadzu LC-8060NX) using similar methods as reported in literature.³⁴ The electrochemical reactions were performed using an IKA ElectraSyn 2.0. Platinum-plated (IKA; product number 0040002852), copper (IKA; product number 0040002847), graphite (IKA; product number 0040002858), and Ag/AgCl non-aqueous reference (IKA; product number 0040002865) electrodes were purchased from IKA and were used as received. Unless stated otherwise, reactions were performed at room temperature (approximately 21 °C).

5.5.2 Experimental Procedures

5.5.2.1 LC-MS/MS Methods

Samples were analyzed via LC-MS/MS using a Shimadzu LC-8060NX (Columbia, Maryland, USA). The chromatographic system consisted of a Nexera binary pump with an autosampler, column oven, photo-diode array detector, and a degasser. A valve in the column oven directed the flow-path to waste or MS/MS after the photodiode array detector. The LC-MS/MS apparatus was equipped with an IonFocus apparatus with a DUIS source. Separations were achieved using a NexLeaf CBX column (2.7 μm , 150 mm x 4.6 mm, equipped with guard column) in the quantitative analysis of Δ^9 -THC and quinone products. Elution gradients utilized Buffer A (0.1% formic acid in water) and Buffer B (0.1% formic acid in acetonitrile) using a flow rate of 1.0 mL min⁻¹ and injection volumes 30-50 μL . The elution method (as % Buffer B in Buffer A) was initiated with a gradient of 70% to 80% for 10 min, followed by a gradient of 80% to 98% for 0.5 min, followed by isocratic 100% for 1.5 min, and then isocratic 70% for 1.5 min. The total run time of this method was 14.0 min. Flow was diverted to waste from 0 to 5.3 min to remove most of the electrolyte. Autosampler and column oven temperatures were 4 °C and 35 °C, respectively. MS/MS data were acquired via using optimized MRM in positive ion mode. Source parameters were nebulizing gas flow 2 L/min, heating gas flow 10 L/min, drying gas flow 6 L/min, interface temperature 350 °C, desolvation line temperature 200 °C, and heat block temperature 450 °C. Standard solutions of Δ^9 -THC/CBN/CBD (Phytocannabinoid Mixture 3, Cayman Chemical) and synthesized THC quinone products **5.2** and **5.3** were prepared for calibration curves over a range of 15 μM – 0.2 nM analyte concentrations with 0.1 M electrolyte present. MRM was used for quantification for each of the following: for Δ^9 -THC (**5.1**, $r_t = 9.28$

min) via 315>123 m/z (CE -15 V), for Δ^9 -THCQ_{para} (**5.2**, $r_t = 9.94$ min) via 329>229 m/z (CE -31 V), and for Δ^9 -THCQ_{ortho} (**5.3**, $r_t = 10.09$ min) via 329>259 m/z (CE -21 V).

5.5.2.2 General Procedure for Electrochemical Oxidation Reactions

A 5 mL ElectraSyn 2.0 vial was equipped with a magnetic stir bar and charged with a solution of Δ^9 -THC in electrolyte solution (3.000 mL, 0.100 M in MeCN) and water (0.400 mL). After thorough mixing via pipet, the solution was sampled to measure the concentration of Δ^9 -THC (**5.1**) via LC-MS/MS. Next, the vial was equipped with an anode and a cathode. Where specified, a reference electrode was utilized (Ag/AgCl reference electrode was filled with electrolyte solution and then soaked overnight prior to performing experiments). In experiments where gas sparging was used, a balloon was filled with the respective gas and equipped with a long needle (22 gauge), which was inserted through the ElectraSyn septum cap and bubbled vigorously into the reaction solution. This vial was then connected to the ElectraSyn 2.0 instrument, and experiments were performed with either constant current or constant potential modes at a stir rate of 400 rpm. In reactions with copper electrodes, precipitates often formed within the first 2 minutes of the reaction. Once the reaction was complete, the reaction was sampled via pipet and diluted with 0.1% formic acid in water before being filtered over a 13 mm nylon syringe filter (0.2 μm) for analysis via LC-MS/MS.

5.5.2.3 Select Results from Electrochemical Oxidation Screening

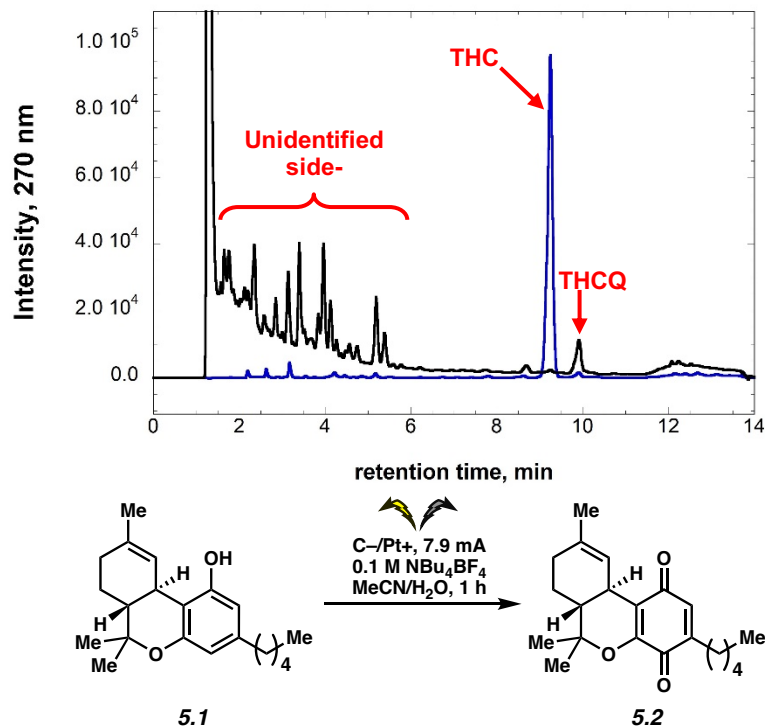


Figure 5.5. Conditions: Δ^9 -THC (**5.1**) (1.0 mM), 8:1 0.1 M NBu₄BF₃ in MeCN:H₂O, 23 °C, 1 h, polarity alternation every 60 s. The blue LC/MS chromatographic trace is of the starting solution. The overlaid black LC/MS chromatographic trace is of the crude reaction mixture. **5.1** is fully consumed, with a small amount of conversion to **5.2**. The majority of the **5.1** has decomposed into unidentified side-products.

Table 5.4. Effects of the anode material and electrochemical condition at μM concentrations of $\Delta^9\text{-THC}$ (5.1). The general procedure for electrochemical oxidation reactions from Section 5.5.2.2 was used with Bu_4NBF_4 as the electrolyte and a platinum film cathode. Reactions were run for 10 minute.

Entry	Anode material	Applied Current	Measured THC Concentration (μM)*	% THC (5.1) Remaining*	Total % Yield THCQ (5.2 + 5.3)*
1	Graphite	3.5 mA, 60 sec alternating polarity	14	0%	0%
2	Platinum film	3.5 mA, 60 sec alternating polarity	13	12%	13%
3	Nickel	3.5 mA, 60 sec alternating polarity	13	0%	0%
4	Boron-doped diamond	3.5 mA, 60 sec alternating polarity	12	0%	3%
5	Copper	3.5 mA, 60 sec alternating polarity	14	97%	1%
6	Copper	3.5 mA, constant polarity	13	95%	4%
7	Copper	2.0 mA, constant polarity	12	97%	0%
8	Copper	6.0 mA, constant polarity	11	67%	1%
9	Copper	10.0 mA, constant polarity	10	63%	7%
10	Copper	14.0 mA, constant polarity	8.7	72%	1%

*Determined from MRM mode of quantification.

Table 5.5. Effects of applied potential at μM concentrations of $\Delta^9\text{-THC}$ (**5.1**). The general procedure for electrochemical oxidation reactions from Section 5.5.2.2 was used with Bu_4NBF_4 as the electrolyte, a copper anode and a platinum film cathode. Reactions were run in a sealed cell under air.

Entry	Applied Potential	Reaction Time (min)	THC Concentration (μM)	% THC (5.1) Remaining*	Total % Yield THCQ (5.2 + 5.3)*
1	+0.27 V	10	11	90%	0%
2	+0.33 V	10	7.5	85%	13%
3	+0.39 V	10	17	69%	19%
4	+0.25 V vs Ag/AgCl	10	18	96%	3%
5	+0.45 V vs Ag/AgCl	10	10	92%	2%
6	+0.65 V vs Ag/AgCl	10	17	82%	2%
7	+0.45 V vs Ag/AgCl	30	9.8	85%	3%
8	+0.45 V vs Ag/AgCl	60	9.6	78%	4%

*Yield determined from MRM mode of quantification.

5.5.2.4 Procedure for the Vaporization, Capture and Subsequent Oxidation of Δ^9 -THC

5.5.2.4.1 Vaporization

150.0 μ L of a 50 mg/mL solution of Δ^9 -THC (**5.1**) in acetonitrile was deposited dropwise onto a mesh, circular drip pad (2.8 cm diameter x 0.2 cm height). The drip pad was dried under a stream of air between drops, and then for 5 continuous minutes following full addition of the solution to evaporate any excess acetonitrile. Approximately 7 mg of Δ^9 -THC (**5.1**) was deposited onto the mesh after drying. At this point, a Volcano Vaporizer was plugged in and the temperature setting was set to 9 (226 °C). After 10 minutes, the yellow control lamp had switched “off”, indicating that the Volcano had reached temperature. A piece of PVC tubing (lab grade, 1/4 x 1/2” ID x OD) was connected to the top of the Volcano filling chamber. The other end of the tubing was connected to a gas dispersion tube (0.31 inch diameter, 170 to 220 μ m pore size) which was situated inside a round bottom flask filled with 30 mL of acetonitrile, such that the porous surface was completely submerged in the solutions. The THC-laden mesh was then placed inside the filling chamber, and the entire chamber was secured to the top of the Volcano. The air-flow was started, and the vaporized Δ^9 -THC (**5.1**) air-stream was bubbled directly into the 30 mL acetonitrile solution. After 10 minutes, the heat was turned off while the air continued to flow for an additional 5 minutes. 250 μ L of this solution was sampled via pipet and diluted with 250 μ L Buffer A for analysis via LC-MS/MS to measure the concentration of Δ^9 -THC (**5.1**) in solution.

5.5.2.4.2 Electrochemical Oxidation

A 5 mL ElectraSyn vial equipped with a stir bar was charged with 3.00 mL of the acetonitrile solution with vaporized Δ^9 -THC (**5.1**) from Section 5.5.2.4.1. Tetrabutylammonium tetrafluoroborate (100 mg, 0.100 M final concentration) and water (0.400 mL) were added to the

vial. 250 μ L of this solution was sampled via pipet and diluted with 250 μ L Buffer A for analysis via LC-MS/MS to measure initial concentrations. The initial concentration of **5.1** in the vapor-transferred solution was measured to be 9.4 μ M with no **5.2** or **5.3** observed. The vial was then equipped with a copper anode, a platinum film cathode, and a reference electrode (Ag/AgCl reference electrode was filled with electrolyte solution and then soaked overnight prior to the performing experiment). This vial was then connected to the ElectraSyn 2.0 instrument, and the solution was subjected to constant potential (+0.45 V with respect to reference electrode) at a stir rate of 400 rpm with polarity switching disabled. Once the reaction was complete, 250 μ L of the reaction was sampled via pipet and diluted with 250 μ L Buffer A for analysis via LC-MS/MS.

Table 5.6. LC-MS/MS analysis at different timepoints for the electrochemical oxidation of vaporized, then captured Δ^9 -THC (**5.1**).

Entry	Reaction time (min)	% THC (5.1) Remaining*	Total % Yield THCQ (5.2 + 5.3)*
1	10	98%	3%
2	20	92%	7%
3	30	88%	11%

*Yield determined from MRM mode of quantification.

5.5.2.5 Chromatographic Comparison of *ortho*- and *para*- Isomers of Δ^9 -THCQ

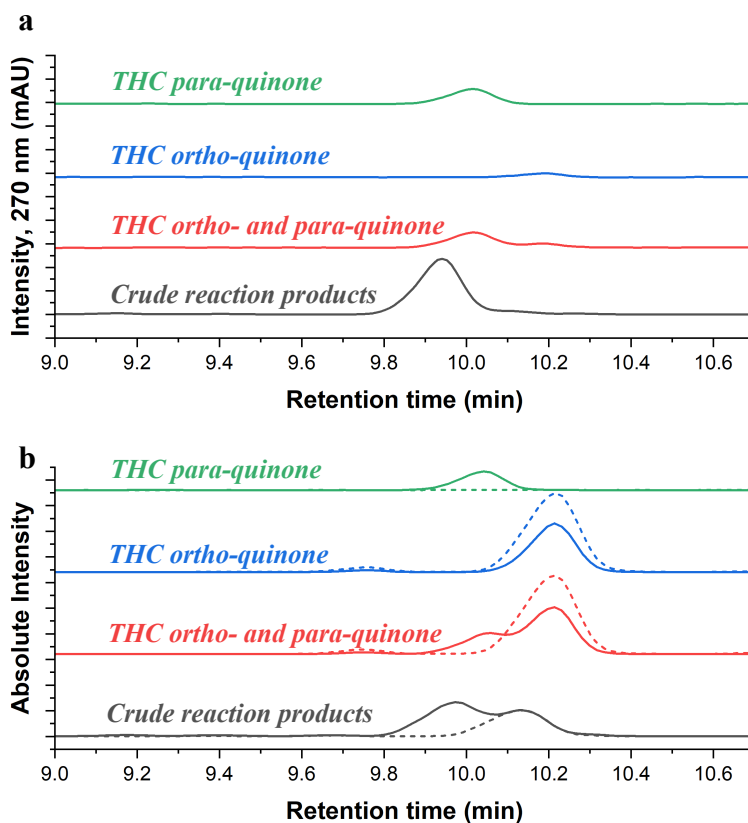
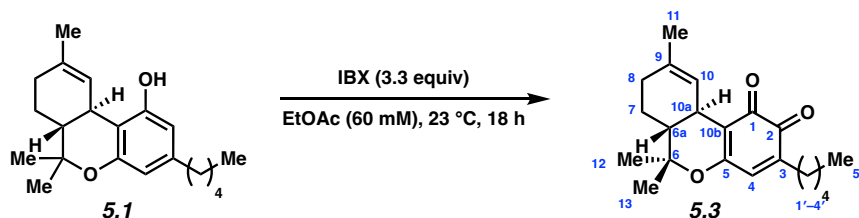


Figure 5.6. Chromatograms of synthesized THC *para*-quinone (**5.2**, green trace), THC *ortho*-quinone (**5.3**, blue trace), a 1:1 mixture of both THC *para*- and *ortho*-quinones (**5.2** + **5.3**, red trace), and the typical crude reaction products from an electro-oxidation reaction with THC (**5.1**, black trace). The chromatogram traces show UV-Vis detection via PDA at 270 nm (a) and LC-MS detection via selected ion mode at 329.25 m/z (b, solid line, THCQ + H⁺), and at 351.25 m/z (b, dashed line, THCQ + Na⁺).

5.5.2.6 Independent Chemical Oxidation of Δ^9 -THC to Δ^9 -THC *ortho*-Quinone (5.3)



Δ^9 -THCQ (**5.3**). A modified procedure for the synthesis of oxidized cannabinol was followed.³⁵ A 1 dram vial was equipped with a magnetic stir bar and flame-dried under reduced pressure. The vial was then cooled to 23 °C under nitrogen. A THC solution (0.40 mL of 25 mg/mL solution in ethanol; 10 mg, 1.00 Eq, 32 μ mol) was added to the vial and concentrated under reduced pressure to give a clear oil. The contents of the vial were then suspended in ethyl acetate (0.53 mL). The mixture was placed in a dry ice and acetone bath (-78 °C) and allowed to cool over 5 min while stirring. After this time, IBX (29 mg, 3.3 Eq, 0.10 mmol) was added in a single portion. The cooling bath was then removed, and the suspension was allowed to stir at 23 °C for 18 h. After this time, the reaction mixture was filtered through a pad of Celite with ethyl acetate (10 mL). The organic mixture was then washed with saturated $\text{Na}_2\text{S}_2\text{O}_3$ (2×15 mL), dried over magnesium sulfate, decanted and concentrated under reduced pressure. The crude material was then purified via preparative TLC using 100% benzene as the mobile phase. The desired product was isolated as a red oil. **THCQ (5.3)**: R_f 0.15 (Benzene); $^1\text{H-NMR}$ (500 MHz, CDCl_3): δ 6.45 (s, 1H, H4), 6.10 (s, 1H, H10), 3.03–2.97 (m, 1H, H10a), 2.37–2.26 (m, 2H, H1'), 2.17–2.09 (m, 2H, H8), 1.86–1.80 (m, 1H, 7 β), 1.64 (s, 3H, H11), 1.62–1.52 (m, 1H, 6a), 1.49–1.44 (m, 3H, H12), 1.41–1.35 (m, 1H, 7 α), 1.35–1.24 (m, 6H, H4', H3', H2'), 1.16 (s, 3H, H13), 0.88 (t, $J = 6.4$ Hz, H5'); $^{13}\text{C-NMR}$ (125 MHz, CDCl_3): 181.4 (C2), 177.6 (C1), 163.2 (C5), 143.2 (C3), 134.5 (C4), 134.2 (C9), 121.7 (C10), 113.4 (10b), 82.9 (C6), 44.8 (C6a), 32.1 (C10a), 31.4 (C3'), 31.2 (C8), 28.7 (C1'), 27.5 (C2'), 27.0 (C12), 24.4 (C7), 23.2 (C11), 22.4 (C4'), 20.6 (C13), 13.9

(C5'); δ IR (film): 3456, 2970, 1729, 1435, 1366; HRMS–APCI (m/z) $[M + H]^+$ calcd for $C_{21}H_{29}O_3^+$, 329.2112; found, 329.2136. δ IR (film): 3456, 2970, 1729, 1435, 1366.

2D NMR spectroscopy was used to provide evidence of the *o*-quinone as opposed to the *p*-quinone and supported an assignment with the alkene in the 9-position, as opposed to the more thermodynamically favored 8-position. The structure of **5.3** was numbered according to modern conventions and was assigned using a variety of NMR techniques. The alkene position was assigned according to COSY interaction between H10a and H10 as well as an HMBC correlation between H10 and C10a, and between H10a and C10. The position of the quinone carbonyl at C2 was assigned according to HMBC correlations between H4 and C2, C5, C10b, and C3.

5.5.2.7 Relevant Photophysical Data for 5.3

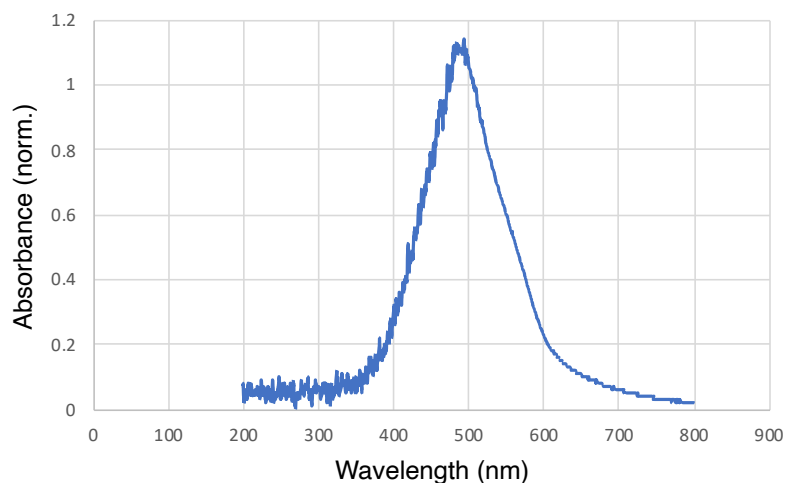


Figure 5.7. UV–Vis absorbance spectrum of **5.3**.

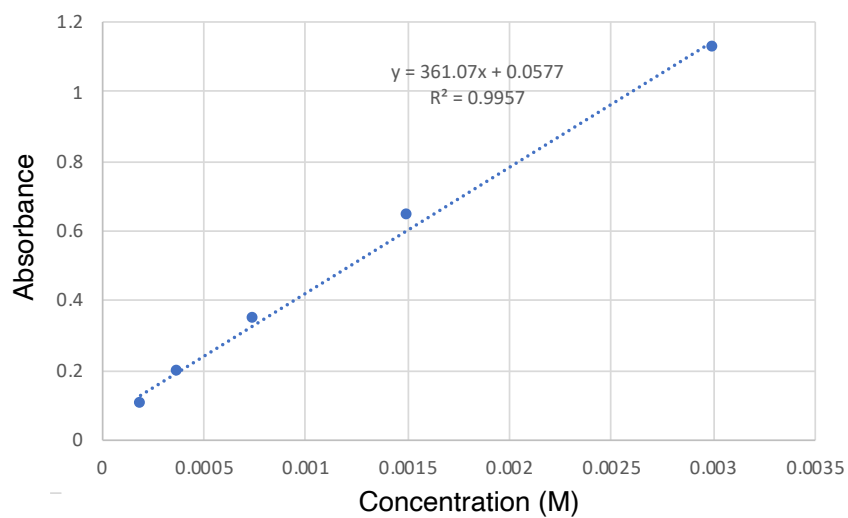


Figure 5.8. Beer-Lambert plot of **5.3** at 495 nm. ($\epsilon = 3.61 \times 10^2 \text{ M}^{-1} \text{ cm}^{-1}$).

5.6 Spectra Relevant to Chapter Five:

Electrochemical Oxidation of Δ^9 -Tetrahydrocannabinol at Nanomolar Concentrations

Christina R. Forbes, Katie A. Spence, Neil K. Garg, and Evan R. Darzi.

Manuscript Submitted.

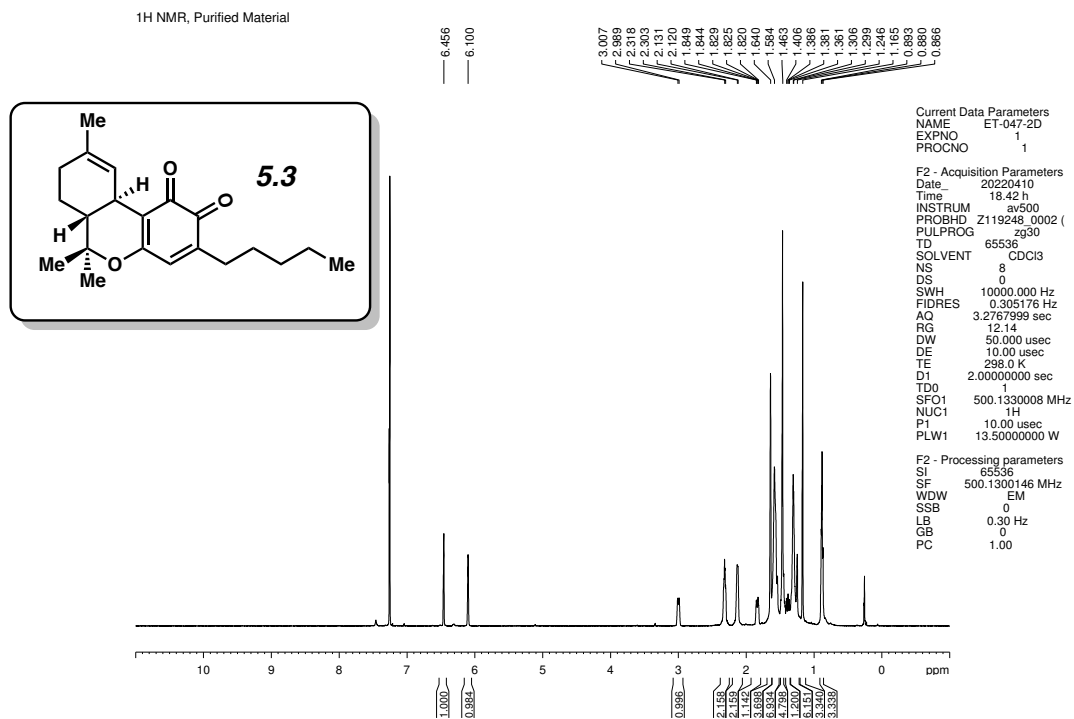


Figure 5.9 ¹H NMR (500 MHz, CDCl₃) of compound **5.3**.

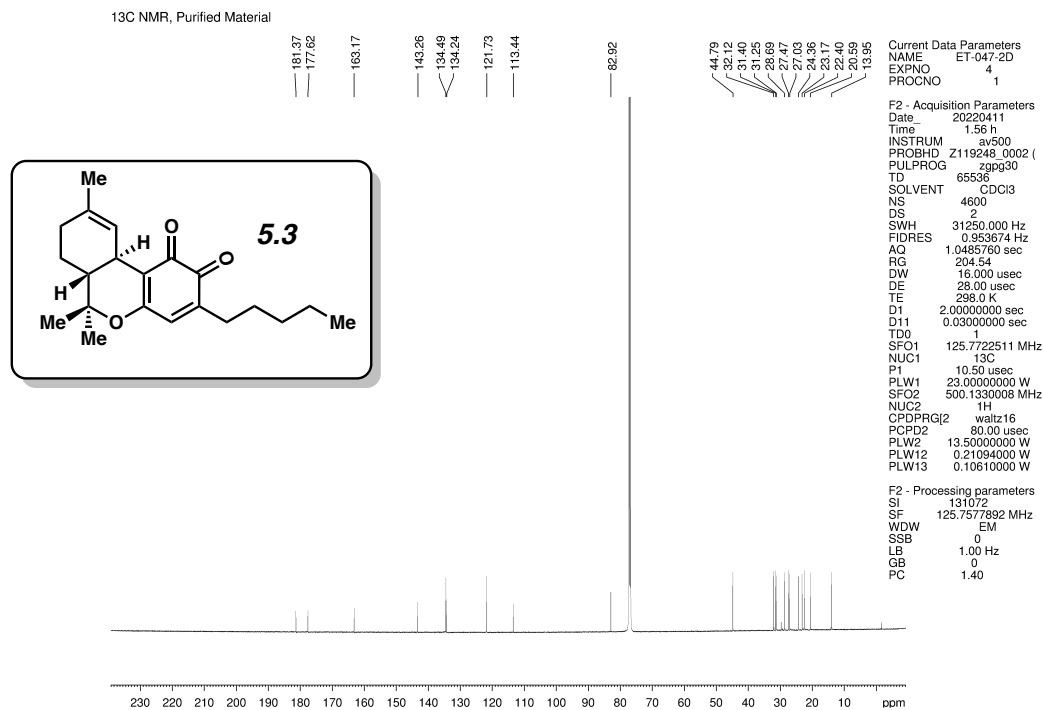
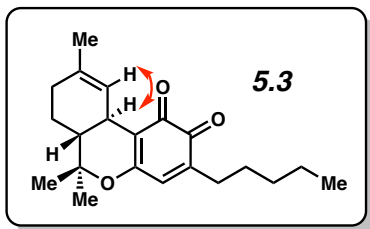
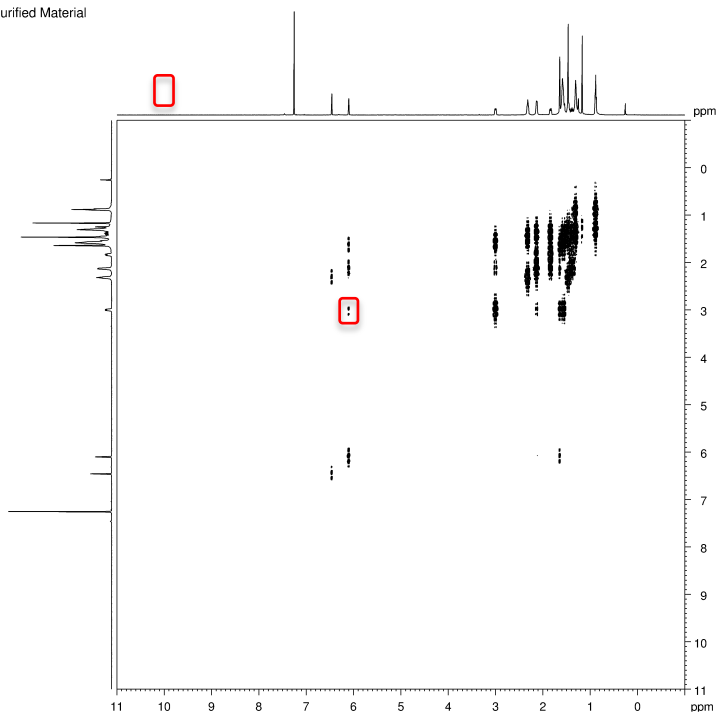


Figure 5.10 ¹³C NMR (125 MHz, CDCl₃) of compound **5.3**.



COSY, Purified Material



```

Current Data Parameters
NAME      ET-047-2b
EXPNO    2
PROCNO   1

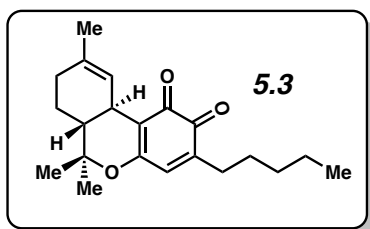
F2 - Acquisition Parameters
Date_    20220410
Time     19:07 h
INSTRUM  av500
PROBHD   Z119248_0002 (
PULPROG  zgpg30
TD       2048
SOLVENT  CDCl3
NS       8
DS       8
SWH      10000.000 Hz
FIDRES   9.755625 Hz
AQ       0.1024000 sec
RG       12.14
DW       50.000 usec
DE       10.00 usec
TE       298.0 K
D0       0.00063727 sec
D1       2.00000000 sec
D13      0.0000400 sec
D18      0.00020000 sec
IN       0.00010000 sec
TDaw     1
SFO1     500.1330008 MHz
NUC1     1H
P1       10.00 usec
P2       20.00 usec
PLW1     13.50000000 W
GPNAM[1] SMSC10.100
GPZ1     10.00 %
GPNAM[2] SMSC10.100
GPZ2     20.00 %
P16      1000.00 usec

F1 - Acquisition parameters
TD       256
SFO1     500.133 MHz
FIDRES   78.125000 Hz
SW       19.995 ppm
FHM0MODE States-TPPI

F2 - Processing parameters
SI       2048
SF       500.1300146 MHz
WDW      SINE
SSB      1
LB       0 Hz
GB       0
PC       1.00

F1 - Processing parameters
SI       2048
MC2      States-TPPI
SF       500.1300146 MHz
WDW      SINE
SSB      0 Hz
GB       0
  
```

Figure 5.11 COSY NMR (125 MHz, CDCl_3) of compound **5.3**.



NOESY, Purified Material

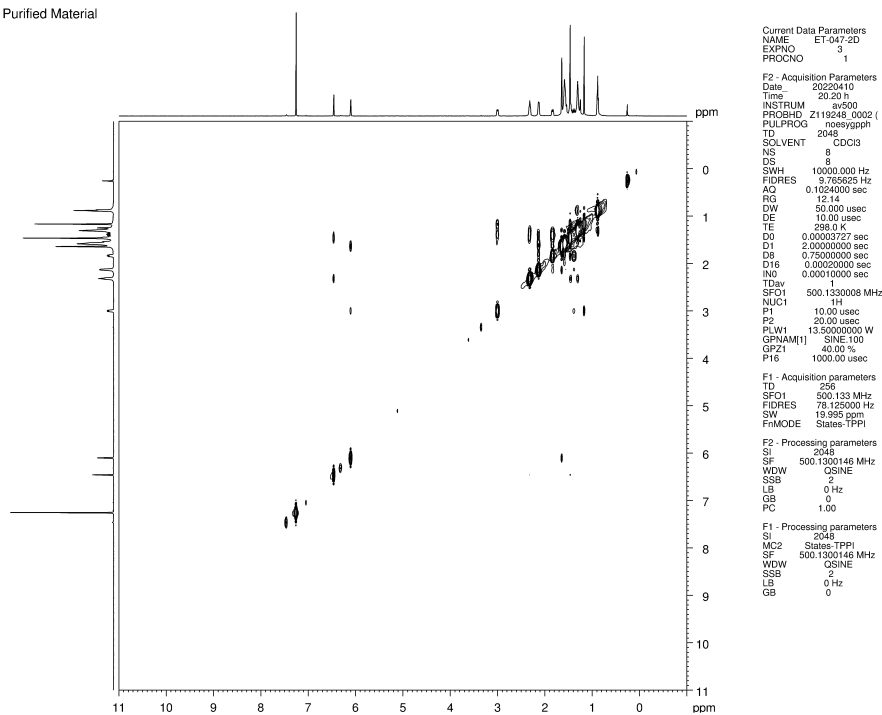
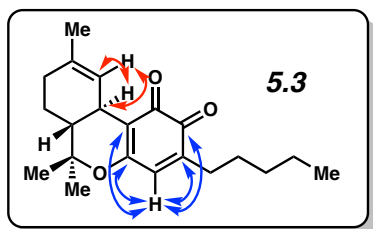


Figure 5.12 NOESY NMR (125 MHz, CDCl₃) of compound 5.3.



HMBC, Purified Material

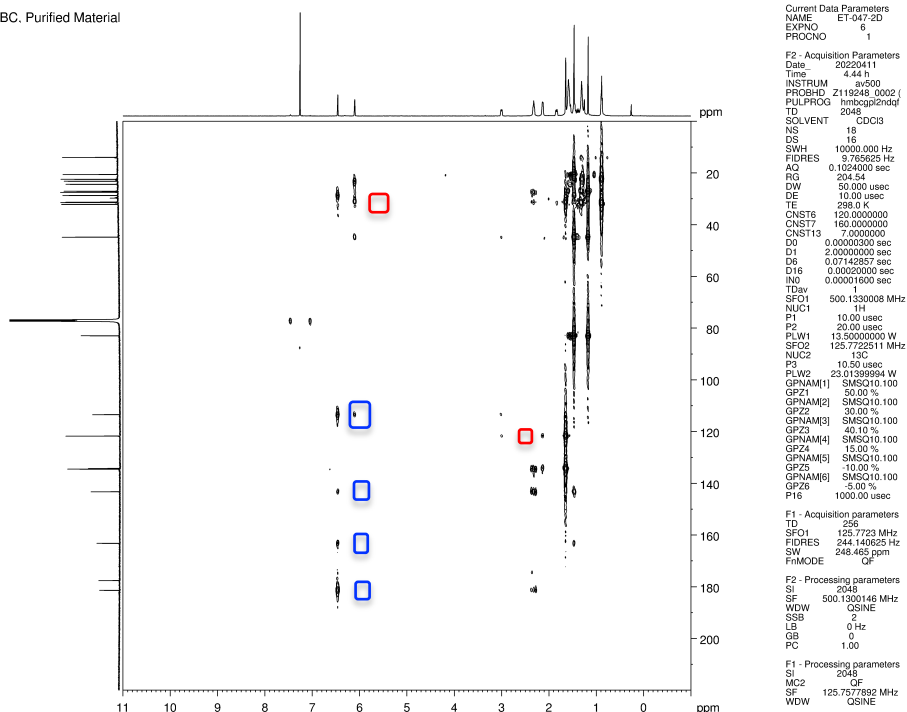
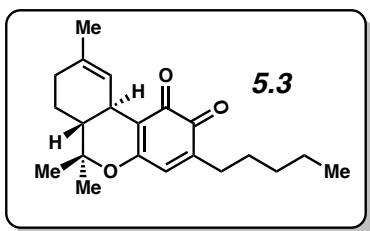
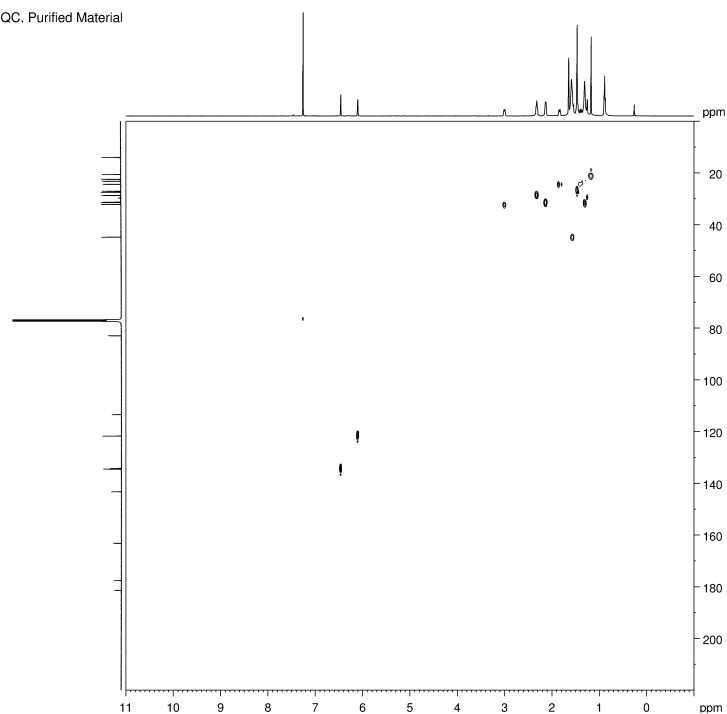


Figure 5.13 HMBC NMR (125 MHz, CDCl₃) of compound 5.3.



HSQC, Purified Material



```

Current Data Parameters
NAME      ET-047-20
EXPNO    1
PROCNO   1

F2 - Acquisition Parameters
Date_    20220411
Time     1.57 h
INSTRUM  av500
PROBHD   Z119248_0002 (
PULPROG  msgecho1pp
TD        2048
SOLVENT  CDCl3
NS        24
DS        6
SWH       10000.000 Hz
FIDRES    9.765625 Hz
AQ        0.1024000 sec
RG        204.54
DW        50.000 usec
DE        10.00 usec
TE        298.0 K
CNST2     145.0000000
D0        0.00000000 sec
D1        1.5000000 sec
D4        0.00172414 sec
D11       0.03000000 sec
D13       0.00000400 sec
D18       0.00020000 sec
D21       0.00345000 sec
NO        0.00001600 sec
TD0       1
ZSOPTNS
SFO1      500.1330008 MHz
NUC1      1H
P1         10.00 usec
P2         20.00 usec
P2B        1000.00 usec
PLW1       13.50000000 W
SFO2      125.7722511 MHz
NUC2      13C
CPDPRG2   garp
P3         10.50 usec
P4         21.00 usec
PCPD2     70.00 usec
PLW2       23.01339994 W
PLW12     0.51789999 W
GPNAM[1]  SMSQ10.100
GPZ1      80.00 %
GPNAM[2]  SMSQ10.100
GPZ2      20.10 %
P16       1000.00 usec

F1 - Acquisition parameters
TD        2048
SFO1      125.7723 MHz
FIDRES    244.146825 Hz
SW        248.465 ppm
FmMODE    Echo-Antiecho

F2 - Processing parameters
SI        2048
SF        500.1300146 MHz
WDW       GSSINE
SSB       2
LB        0 Hz
GB        0
PC        1.00

F1 - Processing parameters
SI        2048
MC2       echo-antiecho
SF        125.7577892 MHz
WDW       GSSINE
SSB       2
  
```

Figure 5.14 HSQC NMR (125 MHz, CDCl_3) of compound 5.3.

5.7 Notes and References

- (1) Caulkins, J. P.; Kilmer, B.; Kleiman, M. A. R. *Marijuana Legalization: What Everyone Needs to Know* 2nd ed.; Oxford University Press, 2016.
- (2) *Summer 2022: A Brief Cannabis Legalization Update*. <https://www.afslaw.com/perspectives/alerts/summer-2022-brief-cannabis-legalization-update> (Accessed 2022-09-26).
- (3) Röhrich, J.; Schimmel, I.; Zörntlein, S.; Becker, J.; Drobnik, S.; Kaufmann, T.; Kuntz, V.; Urban, R. Concentrations of Δ^9 -Tetrahydrocannabinol and 11-nor-9-carboxytetrahydrocannabinol in Blood and Urine After Passive Exposure to Cannabis Smoke in a Coffee Shop. *J. Anal. Toxicol.* **2010**, *34*, 196–203.
- (4) Divagar, M.; Gayathri, R.; Rasool, R.; Shamlee, J. K.; Bhatia, H.; Satija, J.; Sai, V. V. R. Plasmonic fiberoptic absorbance biosensor (P-FAB) for Rapid Detection of SARS-CoV-2 Nucleocapsid Protein. *IEEE Sens. J.* **2021**, *21*, 22758–22766.
- (5) Niedbala, R. S.; Kardos, K. W.; Fritch, D. F.; Kardos, S.; Fries, T.; Waga, J. Detection of Marijuana Use by Oral Fluid and Urine Analysis Following Single-Dose Administration of Smoked and Oral Marijuana. *J. Anal. Toxicol.* **2001**, *25*, 289–303.
- (6) Karschner, E. L.; Schwilke, E. W.; Lowe, R. H.; Darwin, W. D.; Pope, H. G.; Herning, R.; Cadet, J. L.; Huestis, M. A. Do Δ^9 -Tetrahydrocannabinol Concentrations Indicate Recent Use in Chronic Cannabis Users? *Addiction* **2009**, *104*, 2041–2048.
- (7) Khajuria, H.; Nayak, B. P. Detection of Δ^9 -Tetrahydrocannabinol (THC) in Hair Using GC-MS. *Egypt. J. Forensic Sci.* **2013**, *4*, 17–20.

- (8) Verstraete, A. G. Detection times of drugs of abuse in blood, urine, and oral fluid. *Ther. Drug Monit.* **2004**, *26*, 200–205.
- (9) DeGregorio, M. W.; Wurtz, G. T.; Montoya, E.; Kao, C.-J. A comprehensive breath test that confirms recent use of inhaled cannabis within the window of impairment. *Sci. Rep.* **2021**, *11*, 22776.
- (10) Sewell, R. A.; Poling, J.; Sofuoglu, M. The effect of cannabis compared with alcohol on driving. *Am. J. Addict* **2009**, *18*, 185–193.
- (11) Hartman, R. L.; Huestis, M. A. Cannabis effects on driving skills. *Clin. Chem.* **2013**, *59*, 478–492.
- (12) Hartman, R. L.; Brown, T. L.; Milavetz, G.; Spurgin, A.; Pierce, R. S.; Gorelick, D. A.; Gaffney, G.; Huestis, M. A. Cannabis effects on driving lateral control with and without alcohol. *Drug Alcohol Depend.* **2015**, *154*, 25–37.
- (13) Lynn, M. S.; Tang, H. R.; Bechtel, K. L.; Holst, P. A. Compositions and methods for detection of target constituent in exhaled breath. US Patent No. US 9,921,234 B1.
- (14) Lynn, M. S.; Heanue, J. A.; Anekal, S. G.; Limtao, K. M.; Dunk, K. B.; Schuster, J. A. Analyte detection from breath samples. US Patent No, US 11,187.711 B1.
- (15) Lynn, M. S.; Tang, H. R.; Dunk, K. B.; Limtao, K. M.; Jain, H. Detection and measurement of target substance in exhaled breath. UP Patent No. US 11,026,596 B1.
- (16) Hwang, S. I.; Franconi, N. G.; Rothfuss, M. A.; Bocan, K. N.; Bian, L.; White, D. L.; Burkert, S. C.; Euler, R. W.; Sopher, B. J.; Vinay, M. L., Sejdic, E.; Star. A. Tetrahydrocannabinol detection using semiconductor-enriched single-walled carbon nanotube chemiresistors. *ACS Sens.* **2019**, *4*, 2084–2093.

- (17) Star, A.; Huang, S. Tetrahydrocannabinol Sensor. International Patent No. WO 2018/200794 A1.
- (18) Attariwala, R.; Malhi, K.; Yost, R.; Boock, J.; Costanzo, M. T. Device and method for the detection of cannabis and other controlled substances using FAIMS. International Patent No. WO 2017/147687 A2.
- (19) Costanzo, M. T.; Boock, J. J.; Kemperman, R. H. J.; Wei, M. S.; Beekman, C. R.; Yost, R. A. Portable FAIMS: Applications and future perspectives. *Int. J. Mass Spectrom.* **2017**, *422*, 188–196.
- (20) Lai, H.; Corbin, I.; Almirall, J. R. Headspace sampling and detection of cocaine, MDMA, and marijuana via volatile markers in the presence of potential interferences by solid phase microextraction ion mobility spectrometry (SPME-IMS). *Anal. Bioanal. Chem.* **2008**, *392*, 105–113.
- (21) Darzi, E. R.; Garg, N. K. Electrochemical Oxidation of Δ^9 -Tetrahydrocannabinol: A Simple Strategy for Marijuana Detection. *Org. Lett.* **2020**, *22*, 3951–3955.
- (22) Di, H.; Forbes, C. R.; Garg, N. K.; Darzi, E. R. A Cannabinoid Fuel Cell Capable of Producing Current by Oxidizing Δ^9 -Tetrahydrocannabinol. *Org. Lett.* **2022**, *24*, 6705–6710.
- (23) Himes, S. K.; Scheidweiler, K. B.; Beck, O.; Gorelick, D. A.; Desrosiers, N. A.; Huestis, M. A. Cannabinoids in Exhaled Breath Following Controlled Administration of Smoked Cannabis. *Clin. Chem.* **2013**, *59*, 1780–1789.

- (24) Kintz, P.; Mura, P.; Jamey, C.; Raul, J.-S. Detection of Δ^9 -Tetrahydrocannabinol in Exhaled Breath after Cannabis Smoking and Comparison with Oral Fluid. *Forensic Toxicol.* **2017**, *35*, 173–178.
- (25) Luo, Y. R.; Yun, C.; Lynch, K. L. Quantitation of Cannabinoids in Breath Samples Using a Novel Derivatization LC-MS/MS Assay with Ultra-High Sensitivity. *J. Anal. Toxicol.* **2019**, *43*, 331–339.
- (26) Sandford, C.; Edwards, M. A.; Klunder, K. J.; Hickey, D. P.; Li, M.; Barman, K.; Sigman, M. S.; White, H. S.; Minter, S. D. A Synthetic Chemist's Guide to Electroanalytical Tools for Studying Reaction Mechanisms. *Chem. Sci.* **2019**, *10*, 6404–6422.
- (27) Mattoteia, D.; Tagliatela-Scafati, O.; Muñoz, E.; de la Vega, L.; Caprioglio, D.; Appendino, G. Regiodivergent Synthesis of *ortho*- and *para*-Cannabinoquinones. *Eur. J. Org. Chem.* **2020**, 7429–7434.
- (28) Ito, S.; Okada, H.; Katayama, R.; Kunai, A.; Sasaki, K. Direct Conversion of Benzene to Hydroquinone Mediated with Cu(I)/Cu(II) Redox System. *J. Electrochem. Soc.* **1988**, *135*, 2996–3000.
- (29) Ling, K.; Lee, Y.; Macikenas, D.; Protasiewicz, J. D.; Sayre, L. M. Copper(II)-Mediated Autoxidation of Tert -Butylresorcinols. *J. Org. Chem.* **2003**, *68*, 1358–1366.
- (30) Sotaro, I.; Kunai, A.; Okada, H.; Kazuo, S. Direct Conversion of Benzene to Hydroquinone. Cooperative Action of Cu(I) Ion and Dioxygen. *J. Org. Chem.* **1988**, *53*, 296–300.

- (31) Allen, S. E.; Walvoord, R. R.; Padilla-Salinas, R.; Kozlowski, M. C. Aerobic Copper-Catalyzed Organic Reactions. *Chem. Rev.* **2013**, *113*, 6234–6458.
- (32) Bard, A. J.; Faulkner, L. R. *Electrochemical Methods: Fundamentals and Applications*, 2nd ed.; Wiley Global Education, 2000.
- (33) Frigerio, M.; Santagostino, M.; Sputore, S. A User-Friendly Entry to 2-Iodoxybenzoic Acid (IBX). *J. Org. Chem.* **1999**, *64*, 4537–4538.
- (34) Andersson, M.; Scheidweiler, K. B.; Sempio, C.; Barnes, A. J.; Huestis, M. A. Simultaneous Quantification of 11 Cannabinoids and Metabolites in Human Urine by Liquid Chromatography Tandem Mass Spectrometry Using WAX-S Tips. *Anal. Bioanal. Chem.* **2016**, *408*, 6461–6471.
- (35) Mattoteia, D.; Tagliatela-Scafati, O.; Muñoz, E.; de la Vega, L.; Caprioglio, D.; Appendino, G. Regiodivergent Synthesis of *ortho*- and *para*- Cannabinoquinones. *Eur. J. Org. Chem.* **2020**, 7429–7434.